UNIVERSIDAD AUTONOMA DE MADRID

FACULTAD DE CIENCIAS

Departamento de Biología Molecular

EL GEN 7 DE *ALFACORONAVIRUS 1* CONTRARRESTA LA RESPUESTA DEL HUÉSPED Y MODULA LA VIRULENCIA DEL VIRUS

Jazmina L. González Cruz

CSIC
CONSEJO SUPERIOR DE INVESTIGACIONES CIENTÍFICAS

CENTRO NACIONAL DE BIOTECNOLOGÍA

Madrid, Noviembre de 2011

UNIVERSIDAD AUTÓNOMA DE MADRID
FACULTAD DE CIENCIAS
Departamento de Biología Molecular

EL GEN 7 DE *ALFACORONAVIRUS 1* CONTRARRESTA LA RESPUESTA DEL HUÉSPED Y MODULA LA VIRULENCIA DEL VIRUS

Memoria presentada por Jazmina L. González Cruz para optar al grado de Doctor de Ciencias por la Universidad Autónoma de Madrid

Madrid, Noviembre de 2011

El trabajo que se describe en esta memoria ha sido realizado en el Centro Nacional de Biotecnología (CNB-CSIC) bajo la codirección de los Drs. Luis Enjuanes y Sonia Zúñiga.

Madrid, Noviembre de 2011

Fdo. Luis Enjuanes Fdo. Sonia Zúñiga

AGRADECIMIENTOS

Al director de la tesis, el profesor de investigación Luis Enjuanes, gracias por su confianza, su apoyo y por permitirme trabajar en su laboratorio y alcanzar las metas que me había propuesto.

Estos cinco años han sido todo un desafío y aventura para mi, y me gustaría aprovechar esta oportunidad para dejar constancia de lo importantes que habéis sido para mi. Llegué a Madrid arrastrando una maleta más grande que yo y a lo largo de estos años he conseguido tantas cosas que no existen maletas suficientes en el mundo para llevarme todo lo que me habéis dado.

Mi querida Sonia, cómo podría agradecerte todo lo que has hecho por mi como co-directora, pero más importante, como amiga. Gran parte de lo que soy como científica te lo debo a ti, porque me enseñaste lo que sabías con la paciencia de una madre; porque confiaste en mi y me dejaste dar mis primeros pasos sola. Siempre atenta, siempre dispuesta a tenderme una mano. Ha sido maravilloso tenerte para compartir mi pasión por lo que hacemos. Voy a echar de menos nuestras conversaciones de mesa a mesa, o tenerte en el público asintiendo y mirándome con orgullo. Te voy a echar de menos. Sin ti no podría haber hecho nada de esto, y lo peor de todo, sin ti no habría sido tan divertido. Muchísimas gracias.

A mis compañeros del 114. Lorena, aunque dedicase todo el tiempo del mundo creo que no acabaría de entender cómo una persona tan maravillosa y buena cabe en un cuerpito tan pequeño. Gracias por haber estado siempre tanto en los momentos malos como en los buenos. Por haberme aceptado tal y como soy con mis locuras, por haberme hecho reír hasta llorar con tus "lorenadas" y por haberme honrado al incluirme en los momentos que han sido importantes para ti. No importa lo lejos que esté, siempre estaremos la una para la otra.

Marga, muchos estarán de acuerdo conmigo que eres como nuestra madre en el 114. Desde el primer momento que cruzamos esa puerta, nos acoges bajo tu ala, preocupándote no sólo por papeleos sino también por que nos sintamos un poco como en casa. Gracias por todas la veces que has dejado a un lado lo que estabas haciendo y me has ayudado con una gran sonrisa diciendo que no me preocupase que algo se podría hacer. Gracias por tu bondad y buen corazón, y por enseñarme que todos los problemas se pueden solucionar con una sonrisa y preguntándole a la persona adecuada.

Gracias también a mis dos pequeños soles, Martina y Sarhay. Martina, gracias por no hacer caso a todo lo que se te dice, porque sino me hubiese perdido tu alegría y optimismo. Me siento orgullosa de que alguna vez me hayas seguido en mis locuras, aunque eso implicase cruzar los dedos para que todo saliese bien. Sarhay, gracias por dejarme ver realmente quién eres. Eres pura luz y dulzura, nunca dejes que nadie cambie eso porque te hace ver el mundo más hermoso que aquellos que no te entienden, y aunque no lo creas, eso te hace fuerte.

Jose Luis, es mucho lo que hemos pasado en este tiempo y al final siempre queda lo bueno, y yo me llevo muchos recuerdos bonitos de mi amigo, lo cual te agradezco. Eres alguien con un corazón muy noble y no te hace falta nada más que eso para ser feliz, créeme.

Y cómo no agradecer la alegría de los Zipi-Zape del laboratorio, Jose Ángel y Jose Manuel. Jose Ángel, nunca olvidaré los deliciosos dulces de tu país y las expresiones tan simpáticas que traes impresas en tu ADN. Jose Manuel, nos has dado una gran lección a todos nosotros. Me llevo tú gran fuerza y entereza frente a las dificultades, y por supuesto, gracias por "el comentario perfecto". Tu genialidad me ha arrancado lágrimas de risa. Gracias por haberme dejado ver más allá de tu concha, me pareces simplemente una persona brillante.

Fernando, tienes una visión prodigiosa sobre los puntos flacos de las historias, por eso agradezco enormemente tus temidas pero esperadas preguntas porque una vez resueltas siempre mejoraron mi trabajo. De la misma forma agradezco a Isabel por su integridad y profesionalidad. Siempre has estado dispuesta a ayudar y a discutir de igual a igual, lo que me ha resultado muy enriquecedor tanto profesional como personalmente. Carlos, por suerte para mi en estos últimos años he aprendido que se te gana con una sonrisa. Gracias por el apoyo técnico y humano que nos das en el laboratorio. Gracias a Marta y a Pedro, porque hace falta personas como ustedes para entender lo que es ser un buen compañero. Gracias Aitor, por todos los momentos compartidos este tiempo, por enseñarme que Madrid es algo más que edificios y asfalto, y por lo buen compañero que has sido siempre. Tienes un corazón enorme Tori, cuídalo bien. A Silvia, eres un ejemplo de superación. Gracias por tu entusiasmo y las ganas que le pones a todo lo que haces.

No quisiera olvidar a aquellos que conocí a partir de su agradable estancia en el 114. Javi, te has convertido por derecho propio en alguien muy importante para mi. Eres mi "hado padrino", si me permites el título. Siempre has estado para ayudarme y para encender una luz cuando estaba perdida. Tienes un gran corazón y me siento afortunada y agradecida de que seamos amigos. Lo sabes, ¿verdad? Me caíste bien desde el primer momento. Espero que estés siempre. Jose Luis M., que lejos veo el tiempo en el que me regañabas por agitar la botella de medio como una maraca. Agradezco todo lo que me enseñaste y todo lo que aprendí a raíz de haber conocido al chico del extrarradio. Gracias por cuidar de mi… a tu manera. Kike, siempre era productivo preguntarte porque tienes una mente prodigiosa. Aprendí muchas cosas de ti, incluyendo la canción "Maradona" de Calamaro, gracias entre muchas cosas por esos momentos musicales.

Y por supuesto quiero agradecer a mis dos frikis preferidas, Bea y Ana C., las únicas con las que se puede hablar de ciencia con un mojito en la mano. Bea, fuiste mi primera amiga en el 114. Recuerdo cuando nos escapábamos para tumbarnos al sol; los sudokus en los cursos de doctorado; lo inteligente que eres y las ganas de hacer algo importante. Muchas gracias por seguir compartiendo conmigo las batallas del día a día. Mi preciosa Ana, siempre has estado dispuesta a escucharme en los malos momentos y a reírte conmigo en los buenos. Eres pura generosidad, todo lo que tienes lo pones al servicio de quien lo necesite sin esperar nada a cambio. Eso te hace especial. Me siento muy afortunada de haber estado cerca de ti y, a cambio de todo lo que has hecho por mi, tienes una amiga que te quiere y que siempre te acogerá con los brazos abiertos.

A todas las personas del Centro Nacional de Biotecnología con las que he tenido el placer de coincidir a lo largo de estos cinco años. Especialmente a Carlos E., porque siempre tienes una palabra para subirnos el ánimo, y a Fernando Albarrán, por contagiarme tu sonrisa cada vez que paso por esa puerta, sea fin de semana o vacaciones. Y a los amigos que he hecho en otros laboratorios. Joan, menos mal que al final le cogí el punto a tu humor catalán, lo que hizo que las discusiones del almuerzo

fuesen más interesantes y "multiculturales", aunque hablar de libros no es lo tuyo, a menos que se hable de "el millor que li pot passar a un crusant". A Lorena y a Dani, por todos los momentos de ocio que compartimos, bien moviendo la barriga como serpenteando por las montañas y barrancos. A Paloma, por ser tan buena y generosa, y por aguantarme estos años, literalmente.

Al servicio de microscopía confocal. Silvia, tu calidad como profesional y como persona es lo que hace que el servicio que llevas funcione tan bien. Susana, gracias por estar siempre dispuesta a ayudarme con tanta alegría. Me ha encantado trabajar y silbar con ustedes.

Al servicio de genómica, especialmente a Juan Carlos O., por estar siempre dispuesto ha ayudar y a compartir conmigo lo último de lo último en avances tecnológicos… de ocio, claro está.

A mis tres lindas muñequitas, Ana, Nieves e Isa, estoy muy orgullosa de ustedes. Me recuerdan de dónde vengo y que la verdadera amistad resiste al paso del tiempo. Me hacen sentir como en casa. Ana, gracias por tu dulzura, que hace que se despierte en mi la parte más tierna. Y gracias por lo loca que estás, no me regañes pero es la parte que más me gusta de ti porque es maravilloso poder dar rienda suelta a la alegría que uno tiene que contener por las formalidades del mundo adulto. ¡¡¡Viva la pota volona!!! Nieves, mi pequeña brujita, gracias por tu fuerza de carácter, tu determinación y tu buen humor, que han hecho que los momentos más extravagantes de mi vida se parezcan más a una novela rosa que a verdaderos problemas. Así lo malo pesa mucho menos. Mi valiente Isa, gracias por compartir conmigo las batallas perdidas y ganadas. Hemos ido creciendo juntas, alimentándonos la una con la fuerza de la otra, y gracias a eso las dos llegaremos bien alto. Las tres me complementan.

Mario, no sólo me has escuchado en los malos momentos de estos años, sino que, lo más importante, he disfrutado mucho de Madrid a tu lado. Tengo que agradecerte que fueses mi camarada en cada aventura que vivimos por las calles de la gran ciudad. Gracias por ser el mejor compañero de juegos.

Ana N., eres una de las personas más importantes de mi vida. Soy afortunada de que te hayas cruzado en mi camino y así poder compartir contigo un programa de televisión, el poner el árbol de Navidad, un viaje a Portugal…Pequeñas cosas que compartes con alguien cercano; pequeñas cosas que compartes con tu familia. Mil gracias, sabes que te adoro.

Y por último agradecer a lo más importante que tengo en esta vida, mi familia. Habéis sido mi soporte en los momentos en los que flaqueaba, y habéis compartido conmigo los momentos más dulces y alegres de este proceso. Ni un segundo en estos años les he sentido lejos, porque sois parte de mi y todo lo bueno que tengo se lo debo a ustedes. A mis abuelos y tíos, por preguntarme por los bichitos; a mi hermano Ardiel, por las largas conversaciones telefónicas que me ayudaron a dar un enfoque distinto a los problemas; a mi hermana pequeña Ariadna, la mejor amiga que tengo, gracias por haber estado al pie del cañón durante estos cinco años; a mi madre Mª del Carmen, por haberme transmitido tu coraje y la valentía que hace falta para luchar por lo que crees justo; y a mi padre, Florencio, por entenderme y cuidarme, no hay nada que me complazca más que saber que estás orgulloso de mi. Los quiero hasta el ocho acostado.

¿No hay límites, Juan?, pensó, y sonrió.

Su carrera hacia el aprendizaje había empezado...

("Juan Salvador Gaviota", Richard Back)

A mi familia, con la que comparto lazos de sangre y con la que no.

ABREVIATURAS

2'-5'A	5'-trifosfo,2'-5'-oligoadenilatos
2'-5'OAS	2'-5' oligoadenilado sintetasa
aa	Animoácidos
ASFV	Virus de la peste porcina Africana
BAC	Cromosoma artificial de bacteria
BCoV	Coronavirus bovino
BGH	Homona de crecimiento bovino
BHK	Línea celular de riñón de hamster
Bip/GRP78	Proteína de unión a inmunoglobulina o proteína regulada por glucosa-78
BtCoV	Coronavirus de murciélago
BUSB	Beta-glucuronidasa
Cap	7-metil-guanosina
CCoV	Coronavirus canino
cDNA	Ácido deoxirribonucleico complementario
CMV	Citomegalovirus
CoV	Coronavirus
JNK	Quinasa del extremo N-terminal de c-Jun
Hel	Helicasa
CPE	Efecto citopático
CS	Secuencia central conservada
DMEM	Medio Eagle modificado por Dulbecco
DMV	Vesícula de doble membrana
DNA	Ácido deoxirribonucleico
DRBD	Dominio de unión a RNA de doble cadena
dsRNA	RNA de doble cadena
EBV	Virus del Epstein-Barr
EDTA	Ácido etilendiaminotetraacético
eIF2 α	Factor iniciador de la traducción 2α
eIF4G	Factor iniciador de la traducción 4G
EMCV	Virus de la encefalomiocarditis
Endo	Endonucleasa
Exo	Exoncleasa
FBS	Suero fetal de ternera
FDR	Tasa de falsos descubrimientos
FECoV	Coronavirus de la enteritis felina
FIPV	Virus de la peritonitis infecciosa felina
FITC	Isotiocianato de fluoresceina
GADD34	Proteína de parada del crecimiento inducible por lesión del DNA
GAS	Secuencias activadas por interferón-γ
GCN2	Quinasa del control general de la biosíntesis de aminoácidos
HA	Hemaglutinina
HCoV	Coronavirus humano
HCV	Virus de la hepatitis C
HE	Hemaglutinina esterasa
HIV-1	Virus de la inmunodeficiencia humana tipo 1
Hpi	Horas después de la infección
HRI	Quinasa de eIF2α regulada por el grupo hemo
HSV-1	Virus del herpes simple-1
IBV	Virus de la bronquitis infecciosa
ICTV	Comité Internacional de Taxonomía de Virus
IFN	Interferón
IL	Interleuquina
IRF	Factor regulador del interferón
ISG	Gen estimulado por interferón
ISRE	Elemento de respuesta estimulado por interferón
Iκκ	Complejo quinasa
JAK	Quinasa Janus
kb	Kilobase

kDa	Kilodalton
LAMP-1	Proteína-1 asociada a la membrana de los lisosomas
LB	Luria Bertani
MDA-5	Proteína gen-5 asociado a la diferenciación del melanoma
MHC-I	Complejo de histocompatibilidad de tipo I
MHV	Virus de la hepatitis murina
Moi	Multiplicidad de infección
MT	Metiltransferasa
NF-κB	Factor nuclear κB de transcripción
NK	Células *natural killer*
nsp	Proteínas no estructurales
nt	Nucleótido
ORF	Fase abierta de lectura
pAPN	Aminopeptidasa N porcina
pb	Pares de bases
pBAC	Plásmido pBeloBAC11
PBS	Solución salina tamponada con fosfato
PCR	Reacción en cadena de la polimerasa
pfu	Unidades formadoras de placa
PI	Yoduro de propidio
PKR	Quinasa dependiente de RNA de doble cadena
poliA	Tramo de poliadeninas, An
Poly(I:C)	Ácido poliinosínico/policitidílico
PP1	Proteína fostasa-1
PP1c	Subunidad catalítica de la fosfatasa PP1
PRCoV	Coronavirus respiratorio porcino
RdRp	RNA polimerasa dependiente de RNA
RIG-I	Proteína gen-I inducible por ácido retinoico
RLI	Inhibidor de la RNasa L
RMA	Análisis Robusto Multimatricial
RNA	Ácido ribonucleico
RNasa L	Ribonucleasa L
rpm	Revoluciones por minuto
RS	Sentido reverso
RTC	Complejo de replicación-transcripción
rTGEV	Virus recombinante TGEV
RT-qPCR	Transcripción reversa seguida por PCR cuantitativa
SARS	Síndrome respiratorio agudo severo
SDS	Dodecil sulfato sódico
SDS-PAGE	Gel de poliacrilamida con dodecil sulfato sódico
sg RNA	RNA subgenómico
ST	Línea celular de tésticulo de cerdo
STAT	Factor transductor de señal y activador de transcripción
TAE	Tampón Tris-acetado-EDTA
TAR	Región de respuesta a trans-activación
TGEV	Virus de la gastroenteritis porcina transmisible
TLR	Receptor de tipo Toll
Tm	Temperatura de fusión
tRNA	RNA de transferencia
TRS	Secuencia reguladora de la transcripción
TYK2	Tirosin-quinasa 2
UTR	Regiones no traducidas
VS	Sentido viral
VV	Virus vaccinia
ZVAD	Inhibidor N-benziloxicarbonil-Val-Ala-Asp-fluorometiolcetona

I. ÍNDICE

I. ÍNDICE

ÍNDICE DE FIGURAS

ÍNDICE DE TABLAS

II. RESUMEN EN INGLÉS

Transmissible gastroenteritis virus (TGEV) genome contains three accessory genes: 3a, 3b and 7. Gene 7 is only present in members of the species *Alphacoronavirus 1*, and encodes a hydrophobic protein of 78 aa. To study gene 7 function, a recombinant TGEV virus lacking gene 7 was engineered (rTGEV-Δ7). Both the deletion mutant and the parental (rTGEV-*wt*) viruses showed the same growth and viral RNA synthesis kinetics in tissue culture. Nevertheless, cells infected with rTGEV-Δ7 virus showed an increased cytopathic effect caused by an enhanced apoptosis mediated by caspase activation.

Analysis of macromolecular synthesis showed that rTGEV-Δ7 virus infection led to host translational shut-off and increased cellular RNA degradation compared with rTGEV-*wt* infection. An increase of eukaryotic translation initiation factor 2 (eIF2α) phosphorylation and an enhanced nuclease activity were observed in rTGEV-Δ7 virus infected cells. These results suggested that the removal of gene 7 promoted an intensified dsRNA-activated host antiviral response.

A conserved sequence motif that potentially mediates binding to protein phosphatase 1 catalytic subunit (PP1c), a key regulator of the cell antiviral defenses, was identified in protein 7 by bioinformatic analysis. In fact, pull-down assays demonstrated the interaction between PP1 and TGEV protein 7, but not a protein 7 mutant lacking PP1c binding motif. Furthermore, eIF2α was also present in this complex, strongly suggesting a regulation of eIF2α phosphorylation by protein 7. Moreover, the interaction between protein 7 and PP1 was required for eIF2a dephosphotylation and inhibition of cell RNA degradation. These data indicated that TGEV protein 7 counteracted host antiviral response by its association with PP1c.

The analysis of the gene expression profiling in rTGEV-*wt* and rTGEV-Δ7 infected cells using microarrays, showed that the genes differentially expressed were involved in response to virus and inflammation. These results were confirmed by RT-qPCR using specific TaqMan assays, suggesting that the absence of protein 7 during TGEV infection led to enhanced levels of pro-inflammatory cytokines such as IFNβ, TNF, RANTES, CCL2 and CCL4.

Inoculation of newborn piglets with rTGEV-Δ7 and rTGEV-*wt* viruses showed that rTGEV-Δ7 virus led to an accelerated growth kinetics and pathology compared with the parental virus. Furthermore, the increased pathology caused by the rTGEV-Δ7 infection could be due to and exacerbate macrophage activation, as a higher macrophage

infiltration in lung was observed in the animals infected with the deletion mutant virus compared with those infected with the wild type.

Overall, the results indicated that gene 7 counteracted host cell defenses, and modified TGEV virulence increasing TGEV survival. Therefore, the acquisition of gene 7 by the TGEV genome most likely has provided a selective advantage to the virus.

III. INTRODUCCIÓN

1. CLASIFICACIÓN Y CARACTERIZACIÓN DE LOS CORONAVIRUS

El orden de los *Nidovirales*, que incluye a las familias *Coronaviridae*, *Arteriviridae* y *Roniviridae* (Cavanagh y col., 1997; Enjuanes y col., 2000), está compuesto por virus con genoma de RNA no segmentado, de cadena sencilla y polaridad positiva. Los virus de la familia *Coronaviridae* poseen el mayor genoma de RNA conocido, de aproximadamente 30 kb (Gonzalez y col., 2003). La familia *Coronaviridae* se compone de las subfamilias *Coronavirinae*, formada por los géneros Alfa-, Beta- y Gamma-coronavirus, y *Torovirinae*, formada por los géneros torovirus y bafinivirus (http://www.ictvonlineorg/virusTaxonomy.asp, Octubre 2011) (Carstens, 2010; de Groot y col., 2011; de Groot y col., 2010a). Recientemente se ha propuesto un nuevo género, el Deltacoronavirus, aunque todavía no ha sido aprobado por el Comité Internacional de Taxonomía de Virus (ICTV) (Lauber C. y Gorbalenya A.E., 2011, *The XIIth International Nidovirus Symposium*).

Los nidovirus infectan a un amplio rango de hospedadores desde vertebrados mamíferos como humanos, animales domésticos y salvajes, ballenas o murciélagos, hasta distintas especias aviares así como invertebrados, tales como gambas y langostas e insectos (Cowley y col., 2002; Mihindukulasuriya y col., 2008; Sittidilokratna y col., 2002; van der Hoek y col., 2004; Vijaykrishna y col., 2007; Woo y col., 2005a; Zirkel y col., 2011). Los coronavirus (CoVs) de los géneros α y β infectan mamíferos, incluido el hombre, mientras que los CoVs del género γ infectan principalmente aves. Además, recientemente se ha descrito un gran número de especies de CoV, incluidos dentro de los géneros α y β que infectan a murciélagos (Chu y col., 2006; Poon y col., 2005). Los CoVs se asocian principalmente a enfermedades respiratorias, entéricas, hepáticas y del sistema nervioso central (Drosten y col., 2003; Lai and Holmes, 2001; Perlman y col., 2000). Los CoVs humanos causan principalmente infecciones del tracto respiratorio, y son responsables del 10-20% de los catarros comunes (McIntosh y col., 1969). En el año 2003, los CoVs atrajeron la atención mundial debido a la emergencia en China del CoV del síndrome respiratorio agudo severo (SARS-CoV), que infectó a más de 8000 personas de 32 países con una mortalidad del 10% (Drosten y col., 2003; Rota y col., 2003). Desde entonces, se han identificado nuevos CoVs humanos, como el HCoV-NL63 (van der Hoek y col., 2004) y el HCoV-HKU1 (Woo y col., 2005b), que producen neumonías relativamente graves. La identificación de CoV en murciélagos, que son antecesores comunes recientes de los CoVs de los géneros α y β, incluyendo al

SARS-CoV (Chu y col., 2008; Dominguez y col., 2007; Gloza-Rausch y col., 2008; Muller y col., 2007), y de dos aislados de nidovirus en mosquitos, pone de manifiesto la potencial transmisión de estos virus a otras especies, entre ellas a humanos (Parquet y col., 2008; Zirkel y col., 2011; P.T. Nga, E.J. Snijder y A.E. Gorbalenya, comunicación personal).

2. EL VIRUS DE LA GASTROENTERITIS PORCINA TRANSMISIBLE

2.1. Clasificación

En el laboratorio utilizamos el virus de la gastroenteritis porcina transmisible (TGEV) como modelo de CoV. El TGEV es miembro de la especie *Alfacoronavirus 1*, que incluye virus con secuencias altamente relacionadas y que infectan a animales domésticos. Esta especie incluye, además del TGEV, al virus de la peritonitis infecciosa felina (FIPV), el Cov de la enteritis felina (FECoV), el CoV canino (CCoV) y al CoV respiratorio porcino (PRCoV), un mutante de TGEV con tropismo exclusivamente respiratorio. Como característica común, los miembros de esta especie contienen en su genoma el gen 7 después del gen de la nucleocápsida (N). Dependiendo de la especie del virus, contienen una sola ORF (7a), como en el caso del TGEV o PRCoV, o dos ORFs (7a y 7b), como los virus FIPV y CCoV (http//talk.ictvonline.org /media/g/vertebrate-2008/default.aspx, Octubre 2011).

2.2. Epidemiología

El TGEV produce una enteritis muy contagiosa en lechones recién nacidos, con índices de mortalidad próximos al 100% (Saif and Wesley, 1992). La enfermedad, descrita por primera vez en EEUU (Doyle and Hutchings, 1946), se ha identificado en numerosos países europeos, en América central y del sur, en Canadá y en diversos países asiáticos. Actualmente la mayor parte de ganado porcino europeo presenta inmunidad parcial frente al TGEV (Enjuanes and Van der Zeijst, 1995; Pensaert and Van Reeth, 1998) debido a la diseminación de un mutante natural atenuado, el PRCoV. En otros países la diseminación del PRCoV no parece haber sido tan efectiva como en Europa (Woods and Wesley, 1998), y la enfermedad continúa siendo un problema económico para los productores de ganado porcino, particularmente en cabañas porcinas seronegativas de EEUU, Centroamérica, Rusia y China (World Animal Health Organization, http://web.aie.int/wahis/public.php?page=disease, Octubre 2011).

3. ESTRUCTURA DEL GENOMA Y EXPRESIÓN GÉNICA EN CORONAVIRUS

Los CoVs son virus esféricos con una envuelta lipídica, en donde se insertan las proteínas estructurales: de la espícula (S), que confiere a la partícula viral apariencia de corona, dando nombre a la familia, de membrana (M), y de la envuelta (E). En el interior del virión se encuentra la nucleocápsida, formada por el RNA genómico unido a la proteína N (Figura 1A).

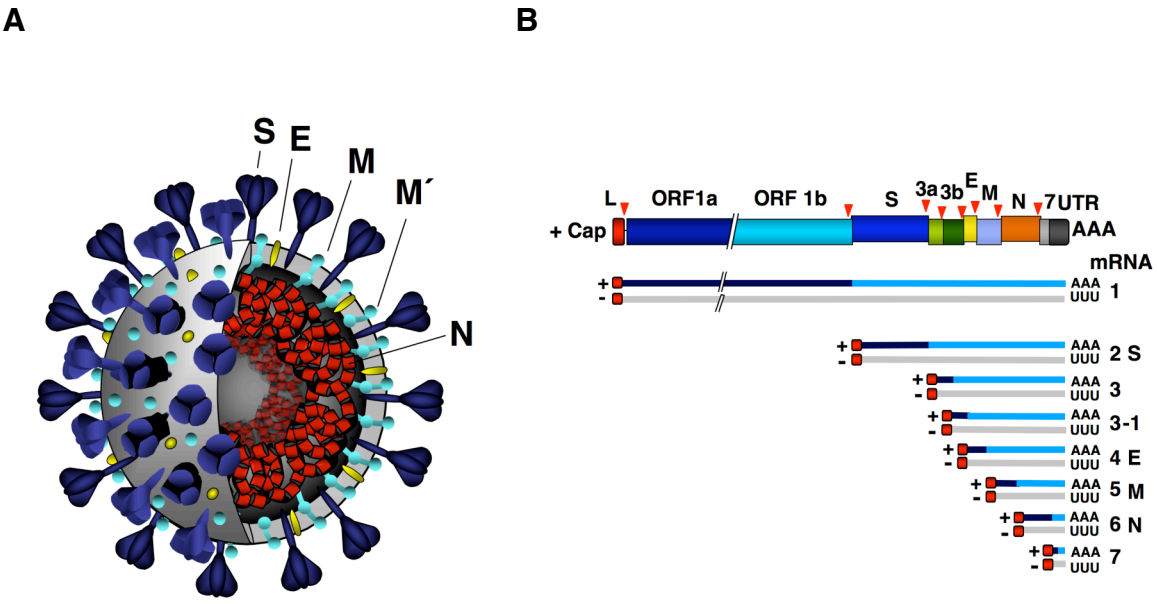

Figura 1. Estructura del virión y expresión génica del coronaTGEV. (A) Modelo de la partícula viral, con los tres niveles estructurales que la conforman: la envuelta lipídica, en la que se insertan las proteínas S, E y M (en dos conformaciones M y M'), la cápsida interna constituida por la proteína N asociada al endodominio C-terminal de la proteína M y la nucleocápsida helicoidal formada por el genoma RNA asociado a la proteína N. (B) Esquema del genoma de TGEV (barra superior), en el que las letras y los números indican genes virales. L, secuencia líder; UTR, región 3' no traducida; AAA, poliA. Los distintos RNAs virales, genómico y subgenómicos, están numerados del 1 al 7 y se indica su polaridad y estructuras terminales comunes. Las secuencias líder y antilíder se muestran en rojo y las secuencias reguladoras de la transcripción (TRSs) se indican con triángulos rojos invertidos.

El genoma de los CoVs consiste en una cadena de RNA sencilla y de polaridad positiva de aproximadamente 30 Kb de longitud (Carstens, 2010; de Groot y col., 2011; Enjuanes y col., 2008b; Gorbalenya y col., 2004; Snijder y col., 2003) (Figura 1B). Estructuralmente, el genoma de los CoVs se asemeja a los mRNAs eucariotas, con una estructura 7-metil-guanosina (Cap) en el extremo 5' (Page y col., 1990), una cola de poliadeninas (poliA) en el extremo 3' (Jacobs y col., 1986), y regiones no traducidas en

ambos extremos (5'UTR y 3'UTR) con una longitud que varia entre los 210 y 530 nt (Brian and Baric, 2005). Los dos tercios 5' terminales del genoma comprenden las fases abiertas de lectura (ORFs) 1a y 1b que codifican la replicasa viral en forma de dos poliproteínas pp1a y pp1ab (Thiel y col., 2003). Las proteínas de la replicasa están implicadas en la replicación del genoma y en la transcripción de los RNAs mensajeros subgenómicos (sg mRNAs). El tercio 3' terminal contiene los genes estructurales en orden: 5'-S-E-M-N-3', y los genes específicos de grupo cuyo número y secuencia varía dependiendo de la cepa de CoV (Carstens, 2010; de Groot y col., 2011; Enjuanes y col., 2008a; Masters, 2006). En la mayor parte de los CoVs, existe un solapamiento entre los genes, bien de secuencias codificantes, o de secuencias reguladoras de la transcripción con secuencias codificantes. Los CoVs replican en el citoplasma y generan un conjunto de sg mRNAs 5' y 3'co-terminales de diferentes tamaños, estructuralmente policistrónicos pero funcionalmente monocistrónicos (Figura 1B). Todos ellos presentan en el extremo 5' la secuencia líder viral, que se incorpora mediante un proceso de síntesis discontinua de RNA dirigido por las secuencias reguladoras de la transcripción (TRSs), formadas por un hexanucleótido central conservado (CS), flanqueado por secuencias variables denominadas 5' y 3' TRSs (Enjuanes y col., 2006b; Sola y col., 2005; Zuñiga y col., 2004).

3.1. Proteínas no estructurales

El complejo de replicación-transcripción (RTC) de CoV está formado por los productos generados a partir de las poliproteínas pp1a y pp1ab y por proteínas celulares. Los productos finales del autoprocesamiento de las poliproteínas pp1a y pp1ab son generalmente 16 proteínas denominadas no estructurales (nsps) (Ziebuhr, 2005). Las proteínas derivadas de la poliproteína pp1a (nsp1 a nsp11) son comunes con las derivadas de la pp1ab (nsp1 a nsp10 y nsp12 a nsp16), excepto la nsp11 que es un polipéptido originado cuando no tiene lugar el salto de fase del ribosoma requerido para la traducción de la pp1ab.

Además de las proteínas esenciales en el RTC, como la RNA polimerasa dependiente de RNA (RdRp, nsp12), o la helicasa (Hel, nsp13), varias proteínas, como la nsp3, nsp4 y nsp6 tienen funciones de andamiaje del complejo del RTC, y reorganización de membranas celulares. Además, las proteínas nsp3 y nsp5 actúan como proteasas para el procesamiento de las poliproteínas (Ziebuhr, 2005; Ziebuhr y col., 2000).

La nsp1 es el primer producto de procesamiento que se observa en células infectadas (Denison y col., 1992; Herold y col., 1998). En el CoV bovino (BCoV) se ha descrito su unión a una secuencia requerida para la replicación (Pfefferle y col., 2009). Sin embargo, su función se desconoce y, de hecho, el virus de la bronquitis infecciosa (IBV), del género γ, no codifica una nsp1 (Gorbalenya y col., 2006; Ziebuhr, 2005).

La proteína nsp2 se incorpora al RTC (Hagemeijer y col., 2010). Aunque aparentemente esta proteína es dispensable para la replicación de los CoVs del género β, se observa una reducción del 50% en el título viral al eliminarla (Graham y col., 2005). Por tanto, su papel en el ciclo viral aún se desconoce.

La proteína nsp3 es multifuncional, y la mayor parte de sus dominios son dispensables para la síntesis de RNA aunque podrían tener un papel en patogénesis (Frieman y col., 2009; Neuman y col., 2008b). La proteína nsp3 interacciona con las proteínas N (Hurst y col., 2010) y E (Alvarez y col., 2010), aunque el papel de estas interacciones no se conoce.

Se ha propuesto que las proteínas nsp7 a nsp10 forman un módulo funcional implicado en la síntesis de RNA (Deming y col., 2007). Las proteínas nsp7 y nsp8 forman un complejo hexadecamérico con propiedades estructurales compatibles con las de un factor de procesividad para la RdRp (Zhai y col., 2005). La nsp8 posee actividad RdRp y probablemente produce los oligonucleótidos cebadores requeridos para la síntesis de RNA por la nsp12 (RdRp) (Imbert y col., 2006; te Velthuis y col., 2010). La proteína nsp9 une RNA de cadena sencilla y podría estabilizar a los RNAs virales durante su síntesis (Egloff y col., 2004; Sutton y col., 2004). Esta proteína forma homodímeros y su oligomerización se requiere para la replicación viral (Miknis y col., 2009). Las nsp8 y 9 del virus de la hepatitis murina (MHV) interaccionan con la RdRp (Brockway y col., 2003) y evidencias genéticas sugieren que también interaccionan con el 3' del genoma viral (Zust y col., 2008). La nsp10 une ácidos nucleicos no específicamente y se ha implicado en síntesis de la cadena negativa de RNA (Matthes y col., 2006; Siddell y col., 2001).

Las nsps 14, 15 y16 codifican actividades de procesamiento de RNA que son únicas en los virus RNA, como exonucleasa (ExoN), endonucleasa (EndoU) y metiltransferasa (MT), respectivamente (Ziebuhr, 2005). Todas estas actividades son necesarias para una síntesis eficiente de RNA (Almazan y col., 2006; Ivanov y col., 2004; Kang y col., 2007). Se ha propuesto que la presencia de estas actividades, especialmente de la nsp14, permite el mantenimiento de los genomas de CoV, de gran tamaño, actuando como un

sistema de corrección de errores (Eckerle y col., 2010; Eckerle y col., 2007; Gorbalenya y col., 2006). La nsp14 de CoV también codifica una proteína con actividad MT en su extremo C-terminal, requerida para la síntesis de RNA (Chen y col., 2009). Es posible que las actividades MT y de la nsp14 y nsp16 actúen de manera coordinada para la incorporación del Cap a los mRNAs virales (Decroly y col., 2008).

3.2. Proteínas estructurales

La proteína S, o proteína de las espículas, se localiza en la envuelta del virión y es el principal inductor de anticuerpos neutralizantes (Delmas y col., 1986; Enjuanes y col., 2007; He y col., 2006; Jiménez y col., 1986; Sanchez y col., 1990; Traggiai y col., 2004; Zhang y col., 2006). La proteína S se encuentra glicosilada, tiene un peso molecular de entre 150-200 kDa, y su forma funcional es un trímero que da el aspecto distintivo a la superficie de los CoVs (Delmas y col., 1990; Song y col., 2004). Esta proteína es importante fundamentalmente en la unión del virus al receptor celular y la fusión de las membranas viral y celular, procesos críticos para la entrada del virus en las células (Gallagher and Buchmeier, 2001). De hecho, la proteína S es la que determina la especificidad de tejido y especie (Sanchez y col., 1992). Trabajos realizados en nuestro laboratorio demostraron que se podían generar virus recombinantes con tropismo respiratorio y entérico (rTGEV-SC11) o sólo respiratorio (rTGEV-SPTV), introduciendo el gen S del TGEV-PUR46-SW11-ST2-C11 o el gen S del TGEV-PTV, respectivamente (Sanchez y col., 1999).

La glicoproteína de membrana M es el componente estructural más abundante de los CoVs (Sturman y col., 1980; Sturman and V., 1977). Es una proteína de entre 25 y 30 kDa, que está formada por un pequeño segmento N-terminal situado hacia el exterior de la partícula viral, tres segmentos transmembrana y un extremo C-terminal orientado hacia el interior del virión y que interacciona con la proteína N. En el caso del TGEV, la proteína M presenta dos topologías, la segunda de ellas con ambos extremos orientados hacia el exterior de la partícula viral (Escors y col., 2001a; Escors y col., 2001b). La proteína M es fundamental para la morfogénesis de CoV (Arndt y col., 2010; Corse and Machamer, 2002, 2003; de Haan y col., 1998a; de Haan y col., 1998b; Fischer y col., 1998).

La proteína E es una proteína transmembrana de entre 8.4 y 12 kDa presente en los viriones en un bajo número de copias (Maeda y col., 2001; Raamsman y col., 2000). Aunque, en general, las proteínas E de los distintos CoVs poseen poca homología de

secuencia, todas comparten la misma organización estructural: un extremo amino terminal corto formado por 8-12 aminoácidos (aa) hidrofóbicos, una zona hidrofóbica de 21-29 aa que contiene de 2-4 cisteínas, y un extremo carboxilo terminal hidrofílico (39-76 aa) (Wilson y col., 2006). La proteína E de CoV comparte características comunes con otras proteínas virales que funcionan como canales iónicos (Torres y col., 2006). La eliminación de la proteína E de TGEV genera virus eficientes en replicación y deficientes en propagación (Ortego y col., 2002). En MHV la proteína E no es esencial, y su eliminación reduce el título viral hasta 3 órdenes de magnitud (Kuo and Masters, 2003). En SARS-CoV, la proteína E tampoco es esencial, pero su eliminación genera virus atenuados *in vivo* (DeDiego y col., 2007) y se ha demostrado que la proteína E es un factor de virulencia que modula la respuesta celular a estrés de retículo y la inflamación (DeDiego y col., 2011).

La proteína N, de entre 43 y 50 kDa, forma parte de la nucleocápsida helicoidal que contiene el genoma viral (Laude and Masters, 1995). Se ha propuesto una organización modular para la proteína N, basada en regiones desordenadas de la proteína, común entre los distintos CoVs (Chang y col., 2006; Zuñiga y col., 2007). En la proteína N se han localizado diferentes dominios de interacción con el RNA (Fan y col., 2005; Huang y col., 2004; Luo y col., 2006; Masters, 1992; Nelson y col., 2000) y de oligomerización (Fan y col., 2005; Hurst y col., 2005; Luo y col., 2006; Yu y col., 2005). La proteína N se une de forma específica a la TRS de la secuencia líder de polaridad positiva (Chen y col., 2007; Sola y col., 2011), secuencias 3'UTR (Zhou y col., 1996), al gen N (Cologna y col., 2000), y a la señal de encapsidación del genoma (Cologna and Hogue, 2000; Molenkamp and Spaan, 1997). La proteína N está fosforilada, lo que ha sido demostrado para CoVs de los tres géneros (Calvo y col., 2005; King and Brian, 1982; Lomniczi and Morser, 1981; Stohlman and Lai, 1979; Zakhartchouk y col., 2005), aunque el papel de esta modificación en el ciclo viral se desconoce. La proteína N posee actividad chaperona de RNA (Zuñiga y col., 2009; Zuñiga y col., 2007), y además de su papel estructural, es necesaria para una síntesis eficiente de RNA (Almazan y col., 2004; Casais y col., 2001; Schelle y col., 2005; Yount y col., 2000) y co-localiza con el RTC (Bost y col., 2001; Verheije y col., 2010). Recientemente, nuestro grupo ha descrito que la proteína N no es necesaria para la replicación de TGEV pero es esencial para la transcripción (Zuñiga y col., 2010).

3.3. Proteínas accesorias o específicas de grupo

Además de los genes comunes a todos los CoVs, (replicasa, S, E, M y N) todos los genomas de estos virus contienen ORFs adicionales (Figura 2). Estos genes accesorios, o específicos de grupo, se encuentran intercalados entre los genes estructurales comunes y van desde un único gen, como el gen 3b del HCoV-NL63, hasta 8 genes, como en el SARS-CoV. La expresión intracelular de estos genes accesorios se ha demostrado sólo en algunos casos.

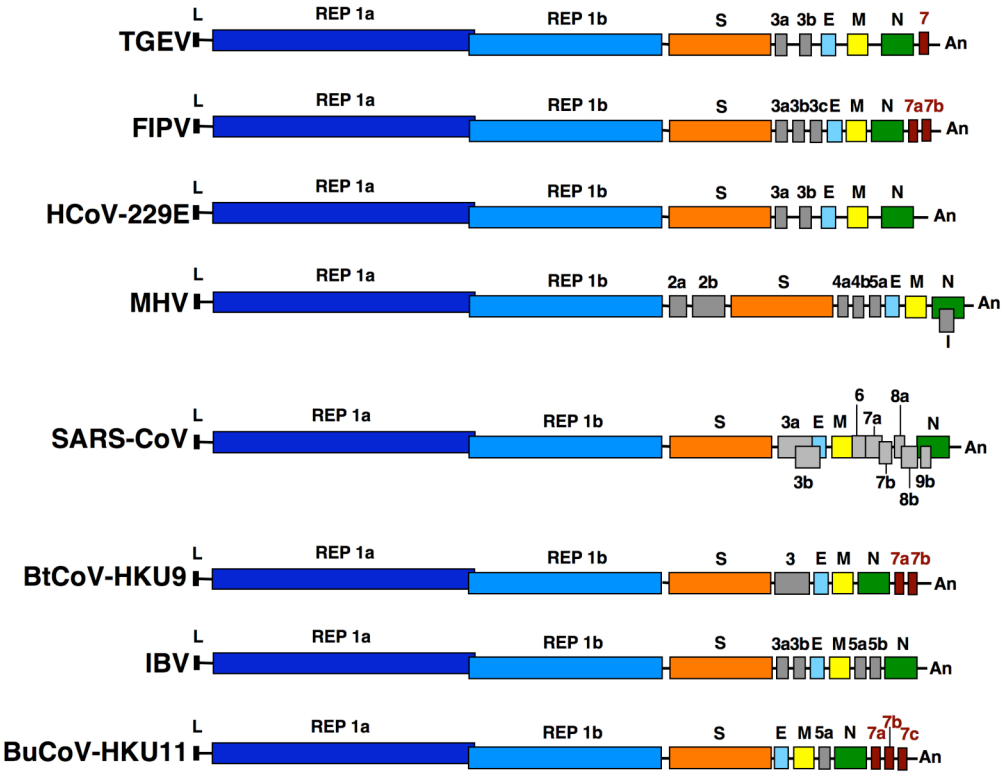

Figura 2. Organización genómica de los CoVs. Organización del genoma de virus representativos de los géneros α, β y γ de CoV. Del género α se representa el genoma del virus de la gastroenteritis transmisible porcina (TGEV) y del CoV de la peritonitis infecciosa felina (FIPV), incluidos en la especie *Alfacoronavirus 1*, y el CoV humano 229E (HCoV-229E). Del género β se representa el genoma del CoV de la hepatitis murina (MHV), de la especie CoVs murinos, el CoV del síndrome respiratorio severo y agudo (SARS-CoV) y el CoV de murciélago universidad de Hon-Kong 9 (BtCoV-HK9). Del género γ se representa el genoma del virus de la bronquitis infecciosa (IBV) y del CoV del bulbul (BuCoV-HKU11), agrupados en la especie CoVs aviares. En gris se representan los genes accesorios. En rojo se representa la posición que ocupan en el genoma los genes 7.

Los genes accesorios de CoV pueden ser estructurales, como por ejemplo el producto del gen 2b o HE de los CoVs del género β (Kienzle y col., 1990; Pfleiderer y col., 1991) y las proteínas 3a, 7a y 9b del SARS-CoV que se han encontrado formando parte del

virión (Huang y col., 2006b; Xu y col., 2009). En general, los genes accesorios han sido nombrados en función del número del sg mRNA a partir del cual se expresan. Sin embargo, esta nomenclatura puede llevar fácilmente a error dado que genes nombrados igual no necesariamente ocupan la misma posición en el genoma, como es el caso de los genes 5a de MHV e IBV, o no poseen homología de secuencia, como los genes 3a del SARS-CoV y de los géneros α y γ.

3.3.1. Genes accesorios localizados entre el gen de la replicasa y de la S

La especie CoV murino es la única que contiene genes accesorios, ORF2a y ORF2b, precediendo al gen que codifica la proteína S. En MHV la eliminación de ambos genes, conjuntamente, resultó en la atenuación completa del virus sin afectar al título viral (de Haan y col., 2002).

La proteína 2a es una proteína no estructural de unos 30 kDa que pertenece a la familia de las 2'-3'ciclo fosfodiesterasas (Mazumder y col., 2002). Estas son enzimas de procesamiento de RNA implicadas en los procesos de maduración del RNA de transferencia (tRNA) (Snijder y col., 2003). Aunque se desconoce el papel concreto de la proteína 2a en el ciclo viral, se ha descrito que un MHV con una proteína 2a conteniendo una mutación puntual es menos virulento, y no replica eficientemente en el cerebro de los ratones infectados, a pesar de que en cultivos celulares la replicación del virus mutante no está afectada (Sperry y col., 2005). Un MHV con una proteína 2a sin actividad fosfodiesterasa no replica en el hígado, aunque es indistinguible del virus parental en sistema nervioso central (Roth-Cross y col., 2009). Recientemente, se ha descrito que esta proteína actúa como antagonista del interferón (IFN) (Zhao L y col., 2011, *The XIIth International Nidovirus Symposium*).

Uno de los genes accesorios mejor caracterizado es la ORF 2b que codifica la proteína hemaglutinina esterasa (HE), uno de los componentes más abundantes en la envuelta de muchos miembros de los CoVs murinos (Brian y col., 1995). La proteína HE forma un segundo grupo de pequeñas espículas que aparecen en la envuelta entre las espículas formadas por los trímeros de la proteína S. Al igual que la proteína S, la proteína HE se encuentra glicosilada, y en su forma madura forma un homodímero que se ha descrito que actúa como cofactor de la proteína S, modulando la entrada del virus en la célula y la especificidad de tejido (Hogue y col., 1989; Kazi y col., 2005; Lissenberg y col., 2005; Popova and Zhang, 2002). Además, la proteína HE podría

prevenir la agregación de la progenie viral, facilitando la diseminación de los virus en el tejido infectado (Cornelissen y col., 1997).

3.3.2. Genes accesorios localizados entre los genes S y E

Los genes accesorios comprendidos entre los genes S y E son las ORFs 3a, 3b, 3c y 4 en todos los géneros de CoV, excepto en la especie CoV murino del género β donde son las ORFs 4 y 5a (Figura 2).

Las proteínas 3a, b y c de la especie *Alfacoronavirus 1* no son esenciales para la replicación en cultivos celulares. En el caso del TGEV, la eliminación de los genes 3a y 3b, solos o combinados, no afecta a la replicación o virulencia del virus (Curtis y col., 2002; Sola y col., 2003; Vaughn y col., 1995). De hecho, nuestro grupo ha generado vectores derivados de TGEV que expresan antígenos heterólogos desde la posición previamente ocupada por los genes 3a y 3b (Cruz y col., 2010; Ribes y col., 2011; Sola y col., 2003). En contraste, los mutantes de FIPV que carecen de los genes 3a, b y c están muy atenuados *in vivo* (Haijema y col., 2004). A diferencia de las proteínas 3a de la especie *Alfacoronavirus 1*, la proteína 3a del SARS-CoV es una proteína estructural que se incorpora en el virión e interacciona con la proteína S (Zeng y col., 2004). Su papel durante el ciclo viral no está claro, aunque recientemente se ha descrito que induce estrés de retículo, y actúa como un inhibidor de la inducción de IFN (Minakshi y col., 2009) y como canal iónico (Wilson y col., 2006). La proteína 3b del SARS-CoV se detecta en células infectadas (Chan y col., 2005), y su sobreexpresión induce la parada del ciclo celular en fase G0/G1 y apoptosis (Yuan y col., 2005). La proteína 3a del IBV, un CoV prototipo del género γ, es una proteína citosólica que no se incorpora en el virión (Pendleton and Machamer, 2005), y la proteína 3b se encuentra en el núcleo de las células infectadas (Shen y col., 2003). Mutantes naturales que carecen de los genes 3a-3b, 3b, o que expresan una proteína 3a de menor tamaño que la nativa, poseen una virulencia similar *in vitro* e *in vivo* a la de los IBVs de genoma completo, lo que indica que estos genes no son necesarios para el crecimiento y la patogénesis viral (Liu y col., 2008; Mardani y col., 2008; Shen y col., 2003).

La secuencia del gen 4 varía entre los diferentes miembros del género Betacoronavirus. En las cepas MHV-JHM y MHV-S, el gen 4 contiene una única ORF, mientras que en el BCoV y la cepa MHV-A59, este gen posee dos ORFs, 4a y 4b (Mounir and Talbot, 1993; Weiss y col., 1993; Yokomori and Lai, 1991). Estos genes

no son esenciales y se han reemplazado para generar vectores de expresión (Baric and Sims, 2005; Fischer y col., 1997).

El gen accesorio 5a de los CoVs murinos, no se encuentra en todas las estirpes de MHV. Recientemente se ha demostrado que el producto de este gen es un antagonista del IFN de tipo I (Koetzner y col., 2010). La eliminación conjunta de los genes 4 y 5a en MHV afecta a la producción de virus, disminuyendo el título viral una unidad logarítmica, y produce una fuerte atenuación del virus (de Haan y col., 2002).

3.3.3. Genes accesorios localizados entre los genes M y N

El IBV contiene dos ORFs accesorias, 5a y 5b, entre los genes M y N que codifican dos proteínas de 7.4 kDa y 9.5 kDa, respectivamente (Jia and Naqi, 1997). Aunque se desconoce el papel de los genes accesorios 5a y 5b, la eliminación del gen 5a no tiene efecto en la replicación del virus en cultivos celulares (Youn y col., 2005).

El SARS-CoV contiene en esa posición del genoma las ORFs 6, 7a, 7b, 8a, 8b y 9b, que carecen de homología con cualquier otro gen de CoV. La generación en nuestro laboratorio de un virus mutante que no expresaba estos seis genes accesorios (SARSCoV-Δ6-9b) confirmó que estos genes eran no esenciales y que además tenían un efecto muy limitado sobre el título viral o la patología causada por la infección (DeDiego y col., 2008). La proteína 6 se incorpora en los viriones, y en la célula infectada se localiza en el retículo endoplásmico y en el aparato de Golgi (Huang y col., 2007; Pewe y col., 2005). Esta proteína interacciona con la proteína nsp8, con lo que podría desempeñar un papel en la replicación viral (Kumar y col., 2007). Se ha demostrado que la proteína 6 induce apoptosis mediada por caspasa 3, estrés y vías de señalización dependientes de la quinasa del extremo N-terminal de c-Jun (JNK) (Ye y col., 2008).

La proteína 7a de SARS-CoV es una proteína estructural y en células infectadas se localiza en el compartimento intermedio (Chen y col., 2005; Fielding y col., 2004; Huang y col., 2006a; Nelson y col., 2005). La proteína 7a interacciona con la nsp3 y las proteínas estructurales S, E y M (Pan y col., 2008; von Brunn y col., 2007). La sobre-expresión de esta proteína produce la parada del ciclo celular en fase G0/G1, la inhibición de la síntesis de proteínas celulares, y la fosforilación de la proteína kinasa activada por mitógeno p38 (Kopecky-Bromberg y col., 2006; Yuan y col., 2006). La proteína 7b es una proteína integral de membrana, que se incorpora en el virión y se localiza en el aparato de Golgi en las células infectadas (Schaecher y col., 2007). Esta

proteína podría interaccionar con las proteínas virales nsp9, nsp16, E, 6, 8b y 9b (Pan y col., 2008; von Brunn y col., 2007). Las proteínas 7a y 7b de SARS-CoV son dispensables para el ciclo viral tanto *in vitro* como *in vivo* (DeDiego y col., 2008; Yount y col., 2005).

Las proteínas 8a y 8b se expresan como proteínas independientes en la mayoría de los aislados del SARS-CoV procedentes de humanos, mientras que en los aislados de animales, y de humanos de una etapa temprana de la epidemia, las proteínas 8a y 8b se encuentran fusionadas en una sola proteína (8ab), aunque el significado biológico de este cambio aún no se ha descrito (Oostra y col., 2007; Yount y col., 2005). La proteína 8a interacciona con las proteínas virales nsp8, nsp15, 8b y 9b, y la proteína 8b interacciona con las proteínas virales nsp3, nsp8, 3a, S, M, 7b, 8a, 9b y N, aunque el papel de estas interacciones en el ciclo del virus se desconoce (Pan y col., 2008; von Brunn y col., 2007).

La expresión de la proteína 9b en células de mamífero ha demostrado que se asocia con vesículas intracelulares y es un componente minoritario del virión, lo cual sugiere un posible papel en el ensamblaje viral (Meier y col., 2006; Neuman y col., 2008a). Esta proteína podría interaccionar con las proteínas virales nsp3, nsp5, nsp7, nsp8, nsp12, nsp13, nsp14, nsp15 y 7b (von Brunn y col., 2007).

3.3.4. Genes accesorios localizados después del gen N

Tradicionalmente los genes localizados después del gen de la N han sido nombrados como gen 7. Así se han descrito los genes 7a, 7b y 7c en miembros de los tres géneros de CoV (Chu y col., 2008; de Groot y col., 2010b; Woo y col., 2007) (Figura 2). Sin embargo, el análisis de la secuencia de estos genes demuestra que no están relacionados entre sí. De hecho, los genes encontrados después del gen de la N, en aislados nuevos de CoV en aves, no se han nombrado como ORF 7 puesto que no son homólogos a otros genes de CoV (Lillehaug y col., 2005). El gen 7 de TGEV es un gen específico de grupo homólogo al gen 7a de la especie *Alfacoronavirus 1*, con una identidad del 72% con las ORF7a del FIPV, CCoV y PRCV (Figura 3A) (Gorbalenya y col., 2006; Lai and Cavanagh, 1997). Recientemente se ha descrito la existencia de una ORF 7 en *Alfacoronavirus* de murciélagos. Sin embargo, su secuencia no está relacionada con los genes 7 de la especie *Alfacoronavirus 1* y se postula que la ORF 7 de los CoVs de murciélagos tiene un origen diferente al del gen 7 de la especie *Alfacoronavirus 1* (Chu y col., 2008).

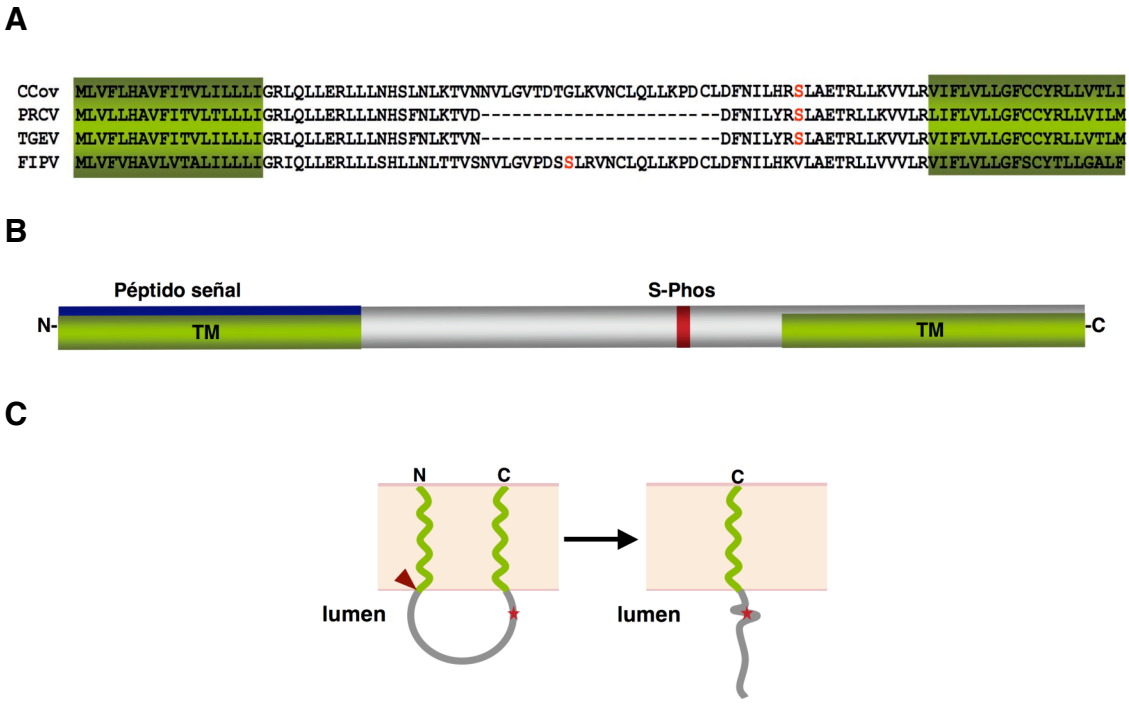

Figura 3. Secuencia y estructura del gen 7 de la especie *Alfacoronavirus 1.* (A) Alineamiento de las proteínas 7a de la especie *Alfacoronavirus 1*, utilizando T-COFFEE (Notredame y col., 2000). Se usaron las secuencias de las proteínas 7a de los CoVs canino (CCoV) y respiratorio porcino (PRCV), del virus de la gastroenteritis tranmisible porcina (TGEV) y del virus de la peritonitis infecciosa felina (FIPV). Los números de acceso de GenBank son: ADB28914.1, ABG89313.1, CAA80842.1 y CAA62190.1, respectivamente. (B) Predicción *in silico* de los dominios presentes en la proteína 7 de TGEV. Dominios transmembrana (TM) están representados en verde [*PredictProtein*, (Rost y col., 2004)], el péptido señal en azul [*Signal P3.0 Server*, (Bendtsen y col., 2004)], y una serina conservada susceptible de ser fosforilada (S-Phos) en rojo [*NetPhos 2.0 Server*, (Blom y col., 1999)]. (C) Topología propuesta para la proteína 7 de TGEV [*PSORTII* (Nakai and Horton, 1999)]. El corte del péptido señal se indica con la cabeza de flecha roja. S-Phos se indica con la estrella roja.

La ORF7 de TGEV codifica una proteína de 78 aa muy hidrofóbica (Tung y col., 1992). La proteína posee dos dominios transmembrana, el primero de los cuales solapa con un péptido señal (Figura 3B). Por ello, la topología propuesta para esta proteína sería la de una proteína integral de membrana de tipo 1 (Figura 3C). De acuerdo con estas predicciones, la proteína 7 se asocia a la membrana del retículo endoplásmico o a la membrana plasmática celular (Tung y col., 1992) durante la infección, aunque también se ha descrito la localización de la proteína 7 en el núcleo de la célula infectada (Garwes y col., 1989). Se ha sugerido que el gen 7 de los CoVs de la especie *Alfacoronavirus 1* está implicado en virulencia. En el FIPV se describió la atenuación del virus al eliminar los genes a y b (FIPV-Δ7ab) (Haijema y col., 2004; Herrewegh y col., 1995; Ortego y col., 2003). En trabajos previos con TGEV, la eliminación del gen

7 dio lugar a un virus atenuado (Haijema y col., 2004; Herrewegh y col., 1995; Ortego y col., 2003). Sin embargo, el papel concreto del gen 7a en atenuación no está claro, ya que el fenotipo del FIPV-Δ7ab es similar al de los FIPV que carecen del gen 7b. Y en el caso del TGEV el virus parental del que se partió para la generación del virus mutante estaba altamente atenuado (Haijema y col., 2004; Herrewegh y col., 1995; Ortego y col., 2003).

4. CICLO INFECTIVO VIRAL

La infección con CoV (Figura 4) comienza con la unión de la proteína S de la superficie de los viriones con el receptor celular, que en el caso del TGEV es la aminopeptidasa N porcina (pAPN) (Delmas y col., 1992), lo que induce la entrada del virus. Una vez liberada la nucleocápsida en el citoplasma de la célula, el RNA genómico es traducido, dando lugar a las poliproteínas pp1a y pp1ab. Éstas se autoprocesan por tres proteasas virales, dando lugar a los componentes virales del RTC.

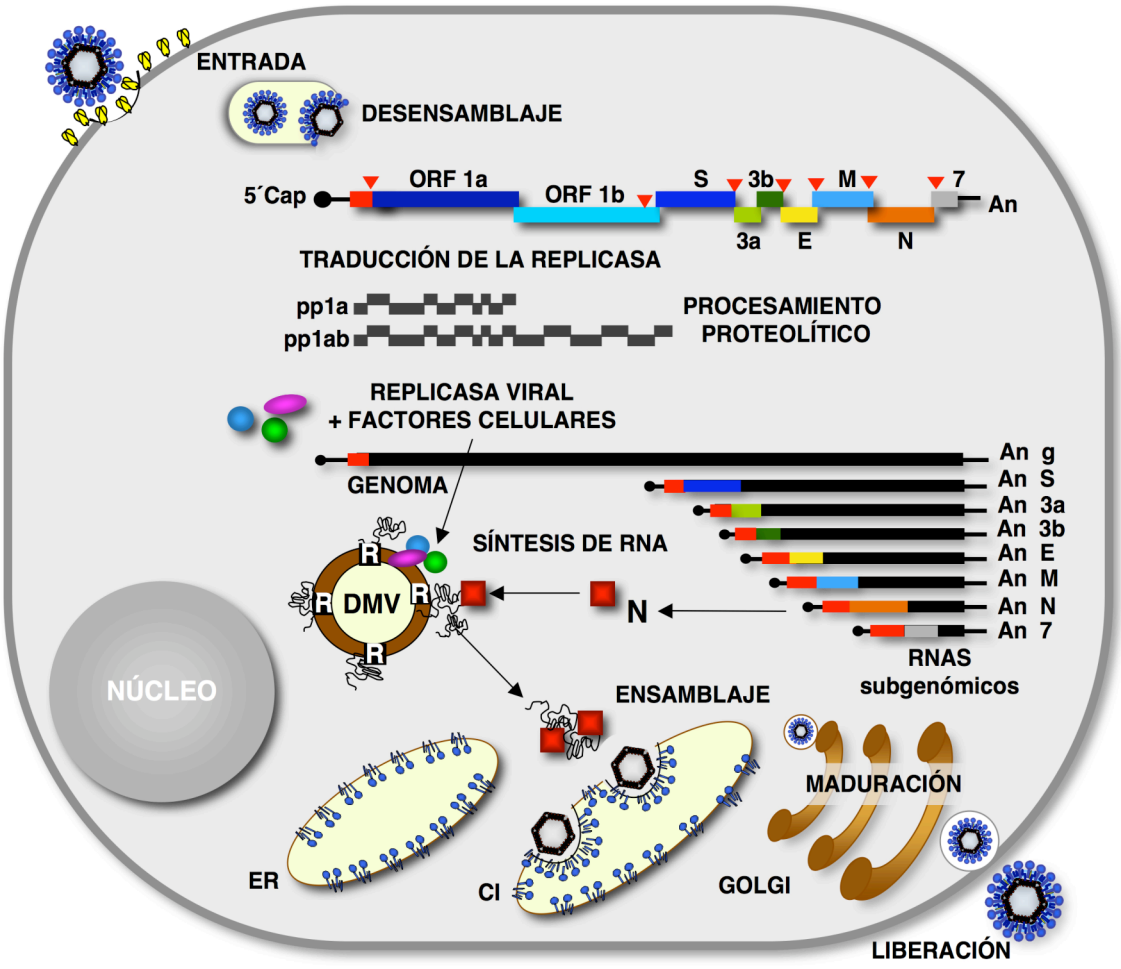

Figura 4. Ciclo infectivo de CoV. Esquema de la infección con el TGEV. Por simplificación, sólo se representan las especies de RNA codificantes, de polaridad positiva. An, poliA; R, complejo de replicación-transcripción; DMV, vesículas de doble membrana; ER, retículo endoplásmico; CI, compartimento intermedio; Golgi, aparato de Golgi.

Este complejo RTC se ensambla en vesículas de doble membrana (Gosert y col., 2002; Nogales y col., 2011; Snijder y col., 2006) y presumiblemente contiene factores celulares. La replicasa utiliza el genoma entrante, de polaridad positiva, como molde para la síntesis de los genomas progenie y de los mensajeros subgenómicos, a través de intermediarios de polaridad negativa de tamaño genómico y subgenómico, respectivamente (Sawicki and Sawicki, 1990; Sawicki y col., 2007). A partir de los mRNAs subgenómicos se traducen las proteínas estructurales y no estructurales del extremo 3' del genoma. Las proteínas de la envuelta S, M y E se insertan en la membrana del retículo endoplásmico, y de allí se translocan a las cisternas del compartimento intermedio. Las nucleocápsidas virales, formadas por los genomas progenie asociados a la proteína N, se asocian con los componentes estructurales integrados en las membranas del compartimento intermedio, a través de la interacción entre la proteína N y el domino C-terminal de la proteína M (Narayanan and Makino, 2001; Sturman y col., 1980). Este proceso induce una invaginación de la membrana y la envoltura de la nucleocápsida que da lugar a los viriones inmaduros. Finalmente, los viriones progenie son exportados en cisternas del aparato de Golgi, donde ocurre su maduración (Salanueva y col., 1999), hasta la membrana plasmática para ser liberados al espacio extracelular, mediante la fusión de las vesículas que los contienen con la membrana plasmática.

5. GENÉTICA REVERSA EN CoV

La manipulación del genoma de CoV mediante genética reversa ha estado limitada por su gran tamaño y por la existencia de regiones tóxicas en el gen de la replicasa que impedían la clonación y crecimiento en bacterias de un DNA complementario (cDNA) infectivo. Inicialmente, los estudios genéticos en CoVs estaban limitados al análisis de RNAs defectivos o de mutantes termosensibles. El primer sistema de manipulación del genoma completo de CoV fue desarrollado originalmente para el MHV (Masters, 1999), y estaba basado en la recombinación dirigida de RNA, aprovechando la alta tasa de recombinación homóloga de este virus. Sin embargo, este sistema no permitía manipular con facilidad el extremo 5' del genoma ni las secuencias próximas al extremo

3' del mismo, por lo que se requerían otros sistemas de genética reversa que permitiesen modificar cualquier secuencia viral.

5.1. Generación de clones infectivos de CoV

El primer clon infectivo de CoV se construyó en nuestro laboratorio para el TGEV y fue ensamblado en un cromosoma artificial de bacteria (BAC) (Almazan y col., 2000). Este sistema limita la cantidad de vector por bacteria a una o dos copias, reduciendo así la toxicidad del cDNA viral durante su propagación en *Escherichia coli*. El ensamblaje se realizó tomando como base un clon cDNA del RNA defectivo natural DI-C (Méndez y col., 1995), formado por cuatro segmentos discontinuos del genoma de TGEV, a partir del cual se reconstruyó el genoma completo. Este procedimiento permitió la localización de la región del gen de la replicasa responsable de la toxicidad del cDNA viral en las bacterias, que se introdujo en un último paso de clonación. El cDNA del TGEV se clonó bajo el promotor del citomegalovirus (CMV), y en un extremo 3' se incluyeron una secuencia de poliA, la secuencia de la ribozima del virus de la hepatitis delta, y la señal de poliadenilación y terminación de la hormona de crecimiento bovina (BGH), para la terminación correcta del RNA. Una vez transfectado el clon infectivo en células eucariotas, el genoma viral se transcribe en el núcleo por la RNA polimerasa II celular. Posteriormente, el RNA viral transcrito se transloca al citoplasma, donde comienza el ciclo infectivo del virus. Esta estrategia se ha utilizado posteriormente con éxito para la generación de clones infectivos de los CoVs humanos HCoV-OC43 (St-Jean y col., 2006) y SARS-CoV (Almazan y col., 2006).

6. RESPUESTA ANTIVIRAL ACTIVADA POR DOBLE CADENA DE RNA

La respuesta inmune innata es la primera línea de defensa antiviral del huésped, y está constituida por una cadena de eventos que promueven, tanto en las células infectadas como en las células vecinas, la inhibición de la síntesis proteica, la activación transcripcional de interferón y otras citoquinas pro-inflamatorias, y en último lugar, la muerte celular. La respuesta antiviral se dispara por el reconocimiento, mediante receptores específicos, de patrones moleculares asociados a patógenos (PAMPs) producidos durante el ciclo viral (Andrejeva y col., 2004; Thompson and Locarnini, 2007; Yoneyama y col., 2004).

El RNA de doble cadena (dsRNA), producido por diferentes tipos de virus como intermediaro de replicación o transcripción, es el PAMP que desencadena la activación

de un mecanismo antiviral, ampliamente caracterizado, que lleva a la inhibición de la síntesis proteica, la inducción transcripcional de genes antivirales, y a la muerte celular (Figura 5) (Medzhitov and Janeway, 1997). El origen del dsRNA viral es diverso. En el caso de los CoVs, se ha descrito la existencia de dsRNA durante la replicación y transcripción (Knoops y col., 2008; Sawicki y col., 2001). Además, el genoma de CoV forma estructuras de RNA complejas, que incluyen zonas de dsRNA (Brian and Baric, 2005; Sola y col., 2011).

La activación de la respuesta antiviral disparada por el dsRNA está mediada principalmente por dos efectores (Figura 5): la quinasa dependiente de dsRNA (PKR), que promueve la fosforilación del factor iniciador de la traducción eucariota 2α (eIF2α), y la 2'-5'oligoadenilato sintetasa (2'-5'OAS), que activa a la ribonucleasa L (RNasa L), responsable de la degradación de RNAs virales y celulares (Bisbal and Silverman, 2007; Dauber and Wolff, 2009; Player and Torrence, 1998; Proud, 1995; Taylor y col., 2005).

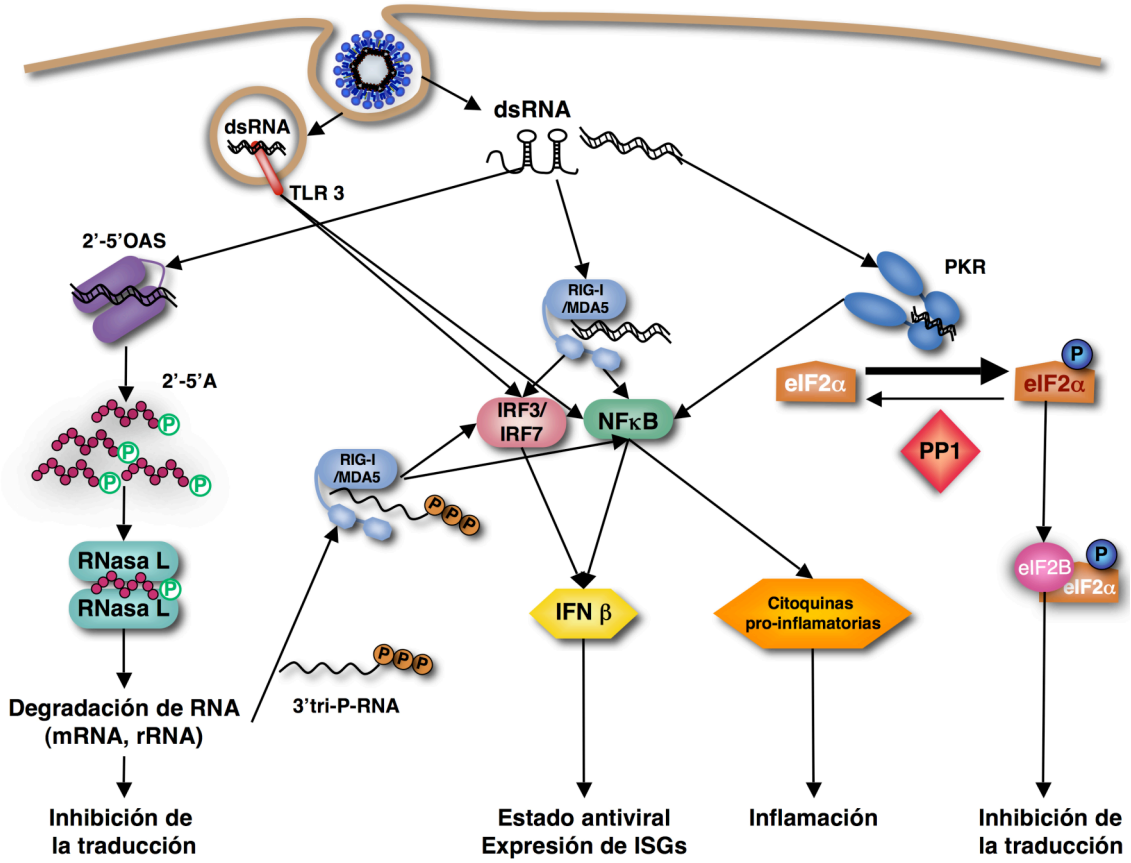

Figura 5. Respuesta antiviral activada por dsRNA. Esquema del reconocimiento del dsRNA y las rutas celulares que se activan.

Además, la producción de IFN por la activación de la respuesta antiviral mediada por dsRNA depende de varios sensores como las proteínas gen-I inducible por ácido retinoico (RIG-I), gen-5 asociado a la diferenciación del melanoma (MDA-5), o el receptor de tipo Toll (TLR)-3 (Figura 5). Todos los efectores y sensores implicados en la respuesta a dsRNA son a su vez inducidos por IFN, lo que contribuye al mantenimiento del estado antiviral (Chakrabarti y col., 2011).

6.1. Ruta de la PKR

PKR es una serin-treonin quinasa activada por dsRNA (Proud, 1995). La proteína PKR se expresa constitutivamente en bajos niveles. La mayor parte de PKR se localiza en el citoplasma de la célula, no fosforilara y asociada con el ribosoma, aunque una pequeña fracción también se localiza en el núcleo de la célula (Barber, 2005). La proteína PKR está compuesta por dos dominios de unión a dsRNA (DRBDs) y un dominio quinasa (Meurs y col., 1990). Los DRBDs unen específicamente dsRNA y ssRNAs con estructuras secundarias, sin especificidad de secuencia (Saunders and Barber, 2003). Cuando los fragmentos de dsRNA se unen a la PKR, se induce un cambio conformacional en la proteína que conlleva el desenmascaramiento del dominio quinasa y la autofosforilación de la proteína (Williams, 2001). Esta proteína PKR activada puede entonces fosforilar distintos sustratos, de los que el más conocido es la subunidad α del factor eIF2 (Samuel, 1979). La fosforilación del factor eIF2α en la serina 51 resulta en la estabilización de la unión del factor eIF2 y el factor eIF2B, lo que provoca que el eIF2 no esté disponible para un nuevo ciclo de traducción y por tanto, se inhiba la síntesis proteica (Samuel, 1993). Esta inhibición se produce incluso cuando sólo el 20% del factor eIF2α celular se encuentra fosforilado (Williams, 2001).

La proteína PKR también promueve la fosforilación del factor inhibidor de kappa β (I$\kappa\beta$), mediante su unión al complejo quinasa I$\kappa\beta$ (I$\kappa\kappa$), lo que lleva a la activación del factor de transcripción nuclear κB (NF-κB) (Gil y col., 2004). También se ha implicado a la proteína PKR en la activación del factor 1 regulador del IFN (IRF1) (Kumar y col., 1997). Por último, se ha observado en distintos tipos celulares que la activación de PKR por dsRNA promueve la activación de la apoptosis (Barber, 2005; Garcia y col., 2006; Williams, 2001).

6.2. Ruta de la 2'-5'OAS y RNasa L

La proteína 2'-5'OAS fue una de las primeras enzimas inducidas por el interferón implicadas en la respuesta antiviral (Hovanessian y col., 1977). En humanos se han descrito cuatro miembros en función de su homología de secuencia: 2'-5'OAS-1, 2'-5'OAS-2, 2'-5'OAS-3 y 2'-5'OAS-L. Hasta la fecha, se han descrito dos formas porcinas: 2'-5'OAS1 y 2'-5'OAS2, que tienen un 75% y 82% de homología con las formas humanas, respectivamente. Después de la unión de dsRNA a los dos dominios de unión a RNA de la 2'-5'OAS1, esta proteína sufre un cambio conformacional que promueve su activación (Hartmann y col., 2003). La función del complejo 2'-5'OAS/RNA es generar 2'-5'oligoadenilatos (2'-5'A) a partir de ATP. Las moléculas de 2'-5'A se unen a la RNasa L provocando un cambio conformacional de esta nucleasa y permitiendo su homodimerización, lo que desenmascara el dominio C-terminal con actividad ribonucleasa y, por tanto, activa a la RNasa L (Cole y col., 1997; Cole y col., 1996; Dong and Silverman, 1995). Las moléculas de 2'-5'A son muy inestables y su defosforilación en el extremo 5', por fosfatasas poco específicas, provoca que estas moléculas sean incapaces de activar a la RNasa L (Silverman, 1985). La activación de la RNasa L da lugar al corte de RNAs celulares y virales en secuencias ricas en poli-uracilo, dejando el extremo 3' tri-fosforilado. Por ello, su actividad resulta en la inhibición generalizada de la traducción (Hassel y col., 1993). Además, la RNasa L degrada preferentemente moléculas de RNA que alternan secuencias ssRNA con dsRNA, como por ejemplo intermediarios de replicación viral, lo que pone de manifiesto el posible efecto antiviral del sistema 2'-5'OAS/RNasa L (Nilsen and Baglioni, 1979).

6.3. RIG-I y MDA5

Además de las proteínas PKR y 2'-5'OAS, que se activan a través de su unión directa a las moléculas de dsRNA, en el citoplasma de la célula existen otros sensores de dsRNA que disparan la transcripción de distintos genes implicados en la producción IFN de tipo I y de citoquinas pro-inflamatorias (Sarkar and Sen, 2004). Las helicasas de RNA citoplasmáticas RIG-I y MDA-5, son elementos fundamentales en el reconocimiento del dsRNA (Foy y col., 2005; Kato y col., 2006; Sumpter y col., 2005). La activación de RIG-I y MDA-5 depende de su interacción directa con moléculas de dsRNA (Yoneyama y col., 2004). Además, recientemente se ha descrito que tanto la helicasa RIG-I como MDA5 actúan amplificando la respuesta inmune innata al

reconocer moléculas de ssRNA 3' o dsRNA 5' tri-fosforiladas (Hornung y col., 2006; Malathi y col., 2007; Pichlmair y col., 2006; Schlee y col., 2009; Schmidt y col., 2009), como los productos de procesamiento generados por la RNasa L (Malathi y col., 2007). Tanto RIG-I como MDA-5 son responsables de la amplificación de la respuesta inmune al estimular la producción de IFN α y β a través de la activación de los factores de transcripción IRF3 y NF-κB (Kato y col., 2006; Xu y col., 2005; Yoneyama y col., 2004).

6.4. Receptor TLR-3

Otro sensor celular de dsRNA es el receptor TLR-3. Esta proteína se localiza fundamentalmente en membranas de vesículas celulares, como endosomas. En la especie porcina hay evidencias de que los macrófagos alveolares usan principalmente TLR-3 para reconocer dsRNA, mientras que otro tipo de macrófagos usan PKR (Uenishi and Shinkai, 2009). Al reconocer el dsRNA, el receptor TLR-3 induce una cascada de señales que activa los factores de transcripción IRF3, NF-κB y AP-1, lo que lleva a la producción de IFN (Matsumoto and Seya, 2008). Sin embargo, TLR-3 no es esencial para la producción de IFN, dado que células que no expresan TLR-3 aún inducen IFN después de una infección viral (Yoneyama y col., 2004).

7. MECANISMOS PARA CONTRARRESTAR LA RESPUESTA ANTIVIRAL ACTIVADA POR dsRNA

La fosforilación del factor eIF2α y la degradación del RNA celular resultan en una inhibición generalizada de la síntesis de proteínas. A este efecto se suman las numerosas moléculas con carácter antiviral, como el IFN, que son producidas por el hospedador. Por lo tanto, debido a los efectos negativos de esta respuesta en la supervivencia viral, muchos virus han desarrollado diferentes estrategias para contrarrestar la respuesta antiviral activada por dsRNA.

Numerosos virus no relacionados codifican proteínas de unión a dsRNA para secuestrar o esconder estas moléculas y, por consiguiente, prevenir el reconocimiento de dsRNA virales por los sensores celulares. Éste es el caso de la proteína U(S)11 del virus del herpes simple-1 (HSV-1), la proteína E3L del virus vaccinia, la proteína σ3 de reovirus, la proteína NS1 del virus de la gripe, y la proteína NSP3 del rotavirus porcino (Bergmann y col., 2000; Cassady and Gross, 2002; Chang y col., 1992; Langland y col.,

1994; Rivas y col., 1998; Watson y col., 1991). Algunas proteínas virales impiden el reconocimiento de dsRNA inhibiendo la acción de los receptores citoplasmáticos RIG-I y MDA-5, como la proteína NS1 del virus de la gripe y la proteína V de paramixovirus, que se unen directamente a RIG-I y a MDA-5, respectivamente (Andrejeva y col., 2004; Mibayashi y col., 2007; Yoneyama y col., 2005). Otra estrategia viral consiste en el bloqueo de las proteínas implicadas en la transducción de la señal desde los sensores de dsRNA hasta los factores de transcripción en el núcleo, éste es el caso de la proteína NS3 del virus de la hepatitis C (HCV), que degrada a la proteína IPS-1, un nodo esencial en la señalización por RIGI y MDA-5 (Meylan y col., 2005).

Algunas proteínas virales ejercen su función interaccionando directamente con las proteínas efectoras de la respuesta activada por dsRNA. Las proteínas U(S)11, E3L, NS5A del virus HCV, y PK2 de baculovirus, se unen directamente a PKR e impiden su activación (Dever y col., 1998; Gale y col., 1997; Peters y col., 2002; Romano y col., 1998). Además, las proteínas E2 de HCV y K3L del virus vaccinia son estructuralmente similares al factor eIF2α y pueden unirse con gran afinidad a la proteína PKR, evitando que el factor de traducción eIF2α se fosforile (Beattie y col., 1991; Taylor y col., 1999).

Algunos virus producen cantidades abundantes de pequeñas moléculas de RNA que actúan como inhibidores de competición de la PKR, como el fragmento VAI de adenovirus, las moléculas EBER-1 y EBER-2 del virus del Epstein-Barr (EBV), o los transcritos de la región de respuesta a trans-activación (TAR) del virus de la inmunodeficiencia humana de tipo 1 (HIV-1) (Gunnery y col., 1990; O'Malley y col., 1986; Sharp y col., 1993). Los virus HSV de tipo 1 y 2 codifican 2'-5'A cortos que bloquean la activación de la ribonucleasa RNasa L (Cayley y col., 1984).

Otros mecanismos consisten, más que en la producción de factores virales, en la modulación de componentes celulares. El virus de la gripe promueve la activación post-transcripcional del inhibidor celular de la PKR, el factor $p58^{IPK}$ (Goodman y col., 2009; Polyak y col., 1996). La proteína γ134.5 del HSV-1, la oncoproteína E6 del papilomavirus, y la proteína DP71L del virus de la peste porcina Africana (ASFV), promueven la defosforilación del factor eIF2α a través de su interacción con la proteína fosfatasa-1 (PP1) (He y col., 1997; Kazemi y col., 2004; Rivera y col., 2007). El virus HSV-1 y el virus de la encefalomiocarditis bloquean la acción de la RNasa L mediante la estimulación de la sobre-expresión de un inhibidor celular de la nucleasa, el inhibidor

de la RNasa L (RLI) (Cayley y col., 1982; Martinand y col., 1999; Martinand y col., 1998).

7.1. Mecanismos para contrarrestar la respuesta activada por dsRNA en CoV

La replicación del los CoVs ocurre en el citoplasma de la célula, y se generan distintas especies de dsRNA que activan la respuesta antiviral del huésped. Por lo tanto, los CoVs han desarrollado distintos mecanismos para evadir esta respuesta. El mecanismo común es la asociación del complejo de replicación-transcripción y de los RNAs virales con membranas celulares en vesículas de doble membrana (DMVs). Las DMVs, descritas en las células infectadas con MHV, SARS-CoV y TGEV (Gosert y col., 2002; Snijder y col., 2006) A. Nogales, L. Enjuanes y F. Almazán, 2011, manuscrito en preparación), conferirían el ambiente y condiciones adecuadas para la síntesis del RNA viral, y además prevendrían la activación de las defensas del huésped ocultando las especies dsRNA de los sensores celulares localizados en el citoplasma de la célula.

Otros mecanismos se basan en evitar el bloqueo de la maquinaria de síntesis proteica modulando factores celulares que intervienen en estos procesos. La proteína N del MHV y la proteína nsp2 del IBV actúan como antagonistas de la proteína PKR (Ye y col., 2007). Además, el IBV induce la sobre-expresión de la proteína de arresto del crecimiento por daño en el DNA 34 (GADD34), que participa en la defosforilación del factor eIF2α (Wang y col., 2009). La proteína N de MHV también evita la degradación del RNA por el sistema de la 2'-5'OAS/RNasa L (Ye y col., 2007). Sin embargo, otros CoVs utilizan la inhibición de la síntesis proteica celular en su propio beneficio. Este es el caso de los CoVs del género β, en los que la proteína nsp1 promueve la degradación de mRNAs del huésped con el objetivo de suprimir la repuesta inmune innata (Kamitani y col., 2006; Tohya y col., 2009). La proteína nsp1 de SARS-CoV se ha implicado además en la inhibición de la síntesis de proteínas mediante su interacción con la subunidad 40S del ribosoma (Kamitani y col., 2009).

8. INTERFERÓN

Los interferones componen una gran familia de citoquinas inducibles que tienen principalmente tres funciones: antiviral, antiproliferativa e inmunomoduladora (Stark y col., 1998). Los IFNs inhiben la replicación y diseminación viral mediante la activación de mecanismos antivirales directos, como la activación de procesos que llevan a apoptosis, y actividades inmunorreguladoras indirectas, como promover la producción

de moléculas del complejo de histocompatibilidad de tipo I (MHC-I) (Haller y col., 2006; Samuel, 2001). Existen tres tipos de interferones: IFN tipo I, que comprende las especies IFN α, β, ω, ε y τ, IFN de tipo II que incluye la especie IFN γ, y el IFN tipo III que abarca las especies IFN-l1, -l2 y -l3 (Kotenko y col., 2003), también conocidos como IL-29, IL-28A e IL-28B, respectivamente (Sheppard y col., 2003). El IFN tipo I se induce en la mayoría de tipos celulares como consecuencia de una infección viral o la exposición a moléculas de dsRNA, por lo que es conocido como "IFN viral" (Samuel, 2001). Por otro lado, el IFN tipo II se secreta principalmente por linfocitos Th1 y células *natural killer* (NK) tras estímulos antigénicos o mitogénicos (Young, 1996). El IFN de tipo III se expresa en las infecciones virales, y señaliza a través de la cascada de las quinasas Janus (JAK) y los factores transductores de señales y activadores de la transcripción (STATs), contribuyendo a los mecanismos antivirales de una manera similar al IFN tipo I pero independientemente de éste (Kotenko y col., 2003).

8.1. Producción de IFN

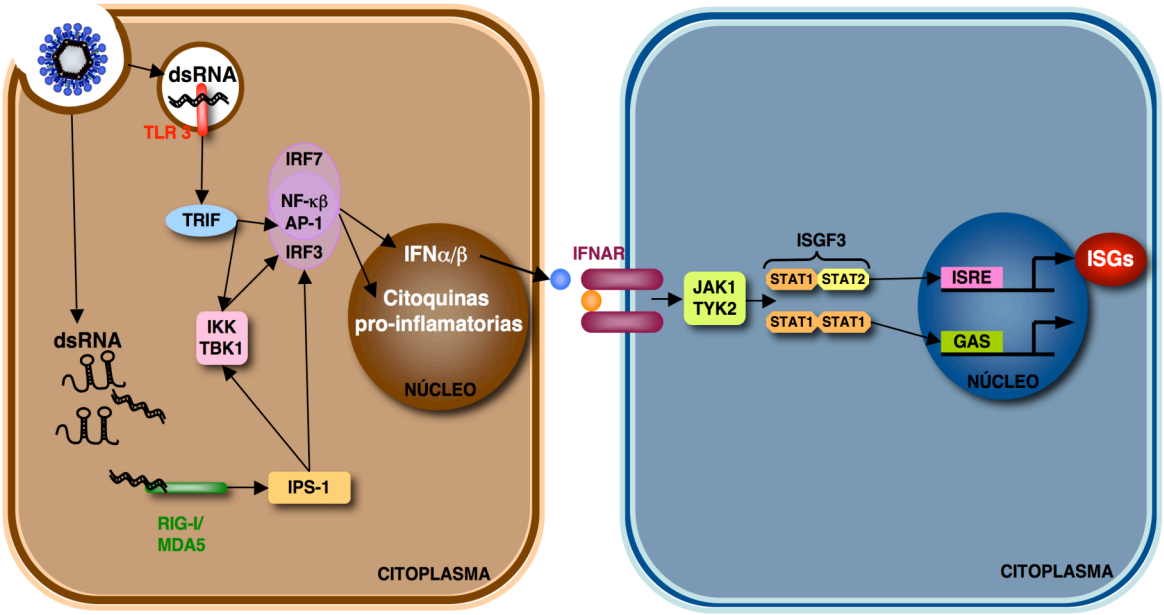

Figura 6. Producción y señalización del IFN. A la izquierda se muestran las rutas que llevan a la producción del IFN. A la derecha se muestran las rutas de señalización por IFN de tipo I.

La mayoría de las células del organismo utilizan un mecanismo clásico para detectar virus y activar la expresión de los genes de IFN tipo I α y β (Haller y col., 2006) (Figuras 5 y 6). Las células infectadas secretan principalmente IFNβ como respuesta

inicial frente a la infección pero, posteriormente se produce una secreción de IFNα durante la fase de amplificación de la respuesta de IFN (Marie y col., 1998). En las células infectadas la unión de moléculas de dsRNA a los sensores citoplasmáticos, RIG-I y MDA-5, resulta en la activación de los factores de transcripción IRF3 y NF-κB, principales reguladores de la expresión de IFNα/β (Haller y col., 2006; Kawai y col., 2005).

8.2. Acción del IFN

El IFN actúa de forma autocrina y paracrina, uniéndose a los receptores de IFN de tipo I localizados en la membrana plasmática de la célula (Figura 6). Estos receptores están compuestos por las subunidades IFNAR1 e IFNAR2 (Brierley and Fish, 2002; Darnell y col., 1994; Platanias, 2005; Uze y col., 1990), que después de su unión al IFN dimerizan y activan a JAK1 y a la tirosin-quinasa 2 (TYK2), localizadas próximas al dominio citoplásmico del receptor. Estas quinasas catalizan la fosforilación de los factores de transcripción STAT1 y STAT2, que formarán el complejo STAT1-STAT2-IRF9, también denominado factor 3 estimulador de IFN (ISGF3), así como el homodímero STAT1, conocido como factor estimulador de IFNγ, que activa la respuesta inmune adaptativa de la célula (Bluyssen y col., 1996; Darnell y col., 1994; Haque and Williams, 1994). Ambos complejos se translocan al núcleo de la célula, y se unen a secuencias de DNA reguladoras de la transcripción, que contienen los elementos de respuesta estimulados por IFN (ISREs) y las secuencias activadas por IFNγ (GAS), respectivamente. Esto lleva a la producción de nuevo IFN de tipo I, citoquinas pro-inflamatorias y a la transcripción de más de 100 genes estimulados por el IFN (ISGs), entre los que se encuentran las proteínas PKR, y 2'-5'OAS, y el MHC-I (Chawla-Sarkar y col., 2003; Garcia-Sastre and Biron, 2006). De este modo se establece una retroalimentación de la ruta del IFN, que permite mantener el estado antiviral.

El interferón de tipo I también activa otros tipos de STAT, como el STAT 3 y STAT 5, que forman homodímeros o heterodímeros STAT1-STAT 3 o STAT5-CrkL (Fish y col., 1999). El homodímero STAT5 tiene funciones pleiotrópicas como el control de la proliferación celular, diferenciación y la apoptosis celular (Heltemes-Harris y col., 2011). El heterodímero STAT5-CrkL activa los elementos GAS (Takaoka and Yanai, 2006). Sin embargo, el papel de estos complejos en la respuesta inmune innata aún no está claro.

8.3. IFN y apoptosis

El IFN influye en la supervivencia celular modulando la expresión de proteínas implicadas en la activación de la inflamación . El tratamiento *in vitro* con IFN tipo I y tipo II produce cambios morfológicos característicos del proceso apoptótico y la inducción de la cascada de caspasas (Balachandran y col., 2000; Barber, 2000; Clemens, 2003; Pokrovskaja y col., 2005; Thyrell y col., 2004; Yanase y col., 2000). Estudios genómicos han identificado más de 15 ISGs que codifican proteínas con funciones pro-apoptóticas, entre las que se encuentran la proteína PKR, la proteína 2'-5'OAS, las caspasas 3 y 8, la proteína galectina 9, XAF-1 y los receptores TRAIL/Apo21 y Fas/CD95 (Chawla-Sarkar y col., 2003). La acción del IFN en la inducción de apoptosis tiene como propósito frenar la infección y evitar la diseminación del patógeno a otras zonas del organismo, con lo que la apoptosis constituye en sí misma un mecanismo de defensa antiviral (Barber, 2000, 2001; Clemens, 2003; Samuel, 2001).

8.4. Antagonistas del IFN en CoV

Los CoVs, como otros virus, han desarrollado distintas estrategias para contrarrestar la respuesta inmune innata. El IFN es un componente crucial en el inicio y mantenimiento de esta respuesta, y por ello los CoVs poseen mecanismos directos o indirectos cuyo objetivo es prevenir la inducción del IFN y su ruta de señalización. Dentro de estos mecanismos se encuentra la asociación del RTC y de los RNAs virales con membranas celulares en DMVs, descrito en el apartado 7.1.

Además, varias proteínas virales se han descrito como antagonistas del IFN, aunque el mecanismo por el cual realizan su papel se desconoce en la mayoría de los casos. La proteína N de MHV y SARS-CoV inhibe la producción de IFN, pero no la cascada de señalización derivada del tratamiento de las células con esta citoquina (Kopecky-Bromberg y col., 2007; Lu y col., 2011; Ye y col., 2007). La proteína nsp3 de MHV y SARS-CoV regula negativamente la producción de IFN inhibiendo la activación del factor IRF3, a través de los dominios PLP2 y PLP1 de nsp3, respectivamente (Frieman y col., 2009; Wang y col., 2011). Además, el dominio PLP1 de la nsp3 de SARS-CoV también inhibe la ruta de señalización mediada por el factor NF-κB (Frieman y col., 2009). Recientemente se ha descrito que el dominio ADP-ribosa-1-fosfatasa de la nsp3 del SARS-CoV y del HCoV-229E, podría actuar como antagonista del IFN, puesto que la eliminación de este dominio aumentó la sensibilidad de estos virus a IFNα (Kuri y col., 2011). De forma similar, se ha demostrado que la 2'-O-metilación del Cap de los

mRNAs virales, llevada a cabo por la proteína viral nsp16, previene la producción de IFN de tipo I y disminuye la sensibilidad a IFN de MHV (Zust y col., 2011). La capacidad de la proteína nsp1 de degradar los mRNAs celulares se ha relacionado con la inhibición específica de la producción de IFN durante la infección de los virus SARS-CoV y MHV (Kamitani y col., 2006; Narayanan y col., 2008). La proteína nsp1 de estos virus también inhibe la ruta de señalización activada por el IFN mediante la inhibición de la fosforilación de STAT1 (Wathelet y col., 2007; Zust y col., 2007). De un modo similar la proteína 6 de SARS-CoV previne la translocación del factor STAT-1 al núcleo de la célula mediante la retención de las proteínas carioferina α1 y β1, implicadas en el transporte nuclear, en las membranas del ER/Golgi (Frieman y col., 2007). Sin embargo, la eliminación del gen 6 del genoma de SARS-CoV no resultó en un aumento en la sensibilidad al IFN de este virus (Zhao y col., 2009), lo que sugiere que existen mecanismos redundantes que antagonizan la acción del IFN. Además, al igual que la ORF6 de SARS-CoV, la ORF 3b de SARS-CoV inhibe tanto la producción del IFN como la ruta de señalización derivada de la producción de esta citoquina (Kopecky-Bromberg y col., 2007). Otras dos proteínas accesorias de MHV, Ns2 y la proteína 5a, se han descrito como posibles antagonistas del IFN, puesto que su eliminación da lugar a fenotipos atenuados más sensibles al IFN que los virus parentales (Koetzner y col., 2010; Roth-Cross y col., 2009; Zhao y col., 2011).

9. INFLAMACIÓN

Además de la producción de IFN, el reconocimiento de los PAMPs durante las infecciones, dispara la transcripción de diversos genes pro-inflamatorios mediante la activación de factores de transcripción como el factor NF-κB (Bonjardim y col., 2009).

El proceso inflamatorio conlleva la producción y secreción de citoquinas y quimioquinas. Aunque en cultivos celulares las células producen estas moléculas, las inflamación es una respuesta en la que intervienen distintos tipos celulares y, por tanto, sus efectos sólo son visibles de forma integral en el contexto del organismo completo. La inflamación se define tradicionalmente por la aparición en zonas localizadas de cuatro síntomas: aumento de la temperatura, dolor, enrojecimiento e hinchazón. Estos síntomas reflejan la acción de las citoquinas, y de otros mediadores de la inflamación, que promueven la dilatación y el incremento de la permeabilidad de los capilares, lo que resulta en un incremento del flujo sanguíneo y la salida de líquido hacia los tejidos afectados.

En etapas tempranas de una infección, las células infectadas del tejido secretan citoquinas pro-inflamatorias específicas como TNF, CCL2, CCL4 o CCL5 (RANTES) (Kohlmeier and Woodland, 2009; Strieter y col., 2002). Estas moléculas promueven el reclutamiento y la diferenciación de células de la línea blanca circulantes en sangre. Estas están constituidas por monocitos, granulocitos y células dendríticas. Los monocitos, una vez se internan en el tejido, se diferencian a macrófagos y junto con los macrófagos residentes son las principales células fagocíticas del sistema inmune innato. Los granulocitos se dividen en basófilos, eosinófilos y neutrófilos, que después de la extravasación aumentan en número durante la respuesta inmune. Los basófilos y eosinófilos están relacionados con la defensa contra parásitos y con las inflamaciones alérgicas, respectivamente. Una de sus principales funciones es la secreción de moléculas que aumentan la permeabilidad de los vasos sanguíneos. Los neutrófilos son células fagocíticas muy importantes del sistema inmune, y son los granulocitos más abundantes durante las infecciones virales. Los macrófagos y los neutrófilos fagocitan y destruyen a las células infectadas, participando tanto en la respuesta inmune innata como en la adaptativa. El reclutamiento de células de la línea blanca en tejidos inflamados amplifica la señal pro-inflamatoria, dado que los macrófagos y neutrófilos activados producen y secretan nuevas citoquinas y quimioquinas.

El equilibrio entre inmunidad e inmunopatología durante una infección está controlado por el balance entre los mecanismos pro- y anti-inflamatorios. Una combinación adecuada de estos mecanismos lleva a la eliminación del virus y a la adquisición de protección frente a nuevas reinfecciones, con un daño mínimo en el tejido del huésped. Sin embargo, una activación excesiva de los mecanismos pro-inflamatorios puede llevar a la eliminación del virus pero causando grandes daños en el tejido (Rouse and Sehrawat, 2010). De hecho, la hipervirulencia de muchos virus se debe más a la respuesta inmune que inducen, que a su propia replicación en el tejido infectado (Peiris y col., 2010; Zampieri y col., 2007).

IV. OBJETIVOS

Los CoVs son importantes patógenos animales y humanos. Tradicionalmente, los genes accesorios de CoV se han relacionado con la modulación de la virulencia viral. Sin embargo, la información que se tiene del papel concreto y el mecanismo de acción de las proteínas que codifican los genes accesorios durante la infección es muy limitada.

El objetivo general de esta tesis es la caracterización de la función de la proteína 7 de la especie *Alfacoronavirus 1*, utilizando como modelo el TGEV. Los objetivos específicos abordados en este trabajo fueron los siguientes:

1. Generación y caracterización en cultivos celulares de un virus recombinante TGEV que no exprese el gen 7.
2. Análisis, en cultivos celulares, de la función del gen 7 durante la infección con el TGEV. Estudio del mecanismo de actuación de la proteína 7 durante la infección.
3. Estudio de la expresión génica del huésped, durante la infección de TGEV, en presencia y ausencia de la proteína 7.
4. Análisis de la relevancia del gen 7 en la virulencia de TGEV y la patología causada por la infección.

V. MATERIALES Y MÉTODOS

1. CÉLULAS EUCARIOTAS

1.1. Líneas celulares

La línea celular ST, derivada de testículo embrionario de cerdo, fue inicialmente desarrollada por McCurklin y Norman (1966) y cedida al laboratorio por L. Kemeney (Nacional Animal Disease Center, Ames, Iowa, EEUU).

La línea celular BHK-pAPN (Delmas y col., 1993), derivada de la línea epitelial de riñón de hamster BHK-21 (ATCC CCL-10) y transformada establemente con el gen que codifica la aminopeptidasa-N porcina, el receptor de TGEV, fue cedida al laboratorio por el Dr. H. Laude (Unité de Virologie Immunologie Moléculaires, Jouy-en-Josas, Francia).

1.2. Cultivo de células eucariotas

Las células se cultivaron a 37ºC en una atmósfera de CO_2 al 7% y 98% de humedad, en medio modificado Dulbecco (DMEM) suplementado con aminoácidos no esenciales al 1% (Sigma), suero fetal de ternera (FBS) al 10% (Bio-Whittaker Europe, Verviers, Bélgica), 2 mM L-glutamina (Sigma) y 5 mg/ml de gentamicina. En el caso de las células BHK-pAPN y ST-HA-7, cada cuatro pases se crecieron las células en presencia del antibiótico de selección geneticina (G418) a una concentración de 1.5 mg/ml. Las líneas celulares se almacenarion mediante congelación en nitrógeno líquido a una densidad de 1-2 x10^6 células/ml en una mezcla 9:1 de FBS:DMSO.

1.3. Generación de células ST que expresan la proteína 7 de TGEV

El gen que codifica la proteína 7 de TGEV, con el *tag* de la hemaglutinina (HA) después del péptido señal, fue clonado en los sitios de restricción *Hin*dI-*Eco*RI del plásmido pcDNA3.1 (Invitrogen) por la empresa GeneArt (Germany). Cuatro microgramos de pc DNA3.1-HA-7 se cortaron con *Sma*I y purificaron con el *QIAquick*® *kit* (QIAGEN), siguiendo las instrucciones del fabricante. Células ST confluentes, crecidas en una placa de 35 mm de diámetro con medio DMEM sin antibióticos, se levantaron con una solución de tripsina-EDTA (25%). La suspensión de células se lavó dos veces con DMEM sin antibiótico, y se transfectó con 4 µg del plásmido lineal y 12 µg de Lipofectamina 2000 (Invitrogen), siguiendo las recomendaciones del proveedor. Las células trasfectadas se sembraron en una placa de 35 mm de diámetro y se incubaron a 37ºC. Trascurridas 24 horas de la transfección reversa, el medio fue reemplazado por medio DMEM suplementado con 10% de FBS y G418 (1.5 mg/ml)

como agente de selección durante cinco pases en cultivos. Las células fueron clonadas en placas de 96 pocillos (M96) y aquellos clones positivos para la expresión de la proteína HA-7, por inmunofluorescencia e inmunodetección (*Western-blot*), fueron amplificados.

2. VIRUS

2.1. Aislados virales

El aislado de TGEV PUR46-MAD (código de acceso *GenBank* AJ271965) (Sánchez y col., 1990) corresponde al clon PUR46-CC120-MAD aislado en el laboratorio, que deriva del aislado Purdue del TGEV, obtenido en el año 1946 en Indiana (EEUU) por Doyle y Hutchings.

Los virus recombinantes rescatados a partir de la transfección del clon infectivo del TGEV (rTGEV) presentan el fondo genético del aislado del TGEV PUR46-MAD con la excepción del gen S, derivado del aislado TGEV PUR46-C11 en el caso de los virus entéricos y del aislado TGEV PTV en el caso de los virus respiratorios (Almazan y col., 2000; Sanchez y col., 1999).

2.2. Crecimiento y titulación del virus en cultivos celulares

Los rTGEV se crecieron y titularon en células ST según lo descrito previamente (Correa y col., 1988). Para la generación de lotes de virus, las células ST se crecieron en monocapas hasta el 100% de confluencia y se infectaron 24 horas después a una multiplicidad de infección (moi) de 1 unidad formadora de placa (pfu) por célula. El sobrenadante de esta infección se recogió entre 16-20 horas después de la infección (hpi) y se almacenó a -70ºC hasta su utilización.

3. BACTERIAS

3.1. Cepas y cultivos de bacterias

La cepa DH10B de *Escherichia coli* (GibcoBRL), cuyo genotipo es F$^-$ *mcr*A Δ(*mrr-hsd*RMS-*mcr*BC) Ø80d*lac*ZΔM15 Δ*lac*X74 *deo*R *rec*A1 *end*A1 *ara*D139 Δ(*ara, leu*)7697 *gal*U *gal*K λ-*rps*L *nup*G, se utilizó de rutina para la clonación de DNA.

Los cultivos bacterianos se realizaron en medio líquido LB (Sambrook and Russell, 2001) a partir del cual se preparó medio sólido añadiendo agar a una concentración de 15 g/l, que se utilizó para el aislamiento de colonias bacterianas. El medio fue suplementado con los antibióticos adecuados (150 µg/ml de ampicilina; 12.5 µg/ml de

cloranfenicol) cuando fue necesario. Los cultivos en medio líquido se crecieron a 30ºC o a 37ºC, según se indique.

3.2. Preparación de bacterias competentes

Las bacterias DH10B competentes para electroporar se prepararon a partir de una colonia única crecida en medio sólido, que se amplificó posteriormente en un litro de medio SOB (20g/l triptona, 5 g/l extracto de levadura, 0.5 g/l NaCl, 0.18 g/l KCl) hasta alcanzar una DO_{550} de 0.7. A continuación el cultivo se enfrió a 4ºC durante 20 min, las baterias se sedimentaron por centrifugación a 4000*xg* furante 15 min, y se lavaron tres veces con una solución de glicerol al 10% previamente enfriada a 4ºC, utilizando un volumen del cultivo inicial para el primer lavado y reduciendo el volumen a la mitad en los lavados sucesivos (1 l, 0.5 l y 0.25 l, respectivamente). En cada lavado las bacterias se resuspendieron a 4ºC y se centrifugaron a 4000*xg* durante 15 min. El sedimento final se resuspendió en 3 ml de glicerol frío 10%, se repartió en partes alícuotas y se congeló a -70ºC hasta su utilización.

3.3. Transformación de bacterias

Las bacterias DH10B competentes se transformaron por electroporación con DNA desalado mediante diálisis con membranas de nitrocelulosa (Millipore). El DNA desalado se mezcló con 50 µl de las bacterias competentes. Esta mezcla se transfirió a una cubeta de electroporación de 0.2 cm (Bio-Rad), donde se aplicó un pulso de 25 µF, 2.5 kV y 200 Ω utilizando un electroporador GenePulser (Bio-Rad). Las bacterias se resuspendieron inmediatamente en 1 ml de medio SOC (Hanahan, 1985), se incubaron a 37ºC con agitación durante 45 min y se sembraron por extensión en superficie sobre placas de medio LB-agar con el antibiótico de selección apropiado.

4. MANIPULACIÓN Y ANÁLISIS DEL DNA

4.1. Plásmidos

Los plásmidos pSL1190 (Pharma Biotech) y pcDNA3.1 (Invitrogen), de alto número de copia, se utilizaron para el clonaje y modificación de cDNAs virales de hasta 9 Kb.
El plásmido pBeloBAC11 (pBAC) (Wang y col., 1997), de 5 Kb, contiene el origen de replicación del factor F de *E. coli* (*oriS*), el gen de resistencia a cloranfenicol (*cat*) y los genes necesarios para mantener una copia única del plásmido por célula (*par*A, *par*B, *par*C y *rep*E). Este vector fue utilizado para el clonaje y modificación de cDNAs virales

de gran tamaño o que contuviesen secuencias tóxicas para su crecimiento en bacterias según lo descrito anteriormente (Almazan y col., 2000; Gonzalez y col., 2002).

4.2. Manipulación y purificación de plásmidos

Para la purificación de plásmidos a partir de cultivos bacterianos a pequeña escala (Minipreps) se utilizó el reactivo *Plasmid Mini Kit* (QIAGEN) según el protocolo del fabricante. Para la purificación de plásmidos de alto número de copia a media y gran escala (Midi- y Maxipreps) se utilizaron los reactivos *Plasmid Midi Kit* y *Plasmid Maxi Kit* (QIAGEN), respectivamente. Los pBACs se purificaron utilizando el reactivo *Large-Construct Kit* (QIAGEN), a partir de cultivos bacterianos que se crecieron a 30ºC durante 18 h aproximadamente, partiendo de un preinóculo de 10 ml de cultivo que se añadió a 500 ml de medio LB que contenía 12.5 µg/ml de cloranfenicol.

Para la purificación de fragmentos de DNA extraídos de geles de agarosa y de productos amplificados mediante reacción en cadena de la polimerasa (PCR) se utilizó el reactivo *QIAquick gel extraction kit* (QIAGEN) o el reactivo *QIAEX II* (QIAGEN) en el caso de fragmentos mayores de 10 kb, siguiendo el protocolo indicado por el fabricante en cada caso.

4.3. Enzimas de restricción y modificación de DNA

Las enzimas de restricción y modificación de DNA (DNA ligasa del fago T4, fosfatasa alcalina de gamba, y el fragmento Klenow de la DNA polimerasa I) se adquirieron de Roche o New England Biolabs. Los tratamientos enzimáticos de restricción, defosforilación o ligación de DNA se hicieron siguiendo protocolos estándar (Sambrook and Russell, 2001). Todas las construcciones generadas se confirmaron mediante secuenciación utilizando un secuenciador automático 373 (Applied Biosystems).

4.4. Amplificación del DNA mediante PCR

Las reacciones de PCR con fines analíticos se realizaron utilizando 2.5 U de la enzima *AmpliTaq DNA polymerase* (Appplied Biosystems) en un volumen de reacción de 50 µl en presencia de 20 pmoles de los oligonucleótidos correspondientes, una mezcla de deoxinucleótidos trifosfato a una concentración final de 0.25 mM, 1.25 mM de $MgCl_2$ y tampón de PCR (10 mM Tris-HCl pH 8.3, 50 mM KCl). En función de la temperatura de fusión de los oligonucleótidos (Tm) y la longitud del fragmento a

amplificar, la reacción de PCR se programó según los ciclos: (a) 94ºC, 5 min; (b) 25-30 ciclos de 94ºC, 1min; (Tm-10ºC), 1min; 72ºC, 1min/Kb; (c) 72ºC, 10 min.

Para la amplificación de fragmentos de DNA con fines preparativos se utilizó la enzima *Platinum Pfx DNA polymerase* (Invitrogen), que posee antividad exonucleasa correctora 3'-5', según las indicaciones del proveedor. Brevemente, para la reacción de PCR se utilizó el mismo programa descrito para la enzima AmpliTaq DNA polimerasa con la excepción de que el tiempo de elongación fue de 2min/Kb.

4.5. Electroforesis de DNA en geles de agarosa

La separación de DNA para estudios analíticos y purificación de bandas de DNA se realizó en geles de agarosa *D*-1 *Medio EEO* (Pronadisa) al 0.8-1.2% disuelta en TAE (40 mM Tris-acetato, 1mM EDTA) con *SYBR®Safe DNA gel stain* 1X (Invitrogen).

5. OBTENCIÓN DE VIRUS RECOMBINANTES

5.1. Construcción de los plásmidos pBAC-TGEV-SPTV-Δ7 y pBAC-TGEV-SC11-Δ7

Para silenciar la expresión del gen 7, se introdujeron un conjunto de mutaciones que permitieron inactivar la secuencia consenso (CS) de la secuencia reguladora de la transcripción (TRS) de la ORF7. Además, se eliminaron los dos primero núcleotidos del codón de inicio de la traducción de la proteína 7. Dichas mutaciones fueron introducidas por PCR solapante usando como molde el plásmido pSL-SPTV-3EMN7, que contiene del núcleotido 20372 al 28087 del genoma de TGEV (Penzes y col., 2001). Los fragmentos de PCR solapantes, con las mutaciones puntuales y eliminaciones, fueron amplificados usando los oligonucleótidos ΔORF7 VS (5'-GCTCGTCTTC CTCCATGCTGTATTTAT-3') y ΔORF7 RS (5'-GATAATTGA TGAGGTAACGAACTGAGCTCGTCTTCGTTACCTATC-3'). El producto final (2700 pb), fue amplificado con los oligonucleótidos externos ΔORF7 VS-Oli 4 *Sph*I RS (5'-CATAGCACAATAGCGTTCTCCACATGCGCATGCA-3') y ΔORF7 RS-Oli 1 *Sph*I VS (5'-GGAGGATTGGGAAGACAATAGCAGGCAT GCTGGGG-3'), fue digerido con *Sph*I y clonado en el mismo lugar de restricción en el pSL-SPTV-3EMN7, dando como resultado el plásmido pSL-SPTV-3EMNΔ7. Para generar el plásmido pBAC-TGEV-SPTV-Δ7, el pSL-SPTV-3EMNΔ7 fue digerido con *Sfo*I-*Bam*HI. Este fragmento, que contenía los núcleotidos del 23464 a 28700 del genoma de TGEV, y las mutaciones necesarias para silenciar el gen 7, fue clonado en el sitio de restricción *Sfo*I-

*Bam*HI del pBAC que contenía el genoma completo de TGEV-SPTV, pBAC-TGEV-SPTV^{FL} (Almazan y col., 2000).

Para generar un rTGEV-Δ7 con tropismo entérico y respiratorio se utilizó como base el genoma del rTGEV-SC11. Con este fin, el plásmido pSL-SPTV-3EMN7 fue digerido con *Sfo*I-*Bam*HI. Este fragmento, fue clonado en el sitio de restricción *Sfo*I-*Bam*HI del pBAC que contenía el genoma completo de TGEV-SC11, pBAC-TGEV-SC11^{FL} (Almazan y col., 2000). Todos los pasos de clonación se comprobaron mediante secuenciación de los fragmentos de PCR y de las zonas de unión donde se introdujeron los fragmentos.

5.2. Transfección y rescate de virus infecciosos a partir de los clones de cDNA

Células BHK-pAPN crecidas al 90% de confluencia en placas de 35-mm de diámetro se transfectaron con 4 µg de los plásmidos pBAC-SPTV-*wt*, pBAC-SPTV-Δ7, pBAC-SC11-*wt* y pBAC-SC11-Δ7, usando 12 µg de Lipofectamina 2000 (Invitrogen), de acuerdo con las instrucciones del fabricante. Después de un periodo de incubación de 6 horas a 37ºC, las células se tripsinizaron con 200 µl de tripsina-EDTA (25%) y se añadieron sobre una monocapa confluente de células ST, susceptibles a la infección viral. Después de un periodo de incubación de 48 h, el sobrenadante de las células (nombrado como pase 0) se recogió y se pasó dos veces sobre monocapas de células ST confluentes. Después de dichos pases, los virus del sobrenadante se clonaron mediante tres pasos sucesivos de purificación de placas de lisis en medio semi-sólido que contenía 0.6% de agarosa. Los virus clonados a partir del pase 1, se amplificaron mediante la infección de células ST crecidas en monocapa en placas de 35 mm de diámetro. Después de 24 h de incubación a 37ºC, el sobrenadante se recogió (nombrado como pase 3) y se cuantificó mediante titulación por formación de placa de lisis siguiendo protocolos previamente descritos (Jiménez y col., 1986).

6. ANÁLISIS DE CITOMETRÍA DE FLUJO

6.1. Cuantificación de la muerte celular

Las diferentes fases del ciclo celular y el porcentaje de células con contenido de DNA sub-G0 (subdiploides) se evaluaron mediante marcaje con ioduro de propidio (PI) y posterior análisis por citometría de flujo. Células ST, sembradas en placas de 35 mm de diámetro, sin infectar o infectadas con los distintos rTGEVs se levantaron con tripsina-EDTA (25%) a distintos tiempos después de la infección, se centrifugaron a

1000 rpm durante 5 minutos y se lavaron con solución salina tamponada con fosfato (PBS) frío. A continuación, se permeabilizaron con 600 µl de etanol frío al 70% en PBS a 4ºC durante 5 minutos. Las células se lavaron tres veces con PBS y se marcaron durante 1 hora con 1 ml de PI (10 µg/ml; Roche) a temperatura ambiente en oscuridad. El porcentaje de células con contenido de DNA subdiploide, que correspondía a células muertas, se determinó por citometría de flujo (*Cytomics^{TM} FC 500*, Beckman Coulter). Los datos se obtuvieron mediante la adquisición de 10.000 células por muestra con las señales de fluorescencia en escala logarítmica y se analizaron con el programa informático *EXPO32analysis*.

6.2. Análisis de la apoptosis

Para cuantificar la apoptosis inducida por la infección de los distintos rTGEVs, se realizó un doble marcaje de las células utilizando la Anexina V, conjugada con el isotiocianato de fluoresceína (FITC) (Roche) y ioduro de propidio (Roche).

Células ST, sembradas en placas de 35 mm de diámetro, sin infectar o infectadas con los distintos rTGEVs se levantaron con tripsina-EDTA (25%) a distintos tiempos después de la infección, se centrifugaron a 1000 rpm durante 5 minutos, y se lavaron dos veces con PBS frío. Las células se resuspendieron en el tampón de incubación de apoptosis (Roche) a una concentración final de 1-10x10^6 células/ml. A 100 µl de la suspensión de células se les añadieron 10 µl de Anexina V-FITC 1X y se incubaron 15 min a 4ºC en oscuridad. Tras el periodo de incubación se añadieron 380 µl de solución de unión (Roche) y 10 µl de PI (Roche). Las muestras se analizaron mediante citometría de flujo (*Cytomics^{TM} FC 500*, Beckman Coulter) con el programa informático *EXPO32analysis* adquiriendo 40000 células por muestra con las señales de fluorescencia en escala logarítmica.

6.3. Cuantificación del nivel de infección

Como dato previo para los experimentos de genómica, el porcentaje de células infectadas se analizó mediante citometría de flujo. Para ello, las células infectadas se levantaron de la placa con una solución de tripsina-EDTA (25%) y se lavaron dos veces con PBS. Las células en suspensión se fijaron durante 30 min a temperatura ambiente con paraformaldehido al 4% en PBS, y se incubaron durante 30 min con la solución de bloqueo y permeabilización que estaba compuesta por 10% FBS, 0.2% saponina en PBS. Se incubaron durante 90 min con un suero monoclonal específico frente a la

proteína N, 3D.C10 (Jimenez y col., 1986), a una dilución 1:500 en la misma solución de bloqueo y permeabilización. A continuación las células se lavaron tres veces con PBS y se incubaron con un anticuerpo secundario anti-ratón conjugado con el fluorocromo Alexa488 (Jackson Immunoresearch), dilución 1:500 en solución de bloqueo, durante 30 min en oscuridad a temperatura ambiente. Después de cada incubación, para eliminar los distintos medios, las células se centrifugaron durante 5 min a 1500*xg*. Todas las incubaciones se realizaron con agitación. Las células en suspensión se lavaron dos veces con PBS y se analizaron en el citómetro de flujo (*Cytomics*^{TM} *FC 500*, Beckman Coulter). El número de eventos analizados fueron 20000.

7. MANIPULACIÓN Y ANÁLISIS DEL RNA

7.1. Extracción del RNA total intracelular

Células ST, crecidas en placas de 35-mm de diámetro, y 24 horas después del 100% de confluencia fueron infectadas con una moi de 5. El RNA total intracelular se extrajo a diferentes horas después de la infección (hpi) usando el reactivo *RNeasy Mini Kit* (QIAGEN), según el protocolo del fabricante. El RNA purificado se cuantificó utilizando un espectofotrómetro NanoDrop ND-1000 (NanoDrop Technologies, EEUU) y se guardó a -70ºC hasta su utilización.

7.2. Análisis del RNA por hibridación DNA-RNA (*Northern Blot*)

El RNA total extraído siguiendo el protocolo describo en el apartado 7.1 se separó en geles desnaturalizantes del 1% de agarosa con 2.2 M de formaldehído, y se transfirieron a membranas de nylon cargadas positivamente, BrightStar^{TM}-*Plus* (Ambion) como se ha descrito anteriormente (Moreno y col., 2008; Zuñiga y col., 2004). La sonda de DNA utilizada, específica de la región 3' UTR del genoma de la cepa PUR46-MAD del TGEV (nt 28300 a 28544) (Penzes y col., 2001), se marcó con biotina usando *BrightSar*^{TM}*Psoralen-Biotin kit* (Ambion), y se detectó usando el *BrigthStar*^{TM} *BioDectect*^{TM} *kit* (Ambion) de acuerdo con las instrucciones del proveedor.

7.3. Análisis del RNA mediante RT-PCR

La síntesis de cDNA o retrotranscripción (RT) se realizó usando el reactivo *High Capacity cDNA RT kit* (Applied biosystems), 100 ng de RNA total intracelular como molde, y los hexanucleótidos al azar provistos en dicho *kit*, en un volumen final de 20

µl. La reacción de RT se incubó durante 10 min a 25ºC y 120 min a 37ºC. La enzima se inactivó mediante incubación a 85ºC durante 5 segundos. Los cDNAs resultantes se guardaron a -20ºC.

Un volumen de 2 µl de cDNA resultante de la reacción de RT se utilizó como molde para su amplificación por PCR, según los protocolos descritos en el apartado 4.4 de esta sección.

7.4. Cuantificación de RNAs virales mediante RT-PCR a tiempo real

Los oligonucleótidos empleados para la cuantificación a tiempo real de subgenómicos mRNAs virales mediante RT-PCR cuantitativa (RT-qPCR) se diseñaron utilizando el programa *Primer Express v2.0* (Applied Bioystem). En todos los casos se comprobó experimentalmente que no formaran dímeros, y se optimizó su concentración en la reacción de PCR entre 300-900 nM (Moreno y col., 2008).

Para la reacción de PCR cuantitativa se utilizó el reactivo *SYBR Green PCR master mix* (Applied Biosystems) según las especificaciones del fabricante. La detección se realizó utilizando un equipo *ABI PRISM 7000* (Applied Biosystems) en un volumen de 25 µl utilizando los parámetros de termociclación: (a) 95ºC, 10 min; (b) 95ºC; 15 seg; (c) 60ºC, 1 min; (40 ciclos). Al final de la reacción de PCR, se añadió un paso de rampa de desnaturalización desde 60ºC (Tm de los oligonucleótidos) hasta 95ºC, para el análisis de la curva de disociación del producto amplificado. Los datos fueron analizados utilizando el programa *ABI PRISM 7000 SDS v.1.2.3* (Applied Biosystems). Para aumentar la fiabilidad de los resultados cada muestra se corrió por triplicado, de tres réplicas biológicas independientes para cada condición. Los valores correspondientes a las medias de los valores de los ciclos de corte (Ct) se usaron para calcular los valores de expresión relativos utilizando el método $2^{-\Delta\Delta Ct}$. El valor de la cantidad de RNA genómico se utilizó como control endógeno para normalizar la cuantificación de los distintos sg mRNAs en cada muestra.

7.5. Cuantificación de RNAs celulares mediante RT-qPCR

La expresión diferencial de los de genes celulares seleccionados se analizó mediante RT-qPCR. Para la reacción de PCR cuantitativa se partió de 2 µl de RT y se utilizó el reactivo *Taqman Universal PCR Master mix* (Applied Biosystems) y ensayos Taqman específicos para los genes seleccionados (Applied Biosystems), en un volumen final de 20 µl, siguiendo las recomendaciones del fabricante. La detección se realizó utilizando

un equipo *ABI PRISM 7000* (Applied Biosystems) en un volumen de 20 µl utilizando los parámetros de termociclación: (a) 50ºC, 2 min; 95ºC; 10 min; (b) 40 ciclos de 95ºCºC, 15 seg; 60ºC, 1 min. Los datos obtenidos a partir de los triplicados de cada muestra, se analizaron utilizando el programa *ABI PRISM 7000 SDS, vs 1.2.3* (Applied Biosystems). Para aumentar la fiabilidad de los resultados, se analizaron las muestras correspondientes a tres replicas biológicas independientes. Los valores correspondientes a las medias de los valores de los ciclos de corte (Ct) se usaron para calcular los valores de expresión relativos utilizando el método $2^{-\Delta\Delta Ct}$. El gen de la beta-glucuronidasa (GUSB) se utilizó como control endógeno para normalizar la cuantificación, dado que se había determinado previamente que su expresión no variaba en las distintas condiciones experimentales.

7.6. Análisis de la integridad del RNA

La integridad del RNA total fue evaluada con un *Bioanalyzer 2100* (Agilent Technologies) siguiendo especificaciones del fabricante, y los datos fueron analizados con el programa informático *2100 Expert* (Agilent Technologies).

Para el estudio de la activación de la RNasa L, células ST al 100% de confluencia crecidas en una placa de 35-mm de diámetro se sometieron a una transfección reversa con 4 µg de ácido poliinosínico/policitidílico [Poly(I:C), Sigma] y 12 µg de *Lipofectamine 2000* (Invitrogen), según lo descrito en el apartado 7.1, el RNA total fue extraído 16 horas después de la transfección, y se analizó su integridad.

En los experimentos de inhibición de la apoptosis, el inhibidor N-benziloxicarbonil-Val-Ala-Asp-fluorometiolcetona (ZVAD) se añadió al medio de cultivos a una concentración final de 100 µM como se ha descrito previamente (Eleouet y col., 1998). Se analizó la integridad del RNA total extraído a las 18 horas después de la infección.

Para evaluar la degradación del RNA celular por el sistema 2'-5'OAS/RNasa L, se utilizaron tres virus recombinantes vaccinia, vvT, vvRL y VV2-5AS, como se había descrito previamente (Domingo-Gil and Esteban, 2006). La expresión de la RNasa L desde el virus VVRL estaba bajo el control del promotor del fago T7 (Diaz-Guerra y col., 1997). La expresión de la polimerasa del fago T7 y de la 2'-5'OAS1 humana, desde los virus vvT y vv2-5AS respectivamente, era constitutiva. Se infectaron células ST a una moi de 2 con el virus vvT7 o con los virus vvT7, vvRL y vv2-5AS. Se recogió el RNA total a las 24 horas después de la infección, y se analizó su integridad.

8. ANÁLISIS DE TRANSCRIPTÓMICA

8.1. Síntesis de RNAs complementarios (cRNAs) biotinilados

Para aumentar la fiabilidad y representatividad de los ensayos de genómica, se realizaron 9 réplicas biológicas. Una vez el RNA total fue extraído como se describe en el apartado 7.1, las muestras se mezclaron de tres en tres obteniéndose al final tres réplicas biológicas que se conservaron a -70ºC hasta el momento de su utilización.

Los RNAs se biotinilaron utilizando el sistema *One cycle traget-labeling kit* (Affimetrix, Santa Clara, CA). Para ello se sinterizaron cDNAs a partir de 5 µg de RNA total, usando un oligonucleótido dT que conteniá el promotor para la RNA polimerasa T7 añadido en el extremo 3'. A continuación se sintetizó la segunda cadena de cDNA y se realizó una transcripción *in vitro* con la enzima RNA polimerasa T7, para producir los cRNAs biotinilados. Las muestras de cRNA biotinilados (15 µg) se fragmentaron en secuencias de 35-200 bases a 94ºC durante 35 min y se añadieron a una concentración final de 0.05 µg/ml en la solución de hibridación que contenía 100 mM de ácido 4-morfolinopropanosulfónico, 1M de Na^+ y 20 mM de EDTA en presencia de 0.01% de Tween 20.

8.2. Hibridación, lavado y procesamiento de las micromatrices de oligonucleótidos

Se hibridaron 10 µg de los cRNAs biotinilados y fragmentados en la solución de hibridación descrita anteriormente en las micromatrices de oligonucleótidos (*microarrays*) porcinos *Genechip Porcine genome array* (Affymetrix, Santa Clara, CA). Estos *microarrays* contienen 23937 grupos de sondas, que corresponden a 20201 genes. Las hibridaciones se realizaron a 45ºC durante 16 horas. Cada *microarray* se lavó y se tiñó con estreptavidina-ficoeritrina y se cuantificó con el escaner *GeneChip® Scanner 3000 7G System* (Affimetrix) según las instrucciones del fabricante.

8.3. Análisis de los datos

8.3.1. Pre-procesamiento de los datos, cálculo de expresión diferencial y estimación de la significación estadística

Para eliminar el ruido de fondo de las señales obtenidas en el proceso de cuantificación y unificar los valores de todas las sondas pertenecientes al mismo gen, se utilizó el método Análisis Robusto Multimatricial (RMA) (Irizarry y col., 2003). Este mismo método se utilizo también para normalizar los resultados de todas las hibridaciones de forma que fueran comparables ente sí. La nomalización se hizo

mediante el ajuste de los cuantiles de todos los conjuntos de intensidades (Bolstad y col., 2003). Durante este paso las intensidades fueron convertidas a escala logarítmica en base 2.

Para cada comparación, se calculó la expresión diferencial de cada gen como la diferencia entre el promedio de las intensidades logarítmicas de las réplicas de cada tipo de muestra a comparar (logRatios). Esta diferencia de logaritmos equivale al logaritmo de la división de las intensidades en escala lineal (tasa de cambio).

Se estimó la significación estadística de la expresión diferencial de los genes, expesada como valores p, con el método limma (Smyth, 2004), una variante del t-test clásico, optimizado para datos de *microarrays* con pocas réplicas. Para compensar la sobreestimación de la significación estadística que se produce cuando se aplica cualquier test estadístico numerosas veces (problema del testeo múltiple), los valores p se ajustaron por el método que controla la tasa de falsos descubrimientos (FDR) (Benjamini and Hochberg, 1995).

Todos los cálculos mencionados se hicieron con los paquetes estadísticos correspondientes de Bioconductor (Gentleman y col., 2004).

8.3.2. Selección de genes relevantes

Se seleccionaron como genes candidatos aquellos con un FDR menor que 0.05 y un logRatio mayor que 1, lo que equivale a una tasa de cambio de 2 veces. Se utilizó el sistema FIESTA viewer (Oliveros y col., 2007) para la evaluación del efecto de la aplicación de filtros estadísticos a los resultados.

8.3.3. Análisis funcional de los resultados

Debido a que el *microarray* porcino está pobremente anotado en la base de datos original de *Affymetrix*, se utilizó una anotación alternativa basada en la homología de los genes de cerdo con los humanos (Tsai y col., 2006). De esta manera se pudo utilizar la anotación de los genes humanos, mucho más completa que la de cerdo, para el análisis funcional de los resultados obtenidos. Así, se utilizó DAVID (Huang da y col., 2009a, b) para estimar a sobre-representación de términos de procesos biológicos (BP) de Gene-Ontology (The Gene Ontology Consortium, 2000) en cada grupo de genes.

9. MANIPULACIÓN Y EVALUACIÓN DE PROTEÍNAS

9.1. Análisis de las proteínas mediante inmunodetección (*Western-blot)*

Células ST, infectadas a una moi de 5, se recogieron a distintas horas después de la infección y se lisaron a 4ºC añadiendo una solución de extracción de proteínas que contenía Tris-HCl pH 7.6 50 mM, NaCl 2 mM, EDTA 2 mM, NP-40 1% y una mezcla de inhibidores de proteasas (*Complete*®, Roche). Cuando los niveles de fosforilación de determinadas proteínas se analizaron, se añadió a la solución de extracción una mezcla de inhibidores de fosfatasas (*PhosSTOP*®, Roche), siguiendo las recomendaciones del proveedor. Para obtener el extracto citoplasmático, las células lisadas se centrifugaron a 4ºC a 13000*xg* y el sobrenadante se conservó a -70ºC hasta el momento de su utilización. Los extractos celulares se resolvieron con una electroforesis utilizando un gel de poliacrilamida con dodecil sulfato sódico (SDS-PAGE). Las proteínas fueron transferidas a una membrana de nitrocelulosa (*Hybond-C*, GE Healthcare) y analizadas como previamente se ha descrito (Sola, 2003). Las membranas fueron incubadas con anticuerpos policlonales (pAbs) específicos para la forma activa de la Caspasa 3 (abcam, 1:10000), PKR (Santa Cruz, 1:200), BiP (Abcam, 1:500), eIF2α (Santa Cruz, 1:2000), eIF2α fosforilado (Invitrogen, 1:500), eIF4G (Santa Cruz, 1:500) y PP1 (Santa Cruz, 1:200). Los anticuerpos monoclonales (mAbs) específicos para el HA (Sigma, 1:1000), PKR total (Santa Cruz, 1:1000), PP1 (Santa Cruz, 1:1000) y β-Actina (Abcam, 1:10000) también fueron usados. La unión del anticuerpo primario se detectó con anticuerpos secundarios, con especificidad para diferentes especies, conjugados a la peroxidasa de rábano, y usando como sustrato quimioluminiscente el *Immobilon Western* (Millipore), siguiendo las recomendaciones del fabricante. Las cantidades de proteínas se estimaron mediante un análisis densitométrico usando el programa *Quantity One 4.6.3* (BioRad). Películas con la apropiada exposición, de al menos tres experimentos independientes, se usaron en todos los casos con resultados similares. Es más, se evaluaron diferentes exposiciones de los mismos experimentos para asegurar que los datos se obtenían a partir de películas con un rango lineal.

9.2. Microscopía de inmunofluorescencia indirecta

Las células ST-HA-7 se crecieron en una placa de 24 pocillos (M24) sobre cubreobjetos de 12 mm de diámetro. Tras alcanzar una confluencia del 50%, las células se lavaron con PBS y se fijaron durante 30 min a temperatura ambiente con paraformaldehido al 4% en PBS. Las células, previamente lavadas con PBS, se

incubaron con una solución de bloqueo y permeabilización que consistía en PBS, 10% FBS, 0.2% saponina. Se incubaron durante 90 min con un suero monoclonal específico frente al *tag* HA (Sigma), dilución 1:500 en la solución de bloqueo y permeabilización. Después la incubación las células se lavaron tres veces con PBS y se incubaron con un anticuerpo secundario anti-ratón conjugado con el fluorocromo Alexa488 (Invitrogen, dilución 1:500 en solución de bloqueo) durante 30 min a temperatura ambiente. Los núcleos se tiñeron durante 20 min con el reactivo de tinción 4'-6'-diamidino-2-fenilidol (DAPI) (Sigma), dilución 1:200 en solución de bloqueo. Los cubreobjetos se lavaron 5 veces con PBS y se montaron sobre portaobjetos con *Prolong®Gold antilade Reagent* (Invitrogen). Las muestras se analizaron mediante microscopía confocal con un microscopio Leica TCS SP5.

9.3. Marcaje metabólico

Células ST un día después de la confluencia y crecidas en P35 se infectaron con una moi de 1, para evitar la muerte de las células debida al el efecto citopático inducido por los virus. Las células se incubaron durante 30 min en medio de deprivación, que consistía en medio DMEM con FBS al 10% sin los aa cisteína (Cys), y metionina (Met). Después del periodo de incubación, el medio fue reemplazado por medio de deprivación con 50 µCi de Cys y Met marcadas radioactivamente con ^{35}S (Taper). Las células se incubaron durante 1 hora a 37ºC. A continuación se lavaron tres veces con PBS completo que contenía Mg^{2+} 50 mM, se levantaron de la placa con ayuda de una espátula estéril y se centrifugaron a 13000*xg*. El precipitado celular se rompió en solución de lisis (Tris-HCl pH 7.6 50 mM, NaCl 2 mM, EDTA 2 mM, NP-40 1%) y una mezcla de inhibidores (*Complete®*, Roche) suplementada con 10U de DNasaI (Roche) y 10U de RNasa A (QIAGEN), y 50 µl de la solución de carga SDS-PAGE 2x (glicerol 20%, SDS 4,6%, β–mercaptoetanol 10%, azul de bromofenol 0,25%). Los extractos celulares fueron sometidos a un ciclo de congelación-descongelación y hervidos a 95ºC durante 10 min. Un volumen de 15 µl de extracto de cada muestra se resolvió en un gel desnaturalizante SDS-PAGE con un gradiente de 2-5%. El gel se secó mediante vacío (*Slab gel dryer EC355*, E-C Apparatus Corporation) sobre papel *Whatman* de 3mm, y se expuso con películas fotográficas para la vizualización de las proteínas marcadas. La marca radioactiva fue estimada mediante análisis densitométricos como se describe en el apartado 9.1.

9.4. Ensayos de coinmunoprecipitación

Tres placas, de 150 mm de diámetro, de células confluentes, se levantaron con ayuda de una espátula estéril y se lavaron dos veces con PBS frío. A partir del sedimento celular se obtuvieron los extractos de proteínas añadiendo 500 µl de tampón de lisis compuesto por IGEPAL 1% en PBS. Las membranas celulares se disgregaron con la ayuda de una pipeta, y se incubaron las muestras en hielo durante 10 min. Posteriormente, las células lisadas se centrifugaron a 10000*xg* a 4ºC. El sobrenadante se mezcló con 200 µl de agarosa conjugada con el anticuerpo monoclonal contra el epítopo HA (Sigma), lavada previamente cinco veces con PBS. Las muestras se incubaron con la resina a 4ºC en agitación durante 24 horas, pasado este tiempo se centrifugaron a 10000*xg* y el sobrenadante se guardó como muestra no unida. Se realizaron tres lavados de 1 min con PBS frío. Tras el último lavado se añadieron 30 µl de buffer de carga 6x (Tris-HCl pH6.8 1M, Glicerol 87%, SDS 10%, azul de bromofenol 1%, β-mercaptoetanol 14.4M) y las muestras junto con la resina se hirvieron a 95ºC durante 3 min. Para la separación de los extractos de la resina de agarosa utilizó una *Wizard*^{TM} *Minicolumn* (Promega) que se centrifugó 1 min a 13000*xg*. Las muestras se guardaron a -20ºC hasta el momento de su utilización. La presencia de la proteína 7 de TGEV, la proteína E de SARS-CoV y de la proteína fosfatasa 1 (PP1) celular fue analizada mediante *Western-blot* utilizando anticuerpos específicos para cada proteína descritos en el apartado 9.1.

10. CARACTERIZACIÓN DE LOS rTGEVs *IN VIVO*

10.1. Análisis de la replicación viral en cerdos

Grupos de 6 cerdos, de dos a tres semanas de edad, no deprivados de colostro y provenientes de madres seronegativas para TGEV, fueron inoculados intranasalmente con 1x10^7 unidades formadoras de placas (pfu) de los rTGEV-SPTV-*wt* y rTGEV-SPTV-Δ7, respectivamente. Los animales fueron monitorizados diariamente con el fin de detectar los síntomas clínicos de la infección. A los 0.5, 1, 2, 3, 4 y 5 días después de la infección se sacrificaron, dos animales por grupo. Los pulmones extraídos de los animales se guardaron en tubos estériles a -20ºC hasta el momento de su utilización.

Para la determinación de los títulos virales, los pulmones enteros se descongelaron, se pesaron y se homogeneizaron en PBS (1:1) a 4ºC utilizando el *Pro-250 tissue homogenizer* (Fisher Scientific). Los homogeneizados se clarificaron mediante centrifugación a baja velocidad, y los títulos virales se determinaron en monocapas de

ST como se ha descrito previamente (Sanchez y col., 1999). Los títulos virales se expresaron como pfu/g de tejido.

10.2. Histopatología de los tejidos de los cerdos infectados

Secciones representativas de pulmón se fijaron con paraformaldehido al 4% y se almacenaron a 4ºC en etanol al 70%. Las muestras se embebieron en parafina y se realizaron cinco secciones de 4 μm de grosor cada 200 μm. El análisis histopatológico se llevó a cabo sobre secciones teñidas con hematoxilina y eosina, realizadas por el servicio de histología del Centro Nacional de Biotecnología (CNB-CSIC, España).

10.3. Inmunohistoquímica

A partir de los bloques de tejido embebidos en parafina, secciones de 4 μm fueron marcadas con anticuerpos contra la proteína M de TGEV y la Caspasa 3 activa. Las muestras fueron desparafinadas a 60ºC durante 30 min y re-hidratadas mediante sucesivas incubaciones en xilol al 100% 10 min dos veces, etanol al 100% 5 min dos veces y etanol al 96% 5 min dos veces. La peroxidasa endógena fue bloqueada con H_2O_2 al 1% diluida en metanol, a 37ºC en oscuridad durante 30 min. Para la detección de la Caspasa 3 procesada, las secciones de tejido se hirvieron en buffer citrato (citrato sódico 8.2 mM, ácido cítrico 1.8 mM) pH 6.5 durante 22 min. Las uniones inespecíficas fueron bloqueadas con albúmina de suero bovino (BSA) al 3% en PBS. Las muestras se incubaron con el anticuerpo monoclonal de ratón específico para la poteína M de TGEV (3B.B3, 1:100) (Jimenez y col., 1986) o con el anticuerpo policlonal de conejo específico para la caspasa 3 activa (abcam, 1:300), respectivamente, diluidos en BSA 1% en PBS, 1 hora a 37ºC. La unión del anticuerpo primario fue revelada con un anticuerpo secundario biotinilado específico para diferentes especies, (Burro-anti ratón, 1:500; Cabra-anti conejo, 1:250) usando el *ABC Peroxidase Staining Kit* y el *Metal Enhanced DAB Substrate Kit* (Pierce), siguiendo las recomendaciones del fabricante.

10.4. Inmunofluorescencia de tejido

Se utilizó la técnica de inmunofluorescenca para detectar dos poblaciones de leucocitos, macrófagos y granulocitos, en cortes de tejido embebidos en parafina procedentes de animales no infectados o infectados con los rTGEV-*wt* y rTGEV-Δ7, respectivamente. Los cortes de tejido se desparafinaron y rehidrataron como se describe en el apartado 10.3. Para la detección de los macrófagos, las secciones de tejido se

hirvieron en buffer citrato (citrato sódico 8.2 mM, ácido cítrico 1.8 mM) pH 6.5 durante 5 min. El tejido se permeabilizó con Tritón X-100 al 0.25% en PBS durante 15 min y las uniones inespecíficas se bloquearon con BSA al 10% y Tritón X-100 al 0.25% en PBS durante 30 min. Las muestras se incubaron 2 horas a temperatura ambiente, con un anticuerpo policlonal de conejo específico para TGEV (1:100) y con el anticuerpo monoclonal de ratón específico para macrófagos 4E9 (J. Dominguez, 1:100), diluidos en BSA al 1% y Tritón X-100 al 0.25% en PBS. Para la detección de la población de granulocitos en los tejidos se realizó el mismo protocolo descrito para la detección de los macrófagos, con la excepción de que el desenmascaramiento antigénico se realizó digiriendo las muestras con Tripsina/EDTA al 0.05% en H_2O durante 30 min a 37ºC. Las muestras se incubaron con el anticuerpo policlonal de conejo específico para TGEV (1:100) y con el anticuerpo monoclonal de ratón específico para granulocitos Mac387 (DAKO, sin diluir), 2 horas a temperatura ambiente. En todos los casos, la unión de los anticuerpos primarios fue revelada con un anticuerpo secundario de cabra anti-conejo conjugado con el fluorocromo Alexa488 y con un anticuerpo secundario de cabra anti-ratón conjugado con el fluorocromo Alexa594 (Invitrogen, dilución 1:250 en solución del anticuerpo primario) durante 30 min a temperatura ambiente. Los núcleos se tiñeron durante 20 min con el reactivo de tinción DAPI (Sigma), dilución 1:200 en solución del anticuerpo primario. Los tejidos se montaron sobre portaobjetos con *Prolong®Gold antilade Reagent* (Invitrogen). Las muestras se analizaron mediante microscopía confocal con un microscopio Leica TCS SP5 y se contrastaron con un filtro de campo claro.

El análisis cuantitativo de los niveles de señal específica para cada anticuerpo se realizó utilizando el programa *MetaMorph*. El número de píxeles positivos al marcaje de macrófagos y granulocitos, respectivamente, se hizo relativo al número de píxeles positivos de la infección con el TGEV.

VI. RESULTADOS

1. GENERACIÓN DE UN TGEV RECOMBINANTE QUE NO EXPRESA EL GEN 7

Con el objeto de estudiar el papel de la proteína 7 durante la infección de TGEV, se generó un rTGEV que no expresaba dicho gen (rTGEV-Δ7). Para silenciar la expresión del gen 7 se introdujeron varios cambios en un clon infectivo del TGEV (Almazan y col., 2000): (i) modificaciones de la TRS del gen 7, que incluyen una mutación puntual en la secuencia CS, que sustituye una A por una G en la posición 28070 del genoma del virus, y la eliminación de los dos últimos nucleótidos de la CS; y (ii) la eliminación de los dos primeros nucleótidos del codón de inicio de la traducción de la proteína 7 (Figura 7A). Las mutaciones introducidas para silenciar la expresión del gen 7 incluyeron un número limitado de cambios en el extremo 3' del genoma, que es necesario para la replicación del virus (Galan y col., 2009; Izeta y col., 1999). Todas las mutaciones introducidas en el cDNA infectivo del TGEV se identificaron en el genoma del rTGEV-Δ7, después de seis pases en cultivos celulares, indicando que eran establemente mantenidas en el genoma del TGEV. La ausencia del mRNA del gen 7 en las células infectadas con el rTGEV-Δ7 se confirmó mediante hibridación de sondas DNA sobre RNA (*Northern-blot*) (Figura 7B).

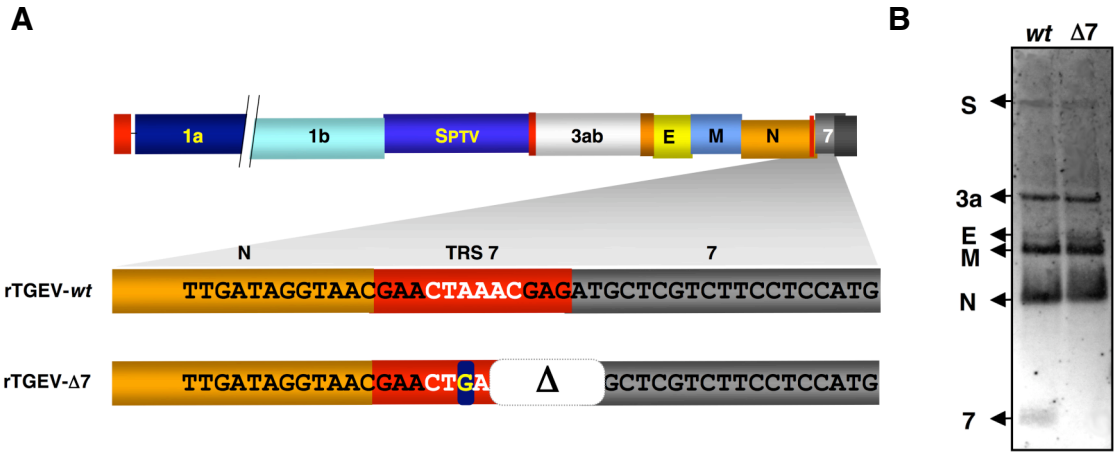

Figura 7. Generación de un virus recombinante TGEV que no expresa el gen 7 (rTGEV-Δ7). (A) Mutaciones introducidas para generar el rTGEV-Δ7. En la parte superior se representa el esquema del genoma del TGEV. Dentro de la TRS7 (rojo), las letras blancas representan la CS. Los nucleótidos mutados se indican con un cuadrado azul, y las partes del genoma eliminadas (Δ) con un cuadrado blanco. (B) *Northern-blot* de los mRNAs subgenómicos producidos por los rTGEVs durante la infección. Se infectaron células ST con los rTGEV-*wt* (*wt*) y rTGEV-Δ7 (Δ7), a una moi de 5. Se extrajo el RNA total a las 8 hpi. Se detectaron los sg mRNAs de las proteínas de la espícula (S), 3a, envuelta (E), membrana (M), nucleocápsida (N), y proteína 7.

El título viral y la acumulación de RNA genómico (gRNA) durante la infección se analizó en cultivos celulares. El RNA intracelular se analizó únicamente en los tiempos después de la infección en los que aún quedaban células viables adheridas a la placa. Los virus parental y mutante mostraron la misma cinética de crecimiento y de acumulación de gRNA (Figura 8). Los títulos del rTGEV-Δ7 se redujeron significativamente transcurridas 24 horas del inicio de la infección, debido a la ausencia de células viables. Este resultado era el esperado dado que, en ausencia de células vivas capaces de producir nuevos virus, el título del TGEV decrece una unidad logarítmica por día debido a su inestabilidad térmica (Laude, 1981). Estos datos mostraron que la proteína 7 no era esencial para la replicación del TGEV en cultivos celulares.

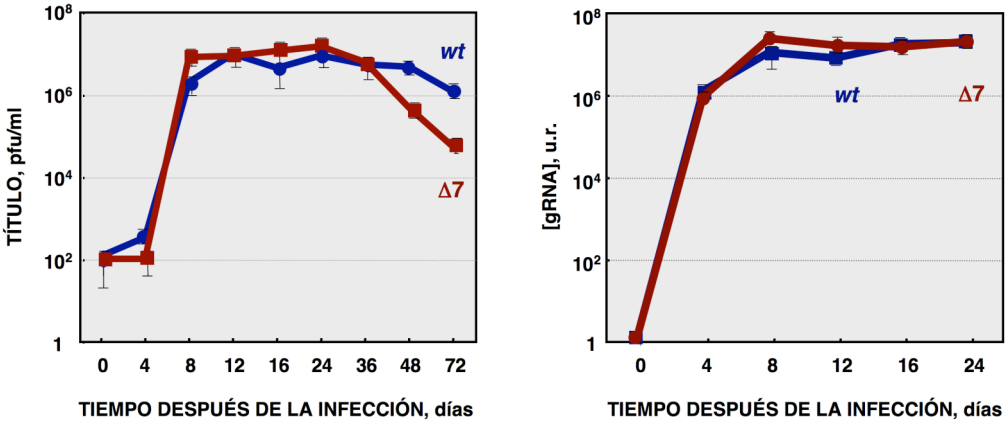

Figura 8. Cinética de crecimiento *in vitro* del rTGEV-Δ7. Se infectaron células ST con los rTGEV-*wt* (*wt*, azul) y rTGEV-Δ7 (Δ7, rojo), a una moi de 5. Se recogieron el medio de cultivo y el RNA intracelular a distintos tiempos después de la infección. Se evaluó el RNA intracelular a aquellos tiempos en los que aún quedaban células viables adheridas a la placa de cultivos. Se analizó el título viral (panel de la izquierda) y la acumulación del RNA genómico viral (gRNA) (panel de la derecha) mediante RT-qPCR. Las barras de error representan las desviaciones estándar de tres experimentos independientes.

2. MUERTE CELULAR INDUCIDA POR LA INFECCIÓN CON EL rTGEV-Δ7

2.1. Efecto citopático causado por el rTGEV-Δ7

El efecto citopático (CPE) inducido por el rTGEV-Δ7, caracterizado por el redondeamiento y levantamiento de las células de la placa, fue similar al causado por el virus silvestre (rTGEV-*wt*). Sin embargo, el rTGEV-Δ7 produjo placas de lisis dos veces mayores (4 mm de diámetro) que las generadas por el virus silvestre (2 mm de diámetro) (Figura 9).

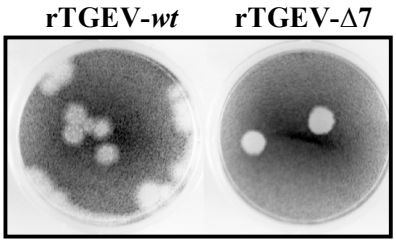

Figura 9. Placas de lisis producidas por el rTGEV-Δ7. Se infectaron células ST con los rTGEV-*wt* y rTGEV-Δ7 y se cubrieron con medio semi-sólido. Las células se fijaron y tiñeron dos días después de la infección.

Además, desde 12 horas después de la infección (hpi), en las células infectadas por el rTGEV-Δ7 los focos de infección fueron mayores que los observados en las células infectadas con el rTGEV-*wt* (Figura 10, panel de la izquierda). Este mayor CPE, muy evidente a las 16 hpi, progresó hasta que casi no quedaron células vivas en la infección con el rTGEV-Δ7 a 24 hpi (Figura 10, panel de la derecha).

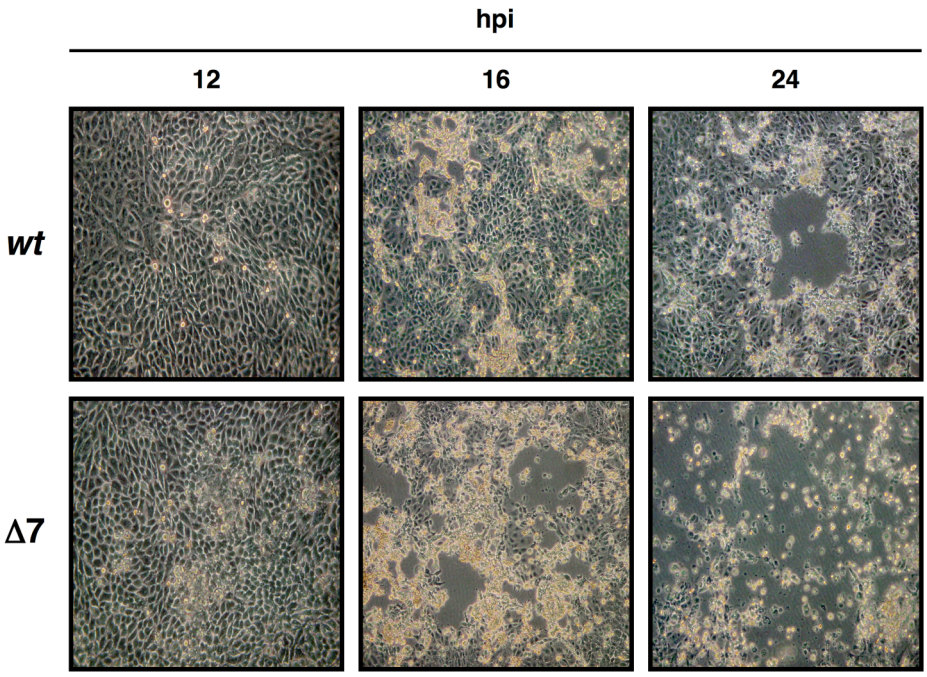

Figura 10. Efecto citopático producido por el rTGEV-Δ7. Se infectaron células ST con los rTGEV-*wt* (*wt*) y rTGEV-Δ7 (Δ7). El efecto citopático producido por ambos virus a 12, 16 y 24 hpi, se analizó mediante microscopía óptica. Las imágenes se tomaron con el objetivo de 40x.

2.2. Cuantificación de la muerte celular causada por el rTGEV-Δ7

La muerte celular inducida por el virus mutante se evaluó mediante citometría de

flujo. Para ello, se permeabilizaron las células y los ácidos nucleicos se tiñeron con yoduro de propidio (PI). El yoduro de propidio es un agente intercalante que se une estequiométricamente a los ácidos nucléicos de doble cadena. La medición de la intensidad de la fluorescencia emitida a partir del PI intercalado, se usa como indicador del contenido de DNA celular (Crissman and Steinkamp, 1973; McCarthy and Fetterhoff, 1989). En las etapas finales de la muerte celular el DNA nuclear es degradado, bien por la acción directa de endonucleasas, como las DNasas I y II y la endonucleasa G (EndoG), o por acción indirecta de proteasas que degradan componentes de la maquinaria de reparación del DNA y del citoesqueleto nuclear (Robertson y col., 2000). La tinción con PI permite distinguir las células en proceso de muerte, o G_0, de las células normales que emiten mayores niveles de fluorescencia al tener el DNA nuclear intacto (Nicoletti y col., 1991; van Engeland y col., 1996). Como se esperaba, el virus silvestre indujo la muerte celular y la degradación del DNA durante la infección (Figura 11), coincidiendo con resultados descritos previamente (Eleouet y col., 1998). El rTGEV-Δ7 también indujo la muerte celular, pero con niveles significativamente mayores que los observados durante la infección del rTGEV-*wt* (Figura 11).

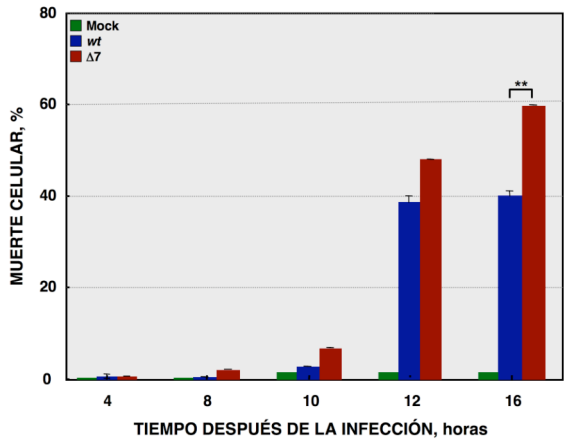

Figura 11. Muerte celular inducida por el rTGEV-Δ7. Cuantificación de la muerte celular inducida por los rTGEV. Células ST se infectaron con los rTGEV-*wt* (*wt*) y rTGEV-Δ7 (Δ7). Las células se recogieron a 4, 8, 10, 12 y 16 hpi y se permeabilizaron y marcaron con yoduro de propidio (PI). La muerte celular se midió mediante citometría de flujo. Las barras de error representan las desviaciones estándar de tres experimentos independientes. **, *p-value*<0.01.

2.3. Apoptosis inducida por el rTGEV-Δ7

El principal componente del efecto citopático inducido por TGEV es la muerte celular programada mediante apoptosis, dado que la inhibición de este proceso previene la muerte celular inducida por la infección (Eleouet y col., 1998; Eleouet y col., 2000; Sirinarumitr y col., 1998). Para analizar si el incremento en la muerte celular observado durante la infección del rTGEV-Δ7 se debía a un aumento en la apoptosis, las células infectadas tanto con el rTGEV-*wt* como el rTGEV-Δ7 se tiñeron simultáneamente con PI y Anexina V. En etapas tempranas de la apoptosis, uno de los cambios de la superficie celular es la translocación de la fosfatidilserina desde la cara interna de la membrana plasmática hacia la cara externa, donde queda expuesta y actúa como señal que es reconocida por los macrófagos encargados de la eliminación de las células apoptóticas (Fadok y col., 1992a; Fadok y col., 1992b; Vermes y col., 1995). La Anexina V es una proteína de unión a fosfolípidos, dependiente de Ca^{2+}, con gran afinidad por la fosfatidilserina (van Engeland y col., 1996). El yoduro de propidio no puede atravesar la membrana celular y, por tanto, se usa como marcador de la integridad de la membrana plasmática (Sasaki y col., 1987). La tinción doble con PI y Anexina V permite distinguir, mediante citometría de flujo, las células que se encuentran en apoptosis temprana y que, por tanto, tienen la membrana plasmática intacta pero la fosfatidilserina expuesta en superficie de la célula (Anexina V^+, PI^-), de las apoptóticas tardías o necróticas, en las que la membrana plasmática finalmente se ha desestructurado (Anexina V^+, PI^+) (van Engeland y col., 1996). Las células sin infectar fueron viables durante todo el experimento (Anexina$^-$, PI^-), lo cual indicó que el tratamiento al que se sometieron las células no indujo la apoptosis por sí mismo (Figura 12). Como se esperaba, el virus silvestre indujo la apoptosis, y la población de células en apoptosis tardía (Anexina V^+, PI^+) fue evidente a las 12 hpi. El virus mutante rTGEV-Δ7 también indujo la apoptosis de las células pero más rápido y con niveles más altos que los que se detectaron en la infección con el virus silvestre, con un incremento de dos veces en el número células apoptóticas a 8 hpi y con sólo un 36% de células vivas a 12 hpi (Figura 12).

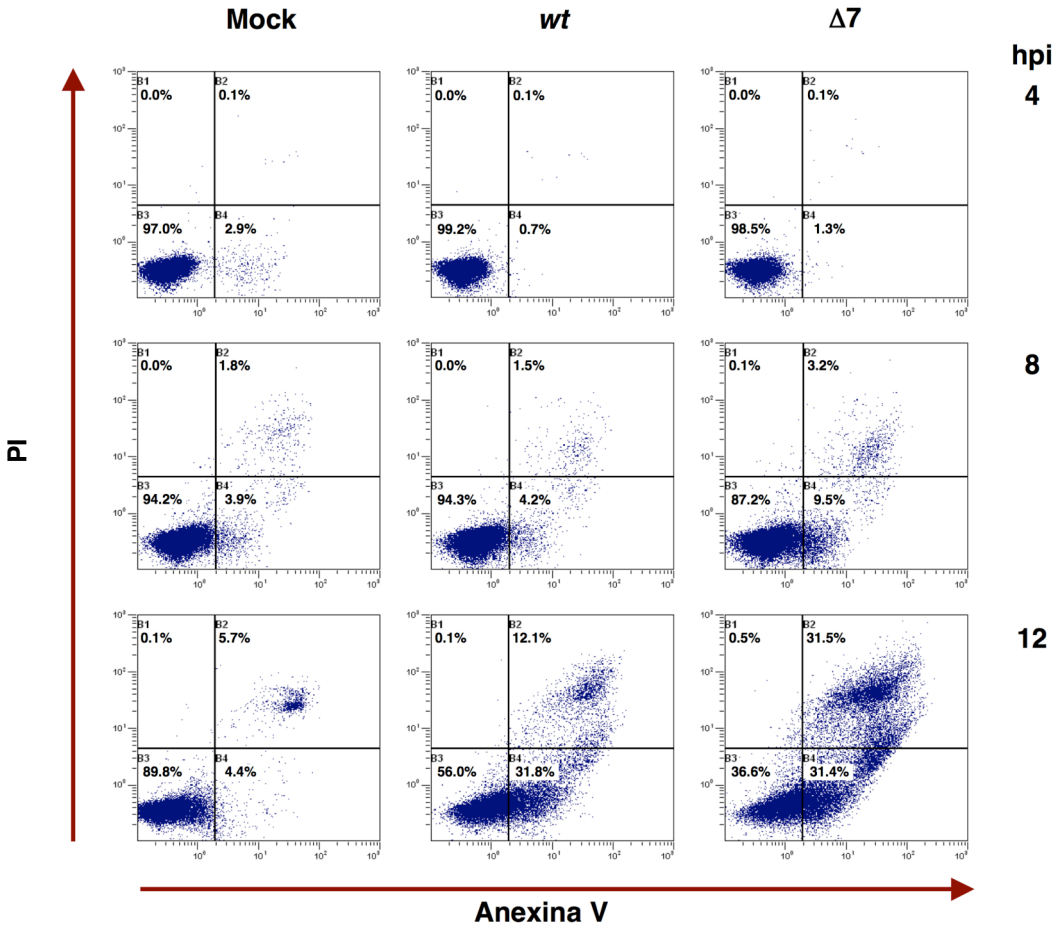

Figura 12. Apoptosis causada por el rTGEV-Δ7. Se evaluaron mediante citometría de flujo los niveles de apoptosis en células sin infectar (Mock) o infectadas con los rTGEV-*wt* (*wt*) y rTGEV-Δ7 (Δ7) a 4, 8 y 12 hpi. Se tiñeron las células con Anexina V y PI para distinguir las células en apoptosis temprana (Anexina V^+, PI^-) de las que se encuentran en apoptosis tardía (Anexina V^+, PI^+).

Según lo descrito previamente, la apoptosis inducida por el TGEV es dependiente de la activación de las caspasas, incluyendo el procesamiento de dos caspasas iniciadoras (caspasa-8 y -9), así como de tres caspasas efectoras que se encuentran en la base de la ruta (caspasa-3, -6 y -7) (Eleouet y col., 2000; Sirinarumitr y col., 1998). La activación de la caspasa 3 promueve el procesamiento de la proteína N del TGEV. Y su inhibición, así como la de otras caspasas, previene la apoptosis inducida por el TGEV (Eleouet y col., 2000). Se analizó la presencia de la caspasa 3 procesada mediante la unión de anticuerpos específicos a la proteína fijada a membranas de nitrocelulosa (*Western-blot*). La infección con el rTGEV-*wt* indujo el corte de la caspasa 3, detectado a partir de 24 hpi (Figura 13). El rTGEV-Δ7 indujo el procesamiento de la caspasa 3 antes que el rTGEV-*wt* (Figura 13).

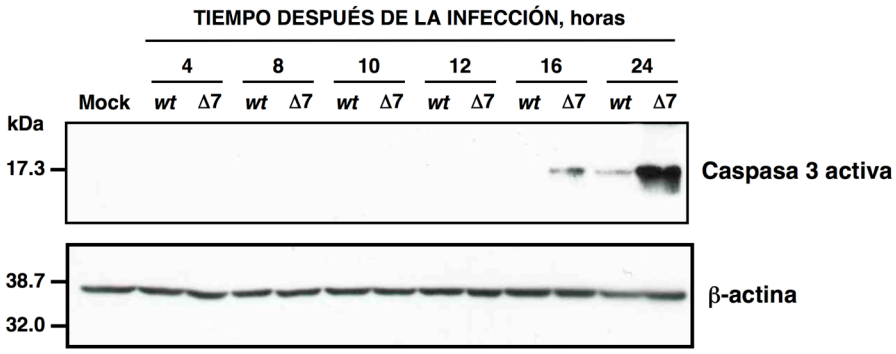

Figura 13. Activación de caspasas durante la infección del rTGEV-Δ7. Detección de la caspasa 3 activa mediante *Western-blot*. Se extrajo la proteína total de células ST infectadas con los rTGEV-*wt* (*wt*) y rTGEV-Δ7 (Δ7), a distintos tiempos después de la infección. Se detectó la caspasa 3 activa utilizando un anticuerpo específico para la forma procesada de la proteína. La proteína β-actina se usó como control de carga.

En conjunto, estos resultados sugirieron que el aumento en el CPE observado durante la infección con el rTGEV-Δ7 se debía a un incremento en la muerte por apoptosis, mediada por la activación de caspasas.

3. EFECTO DE LA ELIMINACIÓN DEL GEN 7 EN LA SÍNTESIS DE PROTEÍNAS

CoVs como el MHV y el SARS-CoV inducen la apoptosis de las células infectadas. Una de las causas de este proceso es que estos virus promueven la inhibición de la traducción (Kamitani y col., 2006; Liu and Zhang, 2007; Narayanan y col., 2008; Raaben y col., 2007; Schwartz y col., 2002; Wei y col., 2007; Zhang y col., 2003). Para determinar si el TGEV desencadenaba la parada de la traducción, y si este proceso estaba implicado en los altos niveles de apoptosis inducidos por la infección con el rTGEV-Δ7, se analizó la síntesis de proteínas *de novo* durante la infección mediante marcaje metabólico. Durante la infección del rTGEV-*wt* no se detectó inhibición de la traducción en los tiempos evaluados (Figura 14), como se ha descrito para otros CoVs tales como IBV y el BCoV (Deregt y col., 1987; Wang y col., 2009). Sin embargo, la infección con el rTGEV-Δ7 inhibió la síntesis de proteínas celulares y virales de forma significativa a partir de las 10 hpi (Figura 14).

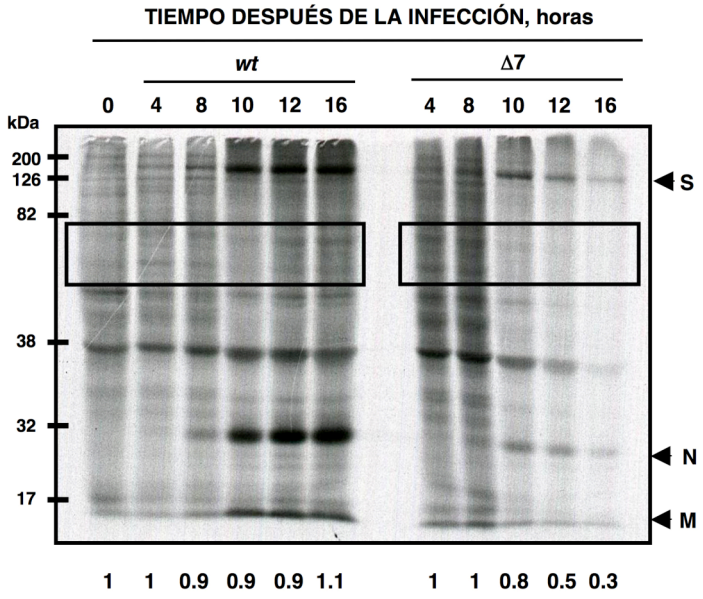

Figura 14. Síntesis *de novo* de proteínas durante la infección con los rTGEVs. Células ST se infectaron a una moi de 1 con los rTGEV-*wt* (*wt*) y rTGEV-Δ7 (Δ7). Las células se marcaron con ^{35}S Met-Cys durante 30 min a distintos tiempos después de la infección. Los extractos de proteínas marcadas se analizaron mediante una electroforesis SDS-PAGE. Los acrónimos S, N y M indican las proteínas virales de la espícula, la nucleocápsida, y la membrana, respectivamente. Los niveles de síntesis de proteínas celulares se determinaron mediante un análisis densitométrico. Los cuadrados negros indican la región utilizada para el análisis densitométrico, y los números la radioactividad de cada carril relativa a la radioactividad de las células sin infectar.

Los mRNAs virales producidos por los CoVs son estructuralmente similares a los del hospedador, dado que contienen una estructura 5'Cap y una cola poli-A en el extremo 3', lo que permite que los CoVs parasiten la maquinaria traduccional celular. Sin embargo, durante la infección de algunos CoVs, como el MHV, los mRNAs virales son traducidos activamente en condiciones de inhibición de la traducción, mediante un mecanismo aún desconocido (Enjuanes y col., 2006a; Kyuwa y col., 1994). Para analizar si los mRNAs virales fueron preferentemente traducidos respecto a los celulares, la cantidad de marca radiactiva correspondiente a la proteína N se tomó como referencia de la síntesis de proteínas virales, y se hizo relativa a la marca total de proteína (proteínas celulares más virales) en cada carril. La relación entre la síntesis de proteína viral y proteína total mostró que no existían diferencias significativas entre la infección del rTGEV-*wt* y la del rTGEV-Δ7 (Figura 15). Este resultado sugería que la ausencia de la proteína 7 durante la infección de TGEV produjo la inhibición de la síntesis de proteínas celulares y virales, probablemente afectando a una etapa común en la traducción.

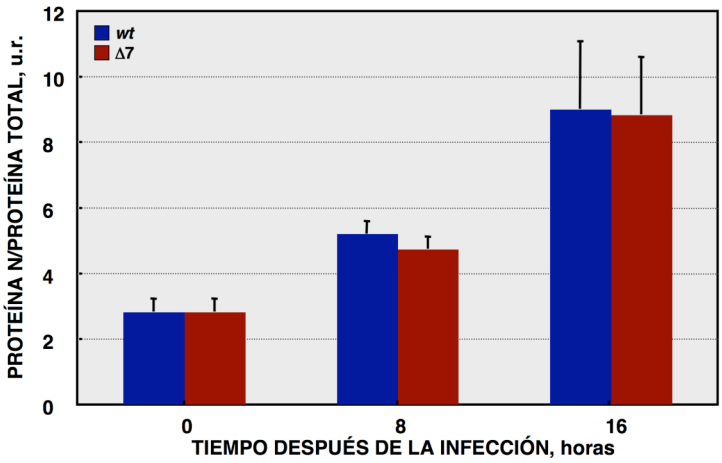

Figura 15. Relación entre la síntesis *de novo* de las proteínas virales y las celulares durante la infección del rTGEV-Δ7. La marca radiactiva correspondiente a la proteína N, estimada por densitometría, se representa en relación a la cantidad de proteína total estimada en cada carril, a las hpi indicadas. Las barras de error representan las desviaciones estándar de tres experimentos independientes. u.r., unidades relativas.

4. ANÁLISIS DE LAS CAUSAS DE LA INHIBICIÓN DE LA TRADUCCIÓN DURANTE LA INFECCIÓN CON EL rTGEV-Δ7

4.1. Efecto de la ausencia de la proteína 7 en la integridad del RNA

Una de las posibles causas de la inhibición de la traducción es una disminución en los niveles de RNA. Por ello, la integridad del RNA total celular se evaluó usando un *Bioanalizer* (Auer y col., 2003; Lin y col., 2009; Scherbik y col., 2006). La infección con el virus silvestre causó un ligero procesamiento del RNA a partir de 12 hpi (Figura 16A), en contraste con la infección con el rTGEV-Δ7, que indujo una más rápida y elevada degradación del RNA celular (Figura 16A). Este dato sugirió que la inhibición de la traducción de las proteínas celulares se debía, en parte, a la degradación de los mRNAs celulares. Además, el incremento en la degradación de la subunidad 28S del RNA ribosómico (Figura 16B), podía estar afectando tanto a la síntesis de proteínas celulares como virales (Iordanov y col., 2000).

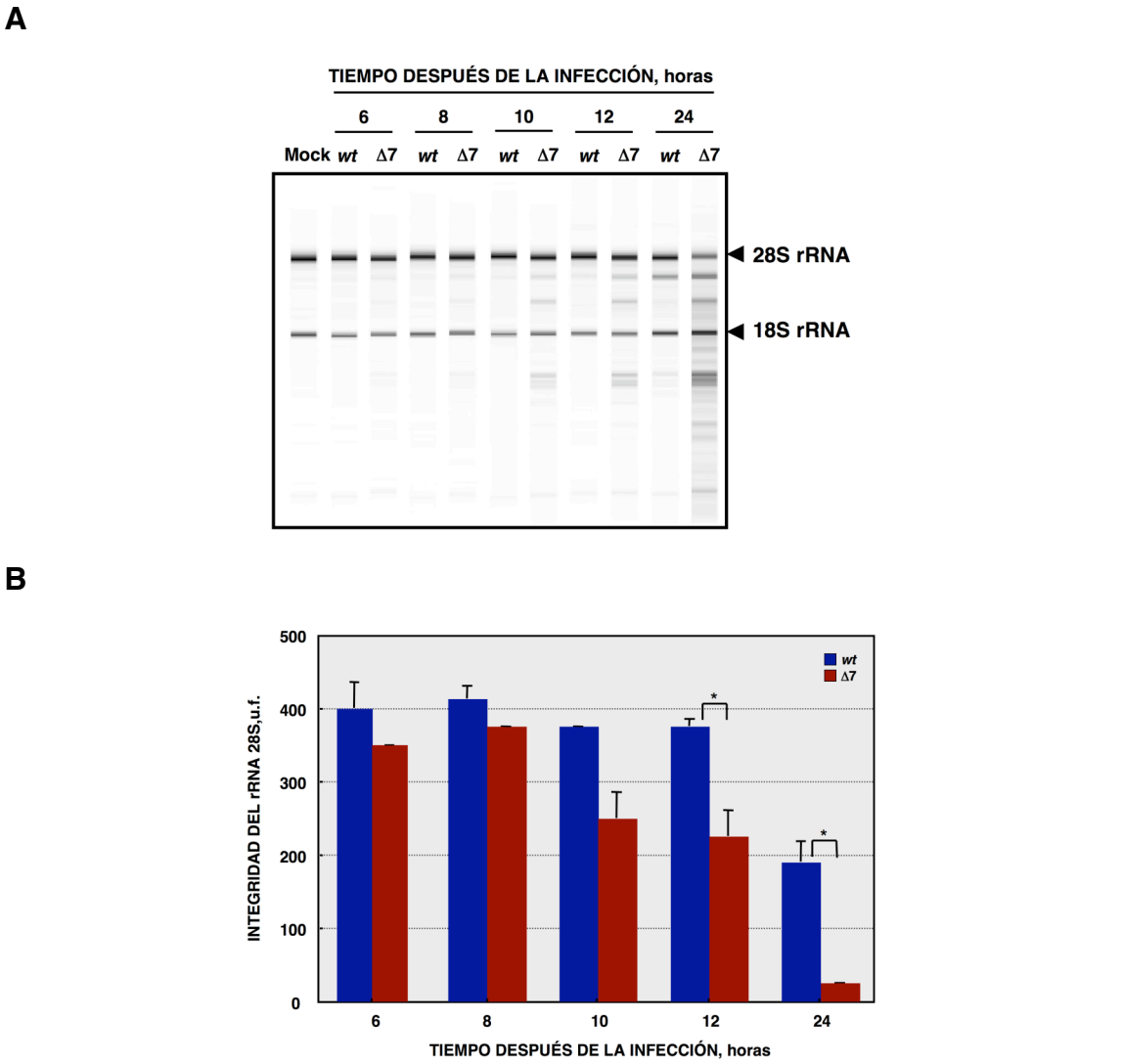

Figura 16. Integridad del RNA celular. (A) El RNA total extraído de células ST infectadas, a distintas hpi, se analizó utilizando un *Bioanalyzer*. Se indica la posición de los RNAs ribosómicos (rRNAs) 28S y 18S. (B) Integridad del rRNA 28S. Representación gráfica de la intensidad de fluorescencia del rRNA 28S, medida con el *Bioanalyzer*, de las muestras infectadas con el rTGEV-*wt* (azul) o rTGEV-Δ7 (rojo), recogidas a distintos tiempos después de la infección. u.f., unidades de fluorescencia. Las barras de error representan las desviaciones estándar de tres experimentos independientes. *, *p-value* < 0.05.

La degradación del RNA podía deberse al proceso de apoptosis. Para estudiar si éste era el caso, se utilizó un inhibidor general de caspasas (ZVAD) que inhibe la apoptosis inducida por el TGEV sin afectar a la producción viral (Eleouet y col., 1998). De hecho, las células ST pre-tratadas con ZVAD e infectadas con los rTGEV-*wt* y rTGEV-Δ7 no mostraron efecto citopático. El análisis de la integridad del RNA total, extraído a partir de células sin tratar o células tratadas con ZVAD, mostró que el patrón de degradación

causado durante la infección del rTGEV-Δ7 era independiente de la apoptosis (Figura 17).

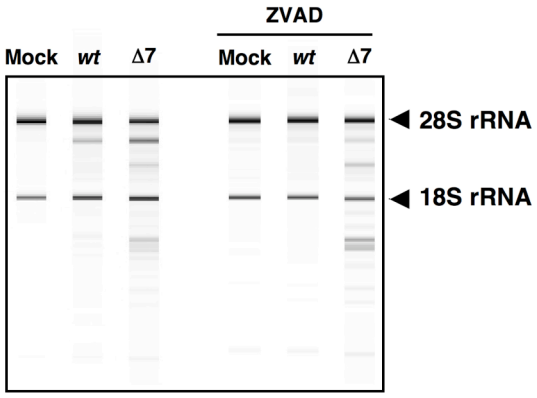

Figura 17. Efecto de la apoptosis en la degradación del RNA celular durante la infección con el rTGEV-Δ7. Células ST tratadas con el inhibidor de caspasas ZVAD, sin infectar (Mock) e infectadas con los rTGEV-*wt* (*wt*) o rTGEV-Δ7 (Δ7). Se extrajo el RNA total y se analizó utilizando un *Bioanalyzer*. Se indica la posición de los rRNAs 28S y 18S.

La degradación del RNA celular podría deberse a la respuesta antiviral inducida por dsRNA. Por ello, se trataron células ST con ácido poliinosínico/policitidílico [Poly(I:C)], que es un potente activador de esta respuesta (Han and Barton, 2002; Lopp y col., 2000; Scherbik y col., 2006). Las células transfectadas con Poly(I:C) mostraron el mismo patrón de degradación de RNA que las infectadas con el rTGEV-Δ7 (Figura 18), al contrario que las células control de la transfección. Estos resultados sugerían que el incremento del procesamiento del RNA celular observado durante la infección del rTGEV-Δ7 se debió a un aumento en la respuesta antiviral inducida por el dsRNA.

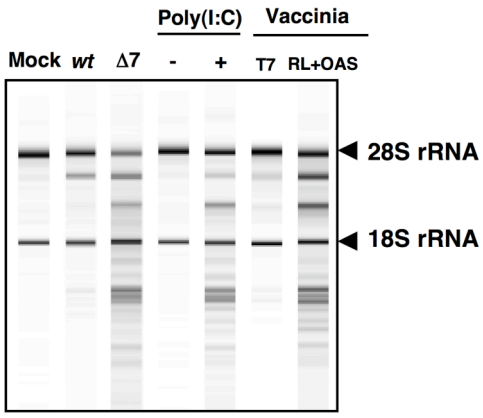

Figura 18. Patrón de degradación del RNA celular. Se transfectaron células ST con Poly(I:C) y el RNA total se

extrajo a las 16 h después de la transfección. Se infectaron células ST con un virus vaccinia (VV) que expresaba la polimerasa del fago T7 (T7) o con el virus T7 junto con los virus VV que expresaban las proteínas 2'-5'OAS y RNase L (RL+OAS). Se extrajo el RNA total a 24hpi. En todos los casos se analizó la integridad del RNA celular utilizando un *Bioanalyzer*.

El principal efector de esta respuesta del huésped es la RNasa L (Han and Barton, 2002; Han y col., 2004; Silverman, 2007). La relevancia de esta nucleasa se estudió utilizando un sistema de virus vaccinia recombinantes (VV). Se ha descrito que el VV no induce una degradación del RNA pronunciada, debido a la presencia de genes virales que inhiben el sistema de la RNasa L. Para activar eficientemente la degradación del RNA por la RNasa L, las células se co-infectan con los VV que expresan la 2'-5'OAS y la RNasa L, respectivamente (Domingo-Gil and Esteban, 2006). Aprovechando el amplio rango de hospedador del virus vaccinia, células porcinas ST se infectaron con el virus VV, o con los virus vaccinia que expresaban la 2'-5'OAS y la RNasa L. Como se esperaba, el virus VV indujo niveles de degradación del RNA muy bajos en las células porcinas (Figura 18). Sin embargo, el patrón de degradación del RNA celular producido por la expresión del sistema de la RNasa L fue idéntico al observado después de la infección con el rTGEV-Δ7. Este resultado sugerió que la RNasa L era la principal nucleasa implicada en el incremento de la degradación del RNA celular inducido por la infección del rTGEV-Δ7.

La activación de la RNasa L requiere de su unión a pequeños 5'-trifosfo,2'-5'-oligoadenilatos (2'-5'A), generados por la 2'-5'OAS (Bisbal and Silverman, 2007; Player and Torrence, 1998) (Figura 19A). En las células los niveles de expresión de la enzima 2'-5'OAS son basales, pero durante una infección estos niveles se incrementan significativamente (Su y col., 2002; Warke y col., 2003). El nivel de expresión del gen de la 2'-5'OAS1 durante la infección de los rTGEV-*wt* y rTGEV-Δ7 fue evaluado mediante RT-PCR cuantitativa (RT-qPCR). Se observó que tanto la infección con el rTGEV-*wt* como la del rTGEV-Δ7 indujeron la expresión de la 2'-5'OAS1 (Figura 19B), como se había descrito previamente (Bosworth y col., 1989) y que, por tanto, la infección por el TGEV activaba esta ruta antiviral. Las pequeñas diferencias observadas en la expresión del gen de la 2'-5'OAS1 entre la infección del virus silvestre y la del virus mutante no explicaban el aumento de la actividad nucleasa observada durante la infección del rTGEV-Δ7 (Figura 19B), dado que los niveles del mRNA de la 2'-5'OAS1 fueron incluso menores en la infección del mutante que los detectados en la del virus parental (Figura 19B).

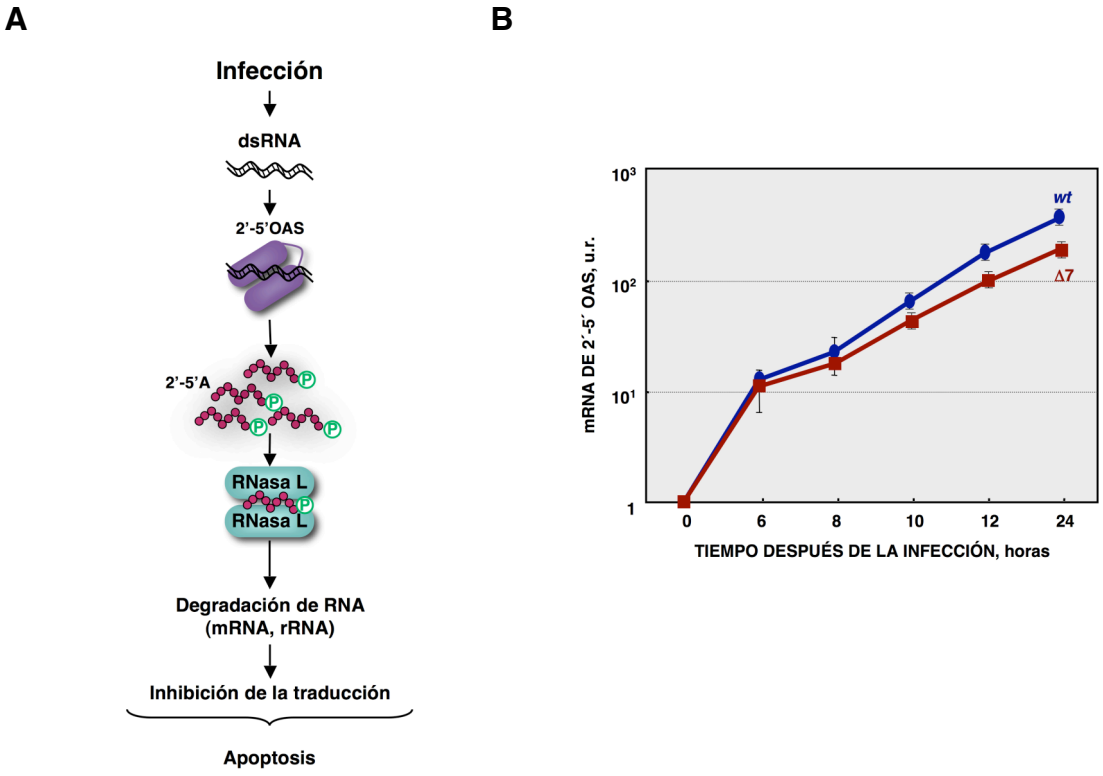

Figura 19. Cuantificación de la expresión de la 2'-5'OAS durante la infección por el rTGEV. (A) Esquema de la activación de la ruta 2'-5'OAS/RNasa L. (B) Cuantificación del mRNA del gen de la 2'-5'OAS1 acumulado durante la infección de los rTGEV-*wt* (azul) o rTGEV-Δ7 (rojo), mediante RT-qPCR, a los tiempos indicados. u.r., unidades relativas. Las barras de error representan las desviaciones estándar de tres experimentos independientes.

4.2. Integridad de los RNAs virales

Los niveles de los mRNAs virales se cuantificaron mediante RT-qPCR y se expresaron como la relación entre las cantidades de mRNA y gRNA. Como ejemplo, no se observaron diferencias significativas en la acumulación de los mRNAs de N y M entre la infección con el rTGEV-*wt* y el rTGEV-Δ7 (Figura 20A). Sin embargo, dado que mediante la RT-qPCR se evalúan fragmentos pequeños de RNA, con esta técnica no se podía discriminar si los mRNA virales estaban siendo procesados. Por tanto, la integridad del RNA viral se evaluó mediante un ensayo *Northern-blot*. Se cargó entre 1.5 y 2 veces más RNA total procedente de células infectadas con el rTGEV-Δ7 que con el rTGEV-*wt,* para distinguir todos los posibles productos de degradación generados durante la infección con el virus mutante. Sorprendentemente, no se detectó degradación de los mRNAs virales durante la infección con los rTGEV-*wt* y rTGEV-Δ7 (Figura 20B). Esto sugirió que los RNAs virales se encontraban protegidos de la actividad nucleasa, aumentada en la infección con el rTGEV-Δ7.

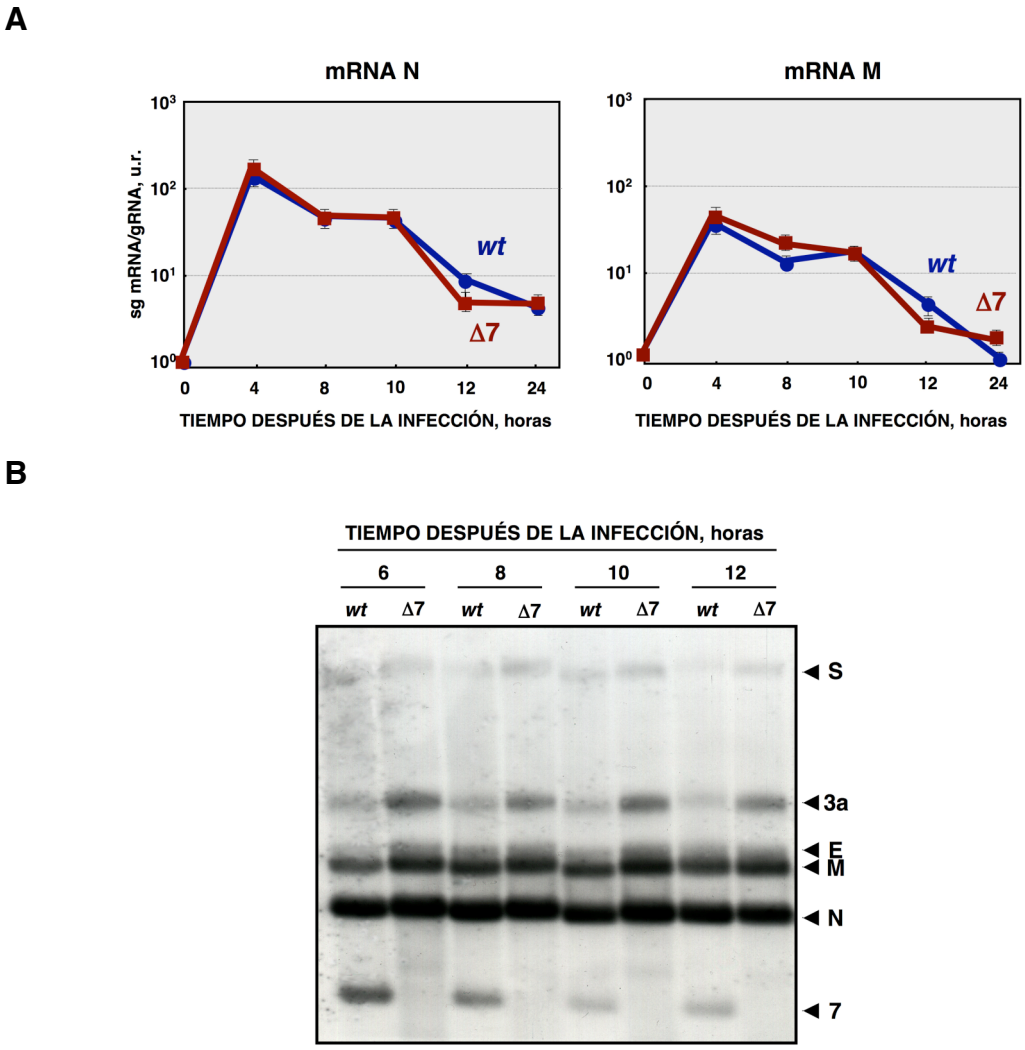

Figura 20. Integridad del RNA viral. (A) Cuantificación de los sg mRNAs de los genes virales N y M acumulados durante la infección con los rTGEV-*wt* (azul) y rTGEV-Δ7 (rojo) mediante RT-qPCR a los tiempos indicados. Se representa la relación entre el sg mRNA y el RNA genómico del virus. u.r., unidades relativas. Las barras de error representan las desviaciones estándar de tres experimentos independientes. (B) Análisis mediante *Northern blot* del sg mRNA viral intracelular. Se infectaron células ST con el rTGEV-*wt* o el rTGEV-Δ7. El RNA total se extrajo a diferentes tiempos después de la infección y se analizó utilizando una sonda complementaria al extremo 3' de todos los sg mRNAs. Para detectar posibles especies de degradación, la cantidad de RNA total cargado de las muestras de la infección con el rTGEV-Δ7 fue de 1.5 a 2 veces superior al de las muestras de la infección con el rTGEV-*wt*. Los mRNAs de las proteínas virales de la espícula (S), envuelta (E), membrana (M), nucleocápsida (N), y las proteínas 3a y 7 se indican a la izquierda.

4.3. Efecto de la ausencia de la proteína 7 en el inicio de la traducción

El bloqueo de la traducción durante la infección con el rTGEV-Δ7. En los apartados anteriores se ha descrito que la ausencia de la proteína 7 durante la infección del TGEV aumentó los niveles de degradación de los mRNAs celulares y los componentes ribosomales. Además de estos factores, existen otros que podrían estar promoviendo la

parada de la traducción. La mayoría de los virus inhiben la traducción de las proteínas celulares mediante la inactivación de uno o varios componentes implicados en la iniciación de la traducción y en la formación del complejo de iniciación dependiente de Cap (Schneider and Mohr, 2003). El factor de iniciación de la traducción 4G (eIF4G) es una de las dianas de la apoptosis inducida por TGEV (Eleouet y col., 2000). Sin embargo, no se detectaron diferencias significativas en el procesamiento del eIF4G durante la infección con el virus silvestre o el virus mutante (Figura 21).

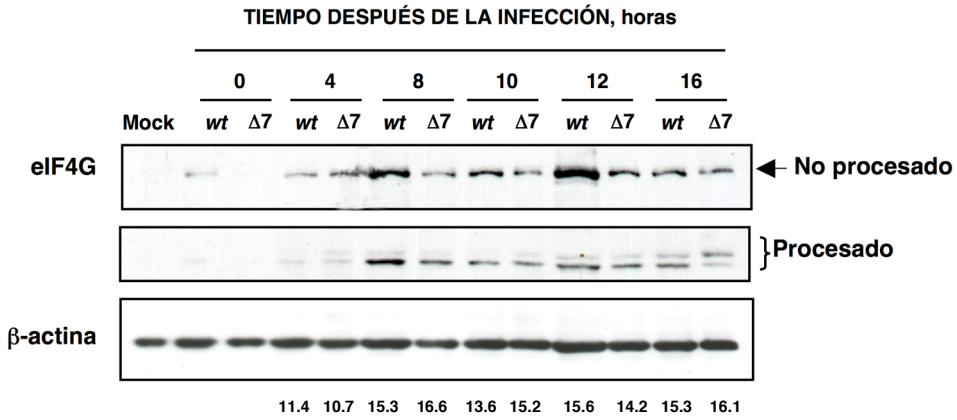

Figura 21. Procesamiento del factor eIF4G durante la infección del rTGEV. Se extrajo la proteína total de células ST sin infectar (Mock) e infectadas, a una moi de 5, con los rTGEV-*wt* (*wt*) y rTGEV-Δ7 (Δ7) a distintos tiempos después de la infección. Se analizó el factor eIF4G sin procesar y procesado mediante *Western-blot* utilizando un anticuerpo que reconocía el extremo C-t de ambas formas. La proteína β-actina se usó como control de carga del experimento. Los números representan la marca relativa de eIF4G procesado respecto al eIF4G total, y el control de carga β-actina.

La síntesis de proteínas suele reducirse cuando las células se encuentran en un estado de estrés, como por ejemplo el causado por la infección viral, mediante la fosforilación de la subunidad α del factor eIF2 en la serina 51 (Hershey, 1991). Los niveles de fosforilación del eIF2α, durante la infección con los virus recombinantes, se analizaron mediante *Western-blot* utilizando anticuerpos específicos para las formas fosforilada (eIF2α-P) y total de la proteína, respectivamente. La infección con el virus silvestre incrementó los niveles de eIF2α-P, alcanzando un máximo a las 8 hpi (Figura 22). Además, la fosforilación del factor eIF2α decreció a tiempos tardíos de la infección, en línea con lo observado para otras infecciones (Brostrom and Brostrom, 1998; Kaufman, 1999). De forma similar, el rTGEV-Δ7 indujo la fosforilación del eIF2α (Figura 22), pero los niveles de eIF2α-P fueron significativamente superiores a los observados en la

infección con el virus silvestre (Figura 22A). Las mayores diferencias entre ambos virus fueron detectadas a las 10 hpi, coincidiendo con la ventana de tiempo en la cual el virus mutante indujo la parada de la traducción (Figura 22B). Este resultado indica que, además de la degradación del RNA celular, el bloqueo en la síntesis de proteínas inducido por el rTGEV-Δ7 se debió al aumento, durante mayor tiempo, de los niveles de eIF2α-P.

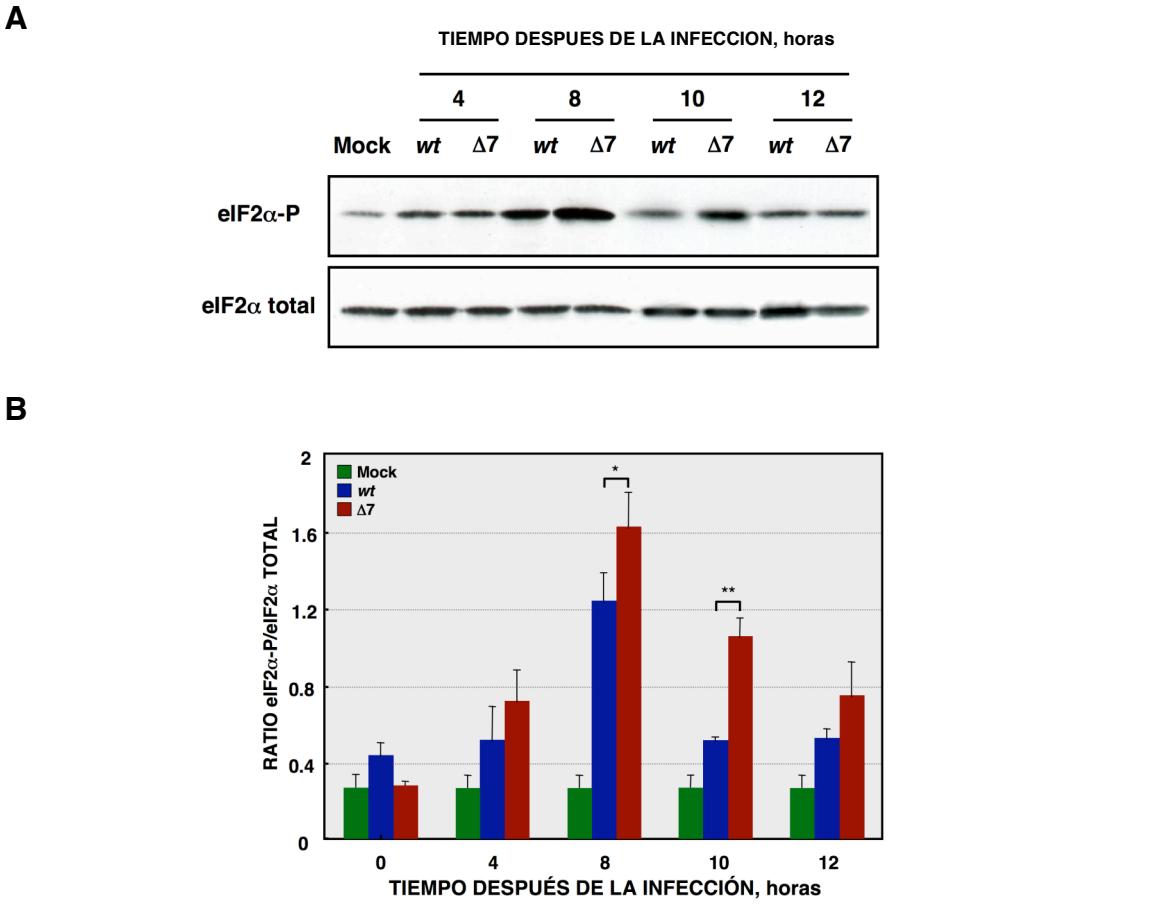

Figura 22. Fosforilación del factor eIF2α durante la infección del rTGEV. (A) Se extrajo la proteína total de células ST sin infectar (Mock) e infectadas, a una moi de 5, con los rTGEV-*wt* (*wt*) y rTGEV-Δ7 (Δ7) a distintos tiempos después de la infección. Se analizó la acumulación del eIF2α total y el eIF2α fosforilado (eIF2α-P) mediante *Western-blot*. (B) Las cantidades de eIF2α y eIF2α-P se estimaron mediante densitometría. La gráfica representa la relación eIF2α-P/eIF2α en células no infectadas (verde) e infectadas con los rTGEV-*wt* (azul) o rTGEV-Δ7 (rojo) a las hpi indicadas. Las barras de error representan las desviaciones estándar de seis experimentos independientes. u.r., unidades relativas. *, p-value < 0.05; **, p-value <0.01.

La proteína de parada del crecimiento inducible por lesión del DNA (GADD34) se induce cuando la célula está bajo ciertos tipos de estrés, y su expresión es directamente

proporcional a los niveles de fosforilación del eIF2α (Novoa y col., 2001). Por tanto, los niveles de mRNA de la GADD34 podrían estar modificados por la infección del rTGEV-Δ7. Se evaluó la expresión de este gen mediante RT-qPCR. La infección con el rTGEV-Δ7 produjo niveles significativamente más altos de mRNA de GADD34 que los inducidos por el virus silvestre (Figura 23). Este resultado estaba en línea con los datos previos, dado que a mayores niveles de eIF2α-P, se observó una mayor expresión de GADD34.

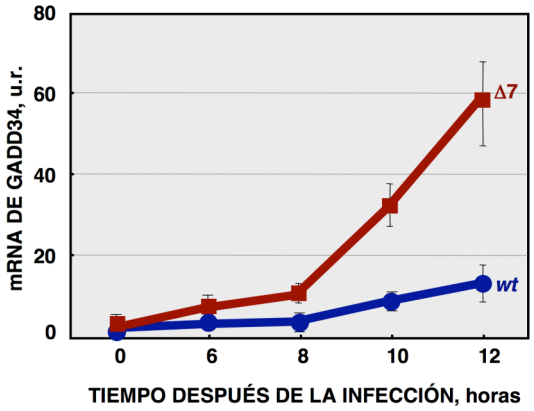

Figura 23. Análisis de la expresión del gen GADD34 porcino. Se analizó mediante RT-qPCR la expresión del gen de la GADD34 porcina durante la infección con los rTGEV-*wt* (azul) o rTGEV-Δ7 (rojo), a los tiempos indicados. Las barras de error representan las desviaciones estándar de tres experimentos independientes. u.r., unidades relativas.

5. LA PROTEÍNA 7 SUMINISTRADA EN *TRANS* REESTABLECE EL FENOTIPO rTGEV-*wt*

Para confirmar que la ausencia de la proteína 7 durante la infección del TGEV era responsable del fenotipo viral observado, se generó una línea de células ST que expresaba establemente la proteína 7 de TGEV con el marcador hemaglutinina (HA) situado después del péptido señal (ST-HA-7) (Figura 24A). La expresión de la proteína 7 se confirmó por inmunofluorescencia (Figura 24B) y *Western-blot* (Figura 24C), utilizando anticuerpos específicos para el marcador HA. Se seleccionaron tres clones de ST-HA-7 con distintos niveles de expresión de la proteína (C1, C2 y C3) (Figura 24B y 24C).

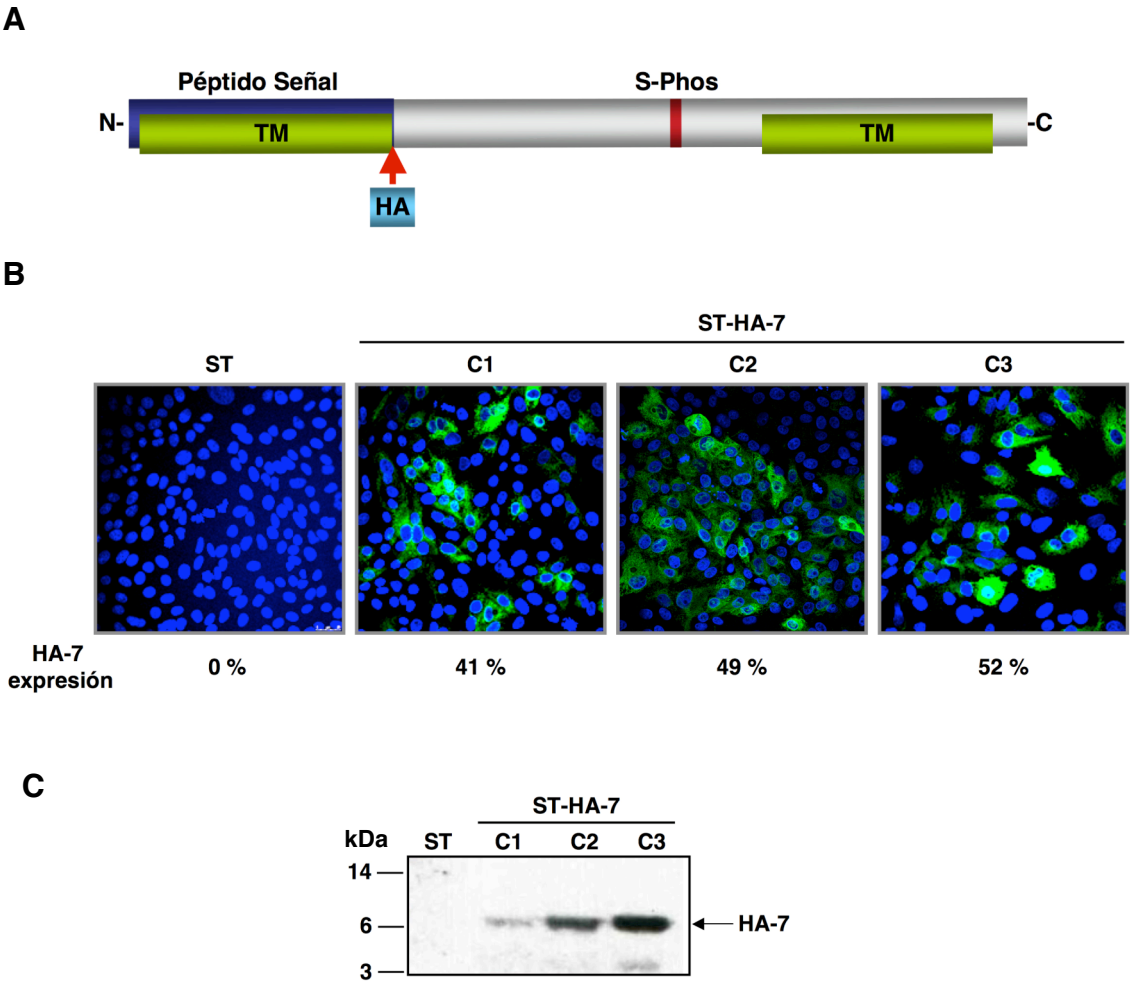

Figura 24. Generación de células ST que expresan la proteína 7 de TGEV en *trans*. (A) Esquema de la proteína 7 de TGEV expresada en las células ST. El marcador de la hemaglutinina (HA, azul claro) se insertó después del péptido señal (azul). (B) Niveles de expresión de la proteína 7, analizados mediante inmunofluorescencia, de tres clones seleccionados de células ST-HA-7 (C1, C2 y C3). La proteína HA-7 se detectó con un anticuerpo anti-HA marcado en verde, y el núcleo se marcó con DAPI (azul). Se indica el porcentaje de células que expresan la proteína HA-7. (C) La acumulación de la proteína HA-7 se evaluó mediante *Western-blot*. Se indica la banda correspondiente a la proteína HA-7 que corresponde con el peso molecular de la proteína HA-7 sin el péptido señal (7 kDa).

La infección de células ST con el rTGEV-Δ7 causó mayores niveles de apoptosis que el rTGEV-*wt*, como se había observado previamente (Figura 25A). Sin embargo, en células ST-HA-7 se redujo significativamente la apoptosis inducida tanto por el rTGEV-Δ7 como por el rTGEV-*wt* (Figura 25A). En células ST la infección con el rTGEV-Δ7 indujo niveles mayores de degradación de RNA que los observados en la infección con el rTGEV-*wt* (Figura 25B). Sin embargo, la expresión de la proteína 7 inhibió la degradación de RNA de forma dependiente de dosis, lo que indicó que la expresión en *trans* de la proteína 7 previno la activación de las nucleasas (Figura 25B).

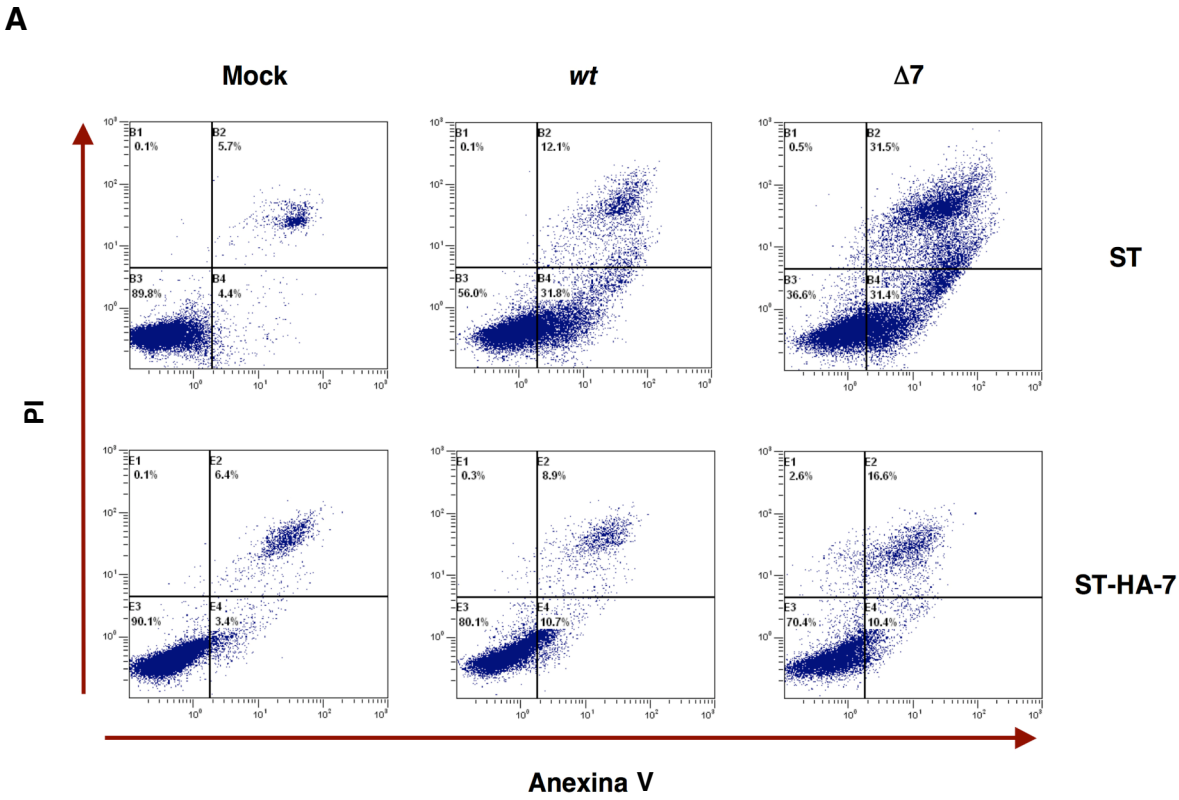

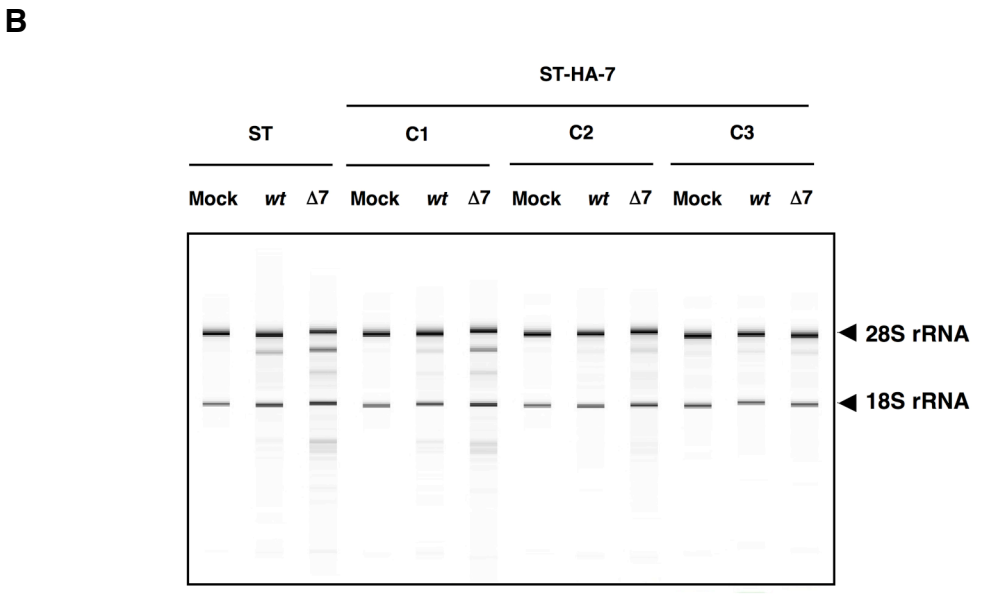

Figura 25. Complementación de la apoptosis y la degradación del RNA celular producidos por el rTGEV-Δ7 mediante la administración de la proteína 7 en *trans*. (A) Se utilizaron células ST o células ST-HA-7 para analizar los niveles de apoptosis mediante citometría de flujo. Se evaluó la apoptosis inducida en las células sin infectar (Mock) y en las células infectadas con el rTGEV-*wt* (*wt*) o con el rTGEV-Δ7 (Δ7) a 12 hpi. Se realizó un doble marcaje de las células con Anexina V y PI para distinguir las células en apoptosis temprana (Anexina V^+, PI^-) de aquellas que se encontraban en apoptosis tardía (Anexina V^+, PI^+). (B) Se infectaron células ST y los tres clones de células ST-HA-7 con los rTGEV-*wt* y rTGEV-Δ7. El RNA total se extrajo a 18 hpi. Se evaluó la integridad del RNA celular utilizando un *Bioanalyzer*. Los rRNAs 28S y 18S se indican a la derecha de la figura.

Los niveles de fosforilación del factor eIF2α (Figura 26A) y de expresión del gen GADD34 (Figura 26B) se redujeron significativamente al suministrar la proteína 7 en *trans*. En conjunto, estos resultados demostraron que el fenotipo del rTGEV-Δ7 se debió exclusivamente a la ausencia de la proteína 7, dado que dicho fenotipo se revertió de una manera dependiente de dosis al administrar la proteína en *trans*.

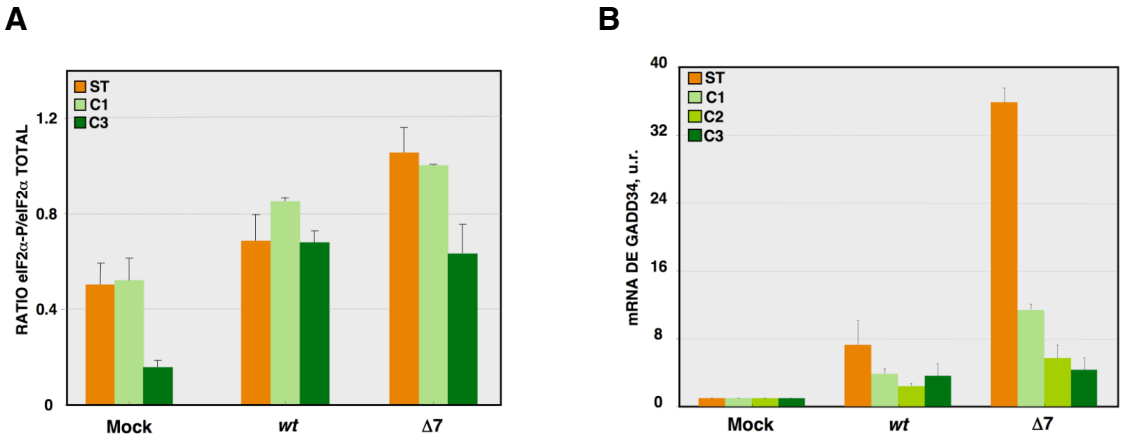

Figura 26. Efecto de la expresión de la proteína 7 de TGEV en *trans* en los niveles de eIF2α-P y de GADD34. (A) Se infectaron células ST y los clones C1 y C3 de las células ST-HA-7 con el rTGEV-*wt* o el rTGEV-Δ7. Se extrajeron las proteínas totales a las 10 hpi y los niveles de eIF2α y eIF2α-P se analizaron mediante *Western-blot*. La cantidad de proteína se estimó mediante densitometría, y se representó la relación eIF2α-P/eIF2α total. Las barras de error representan las desviaciones estándar de seis experimentos independientes. (B) Se infectaron células ST y los clones C1,C2 y C3 de las células ST-HA-7 con el rTGEV-*wt* o el rTGEV-Δ7. Se extrajo el RNA total a las 10 hpi y la expresión del gen GADD34 porcino se analizó mediante RT-qPCR. Las barras de error representan las desviaciones estándar de seis experimentos independientes. u.r., unidades relativas.

6. MECANISMO DE ACCIÓN DE LA PROTEÍNA 7

6.1. Efecto de la ausencia de la proteína 7 sobre las quinasas implicadas en la fosforilación del factor eIF2α

La fosforilación del factor eIF2α está controlada en células de mamífero por cuatro quinasas distintas: la quinasa de eIF2α regulada por el grupo hemo (HRI), la quinasa del control general de la biosíntesis de aa (GCN2), la quinasa activada por dsRNA (PKR), y la quinasa de retículo endoplásmico similar a PKR (PERK). Dado que estas quinasas tienen todas en común el mismo sustrato, su activación genera el mismo efecto en la célula: la inhibición de la traducción celular y la traducción específica de genes de respuesta a estrés (Harding y col., 2002). Las quinasas eIF2 se activan en respuesta a distintos estímulos (Proud, 2005). La quinasa HRI, sintetizada en reticulocitos, participa

en la síntesis de la hemoglobina y se activa en respuesta a la disminución de los niveles del grupo hemo (Matts y col., 1983). La quinasa GCN2 se activa en situaciones de deprivación de nutrientes por la disminución en los niveles de aa (de Haro y col., 1996; Zhu y col., 1996).

Durante la infección viral, los principales responsables de la fosforilación del factor eIF2α son las quinasas PKR y PERK. La quinasa PKR es un componente de la respuesta antiviral del huésped activada por dsRNA. La unión de la proteína PKR al dsRNA promueve la dimerización y activación de la quinasa (Hershey, 1991). La activación de PKR lleva a la fosforilación del eIF2α y a la parada en la síntesis de proteínas (Figura 27A) (Proud, 1995; Taylor y col., 2005). La infección con el rTGEV-*wt* indujo la fosforilación de PKR, con un nivel máximo a las 12 hpi (Figura 27B). No se observaron diferencias significativas entre la infección por los rTGEV-*wt* y rTGEV-Δ7, ni en los niveles de fosforilación de la PKR ni en los niveles de proteína total (Figura 27B), lo que sugirió que las diferencias observadas en la síntesis de proteínas debería tener otro origen.

A

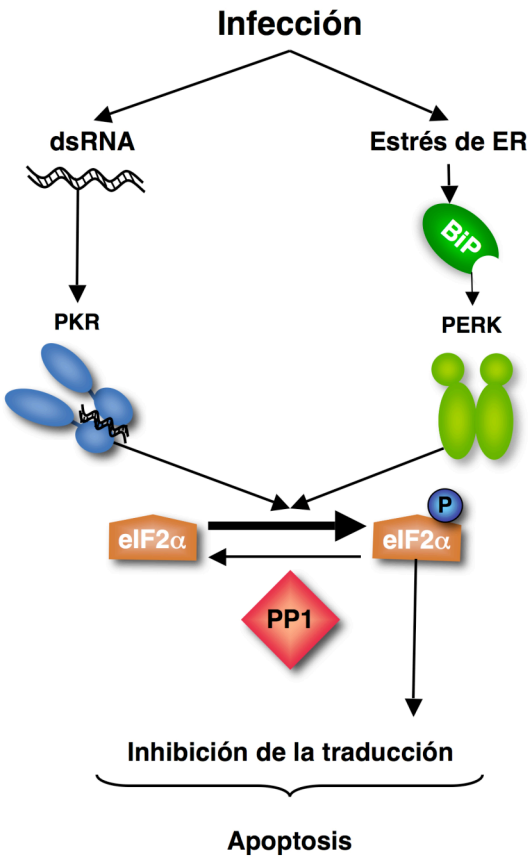

B

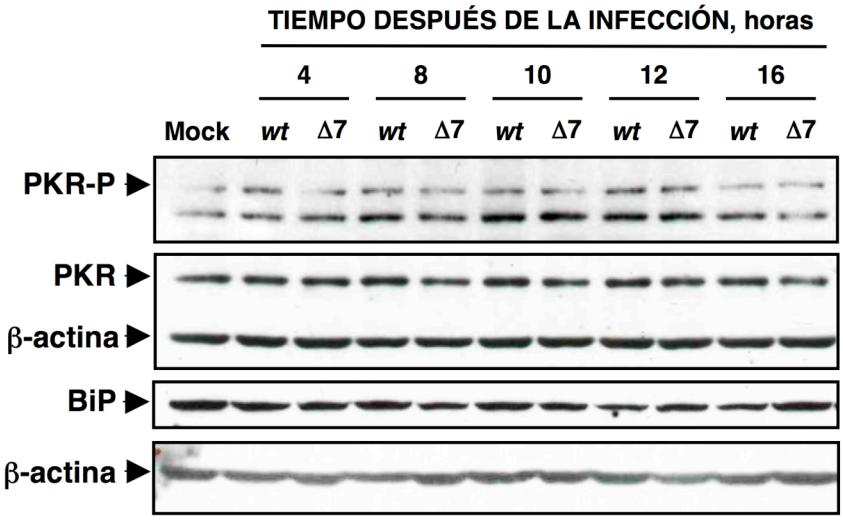

Figura 27. Efecto de la proteína 7 en las quinasas implicadas en la fosforilación del factor eIF2α . (A) Esquema del papel de las enzimas PKR, PERK y PP1 en el balance eIF2α/eIF2α-P. (B) Evaluación mediante *Western-blot* utilizando anticuerpos específicos de los niveles de acumulación de la quinasa PKR fosforilada (PKR-P), la PKR total y la proteína BiP (GRP78) durante la infección con los rTGEV-*wt* y rTGEV-Δ7, a los tiempos indicados. La proteína β-actina se utilizó como control de carga.

Durante la infección viral, la acumulación de proteínas nacientes o mal plegadas en el retículo endoplásmico (ER) causa estrés en este orgánulo, lo que desencadena una respuesta del huésped, que puede llevar también a la fosforilación del eIF2α (Figura 27A) (Schroder and Kaufman, 2005). La proteína PERK se activa cuando existe estrés de ER, y puede participar en la fosforilación del factor eIF2α durante una infección viral (Harding y col., 1999; Shi y col., 1998). Desafortunadamente, los anticuerpos disponibles para detectar la proteína PERK no reconocían la proteína porcina. Sin embargo, como una medida indirecta de la activación de PERK, se evaluó el estrés de ER inducido con la infección del rTGEV-*wt* y con el rTGEV-Δ7. La expresión de la proteína de unión a inmunoglobulina (BiP o GRP78) aumenta en respuesta al estrés de ER, y por ello se utiliza como marcador de este tipo de estrés (He, 2006; Lee, 2001; Luo y col., 2003). Se observaron niveles similares de BiP en las células infectadas con los rTGEV-*wt* y rTGEV-Δ7 (Figura 27B), sugiriendo que la proteína PERK no estaría diferencialmente activada en las células infectadas por el virus mutante que no expresaba el gen 7, respecto a las infectadas con el virus parental.

En conjunto, estos datos sugirieron que un incremento de la actividad quinasa no era el responsable del aumento de la fosforilación del eIF2α durante la infección con el rTGEV-Δ7.

6.2. Efecto de la proteína 7 de TGEV sobre la fosfatasa PP1

Alternativamente, el aumento observado en los niveles de eIF2α-P durante la infección con el rTGEV-Δ7 se podría deber a un incremento en la actividad fosfatasa que contrarresta la función de las quinasas (Figura 27A). La fosfatasa PP1 es la principal serin/treonin fosfatasa encargada de la defosforilación del eIF2α (He y col., 1997; Novoa y col., 2001; Wang y col., 2009). La acumulación de la fosfatasa PP1, evaluada mediante *Western-blot,* fue similar durante las infecciones con los rTGEV-*wt* y rTGEV-Δ7 (Figura 28).

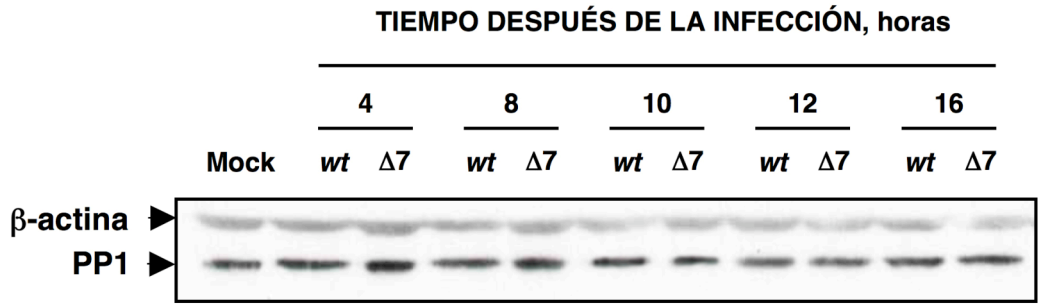

Figura 28. Efecto de la proteína 7 en la acumulación de la fosfatasa PP1. Análisis mediante *Western-blot* de los niveles de acumulación de la fosfatasa PP1 en células ST sin infectar (Mock) o infectadas con los rTGEV-*wt* (*wt*) o rTGEV-Δ7 (Δ7) a los tiempos después de la infección indicados. La proteína β-actina se utilizó como control de carga.

La subunidad catalítica de la fosfatasa PP1 (PP1c) puede interaccionar con más de 50 proteínas reguladoras. La formación de estos complejos determina la especificidad del sustrato, la localización subcelular y la actividad, permitiendo a la fosfatasa PP1 desempeñar numerosas funciones celulares (Aggen y col., 2000; Cohen, 2002). Por tanto, aunque no se detectaron diferencias en los niveles de la proteína PP1c en las células infectadas con los rTGEV-*wt* y rTGEV-Δ7, la proteína 7 podría estar modulando la actividad o la localización de la PP1. Se analizaron los motivos funcionales de la proteína 7 de la especie *Alfacoronavirus 1* utilizando el servidor ELM (Gould y col., 2010; Puntervoll y col., 2003). Se identificó una secuencia, altamente conservada en la proteína 7 de distintos CoVs, que correspondía a la secuencia canónica del motivo de

unión a la subunidad catalítica de la PP1 (Figura 29A). Este motivo consenso de unión a la proteína PP1c incluye una secuencia corta (R/K)VxF, en la cual x es cualquier aa exceptuado aquellos con cadenas laterales hidrofóbicas grandes, rodeado por aa no polares (Figura 29B) (Cohen, 2002). Se ha demostrado que el motivo RVxF es suficiente para mediar la unión con la fosfatasa PP1, mientras que los aa que lo rodean son los responsables de la modulación alostérica de la actividad enzimática de la proteína PP1c (Ajuh y col., 2000; Hsieh-Wilson y col., 1999; Schillace y col., 2001). Hasta la fecha, la presencia de este motivo se ha descrito en tres proteínas virales: la proteína $\gamma_1$34.5 del virus del herpes simple, la proteína E6 del papilomavirus humano y la proteína DP71L del virus de la peste porcina Africana, y en varias proteínas celulares como la proteína GADD34 (Figura 29B). En todos los casos, estas proteínas se unen a la proteína PP1c y promueven la defosforilación del eIF2α (Brush y col., 2003; He y col., 1997; Kazemi y col., 2004; Novoa y col., 2001; Novoa y col., 2003; Rivera y col., 2007).

A

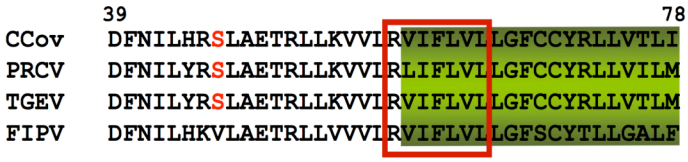

B

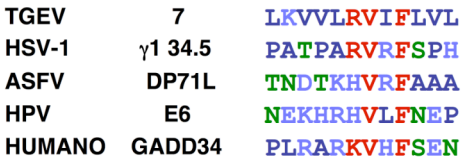

Figura 29. Motivo de la proteína 7a de la especie *Alfacoronavirus 1* que media la unión con la PP1c. (A) Fragmento del alineamiento de las secuencias de las proteínas 7a de la especie *Alfacoronavirus 1*. El motivo canónico de unión a la subunidad catalítica de la proteína PP1 (PP1c) está marcado con una caja roja. (B) El motivo consenso de unión a la proteína PP1c incluye una secuencia corta (R/K)VxF (rojo), rodeada de aa con residuos no polares. Este motivo está en otras proteínas virales y celulares, como la proteína $\gamma_1$34.5 del virus humano del herpes simple-1 (HSV-1), la proteína DP71L del virus de la peste porcina Africana (ASFV), la oncoproteína E6 del papilomavirus humano (HPV), y la proteína humana GADD34. Los números de acceso de *GenBank* son ADB28914.1, P36313, Q65212, ACR78108 y O75807, respectivamente. Se representan en azul oscuro los aa no polares; azul claro, los aa cargados; en verde, los aa polares; y en rojo la secuencia central del motivo de unión a la proteína PP1c.

En este trabajo se ha descrito que tanto el rTGEV-*wt* como el rTGEV-Δ7 inducen la activación una respuesta antiviral en el huésped, lo que lleva a la fosforilación del factor eIF2α. Nosotros proponemos que durante la infección con el rTGEV-*wt* la proteína 7 interaccionaría, a través de su motivo de unión a PP1c, con el complejo de la fosfatasa PP1, promoviendo la defosforilación del eIF2α, y permitiendo la síntesis de proteínas en la célula (Figura 30). Sin embargo, en la infección con el rTGEV-Δ7, no se podrían reducir los niveles del factor eIF2α fosforilado, lo que desencadenaría una parada en la traducción y el daño célular (Figura 30).

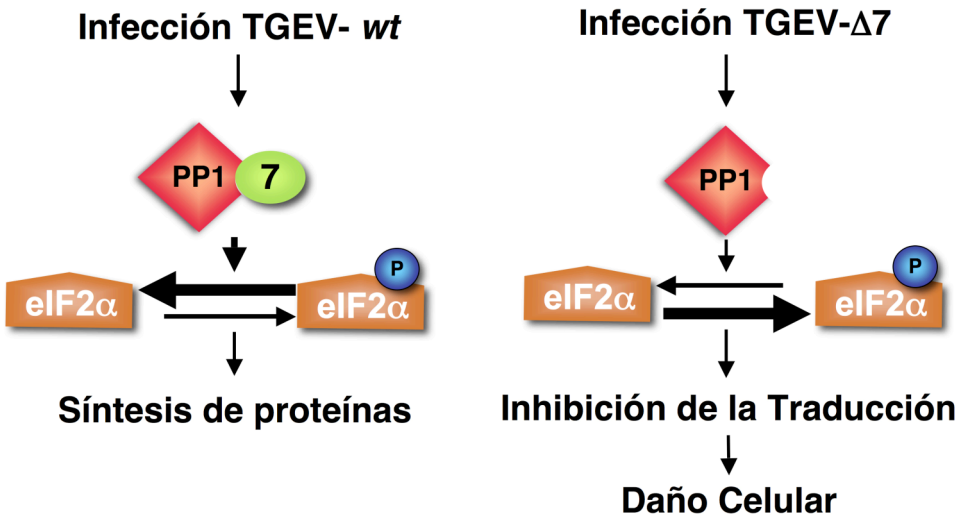

Figura 30. Hipótesis de la función de la proteína 7 de TGEV. Esquema del modelo propuesto de la función de la proteína 7 durante la infección de TGEV.

6.3. Interacción de la proteína 7 con la fosfatasa PP1

Un elemento imprescindible en el modelo propuesto es la interacción de la proteína 7 con la proteína PP1c. Esta interacción se evaluó mediante un ensayo de co-inmunoprecipitación, utilizando células ST-HA-7. La inmunoprecipitación seguida de la inmunodetección con un anticuerpo que reconocía el HA, reveló la presencia de la proteína 7 tanto en la muestra de partida como en los extractos inmunoprecipitados, pero no en los extractos de células ST, tal y como se esperaba (Figura 31). Además se observó que la proteína PP1c inmunoprecipitó junto con la proteína 7 (Figura 31). La proteína de la envuelta (E) del SARS-CoV, que es una proteína pequeña de membrana como la proteína 7 de TGEV, se utilizó como control de la especificidad de la co-inmunoprecipitación. La interacción de la proteína 7 con la PP1c fue específica, puesto

que la proteína E no co-inmunoprecipitó con la proteína PP1c (Figura 31). Se generó una proteína 7 recombinante con el marcador HA y sin el dominio de unión a la proteína PP1c (7-mut). El ensayo de co-inmunoprecipitación mostró que la proteína 7-mut no interaccionaba con la proteína PP1c (Figura 31). En conjunto, estos resultados demostraron la interacción específica de la proteína 7 de TGEV y la proteína del huésped PP1c.

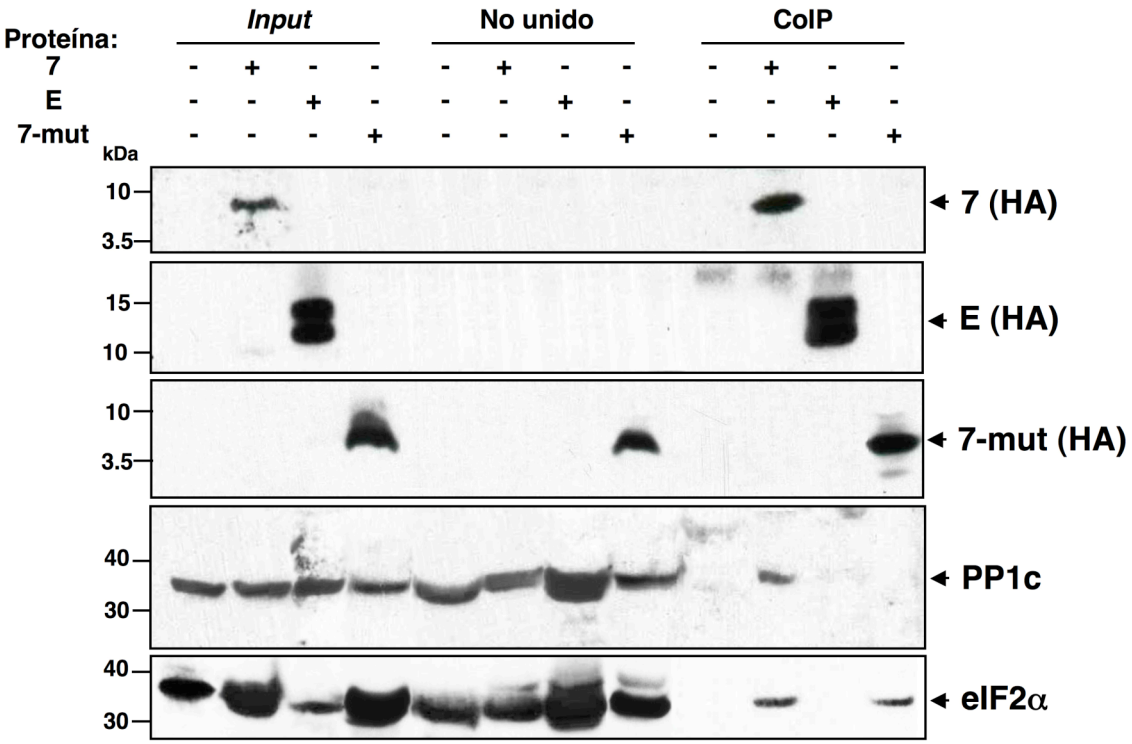

Figura 31. Interacción de la fosfatasa PP1 con la proteína 7 de TGEV. Co-inmunoprecipitación de la proteína 7 de TGEV y la fosfatasa PP1. La interacción entre la proteína 7 de TGEV y la proteína PP1c se evaluó utilizando células ST, ST-HA-7 (7), y células ST que expresaban la proteína E del SARS-CoV E (E) o la proteína 7 de TGEV sin el dominio de unión a la proteína PP1c (7-mut). Los extractos celulares se incubaron con una matriz de agarosa conjugada con el anticuerpo anti-HA. Las muestras de partida (*Input*), de la fracción no unida, y de la elución final (CoIP) se resolvieron mediante SDS-PAGE. La presencia de las proteínas con el marcador HA, la proteína PP1c y el factor eIF2α se analizó mediante *Western-blot* utilizando anticuerpos específicos.

Asimismo, se analizó la presencia del factor eIF2α en las muestras co-inmunoprecipitadas. Éste factor co-inmunoprecipitó específicamente tanto con la proteína 7 nativa como con la proteína mutada (Figura 31), sugiriendo que el factor eIF2α estaba presente en el complejo formado por la proteína 7 de TGEV y la fosfatasa PP1.

Para complementar estor resultados, la interacción proteína 7-PP1c se analizó en el contexto de la infección con el TGEV. Para ello en la co-inmunoprecipitación se utilizaron muestras procedentes de células ST-HA-7 sin infectar o infectadas con el rTGEV-Δ7, para evitar la competición entre la proteína HA-7 y la proteína 7, no marcada, expresada por el virus silvestre. La proteína PP1c co-inmunoprecipitó con la proteína HA-7 en células infectadas con el rTGEV-Δ7 (Figura 32A), indicando que estas proteínas también interaccionaban en el contexto de la infección con el TGEV.

Por otra parte, en las células ST-HA-7 infectadas con el rTGEV-*wt* se observó una disminución en los niveles de PP1c co-inmunoprecipitada por la proteína HA-7 en relación con los niveles detectados en las células infectadas con el rTGEV-Δ7 (Figura 32B). Esto sugirió que la proteína 7, expresada por el rTGEV-*wt*, también interaccionó con la proteína PP1c, y compitió con la proteína HA-7 por esta unión.

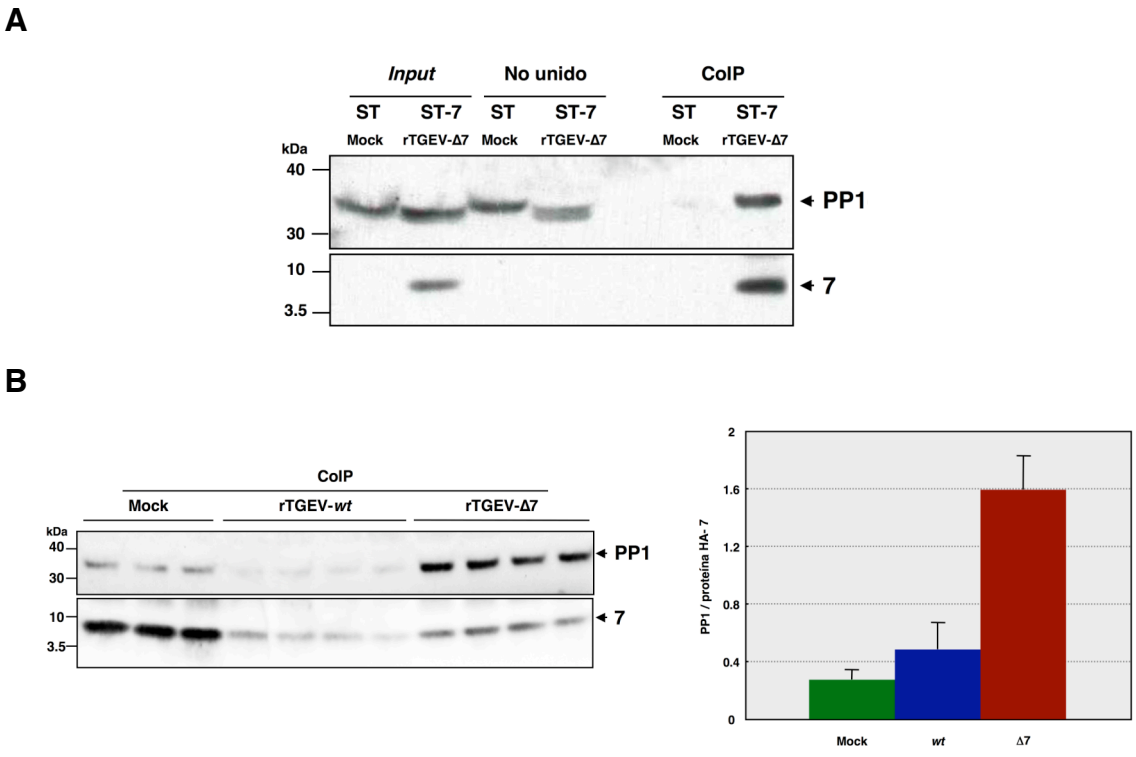

Figura 32. Interacción entre la fosfatasa PP1 y la proteína 7 de TGEV en el contexto de la infección por el TGEV. (A) Células ST sin infectar y células ST-HA-7 infectadas con el rTGEV-Δ7 se utilizaron en un ensayo de co-inmunoprecipitación. Los extractos de células recogidos a 16 hpi se incubaron con la agarosa conjugada con el anticuerpo anti-HA. Las muestras de partida (*Input*), de la fracción no unida, y de la elución final (CoIP) se resolvieron mediante SDS-PAGE. La presencia de la proteína 7 con el marcador HA y la proteína PP1c se analizó mediante *Western-blot* utilizando anticuerpos específicos. (B) Células ST-HA-7 sin infectar e infectadas con los rTGEV-*wt* o rTGEV-Δ7 se utilizaron como muestra en un ensayo de co-inmunoprecipitación como en el apartado (A). Las muestras de la elución final (CoIP) de distintos experimentos se resolvieron mediante SDS-PAGE y la

presencia de la proteína 7 con el marcador HA y la proteína PP1c se analizó mediante *Western-blot.* La gráfica representa la relación entre los niveles de PP1c y de HA-7, estimados por densitometría. Las barras de error representan las desviaciones estándar de cuatro experimentos independientes.

6.4. Efecto de la unión de la proteína 7 y PP1c en la fosforilación del factor eIF2α y la degradación de RNA

Estos resultados, y la presencia del factor eIF2α en el complejo formado por las proteínas 7 y PP1c, indicaron que el efecto de la proteína 7 durante la infección dependía de su unión a la fosfatasa PP1, de acuerdo con la hipótesis de trabajo. Por ello, la degradación del RNA celular y los niveles de fosforilación del factor eIF2α se analizaron en presencia de la proteína 7-mut que no se unía a la proteína PP1c. Células ST se transfectaron con la proteína HA-7-mut. Los niveles de expresión y la localización subcelular de la proteína HA-7-mut eran similares a los observados para la proteína HA-7 tal y como se comprobó por inmunofluorescencia (Figura 33).

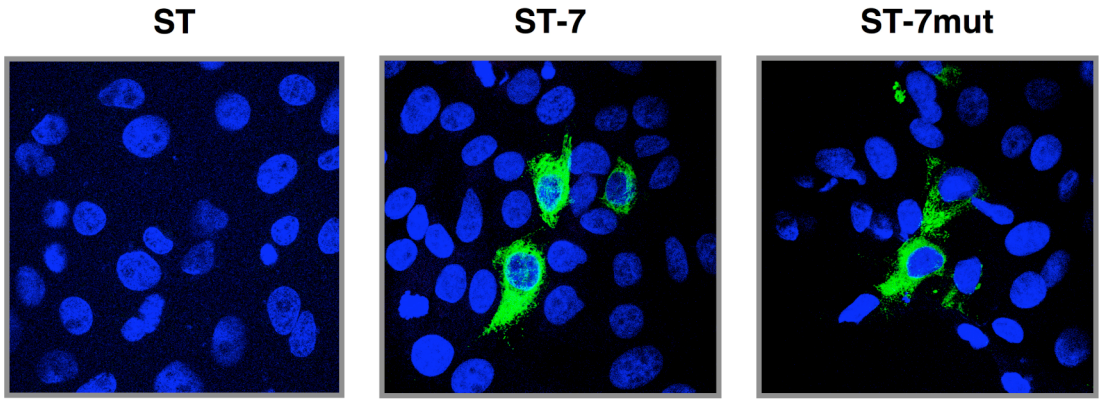

Figura 33. Localización subcelular de las proteínas HA-7 y HA-7-mut en células ST. Las proteínas HA-7 y HA-7-mut se detectaron mediante inmunofluorescencia con un anticuerpo anti-HA marcado en verde y el núcleo se marcó con DAPI (azul).

Como se había observado previamente, la infección con el rTGEV-Δ7 causó un incremento en la degradación de RNA celular (Figura 34A) y en los niveles de fosforilación del factor eIF2α (Figura 34B), comparados con los observados durante la infección con el rTGEV-*wt*. Y la proteína 7 proporcionada en *trans* revertió ambos procesos (Figura 34). Sin embargo, la proteína 7-mut proporcionada en *trans* no redujo los niveles de degradación del RNA ni de fosforilación del factor eIF2α, incrementados por la infección con el rTGEV-Δ7 (Figura 34). Este resultado indicó que la proteína 7

de TGEV modula la degradación del RNA celular y la fosforilación del factor eIF2α a través de su interacción con la fosfatasa PP1.

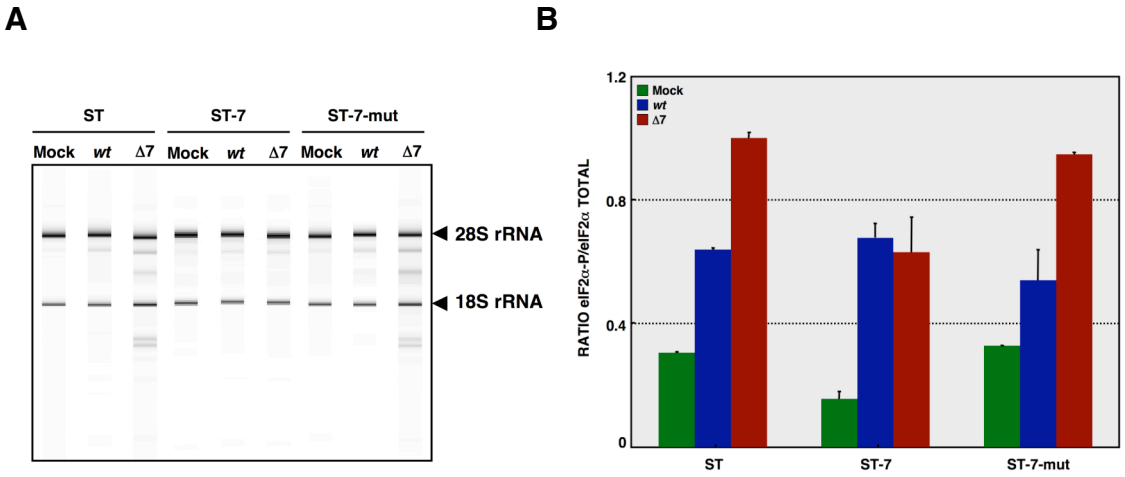

Figura 34. Efecto de la proteína 7 mutante suministrada en *trans* sobre la degradación del RNA y la fosforilación del factor eIF2α. Se utilizaron células ST y las células ST que expresaban la proteína 7 de TGEV nativa (ST-7) o la proteína 7 que carecía del dominio de unión a la proteína PP1c (ST-7-mut). Se evaluaron las células sin infectar (Mock) e infectadas con los rTGEV-*wt* (*wt*) o rTGEV-Δ7 (Δ7). (A) Se extrajo el RNA total a 18hpi y se analizó la integridad del RNA celular utilizando un *Bioanalyzer*. Los rRNAs 28S y 18S rRNAs se indican a la derecha. (B) Se extrajo la proteína total a 10 hpi y los niveles del factor eIF2α total y eIF2α-P se analizaron mediante *Western-blot*. Se estimó la cantidad de cada proteína mediante densitometría. Se representa la relación eIF2α-P/eIF2α. Las barras de error representan las desviaciones estándar de tres experimentos independientes.

7. ANÁLISIS DE LA EXPRESIÓN GÉNICA EN CÉLULAS INFECTADAS CON EL rTGEV-Δ7

Para caracterizar la respuesta celular frente a la infección por los rTGEV-*wt* y rTGEV-Δ7, se estudió el transcriptoma de las células a dos tiempos después de la infección. Se extrajo el RNA total de células ST sin infectar o infectadas con los rTGEV-*wt* y rTGEV-Δ7, a una moi de 5 a tiempos temprano (6 hpi) y tardío (12 hpi) de la infección. Experimentos previos de citometría de flujo demostraron que, con esa moi, el 90% del cultivo celular estaba infectado a 4 hpi. En todos los casos se realizaron 9 infecciones independientes. Para reducir la variabilidad debida al estado de las células al ser infectadas, el RNA de cada variable se obtuvo por combinación de tres cultivos celulares independientes. Asimismo, se realizaron tres experimentos independientes. Los niveles de transcripción de los genes celulares se estudiaron utilizando una matriz de DNA (*microarray*) porcino de Affymetrix que contiene 23937 sondas, que

corresponden a 20201 genes. Para facilitar el análisis funcional posterior, los *microarrays* se reanotaron por homología con los genes humanos (Tsai y col., 2006).

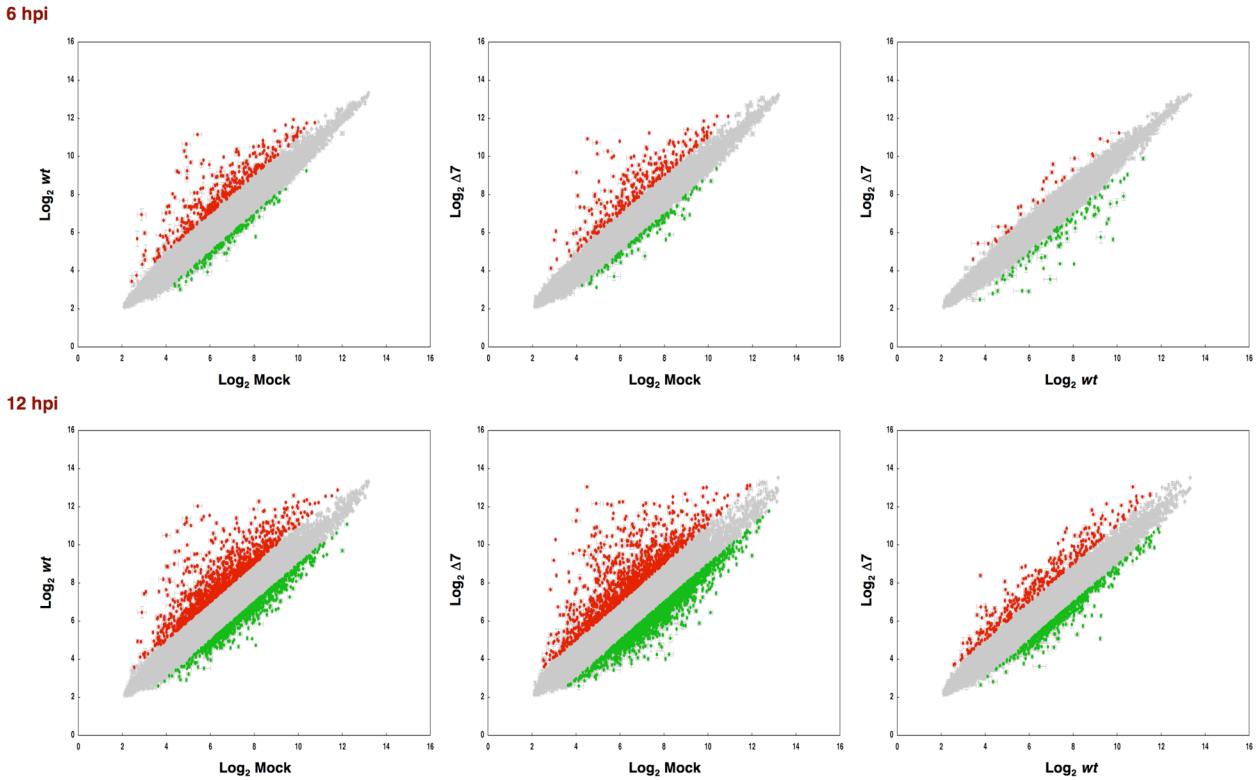

Figura 35. Análisis de la expresión génica en células ST infectadas con los rTGEV-*wt* y rTGEV-Δ7. Visualización de los genes diferencialmente expresados a 6 y 12 hpi en células infectadas con el virus parental (*wt*) o con el virus mutante (Δ7) frente a células no infectadas (Mock) y células infectadas con el rTGEV-Δ7 frente a células infectadas con el rTGEV-*wt*. Los puntos rojos indican genes sobre-expresados, los puntos verdes indican genes que están reprimidos y los puntos grises indican genes cuya expresión no se ve significativamente alterada.

Los cambios en la expresión génica se analizaron aplicando umbrales mínimos con tasas de cambio mayores de 2 o menores de -2, y una tasa de falsos descubrimientos (FDR) menor de 0.05 (Figura 35). El número de sondas que cambiaron su nivel de expresión se resumen en la Tabla I.

TABLA I. Análisis de la expresión génica durante la infección con TGEV.

Comparación[(a)]	hpi	nº de sondas	
		Expresión aumentada	Expresión inhibida
wt vs C$^-$	6	373	148
Δ7 vs C$^-$	6	289	127
Δ7 vs *wt*	6	31	98
wt vs C$^-$	12	1119	768
Δ7 vs C$^-$	12	1259	1782
Δ7 vs *wt*	12	346	525

[(a)] C$^-$, células sin infectar. *wt*, células infectadas con el rTGEV-*wt*. Δ7, células infectadas con el rTGEV-Δ7.

El número de sondas diferencialmente expresadas, al comparar las infecciones con los rTGEV-Δ7 y rTGEV-*wt* (Tabla I), correspondía a 26 y 301 genes sobre-expresados a 6 y 12 hpi, respectivamente, y 84 genes y 466 genes inhibidos a 6 y 12 hpi, respectivamente. El 63% de genes que se sobre-expresaron en la infección con el rTGEV-Δ7, respecto a la del rTGEV-*wt,* a 6 hpi también lo estaban a 12 hpi. La misma tendencia se obtuvo para los genes inhibidos, de modo que el 61% de los genes reprimidos en la infección con el rTGEV-Δ7, respecto a la del rTGEV-*wt,* a 6 hpi también lo estaban a 12 hpi. Estos datos sugirieron que los mecanismos que se activan diferencialmente en la infección del virus mutante respecto a la del virus parental a 6 hpi se mantienen a las 12 hpi, aunque a la expresión diferencial de estos genes se sumen otros afectados a tiempos tardíos de la infección.

7.1. Análisis funcional de los genes diferencialmente expresados

Los genes diferencialmente expresados en la infección con el virus mutante respecto a la del virus parental a 12 hpi, se clasificaron funcionalmente utilizando el programa DAVID (Huang da y col., 2009a, b) y como fuente de anotaciones se usaron los procesos biológicos descritos en *Gene-Ontology* (Ashburner y col., 2000). La mayoría de genes diferencialmente expresados correspondían a respuesta a virus, respuesta de defensa y respuesta inmune (Figura 36).

Figura 36. Grupos biológicos a los que pertenecen los genes diferencialmente expresados en la infección con el rTGEV-Δ7 respecto a la del virus parental. Agrupación de los genes diferencialemente expresados, basada en los términos de procesos biológicos de *Gene Ontology*, a 12 hpi. Se utilizaron en la clasificación sólo aquellos genes con una tasa de cambio >2, o <-2, y un FDR<0.05.

Se realizó un análisis de patrones de expresión de dichos genes en células infectadas frente a células sin infectar, centrándonos en los genes comprendidos en el grupo de respuesta a virus. Este análisis indicó que, en general, los genes activados o reprimidos durante la infección con el virus silvestre también se sobre-activaban o inhibían en la infección con el rTGEV-Δ7. Sin embargo, lo hacían en mayor nivel o a tiempos más tempranos después de la infección con el virus mutante (Figura 37).

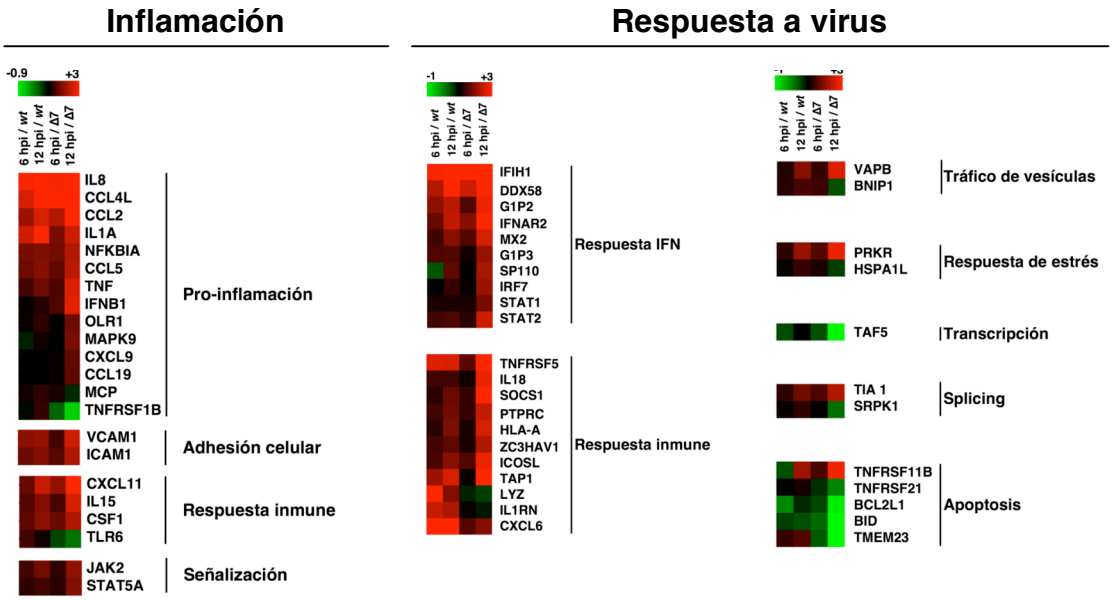

Figura 37. Patrones de expresión de algunos genes representativos del grupo de respuesta a virus. Se agrupan los genes diferencialmente expresados en células ST infectadas con el virus mutante respecto al virus silvestre a 12 hpi. Para aquellos genes reconocidos por más de una sonda, se representa el mayor valor de sobre-expresión o de represión.

Un análisis detallado de la descripción de los genes del grupo de respuesta a virus mostró que, a su vez, se incluían en grupos funcionales implicados en: respuesta inmune, respuesta a IFN, inflamación, factores de transcripción, apoptosis, tráfico de vesículas, activación del complemento, transporte nuclear y respuesta a estrés (Figura 38).

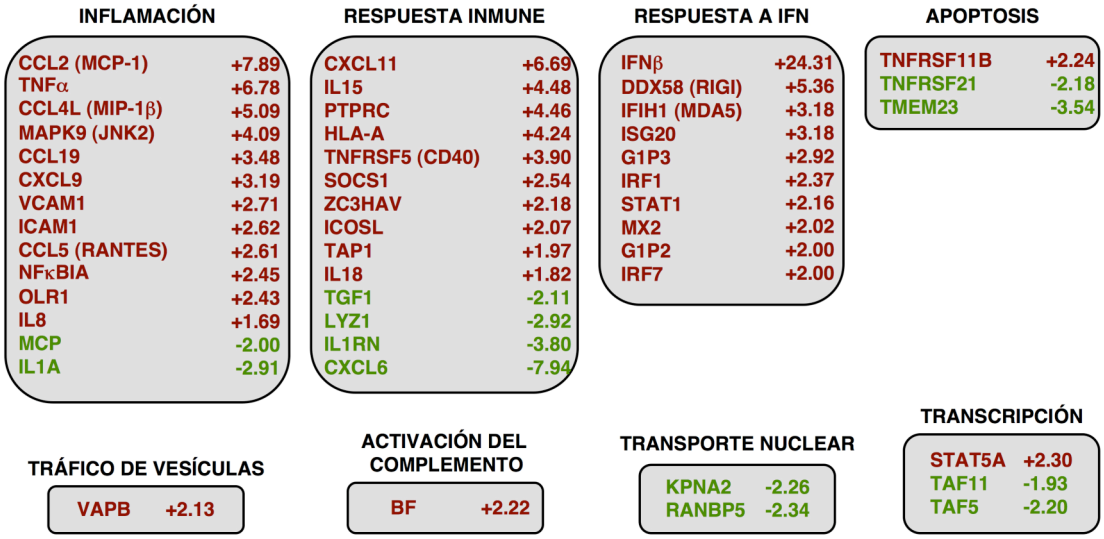

Figura 38. Genes celulares de respuesta a virus diferencialmente expresados en la infección con el rTGEV-Δ7

respecto a la del rTGEV-*wt*. Los genes diferencialmente expresados en células ST infectadas con el virus mutante respecto al virus silvestre a 12 hpi. Para aquellos genes reconocidos por más de una sonda, se representa el valor mayor de sobre-expresión (rojo) o de represión (verde).

Para cuantificar el nivel de expresión mediante RT-qPCR, se seleccionaron 14 genes de entre los grupos biológicos más representativos. Se infectaron células ST con una moi de 5 con los rTGEV-*wt* o rTGEV-Δ7. El RNA total se extrajo a 12 hpi y se analizaron los niveles de expresión de los genes elegidos utilizando ensayos *TaqMan* porcinos específicos para cada gen. En todos los casos, los niveles de expresión del gen de la beta-glucuronidasa (GUSB) se utilizaron para normalizar los datos. El gen GUSB es un gen constitutivo que se utiliza frecuentemente para corregir las pequeñas diferencias en los niveles de RNA de partida utilizados en el análisis de cada muestra (Nelissen y col., 2010; Piorkowska y col., 2011; Zampieri y col., 2010). Además, este gen no cambió su nivel de expresión durante la infección con TGEV, tanto con el virus silvestre como con el virus mutante. Los resultados obtenidos mediante los ensayos RT-qPCR y los *microarrays* fueron similares, con la excepción de la citoquina CXCL9 que sin embargo sigue la misma tendencia con ambas técnicas, y por tanto se validan así los resultados de expresión génica obtenidos (Figura 39).

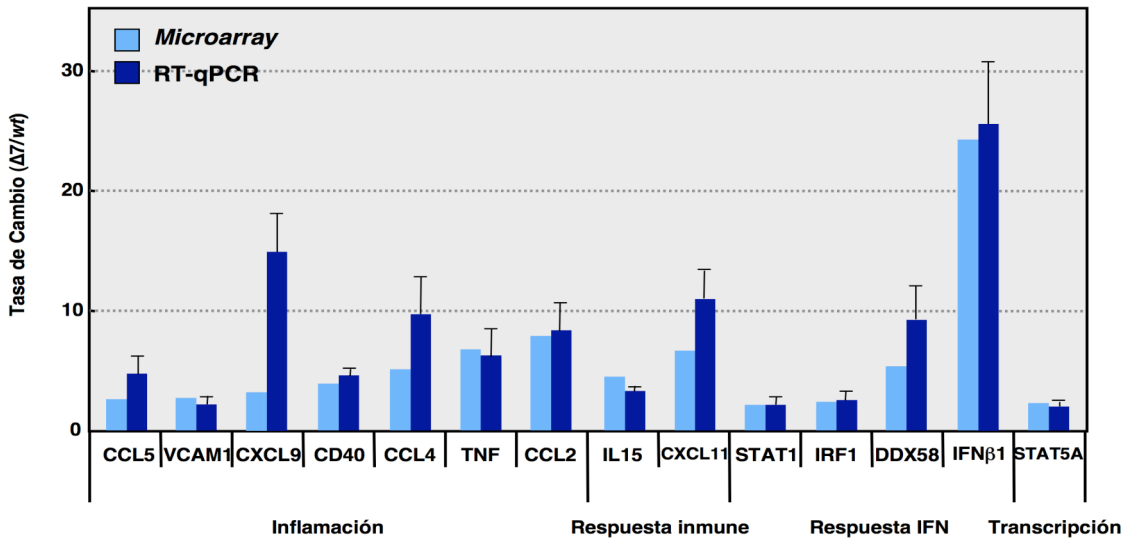

Figura 39. Expresión de genes celulares en la infección con el rTGEV-Δ7 respecto a la del rTGEV-*wt*. Cuantificación del mRNA de 14 genes diferencialmente expresados en la infección con el virus mutante respecto al virus silvestre a 12 hpi, obtenida mediante RT-qPCR utilizando ensayos *TaqMan* específicos. En barras azul claro se representa la tasa de cambio obtenida en los *microarrays,* que es en base al promedio de las intensidades de media de tres réplicas independientes, con un FDR<0.05. En barras azul oscuro se representa la tasa de cambio obtenida mediante RT-qPCR. Las barras de error representan las desviaciones estándar de tres experimentos independientes.

En conjunto estos resultados indicaron que existían diferencias en el patrón de expresión génica entre la infección con el rTGEV-Δ7 y con el rTGEV-*wt*, y que estas diferencias se daban fundamentalmente en genes relacionados con el control de la infección e inflamación. Las diferencias se observaron más en el nivel de expresión de los genes implicados en estos procesos que en el tipo de genes que se veían afectados. Esto sugirió que en la infección del rTGEV-Δ7 se activaron las mismas medidas antivirales que durante la infección con el rTGEV-*wt*, pero más rápidamente y con mayor intensidad.

7.2. Análisis de la expresión de genes implicados en inflamación

Como se describe en esta memoria, en la infección con el rTGEV-Δ7 la respuesta antiviral activada por dsRNA esta sobre-activada. Una de las consecuencias de la activación de esta respuesta antiviral es la inducción de la respuesta inmune innata y la producción de citoquinas pro-inflamatorias. El análisis del transcriptoma celular, utilizando *microarrays,* mostró que la infección con el rTGEV-Δ7 inducía la sobre-expresión de genes pro-inflamatorios en comparación con la infección con el virus silvestre. Por ello se decidió caracterizar la cinética de expresión de nueve genes, implicados en la respuesta pro-inflamatoria, durante la infección con los rTGEV-*wt* y rTGEV-Δ7. Los genes seleccionados se muestran en la Tabla II:

TABLA II. Genes pro-inflamatorios seleccionados.

Actividad	Proteína	Tasa de cambio[(a)]	Función
Inmunidad Innata	IFNβ	23.8 ±8	Antiviral. Activación de las células NK.
	IL-15	3.3 ±0.3	Estimular el crecimiento y proliferación de células T y NK.
	TNF	6.3 ±2.2	Principal mediador de la respuesta inflamatoria aguda. Activación del endotelio para la extravasación. Estimulación de la proliferación y diferenciación de macrófagos y neutrófilos.
Quimioquinas	CCL2 (MCP-1)	8.4 ±2.2	Atrayente de monocitos y basófilos. Relacionada con enfermedades que implican la infiltración de monocitos.
	CCL4L (MIP-β)	9.7 ±3.0	Propiedades pro-inflamatorias y quimio-atrayentes.
	CCL5	4.7 ±1.4	Quimio-atrayente de monocitos, eosinófilos y linfocitos

	(RANTES)		T de memoria. Induce la secreción de histamina de los basófilos y eosinófilos activados.
	CXCL9	15.2 ±3.2	Quimiotaxis de células T activadas. Afecta al crecimiento, movimiento y activación de células que participan en la respuesta inmune e inflamatoria.
	CXCL11	10.9 ±2.2	Quimio-atrayente de células T activadas.
Moléculas de adhesión	VCAM1	2.2 ±0.6	Importante en el reconocimiento célula-célula. Implicada en la adhesión de los leucocitos al endotelio vascular.

[(a)] Comparando infección con rTGEV-Δ7 frente a rTGEV-*wt*, a 12 hpi, mediante RT-qPCR.

Células ST se infectaron con los rTGEV-*wt* y rTGEV-Δ7 a una moi de 5, y se extrajo el RNA total a 8, 10 y 12 hpi. Se analizó la cinética de expresión de los genes seleccionados mediante RT-qPCR utilizando ensayos *TaqMan* específicos para genes porcinos. Como controles se incluyeron los genes JAK2 y TGFβ, dado que su nivel de expresión no cambió diferencialmente entre las infecciones con los dos virus. Los resultados confirmaron que los genes analizados se inducían durante la infección, y que sus cinéticas de expresión eran las similares en la infección con los dos virus (Figura 40). Sin embargo, la infección con el rTGEV-Δ7 indujo niveles de expresión de los genes seleccionados significativamente mayores que la infección con el virus silvestre (Figura 40). La relación entre los niveles de expresión de estos genes y los niveles de las proteínas correspondientes se está analizando. Sin embargo, en casos como el del IFNβ, los datos obtenidos de los análisis de transcriptómica sugieren que se producía mayor nivel de proteína en la infección con el rTGEV-Δ7 comparado con la del rTGEV-*wt*, dado que todos los genes estimulados por IFN que se analizaron se encontraron sobre-expresados.

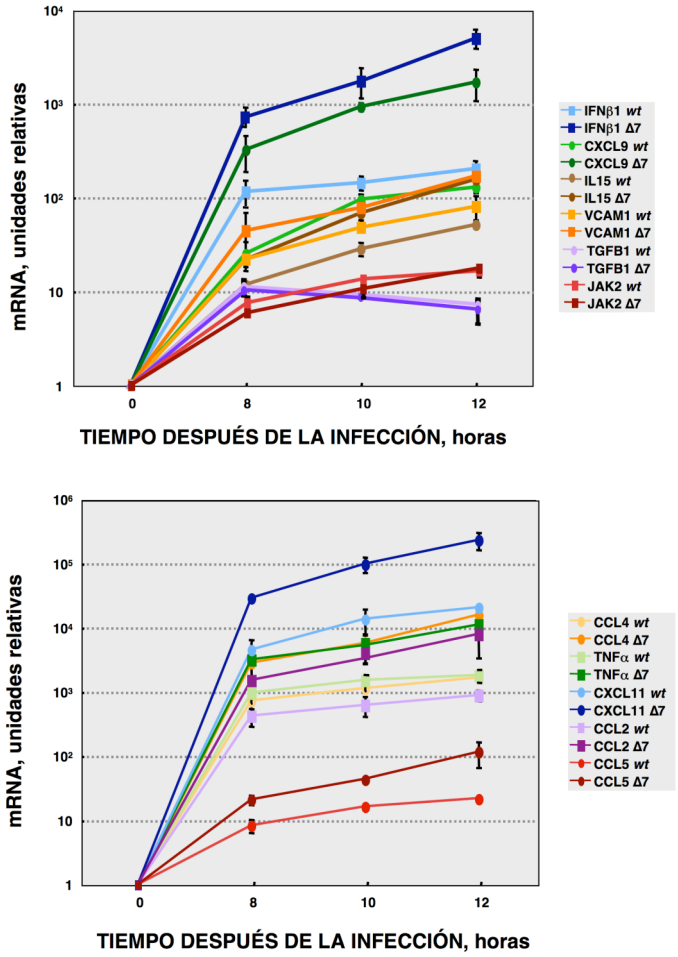

Figura 40. Expresión de genes celulares implicados en inflamación durante las infecciones con los rTGEV-Δ7 y rTGEV-*wt*. Cuantificación del mRNA de los genes seleccionados en la infección con el virus mutante respecto al virus silvestre a 8, 10 y 12 hpi mediante RT-qPCR. En todos los casos los niveles de expresión se han normalizado con la cantidad del mRNA del gen GUSB. Para cada gen se ha utilizado un código de color, utilizando tonos claros del mismo para representar los niveles de expresión del gen en la infección con el rTGEV-*wt* (*wt*), mientras que en líneas oscuras se representan los niveles de expresión en la infección con el rTGEV-Δ7 (Δ7). Las barras de error representan las desviaciones estándar de tres experimentos independientes.

8. FENOTIPO DEL rTGEV-Δ7 *IN VIVO*

8.1. Crecimiento del rTGEV-Δ7 en tejido

La infección de cultivos celulares con el rTGEV-Δ7 en comparación con la infección con el rTGEV-*wt*, mostró un aumento en la muerte celular y un incremento en la expresión de genes pro-inflamatorios. Estos resultados sugerían que la ausencia del gen 7 podría modular la virulencia de TGEV *in vivo*. Por ello, se infectaron lechones con los rTGEV-*wt* y rTGEV-Δ7. Ambos virus mostraron una cinética de crecimiento similar en

pulmón, aunque el virus sin la proteína 7 alcanzó títulos más altos que el virus parental a tiempos tempranos de la infección (Figura 41).

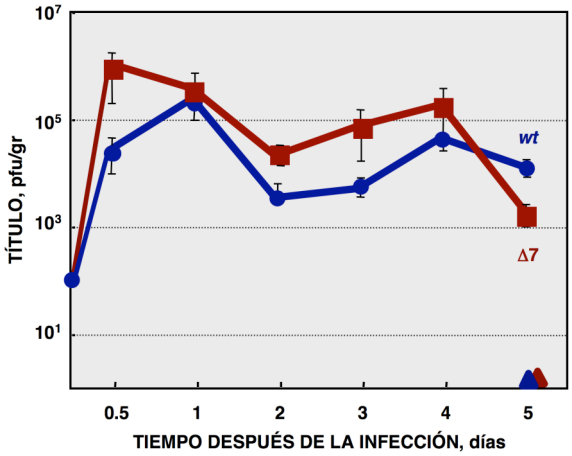

Figura 41. Cinética de crecimiento del rTGEV-Δ7 en pulmón. Lechones de dos a tres días de edad se inocularon con 1×10^7 pfu/animal de los rTGEV-*wt* y rTGEV-Δ7 por dos rutas (oral e intranasal). A los días 0.5, 1, 2, 3, 4 y 5 después de la inoculación se sacrificaron dos animales por grupo, y se extrajeron los pulmones. Los rTGEV-*wt* (*wt*, azul) y rTGEV-Δ7 (Δ7, rojo) recuperados del pulmón se titularon. Los triángulos representan el título de los virus en los animales centinelas. Las barras de error representan las desviaciones estándar de cuatro experimentos independientes.

Las cepas virulentas de TGEV replican en las células epiteliales de las vellosidades intestinales, además de en las células del pulmón, causando diarrea severa en animales recién nacidos (Enjuanes and Van der Zeijst, 1995; Saif and Wesley, 1992; Sanchez y col., 1999). El tropismo respiratorio y entérico de los rTGEVs puede modificarse mediante la introducción de cambios en el gen S (Enjuanes and Van der Zeijst, 1995; Saif and Wesley, 1992; Sanchez y col., 1999). El rTGEV-Δ7 utilizado en este trabajo se generó con tropismo exclusivamente respiratorio, dado que este recombinante era más estable en cultivos celulares. Para estudiar la relevancia de la proteína 7 en virulencia, se generó un recombinante con tropismo entérico y respiratorio, que carecía del gen 7 (rTGEV-SC11-Δ7) (Enjuanes and Van der Zeijst, 1995; Saif and Wesley, 1992; Sanchez y col., 1999). El crecimiento de los rTGEV-SC11-*wt* y rTGEV-SC11-Δ7 en pulmón fue muy similar al observado para los virus silvestre y mutante anteriormente utilizados. Sin embargo, el rTGEV-SC11-Δ7 mostró una cinética de crecimiento acelerada en intestino comparada con la del virus silvestre (Figura 42).

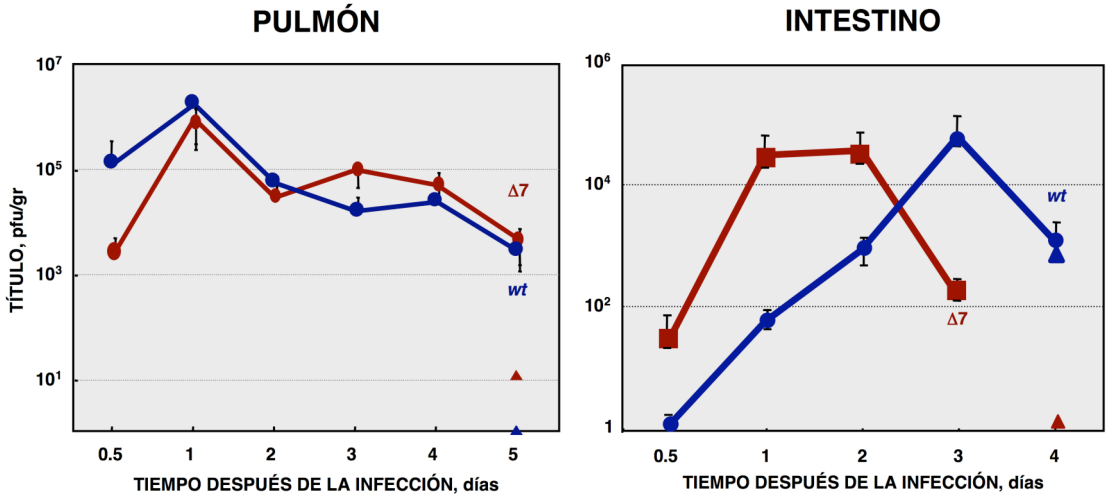

Figura 42. Cinética de crecimiento *in vivo* del rTGEV-SC11-Δ7. Lechones de dos a tres días de edad se inocularon con 1x10^7 pfu/animal de los vius rTGEV-SC11-*wt* (*wt*) y rTGEV-SC11-Δ7 (Δ7) por tres rutas (oral, intranasal e intragástrica). A los tiempos indicados se sacrificaron dos animales por grupo, y se recogieron los pulmones y el intestino. Se representa el título de los rTGEV-*wt* (azul) y rTGEV-Δ7 (rojo) en pulmón y en intestino. Los triángulos representan el título de los virus en los animales centinelas. Las barras de error representan las desviaciones estándar de tres experimentos independientes.

8.2. Patología causada por el rTGEV-Δ7

El título elevado de los virus en el intestino se asoció con una sintomatología más pronunciada (Figura 43A). El porcentaje de supervivencia de los animales infectados con ambos virus fue el mismo (50%). Sin embargo, los animales infectados con el rTGEV-SC11-Δ7 murieron 6 días antes que aquellos infectados con el rTGEV-SC11-*wt* (Figura 43B). Además, sólo se detectó virus en los animales centinelas que se encontraban junto con los cerdos infectados con el virus silvestre (Figura 42). Este resultado indicó que la presencia de la proteína 7 facilitó la supervivencia del animal y la diseminación del virus.

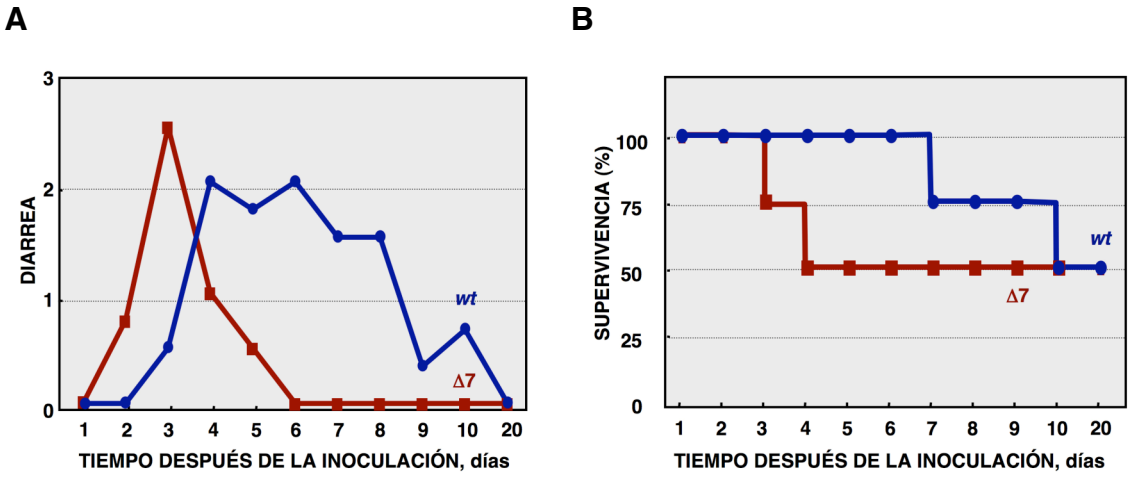

Figura 43. Virulencia del rTGEV-SC11-Δ7. Grupos de 6 lechones de dos a tres días de edad, se inocularon por tres rutas (oral, intranasal e intragástrica), con $1x10^7$ pfu/animal de los vius rTGEV-SC11-*wt* y rTGEV-SC11-Δ7. (A) Se analizaron los síntomas clínicos durante la realización del experimento. Se representa el grado de diarrea: desde 0, animales sanos, hasta 3, diarrea severa. (B) Número de animales supervivientes a los diferentes días después de la inoculación.

El efecto de la ausencia de la proteína 7, durante la infección de lechones por el TGEV se analizó estudiando la histopatología en pulmón. El rTGEV-*wt* causó un engrosamiento de la pared alveolar, enfisema y obstrucción de los conductos aéreos por restos de células apoptóticas y material hialino (Figura 44). La patología inducida por el rTGEV-Δ7 un día después de la infección fue comparable con la observada en los animales 4 días después de la infección con el rTGEV-*wt* (Figura 44). A tiempos más tardíos de infección, además de las lesiones descritas en los animales infectados con el rTGEV-*wt*, en los tejidos infectados con el rTGEV-Δ7 se encontraron edemas generados como consecuencia de una fuerte congestión alveolar (Figura 44).

La detección de antígenos virales por inmunohistoquímica mostró que ambos virus desarrollaban el mismo patrón de infección (Figura 44). El marcaje de la caspasa 3 procesada demostró que el patrón de apoptosis se solapaba con el de las zonas infectadas (Figura 44). En conjunto, estos datos indicaron un daño más extenso y rápido en el tejido de los animales infectados con el rTGEV-Δ7, comparado con el producido por el virus silvestre.

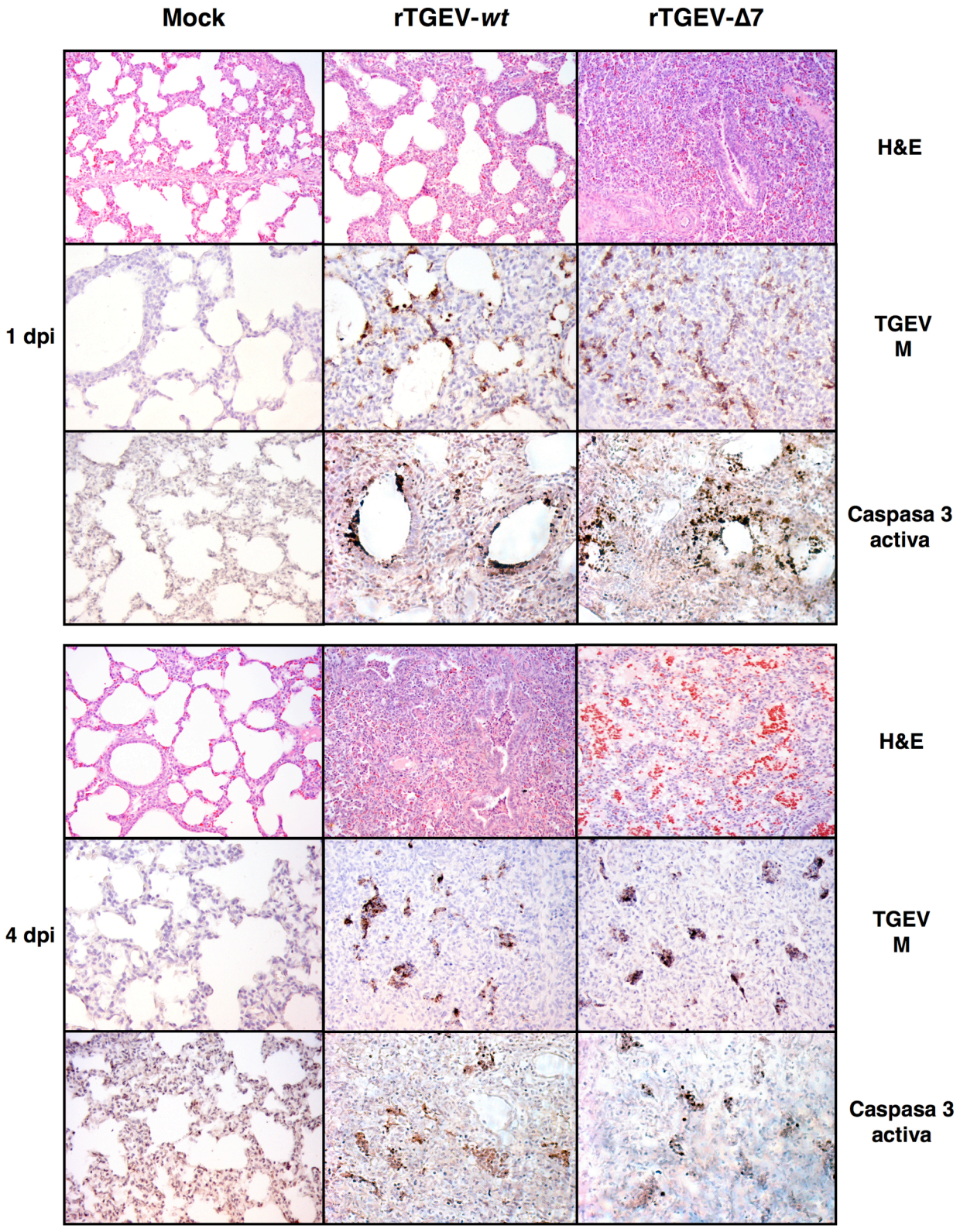

Figura 44. Histopatología de pulmón causada por la infección con el rTGEV-Δ7. Se inocularon, por dos rutas (oral e intranasal), lechones de dos a tres días de edad con 1×10^7 pfu/animal de los rTGEV-*wt* y rTGEV-Δ7. Las muestras de pulmón, recogidas a día 1 y 4 después de la infección, se tiñeron con hematoxilina-eosina (H&E). Se detectaron, con anticuerpos específicos, la proteína de membrana (M) de TGEV, como marcador de la infección, y la caspasa 3 activa, como marcador de apoptosis. Las fotografías se tomaron con un objetivo de 40x.

8.3. Análisis de leucocitos mediadores de inflamación en la infección con el rTGEV-Δ7

El daño en el tejido producido por toxinas o patógenos no sólo se debe a sus efectos directos, sino también a la acción de células del sistema inmune del huésped residentes o infiltradas en el tejido afectado, lo que se ha denominado "inmunopatología mediada por el hospedador" (Zampieri y col., 2007). Una de las principales características de este tipo de patología es la acumulación excesiva de leucocitos, especialmente macrófagos y granulocitos, que a su vez, amplifican el daño al producir citoquinas y otras moléculas pro-inflamatorias. A pesar de que el título en pulmón de los TGEV con y sin gen 7 fue similar, la infección con el rTGEV-Δ7 indujo un mayor daño en el tejido, y en cultivos celulares producía mayores niveles de citoquinas pro-inflamatorias que la infección con el virus parental. Por ello, la patología exacerbada producida por la infección con el virus sin la proteína 7 se podría deber a una sobre-activación de las células implicadas en el daño mediado por el hospedador.

La presencia de macrófagos y granulocitos se evaluó en los tejidos de lechones infectados con los rTGEV-*wt* y rTGEV-Δ7. En primer lugar se caracterizó el tipo celular que los anticuerpos monoclonales 4E9/11 (cedido por el Dr. Javier Domínguez, INIA) y Mac 387 (Termo Scientific, Dako) reconocían en pulmón de cerdo, mediante inmunofluorescencia y microscopía confocal. El anticuerpo 4E9/11 reconoce específicamente la proteína-1 asociada a la membrana de los lisosomas (LAMP-1), o CD170a, porcina. Este anticuerpo reconoce monocitos, macrófagos y granulocitos. Sin embargo, reconoce con mayor intensidad células con un proceso de fagocitosis muy activo, como macrófagos activados. El estudio, mediante microscopía confocal de los cortes de pulmón, reveló que el anticuerpo 4E9/11 marcaba vesículas en el interior de células con núcleos prominentes y no segmentados, que fueron caracterizadas como macrófagos (Figura 45A). El anticuerpo Mac 387 reconoce la proteína humana L1, o calprotectina, que se localiza en el citoplasma de ganulocitos, monocitos y macrófagos. La utilización de este anticuerpo en cortes de pulmón de animales infectados mostró un marcaje citoplasmático intenso de células redondeadas que presentaban un núcleo multilobulado, morfología típica de granulocitos (Figura 45B). En ningún caso se observó que el anticuerpo Mac 387 reconociese macrófagos. Este resultado está en la línea de lo observado por otros autores (Chianini y col., 2001), que describieron que el anticuerpo Mac 387 sólo reconoce granulocitos en el pulmón de cerdo, sugiriendo que

los macrófagos alveolares de cerdo no expresan la proteína L1 en cantidad suficiente como para ser detectada por el anticuerpos.

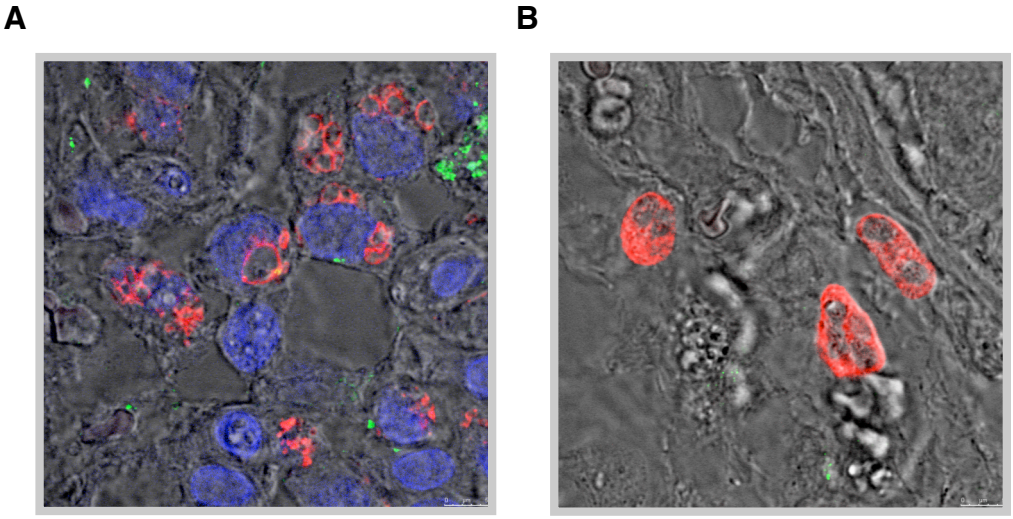

Figura 45. Detección de leucocitos en muestras de pulmón de animales infectados con el rTGEV-Δ7. (A) Las muestras de pulmón procedentes de animales infectados con el rTGEV-Δ7 recogidas a 4 dpi, se marcaron con el anticuerpo 4E9/11 (rojo), que detecta macrófagos, y con un anticuerpo policlonal específico para TGEV (verde). Los núcleos se marcaron con DAPI (azul). (B) Las muestras de pulmón procedentes de animales infectados con el rTGEV-Δ7 recogidas a 4 dpi, se marcaron con el anticuerpo Mac387 (rojo), que detecta granulocitos, y con un anticuerpo policlonal específico para TGEV (verde). La topología del tejido se muestra con escala de grises, mediante la aplicación de un filtro de campo claro. En todos los casos las fotografías se tomaron con microscopía confocal, usando un objetivo de 63x con un aumento electrónico de 5x.

La presencia de granulocitos se analizó en muestras de pulmón de animales sin infectar e infectados con los rTGEV-*wt* o rTGEV-Δ7 respectivamente, a 1 y 4 dpi. Se observó que a tiempos tempranos (1 dpi) los niveles de granulocitos en la infección con el rTGEV-Δ7 fueron superiores que los observados en la infección con el rTGEV-*wt*, correlacionando una mayor patología con un nivel alto de granulocitos infiltrados (Figura 46). Sin embargo, a tiempos tardíos, de 4 dpi, los niveles de granulocitos en ambas infecciones decrecieron a pesar de que se seguían observando lesiones en los pulmones de los animales infectados con ambos virus (Figura 46).

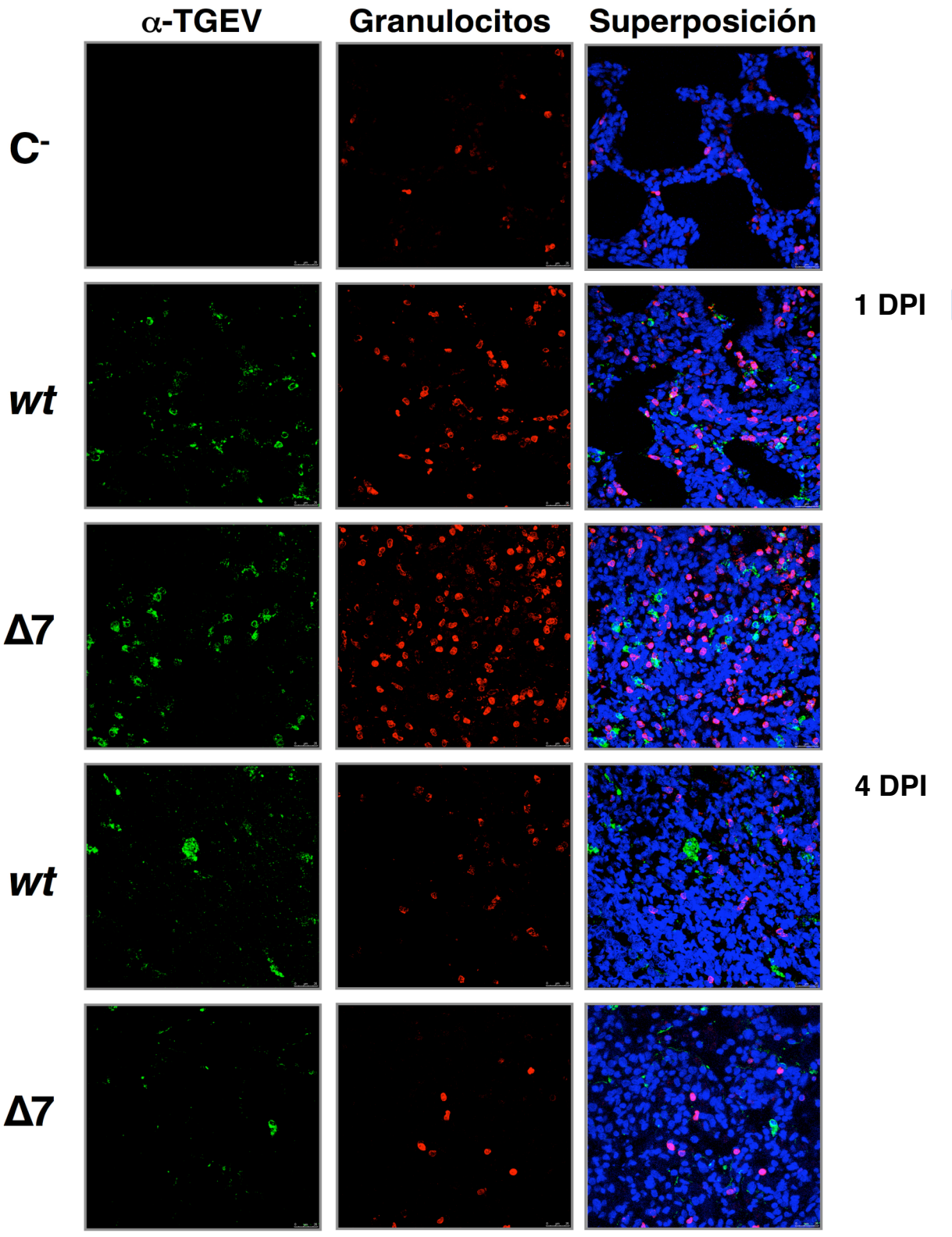

Figura 46. Detección de granulocitos en muestras de pulmón de animales infectados con el rTGEV-Δ7. Las muestras de pulmón procedentes de animales no infectados (C^-) e infectados con el rTGEV-*wt* (*wt*) o con el rTGEV-Δ7 (Δ7) a 1 y 4 dpi, se marcaron con el anticuerpo Mac 387 (rojo), que detecta granulocitos y con el anticuerpo policlonal α-TGEV (verde). Los núcleos se marcaron con DAPI (azul). En todos los casos las fotografías se tomaron con un objetivo de 63x.

La presencia de macrófagos se analizó en muestras de pulmón de animales sin infectar e infectados con los rTGEV-*wt* o rTGEV-Δ7 respectivamente, a 1 y 4 dpi (Figura 47). En los animales sin infectar se observó una marca basal que probablemente correspondía con la población de macrófagos residentes en el tejido (Figura 47). En los tejidos infectados con el rTGEV-*wt* a 1 dpi, los macrófagos se distribuían por el tejido sin un patrón definido (Figura 47). Resultados similares se obtuvieron en los tejidos infectados por el rTGEV-Δ7 a 1 dpi, a pesar de que los espacios alveolares ya se encontraban colapsados y el tejido se encontraba muy dañado (Figura 47). A 4 dpi se observó un reclutamiento de los macrófagos en las zonas donde se localizaba la infección tanto po el virus silvestre como por el virus parental (Figura 47).

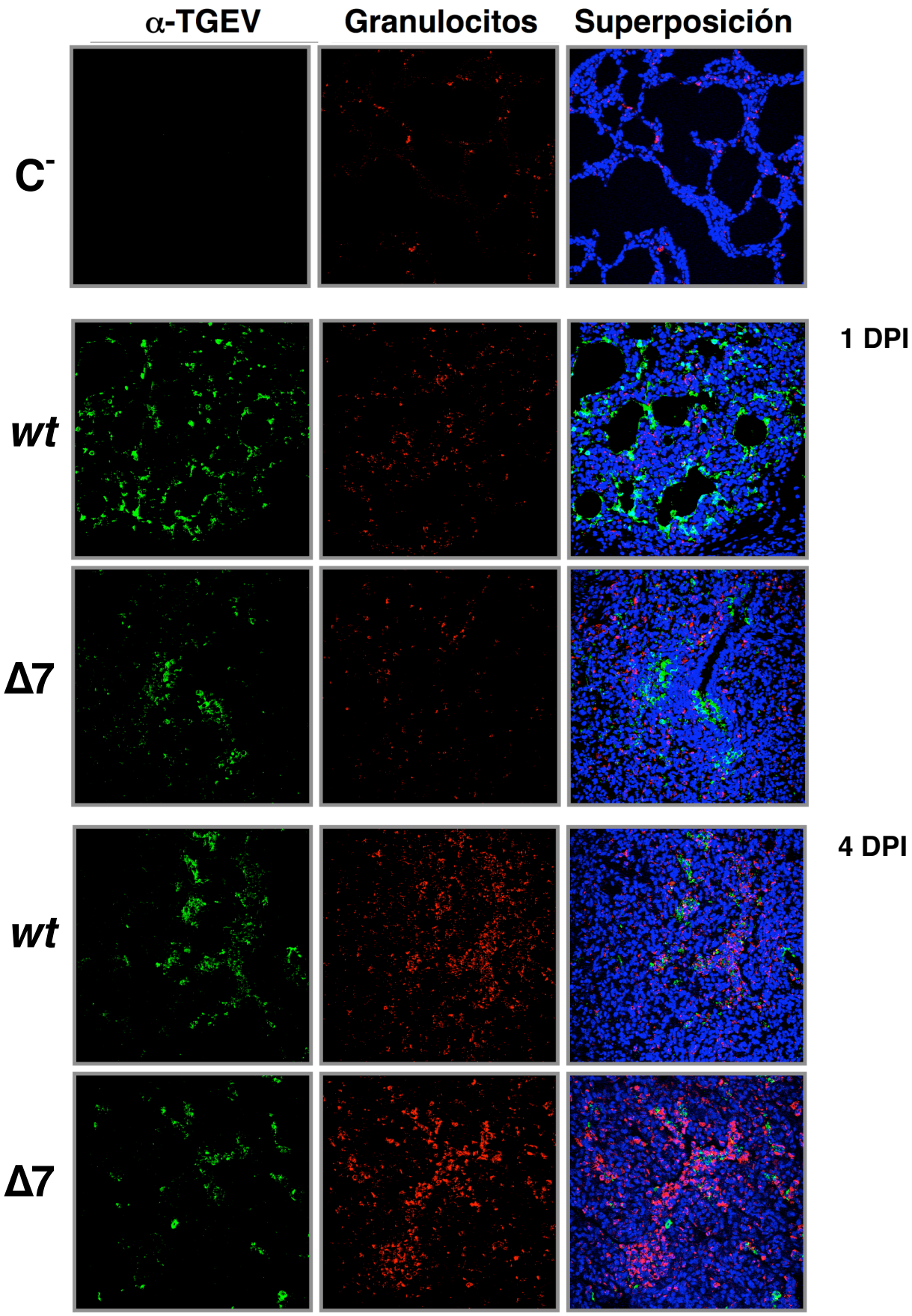

Figura 47. Detección de macrófagos en muestras de pulmón de animales infectados con el rTGEV-Δ7. Las

muestras de pulmón procedentes de animales no infectados (C^-), o infectados con el rTGEV-*wt* (*wt*) o, alternativamente, con el rTGEV-Δ7 (Δ7) a 1 y 4 dpi, se marcaron con el anticuerpo 4E9/11 (rojo), que detecta macrófagos y con el anticuerpo policlonal α-TGEV (verde). Los núcleos se marcaron con DAPI (azul). En todos los casos las fotografías se tomaron con un objetivo de 40x.

La presencia de macrófagos en los tejidos infectados por el rTGEV-Δ7 era más intensa a 4 dpi que en los tejidos infectados con el rTGEV-*wt*. Un análisis detallado de la distribución de la señal del anticuerpo 4E9/11 mostró que las vesículas lisosomales inducidas en los macrófagos por la infección con el virus silvestre eran significativamente menores en tamaño que las inducidas por la infección con el virus sin la proteína 7, lo que sugirió una mayor activación de los macrófagos en los animales infectados con el rTGEV-Δ7 (Figura 48).

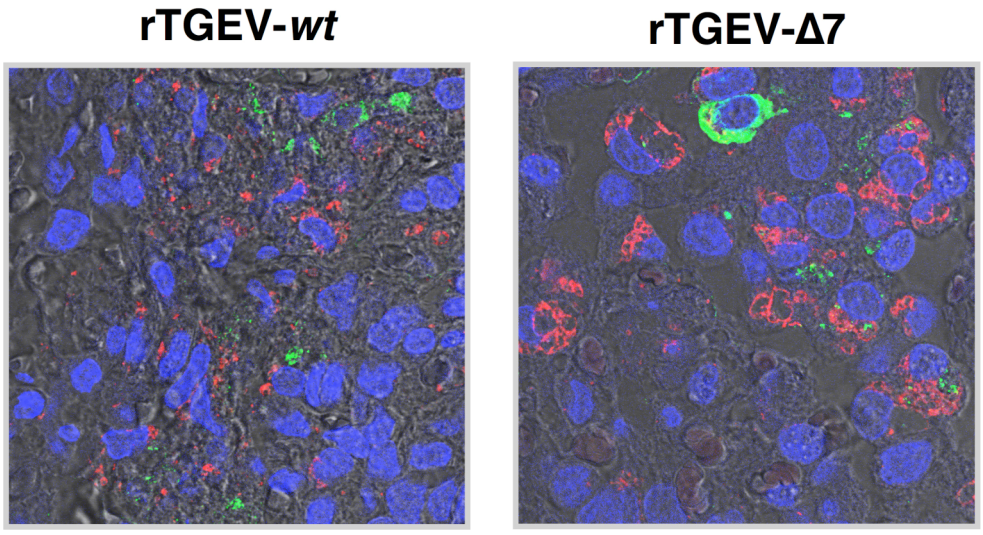

Figura 48. Detalle de células fagocíticas en muestras de pulmón de animales infectados. Las muestras de pulmón procedentes de animales infectados con el rTGEV-*wt* o con el rTGEV-Δ7 a 4 dpi, se marcaron con el anticuerpo 4E9/11 (rojo), que detecta lisosomas y con el anticuerpo policlonal específico de TGEV (verde). Los núcleos se marcaron con DAPI (azul). La topología del tejido se muestra en escala de grises, mediante la aplicación de un filtro de campo claro. En todos los casos las fotografías se tomaron con un objetivo de 63x con un aumento electrónico de 3x.

Para analizar la reducción del tamaño de las vesículas lisosomales y el nivel de reclutamiento de macrófagos en las zonas infectadas, se midió el nivel de señal positiva de los macrófagos (rojo) y se hizo relativa a la señal de la infección (verde), a 1 y 4 dpi. Se observó que no existían diferencias entre ambos virus a 1 dpi (Figura 49). Sin embargo, el rTGEV-Δ7 indujo un mayor reclutamiento y/o activación de macrófagos que el rTGEV-*wt* a 4 dpi (Figura 49), lo que sugiere que la presencia de la proteína 7 en

la infección de TGEV reduce la infiltración de células del sistema inmune.

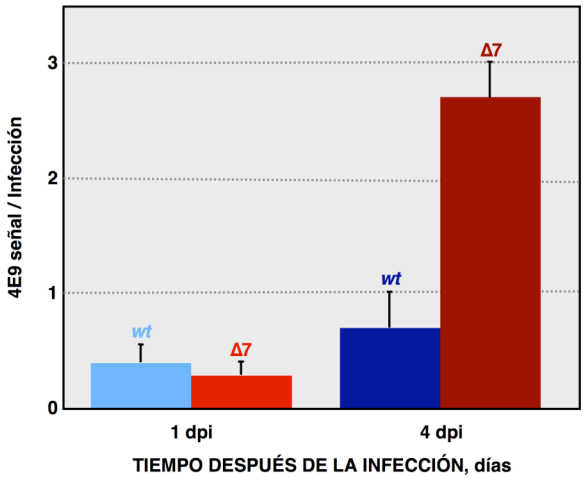

Figura 49. Cuantificación de la señal de lisosomas en muestras de pulmón de animales infectados. Las muestras de pulmón procedentes de animales infectados con el rTGEV-*wt* (*wt*) o con el rTGEV-Δ7 (Δ7) a 1 y 4 dpi, se marcaron con el anticuerpo 4E9/11, que detecta lisosomas y con el anticuerpo policlonal α-TGEV. Se representa la cuantificación del área de señal positiva para el anticuerpo 4E9/11 con el programa *MetaMorph* relativa al área de señal positiva para el anticuerpo α-TGEV de la misma zona, a 1 y 4 dpi. Las barras de error representan las desviaciones estándar de 20 campos observados en 10 muestras independientes.

VII. DISCUSIÓN

En esta tesis se describe la generación y caracterización *in vitro* e *in vivo* de un TGEV mutante que no expresa la proteína 7 para estudiar el papel de esta proteína en la virulencia de CoV. Se ha observado que la proteína 7 de TGEV modificó la respuesta antiviral del huésped activada por dsRNA, mediante un nuevo mecanismo en virus con genoma RNA, que incluye la interacción de la proteína 7 del virus con la fosfatasa celular PP1. Los resultados obtenidos indicaron que el gen 7 actúa como antagonista del IFN, modulando la respuesta inmune innata inducida en la infección por TGEV. Además, se demostró que la presencia del gen 7 modulaba la virulencia de TGEV, reduciendo la patología causada por la infección e incrementando el período de diseminación viral, lo que muy probablemente proporciona una ventaja selectiva para el virus que ha integrado el gen 7.

1. EFECTO DEL GEN 7 EN LA REPLICACIÓN VIRAL

Para generar un TGEV mutante que no expresaba el gen 7 se introdujeron, en el genoma del rTGEV-*wt,* varias modificaciones para silenciar la expresión del gen 7 que no alteraron la estructura de los genes flanqueantes. La caracterización de los virus con y sin proteína 7, tanto en cultivos celulares como *in vivo*, mostró que ambos virus tenían cinéticas de crecimiento y títulos muy similares, aunque el rTGEV-Δ7 era más virulento que el virus silvestre. Sin embargo, la generación de un virus sin gen 7, en el que además se había modificdo varias secuencias delante de cada gen, generó un virus atenuado (Ortego y col., 2003). El virus atenuado incluía una serie de mutaciones adicionales a lo largo del genoma: (i) cinco sitios de restricción insertados al inicio de los genes S, 3a, E, M, N; (ii) la duplicación de las secuencias que preceden a los genes E, M, N y 7, que se requirió para la eliminación del solapamiento de los genes virales. Es más, estas duplicaciones, localizadas muy próximas a las TRS de los genes, contenían TRS adicionales para regular los niveles de expresión de cada gen y probablemente influyeron en los niveles de expresión de estos genes; y (iii) una eliminación de 21 nt, que contenía el codón de inicio de la traducción de la ORF7 y los primeros 17 nt de dicha ORF, que se introdujo para prevenir la expresión del gen 7, lo que sugiere fuertemente que el virus generado por Ortego y cols., estaba atenuado por la innumerables modificaciones del genoma de TGEV, distintas a la eliminación de la expresión del gen 7. Por el contrario, el virus mutante TGEV utilizado en este trabajo sólo incluyó una mutación puntual en la CS del gen 7 y la eliminación de 7 nt,

modificaciones que fueron estables y evitaron la expresión de la proteína 7 con cambios mínimos que no conllevaron la eliminación física del gen 7.

2. EFECTO DE LA PROTEÍNA 7 EN LA RESPUESTA ANTIVIRAL ACTIVADA POR dsRNA

La infección con TGEV activó una ruta antiviral desencadenada por la producción de dsRNA durante los procesos de replicación y transcripción del virus (Figura 50). Esta ruta tiene dos efectores principales: la proteína 2'-5'OAS, responsable de la activación de la RNasa L y la degradación del RNA celular, y la enzima PKR que es responsable de la fosforilación del factor eIF2α (Gantier and Williams, 2007). La activación de esta ruta normalmente desencadena el bloqueo de la maquinaria de traducción de la célula, y la inducción de la apoptosis dependiente de caspasas tanto en las células infectadas como en las células vecinas (Figura 50) (Bisbal and Silverman, 2007; Dauber and Wolff, 2009). En este trabajo se demostró que la proteína 7 de TGEV se unía a la fosfatasa PP1, un regulador clave de la respuesta antiviral, y modulaba la ruta activada por el dsRNA (Figura 50).

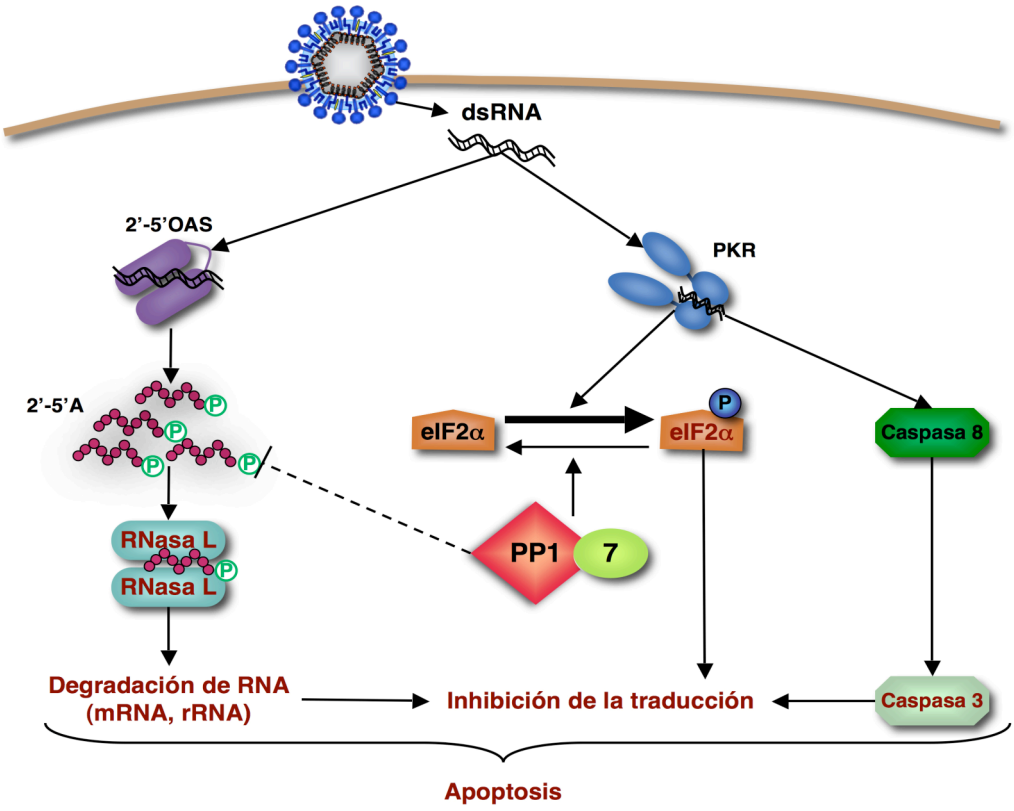

Figura 50. Respuesta antiviral inducida por la dsRNA. Esquema de la respuesta antiviral inducida por dsRNA. Se

representan en letras rojas aquellos puntos modificados durante la infección con el rTGEV-Δ7. En el esquema se incluye la unión de la proteína 7 a la fosfatasa PP1, y sus efectos en las rutas activadas por dsRNA.

En las células infectadas con el rTGEV-Δ7 se observó un incremento en los niveles de fosforilación del factor eIF2α respecto a los niveles detectados en la infección con el rTGEV-*wt*. En esta tesis se postula que los menores niveles de fosforilación del factor eIF2α en la infección con el virus parental se deben a la interacción entre la proteína 7 y el complejo de la proteína PP1c que contrarresta la actividad de la PKR, y no debido a un aumento diferencial de la actividad de PKR en células infectadas con el TGEV con o sin la proteína 7 (Figura 50). Este mecanismo de modulación de la respuesta antiviral no se ha descrito anteriormente en infecciones por virus con genoma de RNA, aunque previamente se han descrito tres proteínas de virus DNA que contienen el dominio de unión a la proteína PP1c. Estas proteínas están codificadas por el virus herpes simple-1 (proteína $\gamma_1$34.5), el papilomavirus humano (proteína E6) y el virus de la peste porcina Africana (proteína DP71L) (He y col., 1997; Kazemi y col., 2004; Rivera y col., 2007). Estas proteínas neutralizan el efecto negativo de la fosforilación del factor eIF2α sobre la síntesis de proteínas, mediante su interacción con la fosfatasa PP1, promoviendo la defosforilación de este factor de traducción (He y col., 1997; Kazemi y col., 2004; Rivera y col., 2007). La confirmación de que la proteína 7 de TGEV afectaba a la traducción, mediante la defosforilación del factor eIF2α, se basó en la observación de que la proteína 7 nativa de TGEV suministrada en *trans* indujo la defosforilación del factor eIF2α. Sin embargo, una proteína 7-mut, que no se unió a la proteína PP1c, no redujo los niveles de fosforilación del factor eIF2α durante la infección con el TGEV-Δ7.

La evaluación de la integridad del RNA en las células infectadas con el rTGEV-Δ7 reveló un incremento en la degradación del RNA celular en comparación con las células infectadas con el rTGEV-*wt*. El patrón de degradación del RNA fue idéntico al observado después de la activación específica de la RNasa L, sugiriendo que esta nucleasa era la responsable de la degradación del RNA durante la infección con el TGEV. La expresión de la enzima 2'-5'OAS1, necesaria para la activación de la RNasa L, aumentó de forma similar en las infecciones con los virus mutante y silvestre. Estos resultados sugirieron que la proteína 7 modulaba la ruta de la 2'-5'OAS en una etapa anterior a la activación de la RNasa L. La activación de la 2'-5'OAS por el dsRNA lleva a la síntesis de los 2'-5'A necesarios para la dimerización y activación de la RNasa L.

Los 2'-5'A son altamente inestables debido a que fácilmente pierden el fosfato del extremo 5' por la acción de múltiples fosfatasas, y estos oligoadenilatos defosforilados no activan eficientemente a la RNasa L (Silverman, 1985). Basándose en los resultados mostrados en esta memoria, se propone que el complejo fosfatasa PP1-proteína 7 podría contrarrestar la activación de la RNasa L mediante la defosforilación de los 2'-5'A (Figura 50). De hecho, la proteína 7 nativa suministrada en *trans* redujo la degradación del RNA, mientras que la proteína 7-mut, que no unía a la proteína PP1c, mantuvo los niveles de degradación del RNA en la infección con el rTGEV-Δ7. Aunque se requieren experimentos adicionales para demostrar el efecto directo del complejo fosfatasa PP1-proteína 7 en la inhibición de la activación de la RNasa L, esta es la primera vez que se relaciona a la fosfatasa PP1 con la ruta antiviral de la 2'-5'OAS/RNasa L.

Sorprendentemente, los mRNAs virales no se degradaron diferencialmente después de la infección con los rTGEV-*wt* o rTGEV-Δ7, lo que sugirió que no eran susceptibles a la acción de las nucleasas. Inicialmente, la protección de estos mRNAs podría estar mediada por su localización en el interior de vesículas de doble membrana (DMVs), inducidas por la infección de CoV, y que se han identificado en células infectadas con MHV (Gosert y col., 2002), SARS-CoV (Snijder y col., 2006), y TGEV (A. Nogales, L. Enjuanes and F. Almazán, manuscrito en preparación). Las DMVs podrían proveer un ambiente óptimo para la síntesis de RNAs virales, y prevenir la acción de componentes de la maquinaria de defensa del huésped, como por ejemplo las nucleasas antivirales.

2.1. Consecuencias de la sobre-activación de las vías de PKR y 2'-5'OAS/RNasa L durante la infección con el rTGEV-Δ7

El rTGEV-Δ7 mostró un efecto citopático aumentado, en relación con el causado por el virus parental, como consecuencia de un proceso de apoptosis acelerado. En línea con estos resultados, se ha descrito que una activación de las rutas de la PKR y del sistema 2'-5'OAS/RNasa L desencadena la apoptosis (Der y col., 1997; Zhou y col., 1997). La cinética de crecimiento de los rTGEV-*wt* y rTGEV-Δ7 fue muy similar, indicando que el incremento en la respuesta antiviral y la apoptosis no comprometió la producción viral. De forma similar, en otros CoVs como el SARS-CoV o el MHV, la inhibición de la expresión de la PKR o la RNasa L, respectivamente, no produjo ningún efecto en el título viral (Ireland y col., 2009; Krahling y col., 2009). Se ha descrito previamente que la inhibición de la apoptosis inducida por la infección del TGEV no genera un aumento en la producción viral (Eleouet y col., 1998). Además, los niveles de acumulación de

proteínas virales fueron similares para los rTGEV-*wt* y rTGEV-Δ7 (datos no mostrados). Esta información, junto con el hecho de que el virus mutante y el silvestre alcanzaron los mismos títulos, sugirió que los niveles de síntesis de proteínas virales durante la infección con el rTGEV-Δ7 eran suficientes para mantener el mismo nivel de progenie viral que produce el virus silvestre.

En conjunto estos resultados sugieren que, al menos para algunos CoVs, la repuesta activada por dsRNA no afecta a la replicación viral. Sin embargo, todos estos CoVs han desarrollado diversas estrategias que contrarrestan la repuesta antiviral activada por dsRNA (Kopecky-Bromberg y col., 2007; Wathelet y col., 2007; Ye y col., 2007). Estas estrategias podrían controlar el efecto deletéreo que una respuesta antiviral exacerbada puede tener en el huésped y, por tanto, en la supervivencia del virus (Garcia-Sastre and Biron, 2006). De hecho, la modulación de las rutas de PKR y 2'-5'OAS/RNasa L suele tener un efecto en la patología producida por CoVs (Ireland y col., 2009; Wang y col., 2009). Los resultados mostrados en esta memoria están en línea con estas observaciones, como se comenta más adelante.

3. PAPEL DE LA PROTEÍNA 7 COMO ANTAGONISTA DE IFN

La principal citoquina diferencialmente sobre-expresada en la infección con el virus sin la proteína 7 respecto a la del virus silvestre fue el IFNβ, un factor clave en el desarrollo de la respuesta antiviral (Biron C, Sen GC, 2001). Los altos niveles de IFNβ junto con la sobre-expresión del factor TNF probablemente contribuyeron a los altos niveles de apoptosis inducidos tanto en células infectadas como no infectadas con el rTGEV-Δ7 debido a la actividad paracrina de ambas citoquinas. En general, las infecciones virales desencadenan la entrada de las células infectadas, y las células de su entorno, en un estado antiviral (Sirinarumitr y col., 1998). Los resultados obtenidos en este trabajo sugirieron que el balance entre el aumento en la apoptosis y en la respuesta antiviral en las células infectadas y las de su entorno, limitó la diseminación del rTGEV-Δ7, dando lugar a títulos de los virus mutante y silvestre similares.

La producción de IFNβ en las células infectadas está estrechamente relacionada con la respuesta antiviral activada por dsRNA (Figura 51). El dsRNA producido durante una infección viral puede ser reconocido por el receptor TLR-3, en las membranas de los endosomas, y los sensores citoplasmáticos RIG-I y MDA5, lo que lleva a la activación de los factores de transcripción IRF3, IRF7, NF-κB y, por tanto, a la producción de IFN

(Figura 51) (Bonjardim y col., 2009; Takeuchi and Akira, 2008). Además, la activación de PKR y de la ruta de la 2'-5'OAS/RNasa L lleva a la producción de IFN, utilizando como efectores a NF-κB y a los sensores citoplasmáticos, respectivamente (Figura 51) (Gil y col., 1999; Malathi y col., 2007).

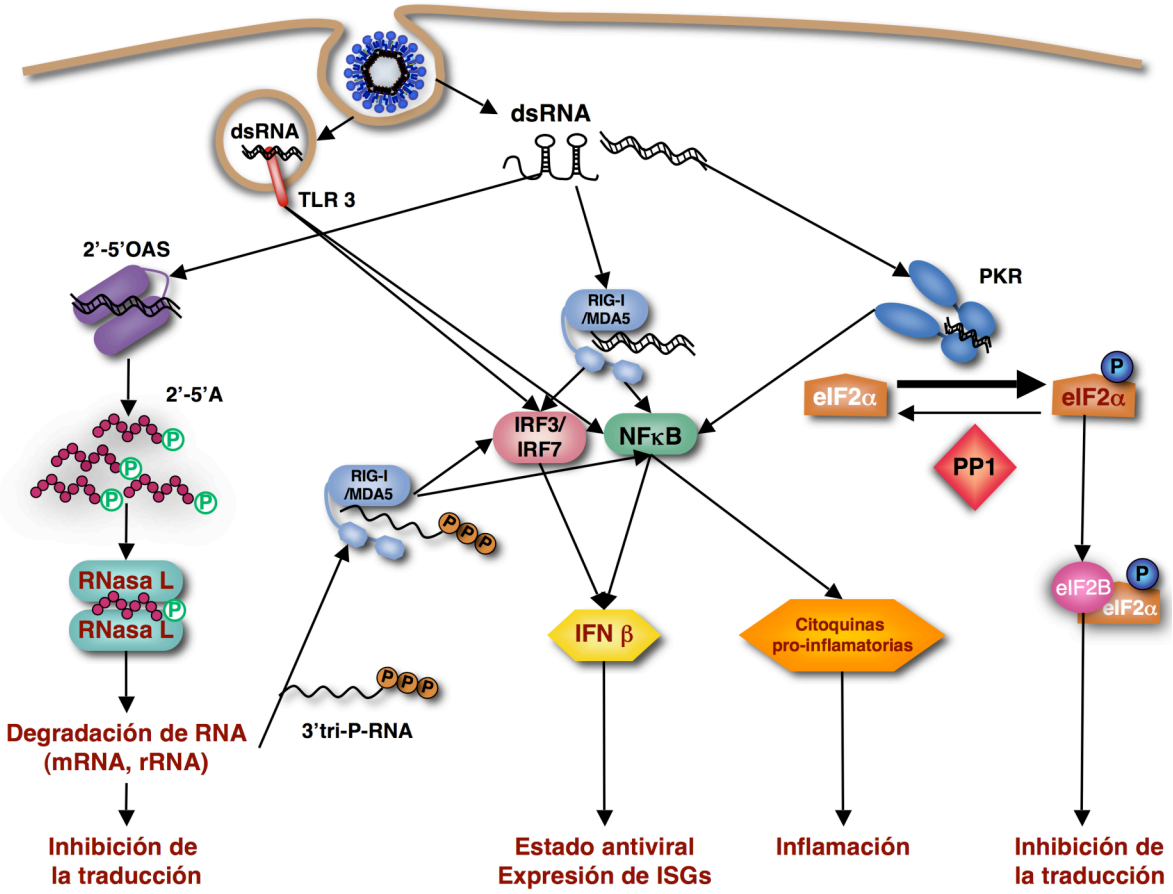

Figura 51. Respuesta antiviral activada por dsRNA e inducción de IFN. Esquema de la respuesta antiviral inducida por dsRNA y la producción de IFN. En texto rojo se muestran los efectos diferenciales en la infección con el rTGEV-Δ7.

La mayor producción de IFNβ por las células infectadas con el rTGEV-Δ7, comparada con la infección con el rTGEV-*wt*, probablemente no se debió a una mayor activación de la PKR, como ya se ha descrito en los resultados, ni a un mayor reconocimiento de RNAs virales por los sensores TLR-3, RIG-I y MDA5, dado que la síntesis de RNAs virales fue similar en ambas infecciones. Por tanto, la mayor activación de la ruta 2'-5'OAS/RNasa L podría ser la causa del aumento en la producción de IFN durante la infección con el rTGEV-Δ7. Recientemente se ha descrito que los productos de degradación generados por la RNasa L son reconocidos por RIG-I

y MDA5, lo que lleva a un aumento en la producción de IFN (Malathi y col., 2007). Además, se ha demostrado que células y ratones deficientes en RNasa L inducen menos IFNβ después del tratamiento con Poly(I:C), o después de las infecciones con los virus Sendai o el virus de la encefalomiocarditis (EMCV), respectivamente (Malathi y col., 2007). En la infección con el rTGEV-Δ7 se produce un gran número de RNAs degradados, probablemente por acción de la RNasa L, que serían reconocidos por RIG-I y MDA5 provocando un aumento en la producción de IFNβ.

Es destacable que varias proteínas de CoV descritas como antagonistas de IFN, tales como la proteína N, o la proteína accesoria 2 de MHV, actúan sobre la ruta de la 2'-5'OAS/RNasa L (Ye y col., 2007);Zhao L. y col., 2011, *The XIIth International Nidovirus Symposium*). Esto sugiere que la activación de esta ruta juega un papel importante en la producción de IFNβ durante la infección de CoV y en el mantenimiento del estado antiviral.

4. EFECTO DE LA PROTEÍNA 7 EN LA PATOLOGÍA CAUSADA POR EL rTGEV

En esta memoria se ha demostrado que el rTGEV-Δ7 era más virulento que el rTGEV-*wt*, probablemente por la inducción de un proceso inflamatorio exacerbado que provocó edema, rotura de vasos sanguíneos y congestión pulmonar en los animales infectados. El mayor daño en el tejido infectado con el rTGEV-Δ7 no estaba relacionado con un título viral mayor que el del rTGEV-*wt*, sino con una respuesta antiviral del huésped exacerbada, de modo similar a lo descrito para virus como el de la gripe o de la hepatitis C (Bantel and Schulze-Osthoff, 2003).

La infección con el rTGEV-Δ7 indujo la sobre-expresión de citoquinas como el TNF, principal mediador de inflamación, y CCL2, CCL4 y CCL5, cuya principal función es el reclutamiento y activación de macrófagos. Además, el rTGEV-Δ7 indujo la sobre-expresión del receptor CD40, que es indispensable para la activación de macrófagos (Hashimoto y col., 2004). De acuerdo con estos resultados, se observó un mayor reclutamiento y activación de macrófagos en los pulmones de los animales infectados con el rTGEV-Δ7. Estos datos sugirieron que los macrófagos estaban implicados en el incremento de la inflamación producida en ausencia de la proteína 7 durante la infección del TGEV. En línea con estas observaciones, la infección de animales que no expresan el receptor de CCL5 con el MHV produce una disminución en la patología causada por el virus, debido a un menor reclutamiento de macrófagos (Glass y col.,

2001). En conjunto, el aumento del daño en el tejido infectado con el rTGEV-Δ7 estaría causado, en parte, por el reclutamiento masivo de macrófagos hiper-activados mediado por la sobre-expresión de citoquinas pro-inflamatorias como IFNβ, TNF, CCL2, CCL4 y CCL5, o receptores como CD40. Es más, la recuperación del daño pulmonar fue más lenta en los animales infectados con el rTGEV-Δ7 que en los infectados con el rTGEV-*wt*, dado que los animales infectados con el virus sin la proteína 7 mostraron un mayor número de lesiones a 4 dpi que los infectados con el virus silvestre (datos no mostrados).

En varias infecciones virales se ha descrito que una producción exacerbada de citoquinas pro-inflamatorias y un reclutamiento excesivo de células del sistema inmune lleva a la destrucción del tejido y contribuye a la patología causada por la infección (Huang y col., 2005; Theron y col., 2005; Walsh y col., 2011). Esta inmunopatología se denomina "tormenta de citoquinas" o hipercitoquinemia (Ferrara y col., 1993) y se cree que podría ser la causa de la extremada virulencia de virus como la cepa pandémica de gripe A/H5N1 o el SARS-CoV (Theron y col., 2005; Walsh y col., 2011). Se ha observado que la infección con el virus de la gripe A/H5N1 desencadena la sobre-producción de TNF, IFNα/β, CCL2, CCL4 y CCL5, lo que podría ser responsable de la inusual severidad de la sintomatología clínica causada por esta cepa viral (Cheung y col., 2002). Además se ha descrito que el daño de pulmón en los pacientes infectados con el virus SARS-CoV persiste después de la reducción del título viral, lo que sugiere que el mayor componente en la patología es de origen inmunológico (Peiris y col., 2003; Theron y col., 2005).

Estas observaciones junto con los resultados obtenidos en este trabajo, sugerían que la respuesta antiviral exacerbada desencadenada por la infección con el rTGEV-Δ7, podría ser la causa de una inmunopatología responsable del aumento en la gravedad de las lesiones en el tejido, tal y como se observó en los animales infectados con el rTGEV-Δ7. Además, los lechones infectados con los TGEV entéricos virulentos que no expresaban la proteína 7, desarrollaron antes síntomas clínicos más agudos que los infectados con el virus parental. Esta elevada virulencia resultó en una muerte más rápida del huésped, que también afectó a la supervivencia a largo plazo del propio virus, dado que éste precisa del hospedador para su propagación. Desde un punto de vista evolutivo, los resultados presentados en este trabajo sugieren que los CoVs de la especie *Alfacoronavirus 1* pueden haber adquirido el gen 7 para contrarrestar las defensas del huésped con el objetivo de prevenir lesiones agudas en el tejido debidas a una respuesta

inmune innata exacerbada. Por tanto, la proteína 7 podría beneficiar tanto al hospedador, reduciendo la patología causada por la infección, como al virus, ampliando el período de replicación y diseminación viral.

VIII. CONCLUSIONES

1. La proteína 7 no es esencial en la replicación del TGEV tanto *in vitro* como *in vivo*.
2. La ausencia de la proteína 7 durante la infección con TGEV aumenta el efecto citopático del virus debido a un incremento de la muerte celular por apoptosis, mediada por la activación de caspasas.
3. La infección con el virus defectivo rTGEV-Δ7 causa la inhibición de la traducción de las proteínas celulares y virales. Esta inhibición se debió a un aumento de la fosforilación del factor eIF2α y de la degradación de RNAs celulares por la RNasa L en comparación con las producidas por el rTGEV-*wt*.
4. La expresión de la proteína 7 en *trans* durante la infección del rTGEV-Δ7, disminuye la apoptosis, los niveles de fosforilación del factor eIF2α, y la degradación del RNA celular a niveles similares a los observados en la infección con el rTGEV-*wt*. Por lo tanto, el fenotipo del rTGEV-Δ7 se debe exclusivamente a la ausencia de la expresión de la proteína 7.
5. Los niveles aumentados de fosforilación del factor eIF2α en la infección con el rTGEV-Δ7 no se deben a un incremento de la actividad de las quinasas PKR y PERK o a una disminución en la acumulación de la fosfatasa PP1, en comparación con la infección con el virus parental.
6. Se identificó la secuencia canónica de unión a la fosfatasa PP1 en las proteínas 7a de la especie *Alfacoronavirus 1*. La proteína 7 de TGEV, expresada o producida por el virus durante la infección, se une a la fosfatasa PP1. Esta interacción es necesaria para la función de la proteína 7 durante el ciclo viral. La presencia del factor eIF2α en el complejo proteína 7-PP1 sugiere que una de las funciones de la proteína 7 es la modulación de la fosforilación de la proteína 7.
7. La comparación de la expresión génica de células no infectadas respecto a células infectadas con el rTGEV-Δ7 o con el rTGEV-*wt* muestra que, en general, los genes activados o reprimidos son los mismos en ambas infecciones. Sin embargo, en la infección con el virus mutante estos genes se sobre-activan o inhiben a mayores niveles o a tiempos más tempranos de la infección. Los genes diferencialmente expresados en la infección del rTGEV-Δ7 respecto a la del rTGEV-*wt* se relacionan con el control de la infección y de la inflamación.
8. Los experimento *in vivo* con lechones muestran que el rTGEV-Δ7 es más virulento que el virus parental. El análisis de cortes histológicos de pulmón muestra que hay un mayor reclutamiento de células del sistema inmune implicadas en procesos

inflamatorios en los animales infectados con el virus mutante que con el virus silvestre

IX. BIBLIOGRAFÍA

Aggen, J.B., Nairn, A.C., Chamberlin, R., 2000. Regulation of protein phosphatase-1. Chem. Biol. 7, R13-23.

Ajuh, P.M., Browne, G.J., Hawkes, N.A., Cohen, P.T., Roberts, S.G., Lamond, A.I., 2000. Association of a protein phosphatase 1 activity with the human factor C1 (HCF) complex. Nucleic Acids Res 28, 678-686.

Almazan, F., DeDiego, M.L., Galan, C., Escors, D., Alvarez, E., Ortego, J., Sola, I., Zuñiga, S., Alonso, S., Moreno, J.L., Nogales, A., Capiscol, C., Enjuanes, L., 2006. Construction of a SARS-CoV infectious cDNA clone and a replicon to study coronavirus RNA synthesis. J. Virol. 80, 10900-10906.

Almazan, F., Galan, C., Enjuanes, L., 2004. The nucleoprotein is required for efficient coronavirus genome replication. J. Virol. 78, 12683-12688.

Almazan, F., Gonzalez, J.M., Penzes, Z., Izeta, A., Calvo, E., Plana-Duran, J., Enjuanes, L., 2000. Engineering the largest RNA virus genome as an infectious bacterial artificial chromosome. Proc. Natl. Acad. Sci. USA 97, 5516-5521.

Alvarez, E., DeDiego, M.L., Nieto-Torres, J.L., Jimenez-Guardeno, J.M., Marcos-Villar, L., Enjuanes, L., 2010. The envelope protein of severe acute respiratory syndrome coronavirus interacts with the non-structural protein 3 and is ubiquitinated. Virology 402, 281-291.

Andrejeva, J., Childs, K.S., Young, D.F., Carlos, T.S., Stock, N., Goodbourn, S., Randall, R.E., 2004. The V proteins of paramyxoviruses bind the IFN-inducible RNA helicase, mda-5, and inhibit its activation of the IFN-beta promoter. Proc. Natl. Acad. Sci. USA 101, 17264-17269.

Arndt, A.L., Larson, B.J., Hogue, B.G., 2010. A conserved domain in the coronavirus membrane protein tail is important for virus assembly. J. Virol. 84, 11418-11428.

Ashburner, M., Ball, C.A., Blake, J.A., Botstein, D., Butler, H., Cherry, J.M., Davis, A.P., Dolinski, K., Dwight, S.S., Eppig, J.T., Harris, M.A., Hill, D.P., Issel-Tarver, L., Kasarskis, A., Lewis, S., Matese, J.C., Richardson, J.E., Ringwald, M., Rubin, G.M., Sherlock, G., 2000. Gene ontology: tool for the unification of biology. The Gene Ontology Consortium. Nat. Genet. 25, 25-29.

Auer, H., Lyianarachchi, S., Newsom, D., Klisovic, M.I., Marcucci, G., Kornacker, K., 2003. Chipping away at the chip bias: RNA degradation in microarray analysis. Nat. Genet. 35, 292-293.

Balachandran, S., Roberts, P.C., Kipperman, T., Bhalla, K.N., Compans, R.W., Archer, D.R., Barber, G.N., 2000. Alpha/beta interferons potentiate virus-induced apoptosis through activation of the FADD/Caspase-8 death signaling pathway. J Virol 74, 1513-1523.

Bantel, H., Schulze-Osthoff, K., 2003. Apoptosis in hepatitis C virus infection. Cell Death Differ. 10 Suppl 1, S48-S58.

Barber, G.N., 2000. The interferons and cell death: guardians of the cell or accomplices of apoptosis? Semin Cancer Biol 10, 103-111.

Barber, G.N., 2001. Host defense, viruses and apoptosis. Cell Death Differ. 8, 113-126.

Barber, G.N., 2005. The dsRNA-dependent protein kinase, PKR and cell death. Cell Death Differ 12, 563-570.

Baric, R.S., Sims, A.C., 2005. Development of mouse hepatitis virus and SARS-CoV infectious cDNA constructs, in: Enjuanes, L. (Ed.), Curr. Top. Microbiol. Immunol. Springer, pp. 229-252.

Beattie, E., Tartaglia, J., Paoletti, E., 1991. Vaccinia virus-encoded eIF-2 alpha homolog abrogates the antiviral effect of interferon. Virology 183, 419-422.

Bendtsen, J.D., Nielsen, H., von Heijne, G., Brunak, S., 2004. Improved prediction of signal peptides: SignalP 3.0. J. Mol. Biol. 340, 783-795.

Benjamini, Y., Hochberg, Y., 1995. Controlling the false discovery rate: a practical and powerful approach to multiple testing. J. Roy. Stat. Soc. B 57, 289-300.

Bergmann, M., Garcia-Sastre, A., Carnero, E., Pehamberger, H., Wolff, K., Palese, P., Muster, T., 2000. Influenza virus NS1 protein counteracts PKR-mediated inhibition of replication. J. Virol. 74, 6203-6206.

Bisbal, C., Silverman, R.H., 2007. Diverse functions of RNase L and implications in pathology. Biochimie 89, 789-798.

Blom, N., Gammeltoft, S., Brunak, S., 1999. Sequence and structure-based prediction of eukaryotic protein phosphorylation sites. J. Mol. Biol. 294, 1351-1362.

Bluyssen, A.R., Durbin, J.E., Levy, D.E., 1996. ISGF3 gamma p48, a specificity switch for interferon activated transcription factors. Cytokine Growth Factor Rev 7, 11-17.

Bolstad, B.M., Irizarry, R.A., Astrand, M., Speed, T.P., 2003. A comparison of normalization methods for high density oligonucleotide array data based on variance and bias. Bioinformatics 19, 185-193.

Bonjardim, C.A., Ferreira, P.C., Kroon, E.G., 2009. Interferons: signaling, antiviral and viral evasion. Immunol Lett 122, 1-11.

Bost, A.G., Prentice, E., Denison, M.R., 2001. Mouse hepatitis virus replicase protein complexes are translocated to sites of M protein accumulation in the ERGIC at late times of infection. Virology 285, 21-29.

Bosworth, B.T., MacLachlan, N.J., Johnston, M.I., 1989. Induction of the 2-5A system by interferon and transmissible gastroenteritis virus. J. Interferon Res. 9, 731-739.

Brian, D.A., Baric, R.S., 2005. Coronavirus genome structure and replication. Curr. Top. Microbiol. Immunol. 287, 1-30.

Brian, D.A., Hogue, B.G., Kienzle, T.E., 1995. The coronavirus hemagglutinin esterase glycoprotein, in: Siddell, S.G. (Ed.), The coronaviridae. Plenum press, New York, pp. 165-176.

Brierley, M.M., Fish, E.N., 2002. Review: IFN-alpha/beta receptor interactions to biologic outcomes: understanding the circuitry. J Interferon Cytokine Res 22, 835-845.

Brockway, S.M., Clay, C.T., Lu, X.T., Denison, M.R., 2003. Characterization of the expression, intracellular localization, and replication complex association of the putative mouse hepatitis virus RNA-dependent RNA polymerase. J. Virol. 77, 10515-10527.

Brostrom, C.O., Brostrom, M.A., 1998. Regulation of translational initiation during cellular responses to stress. Prog. Nucleic Acid Res. Mol. Biol. 58, 79-125.

Brush, M.H., Weiser, D.C., Shenolikar, S., 2003. Growth arrest and DNA damage-inducible protein GADD34 targets protein phosphatase 1 alpha to the endoplasmic reticulum and promotes dephosphorylation of the alpha subunit of eukaryotic translation initiation factor 2. Mol. Cell Biol. 23, 1292-1303.

Calvo, E., Escors, D., Lopez, J.A., Gonzalez, J.M., Alvarez, A., Arza, E., Enjuanes, L., 2005. Phosphorylation and subcellular localization of transmissible gastroenteritis virus nucleocapsid protein in infected cells. J. Gen. Virol. 86, 2255-2267.

Carstens, E.B., 2010. Ratification vote on taxonomic proposals to the International Committee on Taxonomy of Viruses (2009). Arch. Virol. 155, 133-146.

Casais, R., Thiel, V., Siddell, S.G., Cavanagh, D., Britton, P., 2001. Reverse genetics system for the avian coronavirus infectious bronchitis virus. J. Virol. 75, 12359-12369.

Cassady, K.A., Gross, M., 2002. The herpes simplex virus type 1 U(S)11 protein interacts with protein kinase R in infected cells and requires a 30-amino-acid sequence adjacent to a kinase substrate domain. J. Virol. 76, 2029-2035.

Cavanagh, D., Brian, D.A., Britton, P., Enjuanes, L., Horzinek, M.C., Lai, M.M.C., Laude, H., Plagemann, P.G.W., Siddell, S., Spaan, W., Talbot, P.J., 1997. *Nidovirales*: a new order comprising *Coronaviridae* and *Arteriviridae*. Arch. Virol. 142, 629-635.

Cayley, P.J., Davies, J.A., McCullagh, K.G., Kerr, I.M., 1984. Activation of the ppp(A2'p)nA system in interferon-treated, herpes simplex virus-infected cells and evidence for novel inhibitors of the ppp(A2'p)nA-dependent RNase. Eur. J. Biochem. 143, 165-174.

Cayley, P.J., Knight, M., Kerr, I.M., 1982. Virus-mediated inhibition of the ppp(A2'p)nA system and its prevention by interferon. Biochem. Biophys. Res. Commun. 104, 376-382.

Chakrabarti, A., Jha, B.K., Silverman, R.H., 2011. New insights into the role of RNase L in innate immunity. J Interferon Cytokine Res 31, 49-57.

Chan, W.S., Wu, C., Chow, S.C., Cheung, T., To, K.F., Leung, W.K., Chan, P.K., Lee, K.C., Ng, H.K., Au, D.M., Lo, A.W., 2005. Coronaviral hypothetical and structural proteins were found in the intestinal surface enterocytes and pneumocytes of severe acute respiratory syndrome (SARS). Mod. Pathol. 18, 1432-1439.

Chang, C.K., Sue, S.C., Yu, T.H., Hsieh, C.M., Tsai, C.K., Chiang, Y.C., Lee, S.J., Hsiao, H.H., Wu, W.J., Chang, W.L., Lin, C.H., Huang, T.H., 2006. Modular organization of SARS coronavirus nucleocapsid protein. J. Biomed. Sci. 13, 59-72.

Chang, H.W., Watson, J.C., Jacobs, B.L., 1992. The E3L gene of vaccinia virus encodes an inhibitor of the interferon-induced, double-stranded RNA-dependent protein kinase. Proc. Natl. Acad. Sci. USA 89, 4825-4829.

Chawla-Sarkar, M., Lindner, D.J., Liu, Y.F., Williams, B.R., Sen, G.C., Silverman, R.H., Borden, E.C., 2003. Apoptosis and interferons: role of interferon-stimulated genes as mediators of apoptosis. Apoptosis 8, 237-249.

Chen, C.Y., Chang, C.K., Chang, Y.W., Sue, S.C., Bai, H.I., Riang, L., Hsiao, C.D., Huang, T.H., 2007. Structure of the SARS coronavirus nucleocapsid protein RNA-binding dimerization domain suggests a mechanism for helical packaging of viral RNA. J. Mol. Biol. 368, 1075-1086.

Chen, Y., Cai, H., Pan, J., Xiang, N., Tien, P., Ahola, T., Guo, D., 2009. Functional screen reveals SARS coronavirus nonstructural protein nsp14 as a novel cap N7 methyltransferase. Proc Natl Acad Sci U S A 106, 3484-3489.

Chen, Y.Y., Shuang, B., Tan, Y.X., Meng, M.J., Han, P., Mo, X.N., Song, Q.S., Qiu, X.Y., Luo, X., Gan, Q.N., Zhang, X., Zheng, Y., Liu, S.A., Wang, X.N., Zhong, N.S., Ma, D.L., 2005. The protein X4 of severe acute respiratory syndrome-associated coronavirus is expressed on both virus-infected cells and lung tissue of severe acute respiratory syndrome patients and inhibits growth of Balb/c 3T3 cell line. Chin. Med. J. (Engl) 118, 267-274.

Cheung, C.Y., Poon, L.L., Lau, A.S., Luk, W., Lau, Y.L., Shortridge, K.F., Gordon, S., Guan, Y., Peiris, J.S., 2002. Induction of proinflammatory cytokines in human macrophages by influenza A (H5N1) viruses: a mechanism for the unusual severity of human disease? Lancet 360, 1831-1837.

Chianini, F., Majo, N., Segales, J., Dominguez, J., Domingo, M., 2001. Immunohistological study of the immune system cells in paraffin-embedded tissues of conventional pigs. Vet Immunol Immunopathol 82, 245-255.

Chu, D.K., Peiris, J.S., Chen, H., Guan, Y., Poon, L.L., 2008. Genomic characterizations of bat coronaviruses (1A, 1B and HKU8) and evidence for co-infections in Miniopterus bats. J. Gen. Virol. 89, 1282-1287.

Chu, D.K., Poon, L.L., Chan, K.H., Chen, H., Guan, Y., Yuen, K.Y., Peiris, J.S., 2006. Coronaviruses in bent-winged bats (Miniopterus spp.). J. Gen. Virol. 87, 2461-2246.

Clemens, M.J., 2003. Interferons and apoptosis. J Interferon Cytokine Res 23, 277-292.

Cohen, P.T., 2002. Protein phosphatase 1--targeted in many directions. J. Cell Sci. 115, 241-256.

Cole, J.L., Carroll, S.S., Blue, E.S., Viscount, T., Kuo, L.C., 1997. Activation of RNase L by 2',5'-oligoadenylates. Biophysical characterization. J Biol Chem 272, 19187-19192.

Cole, J.L., Carroll, S.S., Kuo, L.C., 1996. Stoichiometry of 2',5'-oligoadenylate-induced dimerization of ribonuclease L. A sedimentation equilibrium study. J Biol Chem 271, 3979-3981.

Cologna, R., Hogue, B.G., 2000. Identification of a bovine coronavirus packaging signal. J. Virol. 74, 580-583.

Cologna, R., Spagnolo, J.F., Hogue, B.G., 2000. Identification of nucleocapsid binding sites within coronavirus-defective genomes. Virology 277, 235-249.

Cornelissen, L.A.H.M., Wierda, C.M.H., Van Der Meer, F.J., Herrewegh, A.P.M., Horzinek, M.C., Egberonk, H.F., Groot, R.J., 1997. Hemagglutinin-esterase, a novel structural protein of torovirus. J. Virol. 71, 5277-5286.

Correa, I., Jiménez, G., Suñé, C., Bullido, M.J., Enjuanes, L., 1988. Antigenic structure of the E2 glycoprotein from transmissible gastroenteritis coronavirus. Virus Res. 10, 77-94.

Corse, E., Machamer, C.E., 2002. The cytoplasmic tail of infectious bronchitis virus E protein directs Golgi targeting. J. Virol. 76, 1273-1284.

Corse, E., Machamer, C.E., 2003. The cytoplasmic tails of infectious bronchitis virus E and M proteins mediate their interaction. Virology 312, 25-34.

Cowley, J.A., Dimmock, C.M., Walker, P.J., 2002. Gill-associated nidovirus of Penaeus monodon prawns transcribes 3'-coterminal subgenomic mRNAs that do not possess 5'-leader sequences. J Gen Virol 83, 927-935.

Crissman, H.A., Steinkamp, J.A., 1973. Rapid, simultaneous measurement of DNA, protein, and cell volume in single cells from large mammalian cell populations. J Cell Biol 59, 766-771.

Cruz, J.L., Zuniga, S., Becares, M., Sola, I., Ceriani, J.E., Juanola, S., Plana, J., Enjuanes, L., 2010. Vectored vaccines to protect against PRRSV. Virus Res 154, 150-160.

Curtis, K.M., Yount, B., Baric, R.S., 2002. Heterologous gene expression from transmissible gastroenteritis virus replicon particles. J. Virol. 76, 1422-1434.

Darnell, J.E., Jr., Kerr, I.M., Stark, G.R., 1994. Jak-STAT pathways and transcriptional activation in response to IFNs and other extracellular signaling proteins. Science 264, 1415-1421.

Dauber, B., Wolff, T., 2009. Activation of the Antiviral Kinase PKR and Viral Countermeasures. Viruses 1, 523-544.

de Groot, R.J., Cowley, J.A., Enjuanes, L., Faaberg, K.S., Perlman, S., Rottier, P.J.M., Snijder, E.J., Ziebuhr, J., Gorbalenya, A.E., 2011. The Positive Stranded ssRNA Viruses, Virus taxonomy.

de Groot, R.J., Ziebuhr, J., Poon, L.L., Woo, P.C., Talbot, P., Rottier, P.J.M., Holmes, K.V., Baric, R., Perlman, S., Enjuanes, L., Gorbalenya, A.E., 2010a. Taxonomic structure of the Coronaviridae, in: Fauquet, C.M., Mayo, M.A., Maniloff, J., Desselberg, U., King, A. (Eds.), Virus Taxonomy. International Committee on Taxonomy of Viruses. Academic Press, p. in press.

de Groot, R.J., Ziebuhr, J., Poon, L.L., Woo, P.C., Talbot, P., Rottier, P.J.M., Holmes, K.V., Baric, R., Perlman, S., Enjuanes, L., Gorbalenya, A.E., 2010b. Taxonomic structure of the Coronaviridae, in: Fauquet, C.M., Mayo, M.A., Maniloff, J., Desselberg, U., King, A. (Eds.), Virus Taxonomy. International Committee on Taxonomy of Viruses. Academic Press.

de Haan, C.A.M., Kuo, L., Masters, P.S., Vennema, H., Rottier, P.J.M., 1998a. Coronavirus particle assembly: primary structure requirements of the membrane protein. J. Virol. 72, 6838-6850.

de Haan, C.A.M., Masters, P.S., Shen, S., Weiss, S., Rottier, P.J.M., 2002. The group-specific murine coronavirus genes are not essential, but their deletion, by reverse genetics, is attenuating in the natural host. Virology 296, 177-189.

de Haan, C.A.M., Vennema, H., Rottier, P.J.M., 1998b. Coronavirus envelope assembly is sensitive to changes in the terminal regions of the viral M protein. Adv. Exp. Med. Biol. 440, 367-376.

de Haro, C., Mendez, R., Santoyo, J., 1996. The eIF-2alpha kinases and the control of protein synthesis. FASEB J 10, 1378-1387.

Decroly, E., Imbert, I., Coutard, B., Bouvet, M., Selisko, B., Alvarez, K., Gorbalenya, A.E., Snijder, E.J., Canard, B., 2008. Coronavirus nonstructural protein 16 is a cap-0 binding enzyme possessing (nucleoside-2'O)-methyltransferase activity. J Virol 82, 8071-8084.

DeDiego, M.L., Alvarez, E., Almazan, F., Rejas, M.T., Lamirande, E., Roberts, A., Shieh, W.J., Zaki, S.R., Subbarao, K., Enjuanes, L., 2007. A severe acute respiratory syndrome coronavirus that lacks the E gene is attenuated in vitro and in vivo. J. Virol. 81, 1701-1713.

DeDiego, M.L., Nieto-Torres., J.L., Jimenez-Guardeño, J.M., Regla-Nava, J.A., Alvarez, E., Oliveros, J.C., Zhao, J., Fett, C., Perlman, S., Enjuanes, L., 2011. Severe acute respiratory syndrome coronavirus envelope protein regulates stress response and inflammation. PLoS Pathog., In press.

DeDiego, M.L., Pewe, L., Alvarez, E., Rejas, M.T., Perlman, S., Enjuanes, L., 2008. Pathogenicity of severe acute respiratory coronavirus deletion mutants in hACE-2 transgenic mice. Virology 376, 379-389.

Delmas, B., Gelfi, J., L'Haridon, R., Vogel, L.K., Norén, O., Laude, H., 1992. Aminopeptidase N is a major receptor for the enteropathogenic coronavirus TGEV. Nature 357, 417-420.

Delmas, B., Gelfi, J., Laude, H., 1986. Antigenic structure of transmissible gastroenteritis virus. II. Domains in the peplomer glycoprotein. J. Gen. Virol. 67, 1405-1418.

Delmas, B., Gelfi, J., Sjöström, H., Noren, O., Laude, H., 1993. Further characterization of aminopeptidase-N as a receptor for coronaviruses. Adv. Exp. Med. Biol. 342, 293-298.

Delmas, B., Rasschaert, D., Godet, M., Gelfi, J., Laude, H., 1990. Four major antigenic sites of the coronavirus transmissible gastroenteritis virus are located on the amino-terminal half of spike glycoprotein S. J. Gen. Virol. 71, 1313-1323.

Deming, D.J., Graham, R.L., Denison, M.R., Baric, R.S., 2007. Processing of open reading frame 1a replicase proteins nsp7 to nsp10 in murine hepatitis virus strain A59 replication. J Virol 81, 10280-10291.

Denison, M.R., Zoltick, P.W., Hughes, S.A., Giangreco, B., Olson, A.L., Perlman, S., Leibowitz, J.L., Weiss, S.R., 1992. Intracellular processing of the N-terminal ORF-1a proteins of the coronavirus MHV-A59 requires multiple proteolytic events. Virology 189, 274-284.

Der, S.D., Yang, Y.L., Weissmann, C., Williams, B.R., 1997. A double-stranded RNA-activated protein kinase-dependent pathway mediating stress-induced apoptosis. Proc Natl Acad Sci U S A 94, 3279-3283.

Deregt, D., Sabara, M., Babiuk, L.A., 1987. Structural proteins of bovine coronavirus and their intracellular processing. J. Gen. Virol., 2863-2877.

Dever, T.E., Sripriya, R., McLachlin, J.R., Lu, J., Fabian, J.R., Kimball, S.R., Miller, L.K., 1998. Disruption of cellular translational control by a viral truncated eukaryotic translation initiation factor 2alpha kinase homolog. Proc. Natl. Acad. Sci. USA 95, 4164-4169.

Diaz-Guerra, M., Rivas, C., Esteban, M., 1997. Inducible expression of the 2-5A synthetase/RNase L system results in inhibition of vaccinia virus replication. Virology 227, 220-228.

Domingo-Gil, E., Esteban, M., 2006. Role of mitochondria in apoptosis induced by the 2-5A system and mechanisms involved. Apoptosis 11, 725-738.

Dominguez, S.R., O'Shea, T.J., Oko, L.M., Holmes, K.V., 2007. Detection of group 1 coronaviruses in bats in North America. Emerg. Infect. Dis. 13, 1295-1300.

Dong, B., Silverman, R.H., 1995. 2-5A-dependent RNase molecules dimerize during activation by 2-5A. J Biol Chem 270, 4133-4137.

Doyle, L.P., Hutchings, L.M., 1946. A transmissible gastroenteritis in pigs. J. Amer. Vet. Med. Assoc. 108, 257-259.

Drosten, C., Gunther, S., Preiser, W., van der Werf, S., Brodt, H.R., Becker, S., Rabenau, H., Panning, M., Kolesnikova, L., Fouchier, R.A., Berger, A., Burguiere, A.M., Cinatl, J., Eickmann, M., Escriou, N., Grywna, K., Kramme, S., Manuguerra, J.C., Muller, S., Rickerts, V., Sturmer, M., Vieth, S., Klenk, H.D., Osterhaus, A.D., Schmitz, H., Doerr, H.W., 2003. Identification of a novel coronavirus in patients with severe acute respiratory syndrome. N. Engl. J. Med. 348, 1967-1976.

Eckerle, L.D., Becker, M.M., Halpin, R.A., Li, K., Venter, E., Lu, X., Scherbakova, S., Graham, R.L., Baric, R.S., Stockwell, T.B., Spiro, D.J., Denison, M.R., 2010. Infidelity of SARS-CoV Nsp14-exonuclease mutant virus replication is revealed by complete genome sequencing. PLoS Pathog 6, e1000896.

Eckerle, L.D., Lu, X., Sperry, S.M., Choi, L., Denison, M.R., 2007. High fidelity of murine hepatitis virus replication is decreased in nsp14 exoribonuclease mutants. J. Virol. 81, 12135-12144.

Egloff, M.P., Ferron, F., Campanacci, V., Longhi, S., Rancurel, C., Dutartre, H., Snijder, E.J., Gorbalenya, A.E., Cambillau, C., Canard, B., 2004. The severe acute respiratory syndrome-coronavirus replicative protein nsp9 is a single-stranded RNA-binding subunit unique in the RNA virus world. Proc. Natl. Acad. Sci. USA 101, 3792-3796.

Eleouet, J.F., Chilmonczyk, S., Besnardeau, L., Laude, H., 1998. Transmissible gastroenteritis coronavirus induces programmed cell death in infected cells through a caspase-dependent pathway. J. Virol. 72, 4918-4924.

Eleouet, J.F., Slee, E.A., Saurini, F., Castagné, N., Poncet, D., Garrido, C., Solary, E., Martin, S.J., 2000. The viral nucleocapsid protein of transmissible gastroenteritis coronavirus (TGEV) is cleaved by caspase-6 and -7 during TGEV-induced apoptosis. J. Virol. 74, 3975-3983.

Enjuanes, L., Almazan, F., Sola, I., Zuniga, S., 2006a. Biochemical aspects of coronavirus replication and virus-host interaction. Annu. Rev. Microbiol. 60, 211-230.

Enjuanes, L., Almazan, F., Sola, I., Zuniga, S., Alvarez, E., Reguera, J., Capiscol, C., 2006b. Biochemical aspects of coronavirus replication. Adv. Exp. Med. Biol. 581, 13-24.

Enjuanes, L., Gorbalenya, A.E., de Groot, R.J., Cowley, J.A., Ziebuhr, J., Snijder, E.J., 2008a. The Nidovirales, in: Mahy, B.W.J., Van Regenmortel, M., Walker, P., Majumder-Russell, D. (Eds.), Encyclopedia of Virology, Third Edition. Elsevier Ltd., Oxford, pp. 419-430.

Enjuanes, L., Sola, I., Zuñiga, S., Almazán, F., 2008b. Coronavirus replication and interaction with host, in: Mettenleiter, T.C., Sobrino, F. (Eds.), Animal viruses. Molecular biology. Caister Academic Press, Norfolk, pp. 149-202.

Enjuanes, L., Sola, I., Zuñiga, S., Ortego, J., 2007. Expression vectors based on coronavirus genomes, in: Hefferon, K.L. (Ed.), Virus expression vectors. Tranworld Research Network, Kerala, pp. 147-182.

Enjuanes, L., Spaan, W., Snijder, E., Cavanagh, D., 2000. *Nidovirales*, in: van Regenmortel, M.H.V., Fauquet, C.M., Bishop, D.H.L., Carstens, E.B., Estes, M.K., Lemon, S.M., Maniloff, J., Mayo, M.A., McGeoch, D.J., Pringle, C.R., Wickner, R.B. (Eds.), Virus taxonomy. Seventh report of the international committee on taxonomy of viruses. Academic Press, New York, pp. 827-834.

Enjuanes, L., Van der Zeijst, B.A.M., 1995. Molecular basis of transmissible gastroenteritis coronavirus epidemiology, in: Siddell, S.G. (Ed.), The *Coronaviridae*. Plenum Press, New York, pp. 337-376.

Escors, D., Camafeita, E., Ortego, J., Laude, H., Enjuanes, L., 2001a. Organization of two transmissible gastroenteritis coronavirus membrane protein topologies within the virion and core. J. Virol. 75, 12228-12240.

Escors, D., Ortego, J., Enjuanes, L., 2001b. The membrane M protein of the transmissible gastroenteritis coronavirus binds to the internal core through the carboxy-terminus. Adv. Exp. Med. Biol. 494, 589-593.

Fadok, V.A., Savill, J.S., Haslett, C., Bratton, D.L., Doherty, D.E., Campbell, P.A., Henson, P.M., 1992a. Different populations of macrophages use either the vitronectin receptor or the phosphatidylserine receptor to recognize and remove apoptotic cells. J Immunol 149, 4029-4035.

Fadok, V.A., Voelker, D.R., Campbell, P.A., Cohen, J.J., Bratton, D.L., Henson, P.M., 1992b. Exposure of phosphatidylserine on the surface of apoptotic lymphocytes triggers specific recognition and removal by macrophages. J Immunol 148, 2207-2216.

Fan, H., Ooi, A., Tan, Y.W., Wang, S., Fang, S., Liu, D.X., Lescar, J., 2005. The nucleocapsid protein of coronavirus infectious bronchitis virus: crystal structure of its N-terminal domain and multimerization properties. Structure 13, 1859-1868.

Ferrara, J.L., Abhyankar, S., Gilliland, D.G., 1993. Cytokine storm of graft-versus-host disease: a critical effector role for interleukin-1. Transplant Proc 25, 1216-1217.

Fielding, B.C., Tan, Y.J., Shuo, S., Tan, T.H., Ooi, E.E., Lim, S.G., Hong, W., Goh, P.Y., 2004. Characterization of a unique group-specific protein (U122) of the severe acute respiratory syndrome coronavirus. J. Virol. 78, 7311-7318.

Fischer, F., Stegen, C.F., Koetzner, C.A., Masters, P.S., 1997. Analysis of a recombinant mouse hepatitis virus expressing a foreign gene reveals a novel aspect of coronavirus transcription. J. Virol. 71, 5148-5160.

Fischer, F., Stegen, C.F., Masters, P.S., Samsonoff, W.A., 1998. Analysis of constructed E gene mutants of mouse hepatitis virus confirms a pivotal role for E protein in coronavirus assembly. J. Virol. 72, 7885-7894.

Fish, E.N., Uddin, S., Korkmaz, M., Majchrzak, B., Druker, B.J., Platanias, L.C., 1999. Activation of a CrkL-stat5 signaling complex by type I interferons. J Biol Chem 274, 571-573.

Foy, E., Li, K., Sumpter, R., Jr., Loo, Y.M., Johnson, C.L., Wang, C., Fish, P.M., Yoneyama, M., Fujita, T., Lemon, S.M., Gale, M., Jr., 2005. Control of antiviral defenses through hepatitis C virus disruption of retinoic acid-inducible gene-I signaling. Proc Natl Acad Sci U S A 102, 2986-2991.

Frieman, M., Ratia, K., Johnston, R.E., Mesecar, A.D., Baric, R.S., 2009. Severe acute respiratory syndrome coronavirus papain-like protease ubiquitin-like domain and catalytic domain regulate antagonism of IRF3 and NF-kappaB signaling. J. Virol. 83, 6689-6705.

Frieman, M., Yount, B., Heise, M., Kopecky-Bromberg, S.A., Palese, P., Baric, R.S., 2007. Severe acute respiratory syndrome coronavirus ORF6 antagonizes STAT1 function by sequestering nuclear import factors on the rough endoplasmic reticulum/Golgi membrane. J. Virol. 81, 9812-9824.

Galan, C., Sola, I., Nogales, A., Thomas, B., Akoulitchev, A., Enjuanes, L., Almazan, F., 2009. Host cell proteins interacting with the 3' end of TGEV coronavirus genome influence virus replication. Virology 391, 304-314.

Gale, M.J., Jr., Korth, M.J., Tang, N.M., Tan, S.L., Hopkins, D.A., Dever, T.E., Polyak, S.J., Gretch, D.R., Katze, M.G., 1997. Evidence that hepatitis C virus resistance to interferon is mediated through repression of the PKR protein kinase by the nonstructural 5A protein. Virology 230, 217-227.

Gallagher, T.M., Buchmeier, M.J., 2001. Coronavirus spike proteins in viral entry and pathogenesis. Virology 279, 371-374.

Gantier, M.P., Williams, B.R., 2007. The response of mammalian cells to double-stranded RNA. Cytokine Growth Factor Rev. 18, 363-371.

Garcia, M.A., Gil, J., Ventoso, I., Guerra, S., Domingo, E., Rivas, C., Esteban, M., 2006. Impact of protein kinase PKR in cell biology: from antiviral to antiproliferative action. Microbiol Mol Biol Rev 70, 1032-1060.

Garcia-Sastre, A., Biron, C.A., 2006. Type 1 interferons and the virus-host relationship: a lesson in detente. Science 312, 879-882.

Garwes, D.J., Stewart, F., Britton, P., 1989. The polypeptide of Mr 14000 of porcine transmissible gastroenteritis virus: Gene assignment and intracellular location. J. Gen. Virol. 70, 2495-2499.

Gentleman, R.C., Carey, V.J., Bates, D.M., Bolstad, B., Dettling, M., Dudoit, S., Ellis, B., Gautier, L., Ge, Y., Gentry, J., Hornik, K., Hothorn, T., Huber, W., Iacus, S., Irizarry, R., Leisch, F., Li, C., Maechler, M., Rossini, A.J., Sawitzki, G., Smith, C., Smyth, G., Tierney, L., Yang, J.Y., Zhang, J., 2004. Bioconductor: open software development for computational biology and bioinformatics. Genome Biol. 5, R80.

Gil, J., Alcami, J., Esteban, M., 1999. Induction of apoptosis by double-stranded-RNA-dependent protein kinase (PKR) involves the alpha subunit of eukaryotic translation initiation factor 2 and NF-kappaB. Mol Cell Biol 19, 4653-4663.

Gil, J., Garcia, M.A., Gomez-Puertas, P., Guerra, S., Rullas, J., Nakano, H., Alcami, J., Esteban, M., 2004. TRAF family proteins link PKR with NF-kappa B activation. Mol Cell Biol 24, 4502-4512.

Glass, W.G., Liu, M.T., Kuziel, W.A., Lane, T.E., 2001. Reduced macrophage infiltration and demyelination in mice lacking the chemokine receptor CCR5 following infection with a neurotropic coronavirus. Virology 288, 8-17.

Gloza-Rausch, F., Ipsen, A., Seebens, A., Gottsche, M., Panning, M., Felix Drexler, J., Petersen, N., Annan, A., Grywna, K., Muller, M., Pfefferle, S., Drosten, C., 2008. Detection and prevalence patterns of group I coronaviruses in bats, northern Germany. Emerg. Infect. Dis. 14, 626-631.

Gonzalez, J.M., Gomez-Puertas, P., Cavanagh, D., Gorbalenya, A.E., Enjuanes, L., 2003. A comparative sequence analysis to revise the current taxonomy of the family Coronaviridae. Arch. Virol. 148, 2207-2235.

Gonzalez, J.M., Penzes, Z., Almazan, F., Calvo, E., Enjuanes, L., 2002. Stabilization of a full-length infectious cDNA clone of transmissible gastroenteritis coronavirus by insertion of an intron. J. Virol. 76, 4655-4661.

Goodman, A.G., Fornek, J.L., Medigeshi, G.R., Perrone, L.A., Peng, X., Dyer, M.D., Proll, S.C., Knoblaugh, S.E., Carter, V.S., Korth, M.J., Nelson, J.A., Tumpey, T.M., Katze, M.G., 2009. P58(IPK): a novel "CIHD" member of the host innate defense response against pathogenic virus infection. PLoS Pathog. 5, e1000438.

Gorbalenya, A.E., Enjuanes, L., Ziebuhr, J., Snijder, E.J., 2006. Nidovirales: evolving the largest RNA virus genome. Virus Res. 117, 17-37.

Gorbalenya, A.E., Snijder, E.J., Spaan, W.J., 2004. Severe acute respiratory syndrome coronavirus phylogeny: toward consensus. J. Virol. 78, 7863-7866.

Gosert, R., Kanjanahaluethai, A., Egger, D., Bienz, K., Baker, S.C., 2002. RNA replication of mouse hepatitis virus takes place at double-membrane vesicles. J. Virol. 76, 3697-3708.

Gould, C.M., Diella, F., Via, A., Puntervoll, P., Gemund, C., Chabanis-Davidson, S., Michael, S., Sayadi, A., Bryne, J.C., Chica, C., Seiler, M., Davey, N.E., Haslam, N., Weatheritt, R.J., Budd, A., Hughes, T., Pas, J., Rychlewski, L., Trave, G., Aasland, R., Helmer-Citterich, M., Linding, R., Gibson, T.J., 2010. ELM: the status of the 2010 eukaryotic linear motif resource. Nucleic Acids Res. 38, 1-14.

Graham, R.L., Sims, A.C., Brockway, S.M., Baric, R.S., Denison, M.R., 2005. The nsp2 replicase proteins of murine hepatitis virus and severe acute respiratory syndrome coronavirus are dispensable for viral replication. J. Virol. 79, 13399-13411.

Gunnery, S., Rice, A.P., Robertson, H.D., Mathews, M.B., 1990. Tat-responsive region RNA of human immunodeficiency virus 1 can prevent activation of the double-stranded-RNA-activated protein kinase. Proc. Natl. Acad. Sci. USA 87, 8687-8691.

Hagemeijer, M.C., Verheije, M.H., Ulasli, M., Shaltiel, I.A., de Vries, L.A., Reggiori, F., Rottier, P.J., de Haan, C.A., 2010. Dynamics of coronavirus replication-transcription complexes. J Virol 84, 2134-2149.

Haijema, B.J., Volders, H., Rottier, P.J., 2004. Live, attenuated coronavirus vaccines through the directed deletion of group-specific genes provide protection against feline infectious peritonitis. J. Virol. 78, 3863-3871.

Haller, O., Kochs, G., Weber, F., 2006. The interferon response circuit: induction and suppression by pathogenic viruses. Virology 344, 119-130.

Han, J.Q., Barton, D.J., 2002. Activation and evasion of the antiviral 2'-5' oligoadenylate synthetase/ribonuclease L pathway by hepatitis C virus mRNA. RNA 8, 512-525.

Han, J.Q., Wroblewski, G., Xu, Z., Silverman, R.H., Barton, D.J., 2004. Sensitivity of hepatitis C virus RNA to the antiviral enzyme ribonuclease L is determined by a subset of efficient cleavage sites. J. Interferon Cytokine Res. 24, 664-676.

Hanahan, D., 1985. Techniques for transformation of *E. coli*, in: Glover, D.H. (Ed.), DNA Cloning. A Practical Approach. IRL Press Oxford, Oxford, pp. 109-136.

Haque, S.J., Williams, B.R., 1994. Identification and characterization of an interferon (IFN)-stimulated response element-IFN-stimulated gene factor 3-independent signaling pathway for IFN-alpha. J Biol Chem 269, 19523-19529.

Harding, H.P., Calfon, M., Urano, F., Novoa, I., Ron, D., 2002. Transcriptional and translational control in the Mammalian unfolded protein response. Annu Rev Cell Dev Biol 18, 575-599.

Harding, H.P., Zhang, Y., Ron, D., 1999. Protein translation and folding are coupled by an endoplasmic-reticulum-resident kinase. Nature 397, 271-274.

Hartmann, R., Justesen, J., Sarkar, S.N., Sen, G.C., Yee, V.C., 2003. Crystal structure of the 2'-specific and double-stranded RNA-activated interferon-induced antiviral protein 2'-5'-oligoadenylate synthetase. Mol Cell 12, 1173-1185.

Hashimoto, N., Kawabe, T., Imaizumi, K., Hara, T., Okamoto, M., Kojima, K., Shimokata, K., Hasegawa, Y., 2004. CD40 plays a crucial role in lipopolysaccharide-induced acute lung injury. Am J Respir Cell Mol Biol 30, 808-815.

Hassel, B.A., Zhou, A., Sotomayor, C., Maran, A., Silverman, R.H., 1993. A dominant negative mutant of 2-5A-dependent RNase suppresses antiproliferative and antiviral effects of interferon. EMBO J 12, 3297-3304.

He, B., 2006. Viruses, endoplasmic reticulum stress, and interferon responses. Cell Death Differ. 13, 393-403.

He, B., Gross, M., Roizman, B., 1997. The gamma(1)34.5 protein of herpes simplex virus 1 complexes with protein phosphatase 1alpha to dephosphorylate the alpha subunit of the eukaryotic translation initiation factor 2 and preclude the shutoff of protein synthesis by double-stranded RNA-activated protein kinase. Proc. Natl. Acad. Sci. USA 94, 843-848.

He, Y., Li, J., Heck, S., Lustigman, S., Jiang, S., 2006. Antigenic and immunogenic characterization of recombinant baculovirus-expressed severe acute respiratory syndrome coronavirus spike protein: implication for vaccine design. J. Virol. 80, 5757-5767.

Heltemes-Harris, L.M., Willette, M.J., Vang, K.B., Farrar, M.A., 2011. The role of STAT5 in the development, function, and transformation of B and T lymphocytes. Ann N Y Acad Sci 1217, 18-31.

Herold, J., Gorbalenya, A.E., Thiel, V., Schelle, B., Siddell, S.G., 1998. Proteolytic processing at the amino terminus of human coronavirus 229E gene 1-encoded polyproteins: identification of a papin-like proteinase and its substrate. J. Virol. 72, 910-918.

Herrewegh, A.A.P.M., Vennema, H., Horzinek, M.C., Rottier, P.J.M., Groot, P.J., 1995. The molecular genetics of feline coronavirus comparative sequence analysis of the ORF7a/7b transcription unit of different biotypes. Virology 212, 622-631.

Hershey, J.W., 1991. Translational control in mammalian cells. Annu Rev Biochem 60, 717-755.

Hogue, B.G., Kienzle, T.E., Brian, D.A., 1989. Synthesis and processing of the bovine enteric coronavirus haemagglutinin protein. J. Gen. Virol. 70, 345-352.

Hornung, V., Ellegast, J., Kim, S., Brzozka, K., Jung, A., Kato, H., Poeck, H., Akira, S., Conzelmann, K.K., Schlee, M., Endres, S., Hartmann, G., 2006. 5'-Triphosphate RNA is the ligand for RIG-I. Science 314, 994-997.

Hovanessian, A.G., Brown, R.E., Kerr, I.M., 1977. Synthesis of low molecular weight inhibitor of protein synthesis with enzyme from interferon-treated cells. Nature 268, 537-540.

Hsieh-Wilson, L.C., Allen, P.B., Watanabe, T., Nairn, A.C., Greengard, P., 1999. Characterization of the neuronal targeting protein spinophilin and its interactions with protein phosphatase-1. Biochemistry 38, 4365-4373.

Huang, C., Ito, N., Tseng, C.T., Makino, S., 2006a. Severe acute respiratory syndrome coronavirus 7a accessory protein is a viral structural protein. J. Virol. 80, 7287-7294.

Huang, C., Narayanan, K., Ito, N., Peters, C.J., Makino, S., 2006b. Severe acute respiratory syndrome coronavirus 3a protein is released in membranous structures from 3a protein-expressing cells and infected cells. J. Virol. 80, 210-217.

Huang, C., Peters, C.J., Makino, S., 2007. Severe acute respiratory syndrome coronavirus accessory protein 6 is a virion-associated protein and is released from 6 protein-expressing cells. J. Virol. 81, 5423-5426.

Huang da, W., Sherman, B.T., Lempicki, R.A., 2009a. Bioinformatics enrichment tools: paths toward the comprehensive functional analysis of large gene lists. Nucleic Acids Res 37, 1-13.

Huang da, W., Sherman, B.T., Lempicki, R.A., 2009b. Systematic and integrative analysis of large gene lists using DAVID bioinformatics resources. Nat Protoc 4, 44-57.

Huang, K.J., Su, I.J., Theron, M., Wu, Y.C., Lai, S.K., Liu, C.C., Lei, H.Y., 2005. An interferon-gamma-related cytokine storm in SARS patients. J Med Virol 75, 185-194.

Huang, Q., Yu, L., M., P.A., Gunasekera, A., Liu, Z., Xu, N., Hajduk, P., Mack, J., W., F.S., Olejniczak, E.T., 2004. Structure of the N-ternimal RNA-binding domain of the SARS CoV nucleocapsid protein. Biochemistry 20, 6059-6063.

Hurst, K.R., Kuo, L., Koetzner, C.A., Ye, R., Hsue, B., Masters, P.S., 2005. A major determinant for membrane protein interaction localizes to the carboxy-terminal domain of the mouse coronavirus nucleocapsid protein. J. Virol. 79, 13285-13297.

Hurst, K.R., Ye, R., Goebel, S.J., Jayaraman, P., Masters, P.S., 2010. An interaction between the nucleocapsid protein and a component of the replicase-transcriptase complex is crucial for the infectivity of coronavirus genomic RNA. J Virol 84, 10276-10288.

Imbert, I., Guillemot, J.C., Bourhis, J.M., Bussetta, C., Coutard, B., Egloff, M.P., Ferron, F., Gorbalenya, A.E., Canard, B., 2006. A second, non-canonical RNA-dependent RNA polymerase in SARS coronavirus. EMBO J. 25, 4933-4942.

Iordanov, M.S., Paranjape, J.M., Zhou, A., Wong, J., Williams, B.R., Meurs, E.F., Silverman, R.H., Magun, B.E., 2000. Activation of p38 mitogen-activated protein kinase and c-Jun NH(2)-terminal kinase by double-stranded RNA and encephalomyocarditis virus: involvement of RNase L, protein kinase R, and alternative pathways. Mol. Cell Biol. 20, 617-627.

Ireland, D.D., Stohlman, S.A., Hinton, D.R., Kapil, P., Silverman, R.H., Atkinson, R.A., Bergmann, C.C., 2009. RNase L mediated protection from virus induced demyelination. PLoS Pathog 5, e1000602.

Irizarry, R.A., Hobbs, B., Collin, F., Beazer-Barclay, Y.D., Antonellis, K.J., Scherf, U., Speed, T.P., 2003. Exploration, normalization, and summaries of high density oligonucleotide array probe level data. Biostatistics 4, 249-264.

Ivanov, K.A., Thiel, V., Dobbe, J.C., van der Meer, Y., Snijder, E.J., Ziebuhr, J., 2004. Multiple enzymatic activities associated with severe acute respiratory syndrome coronavirus helicase. J. Virol. 78, 5619-5632.

Izeta, A., Smerdou, C., Alonso, S., Penzes, Z., Mendez, A., Plana-Duran, J., Enjuanes, L., 1999. Replication and packaging of transmissible gastroenteritis coronavirus-derived synthetic minigenomes. J. Virol. 73, 1535-1545.

Jacobs, L., Van der Zeijst, B.A.M., Horzinek, M., 1986. Characterization and translation of transmissible gastroenteritis virus mRNAs. J. Virol. 57, 1010-1015.

Jia, W., Naqi, S.A., 1997. Sequence analysis of gene 3, gene 4 and gene 5 of avian infectious bronchitis virus strain CU-T2. Gene 189, 189-193.

Jiménez, G., Castro, J.M., del Pozo, M., Correa, I., de la Torre, J.M., Enjuanes, L., 1986. Identification of a Coronavirus inducing porcine gastroenteritis in Spain, 9th Congress I.P.V.S., Barcelona.

Jimenez, G., Correa, I., Melgosa, M.P., Bullido, M.J., Enjuanes, L., 1986. Critical epitopes in transmissible gastroenteritis virus neutralization. J. Virol. 60, 131-139.

Kamitani, W., Huang, C., Narayanan, K., Lokugamage, K.G., Makino, S., 2009. A two-pronged strategy to suppress host protein synthesis by SARS coronavirus Nsp1 protein. Nat. Struct. Mol. Biol. 16, 1134-1140.

Kamitani, W., Narayanan, K., Huang, C., Lokugamage, K., Ikegami, T., Ito, N., Kubo, H., Makino, S., 2006. Severe acute respiratory syndrome coronavirus nsp1 protein suppresses host gene expression by promoting host mRNA degradation. Proc. Natl. Acad. Sci. USA 103, 12885-12890.

Kang, H., Bhardwaj, K., Li, Y., Palaninathan, S., Sacchettini, J., Guarino, L., Leibowitz, J.L., Kao, C.C., 2007. Biochemical and genetic analyses of murine hepatitis virus Nsp15 endoribonuclease. J Virol 81, 13587-13597.

Kato, H., Takeuchi, O., Sato, S., Yoneyama, M., Yamamoto, M., Matsui, K., Uematsu, S., Jung, A., Kawai, T., Ishii, K.J., Yamaguchi, O., Otsu, K., Tsujimura, T., Koh, C.S., Reis e Sousa, C., Matsuura, Y., Fujita, T., Akira, S., 2006. Differential roles of MDA5 and RIG-I helicases in the recognition of RNA viruses. Nature 441, 101-105.

Kaufman, R.J., 1999. Stress signaling from the lumen of the endoplasmic reticulum: coordination of gene transcriptional and translational controls. Genes Dev. 13, 1211-1233.

Kawai, T., Takahashi, K., Sato, S., Coban, C., Kumar, H., Kato, H., Ishii, K.J., Takeuchi, O., Akira, S., 2005. IPS-1, an adaptor triggering RIG-I- and Mda5-mediated type I interferon induction. Nat Immunol 6, 981-988.

Kazemi, S., Papadopoulou, S., Li, S., Su, Q., Wang, S., Yoshimura, A., Matlashewski, G., Dever, T.E., Koromilas, A.E., 2004. Control of alpha subunit of eukaryotic translation initiation factor 2 (eIF2 alpha) phosphorylation by the human papillomavirus type 18 E6 oncoprotein: implications for eIF2 alpha-dependent gene expression and cell death. Mol. Cell Biol. 24, 3415-3429.

Kazi, L., Lissenberg, A., Watson, R., de Groot, R.J., Weiss, S.R., 2005. Expression of hemagglutinin esterase protein from recombinant mouse hepatitis virus enhances neurovirulence. J. Virol. 79, 15064-15073.

Kienzle, T.E., Abraham, S., Hogue, B.G., Brian, D.A., 1990. Structure and orientation of expressed bovine coronavirus hemagglutinin-esterase protein. J Virol 64, 1834-1838.

King, B., Brian, D.A., 1982. Bovine coronavirus structural proteins. J. Virol. 42, 700-707.

Knoops, K., Kikkert, M., Worm, S.H., Zevenhoven-Dobbe, J.C., van der Meer, Y., Koster, A.J., Mommaas, A.M., Snijder, E.J., 2008. SARS-coronavirus replication is supported by a reticulovesicular network of modified endoplasmic reticulum. PLoS Biol. 6, e226.

Koetzner, C.A., Kuo, L., Goebel, S.J., Dean, A.B., Parker, M.M., Masters, P.S., 2010. Accessory protein 5a is a major antagonist of the antiviral action of interferon against murine coronavirus. J. Virol. 84, 8262-8274.

Kohlmeier, J.E., Woodland, D.L., 2009. Immunity to respiratory viruses. Annu Rev Immunol 27, 61-82.

Kopecky-Bromberg, S.A., Martinez-Sobrido, L., Frieman, M., Baric, R.A., Palese, P., 2007. Severe acute respiratory syndrome coronavirus open reading frame (ORF) 3b, ORF 6, and nucleocapsid proteins function as interferon antagonists. J. Virol. 81, 548-557.

Kopecky-Bromberg, S.A., Martinez-Sobrido, L., Palese, P., 2006. 7a protein of severe acute respiratory syndrome coronavirus inhibits cellular protein synthesis and activates p38 mitogen-activated protein kinase. J. Virol. 80, 785-793.

Kotenko, S.V., Gallagher, G., Baurin, V.V., Lewis-Antes, A., Shen, M., Shah, N.K., Langer, J.A., Sheikh, F., Dickensheets, H., Donnelly, R.P., 2003. IFN-lambdas mediate antiviral protection through a distinct class II cytokine receptor complex. Nat Immunol 4, 69-77.

Krahling, V., Stein, D.A., Spiegel, M., Weber, F., Muhlberger, E., 2009. Severe acute respiratory syndrome coronavirus triggers apoptosis via protein kinase R but is resistant to its antiviral activity. J Virol 83, 2298-2309.

Kumar, A., Yang, Y.L., Flati, V., Der, S., Kadereit, S., Deb, A., Haque, J., Reis, L., Weissmann, C., Williams, B.R., 1997. Deficient cytokine signaling in mouse embryo fibroblasts with a targeted deletion in the PKR gene: role of IRF-1 and NF-kappaB. EMBO J 16, 406-416.

Kumar, P., Gunalan, V., Liu, B., Chow, V.T., Druce, J., Birch, C., Catton, M., Fielding, B.C., Tan, Y.J., Lal, S.K., 2007. The nonstructural protein 8 (nsp8) of the SARS coronavirus interacts with its ORF6 accessory protein. Virology 366, 293-303.

Kuo, L., Masters, P.S., 2003. The small envelope protein E is not essential for murine coronavirus replication. J. Virol. 77, 4597-4608.

Kuri, T., Eriksson, K.K., Putics, A., Zust, R., Snijder, E.J., Davidson, A.D., Siddell, S.G., Thiel, V., Ziebuhr, J., Weber, F., 2011. The ADP-ribose-1"-monophosphatase domains

of severe acute respiratory syndrome coronavirus and human coronavirus 229E mediate resistance to antiviral interferon responses. J Gen Virol 92, 1899-1905.

Kyuwa, S., Cohen, M., Nelson, G., Tahara, S.M., Stohlman, S.A., 1994. Modulation of cellular macromolecular synthesis by coronavirus: implication for pathogenesis. J. Virol. 68, 6815-6819.

Lai, M.M.C., Cavanagh, D., 1997. The molecular biology of coronaviruses. Adv. Virus Res. 48, 1-100.

Lai, M.M.C., Holmes, K.V., 2001. Coronaviridae: The viruses and their replication, in: Knipe, D.M., Howley, P.M. (Eds.), Fields Virology, Fourth ed. Lippincott Williams & Wilkins, Philadelphia, pp. 1163-1185.

Langland, J.O., Pettiford, S., Jiang, B., Jacobs, B.L., 1994. Products of the porcine group C rotavirus NSP3 gene bind specifically to double-stranded RNA and inhibit activation of the interferon-induced protein kinase PKR. J. Virol. 68, 3821-3829.

Laude, H., 1981. Thermal inactivation studies of a coronavirus, transmissible gastroenteritis virus. J. Gen. Virol. 56, 235-240.

Laude, H., Masters, P.S., 1995. The coronavirus nucleocapsid protein, in: Siddell, S.G. (Ed.), The coronaviridae. Plenum press, New York, pp. 141-158.

Lee, A.S., 2001. The glucose-regulated proteins: stress induction and clinical applications. Trends Biochem. Sci. 26, 504-510.

Lillehaug, A., Monceyron Jonassen, C., Bergsjo, B., Hofshagen, M., Tharaldsen, J., Nesse, L.L., Handeland, K., 2005. Screening of feral pigeon (Colomba livia), mallard (Anas platyrhynchos) and graylag goose (Anser anser) populations for Campylobacter spp., Salmonella spp., avian influenza virus and avian paramyxovirus. Acta Vet Scand 46, 193-202.

Lin, R.J., Yu, H.P., Chang, B.L., Tang, W.C., Liao, C.L., Lin, Y.L., 2009. Distinct antiviral roles for human 2',5'-oligoadenylate synthetase family members against dengue virus infection. J Immunol 183, 8035-8043.

Lissenberg, A., Vrolijk, M.M., van Vliet, A.L., Langereis, M.A., de Groot-Mijnes, J.D., Rottier, P.J., de Groot, R.J., 2005. Luxury at a cost? Recombinant mouse hepatitis viruses expressing the accessory hemagglutinin esterase protein display reduced fitness in vitro. J. Virol. 79, 15054-15063.

Liu, S., Zhang, Q., Chen, J., Han, Z., Shao, Y., Kong, X., Tong, G., 2008. Identification of the avian infectious bronchitis coronaviruses with mutations in gene 3. Gene 412, 12-25.

Liu, Y., Zhang, X., 2007. Murine coronavirus-induced oligodendrocyte apoptosis is mediated through the activation of the Fas signaling pathway. Virology 360, 364-375.

Lomniczi, B., Morser, J., 1981. Polypeptides of infectious bronchitis virus. I. Polypeptides of the virion. J. Gen. Virol. 55, 155-164.

Lopp, A., Kuusksalu, A., Samuel, K., Kelve, M., 2000. Expression and activity of 2-5A synthetase in the course of differentiation and apoptosis of PC12 cells. Cytokine 12, 737-741.

Lu, X., Pan, J., Tao, J., Guo, D., 2011. SARS-CoV nucleocapsid protein antagonizes IFN-beta response by targeting initial step of IFN-beta induction pathway, and its C-terminal region is critical for the antagonism. Virus Genes 42, 37-45.

Luo, H., Chen, J., Chen, K., Shen, X., Jiang, H., 2006. Carboxyl terminus of severe acute respiratory syndrome coronavirus nucleocapsid protein: self-association analysis and nucleic acid binding characterization. Biochemistry 45, 11827-11835.

Luo, S., Baumeister, P., Yang, S., Abcouwer, S.F., Lee, A.S., 2003. Induction of Grp78/BiP by translational block: activation of the Grp78 promoter by ATF4 through

and upstream ATF/CRE site independent of the endoplasmic reticulum stress elements. J. Biol. Chem. 278, 37375-37385.
Maeda, J., Repass, J.F., Maeda, A., Makino, S., 2001. Membrane topology of coronavirus E protein. Virology 281, 163-169.
Malathi, K., Dong, B., Gale, M., Jr., Silverman, R.H., 2007. Small self-RNA generated by RNase L amplifies antiviral innate immunity. Nature 448, 816-819.
Mardani, K., Noormohammadi, A.H., Hooper, P., Ignjatovic, J., Browning, G.F., 2008. Infectious bronchitis viruses with a novel genomic organization. J Virol 82, 2013-2024.
Marie, I., Durbin, J.E., Levy, D.E., 1998. Differential viral induction of distinct interferon-alpha genes by positive feedback through interferon regulatory factor-7. EMBO J 17, 6660-6669.
Martinand, C., Montavon, C., Salehzada, T., Silhol, M., Lebleu, B., Bisbal, C., 1999. RNase L inhibitor is induced during human immunodeficiency virus type 1 infection and down regulates the 2-5A/RNase L pathway in human T cells. J Virol 73, 290-296.
Martinand, C., Salehzada, T., Silhol, M., Lebleu, B., Bisbal, C., 1998. RNase L inhibitor (RLI) antisense constructions block partially the down regulation of the 2-5A/RNase L pathway in encephalomyocarditis-virus-(EMCV)-infected cells. Eur. J. Biochem. 254, 248-255.
Masters, P.S., 1992. Localization of an RNA-binding domain in the nucleocapsid protein of the coronavirus mouse hepatitis virus. Arch. Virol. 125, 141-160.
Masters, P.S., 1999. Reverse genetics of the largest RNA viruses. Adv. Virus Res. 53, 245-264.
Masters, P.S., 2006. The molecular biology of coronaviruses. Adv. Virus Res. 66, 193-292.
Matsumoto, M., Seya, T., 2008. TLR3: interferon induction by double-stranded RNA including poly(I:C). Adv Drug Deliv Rev 60, 805-812.
Matthes, N., Mesters, J.R., Coutard, B., Canard, B., Snijder, E.J., Moll, R., Hilgenfeld, R., 2006. The non-structural protein Nsp10 of mouse hepatitis virus binds zinc ions and nucleic acids. FEBS Lett 580, 4143-4149.
Matts, R.L., Levin, D.H., London, I.M., 1983. Effect of phosphorylation of the alpha-subunit of eukaryotic initiation factor 2 on the function of reversing factor in the initiation of protein synthesis. Proc Natl Acad Sci U S A 80, 2559-2563.
Mazumder, R., Iyer, L.M., Vasudevan, S., Aravind, L., 2002. Detection of novel members, structure-function analysis and evolutionary classification of the 2H phosphoesterase superfamily. Nucleic Acids Res 30, 5229-5243.
McCarthy, R.C., Fetterhoff, T.J., 1989. Issues for quality assurance in clinical flow cytometry. Arch Pathol Lab Med 113, 658-666.
McIntosh, K., Kapikian, A.Z., Hardison, K.A., Hartley, J.W., Chanock, R.M., 1969. Antigenic relationships among the coronaviruses of man and between human and animal coronaviruses. J. Immunol. 102, 1109-1118.
Medzhitov, R., Janeway, C.A., Jr., 1997. Innate immunity: the virtues of a nonclonal system of recognition. Cell 91, 295-298.
Meier, C., Aricescu, A.R., Assenberg, R., Aplin, R.T., Gilbert, R.J., Grimes, J.M., Stuart, D.I., 2006. The crystal structure of ORF-9b, a lipid binding protein from the SARS coronavirus. Structure 14, 1157-1165.
Méndez, A., Smerdou, C., Gebauer, F., Izeta, A., Enjuanes, L., 1995. Structure and encapsidation of transmissible gastroenteritis coronavirus (TGEV) defective interfering genomes. Adv. Exp. Med. Biol. 380, 583-589.
Meurs, E., Chong, K., Galabru, J., Thomas, N.S., Kerr, I.M., Williams, B.R., Hovanessian, A.G., 1990. Molecular cloning and characterization of the human double-stranded RNA-activated protein kinase induced by interferon. Cell 62, 379-390.

Meylan, E., Curran, J., Hofmann, K., Moradpour, D., Binder, M., Bartenschlager, R., Tschopp, J., 2005. Cardif is an adaptor protein in the RIG-I antiviral pathway and is targeted by hepatitis C virus. Nature 437, 1167-1172.

Mibayashi, M., Martinez-Sobrido, L., Loo, Y.M., Cardenas, W.B., Gale, M., Jr., Garcia-Sastre, A., 2007. Inhibition of retinoic acid-inducible gene I-mediated induction of beta interferon by the NS1 protein of influenza A virus. J Virol 81, 514-524.

Mihindukulasuriya, K.A., Wu, G., St Leger, J., Nordhausen, R.W., Wang, D., 2008. Identification of a novel coronavirus from a beluga whale by using a panviral microarray. J. Virol. 82, 5084-5088.

Miknis, Z.J., Donaldson, E.F., Umland, T.C., Rimmer, R.A., Baric, R.S., Schultz, L.W., 2009. Severe acute respiratory syndrome coronavirus nsp9 dimerization is essential for efficient viral growth. J Virol 83, 3007-3018.

Minakshi, R., Padhan, K., Rani, M., Khan, N., Ahmad, F., Jameel, S., 2009. The SARS Coronavirus 3a protein causes endoplasmic reticulum stress and induces ligand-independent downregulation of the type 1 interferon receptor. PLoS One 4, e8342.

Molenkamp, R., Spaan, W.J.M., 1997. Identification of a specific interaction between the coronavirus mouse hepatitis virus A59 nucleocapsid protein and packaging signal. Virology 239, 78-86.

Moreno, J.L., Zuniga, S., Enjuanes, L., Sola, I., 2008. Identification of a coronavirus transcription enhancer. J. Virol. 82, 3882-3893.

Mounir, S., Talbot, P.J., 1993. Human coronavirus OC43 RNA-4 lacks 2 open reading frames located downstream of the S gene of bovine coronavirus. Virology 192, 355-360.

Muller, M.A., Paweska, J.T., Leman, P.A., Drosten, C., Grywna, K., Kemp, A., Braack, L., Sonnenberg, K., Niedrig, M., Swanepoel, R., 2007. Coronavirus antibodies in African bat species. Emerg. Infect. Dis. 13, 1367-1370.

Nakai, K., Horton, P., 1999. PSORT: a program for detecting sorting signals in proteins and predicting their subcellular localization. Trends Biochem. Sci. 24, 34-36.

Narayanan, K., Huang, C., Lokugamage, K., Kamitani, W., Ikegami, T., Tseng, C.T., Makino, S., 2008. Severe acute respiratory syndrome coronavirus nsp1 suppresses host gene expression, including that of type I interferon, in infected cells. J. Virol. 82, 4471-4479.

Narayanan, K., Makino, S., 2001. Cooperation of an RNA packaging signal and a viral envelope protein in coronavirus RNA Packaging. J. Virol. 75, 9059-9067.

Nelissen, K., Smeets, K., Mulder, M., Hendriks, J.J., Ameloot, M., 2010. Selection of reference genes for gene expression studies in rat oligodendrocytes using quantitative real time PCR. J Neurosci Methods 187, 78-83.

Nelson, C.A., Pekosz, A., Lee, C.A., Diamond, M.S., Fremont, D.H., 2005. Structure and intracellular targeting of the SARS-coronavirus Orf7a accessory protein. Structure 13, 75-85.

Nelson, G.W., Stohlman, S.A., Tahara, S.M., 2000. High affinity interaction between nucleocapsid protein and leader/intergenic sequence of mouse hepatitis virus RNA. J. Gen. Virol. 81, 181-188.

Neuman, B.W., Adair, B.D., Yeager, M., Buchmeier, M.J., 2008a. Purification and electron cryomicroscopy of coronavirus particles. Methods Mol Biol 454, 129-136.

Neuman, B.W., Joseph, J.S., Saikatendu, K.S., Serrano, P., Chatterjee, A., Johnson, M.A., Liao, L., Klaus, J.P., Yates, J.R., 3rd, Wuthrich, K., Stevens, R.C., Buchmeier, M.J., Kuhn, P., 2008b. Proteomics analysis unravels the functional repertoire of coronavirus nonstructural protein 3. J. Virol. 82, 5279-5294.

Nicoletti, I., Migliorati, G., Pagliacci, M.C., Grignani, F., Riccardi, C., 1991. A rapid and simple method for measuring thymocyte apoptosis by propidium iodide staining and flow cytometry. J Immunol Methods 139, 271-279.

Nilsen, T.W., Baglioni, C., 1979. Mechanism for discrimination between viral and host mRNA in interferon-treated cells. Proc Natl Acad Sci U S A 76, 2600-2604.

Nogales, A., Galan, C., Marquez-Jurado, S., Garcia-Gallo, M., Kremer, L., Enjuanes, L., Almazan, F., 2011. Immunogenic characterization and epitope mapping of transmissible gastroenteritis virus RNA dependent RNA polymerase. J Virol Methods 175, 7-13.

Notredame, C., Higgins, D.G., Heringa, J., 2000. T-Coffee: A novel method for fast and accurate multiple sequence alignment. J. Mol. Biol. 302, 205-217.

Novoa, I., Zeng, H., Harding, H.P., Ron, D., 2001. Feedback inhibition of the unfolded protein response by GADD34-mediated dephosphorylation of eIF2alpha. J. Cell Biol. 153, 1011-1022.

Novoa, I., Zhang, Y., Zeng, H., Jungreis, R., Harding, H.P., Ron, D., 2003. Stress-induced gene expression requires programmed recovery from translational repression. EMBO J. 22, 1180-1187.

O'Malley, R.P., Mariano, T.M., Siekierka, J., Mathews, M.B., 1986. A mechanism for the control of protein synthesis by adenovirus VA RNAI. Cell 44, 391-400.

Oliveros, L.B., Domeniconi, M.A., Vega, V.A., Gatica, L.V., Brigada, A.M., Gimenez, M.S., 2007. Vitamin A deficiency modifies lipid metabolism in rat liver. Br J Nutr 97, 263-272.

Oostra, M., de Haan, C.A., Rottier, P.J., 2007. The 29-nucleotide deletion present in human but not in animal severe acute respiratory syndrome coronaviruses disrupts the functional expression of open reading frame 8. J. Virol. 81, 13876-13888.

Ortego, J., Escors, D., Laude, H., Enjuanes, L., 2002. Generation of a replication-competent, propagation-deficient virus vector based on the transmissible gastroenteritis coronavirus genome. J. Virol. 76, 11518-11529.

Ortego, J., Sola, I., Almazan, F., Ceriani, J.E., Riquelme, C., Balasch, M., Plana, J., Enjuanes, L., 2003. Transmissible gastroenteritis coronavirus gene 7 is not essential but influences in vivo virus replication and virulence. Virology 308, 13-22.

Page, K.W., Britton, P., Boursnell, M.E.G., 1990. Sequence analysis of the leader RNA of two porcine coronaviruses: transmissible gastroenteritis coronavirus and porcine respiratory coronavirus. Virus Genes 4, 289-301.

Pan, J., Peng, X., Gao, Y., Li, Z., Lu, X., Chen, Y., Ishaq, M., Liu, D., Dediego, M.L., Enjuanes, L., Guo, D., 2008. Genome-wide analysis of protein-protein interactions and involvement of viral proteins in SARS-CoV replication. PLoS ONE 3, e3299.

Parquet, M.C., Nga, P.T., Nabeshima, T., Yu, F., Posadas, G., Thuy, N.T., Inoue, S., Ito, T., Ichinose, A., Gorbalenya, A.E., Snijder, E.J., Morita, K., 2008. Identification of the first insect nidovirus isolated from mosquitoes in Vietman, The XIth Internacional Nidovirus Symposium St. Catherine's College, Oxford, UK., p. 46.

Peiris, J.S., Chu, C.M., Cheng, V.C., Chan, K.S., Hung, I.F., Poon, L.L., Law, K.I., Tang, B.S., Hon, T.Y., Chan, C.S., Chan, K.H., Ng, J.S., Zheng, B.J., Ng, W.L., Lai, R.W., Guan, Y., Yuen, K.Y., 2003. Clinical progression and viral load in a community outbreak of coronavirus-associated SARS pneumonia: a prospective study. Lancet 361, 1767-1772.

Peiris, J.S., Hui, K.P., Yen, H.L., 2010. Host response to influenza virus: protection versus immunopathology. Curr Opin Immunol 22, 475-481.

Pendleton, A.R., Machamer, C.E., 2005. Infectious bronchitis virus 3a protein localizes to a novel domain of the smooth endoplasmic reticulum. J Virol 79, 6142-6151.

Pensaert, M., Van Reeth, K., 1998. Porcine epidemic diarrhea and porcine respiratory coronavirus. Proc. Ame. Ass. Swi. Pract., 433-436.

Penzes, Z., Gonzalez, J.M., Calvo, E., Izeta, A., Smerdou, C., Mendez, A., Sanchez, C.M., Sola, I., Almazan, F., Enjuanes, L., 2001. Complete genome sequence of transmissible gastroenteritis coronavirus PUR46-MAD clone and evolution of the purdue virus cluster. Virus Genes 23, 105-118.

Perlman, S., Lane, T.E., Buchmeier, M.J., 2000. Coronavirus: hepatitis, peritonitis, and central nervous system disease, in: Cunningham, M.W., Fujinami, R.S. (Eds.), Effects of microbes on the immune system. Lippincott Williams and Wilkins, Philadelphia, pp. 331-348.

Peters, G.A., Khoo, D., Mohr, I., Sen, G.C., 2002. Inhibition of PACT-mediated activation of PKR by the herpes simplex virus type 1 Us11 protein. J. Virol. 76, 11054-11064.

Pewe, L., Zhou, H., Netland, J., Tangudu, C., Olivares, H., Shi, L., Look, D., Gallagher, T., Perlman, S., 2005. A severe acute respiratory syndrome-associated coronavirus-specific protein enhances virulence of an attenuated murine coronavirus. J. Virol. 79, 11335-11342.

Pfefferle, S., Oppong, S., Drexler, J.F., Gloza-Rausch, F., Ipsen, A., Seebens, A., Muller, M.A., Annan, A., Vallo, P., Adu-Sarkodie, Y., Kruppa, T.F., Drosten, C., 2009. Distant relatives of severe acute respiratory syndrome coronavirus and close relatives of human coronavirus 229E in bats, Ghana. Emerg. Infect. Dis. 15, 1377-1384.

Pfleiderer, M., Routledge, E., Herrler, G., Siddell, S.G., 1991. High level transient expression of the murine coronavirus haemagglutinin-esterase. J Gen Virol 72 (Pt 6), 1309-1315.

Pichlmair, A., Schulz, O., Tan, C.P., Naslund, T.I., Liljestrom, P., Weber, F., Reis e Sousa, C., 2006. RIG-I-mediated antiviral responses to single-stranded RNA bearing 5'-phosphates. Science 314, 997-1001.

Piorkowska, K., Oczkowicz, M., Rozycki, M., Ropka-Molik, K., Piestrzynska-Kajtoch, A., 2011. Novel porcine housekeeping genes for real-time RT-PCR experiments normalization in adipose tissue: assessment of leptin mRNA quantity in different pig breeds. Meat Sci 87, 191-195.

Platanias, L.C., 2005. Mechanisms of type-I- and type-II-interferon-mediated signalling. Nat Rev Immunol 5, 375-386.

Player, M.R., Torrence, P.F., 1998. The 2-5A system: modulation of viral and cellular processes through acceleration of RNA degradation. Pharmacol. Ther. 78, 55-113.

Pokrovskaja, K., Panaretakis, T., Grander, D., 2005. Alternative signaling pathways regulating type I interferon-induced apoptosis. J Interferon Cytokine Res 25, 799-810.

Polyak, S.J., Tang, N., Wambach, M., Barber, G.N., Katze, M.G., 1996. The P58 cellular inhibitor complexes with the interferon-induced, double-stranded RNA-dependent protein kinase, PKR, to regulate its autophosphorylation and activity. J. Biol. Chem. 271, 1702-1707.

Poon, L.L., Chu, D.K., Chan, K.H., Wong, O.K., Ellis, T.M., Leung, Y.H., Lau, S.K., Woo, P.C., Suen, K.Y., Yuen, K.Y., Guan, Y., Peiris, J.S., 2005. Identification of a novel coronavirus in bats. J. Virol. 79, 2001-2009.

Popova, R., Zhang, X., 2002. The spike but not the hemagglutinin/esterase protein of bovine coronavirus is necessary and sufficient for viral infection. Virology 294, 222-236.

Proud, C.G., 1995. PKR: a new name and new roles. Trends Biochem. Sci. 20, 241-246.

Proud, C.G., 2005. eIF2 and the control of cell physiology. Semin. Cell Dev. Biol. 16, 3-12.

Puntervoll, P., Linding, R., Gemund, C., Chabanis-Davidson, S., Mattingsdal, M., Cameron, S., Martin, D.M., Ausiello, G., Brannetti, B., Costantini, A., Ferre, F., Maselli, V., Via, A., Cesareni, G., Diella, F., Superti-Furga, G., Wyrwicz, L., Ramu, C., McGuigan, C., Gudavalli, R., Letunic, I., Bork, P., Rychlewski, L., Kuster, B., Helmer-Citterich, M., Hunter, W.N., Aasland, R., Gibson, T.J., 2003. ELM server: A new resource for investigating short functional sites in modular eukaryotic proteins. Nucleic Acids Res. 31, 3625-3630.

Raaben, M., Koerkamp, M.J., Rottier, P.J., de Haan, C.A., 2007. Mouse hepatitis coronavirus replication induces host translational shutoff and mRNA decay, with concomitant formation of stress granules and processing bodies. Cell Microbiol. 9, 2218-2229.

Raamsman, M.J.B., Locker, J.K., de Hooge, A., de Vries, A.A.F., Griffiths, G., Vennema, H., Rottier, P.J.M., 2000. Characterization of the coronavirus mouse hepatitis virus strain A59 small membrane protein E. J. Virol. 74, 2333-2342.

Ribes, J.M., Ortego, J., Ceriani, J., Montava, R., Enjuanes, L., Buesa, J., 2011. Transmissible gastroenteritis virus (TGEV)-based vectors with engineered murine tropism express the rotavirus VP7 protein and immunize mice against rotavirus. Virology 410, 107-118.

Rivas, C., Gil, J., Melkova, Z., Esteban, M., Diaz-Guerra, M., 1998. Vaccinia virus E3L protein is an inhibitor of the interferon (i.f.n.)-induced 2-5A synthetase enzyme. Virology 243, 406-414.

Rivera, J., Abrams, C., Hernaez, B., Alcazar, A., Escribano, J.M., Dixon, L., Alonso, C., 2007. The MyD116 African swine fever virus homologue interacts with the catalytic subunit of protein phosphatase 1 and activates its phosphatase activity. J. Virol. 81, 2923-2929.

Robertson, J.D., Gogvadze, V., Zhivotovsky, B., Orrenius, S., 2000. Distinct pathways for stimulation of cytochrome c release by etoposide. J Biol Chem 275, 32438-32443.

Romano, P.R., Zhang, F., Tan, S.L., Garcia-Barrio, M.T., Katze, M.G., Dever, T.E., Hinnebusch, A.G., 1998. Inhibition of double-stranded RNA-dependent protein kinase PKR by vaccinia virus E3: role of complex formation and the E3 N-terminal domain. Mol. Cell Biol. 18, 7304-7316.

Rost, B., Yachdav, G., Liu, J., 2004. The PredictProtein server. Nucleic. Acids Res. 32, W321-W326.

Rota, P.A., Oberste, M.S., Monroe, S.S., Nix, W.A., Campganoli, R., Icenogle, J.P., Peñaranda, S., Bankamp, B., Maher, K., Chen, M.-H., Tong, S., Tamin, A., Lowe, L., Frace, M., DeRisi, J.L., Chen, Q., Wang, D., Erdman, D.d., Peret, T.C.T., Burns, C., Ksiazek, T.G., Rollin, P.E., Sanchez, A., Liffick, S., Holloway, B., Limor, J., McCaustland, K., Olsen-Rassmussen, M., Fouchier, R., Gunther, S., Osterhaus, A.D.M.E., Drosten, C., Pallansch, M.A., Anderson, L.J., Bellini, W.J., 2003. Characterization of a novel coronavirus associated with severe acute respiratory syndrome. Science 300, 1394-1399.

Roth-Cross, J.K., Stokes, H., Chang, G., Chua, M.M., Thiel, V., Weiss, S.R., Gorbalenya, A.E., Siddell, S.G., 2009. Organ-specific attenuation of murine hepatitis virus strain A59 by replacement of catalytic residues in the putative viral cyclic phosphodiesterase ns2. J Virol 83, 3743-3753.

Rouse, B.T., Sehrawat, S., 2010. Immunity and immunopathology to viruses: what decides the outcome? Nat Rev Immunol 10, 514-526.

Saif, L.J., Wesley, R.D., 1992. Transmissible gastroenteritis, in: Leman, A.D., Straw, B.E., Mengeling, W.L., D'Allaire, S., Taylor, D.J. (Eds.), Diseases of Swine, 7th ed. Wolfe Publishing Ltd, Ames. Iowa, pp. 362-386.

Salanueva, I.J., Carrascosa, J.L., Risco, C., 1999. Structural maturation of the transmissible gastroenteritis coronavirus. J. Virol. 73, 7952-7964.

Sambrook, J., Russell, D.W., 2001. Molecular cloning: A laboratory manual, 3rd ed. Cold Spring Harbor Laboratory Press, Cold Spring Harbor, New York.

Samuel, C.E., 1979. Mechanism of interferon action: phosphorylation of protein synthesis initiation factor eIF-2 in interferon-treated human cells by a ribosome-associated kinase processing site specificity similar to hemin-regulated rabbit reticulocyte kinase. Proc Natl Acad Sci U S A 76, 600-604.

Samuel, C.E., 1993. The eIF-2 alpha protein kinases, regulators of translation in eukaryotes from yeasts to humans. J Biol Chem 268, 7603-7606.

Samuel, C.E., 2001. Antiviral actions of interferons. Clin. Microbiol. Rev. 14, 778-809.

Sanchez, C.M., Gebauer, F., Suñe, C., Mendez, A., Dopazo, J., Enjuanes, L., 1992. Genetic evolution and tropism of transmissible gastroenteritis coronaviruses. Virology 190, 92-105.

Sanchez, C.M., Izeta, A., Sánchez-Morgado, J.M., Alonso, S., Sola, I., Balasch, M., Plana-Duran, J., Enjuanes, L., 1999. Targeted recombination demonstrates that the spike gene of transmissible gastroenteritis coronavirus is a determinant of its enteric tropism and virulence. J. Virol. 73, 7607-7618.

Sanchez, C.M., Jiménez, G., Laviada, M.D., Correa, I., Suñe, C., Bullido, M.J., Gebauer, F., Smerdou, C., Callebaut, P., Escribano, J.M., Enjuanes, L., 1990. Antigenic homology among coronaviruses related to transmissible gastroenteritis virus. Virology 174, 410-417.

Sarkar, S.N., Sen, G.C., 2004. Novel functions of proteins encoded by viral stress-inducible genes. Pharmacol Ther 103, 245-259.

Sasaki, D.T., Dumas, S.E., Engleman, E.G., 1987. Discrimination of viable and non-viable cells using propidium iodide in two color immunofluorescence. Cytometry 8, 413-420.

Saunders, L.R., Barber, G.N., 2003. The dsRNA binding protein family: critical roles, diverse cellular functions. FASEB J 17, 961-983.

Sawicki, D.L., Wang, T., Sawicki, S.G., 2001. The RNA structures engaged in replication and transcription of the A59 strain of mouse hepatitis virus. J. Gen. Virol. 82, 386-396.

Sawicki, S.G., Sawicki, D.L., 1990. Coronavirus transcription: subgenomic mouse hepatitis virus replicative intermediates function in RNA synthesis. J. Virol. 64, 1050-1056.

Sawicki, S.G., Sawicki, D.L., Siddell, S.G., 2007. A contemporary view of coronavirus transcription. J. Virol. 81, 20-29.

Schaecher, S.R., Mackenzie, J.M., Pekosz, A., 2007. The ORF7b protein of SARS-CoV is expressed in virus-infected cells and incorporated into SARS-CoV particles. J. Virol. 81, 718-731.

Schelle, B., Karl, N., Ludewig, B., Siddell, S.G., Thiel, V., 2005. Selective replication of coronavirus genomes that express nucleocapsid protein. J. Virol. 79, 6620-6630.

Scherbik, S.V., Paranjape, J.M., Stockman, B.M., Silverman, R.H., Brinton, M.A., 2006. RNase L plays a role in the antiviral response to West Nile virus. J. Virol. 80, 2987-2999.

Schillace, R.V., Voltz, J.W., Sim, A.T., Shenolikar, S., Scott, J.D., 2001. Multiple interactions within the AKAP220 signaling complex contribute to protein phosphatase 1 regulation. J Biol Chem 276, 12128-12134.

Schlee, M., Roth, A., Hornung, V., Hagmann, C.A., Wimmenauer, V., Barchet, W., Coch, C., Janke, M., Mihailovic, A., Wardle, G., Juranek, S., Kato, H., Kawai, T., Poeck, H., Fitzgerald, K.A., Takeuchi, O., Akira, S., Tuschl, T., Latz, E., Ludwig, J., Hartmann,

G., 2009. Recognition of 5' triphosphate by RIG-I helicase requires short blunt double-stranded RNA as contained in panhandle of negative-strand virus. Immunity 31, 25-34.

Schmidt, A., Schwerd, T., Hamm, W., Hellmuth, J.C., Cui, S., Wenzel, M., Hoffmann, F.S., Michallet, M.C., Besch, R., Hopfner, K.P., Endres, S., Rothenfusser, S., 2009. 5'-triphosphate RNA requires base-paired structures to activate antiviral signaling via RIG-I. Proc Natl Acad Sci U S A 106, 12067-12072.

Schneider, R.J., Mohr, I., 2003. Translation initiation and viral tricks. Trends Biochem. Sci. 28, 130-136.

Schroder, M., Kaufman, R.J., 2005. The mammalian unfolded protein response. Annu. Rev. Biochem. 74, 739-789.

Schwartz, T., Fu, L., Lavi, E., 2002. Differential induction of apoptosis in demyelinating and nondemyelinating infection by mouse hepatitis virus. J. Neurovirol. 8, 392-399.

Sharp, T.V., Schwemmle, M., Jeffrey, I., Laing, K., Mellor, H., Proud, C.G., Hilse, K., Clemens, M.J., 1993. Comparative analysis of the regulation of the interferon-inducible protein kinase PKR by Epstein-Barr virus RNAs EBER-1 and EBER-2 and adenovirus VAI RNA. Nucleic Acids Res. 21, 4483-4490.

Shen, S., Wen, Z.L., Liu, D.X., 2003. Emergence of a coronavirus infectious bronchitis virus mutant with a truncated 3b gene: functional characterization of the 3b protein in pathogenesis and replication. Virology 311, 16-27.

Sheppard, P., Kindsvogel, W., Xu, W., Henderson, K., Schlutsmeyer, S., Whitmore, T.E., Kuestner, R., Garrigues, U., Birks, C., Roraback, J., Ostrander, C., Dong, D., Shin, J., Presnell, S., Fox, B., Haldeman, B., Cooper, E., Taft, D., Gilbert, T., Grant, F.J., Tackett, M., Krivan, W., McKnight, G., Clegg, C., Foster, D., Klucher, K.M., 2003. IL-28, IL-29 and their class II cytokine receptor IL-28R. Nat Immunol 4, 63-68.

Shi, Y., Vattem, K.M., Sood, R., An, J., Liang, J., Stramm, L., Wek, R.C., 1998. Identification and characterization of pancreatic eukaryotic initiation factor 2 alpha-subunit kinase, PEK, involved in translational control. Mol. Cell Biol. 18, 7499-7509.

Siddell, S.G., Sawicki, D., Meyer, Y., Thiel, V., Sawicki, S., 2001. Identification of the mutations responsible for the phenotype of three MHV RNA-negative ts mutants. Adv. Exp. Med. Biol. 494, 453-458.

Silverman, R.H., 1985. Functional analysis of 2-5A-dependent RNase and 2-5a using 2',5'-oligoadenylate-cellulose. Anal. Biochem. 144, 450-460.

Silverman, R.H., 2007. Viral encounters with 2',5'-oligoadenylate synthetase and RNase L during the interferon antiviral response. J. Virol. 81, 12720-12729.

Sirinarumitr, T., Kluge, J.P., Paul, P.S., 1998. Transmissible gastroenteritis virus induced apoptosis in swine testes cell cultures. Arch. Virol. 143, 2471-2485.

Sittidilokratna, N., Hodgson, R.A., Cowley, J.A., Jitrapakdee, S., Boonsaeng, V., Panyim, S., Walker, P.J., 2002. Complete ORF1b-gene sequence indicates yellow head virus is an invertebrate nidovirus. Dis Aquat Organ 50, 87-93.

Smyth, G.K., 2004. Linear models and empirical bayes methods for assessing differential expression in microarray experiments. Stat. Appl. Genet. Mol. Biol. 3, Article3.

Snijder, E.J., Bredenbeek, P.J., Dobbe, J.C., Thiel, V., Ziebuhr, J., Poon, L.L.M., Guan, Y., Rozanov, M., Spaan, W.J.M., Gorbalenya, A.E., 2003. Unique and conserved features of genome and proteome of SARS-coronavirus, an early split-off from the coronavirus group 2 lineage. J. Mol. Biol. 331, 991-1004.

Snijder, E.J., van der Meer, Y., Zevenhoven-Dobbe, J., Onderwater, J.J., van der Meulen, J., Koerten, H.K., Mommaas, A.M., 2006. Ultrastructure and origin of membrane vesicles associated with the severe acute respiratory syndrome coronavirus replication complex. J. Virol. 80, 5927-5940.

Sola, I., Alonso, S., Zúñiga, S., Balach, M., Plana-Durán, J., Enjuanes, L., 2003. Engineering transmissible gastroenteritis virus genome as an expression vector inducing latogenic immunity. J. Virol. 77, 4357-4369.

Sola, I., Galan, C., Mateos-Gomez, P.A., Palacio, L., Zuniga, S., Cruz, J.L., Almazan, F., Enjuanes, L., 2011. The polypyrimidine tract-binding protein affects coronavirus RNA accumulation levels and relocalizes viral RNAs to novel cytoplasmic domains different from replication-transcription sites. J Virol 85, 5136-5149.

Sola, I., Moreno, J.L., Zuñiga, S., Alonso, S., Enjuanes, L., 2005. Role of nucleotides immediately flanking the transcription-regulating sequence core in coronavirus subgenomic mRNA synthesis. J. Virol. 79, 2506-2516.

Song, H.C., Seo, M.Y., Stadler, K., Yoo, B.J., Choo, Q.L., Coates, S.R., Uematsu, Y., Harada, T., Greer, C.E., Polo, J.M., Pileri, P., Eickmann, M., Rappuoli, R., Abrignani, S., Houghton, M., Han, J.H., 2004. Synthesis and characterization of a native, oligomeric form of recombinant severe acute respiratory syndrome coronavirus spike glycoprotein. J. Virol. 78, 10328-10335.

Sperry, S.M., Kazi, L., Graham, R.L., Baric, R.S., Weiss, S.R., Denison, M.R., 2005. Single-amino-acid substitutions in open reading frame (ORF) 1b-nsp14 and ORF 2a proteins of the coronavirus mouse hepatitis virus are attenuating in mice. J. Virol. 79, 3391-3400.

St-Jean, J.R., Desforges, M., Almazan, F., Jacomy, H., Enjuanes, L., Talbot, P.J., 2006. Recovery of a neurovirulent human coronavirus OC43 from an infectious cDNA clone. J. Virol. 80, 3670-3674.

Stark, G.R., Kerr, I.M., Williams, B.R., Silverman, R.H., Schreiber, R.D., 1998. How cells respond to interferons. Annu. Rev. Biochem. 67, 227-264.

Stohlman, S.A., Lai, M.M., 1979. Phosphoproteins of murine hepatitis viruses. J. Virol. 32, 672-675.

Strieter, R.M., Belperio, J.A., Keane, M.P., 2002. Cytokines in innate host defense in the lung. J Clin Invest 109, 699-705.

Sturman, L.S., Holmes, K.V., Behnke, J., 1980. Isolation of coronavirus envelope glycoproteins and interaction with the viral nucleocapsid. J. Virol. 33, 449-462.

Sturman, L.S., V., H.K., 1977. Characterization of a coronavirus. II. Glycoproteins of the viral envelope: tryptic peptide analysis. Virology 77, 650-660.

Su, A.I., Pezacki, J.P., Wodicka, L., Brideau, A.D., Supekova, L., Thimme, R., Wieland, S., Bukh, J., Purcell, R.H., Schultz, P.G., Chisari, F.V., 2002. Genomic analysis of the host response to hepatitis C virus infection. Proc. Natl. Acad. Sci. USA 99, 15669-15674.

Sumpter, R., Jr., Loo, Y.M., Foy, E., Li, K., Yoneyama, M., Fujita, T., Lemon, S.M., Gale, M., Jr., 2005. Regulating intracellular antiviral defense and permissiveness to hepatitis C virus RNA replication through a cellular RNA helicase, RIG-I. J. Virol. 79, 2689-2699.

Sutton, G., Fry, E., Carter, L., Sainsbury, S., Walter, T., Nettleship, J., Berrow, N., Owens, R., Gilbert, R., Davidson, A., Siddell, S., Poon, L.L., Diprose, J., Alderton, D., Walsh, M., Grimes, J.M., Stuart, D.I., 2004. The nsp9 replicase protein of SARS-coronavirus, structure and functional insights. Structure 12, 341-353.

Takaoka, A., Yanai, H., 2006. Interferon signalling network in innate defence. Cell Microbiol 8, 907-922.

Takeuchi, O., Akira, S., 2008. MDA5/RIG-I and virus recognition. Curr Opin Immunol 20, 17-22.

Taylor, D.R., Shi, S.T., Romano, P.R., Barber, G.N., Lai, M.M., 1999. Inhibition of the interferon-inducible protein kinase PKR by HCV E2 protein. Science 285, 107-110.

Taylor, S.S., Haste, N.M., Ghosh, G., 2005. PKR and eIF2alpha: integration of kinase dimerization, activation, and substrate docking. Cell 122, 823-825.

te Velthuis, A.J., Arnold, J.J., Cameron, C.E., van den Worm, S.H., Snijder, E.J., 2010. The RNA polymerase activity of SARS-coronavirus nsp12 is primer dependent. Nucleic Acids Res 38, 203-214.

Theron, M., Huang, K.J., Chen, Y.W., Liu, C.C., Lei, H.Y., 2005. A probable role for IFN-gamma in the development of a lung immunopathology in SARS. Cytokine 32, 30-38.

Thiel, V., Ivanov, K.A., Putics, A., Hertzig, T., Schelle, B., Bayer, S., Wessbrich, B., Snijder, E.J., Rabenau, H., Doerr, H.W., Gorbalenya, A.E., Ziebuhr, J., 2003. Mechanisms and enzymes involved in SARS coronavirus genome expression. J. Gen. Virol. 84, 2305-2315.

Thompson, A.J., Locarnini, S.A., 2007. Toll-like receptors, RIG-I-like RNA helicases and the antiviral innate immune response. Immunol Cell Biol 85, 435-445.

Thyrell, L., Hjortsberg, L., Arulampalam, V., Panaretakis, T., Uhles, S., Dagnell, M., Zhivotovsky, B., Leibiger, I., Grander, D., Pokrovskaja, K., 2004. Interferon alpha-induced apoptosis in tumor cells is mediated through the phosphoinositide 3-kinase/mammalian target of rapamycin signaling pathway. J Biol Chem 279, 24152-24162.

Tohya, Y., Narayanan, K., Kamitani, W., Huang, C., Lokugamage, K., Makino, S., 2009. Suppression of host gene expression by nsp1 proteins of group 2 bat coronaviruses. J. Virol. 83, 5282-5288.

Torres, J., Parthasarathy, K., Lin, X., Saravanan, R., Liu, D.X., 2006. Model of a putative pore: the pentameric alpha-helical bundle of SARS coronavirus E protein in lipid bilayers. Biophys. J. 91, 938-947.

Traggiai, E., Becker, S., Subbarao, K., Kolesnikova, L., Uematsu, Y., Gismondo, M.R., Murphy, B.R., Rappuoli, R., Lanzavecchia, A., 2004. An efficient method to make human monoclonal antibodies from memory B cells: potent neutralization of SARS coronavirus. Nat. Med. 10, 871-875.

Tsai, S., Cassady, J.P., Freking, B.A., Nonneman, D.J., Rohrer, G.A., Piedrahita, J.A., 2006. Annotation of the Affymetrix porcine genome microarray. Anim Genet 37, 423-424.

Tung, F.Y.T., Abraham, S., Sethna, M., Hung, S.L., Sethna, P., Hogue, B.G., Brian, D.A., 1992. The 9-kDa hydrophobic protein encoded at the 3' end of the porcine transmissible gastroenteritis coronavirus genome is membrane-associated. Virology 186, 676-683.

Uenishi, H., Shinkai, H., 2009. Porcine Toll-like receptors: the front line of pathogen monitoring and possible implications for disease resistance. Dev Comp Immunol 33, 353-361.

Uze, G., Lutfalla, G., Gresser, I., 1990. Genetic transfer of a functional human interferon alpha receptor into mouse cells: cloning and expression of its cDNA. Cell 60, 225-234.

van der Hoek, L., Pyrc, K., Jebbink, M.F., Vermeulen-Oost, W., Berkhout, R.J., Wolthers, K.C., Wertheim-van Dillen, P.M., Kaandorp, J., Spaargaren, J., Berkhout, B., 2004. Identification of a new human coronavirus. Nat. Med. 10, 368-373.

van Engeland, M., Ramaekers, F.C., Schutte, B., Reutelingsperger, C.P., 1996. A novel assay to measure loss of plasma membrane asymmetry during apoptosis of adherent cells in culture. Cytometry 24, 131-139.

Vaughn, R.M., Halbur, P.G., Paul, P.S., 1995. Sequence comparison of porcine respiratory coronaviruses isolates reveals heterogeneity in the S, 3, and 3-1 genes. J. Virol. 69, 3176-3184.

Verheije, M.H., Hagemeijer, M.C., Ulasli, M., Reggiori, F., Rottier, P.J., Masters, P.S., de Haan, C.A., 2010. The coronavirus nucleocapsid protein is dynamically associated with the replication-transcription complexes. J Virol 84, 11575-11579.

Vermes, I., Haanen, C., Steffens-Nakken, H., Reutelingsperger, C., 1995. A novel assay for apoptosis. Flow cytometric detection of phosphatidylserine expression on early apoptotic cells using fluorescein labelled Annexin V. J Immunol Methods 184, 39-51.

Vijaykrishna, D., Smith, G.J., Zhang, J.X., Peiris, J.S., Chen, H., Guan, Y., 2007. Evolutionary insights into the ecology of coronaviruses. J. Virol. 81, 4012-4020.

von Brunn, A., Teepe, C., Simpson, J.C., Pepperkok, R., Friedel, C.C., Zimmer, R., Roberts, R., Baric, R., Haas, J., 2007. Analysis of Intraviral Protein-Protein Interactions of the SARS Coronavirus ORFeome. PLoS ONE 2, 1-11.

Walsh, K.B., Teijaro, J.R., Wilker, P.R., Jatzek, A., Fremgen, D.M., Das, S.C., Watanabe, T., Hatta, M., Shinya, K., Suresh, M., Kawaoka, Y., Rosen, H., Oldstone, M.B., 2011. Suppression of cytokine storm with a sphingosine analog provides protection against pathogenic influenza virus. Proc Natl Acad Sci U S A 108, 12018-12023.

Wang, G., Chen, G., Zheng, D., Cheng, G., Tang, H., 2011. PLP2 of mouse hepatitis virus A59 (MHV-A59) targets TBK1 to negatively regulate cellular type I interferon signaling pathway. PLoS One 6, e17192.

Wang, K., Boysen, C., Shizuya, H., Simon, M.I., Hood, L., 1997. Complete nucleotide sequence of two generations of a bacterial artificial chromosome cloning vector. BioTechniques 23, 992-994.

Wang, X., Liao, Y., Yap, P.L., Png, K.J., Tam, J.P., Liu, D.X., 2009. Inhibition of protein kinase R activation and upregulation of GADD34 expression play a synergistic role in facilitating coronavirus replication by maintaining de novo protein synthesis in virus-infected cells. J. Virol. 83, 12462-12472.

Warke, R.V., Xhaja, K., Martin, K.J., Fournier, M.F., Shaw, S.K., Brizuela, N., de Bosch, N., Lapointe, D., Ennis, F.A., Rothman, A.L., Bosch, I., 2003. Dengue virus induces novel changes in gene expression of human umbilical vein endothelial cells. J. Virol. 77, 11822-11832.

Wathelet, M.G., Orr, M., Frieman, M.B., Baric, R.S., 2007. Severe acute respiratory syndrome coronavirus evades antiviral signaling: role of nsp1 and rational design of an attenuated strain. J. Virol. 81, 11620-11633.

Watson, J.C., Chang, H.W., Jacobs, B.L., 1991. Characterization of a vaccinia virus-encoded double-stranded RNA-binding protein that may be involved in inhibition of the double-stranded RNA-dependent protein kinase. Virology 185, 206-216.

Wei, L., Sun, S., Xu, C.H., Zhang, J., Xu, Y., Zhu, H., Peh, S.C., Korteweg, C., McNutt, M.A., Gu, J., 2007. Pathology of the thyroid in severe acute respiratory syndrome. Hum. Pathol. 38, 95-102.

Weiss, S.R., Zoltick, P.W., Leibowitz, J.L., 1993. The ns 4 gene of mouse hepatitis virus (MHV), strain A-59 contains 2 ORFs and thus differs from ns 4 of the JHM and S strains. Arch. Virol. 129, 301-309.

Williams, B.R., 2001. Signal integration via PKR. Sci STKE 2001, re2.

Wilson, L., Gage, P., Ewart, G., 2006. Validation of coronavirus E proteins ion channels as targets for antiviral drugs, in: Perlman, S., Holmes, K. (Eds.), The Nidovirus: Towards control of SARS and other nidovirus diseases. Springer, New York, pp. 573-578.

Woo, P.C., Lau, S.K., Chu, C.M., Chan, K.H., Tsoi, H.W., Huang, Y., Wong, B.H., Poon, R.W., Cai, J.J., Luk, W.K., Poon, L.L., Wong, S.S., Guan, Y., Peiris, J.S., Yuen, K.Y., 2005a. Characterization and complete genome sequence of a novel coronavirus, coronavirus HKU1, from patients with pneumonia. J. Virol. 79, 884-895.

Woo, P.C., Lau, S.K., Tsoi, H.W., Huang, Y., Poon, R.W., Chu, C.M., Lee, R.A., Luk, W.K., Wong, G.K., Wong, B.H., Cheng, V.C., Tang, B.S., Wu, A.K., Yung, R.W., Chen, H., Guan, Y., Chan, K.H., Yuen, K.Y., 2005b. Clinical and molecular epidemiological features of coronavirus HKU1-associated community-acquired pneumonia. J. Infect. Dis. 192, 1898-1907.

Woo, P.C., Wang, M., Lau, S.K., Xu, H., Poon, R.W., Guo, R., Wong, B.H., Gao, K., Tsoi, H.W., Huang, Y., Li, K.S., Lam, C.S., Chan, K.H., Zheng, B.J., Yuen, K.Y., 2007. Comparative analysis of twelve genomes of three novel group 2c and group 2d coronaviruses reveals unique group and subgroup features. J. Virol. 81, 1574-1585.

Woods, R.D., Wesley, R.D., 1998. Transmissible gastroenteritis coronavirus carrier sow. Adv. Exp. Med. Biol. 440, 641-648.

Xu, K., Zheng, B.J., Zeng, R., Lu, W., Lin, Y.P., Xue, L., Li, L., Yang, L.L., Xu, C., Dai, J., Wang, F., Li, Q., Dong, Q.X., Yang, R.F., Wu, J.R., Sun, B., 2009. Severe acute respiratory syndrome coronavirus accessory protein 9b is a virion-associated protein. Virology 388, 279-285.

Xu, L.G., Wang, Y.Y., Han, K.J., Li, L.Y., Zhai, Z., Shu, H.B., 2005. VISA is an adapter protein required for virus-triggered IFN-beta signaling. Mol Cell 19, 727-740.

Yanase, N., Ohshima, K., Ikegami, H., Mizuguchi, J., 2000. Cytochrome c release, mitochondrial membrane depolarization, caspase-3 activation, and Bax-alpha cleavage during IFN-alpha-induced apoptosis in Daudi B lymphoma cells. J Interferon Cytokine Res 20, 1121-1129.

Ye, Y., Hauns, K., Langland, J.O., Jacobs, B.L., Hogue, B.G., 2007. Mouse hepatitis coronavirus A59 nucleocapsid protein is a type I interferon antagonist. J. Virol. 81, 2554-2563.

Ye, Z., Wong, C.K., Li, P., Xie, Y., 2008. A SARS-CoV protein, ORF-6, induces caspase-3 mediated, ER stress and JNK-dependent apoptosis. Biochim. Biophys. Acta 1780, 1383-1387.

Yokomori, K., Lai, M.M.C., 1991. Mouse hepatitis virus S RNA sequence reveals that nonstructural proteins NS 4 and NS 5a are not essential for murine coronavirus replication. J. Virol. 65, 5605-5608.

Yoneyama, M., Kikuchi, M., Matsumoto, K., Imaizumi, T., Miyagishi, M., Taira, K., Foy, E., Loo, Y.M., Gale, M., Jr., Akira, S., Yonehara, S., Kato, A., Fujita, T., 2005. Shared and unique functions of the DExD/H-box helicases RIG-I, MDA5, and LGP2 in antiviral innate immunity. J Immunol 175, 2851-2858.

Yoneyama, M., Kikuchi, M., Natsukawa, T., Shinobu, N., Imaizumi, T., Miyagishi, M., Taira, K., Akira, S., Fujita, T., 2004. The RNA helicase RIG-I has an essential function in double-stranded RNA-induced innate antiviral responses. Nat. Immunol. 5, 730-737.

Youn, S., Leibowitz, J.L., Collisson, E.W., 2005. In vitro assembled, recombinant infectious bronchitis viruses demonstrate that the 5a open reading frame is not essential for replication. Virology 332, 206-215.

Young, H.A., 1996. Regulation of interferon-gamma gene expression. J Interferon Cytokine Res 16, 563-568.

Yount, B., Curtis, K.M., Baric, R.S., 2000. Strategy for systematic assembly of large RNA and DNA genomes: the transmissible gastroenteritis virus model. J. Virol. 74, 10600-10611.

Yount, B., Roberts, R.S., Sims, A.C., Deming, D., Frieman, M.B., Sparks, J., Denison, M.R., Davis, N., Baric, R.S., 2005. Severe acute respiratory syndrome coronavirus group-specific open reading frames encode nonessential functions for replication in cell cultures and mice. J. Virol. 79, 14909-14922.

Yu, I.M., Gustafson, C.L., Diao, J., Burgner, J.W., 2nd, Li, Z., Zhang, J., Chen, J., 2005. Recombinant severe acute respiratory syndrome (SARS) coronavirus nucleocapsid protein forms a dimer through its C-terminal domain. J. Biol. Chem. 280, 23280-23286.

Yuan, X., Shan, Y., Zhao, Z., Chen, J., Cong, Y., 2005. G0/G1 arrest and apoptosis induced by SARS-CoV 3b protein in transfected cells. Virol. J. 2, 66.

Yuan, X., Wu, J., Shan, Y., Yao, Z., Dong, B., Chen, B., Zhao, Z., Wang, S., Chen, J., Cong, Y., 2006. SARS coronavirus 7a protein blocks cell cycle progression at G0/G1 phase via the cyclin D3/pRb pathway. Virology 346, 74-85.

Zakhartchouk, A.N., Viswanathan, S., Mahony, J.B., Gauldie, J., Babiuk, L.A., 2005. Severe acute respiratory syndrome coronavirus nucleocapsid protein expressed by an adenovirus vector is phosphorylated and immunogenic in mice. J. Gen. Virol. 86, 211-215.

Zampieri, C.A., Sullivan, N.J., Nabel, G.J., 2007. Immunopathology of highly virulent pathogens: insights from Ebola virus. Nat Immunol 8, 1159-1164.

Zampieri, M., Ciccarone, F., Guastafierro, T., Bacalini, M.G., Calabrese, R., Moreno-Villanueva, M., Reale, A., Chevanne, M., Burkle, A., Caiafa, P., 2010. Validation of suitable internal control genes for expression studies in aging. Mech Ageing Dev 131, 89-95.

Zeng, R., Yang, R.F., Shi, M.D., Jiang, M.R., Xie, Y.H., Ruan, H.Q., Jiang, X.S., Shi, L., Zhou, H., Zhang, L., Wu, X.D., Lin, Y., Ji, Y.Y., Xiong, L., Jin, Y., Dai, E.H., Wang, X.Y., Si, B.Y., Wang, J., Wang, H.X., Wang, C.E., Gan, Y.H., Li, Y.C., Cao, J.T., Zuo, J.P., Shan, S.F., Xie, E., Chen, S.H., Jiang, Z.Q., Zhang, X., Wang, Y., Pei, G., Sun, B., Wu, J.R., 2004. Characterization of the 3a protein of SARS-associated coronavirus in infected vero E6 cells and SARS patients. J. Mol. Biol. 341, 271-279.

Zhai, Y., Sun, F., Li, X., Pang, H., Xu, X., Bartlam, M., Rao, Z., 2005. Insights into SARS-CoV transcription and replication from the structure of the nsp7-nsp8 hexadecamer. Nat Struct Mol Biol 12, 980-986.

Zhang, L., Zhang, F., Yu, W., He, T., Yu, J., Yi, C.E., Ba, L., Li, W., Farzan, M., Chen, Z., Yuen, K.Y., Ho, D., 2006. Antibody responses against SARS coronavirus are correlated with disease outcome of infected individuals. J. Med. Virol. 78, 1-8.

Zhang, Q.L., Ding, Y.Q., He, L., Wang, W., Zhang, J.H., Wang, H.J., Cai, J.J., Geng, J., Lu, Y.D., Luo, Y.L., 2003. Detection of cell apoptosis in the pathological tissues of patients with SARS and its significance. Di Yi Jun Yi Da Xue Xue Bao 23, 770-773.

Zhao, J., Falcon, A., Zhou, H., Netland, J., Enjuanes, L., Perez Brena, P., Perlman, S., 2009. Severe acute respiratory syndrome coronavirus protein 6 is required for optimal replication. J Virol 83, 2368-2373.

Zhao, L., Rose, K.M., Elliott, R., Van Rooijen, N., Weiss, S.R., 2011. Cell type-specific type I interferon antagonism influences organ tropism of murine coronavirus. J Virol.

Zhou, A., Paranjape, J., Brown, T.L., Nie, H., Naik, S., Dong, B., Chang, A., Trapp, B., Fairchild, R., Colmenares, C., Silverman, R.H., 1997. Interferon action and apoptosis are defective in mice devoid of 2',5'-oligoadenylate-dependent RNase L. EMBO J 16, 6355-6363.

Zhou, M., Williams, A.K., Chung, S.I., Wang, L., Collisson, E.W., 1996. The infectious bronchitis virus nucleocapsid protein binds RNA sequences in the 3' terminus of the genome. Virology 217, 191-199.

Zhu, S., Sobolev, A.Y., Wek, R.C., 1996. Histidyl-tRNA synthetase-related sequences in GCN2 protein kinase regulate in vitro phosphorylation of eIF-2. J Biol Chem 271, 24989-24994.

Ziebuhr, J., 2005. The coronavirus replicase, in: Enjuanes, L. (Ed.), Coronavirus replication and reverse genetics. Springer-Verlag, Berlin Heidelberg, Germany, pp. 57-94.

Ziebuhr, J., Snijder, E.J., Gorbalenya, A.E., 2000. Virus-encoded proteinases and proteolytic processing in the *Nidovirales*. J. Gen. Virol. 81, 853-879.

Zirkel, F., Kurth, A., Quan, P.L., Briese, T., Ellerbrok, H., Pauli, G., Leendertz, F.H., Lipkin, W.I., Ziebuhr, J., Drosten, C., Junglen, S., 2011. An insect nidovirus emerging from a primary tropical rainforest. MBio 2.

Zuñiga, S., Cruz, J.L., Sola, I., Mateos-Gomez, P.A., Palacio, L., Enjuanes, L., 2010. Coronavirus nucleocapsid protein facilitates template switching and is required for efficient transcription. J. Virol. 84, 2169-2175.

Zuñiga, S., Sola, I., Alonso, S., Enjuanes, L., 2004. Sequence motifs involved in the regulation of discontinuous coronavirus subgenomic RNA synthesis. J. Virol. 78, 980-994.

Zuñiga, S., Sola, I., Cruz, J.L., Enjuanes, L., 2009. Role of RNA chaperones in virus replication. Virus Res. 139, 253-266.

Zuñiga, S., Sola, I., Moreno, J.L., Sabella, P., Plana-Duran, J., Enjuanes, L., 2007. Coronavirus nucleocapsid protein is an RNA chaperone. Virology 357, 215-227.

Zust, R., Cervantes-Barragan, L., Habjan, M., Maier, R., Neuman, B.W., Ziebuhr, J., Szretter, K.J., Baker, S.C., Barchet, W., Diamond, M.S., Siddell, S.G., Ludewig, B., Thiel, V., 2011. Ribose 2'-O-methylation provides a molecular signature for the distinction of self and non-self mRNA dependent on the RNA sensor Mda5. Nat Immunol 12, 137-143.

Zust, R., Cervantes-Barragan, L., Kuri, T., Blakqori, G., Weber, F., Ludewig, B., Thiel, V., 2007. Coronavirus non-structural protein 1 is a major pathogenicity factor: implications for the rational design of coronavirus vaccines. PLoS Pathog. 3, e109.

Zust, R., Miller, T.B., Goebel, S.J., Thiel, V., Masters, P.S., 2008. Genetic interactions between an essential 3' cis-acting RNA pseudoknot, replicase gene products, and the extreme 3' end of the mouse coronavirus genome. J. Virol. 82, 1214-1228.

X. ANEXOS

OPEN ACCESS Freely available online

PLoS PATHOGENS

Coronavirus Gene 7 Counteracts Host Defenses and Modulates Virus Virulence

Jazmina L. G. Cruz[1], Isabel Sola[1], Martina Becares[1], Berta Alberca[2], Joan Plana[2], Luis Enjuanes[1]*, Sonia Zuñiga[1]

1 Centro Nacional de Biotecnología, CNB, CSIC, Department of Molecular and Cell Biology, Darwin 3, Campus Universidad Autónoma de Madrid, Cantoblanco, Madrid, Spain, **2** Pfizer Animal Health, Girona, Spain

Abstract

Transmissible gastroenteritis virus (TGEV) genome contains three accessory genes: 3a, 3b and 7. Gene 7 is only present in members of coronavirus genus a1, and encodes a hydrophobic protein of 78 aa. To study gene 7 function, a recombinant TGEV virus lacking gene 7 was engineered (rTGEV-Δ7). Both the mutant and the parental (rTGEV-*wt*) viruses showed the same growth and viral RNA accumulation kinetics in tissue cultures. Nevertheless, cells infected with rTGEV-Δ7 virus showed an increased cytopathic effect caused by an enhanced apoptosis mediated by caspase activation. Macromolecular synthesis analysis showed that rTGEV-Δ7 virus infection led to host translational shut-off and increased cellular RNA degradation compared with rTGEV-*wt* infection. An increase of eukaryotic translation initiation factor 2 (eIF2α) phosphorylation and an enhanced nuclease, most likely RNase L, activity were observed in rTGEV-Δ7 virus infected cells. These results suggested that the removal of gene 7 promoted an intensified dsRNA-activated host antiviral response. In protein 7 a conserved sequence motif that potentially mediates binding to protein phosphatase 1 catalytic subunit (PP1c), a key regulator of the cell antiviral defenses, was identified. We postulated that TGEV protein 7 may counteract host antiviral response by its association with PP1c. In fact, pull-down assays demonstrated the interaction between TGEV protein 7, but not a protein 7 mutant lacking PP1c binding motif, with PP1. Moreover, the interaction between protein 7 and PP1 was required, during the infection, for eIF2α dephosphorylation and inhibition of cell RNA degradation. Inoculation of newborn piglets with rTGEV-Δ7 and rTGEV-*wt* viruses showed that rTGEV-Δ7 virus presented accelerated growth kinetics and pathology compared with the parental virus. Overall, the results indicated that gene 7 counteracted host cell defenses, and modified TGEV persistence increasing TGEV survival. Therefore, the acquisition of gene 7 by the TGEV genome most likely has provided a selective advantage to the virus.

Citation: Cruz JLG, Sola I, Becares M, Alberca B, Plana J, et al. (2011) Coronavirus Gene 7 Counteracts Host Defenses and Modulates Virus Virulence. PLoS Pathog 7(6): e1002090. doi:10.1371/journal.ppat.1002090

Editor: Ralph S. Baric, University of North Carolina at Chapel Hill, United States of America

Received November 4, 2010; **Accepted** April 12, 2011; **Published** June 9, 2011

Funding: This work was supported by grants from Ministry of Science and Innovation of Spain (BIO2007-60978, BIO2010-16705), U.S. National Institutes of Health (ARRA-W000151845), and the European Community's Seventh Framework Programme (FP7/2007-2013) under the projects "EMPERIE" (EC Grant Agreement number 223498), and "PoRRSCon" (EC Grant Agreement number 245141). The funders had no role in study design, data collection and analysis, decision to publish, or preparation of the manuscript.

Competing Interests: The authors have declared that no competing interests exist.

* E-mail: L.Enjuanes@cnb.csic.es

Introduction

The order *Nidovirales* comprises enveloped single-stranded, positive-sense RNA viruses. The *Nidovirales* includes the *Coronaviridae* that contains viruses with the largest known RNA genome, of around 30 Kb [1,2]. Coronaviruses (CoVs) have been classified into 3 genera, α, β and γ {de Groot, 2010 #9759}. They are the causative agents of a variety of human and animal diseases. In humans, CoVs produce respiratory tract infections, causing from the common cold to severe pneumonia and acute respiratory distress syndrome (ARDS) that may result in death [3,4,5]. In animals, CoVs also cause life-threatening diseases, such as severe enteric and respiratory tract infections, and are economically important pathogens [6]. Nevertheless, there is limited information about the molecular mechanisms governing CoV virulence and pathogenesis.

Double-stranded RNA (dsRNA), produced by RNA viruses as a replication intermediate, is the pathogen-associated molecular pattern that mediates the activation of a well-characterized antiviral mechanism leading to viral protein synthesis shut down [7]. This pathway includes the activation of double-stranded RNA-dependent protein kinase (PKR), leading to eukaryotic translation initiation factor 2 (eIF2α) phosphorylation, and the activation of the 2′-5′-oligoadenylate synthetase (2′-5′OAS) and its effector enzyme, the ribonuclease L (RNase L), responsible for RNA degradation [8,9,10,11,12]. Due to the deleterious effects of this response on virus survival, many viruses have developed different strategies that counteract the host antiviral response triggered by the dsRNA. These mechanisms are mediated by viral proteins or RNAs [13,14,15,16,17,18,19,20,21,22], or by the modification of cellular components [23,24,25,26,27].

CoV replication occurs in the cytoplasm, leading to dsRNA species that trigger the host antiviral response. To overcome these defenses, CoVs have developed several strategies. A general mechanism for all CoVs is the induction of structures in infected cells that may hide viral RNAs from the cellular sensors [28,29]. Some CoVs downregulate host gene expression. In fact, it has been proposed that genus β CoV non structural protein (nsp)1

Author Summary

Innate immune response is the first line of antiviral defense. Viruses have developed diverse strategies to evade this deleterious response, ensuring their survival. Several CoV accessory genes play a central role in these pathways. Nevertheless, the molecular mechanisms by which they exert their function are still unknown. The generation of a rTGEV without gene 7 expression allowed us to study the role of protein 7 in the modulation of the antiviral response. The absence of protein 7 during TGEV infection caused an enhanced apoptosis and a translational shutoff, due to an increased cellular RNA degradation and eIF2α phosphorylation. We identified a protein phosphatase 1 (PP1) binding motif in protein 7, and a TGEV protein 7-PP1 interaction was demonstrated. We propose a novel mechanism to counteract dsRNA-induced antiviral response by RNA viruses. *In vitro* results were in agreement with the enhanced virulence of the gene 7 deletion mutant virus in infected piglets. Our results demonstrated that protein 7 modifies TGEV virulence, reducing virus pathology and increasing the period of virus shedding. This effect also benefits the host decreasing clinical disease and extending its survival. These observations could justify the incorporation and maintenance of gene 7 to genus a1 CoVs during their evolution.

protein promotes host mRNA degradation in order to suppress host innate immune response [30,31]. Severe acute respiratory syndrome (SARS)-CoV nsp1 has also been involved in the inhibition of the 40S ribosomal subunit translational activity [30]. Moreover, several CoVs may also prevent the translational shutoff due to the antiviral response, using viral components or modulating cellular factors. Infectious bronchitis virus (IBV) nsp2 acts as a PKR antagonist [32], and MHV N protein antagonizes 2′-5′ OAS activity [33]. IBV also induces the over-expression of growth arrest DNA-damage 34 (GADD34) protein, which participates in eIF2α dephosphorylation [32].

The 5′ two thirds of CoV genome encode the replicase proteins that are expressed from two overlapping open reading frames (ORFs) 1a and 1b [34]. The 3′ one third of the genome contains the genes encoding structural proteins and a set of accessory genes, whose sequence and number differ between the different species of CoV [1,35]. Traditionally, CoV accessory genes have been related to virulence modulation, such as mouse hepatitis virus (MHV) gene 5a that determines the interferon (IFN) resistance of the different MHV strains [36]. SARS-CoV contains the largest number of accessory genes and it has been proposed that these genes could be responsible for its high virulence [37,38]. The role of some structural genes, such as SARS-CoV genes E and 6, on CoV pathogenesis has been demonstrated [39,40,41,42]. Nevertheless, the role of other SARS-CoV accessory genes in virus replication and pathogenesis is still under study, as SARS-CoV mutants lacking different combinations of these genes revealed that they had limited impact on virus replication and pathogenesis [37,38].

TGEV is a genus a1 CoV that contains three accessory genes: 3a, 3b and 7 [43,44,45]. The deletion of gene cluster 3ab demonstrated that these genes were not essential for *in vitro* and *in vivo* viral replication [45]. TGEV gene 7 is located at the 3′end of the genome, being the last ORF. In general, ORFs located in CoV genomes downstream of nucleocapsid (N) gene have been named as gene 7. And, one to three genes, 7a, 7b and 7c, have been described for several CoVs of genus α, β4 and γ3 at the end of their genomes [35,46,47] [48]. Nevertheless, most of these genes are not related to each other (J.L.G. Cruz, S. Zuñiga and L. Enjuanes, unpublished observations). In fact, new genes located in avian CoVs genomes after the N gene have been named differently as they showed no sequence homology to any other CoV genes [49]. TGEV protein 7 is similar to protein 7a of CoV genus α1, with a 72% homology to feline infectious peritonitis virus (FIPV), canine (CCoV) and porcine respiratory (PRCV) CoVs 7a proteins (Figure 1A) [50,51]. The function of protein 7 has not been identified, and it has been proposed that it could play a role in virulence [52,53]. The 7ab cluster deletion in FIPV (FIPV-Δ7ab) resulted in virus attenuation [54]. Nevertheless, the specific role that gene 7a plays in attenuation is not clear, as FIPV-Δ7ab phenotype was similar to the one observed for a FIPV isolate lacking only gene 7b [55].

To study gene 7 function, a recombinant TGEV virus missing gene 7 was engineered. This deletion mutant virus induced an intensified host antiviral response, including enhanced nuclease activity and eIF2α phosphorylation, leading to an increase in cell death by apoptosis. The interaction of TGEV protein 7 with PP1c was also demonstrated. Inoculation of piglets with gene 7 deletion mutant and wild-type viruses showed that virus missing gene 7 produced accelerated growth kinetics and pathology compared with that caused by the parental virus. Overall, these results indicate that TGEV gene 7 is a virulence gene that modulates host cell defenses and extends the period of virus dissemination.

Results

Generation of recombinant TGEV virus (rTGEV) lacking gene 7

TGEV ORF 7 encodes a 78 amino acid hydrophobic protein. The structure predicted for protein 7 contains two transmembrane domains (TM) at the amino- (aa 1–18) and carboxy-termini (aa 60–78), of the protein. The N-terminal TM domain overlaps with a signal peptide (aa 1–24) (Figure 1A). The predicted membrane topology locates the middle part of the protein towards the lumen of a membrane structure (Figure 1A). During TGEV infection, protein 7 was detected associated to the endoplasmatic reticulum (ER) and plasma membranes [56].

To study the role of protein 7 during TGEV infection, an rTGEV virus lacking gene 7 (rTGEV-Δ7) was engineered (Figure 1B) [57]. To avoid gene 7 expression, several modifications that led to an inactive ORF7 transcription regulating core sequence (CS) were introduced (Figure 1B, left panel). The two first nts of protein 7 translation start codon were also removed (Figure 1B, left panel). These mutations introduced into the TGEV infectious cDNA, were predicted to knock down gene 7 expression with minimum alteration to the 3′end of the viral genome, which is required for viral replication [58,59]. All the mutations introduced in the cDNA were present in the recovered rTGEV-Δ7 virus, after 6 passages in tissue culture of a plaque-purified virus, indicating that they were stably maintained in the rTGEV genome. The absence of subgenomic mRNA-7 in rTGEV-Δ7 infected cells was confirmed by Northern-blot (Figure 1B, right panel). Viral titer and genomic RNA (gRNA) levels were analyzed. Intracellular RNA was only analyzed during those times post infection in which viable cells were bound to the plate (up to 24 hpi). Both mutant and parental viruses showed the same virus growth kinetics and gRNA accumulation (Figure 1C). The rTGEV-Δ7 virus titer decreased after 24 hours post infection (hpi) due to the absence of live cells. This result was expected, rTGEV-Δ7 virus titer decreased at a ratio of 1 log unit per day due to thermal instability and to the absence of viable cells, at this time

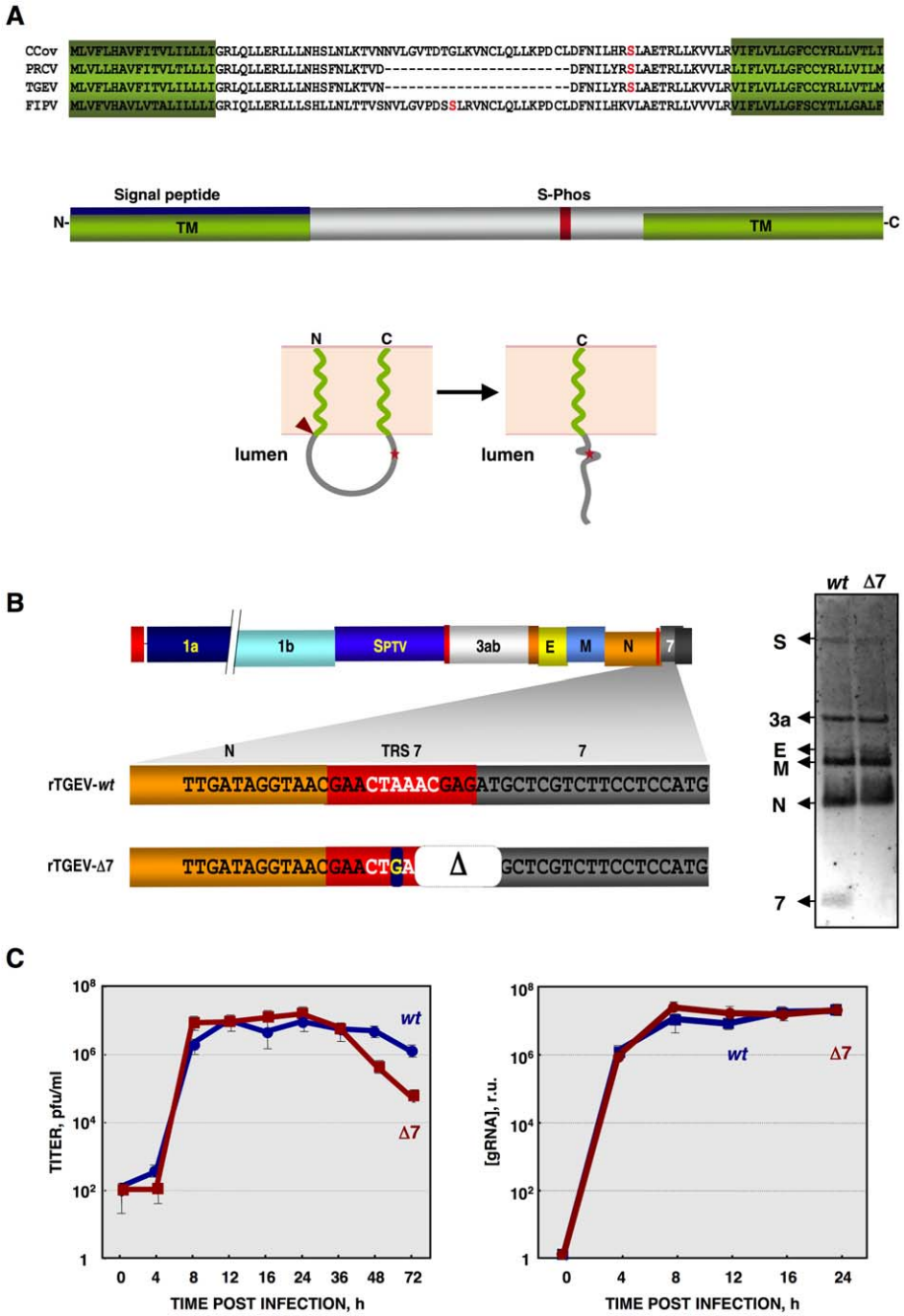

Figure 1. Generation of a recombinant TGEV virus lacking protein 7 expression (rTGEV-Δ7). (A) Genus α1 CoV protein 7a sequence alignment, using T-COFFEE [135]. Protein 7a sequences from the canine (CCoV) and porcine respiratory (PRCV) CoVs, transmissible gastroenteritis (TGEV) and feline infectious peritonitis (FIPV) viruses were used. GenBank accession numbers are ADB28914.1, ABG89313.1, CAA80842.1, and CAA62190.1, respectively. *In silico* prediction of TGEV protein 7 domains is represented. Transmembrane domains (TM) are in green [*PredictProtein*, [136]], the signal peptide in blue [*Signal P3.0 Server*, [137]], and a conserved phosphorilable Serine in red (S-Phos) [*NetPhos 2.0 Server*, [138]]. The predicted topology of TGEV protein 7 is also represented in lower panel [*PSORTII* [139]]. Signal peptide cleavage is indicated by a red arrowhead. S-Phos is indicated by a red star. (B) Mutations introduced to generate a rTGEV-Δ7 virus, right panel. The scheme of TGEV gRNA is shown in the upper part. The white letters represent the CS. Nucleotide change is indicated with a blue square, and the deletion (Δ) as a white square. Northern blot of subgenomic mRNAs (sgmRNAs) produced during rTGEV infections, right panel. ST cells were infected with rTGEV-*wt* (*wt*) and rTGEV-Δ7 (Δ7) viruses, at a moi of 5. Total RNA was extracted at 8 hpi. The sgmRNAs for the spike (S), 3a, envelope (E), membrane (M), nucleocapsid (N) proteins, and protein 7 were detected. (C) *In vitro* growth kinetics of the rTGEV viruses. ST cells were infected with the rTGEV-*wt* (*wt*, blue) and rTGEV-Δ7 (Δ7, red) viruses, at a moi of 5. Culture medium and total intracellular RNA were collected at different hours post infection. Intracellular RNA was only analyzed during those hours post infection in which viable cells were bound to the plate. Viral titers (left panel), and genomic RNA (gRNA) amounts (right panel), determined by RT-qPCR, were analyzed. Error bars represent the standard deviation from three independent experiments.
doi:10.1371/journal.ppat.1002090.g001

post-infection, that could produce new virus [60]. These data confirmed that protein 7 was not essential for TGEV replication in cell culture.

Cell death caused by rTGEV-Δ7 infection

The cytopathic effect (CPE), characterized by the rounding and detachment of the cells, induced by rTGEV-Δ7 virus was similar to that caused by the wild-type (rTGEV-*wt*) virus. Nevertheless, 2-fold larger plaques were produced by rTGEV-Δ7 (4 mm diameter), compared with those caused by the parental virus (2 mm diameter) (data not shown). Accordingly, in rTGEV-Δ7 infected cells the infectious foci were larger than those observed in rTGEV-*wt* infected ones at 16 hpi (Figure 2A, left panels). This increased CPE progressed until almost no viable cells remained in the rTGEV-Δ7 infection at 24 hpi (Figure 2A, right panels). The cell death induced by the rTGEV-Δ7 virus was analyzed by permeabilization, propidium iodide (PI) staining and flow cytometry (Figure 2B). This technique distinguishes dying or subdiploid cells from normal cells that emit a high PI fluorescence signal [61,62]. As expected, the wild-type virus induced cell death and DNA degradation during the infection (Figure 2B) [63]. Interestingly, rTGEV-Δ7 caused a significant increase in cell death compared with that caused by rTGEV-*wt* infection (Figure 2B).

Apoptosis induced by rTGEV-Δ7 virus

The main cause of the cytopathic effect induced by TGEV infection is apoptosis programmed cell death [63,64,65]. To analyze whether the increased cell death during rTGEV-Δ7 infection was due to an enhanced apoptosis, cells infected either with rTGEV-*wt* or rTGEV-Δ7 were simultaneously stained with PI and Annexin V, and monitored by flow cytometry. Mock infected cells remained viable (Annexin V^-, PI^-) throughout the experiment, indicating that the treatment did not induce apoptosis by itself (Figure 3A). As expected, the wild-type virus infection induced apoptosis (Annexin V^+), and a cell population in late apoptosis (Annexin V^+, PI^+) was evident at 12 hpi (Figure 3A). Mutant rTGEV-Δ7 also triggered apoptosis but faster and stronger than that caused by the rTGEV-*wt* virus, with a 2-fold increase in apoptotic cells at 8 hpi and only 36% live cells at 12 hpi (Figure 3A).

It has previously been reported that TGEV virus induces apoptosis following a caspase dependent pathway that involves the processing of two initiator proteases (caspase 8 and 9), as well as three downstream effector caspases (caspase 3, 6 and 7) [64,65]. Caspase 3 activation leads to TGEV N protein cleavage [64], and inhibition of caspase 3 processing, among others caspases, prevents TGEV induced apoptosis [63]. To determine the potential influence of gene 7 on caspase dependent apoptosis, the presence of the processed form of caspase 3 was analyzed by Western-blot using specific antibodies. TGEV infection induced the cleavage of caspase 3 (Figure 3B) and, as a consequence, cleaved N protein was also detected (data not shown), as expected [64]. Moreover, the rTGEV-Δ7 triggered caspase 3 processing faster than the wild-type virus. These results indicated that the increased CPE observed in rTGEV-Δ7 infected cells was most likely due to an enhanced apoptosis mediated by caspase activation.

Effect of gene 7 deletion on macromolecular synthesis

CoVs such as MHV or SARS-CoV, cause translational shutoff and lead to apoptosis increase [30,66,67,68,69,70,71]. To determine whether this was also the case for TGEV-Δ7 virus, *de novo* protein synthesis during the infection was evaluated by metabolic labeling. No translational stall was detected during rTGEV-*wt* infection (Figure 4A), as described for other CoVs such as IBV and bovine coronavirus (BCoV), or MHV at early times post infection [32,33,72]. In contrast, rTGEV-Δ7 infection inhibited host translational machinery, an effect detected from 10 hpi. This translational stop affected both cellular and viral protein synthesis (Figure 4A). CoVs produce viral mRNAs that are structurally similar to those produced by their host (5′ CAP-structure and poly A at the 3′end), allowing CoVs to parasitize the host translational machinery. In some CoVs, such as MHV, selective viral protein synthesis occurs concomitantly with host translational inhibition, using a mechanism not fully characterized [73,74]. To study the mechanism responsible for protein synthesis reduction in TGEV-Δ7 infection, and to analyze whether viral mRNAs were preferentially translated, the amount of radiolabeled N protein, taken as reference for viral protein synthesis, was related to the total amount of protein (viral plus cellular) per well (Figure 4B). The ratio of viral to total protein synthesis showed no significant differences between rTGEV-*wt* and rTGEV-Δ7 infected cells (Figure 4B). In addition, no differences in viral proteins accumulation were observed at this times post infection (data not shown). These results suggested that protein synthesis at early times post infection was responsible for the virus that was still being produced after translational shutoff. This result suggested that the absence of protein 7 during TGEV infection led to protein synthesis inhibition most likely by inhibiting a cell translation step common to cellular and viral protein synthesis.

In principle, RNA decay could be responsible for the observed translational shutoff. Therefore, total cellular RNA integrity was evaluated using a Bioanalyzer [75,76,77]. Wild-type virus infection induced a modest RNA processing, especially at 24 hpi (Figure 5A). In contrast, rTGEV-Δ7 infection induced a faster and stronger cellular RNA degradation (Figure 5A). This data indicated that the cellular translational shutoff could be due, at least in part, to cellular mRNA degradation. Moreover, the increase in 28S rRNA degradation (Figure 5B), could affect both cellular and viral protein synthesis [78]. Nucleases activated by cell apoptosis could be responsible for the observed RNA degradation [79]. To study whether this was the case, we took advantage of the previous description of the inhibition of TGEV induced apoptosis by the addition of caspases inhibitor ZVAD, without affecting virus production [63]. In fact, after infection of ST cells with *wt* or rTGEV-Δ7 viruses in the presence of ZVAD, no CPE was observed. Total RNA was extracted from non-treated or ZVAD-treated cells, and the same RNA degradation patterns were observed in both cases (Figure 5C), indicating that the increased RNA degradation caused by rTGEV-Δ7 virus was independent of nucleases activated by cell apoptosis. To determine whether the observed cellular RNA cleavage was due to a dsRNA induced antiviral response, ST cells were treated with polyinosinic-polycytidylic acid [Poly(I:C)], which is a potent activator of this type of response [77,80,81]. Cells transfected with Poly(I:C) showed the same RNA degradation pattern as those infected with the rTGEV-Δ7 and parental viruses (Figure 5D), in contrast to mock treated cells. These results suggested that the cellular RNA cleavage increase, during rTGEV-Δ7 infection, was due to an enhancement of dsRNA induced antiviral activity. In general, the main effector of this process is RNase L [81,82,83]. To further analyze the relevance of this nuclease during TGEV infection, a recombinant vaccinia virus (VV) system was used. It was previously described that VV does not induce strong RNA degradation, due to the presence of viral genes that inhibit the RNase L system. To efficiently trigger dsRNA activated RNA degradation by RNase L, cells must be infected by VV expressing 2′-5′ OAS and RNase L [84]. Taking advantage of the wide host range of VV, porcine ST cells were infected with VV, or VVs

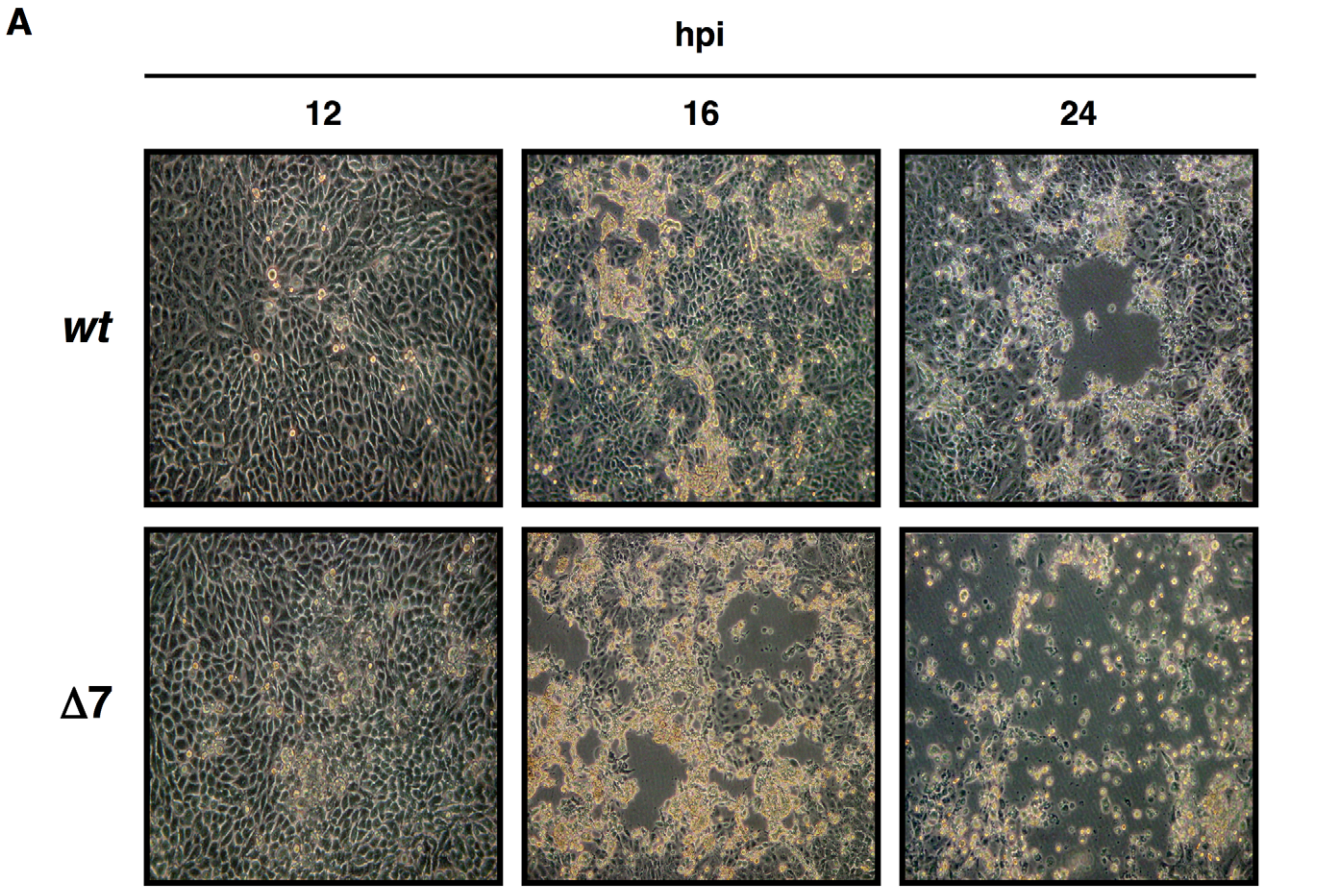

Figure 2. Cell death caused by rTGEV-Δ7. (A) ST cells were infected with rTGEV-*wt* and rTGEV-Δ7 (Δ7) viruses. The cytophatic effect induced by both viruses was analyzed by optical microscopy, at 12, 16 and 24 hpi. Images were taken with a 40x objective. (B) Quantification of cell death induced by rTGEV viruses. ST cells were infected with rTGEV-*wt* (*wt*) and rTGEV-Δ7 (Δ7) viruses. Cells were collected at 4, 8, 10, 12 and 16 hpi, permeabilized, and stained with propidium iodide. Dead cell population was measured by flow cytometry. Error bars indicate the standard deviation from three independent experiments. **, p-value$<$0.01.
doi:10.1371/journal.ppat.1002090.g002

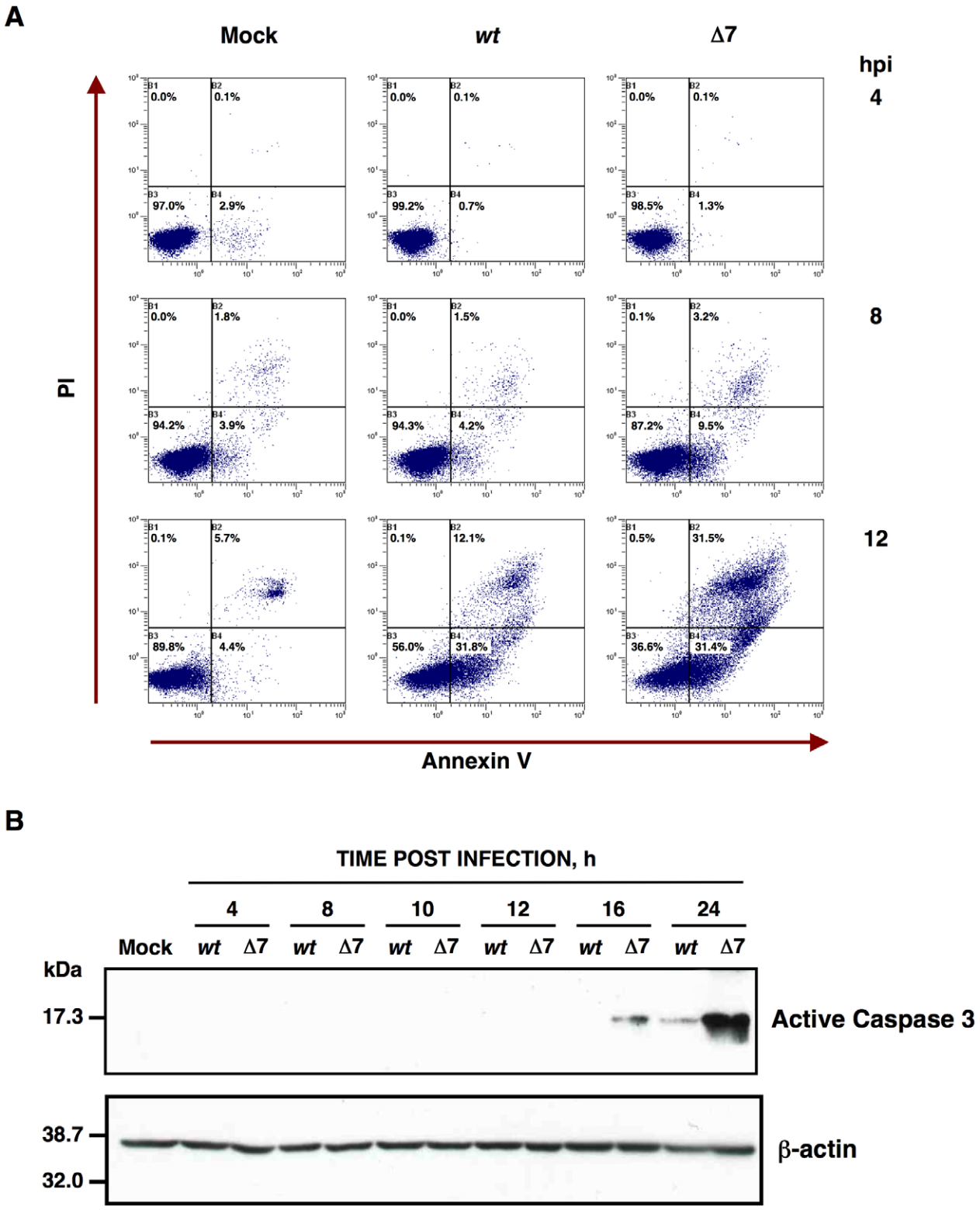

Figure 3. Apoptosis caused by rTGEV-Δ7. (A) Apoptosis levels in mock, rTGEV-*wt* (*wt*) and rTGEV-Δ7 (Δ7) infected cells were evaluated at 4, 8 and 12 hpi, by flow cytometry. Annexin V-PI double staining was performed to differentiate cells in early apoptosis (Annexin V^+, PI^-) from those in late apoptosis (Annexin V^+, PI^+) stages. (B) Detection of active caspase 3 by Western-blot. Total protein was extracted from ST cells infected with rTGEV-*wt* (*wt*) and rTGEV-Δ7 (Δ7) viruses, at the indicated times post infection. Active caspase 3 was detected using specific antibodies for the cleaved form. β-actin was detected as a loading control.
doi:10.1371/journal.ppat.1002090.g003

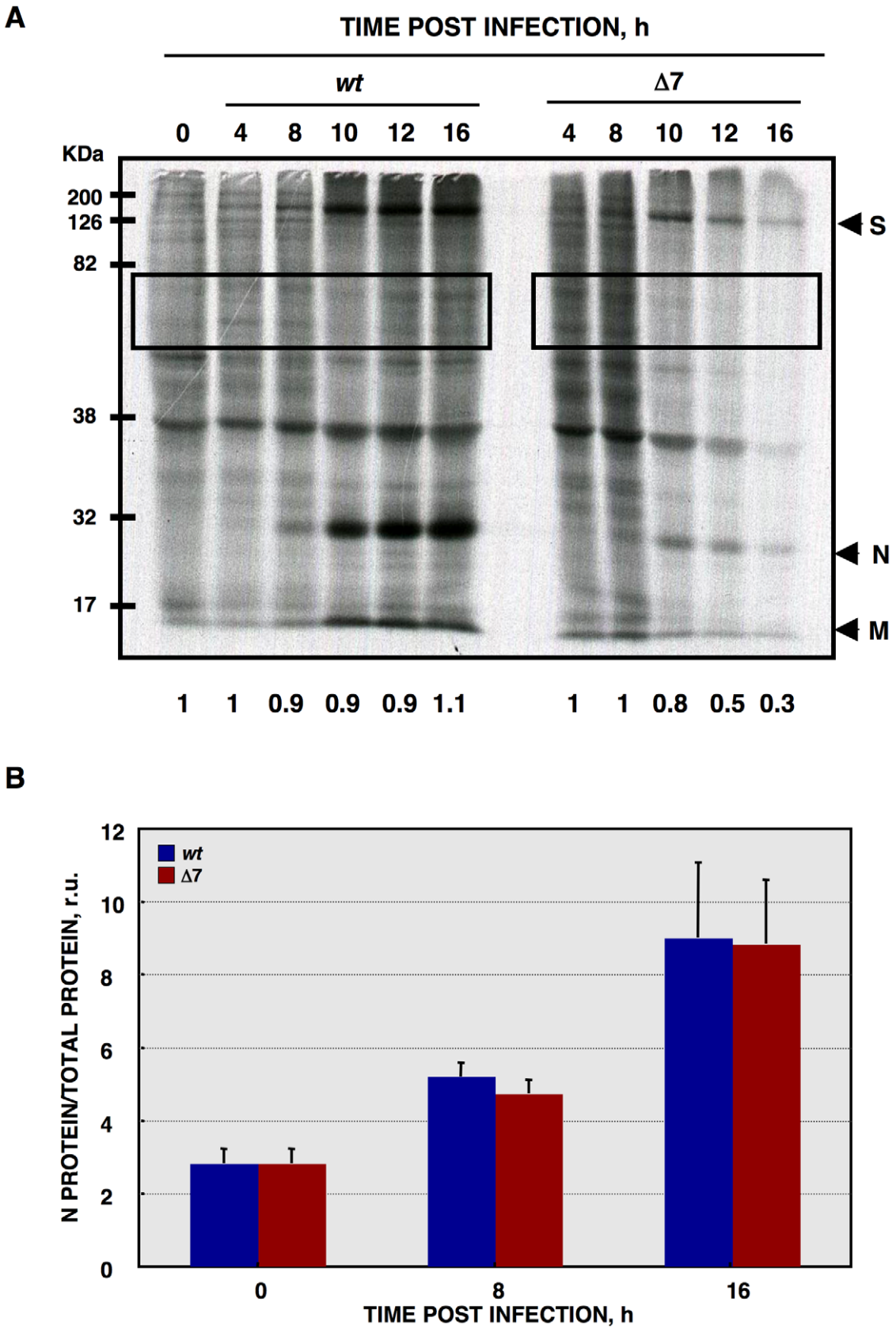

Figure 4. ***De novo*** **protein synthesis in rTGEV infections.** (A) At the indicated times post infection, ST cells were infected at a moi of 1 with rTGEV-*wt* (*wt*) and rTGEV-Δ7 (Δ7) viruses. Cells were labeled with ^{35}S Met-Cys for 30 min. Protein extracts were obtained and SDS-PAGE electrophoresis was performed to detect labeled proteins. Viral spike (S), nucleocapsid (N), and membrane (M) proteins are indicated. Densitometric

analysis was performed to determine the levels of host protein synthesis. The boxes represent the region of the gel used for densitometry analysis, and the numbers below represent the relative radioactivity compared with mock-infected cells. (B) Viral-to-cell protein synthesis ratio. The amount of radiolabeled N protein, estimated by densitometry, was related to the estimated total amount of protein, at the indicated hpi. Error bars indicate the standard deviation from three independent experiments. r.u., relative units.
doi:10.1371/journal.ppat.1002090.g004

expressing 2′-5′ OAS and RNase L. As expected, VV induced a very slight RNA degradation, that was increased by the co-expression of 2′-5′ OAS and RNase L (Figure 5D). Moreover, the RNA degradation pattern produced by the expression of RNase L system was identical to the one observed after rTGEV-Δ7 infection, strongly suggesting that RNaseL is the main nuclease involved in the increased RNA degradation after rTGEV-Δ7 infection.

The activation of RNase L requires its binding to small 5′-triphosphorylated,2′-5′-oligoadenylates (2′-5′A), generated by the 2′-5′A synthetase (2′-5′OAS) [10,11] (Figure 6A). In non-infected cells 2′-5′OAS is expressed at background levels that are significantly increased during some viral infections [85,86]. Therefore, 2′-5′OAS1 expression during infection by rTGEV-*wt* and rTGEV-Δ7 was evaluated by quantitative RT-PCR (RT-qPCR). TGEV-*wt* infection induced the expression of the 2′-5′OAS1, as expected (Figure 6B) [87]. rTGEV-Δ7 infection also activated this pathway. Nevertheless, the slight differences in 2′-5′OAS1 gene expression between rTGEV-*wt* and rTGEV-Δ7 infections could not explain the enhanced nuclease activity observed during mutant virus infection (Figure 6B), as 2′-5′OAS1 mRNA level was even lower for rTGEV-Δ7 than for rTGEV-*wt* virus (Figure 6B).

Viral mRNA levels were measured by RT-qPCR, as the ratio between mRNA and gRNA amounts. No significant differences were observed between rTGEV-Δ7 and rTGEV-*wt* viruses, for the accumulation kinetics of both N and M protein mRNAs (Figure 7A). Nevertheless, RT-qPCR evaluation did not rule out whether viral rTGEV-Δ7 mRNAs could have been degraded, as the cellular RNAs were. Therefore, viral RNA integrity was evaluated by Northern blot assay. The total RNA amount loaded from rTGEV-Δ7 infected cells was 1.5 to 2 fold higher than that loaded from rTGEV-*wt* infected ones, in order to detect possible degradation species. No degradation of viral mRNAs was detected after infection by rTGEV-*wt* or rTGEV-Δ7 (Figure 7B), suggesting that viral RNAs were not degraded by the increased nuclease activity.

Effect of protein 7 absence on translation initiation

Several mechanisms may account for the observed translational blockage. We have shown that the absence of protein 7 during TGEV infection enhanced the degradation of cellular mRNAs and ribosomal components. In addition, other factors could promote translational stall. In fact, many viruses interact with translation machinery components [88]. Eukaryotic initiation factor 4G (eIF4G) is a well-characterized target of the TGEV-induced apoptosis [64]. No difference was found in eIF4G processing at different times post infection by wild-type or mutant viruses (data not shown).

Protein synthesis is frequently reduced when cells are under stress, such as that caused by virus infection, by increasing the phosphorylation levels of the eIF2α subunit at serine 51 [89]. eIF2α phosphorylation, during rTGEV infection, was analyzed by Western-blot using antibodies specific for the phosphorylated (eIF2α-P) and total forms of this factor, respectively. Wild-type infection increased eIF2α-P levels (Figure 8A), reaching a maximum at 8 hpi (Figure 8B). As previously described, for other stress conditions, eIF2α-P levels decreased at late times post-infection [90,91]. Similarly, rTGEV-Δ7 infection also induced eIF2α phosphorylation (Figure 8A) but to significantly higher levels than those observed during rTGEV-*wt* infection (Figures 8A and 8B). Interestingly, the highest difference was detected at 10 hpi, concomitantly with the time at which the mutant virus induced the translational shutoff (Figure 8B). The increased eIF2α phosphorylation was maintained, although at different levels, from 8hpi to 10 hpi, what could be sufficient to account for the translational shutoff, according to previously published studies [92,93]. Altogether, this result indicated that, besides cellular RNA degradation, rTGEV-Δ7-induced translational shutoff is probably due to an increased and sustained eIF2α phosphorylation.

Growth arrest DNA-damage 34 (GADD34) protein is induced by cell stress, and its expression levels are upregulated on increased eIF2α phosphorylation conditions [94]. Therefore, GADD34 mRNA levels could have been modified during rTGEV-Δ7 infection, and were quantified by RT-qPCR. Infection by rTGEV-Δ7 virus induced significantly higher levels of GADD34 mRNA than the rTGEV-*wt* virus (Figure S1). This data correlated with the previous results, as higher eIF2α-P levels, in mutant virus infection, led to GADD34 increased expression.

Protein 7 provided *in trans* restored rTGEV-*wt* phenotype

To assess whether the absence of protein 7 during TGEV infection was responsible for the observed phenotype, ST cells stably expressing TGEV protein 7 (ST-HA-7) were generated. In order to detect protein 7, a hemagglutinin (HA) tag was inserted between the signal peptide and the rest of the protein (Figure 9A). Protein 7 expression was confirmed by immunofluorescence and Western-blot analysis (Figure 9B). Three ST-HA-7 cellular clones (C1, C2 and C3), with different protein 7 expression levels were selected (Figure 9B). The effect of protein 7 provided *in trans* on apoptosis and cellular RNA degradation was analyzed. Infection of ST cells by rTGEV-Δ7 caused a stronger apoptosis than the rTGEV-*wt* virus, as previously observed (Figure 9C). Protein 7 provided *in trans* significantly reduced apoptosis both in rTGEV-Δ7 infected cells and in rTGEV-*wt* infected ones (Figure 9C). Moreover, infection of ST cells by rTGEV-Δ7 caused higher RNA degradation than the rTGEV-*wt* virus, as previously described (Figure 9D). The amount of protein 7 directly correlated with the inhibition of RNA degradation, suggesting that protein 7 expression *in trans* prevented nuclease activation (Figure 9D). Furthermore, GADD34 mRNA expression (Figure S2A) and eIF2α phosphorylation levels (Figure S2B) were reduced by protein 7 expression *in trans*. Altogether, these results demonstrated that the specific phenotype of the rTGEV-Δ7 virus was due to TGEV protein 7 absence, as it was reverted to the rTGEV-*wt* phenotype, in a dose-dependent manner, by providing protein 7 *in trans*.

Effect of protein 7 absence on the antiviral response induced by dsRNA

The activation of an antiviral response pathway triggered by the dsRNA produced during viral infections leads to eIF2α phosphorylation that results in translational shutoff [10,95,96]. The dsRNA-activated protein kinase (PKR) is a component of dsRNA induced antiviral response. PKR dimerization, and subsequent activation by autophosphorylation, is mediated by its binding to dsRNA [89].

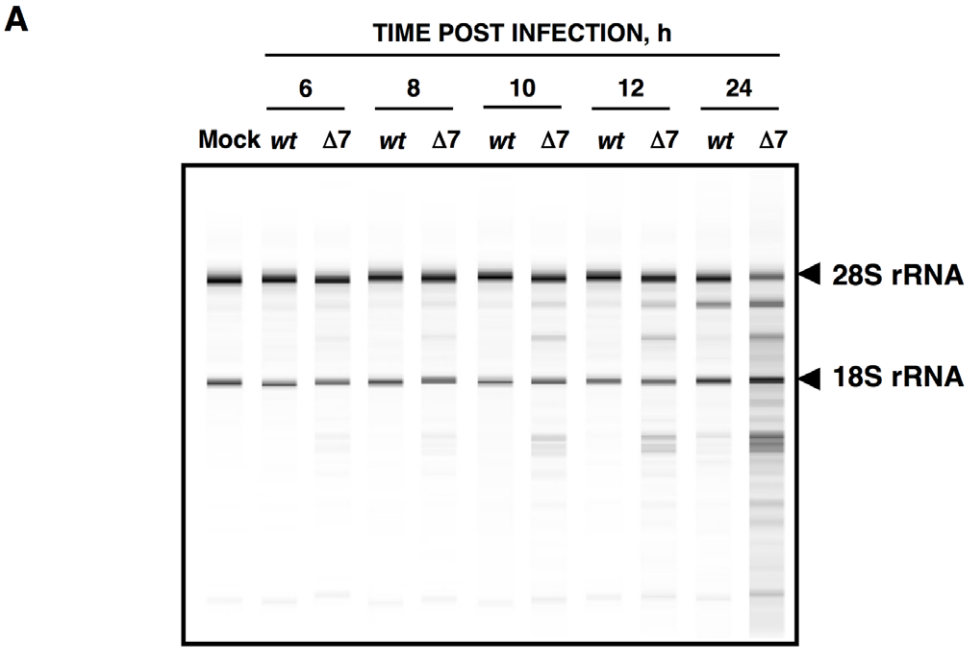
A
TIME POST INFECTION, h
6
8
10
12
24
Mock wt Δ7 wt Δ7 wt Δ7 wt Δ7 wt Δ7
28S rRNA
18S rRNA

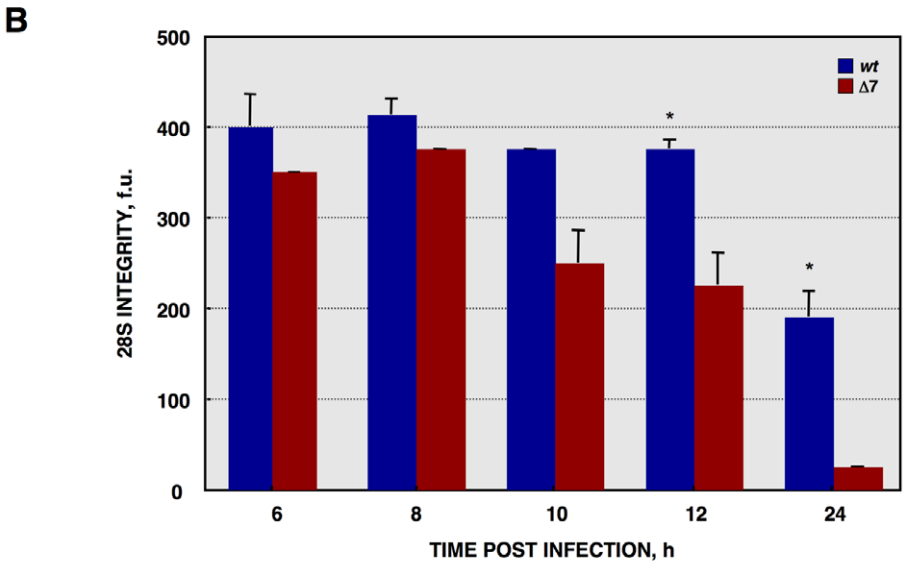
B
28S INTEGRITY, f.u.
500
400
300
200
100
0
wt
Δ7
*
*
6
8
10
12
24
TIME POST INFECTION, h

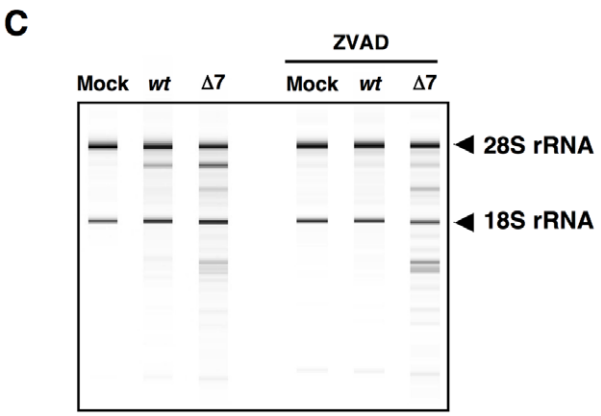
C
ZVAD
Mock wt Δ7 Mock wt Δ7
28S rRNA
18S rRNA

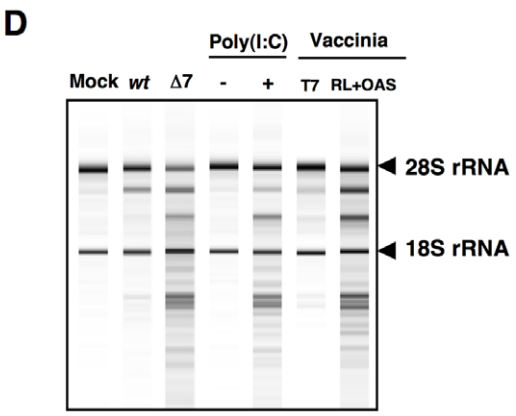
D
Poly(I:C)
Vaccinia
Mock wt Δ7 - + T7 RL+OAS
28S rRNA
18S rRNA

Figure 5. Cellular RNA integrity. (A) Total RNA extracted from infected ST cells, at indicated times post infection, was analyzed using a Bioanalyzer. The position of 28S and 18S rRNAs are indicated. (B) 28S rRNA integrity. Graph of 28S fluorescence intensity, as measured by Bioanalyzer, in the RNA samples from ST cells infected with rTGEV-*wt* (blue) or rTGEV-Δ7 (red), collected at different times post infection. f.u., fluorescence units. Error bars indicate the standard deviation from three independent experiments. *, p-value <0.05. (C) ST cells were treated with caspase inhibitor ZVAD, and infected. Total RNA was extracted and analyzed using a Bioanalyzer. (D) ST cells were transfected with Poly(I:C), and total RNA was extracted 16 hours post transfection. ST cells were also infected with a vaccinia virus expressing T7 polymerase (T7), or with the vaccinia expressing T7 polymerase, and two additional vaccinia viruses expressing 2′-5′ OAS and RNase L (RL+OAS). Total RNA was extracted 24 hpi. In all cases, cell RNA integrity was analyzed using a Bioanalyzer.
doi:10.1371/journal.ppat.1002090.g005

Activation of PKR leads to eIF2α phosphorylation and translation inhibition (Figure S3A) [9,12]. Infection by wild-type TGEV induced PKR phosphorylation, with a maximum at 12 hpi (Figure S3B). Nevertheless, no significant differences were observed between rTGEV-*wt* and rTGEV-Δ7 virus infections, either in PKR-phosphorylation levels or total PKR protein accumulation (Figure S3B).

During viral infection, the accumulation of nascent or misfolded proteins in the endoplasmic reticulum (ER) can trigger an ER stress pathway, which could also lead to translational stall by eIF2α phosphorylation (Figure S3A) [97]. PKR-like endoplasmic reticulum kinase (PERK) is activated by ER stress, and could participate in eIF2α phosphorylation during viral infection [98,99]. Activation of PERK requires the prior activation of the ER chaperone immunoglobulin heavy-chain binding protein (BiP), a biomarker for the onset of the ER stress [100,101]. Similar levels of BiP were observed in rTGEV-*wt* or in rTGEV-Δ7 infected cells during infection (Figure S3B), suggesting that PERK would not be differentially activated in the cells infected with the gene 7 deletion mutant virus with respect to those infected with the parental virus. These data strongly suggested that an increased kinase activity was not responsible for the increased eIF2α phosphorylation during rTGEV-Δ7 virus infection.

Interaction of protein 7 and PP1

The enhanced eIF2α phosphorylation observed during rTGEV-Δ7 virus infection could be alternatively due to a decrease in the phosphatase activity that counteracts the kinases function (Figure S3A). Protein phosphatase 1 (PP1) is one of the major Ser/Thr phosphatases, and is the main enzyme responsible of the eIF2α dephosphorylation [32,94,102]. PP1 expression was evaluated by Western-blot, and similar protein levels were detected in both rTGEV-*wt* and rTGEV-Δ7 infected cells (Figure S3C).

The PP1 catalytic subunit (PP1c) can interact with more than 50 regulatory partners. The formation of these complexes determines its substrate specificity, sub-cellular location and activity, allowing PP1 to participate in numerous cellular functions [103,104]. Therefore, although a decrease in PP1 levels was not detected in rTGEV-Δ7 infected cells, compared with rTGEV-*wt* infected ones, protein 7 could modulate PP1 activity. To study this possibility, the functional motifs of CoV genus a1 protein 7 were analyzed using the ELM server [105,106]. A highly conserved sequence at the C-terminus of the protein was identified as the canonical PP1c-binding motif (Figure 10A). The consensus PP1c-binding motif includes a short sequence (R/K)VxF, in which x is any amino acid except those with large hydrophobic residues, surrounded by non-polar residues (Figure 10B) [103]. Previous

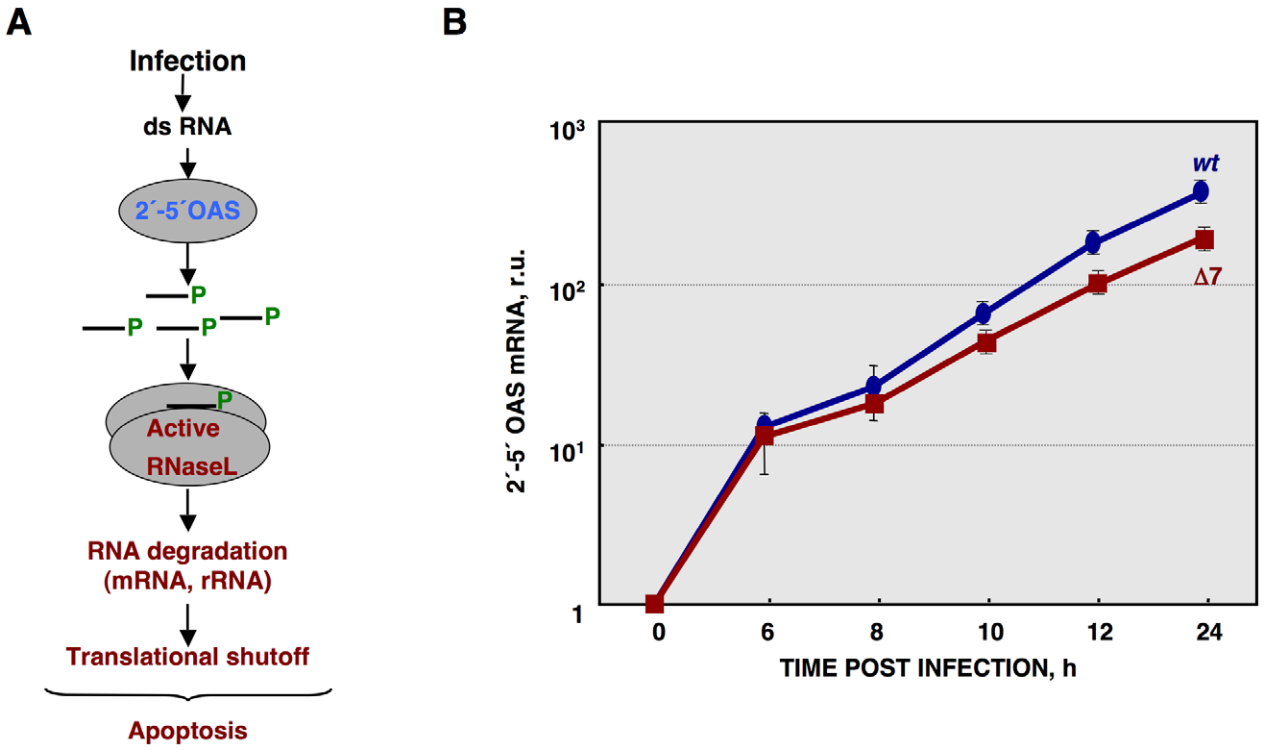

Figure 6. Quantification of 2′-5′OAS expression during rTGEV infection. (A) Scheme of 2′-5′OAS/RNase L activation pathway. (B) Quantification of porcine 2′-5′OAS mRNA accumulation during rTGEV-*wt* (blue) or rTGEV-Δ7 (red) infections, by RT-qPCR, at indicated time post infection. r.u., relative units. Error bars indicate the standard deviation from three independent experiments.
doi:10.1371/journal.ppat.1002090.g006

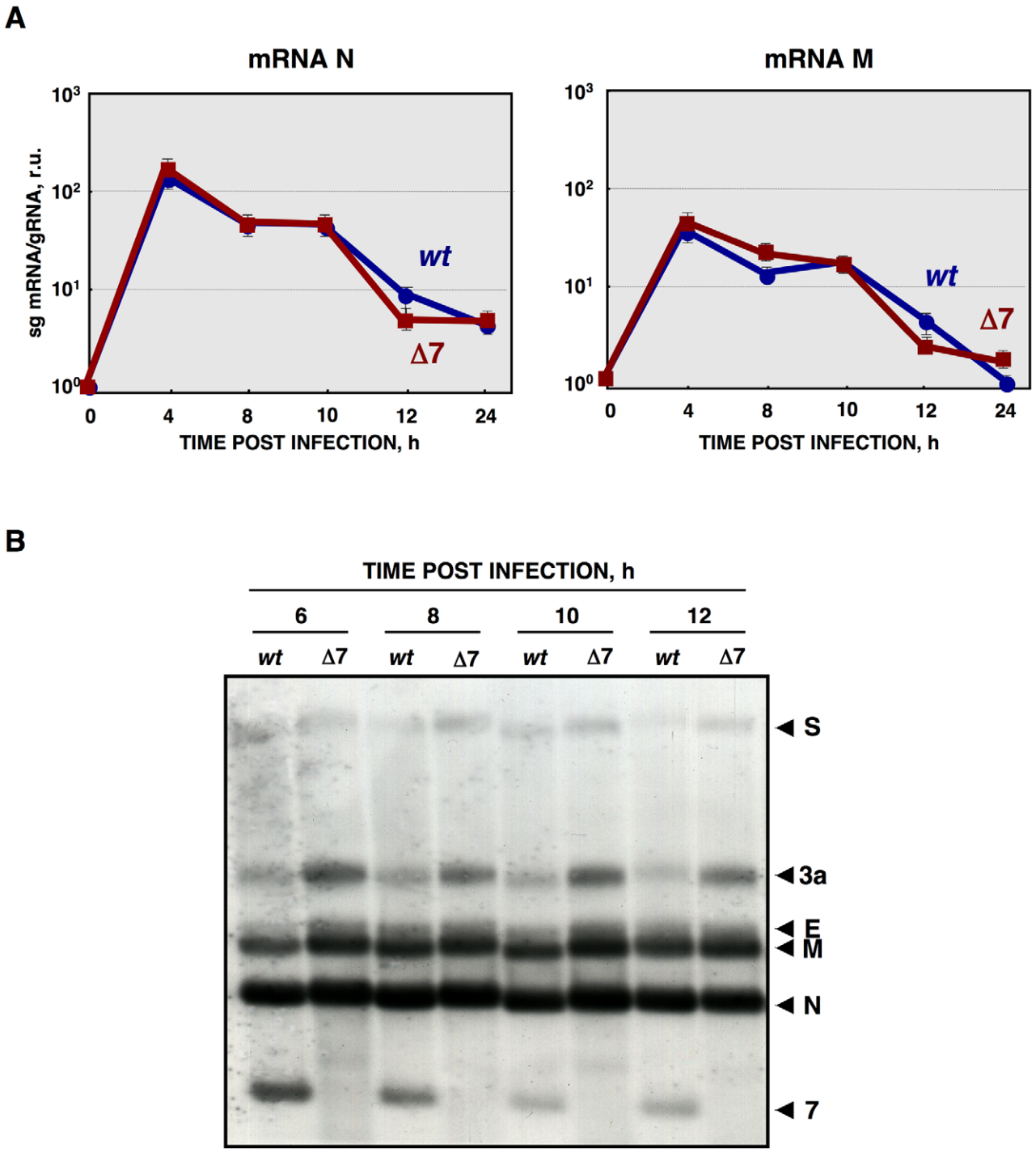

Figure 7. Viral RNA integrity. (A) Quantification of viral N and M sg mRNAs accumulation during rTGEV-*wt* (blue) or rTGEV-Δ7 (red) infections by RT-qPCR at indicated hpi. The ratio of sg mRNA to genomic RNA is represented. r.u., relative units. Error bars indicate the standard deviation from three independent experiments. (B) Northern blot analysis of intracellular viral sg mRNAs. ST cells were infected with rTGEV-*wt* or rTGEV-Δ7 viruses. Total RNA was extracted at indicated hours post infection and analyzed by Northern blot using a probe complementary to the 3′ end of all sg mRNAs. Total RNA amount loaded from rTGEV-Δ7 infected cells was 1.5 to 2 fold higher than that loaded from rTGEV-*wt* infected ones, in order to detect possible degradation species. Viral mRNAs for the spike (S), 3a, envelope (E), membrane (M), nucleocapsid (N) proteins, and protein 7 are indicated on the left.
doi:10.1371/journal.ppat.1002090.g007

studies have demonstrated that the RVxF motif is sufficient to mediate PP1 binding, whereas the surrounding amino acids are responsible for PP1 binding and allosteric modulation of the enzyme activity [107,108,109]. This motif is also present in three viral and several cell proteins, such as herpex simplex virus 1 $\gamma_1$34.5, human papilomavirus E6 oncoprotein and African swine fever virus DP71L, and mammalian GADD34 proteins (Figure 10B). In all cases, these proteins bind PP1c and promote

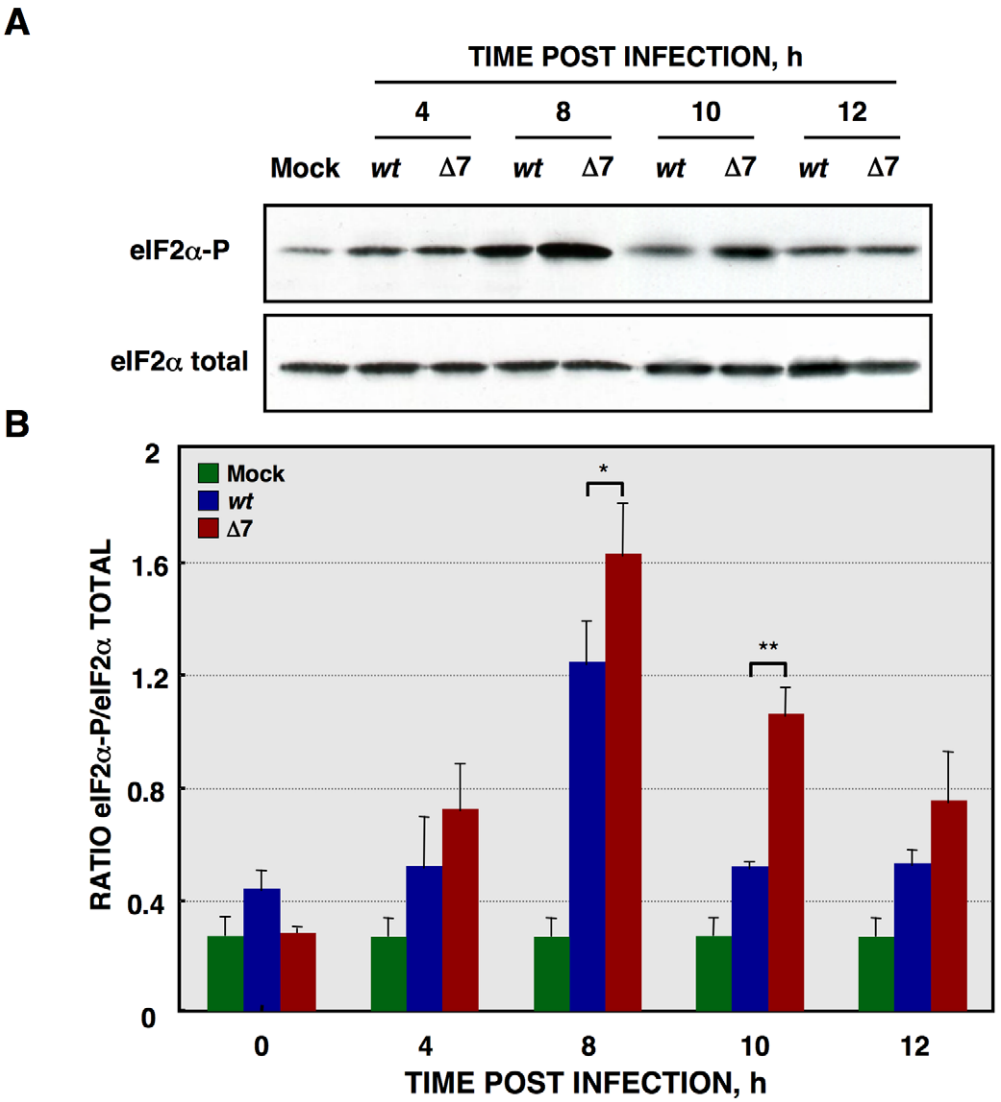

Figure 8. eIF2α phosphorylation during rTGEV infection. (A) Total protein was extracted, at indicated times post infection, from ST cells infected at a moi of 5 with rTGEV-*wt* (*wt*) and rTGEV-Δ7 (Δ7) viruses. Accumulation of total eIF2α and phosphorylated eIF2α (eIF2α-P), was analyzed by Western-blot. (B) eIF2α and eIF2α-P amounts were estimated by densitometric analysis. The graph represented eIF2α/eIF2α-P ratio in mock (green), rTGEV-*wt* (blue) and rTGEV-Δ7 (red) infected cells at indicated hpi. Error bars indicate the standard deviation from six independent experiments. r.u., relative units. *, p-value <0.05; **, p-value <0.01.
doi:10.1371/journal.ppat.1002090.g008

eIF2α dephosphorylation [94,102,110,111,112,113]. We have observed that both rTGEV-*wt* and rTGEV-Δ7 virus infections trigger the cell antiviral response, leading to an increased eIF2α-P level. We hypothesized that during rTGEV-*wt* infection protein 7 may interact through its PP1c-binding motif with the PP1 complex, promoting eIF2α dephosphorylation, leading to normal protein synthesis (Figure 10C). In contrast, in rTGEV-Δ7 infection, the virus could not counteract the high eIF2α-P levels, causing translational shutoff and cell damage (Figure 10C). TGEV protein 7-PP1 interaction was evaluated using a pull-down assay with ST-HA-7 cells extracts. Immunoprecipitation with anti-HA-agarose followed by immunoblotting with anti-HA showed the presence of protein 7 in both the ST-HA-7 input and immunoprecipitated extracts, but not in ST cells extracts, as expected (Figure 10D). Immunoblotting with anti-PP1 confirmed that PP1c was pulled-down together with protein 7 (Figure 10D). HA-tagged SARS-CoV E protein, which is also a small viral membrane protein was used as a control bait for immunoprecipitation. The interaction between protein 7 and PP1 was specific, as E protein did not co-immunoprecipitate PP1protein (Figure 10D). Moreover, an HA-tagged protein 7 mutant, lacking PP1 binding motif, did not co-immunoprecipitate PP1 protein. Altogether, this results demonstrated TGEV protein 7-PP1 interaction. The presence of eIF2α on the co-immunoprecipitated samples was also analyzed. This factor was specifically co-immunoprecipitated both by native and mutant TGEV protein 7 (Figure 10D), suggesting that eIF2α was present in the complex formed by TGEV protein 7 and PP1. Furthermore, the interaction between protein 7 and PP1 was also evaluated in the context of TGEV infection. ST-HA-7 cells were mock infected or infected with rTGEV-Δ7, to avoid competition with the non-tagged protein 7 encoded by the wild-type virus. PP1 co-immunoprecipitated with HA-tagged protein 7 in rTGEV-Δ7 infected cells (Figure S4), indicating that TGEV protein 7 also interacts with PP1 in the

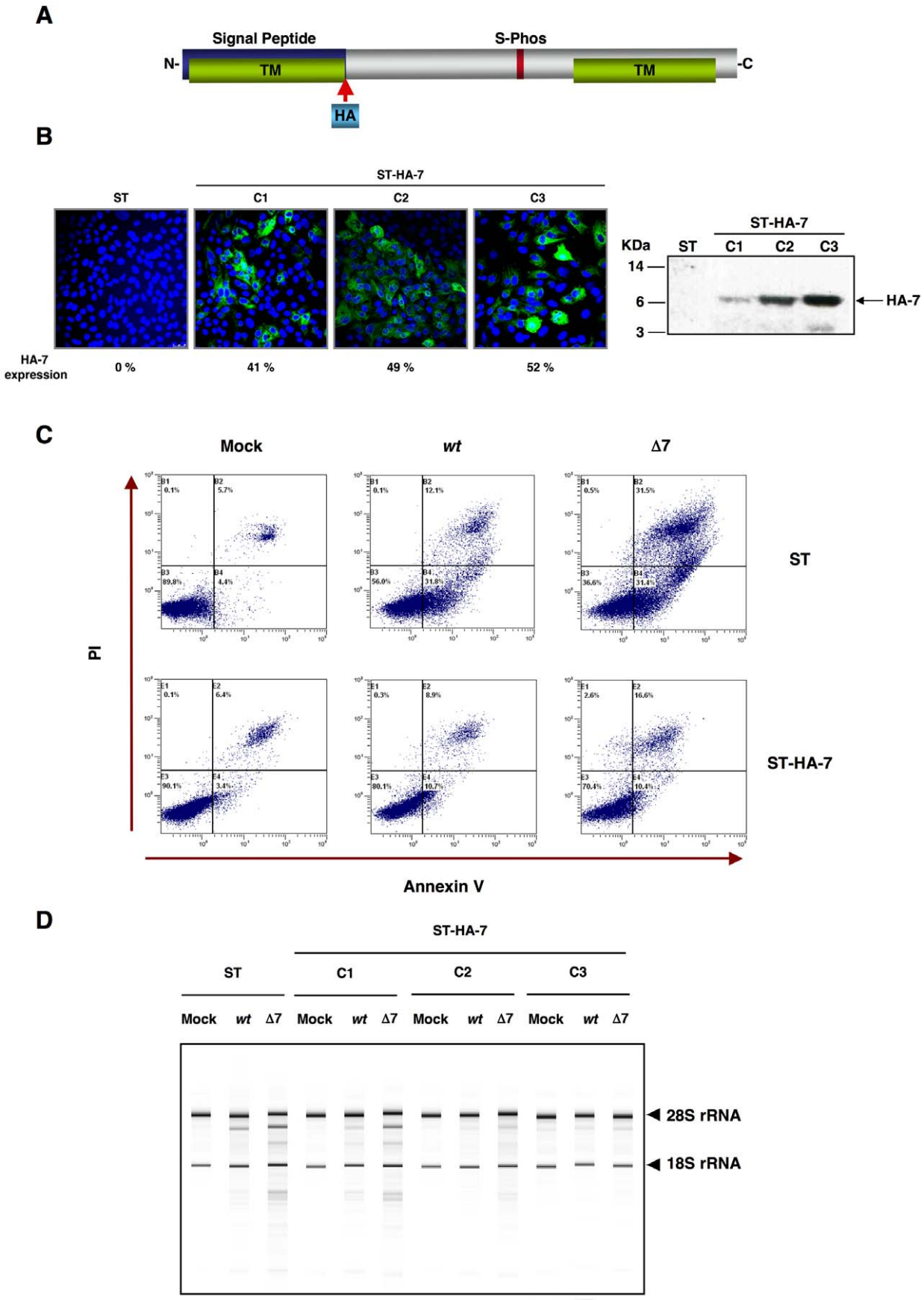
A
Signal Peptide
S-Phos
N-
TM
TM
-C
HA
B
ST-HA-7
ST
C1
C2
C3
HA-7 expression
0 %
41 %
49 %
52 %
KDa
14
6
3
HA-7
C
Mock
wt
Δ7
PI
ST
ST-HA-7
Annexin V
D
ST-HA-7
ST
C1
C2
C3
Mock
wt
Δ7
28S rRNA
18S rRNA

Figure 9. Complementation of rTGEV-Δ7 produced apoptosis and RNA degradation by protein 7 provided *in trans*. Generation of ST cells expressing TGEV protein 7 *in trans*. (A) Scheme of TGEV protein 7 expressed by the gene transfected into ST cells. Hemaglutinin tag (HA, light blue) was inserted after signal peptide (blue). (B) Protein 7 expression levels for the three ST-HA-7 selected cellular clones (C1, C2 and C3), were analyzed by immunofluorescence (left). Tagged protein 7 was detected with an anti-HA antibody stained in green, and cell nucleus were stained in blue. Percentage of HA-7 expressing cells is indicated. HA-7 protein accumulation was evaluated by Western-blot (right). HA-7 band is indicated, and corresponds to tagged protein cleaved form (7 KDa). (C) ST cells, or ST cells expressing HA-tagged protein 7 (ST-HA-7) were used to analyze apoptosis levels by flow cytometry. Apoptosis levels in mock, rTGEV-*wt* (*wt*) and rTGEV-Δ7 (Δ7) infected cells were evaluated at 12 hpi. Annexin V-PI double staining was performed to differentiate cells in early apoptosis (Annexin V^+, PI^-) from those in late apoptosis (Annexin V^+, PI^+) stages. (D) ST cells and the three ST-HA-7 cell clones obtained were mock, rTGEV-*wt* or rTGEV-Δ7 infected. Total RNA was extracted at 18 hpi. Cellular RNA integrity was analyzed using a Bioanalyzer. 28S and 18S rRNAs are indicated on the right.
doi:10.1371/journal.ppat.1002090.g009

context of TGEV infection. Moreover, in rTGEV-*wt* infected ST-HA-7 cells, a decrease in the PP1 co-immunoprecipitated by HA-tagged protein 7 was observed in relation to the rTGEV-Δ7 infected cells (Figure S4B), indicating that protein 7, expressed from rTGEV-*wt* virus, also interacts with PP1, and competed with tagged HA-7 protein for the binding to PP1.

To further evaluate the role of the PP1-protein 7 interaction on the rTGEV-Δ7 observed phenotype, RNA degradation and eIF2α phosphorylation levels were analyzed in the presence of the protein 7 mutant that did not bind to PP1. ST cells were transfected with the HA-tagged protein 7 mutant, and the expression of this protein was confirmed by immunofluorescence (data not shown). As previously observed, rTGEV-Δ7 virus caused an increased RNA degradation (Figure 11A) and eIF2α phosphorylation (Figure 11B). Interestingly, protein 7 mutant provided *in trans* did not reduce the RNA degradation and eIF2α phosphorylation caused by rTGEV-Δ7 virus (Figure 11), although eIF2α was also pulled-down by protein 7 mutant. This data strongly indicated that native TGEV protein 7 modulated RNA degradation and eIF2α phosphorylation by its interaction with PP1 protein, supporting our working hypothesis.

In vivo phenotype of rTGEV-Δ7

Newborn piglets were infected with rTGEV-*wt* and rTGEV-Δ7 viruses. Both viruses showed similar growth kinetics in the lung, although gene 7 deletion mutant virus reached higher titers than the parental virus at early times post infection (Figure 12A). Virulent TGEV strains replicate in the villious epithelial cells of the small intestine and in lung cells, causing severe diarrhea in newborn piglets [57,114,115]. The respiratory and enteric tropism of the rTGEVs can be modified by the introduction of an S gene from a virulent strain [57,114,115]. The rTGEV-Δ7 deletion mutant used throughout this paper was generated with an exclusively respiratory tropism (see Materials and Methods). To study the relevance of protein 7 in a virulent virus, a recombinant virus with respiratory and enteric tropism, lacking the expression of the gene 7 (rTGEV-SC11-Δ7) was engineered [57]. Growth in lung of rTGEV-SC11-*wt* and rTGEV-SC11-Δ7 viruses was similar to that of the previous mutant and wild-type viruses (data not shown). Interestingly, the rTGEV-SC11-Δ7 showed accelerated growth kinetics in gut, compared to the wild-type virus (Figure 12B). This behavior correlated with more pronounced clinical symptoms (Figure S5A). Both rTGEV-SC11-*wt* and rTGEV-SC11-Δ7 infected animals had the same final survival ratio (50%) (Figure S5B). Nevertheless, animals infected with rTGEV-SC11-Δ7 died six days before that those infected with rTGEV-SC11-*wt* (Figure S5B). Accordingly, virus was detected only in sentinel animals in contact with rTGEV-*wt* infected piglets, but not in those in close proximity to the rTGEV-SC11-Δ7 infected animals (Figure 12B). This result suggested that the presence of protein 7 facilitated animal survival and virus shedding.

Histopathology of lungs from animals infected with rTGEV-*wt* and rTGEV-Δ7 viruses was analyzed. Lung injury caused by rTGEV-*wt* consisted in alveolar wall thickening, emphysemas, and obstruction of the conducting airways by cell debris (Figure 13). rTGEV-Δ7 pathology at 1dpi was comparable with that observed in piglets 4 days post rTGEV-*wt* infection, indicating that tissue injury caused by the gene 7 deletion mutant virus was faster than that due to the wild-type virus (Figure 13). In addition to the lesions described in rTGEV-*wt* infected animals, in rTGEV-Δ7 infected tissue edema was also observed as a consequence of strong alveolar congestion (Figure 13).

Virus antigen immunodetection showed the same infection pattern for both viruses (Figure 13), and the active caspase 3 pattern overlapped with those areas in which viral infectious foci were detected (Figure 13). Taken together the results indicated a faster lung infection and more extensive injury caused by rTGEV-Δ7 virus.

Discussion

This study shows that TGEV protein 7 modified the antiviral response, and that the presence of gene 7 attenuated virus virulence. TGEV infection led to the activation of an antiviral pathway triggered by the dsRNA produced during the virus cycle (Figure 14). This pathway has two main effectors: 2′-5′OAS that leads to RNase L activation and RNA degradation, and PKR that is responsible of eIF2α phosphorylation [116]. In general, the activation of this pathway leads to blocking of the cell translational machinery, and induction of caspase-dependent apoptosis of infected and neighboring cells (Figure 14) [8,10]. Interestingly, we have shown that TGEV protein 7 bound PP1, a key regulator of the cell antiviral defenses, and we proposed that this binding modulates dsRNA-activated pathway.

In rTGEV-Δ7 infected cells, an increased eIF2α phosphorylation was observed over rTGEV-*wt* infection, although enhanced kinase activation was not detected. Interaction of protein 7 with the PP1c complex may counteract PKR activity (Figure 14). This is a novel mechanism not previously observed in the RNA viruses. Nevertheless, a similar mechanism was previously described for three DNA virus proteins containing a PP1c-binding motif, encoded by herpex simplex virus-1 ($\gamma_1$34.5 protein), papilomavirus (E6 protein) and African swine fever virus (DP71L protein) (Figure 10B) [102,110,111]. These proteins counteract the negative effect of the eIF2α phosphorylation on cellular and viral protein synthesis through their interaction with the PP1 complex. This interaction promotes dephosphorylation of eIF2α [102,110,111]. In fact, while native TGEV protein 7 provided *in trans* decreased eIF2α phosphorylation, a protein 7 mutant that did not bound PP1 was unable to reduce eIF2α phosphorylation levels.

The evaluation of cellular RNA integrity in rTGEV-Δ7 infected cells revealed an increase of cellular RNA degradation compared with rTGEV-*wt* virus infected cells. The degradation pattern was

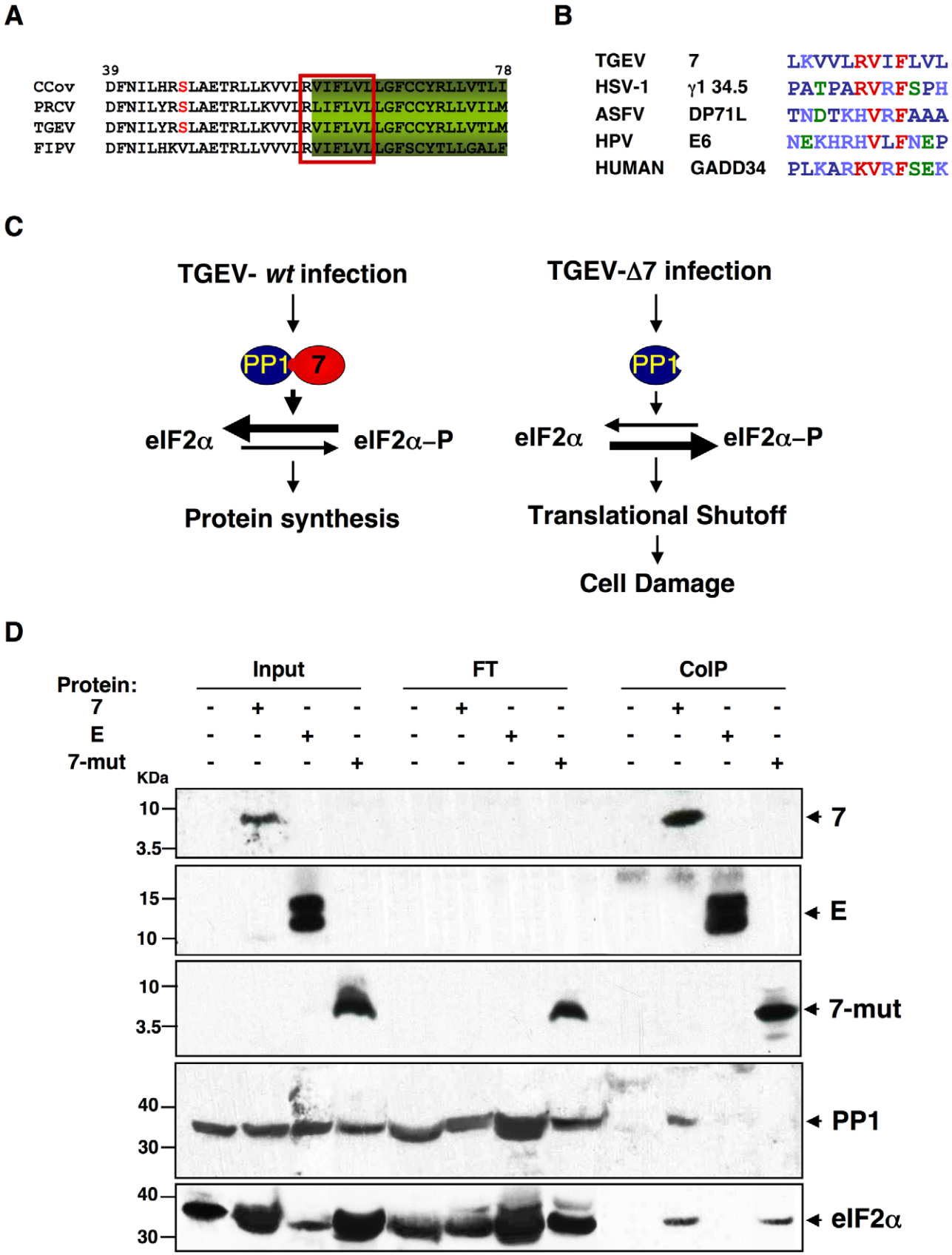

Figure 10. PP1c binding motif in genus α1 CoV protein 7. (A) Fragment from the alignment of genus α1 CoV 7a proteins. Canonical PP1c-binding motif is represented by the red box [ELM server [105,106]]. (B) Consensus PP1 binding motif, including a short sequence (R/K)VxF (red), surrounded by non-polar residues. This motif is present in other viral and cellular proteins, such as human simplex virus-1 (HSV-1) $\gamma_1$34.5, African

swine fever virus (ASFV) DP71L, human papilomavirus (HPV) E6 oncoprotein, and human growth arrest DNA-damage 34 (GADD34). GenBank accession numbers are ADB28914.1, P36313, Q65212, ACR78108 and O75807, respectively. Dark blue, non-polar aa; light blue, basic aa; green, polar aa; and red, PP1 binding motif core sequence. (C) Proposed model for protein 7 function during TGEV infection. (D) Coimmunoprecipitation of TGEV protein 7 and PP1. TGEV protein 7-PP1 interaction was evaluated using ST cells, ST-HA-7 cells (7), or ST cells transiently expressing SARS-CoV E protein (E), or a protein 7 mutant lacking the PP1 binding motif (7-mut). Cell extracts were incubated with anti-HA agarose. Input, flow through (FT), and final elution (CoIP) samples were resolved by SDS-PAGE. The presence of HA-tagged proteins, PP1 and eIF2α was analyzed by Western-blot using specific antibodies.

doi:10.1371/journal.ppat.1002090.g010

identical to that observed after specific RNase L activation, suggesting that this nuclease was the responsible for RNA degradation during TGEV infection. Interestingly, 2′-5′OAS1 expression, which is required for RNase L activation, was similarly increased after infection with both rTGEV-*wt* and rTGEV-Δ7 viruses. These results suggested that protein 7 may be modulating the 2′-5′OAS pathway at a level prior to RNase L activation (Figure 14). Activation of 2′-5′OAS by dsRNA leads to the synthesis of 5′-triphosphorylated, 2′-5′-oligoadenylates (2′-5′A) required for RNase L dimerization and activation. The 2′-5′A are highly unstable due to their potential dephosphorylation at the 5′end by general phosphatases, leaving the core oligoadenylate that does not efficiently activate RNase L [117]. We propose that the complex PP1-protein 7 may counteract RNase L activation through the dephosphorylation of 2′-5′A. In fact, native TGEV protein 7 provided *in trans* reduced RNA degradation, while a protein 7 mutant that did not bound PP1 was unable to decrease RNA degradation. To our knowledge, this is the first report involving PP1 protein on the dsRNA induced RNA degradation pathway. Surprisingly, viral mRNAs were not differentially degraded after infection with rTGEV-*wt* or rTGEV-Δ7, indicating that these mRNAs may be hidden from nuclease activity. Initially, protection of these mRNAs could be mediated by their sheltering in double-membrane vesicles (DMVs), induced by CoV infection, and identified in MHV [28], SARS-CoV [29], and TGEV infected cells (A. Nogales, L. Enjuanes and F. Almazán, unpublished results). DMVs may provide an environment for viral RNA synthesis, and prevent the action of components of host defenses, such as antiviral nucleases. The mechanisms for viral mRNA protection at later stages of the viral cycle will require further studies.

We demonstrated that rTGEV-Δ7 showed an enhanced CPE, in relation to that caused by rTGEV-*wt*, which was a consequence of the acceleration of apoptosis characterized by a faster activation of caspase 3. In agreement with our results, it has previously been described that the activation of PKR and 2′-5′OAS/RNase L pathways generally leads to apoptosis [118,119]. Furthermore, apoptosis initiated by RNase L requires caspase 3 activity [120]. Interestingly, the growth kinetics of both viruses was similar, indicating that the increased antiviral response and apoptosis, did not compromise virus replication. It has been previously described that inhibition of TGEV-induced apoptosis did not enhance viral production [63]. Similarly, in other CoVs, such as SARS-CoV or MHV, downregulation of PKR or RNase L, respectively, did not affect virus growth [96,121]. Altogether these results suggest that, at least for these CoVs, the dsRNA-activated response did not affect viral replication. Nevertheless, all these CoVs have developed strategies to counteract the dsRNA antiviral response [33,122,123]. These strategies could control the deleterious effect that an exacerbated antiviral response may cause in the host, and therefore in long term virus survival [124]. In fact, rTGEV-Δ7 virus showed an accelerated growth kinetics *in vivo* compared to rTGEV-*wt*. This effect was probably due to a premature cell death in the rTGEV-Δ7 infected animal tissue that promoted a faster initial propagation of the virus.

To generate the rTGEV-Δ7 analyzed here, minimal modifications required to avoid gene 7 expression were introduced in a TGEV-wt backbone. A previously evaluated rTGEV without gene 7 expression showed full attenuation, with 100% survival of infected piglets [52], what is at variance (but not in contradiction) with the results presented in this work. Fortunately, the two deletion mutant viruses used in the Ortego et al 2003 paper and the one used here are completely different. The mutant virus in the Ortego's paper was derived from a already highly attenuated virus, only causing 20% piglet death after virus administration. It is essential to realize that this virus already included many additional attenuating genome changes: (i) five engineered restriction sites preceding genes 3a, E, M, N and 7; (ii) the duplication of sequences preceding these genes, required to avoid gene overlapping. Furthermore this duplicated sequences, located close to the gene TRS, contained an additional TRS that regulate the expression levels of each gene, what probably influenced the expression levels of these viral genes; and (iii) a deletion spanning 21 nt upstream ORF7 start codon and the first 17 nt of this ORF, that was introduced to prevent the expression of gene 7. In contrast, the TGEV deletion mutant used in this work only included a point mutation in gene 7 CS and a 7 nt deletion to prevent the production of protein 7. Therefore, the changes observed in the pathogenicity of the Ortego's recombinant virus could not be exclusively assigned to gene 7 absence, in contrast to the results presented in this paper.

In general, viral infection leads to a strong antiviral state in infected and neighboring cells [65]. We postulate that the balance between enhanced apoptosis and the bystander effect compromised and limited rTGEV-Δ7 virus tissue dissemination. Preliminary results from high throughput gene expression analysis supported this proposal (data not shown). In fact, in agreement with this postulate, rTGEV-Δ7 infected piglets showed an accelerated pathology when compared with the rTGEV-*wt* infected ones. Furthermore, the recovery from the inflammatory response was slower in rTGEV-Δ7 infected animals than in rTGEV-*wt* ones as lungs infected by the rTGEV-Δ7 showed more lesions at 4 dpi than those infected with the rTGEV-*wt*. Current work in our lab is directed at analyzing whether the removal of gene 7 in rTGEV leads to an infection with an enhanced innate immune response.

The results obtained suggested that while a balanced immune response promotes virus clearance and tissue reparation, an exacerbated innate immune response could result in immune pathology and subsequent tissue damage, as observed in rTGEV-Δ7 infected piglets. Similar effects have been described for other viruses, such as human hepatitis C virus [125], in which tissue damage was associated to the development of an exacerbated host antiviral response and not with viral replication. Moreover, piglets infected with a TGEV virulent enteric strain lacking protein 7 expression (rTGEV-SC11-Δ7), developed a faster and more pronounced clinical disease. High pathogenicity resulted in a more rapid host elimination, affecting virus long-term survival as the host is essential for virus propagation. From an evolutionary point of view, our results suggested that CoVs genus α1 might have

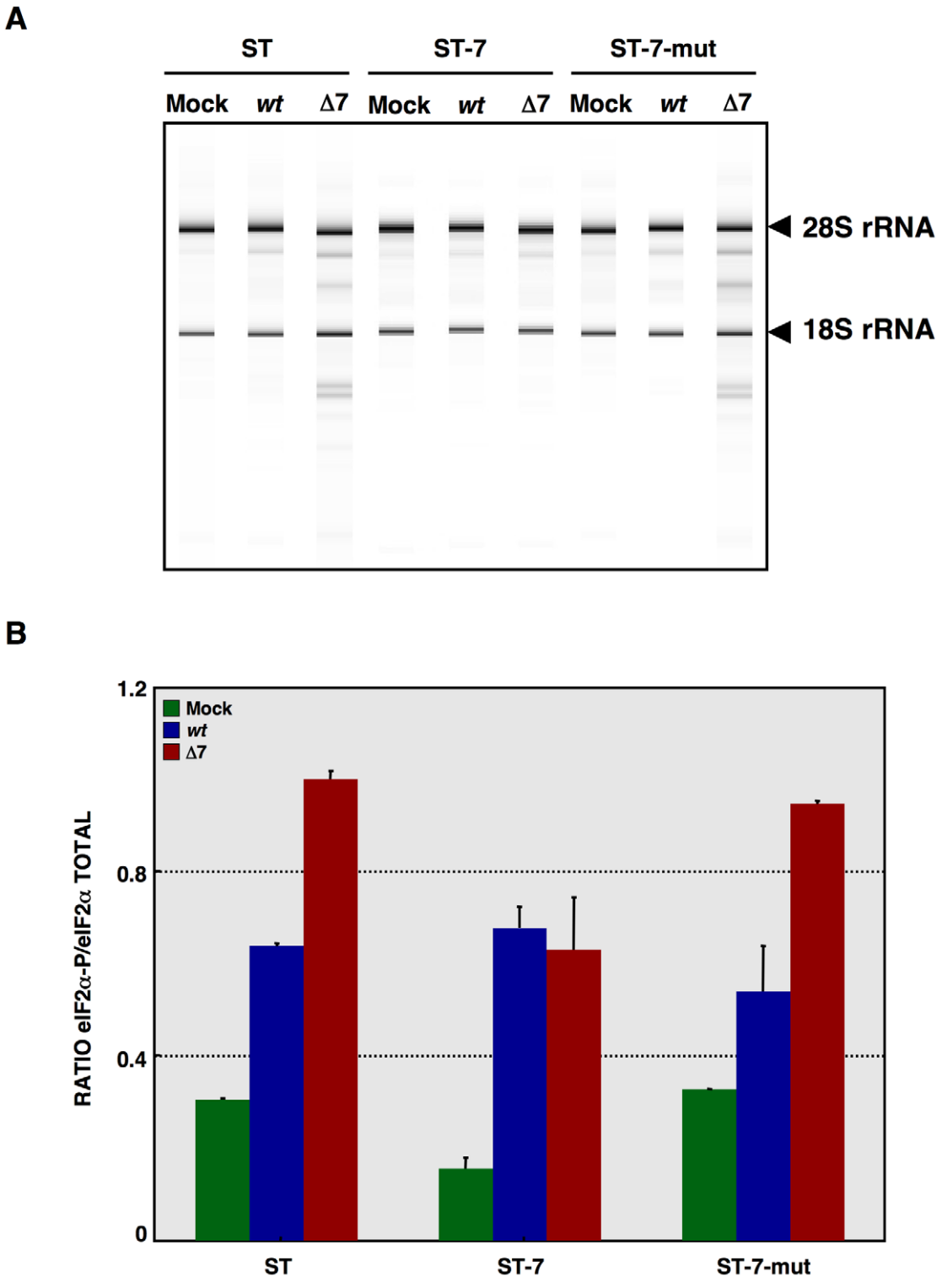

Figure 11. Effect of mutated protein 7 provided *in trans* on RNA degradation and eIF2α phosphorylation. ST cells, or ST cells expressing native TGEV protein 7 or the mutated protein 7 lacking PP1 binding motif were used. Cells were mock infected or rTGEV-*wt* (*wt*) and rTGEV-Δ7 (Δ7) infected. (A) Total RNA was extracted at 18 hpi and cell RNA integrity was analyzed using a Bioanalyzer. 28S and 18S rRNAs are indicated on the right. (B) Total protein was extracted at 10 hpi and eIF2α and eIF2α-P protein levels were analyzed by Western-blot. Protein amounts were estimated by densitometry, and the ratio of eIF2α-P to total eIF2α was represented. Error bars represented the standard deviation of three independent experiments.

doi:10.1371/journal.ppat.1002090.g011

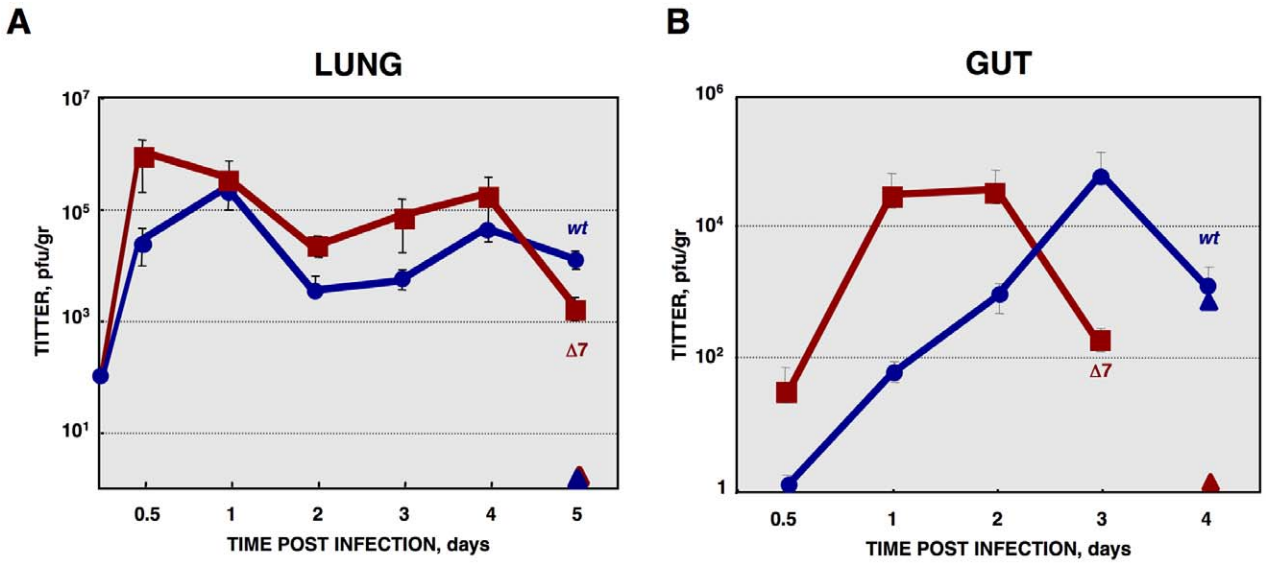

Figure 12. *In vivo* growth kinetics of rTGEV-Δ7 virus. (A) Two- to three-day-old piglets were inoculated with 1×10^7 pfu/pig of rTGEV-*wt* and rTGEV-Δ7 viruses by two routes (oral and nasal) in combination. At 0.5, 1, 2, 3, 4 and 5 days post inoculation two animals per group were sacrificed, and the lungs were harvested. rTGEV-*wt* (blue) and rTGEV-Δ7 (red), recovered from lung, were titrated. Triangles indicated sentinel animals. (B) Two- to three-day-old piglets were inoculated with 1×10^7 pfu/pig of rTGEV-SC11-*wt* and rTGEV-SC11-Δ7 viruses by three routes (oral, intranasal and intragastric) in combination. At indicated days post inoculation two animals per group were sacrificed, and the lung and the gut were harvested. rTGEV-SC11-*wt* (blue) and rTGEV-SC11-Δ7 (red) titers in gut are represented. Triangles indicate sentinel animals. Error bars indicate the standard deviation from three independent experiments.
doi:10.1371/journal.ppat.1002090.g012

acquired gene 7 to counteract host defenses with the aim of preventing overwhelming tissue damage due to an exacerbated innate immune response. Protein 7 would then benefit both the host, reducing the pathology caused by the infection, and the virus, allowing longer virus persistence and dissemination.

Materials and Methods

Ethics statement

Animal experimental protocols were in strict accordance with EU guidelines 2010/63/UE, and Spain national law RD 1201/2005, about protection of animals used for experimentation and other scientific purposes, and national law 32/2007, about animal welfare in their exploitation, transport, experimentation and sacrifice. The experiments were performed in an animal facility at Pfizer Animal Health, Girona (Permit numbers G9900005 and G9900007), and were approved by the in site ethical review committee (Comitè Ètic d'Experimentació Animal).

Cells

Baby hamster kidney (BHK) cells stably transformed with the porcine amino peptidase N gene (BHK-pAPN) [126] were grown in Dulbecco's modified medium (DMEM) supplemented with 5% fetal bovine serum (FBS) and G418 (1.5 mg/ml) as a selection agent. Swine testis (ST) cells were grown in DMEM supplemented with 10% FBS [127].

Generation of ST cells expressing TGEV protein 7

The gene for TGEV protein 7, with hemaglutinin tag (HA) inserted after the signal peptide, cloned in *Hind*III-*Eco*RI restrictions sites in the plasmid pcDNA 3.1, was purchased from GenArt (Germany). Four micrograms of pcDNA 3.1-HA-7 were linearized with *Sma*I, and purified using QIAquick Kit (Qiagen) according to the manufacturers specifications. The linearized plasmid was used for reverse transfection of ST cells with 12 µl of Lipofectamine 2000 (Invitrogen), as recommended by the manufacturer. Cells were grown in DMEM supplemented with 10% FBS and G418 (1.5 mg/ml) as a selection agent. Cells were cloned and positive clones for HA-7 expression, by immunofluoresce and Western-blot, were amplified.

Generation of ST cells transiently expressing TGEV protein 7-mut or SARS-CoV E protein

A pcDNA 3.1 plasmids, with TGEV 7-mut gene cloned in *Hind*III-*Eco*RI restrictions sites, was purchased from GenArt (Germany). This plasmid, pcDNA3.1-7-mut, encodes TGEV protein 7 with a deletion comprising amino acids 59 to 62, which include the PP1 binding motif (R/K)VxF, with an HA tag inserted after the signal peptide. Plasmid pcDNA3.1-E, encoding SARS-CoV E protein, with an HA tag in its amino-terminus, was previously obtained in our laboratory (E. Alvarez, M. L. DeDiego and L. Enjuanes, unpublished results). For transient expression experiments, circular plasmids were used for reverse transfection of ST cells as described above.

Construction of the plasmid pBAC-TGEV-Δ7

A recombinant TGEV virus was engineered using a TGEV-SPTV genetic background, with respiratory tropism and adapted to tissue cultures [57]. The mutations required to knock down gene 7 expression were introduced by overlapping PCR using as a template the plasmid pSL-3EMN7, comprising nucleotides 20,372 to 28,087 of TGEV genome [128]. Overlapping PCR fragments, with point mutations and deletions, were amplified using oligonucleotides ΔORF7 VS (5′-GCTCGTCTTCCTCCATGCTGTATTTAT-3′) and ΔORF7 RS (5′-GATAATTGATGAGGTAACGAACTGAGCTCGTCTTCGTTACCTATC-3′).

The final PCR product (2700 bp), amplified with outer oligonucleotides ΔORF7 VS-Oli 4 *Sph*I RS (5′-CATAGCACAA-

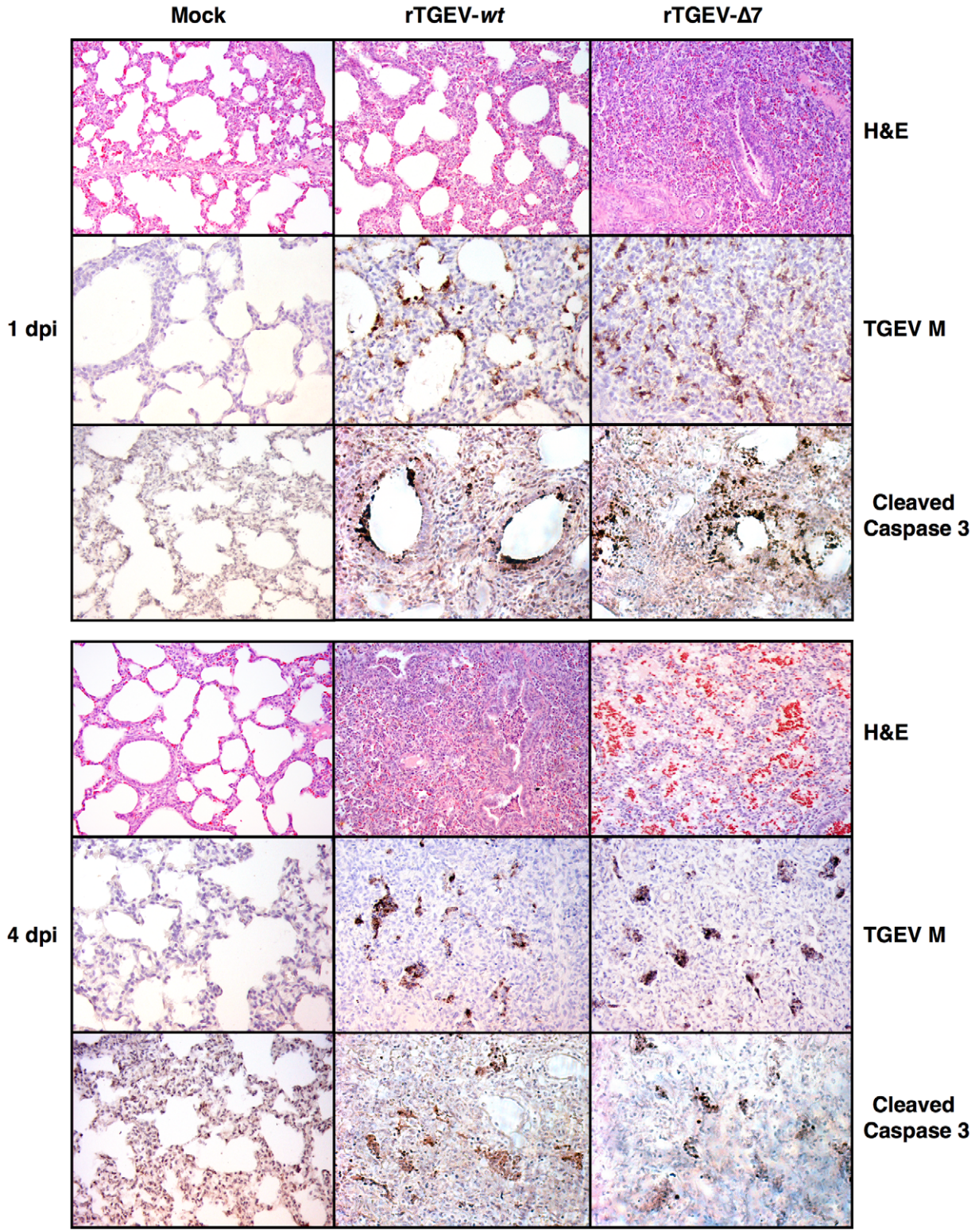

Figure 13. Lung histopathology caused by rTGEV-Δ7 infection. Two- to three-day-old piglets were inoculated with 1×10^7 pfu/pig of rTGEV-*wt* and rTGEV-Δ7. Lung samples, collected at 1 and 4 days post infection, were stained with hematoxylin-eosin (H&E). Pictures were obtained with a 10x objective. TGEV membrane protein (M) and cleaved caspase 3, were also immunodetected with specific antibodies. Pictures were obtained with a 20x objective.
doi:10.1371/journal.ppat.1002090.g013

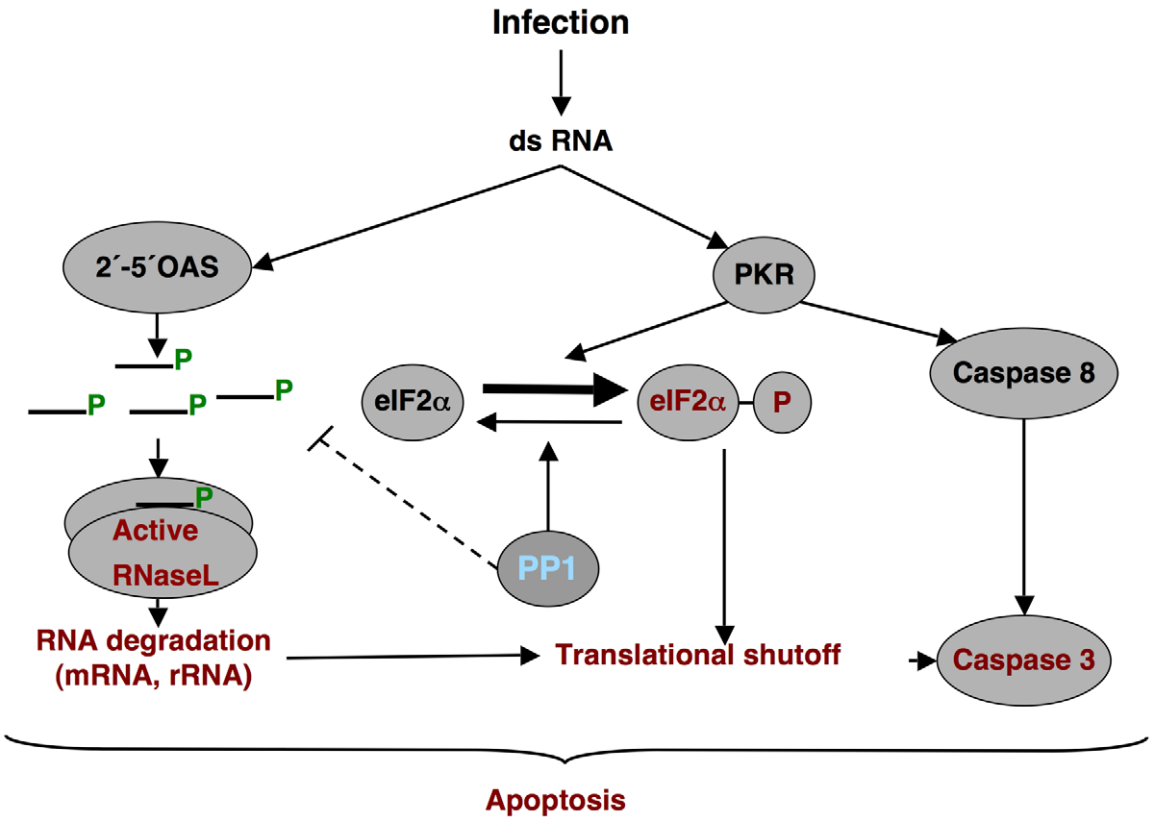

Figure 14. dsRNA induced antiviral pathway. Schematic overview of the dsRNA-induced antiviral pathway analyzed. Differential effects observed during rTGEV-Δ7 infection are in red. PP1, the proposed target of protein 7, is in blue.
doi:10.1371/journal.ppat.1002090.g014

TAGCGTTCTCCACATGCGCATGCA-3′*) and ΔORF7 RS-Oli 1* Sph*I VS (*5′-GGAGGATTGGGAAGACAATAGCAGG-CATGCTGGGG-3′), was digested with *Sph*I and cloned in the same restriction site of pSL-3EMN7, leading to pSL-3EMNΔ7. To generate the plasmid pBAC-TGEV-SPTV-Δ7, pSL-3EMNΔ7 was digested with *Sfo*I-*Bam*HI. This fragment, containing nt 23,464 to 28,700 of the TGEV genome, and including the mutations, was cloned in the same restriction sites of the full-length pBAC-TGEV-SPTV^{FL} [129]. To generate a rTGEV-Δ7 virus with both enteric and respiratory tropism a TGEV-SC11 virus backbone was used [57]. To this end, the pSL-3EMNΔ7 *Sfo*I-*Bam*HI fragment was cloned in the same restriction sites of the full-length pBAC-TGEV-SC11^{FL} [129]. All cloning steps were checked by sequencing of the PCR fragments and cloning junctions.

Transfection and recovery of infectious virus

BHK-pAPN cells were grown to 95% confluence on 35-mm-diameter plates and transfected with 4 µg of infectious cDNA using 12 µl of Lipofectamine 2000 (Invitrogen), according to the manufacturer's specifications. After 6 h of incubation at 37°C, cells were trypsinized and plated over a confluent ST monolayer grown in 35-mm-diameter plate. Recombinant TGEV (rTGEV) viruses were recovered, grown and titrated as previously described [130,131].

RNA extraction and analysis

One day after confluence ST cells, grown on 35-mm-diameters plates, were infected at a multiplicity of infection (moi) of 5. Total intracellular RNA was extracted at different hours post-infection (hpi) using the RNeasy Mini Kit (Qiagen), according to the manufacturer's instructions. Viral sg mRNAs were evaluated by Northern blot and RT-qPCR analyses, following standard procedures set up in our laboratory [131,132]. Cellular gene expression was analyzed by using a custom TaqMan gene expression assay (Applied Biosystems) specific for porcine 2′,5′oligoadenylate synthetase 1 (2′,5′OAS1) (Table 1), and growth arrest DNA-damage 34 (GADD34) (Table 1). Data were acquired with an ABI PRISM 7000 sequence detection system and analyzed with ABI PRISM 7000 SDS version 1.2.3 software (Applied Biosystems). Total cell RNA integrity was evaluated with a Bioanalyzer 2100 (Agilent Technologies) following the manufacturer's recommendations, and analyzed with 2100 Expert software (Agilent Technologies). Four micrograms of polyinosynic-polycytidylic acid [Poly (I:C), Sigma] were used for reverse transfection of ST cells with 12 µg of Lipofectamine 2000 (Invitrogen), as recommended by the manufacturer. Total RNA was extracted 16 hours post transfection, and cell RNA integrity was analyzed as described above. For apoptosis inhibition experiments, caspase inhibitor inhibitor N-benzyloxycarbonyl-Val-Ala-Asp-fluoromethylketone (ZVAD.fmk) was added to the cell culture medium at a concentration of 100 µM as previously described [63]. Total RNA was extracted 18 hours post infection, and cell RNA integrity was analyzed as described above.

Expression of RNase L system from recombinant vaccinia viruses

To evaluate the cellular RNA degradation by the 2-5OAS/RNase L system, three recombinant vaccinia viruses, vvT7, vvRL and vv2-5AS, were used as previously described [84]. Expression of RNase L from vvRL, was under the control of T7 promoter

Table 1. Accession numbers of proteins mentioned in the text.

PROTEIN	SPECIES [a]	ID	DATABASE
β-actin	Porcine	Q7M3B0	UniProtKB (unreviewed)
	Human	P60709	UniProtKB
BiP	Porcine	P34935	UniProtKB
	Human	P11021	UniProtKB
Caspase 3	Porcine	Q95ND5	UniProtKB
eIF2α	Porcine	P20460 [b]	UniProtKB
	Human	Q9BY44	UniProtKB
eIF4G	Porcine	– [c]	–
	Human	Q04637	UniProtKB
GADD34	Porcine	ENSSSCT00000003504	ENSEMBL
OAS1	Porcine	Q29599	UniProtKB
PERK	Porcine	ENSSSCP00000008763	ENSEMBL
	Human	Q9NZJ5	UniProtKB
PKR	Porcine	Q865A4	UniProtKB (unreviewed)
	Human	P19525	UniProtKB
PP1	Porcine	–	–
	Human	P62136	UniProtKB
RNaseL	Porcine	A5H025	UniProtKB (unreviewed)
	Human	Q05823	UniProtKB

(a) The work was performed in porcine cells, but human IDs are also provided when antibodies for human proteins were used.
(b) Available sequence corresponds to a 70 aa fragment.
(c) Sequence not available.
doi:10.1371/journal.ppat.1002090.t001

[133]. Expression of T7 polymerase and human 2-5OAS1, produced by vvT7 and vv-2-5AS respectively, was constitutive. ST cells were infected at a moi of 2 with vvT7 or vvT7, vvRL and vv2-5AS. Total RNA was harvested at 24 hpi, and analyzed by a Bioanalyzer as described above.

Protein analysis by Western blotting

ST cells were infected at a moi of 5, harvested at different hpi, and protein extracts were obtained as previously described [59]. When protein phosphorylation levels were analyzed, a phosphatase inhibitor cocktail (PhosSTOP, Roche) was added to the extraction buffer. Cell lysates were separated by sodium dodecyl sulfate-polyacrylamide gel electrophoresis (SDS-PAGE). Proteins were transferred to a nitrocellulose membrane (Hybond-C, GE Healthcare) and analyzed as described [45]. The membranes were incubated with polyclonal antibodies (pAbs) specific for active Caspase 3 protein (abcam, 1:10,000), PKR (Santa Cruz, 1:200), BiP (Abcam, 1:500), eIF2α (Santa Cruz, 1:2000), phosphorylated eIF2α (Invitrogen, 1:500) and PP1c (Santa Cruz, 1:200). Monoclonal antibodies (mAbs) specific for HA (Sigma, 1:1000), total PKR (Santa Cruz, 1:1000), PP1c (Santa Cruz, 1:1000) and β-Actin (Abcam, 1:10,000) were also used. Protein accession numbers are detailed in Table 1. Bound primary antibodies were detected with horseradish peroxidase-conjugated antibodies specific for the different species, using the Immobilon Western chemiluminescent substrate (Millipore), following the manufacturers recommendations. Protein amounts were estimated by densitometric analysis using Quantity One 4.6.3 software (BioRad). At least three different experiments and appropriate gel exposures were used in all cases with similar results. In addition, different exposures of the same experiment were analyzed to assure that data were obtained from films within linear range.

Immunofluorescence

ST-HA-7 cells were fixed with 4% paraformaldehyde and permeabilized with 0.2% saponin in phosphate-buffered saline (PBS) and 10% FBS. Monoclonal antibody specific for HA (Sigma, 1:500) was used. Bound primary antibody was detected with AlexaFluor488 conjugated antibody specific for mouse (Invitrogen, 1:500). Cell nucleus were stained with 4′,6-diamidino-2-phenylindole (DAPI) (Sigma, 1:200).

Metabolic labeling

One day post-confluence ST cells, grown on 35-mm-diameters plates were infected at a moi of 1 to avoid strong cytopathic effect (CPE). The cells were incubated 30 min in cysteine- and methionine- free modified Eagles medium with 10% FBS (starvation medium). The medium was then replaced by starvation medium containing 50 μCi ^{35}S/ml labeled Met and Cys (Taper). Cells were incubated at 37°C for 1 hour, washed with PBS containing 50 mM Ca^{2+} and 50 mM Mg^{2+}, and pelleted. The cells were broken in 50 μl of lysis buffer [59] supplemented with a nuclease mix (10U DNaseI from Roche, 10 μg RNase A from Qiagen) and 50 μl of SDS-PAGE loading buffer 2x [134]. Total protein lysates were subjected to one freeze-thaw cycle and then boiled at 95°C for 10 min, 15 μl of each sample were separated by 5-15% gradient SDS-PAGE. The gel was dried under vacuum onto Whatman 3 MM paper and exposed for protein product visualization. Label was estimated by densitometric analysis as described above.

Cell death analysis

To quantify cell death levels, ST cells were permeabilized and stained with vital dye propidium iodide (PI) (Roche) following standard procedures (Nicoletti I., 1991). The cell death population (genomic content <2 n) was quantified by flow cytometry. Apoptosis was evaluated by flow cytometry using fluorescein isothiocyanate (FITC) conjugated Annexin V (Roche), specifically binding apoptotic cells, as previously described [61]. Annexin V plus PI double staining was performed to differentiate cells in early apoptosis (Annexin V^+, PI^-) from those in late apoptosis (Annexin V^+, PI^+) stage.

Co-immunoprecipitation

Cell extracts from ST-HA-7 cells, expressing TGEV HA-tagged protein 7, or ST cells transiently expressing HA-tagged coronavirus proteins 7-mut or E were incubated with a mAb anti-HA agarose conjugated (1:1, Sigma), following the manufacturers recommendations. The presence of viral proteins 7, 7-mut and E, and cell proteins PP1 and eIF2α in the eluted samples was analyzed by Western-blot using specific antibodies as described above.

In vivo growth kinetics

Two- to three-day-old non-colostrum-deprived piglets, born from TGEV seronegative sows, were inoculated with virus (1×10^7 pfu/pig) following standard procedures [57]. Briefly, for respiratory tropism viruses animals were infected by two different routes (oral and intranasal) in combination. For enteric tropism viruses, animals were infected by three routes (intranasal, oral and intragastric) in combination. Infected animals were monitored daily to detect symptoms of disease and death. At 0.5, 1, 2, 3, 4 and 5 days post-inoculation (dpi) two animals per group were

sacrificed, and the lungs were collected. In order to evaluate representative samples, tissue extracts were obtained by homogenizing the whole organs at 4°C by using a Pro-250 tissue homogenizer (Fisher Scientific). Virus titers were determined in lung extracts following procedures set up in the laboratory [57].

Immunohistochemistry

Lung representative sections were fixed with 4% paraformaldehyde and stored in 70% ethanol at 4°C. Paraffin embedding, sectioning and hematoxylin-eosin staining (H&E) were performed by the histology service in the National Center of Biotechnology (CNB, Spain). 4 micron sections were immunostained for TGEV membrane (M) protein and cleaved caspase 3. Briefly, samples were deparaffined at 60°C and rehydrated by successive incubations in 100% xylol, 100% ethanol and 96% ethanol. Endogenous peroxidase was blocked at 37°C in darkness with 1% H_2O_2 diluted in methanol. For cleaved caspase 3 detection, tissue sections were boiled in citrate buffer (8.2 mM sodium citrate; 1.8 mM citric acid) pH 6.5. Unspecific binding was blocked with 3% bovine serum albumin (BSA) in PBS. Samples were incubated with a mAb specific for TGEV M protein (3B.B3, 1:100) [130] or with a pAb specific for active caspase 3 protein (abcam, 1:300), respectively. Bound primary antibodies were detected with biotinylated antibodies specific for the different species, using the ABC Peroxidase Staining Kit and Metal Enhanced DAB Substrate Kit (Pierce), following the manufacturers recommendations.

Supporting Information

Figure S1 Porcine GADD34 expression. The expression of porcine GADD34, during rTGEV-*wt* (blue) or rTGEV-Δ7 (red) infections at indicated hpi, was analyzed by RT-qPCR. Error bars indicate the standard deviation from three independent experiments. r.u., relative units.
(TIF)

Figure S2 Decreased eIF2α-P by expression of TGEV protein 7 *in trans*. (A) ST cells and ST-HA-7 clones C1, C2 and C3 were infected with rTGEV-*wt* or rTGEV-Δ7. Total RNA was extracted at 10 hpi and porcine GADD34 expression was analyzed by RT-qPCR. r.u., relative units. Error bars represented the standard deviation of three independent experiments. (B) ST cells and ST-HA-7 clones C1 and C3 were infected with rTGEV-*wt* or rTGEV-Δ7. Total protein was extracted at 10 hpi and eIF2α and eIF2α-P protein levels were analyzed by Western-blot. Protein amounts were estimated by densitometry, and the ratio of eIF2α-P to total eIF2α was represented. Error bars represented the standard deviation of three independent experiments.
(TIF)

Figure S3 Effect of protein 7 on kinases implicated in eIF2α phosphorylation. (A) Scheme of eIF2α/eIF2α-P equilibrium influenced by PKR, PERK and PP1 activity. (B) Evaluation of phosphorylated PKR (PKR-P), total PKR and BiP accumulation during rTGEV-*wt* or rTGEV-Δ7 infections, at indicated hpi, by Western-blot using specific antibodies. β-actin was detected as loading control. (C) Analysis of PP1 accumulation in ST cells infected with rTGEV-*wt* or rTGEV-Δ7 at indicated times post infection, by Western-blot using a specific antibody. β-actin was detected as loading control.
(TIF)

Figure S4 Interaction between PP1 and TGEV protein 7 in the context of TGEV infection. (A) ST mock infected cells, or ST-HA-7 cells infected with rTGEV-Δ7 were used for immunoprecipitation. Cell extracts from 16 hpi were incubated with anti-HA agarose. Input, flow through (FT), and final elution (CoIP) samples were resolved by SDS-PAGE. The presence of HA-tagged protein 7 and PP1 was analyzed by Western-blot using specific antibodies. (B) ST-HA-7 mock infected cells, or infected with rTGEV-*wt* or rTGEV-Δ7 viruses were used for immunoprecipitation as in (A). Co-immunoprecipitated (Co-IP) samples from different experiments were resolved by SDS-PAGE, and HA-tagged protein 7 and PP1 were detected by Western-blot. The graph represents the ratio between PP1 and HA-7 protein, estimated by densitometry. Error bars represent the standard deviation from the different experiments.
(TIF)

Figure S5 *In vivo* rTGEV-SC11-Δ7 virulence. Three-day-old piglets were inoculated with 1×10^7 pfu/animal of rTGEV-SC11-*wt* or rTGEV-SC11-Δ7 viruses, by three routes (oral, intranasal and intragastric) in combination. (A) Clinical symptoms were analyzed during the experiment. The degree of diarrhea was represented: from 0, meaning healthy animal, to 3, meaning acute diarrhea. (B) Number of surviving piglets at different days post inoculation.
(TIF)

Acknowledgments

We thank J.M. Nieto and I. Casanova for their assistance in the interpretation of histopathology samples, and F. Almazan and E. Alvarez for the design and generation of rTGEV-SC11-Δ7 virus. We are also grateful to M. Esteban and A. Cáceres for providing vaccinia viruses for RNase L system expression. We also thank C.M. Sánchez, S. Ros, and M. González for technical assistance. J.L.G.C. received contract from Community of Madrid. S.Z., I.S. and M.B. received contracts from the EU.

Author Contributions

Conceived and designed the experiments: JLGC LE SZ. Performed the experiments: JLGC MB SZ. Analyzed the data: JLGC IS MB LE SZ. Contributed reagents/materials/analysis tools: JLGC MB BA JP SZ. Wrote the paper: JLGC LE SZ. Animal experiments: BA JP.

References

1. Enjuanes L, Gorbalenya AE, de Groot RJ, Cowley JA, Ziebuhr J, et al. (2008) The Nidovirales. In: Mahy BWJ, Van Regenmortel M, Walker P, Majumder-Russell D, eds. Encyclopedia of Virology, Third Edition. Oxford: Elsevier Ltd. pp 419–430.
2. Masters PS (2006) The molecular biology of coronaviruses. Adv Virus Res 66: 193–292.
3. Denison MR (1999) The common cold. Rhinoviruses and coronaviruses. In: Dolin R, Wringht PF, eds. Viral infections of the respiratory tract. New York: Marcel Dekker, Inc. pp 253–280.
4. Drosten C, Gunther S, Preiser W, van der Werf S, Brodt HR, et al. (2003) Identification of a novel coronavirus in patients with severe acute respiratory syndrome. N Engl J Med 348: 1967–1976.
5. Holmes KV, Enjuanes L (2003) The SARS coronavirus: a postgenomic era. Science 300: 1377–1378.
6. Perlman S, Pewe L (1998) Role of CTL escape mutants in demyelination induced by mouse hepatitis virus, strain JHM. Adv Exp Med Biol 440: 515–520.
7. Medzhitov R, Janeway CA, Jr. (1997) Innate immunity: the virtues of a nonclonal system of recognition. Cell 91: 295–298.
8. Dauber B, Wolff T (2009) Activation of the Antiviral Kinase PKR and Viral Countermeasures. Viruses 1: 523–544.
9. Taylor SS, Haste NM, Ghosh G (2005) PKR and eIF2alpha: integration of kinase dimerization, activation, and substrate docking. Cell 122: 823–825.
10. Bisbal C, Silverman RH (2007) Diverse functions of RNase L and implications in pathology. Biochimie 89: 789–798.
11. Player MR, Torrence PF (1998) The 2-5A system: modulation of viral and cellular processes through acceleration of RNA degradation. Pharmacol Ther 78: 55–113.

12. Proud CG (1995) PKR: a new name and new roles. Trends Biochem Sci 20: 241–246.
13. Cassady KA, Gross M (2002) The herpes simplex virus type 1 U(S)11 protein interacts with protein kinase R in infected cells and requires a 30-amino-acid sequence adjacent to a kinase substrate domain. J Virol 76: 2029–2035.
14. Watson JC, Chang HW, Jacobs BL (1991) Characterization of a vaccinia virus-encoded double-stranded RNA-binding protein that may be involved in inhibition of the double-stranded RNA-dependent protein kinase. Virology 185: 206–216.
15. Chang HW, Watson JC, Jacobs BL (1992) The E3L gene of vaccinia virus encodes an inhibitor of the interferon-induced, double-stranded RNA-dependent protein kinase. Proc Natl Acad Sci USA 89: 4825–4829.
16. Bergmann M, Garcia-Sastre A, Carnero E, Pehamberger H, Wolff K, et al. (2000) Influenza virus NS1 protein counteracts PKR-mediated inhibition of replication. J Virol 74: 6203–6206.
17. Langland JO, Pettiford S, Jiang B, Jacobs BL (1994) Products of the porcine group C rotavirus NSP3 gene bind specifically to double-stranded RNA and inhibit activation of the interferon-induced protein kinase PKR. J Virol 68: 3821–3829.
18. Rivas C, Gil J, Melkova Z, Esteban M, Diaz-Guerra M (1998) Vaccinia virus E3L protein is an inhibitor of the interferon (i.f.n.)-induced 2-5A synthetase enzyme. Virology 243: 406–414.
19. Peters GA, Khoo D, Mohr I, Sen GC (2002) Inhibition of PACT-mediated activation of PKR by the herpes simplex virus type 1 Us11 protein. J Virol 76: 11054–11064.
20. Romano PR, Zhang F, Tan SL, Garcia-Barrio MT, Katze MG, et al. (1998) Inhibition of double-stranded RNA-dependent protein kinase PKR by vaccinia virus E3: role of complex formation and the E3 N-terminal domain. Mol Cell Biol 18: 7304–7316.
21. Gale MJ, Jr., Korth MJ, Tang NM, Tan SL, Hopkins DA, et al. (1997) Evidence that hepatitis C virus resistance to interferon is mediated through repression of the PKR protein kinase by the nonstructural 5A protein. Virology 230: 217–227.
22. Dever TE, Sripriya R, McLachlin JR, Lu J, Fabian JR, et al. (1998) Disruption of cellular translational control by a viral truncated eukaryotic translation initiation factor 2alpha kinase homolog. Proc Natl Acad Sci USA 95: 4164–4169.
23. O'Malley RP, Mariano TM, Siekierka J, Mathews MB (1986) A mechanism for the control of protein synthesis by adenovirus VA RNAI. Cell 44: 391–400.
24. Sharp TV, Schwemmle M, Jeffrey I, Laing K, Mellor H, et al. (1993) Comparative analysis of the regulation of the interferon-inducible protein kinase PKR by Epstein-Barr virus RNAs EBER-1 and EBER-2 and adenovirus VAI RNA. Nucleic Acids Res 21: 4483–4490.
25. Gunnery S, Rice AP, Robertson HD, Mathews MB (1990) Tat-responsive region RNA of human immunodeficiency virus 1 can prevent activation of the double-stranded-RNA-activated protein kinase. Proc Natl Acad Sci USA 87: 8687–8691.
26. Polyak SJ, Tang N, Wambach M, Barber GN, Katze MG (1996) The P58 cellular inhibitor complexes with the interferon-induced, double-stranded RNA-dependent protein kinase, PKR, to regulate its autophosphorylation and activity. J Biol Chem 271: 1702–1707.
27. Goodman AG, Fornek JL, Medigeshi GR, Perrone LA, Peng X, et al. (2009) P58(IPK): a novel "CIHD" member of the host innate defense response against pathogenic virus infection. PLoS Pathog 5: e1000438.
28. Gosert R, Kanjanahaluethai A, Egger D, Bienz K, Baker SC (2002) RNA replication of mouse hepatitis virus takes place at double-membrane vesicles. J Virol 76: 3697–3708.
29. Snijder EJ, van der Meer Y, Zevenhoven-Dobbe J, Onderwater JJ, van der Meulen J, et al. (2006) Ultrastructure and origin of membrane vesicles associated with the severe acute respiratory syndrome coronavirus replication complex. J Virol 80: 5927–5940.
30. Kamitani W, Narayanan K, Huang C, Lokugamage K, Ikegami T, et al. (2006) Severe acute respiratory syndrome coronavirus nsp1 protein suppresses host gene expression by promoting host mRNA degradation. Proc Natl Acad Sci USA 103: 12885–12890.
31. Tohya Y, Narayanan K, Kamitani W, Huang C, Lokugamage K, et al. (2009) Suppression of host gene expression by nsp1 proteins of group 2 bat coronaviruses. J Virol 83: 5282–5288.
32. Wang X, Liao Y, Yap PL, Png KJ, Tam JP, et al. (2009) Inhibition of protein kinase R activation and upregulation of GADD34 expression play a synergistic role in facilitating coronavirus replication by maintaining de novo protein synthesis in virus-infected cells. J Virol 83: 12462–12472.
33. Ye Y, Hauns K, Langland JO, Jacobs BL, Hogue BG (2007) Mouse hepatitis coronavirus A59 nucleocapsid protein is a type I interferon antagonist. J Virol 81: 2554–2563.
34. Brierley I, Digard P, Inglis SC (1989) Characterization of an efficient coronavirus ribosomal frameshifting signal: requirement for an RNA pseudoknot. Cell 57: 537–547.
35. de Groot RJ, Ziebuhr J, Poon LL, Woo PC, Talbot P, et al. (2010) Taxonomic structure of the Coronaviridae. In: Fauquet CM, Mayo MA, Maniloff J, Desselberg U, King A, eds. Virus Taxonomy International Committee on Taxonomy of Viruses: Academic Press.
36. Koetzner CA, Kuo L, Goebel SJ, Dean AB, Parker MM, et al. (2010) Accessory protein 5a is a major antagonist of the antiviral action of interferon against murine coronavirus. J Virol 84: 8262–8274.
37. Yount B, Roberts RS, Sims AC, Deming D, Frieman MB, et al. (2005) Severe acute respiratory syndrome coronavirus group-specific open reading frames encode nonessential functions for replication in cell cultures and mice. J Virol 79: 14909–14922.
38. DeDiego ML, Pewe L, Alvarez E, Rejas MT, Perlman S, et al. (2008) Pathogenicity of severe acute respiratory coronavirus deletion mutants in hACE-2 transgenic mice. Virology 376: 379–389.
39. DeDiego ML, Alvarez E, Almazan F, Rejas MT, Lamirande E, et al. (2007) A severe acute respiratory syndrome coronavirus that lacks the E gene is attenuated in vitro and in vivo. J Virol 81: 1701–1713.
40. Dediego ML, Pewe L, Alvarez E, Rejas MT, Perlman S, et al. (2008) Pathogenicity of severe acute respiratory coronavirus deletion mutants in hACE-2 transgenic mice. Virology 376: 379–389.
41. Tangudu C, Olivares H, Netland J, Perlman S, Gallagher T (2007) Severe acute respiratory syndrome coronavirus protein 6 accelerates murine coronavirus infections. J Virol 81: 1220–1229.
42. Pewe L, Zhou H, Netland J, Tangudu C, Olivares H, et al. (2005) A severe acute respiratory syndrome-associated coronavirus-specific protein enhances virulence of an attenuated murine coronavirus. J Virol 79: 11335–11342.
43. Brian DA, Baric RS (2005) Coronavirus genome structure and replication. Curr Top Microbiol Immunol 287: 1–30.
44. Enjuanes L, Almazan F, Ortego J (2003) Virus-based vectors for gene expression in mammalian cells: Coronavirus. In: Makrides SC, ed. Gene Transfer and Expression in Mammalian cells: Elsevier Science B.V. pp 151–168.
45. Sola I, Alonso S, Zúñiga S, Balach M, Plana-Durán J, et al. (2003) Engineering transmissible gastroenteritis virus genome as an expression vector inducing latogenic immunity. J Virol 77: 4357–4369.
46. Chu DK, Peiris JS, Chen H, Guan Y, Poon LL (2008) Genomic characterizations of bat coronaviruses (1A, 1B and HKU8) and evidence for co-infections in Miniopterus bats. J Gen Virol 89: 1282–1287.
47. Woo PC, Wang M, Lau SK, Xu H, Poon RW, et al. (2007) Comparative analysis of twelve genomes of three novel group 2c and group 2d coronaviruses reveals unique group and subgroup features. J Virol 81: 1574–1585.
48. Woo PC, Lau SK, Lam CS, Lai KK, Huang Y, et al. (2009) Comparative analysis of complete genome sequences of three avian coronaviruses reveals a novel group 3c coronavirus. J Virol 83: 908–917.
49. Jonassen CM, Kofstad T, Larsen IL, Lovland A, Handeland K, et al. (2005) Molecular identification and characterization of novel coronaviruses infecting graylag geese (Anser anser), feral pigeons (Columbia livia) and mallards (Anas platyrhynchos). J Gen Virol 86: 1597–1607.
50. Gorbalenya AE, Enjuanes L, Ziebuhr J, Snijder EJ (2006) Nidovirales: evolving the largest RNA virus genome. Virus Res 117: 17–37.
51. Lai MMC, Cavanagh D (1997) The molecular biology of coronaviruses. Adv Virus Res 48: 1–100.
52. Ortego J, Sola I, Almazan F, Ceriani JE, Riquelme C, et al. (2003) Transmissible gastroenteritis coronavirus gene 7 is not essential but influences in vivo virus replication and virulence. Virology 308: 13–22.
53. de Haan CAM, Masters PS, Shen S, Weiss S, Rottier PJM (2002) The group-specific murine coronavirus genes are not essential, but their deletion, by reverse genetics, is attenuating in the natural host. Virology 296: 177–189.
54. Haijema BJ, Volders H, Rottier PJ (2004) Live, attenuated coronavirus vaccines through the directed deletion of group-specific genes provide protection against feline infectious peritonitis. J Virol 78: 3863–3871.
55. Herrewegh AAPM, Vennema H, Horzinek MC, Rottier PJM, Groot PJ (1995) The molecular genetics of feline coronavirus comparative sequence analysis of the ORF7a/7b transcription unit of different biotypes. Virology 212: 622–631.
56. Tung FYT, Abraham S, Sethna M, Hung SL, Sethna P, et al. (1992) The 9-kDa hydrophobic protein encoded at the 3′ end of the porcine transmissible gastroenteritis coronavirus genome is membrane-associated. Virology 186: 676–683.
57. Sanchez CM, Izeta A, Sánchez-Morgado JM, Alonso S, Sola I, et al. (1999) Targeted recombination demonstrates that the spike gene of transmissible gastroenteritis coronavirus is a determinant of its enteric tropism and virulence. J Virol 73: 7607–7618.
58. Izeta A, Smerdou C, Alonso S, Penzes Z, Mendez A, et al. (1999) Replication and packaging of transmissible gastroenteritis coronavirus-derived synthetic minigenomes. J Virol 73: 1535–1545.
59. Galan C, Sola I, Nogales A, Thomas B, Akoulitchev A, et al. (2009) Host cell proteins interacting with the 3′ end of TGEV coronavirus genome influence virus replication. Virology 391: 304–314.
60. Laude H (1981) Thermal inactivation studies of a coronavirus, transmissible gastroenteritis virus. J Gen Virol 56: 235–240.
61. van Engeland M, Ramaekers FC, Schutte B, Reutelingsperger CP (1996) A novel assay to measure loss of plasma membrane asymmetry during apoptosis of adherent cells in culture. Cytometry 24: 131–139.
62. Nicoletti I, Migliorati G, Pagliacci MC, Grignani F, Riccardi C (1991) A rapid and simple method for measuring thymocyte apoptosis by propidium iodide staining and flow cytometry. J Immunol Methods 139: 271–279.
63. Eleouet JF, Chilmonczyk S, Besnardeau L, Laude H (1998) Transmissible gastroenteritis coronavirus induces programmed cell death in infected cells through a caspase-dependent pathway. J Virol 72: 4918–4924.
64. Eleouet JF, Slee EA, Saurini F, Castagné N, Poncet D, et al. (2000) The viral nucleocapsid protein of transmissible gastroenteritis coronavirus (TGEV) is

cleaved by caspase-6 and -7 during TGEV-induced apoptosis. J Virol 74: 3975–3983.
65. Sirinarumitr T, Kluge JP, Paul PS (1998) Transmissible gastroenteritis virus induced apoptosis in swine testis cell cultures. Arch Virol 143: 2471–2485.
66. Zhang QL, Ding YQ, He L, Wang W, Zhang JH, et al. (2003) Detection of cell apoptosis in the pathological tissues of patients with SARS and its significance. Di Yi Jun Yi Da Xue Xue Bao 23: 770–773.
67. Wei L, Sun S, Xu CH, Zhang J, Xu Y, et al. (2007) Pathology of the thyroid in severe acute respiratory syndrome. Hum Pathol 38: 95–102.
68. Narayanan K, Huang C, Lokugamage K, Kamitani W, Ikegami T, et al. (2008) Severe acute respiratory syndrome coronavirus nsp1 suppresses host gene expression, including that of type I interferon, in infected cells. J Virol 82: 4471–4479.
69. Schwartz T, Fu L, Lavi E (2002) Differential induction of apoptosis in demyelinating and nondemyelinating infection by mouse hepatitis virus. J Neurovirol 8: 392–399.
70. Raaben M, Koerkamp MJ, Rottier PJ, de Haan CA (2007) Mouse hepatitis coronavirus replication induces host translational shutoff and mRNA decay, with concomitant formation of stress granules and processing bodies. Cell Microbiol 9: 2218–2229.
71. Liu Y, Zhang X (2007) Murine coronavirus-induced oligodendrocyte apoptosis is mediated through the activation of the Fas signaling pathway. Virology 360: 364–375.
72. Deregt D, Babiuck LA (1987) Monoclonal antibodies to bovine coronavirus: characteristics and topographical mapping of neutralizing epitopes on the E2 and E3 glycoproteins. Virology 68: 41–420.
73. Kyuwa S, Cohen M, Nelson G, Tahara SM, Stohlman SA (1994) Modulation of cellular macromolecular synthesis by coronavirus: implication for pathogenesis. J Virol 68: 6815–6819.
74. Enjuanes L, Almazan F, Sola I, Zuniga S (2006) Biochemical aspects of coronavirus replication and virus-host interaction. Annu Rev Microbiol 60: 211–230.
75. Auer H, Lyianarachchi S, Newsom D, Klisovic MI, Marcucci G, et al. (2003) Chipping away at the chip bias: RNA degradation in microarray analysis. Nat Genet 35: 292–293.
76. Lin RJ, Yu HP, Chang BL, Tang WC, Liao CL, et al. (2009) Distinct antiviral roles for human 2′,5′-oligoadenylate synthetase family members against dengue virus infection. J Immunol 183: 8035–8043.
77. Scherbik SV, Paranjape JM, Stockman BM, Silverman RH, Brinton MA (2006) RNase L plays a role in the antiviral response to West Nile virus. J Virol 80: 2987–2999.
78. Iordanov MS, Paranjape JM, Zhou A, Wong J, Williams BR, et al. (2000) Activation of p38 mitogen-activated protein kinase and c-Jun NH(2)-terminal kinase by double-stranded RNA and encephalomyocarditis virus: involvement of RNase L, protein kinase R, and alternative pathways. Mol Cell Biol 20: 617–627.
79. Widlak P, Garrard WT (2005) Discovery, regulation, and action of the major apoptotic nucleases DFF40/CAD and endonuclease G. J Cell Biochem 94: 1078–1087.
80. Lopp A, Kuusksalu A, Samuel K, Kelve M (2000) Expression and activity of 2-5A synthetase in the course of differentiation and apoptosis of PC12 cells. Cytokine 12: 737–741.
81. Han JQ, Barton DJ (2002) Activation and evasion of the antiviral 2′-5′ oligoadenylate synthetase/ribonuclease L pathway by hepatitis C virus mRNA. RNA 8: 512–525.
82. Silverman RH (2007) Viral encounters with 2′,5′-oligoadenylate synthetase and RNase L during the interferon antiviral response. J Virol 81: 12720–12729.
83. Han JQ, Wroblewski G, Xu Z, Silverman RH, Barton DJ (2004) Sensitivity of hepatitis C virus RNA to the antiviral enzyme ribonuclease L is determined by a subset of efficient cleavage sites. J Interferon Cytokine Res 24: 664–676.
84. Domingo-Gil E, Esteban M (2006) Role of mitochondria in apoptosis induced by the 2-5A system and mechanisms involved. Apoptosis 11: 725–738.
85. Su AI, Pezacki JP, Wodicka L, Brideau AD, Supekova L, et al. (2002) Genomic analysis of the host response to hepatitis C virus infection. Proc Natl Acad Sci USA 99: 15669–15674.
86. Warke RV, Xhaja K, Martin KJ, Fournier MF, Shaw SK, et al. (2003) Dengue virus induces novel changes in gene expression of human umbilical vein endothelial cells. J Virol 77: 11822–11832.
87. Bosworth BT, MacLachlan NJ, Johnston MI (1989) Induction of the 2-5A system by interferon and transmissible gastroenteritis virus. J Interferon Res 9: 731–739.
88. Schneider RJ, Mohr I (2003) Translation initiation and viral tricks. Trends Biochem Sci 28: 130–136.
89. Hershey JW (1991) Translational control in mammalian cells. Annu Rev Biochem 60: 717–755.
90. Brostrom CO, Brostrom MA (1998) Regulation of translational initiation during cellular responses to stress. Prog Nucleic Acid Res Mol Biol 58: 79–125.
91. Kaufman RJ (1999) Stress signaling from the lumen of the endoplasmic reticulum: coordination of gene transcriptional and translational controls. Genes Dev 13: 1211–1233.
92. Proud CG (2005) eIF2 and the control of cell physiology. Semin Cell Dev Biol 16: 3–12.
93. Scheuner D, Patel R, Wang F, Lee K, Kumar K, et al. (2006) Double-stranded RNA-dependent protein kinase phosphorylation of the alpha-subunit of eukaryotic translation initiation factor 2 mediates apoptosis. J Biol Chem 281: 21458–21468.
94. Novoa I, Zeng H, Harding HP, Ron D (2001) Feedback inhibition of the unfolded protein response by GADD34-mediated dephosphorylation of eIF2alpha. J Cell Biol 153: 1011–1022.
95. Meurs E, Chong K, Galabru J, Thomas NS, Kerr IM, et al. (1990) Molecular cloning and characterization of the human double-stranded RNA-activated protein kinase induced by interferon. Cell 62: 379–390.
96. Ireland DD, Stohlman SA, Hinton DR, Kapil P, Silverman RH, et al. (2009) RNase L mediated protection from virus induced demyelination. PLoS Pathog 5: e1000602.
97. Schroder M, Kaufman RJ (2005) The mammalian unfolded protein response. Annu Rev Biochem 74: 739–789.
98. Harding HP, Zhang Y, Ron D (1999) Protein translation and folding are coupled by an endoplasmic-reticulum-resident kinase. Nature 397: 271–274.
99. Shi Y, Vattem KM, Sood R, An J, Liang J, et al. (1998) Identification and characterization of pancreatic eukaryotic initiation factor 2 alpha-subunit kinase, PEK, involved in translational control. Mol Cell Biol 18: 7499–7509.
100. Luo S, Baumeister P, Yang S, Abcouwer SF, Lee AS (2003) Induction of Grp78/BiP by translational block: activation of the Grp78 promoter by ATF4 through and upstream ATF/CRE site independent of the endoplasmic reticulum stress elements. J Biol Chem 278: 37375–37385.
101. Lee AS (2001) The glucose-regulated proteins: stress induction and clinical applications. Trends Biochem Sci 26: 504–510.
102. He B, Gross M, Roizman B (1997) The gamma(1)34.5 protein of herpes simplex virus 1 complexes with protein phosphatase 1alpha to dephosphorylate the alpha subunit of the eukaryotic translation initiation factor 2 and preclude the shutoff of protein synthesis by double-stranded RNA-activated protein kinase. Proc Natl Acad Sci USA 94: 843–848.
103. Cohen PT (2002) Protein phosphatase 1–targeted in many directions. J Cell Sci 115: 241–256.
104. Aggen JB, Nairn AC, Chamberlin R (2000) Regulation of protein phosphatase-1. Chem Biol 7: R13–23.
105. Gould CM, Diella F, Via A, Puntervoll P, Gemund C, et al. (2010) ELM: the status of the 2010 eukaryotic linear motif resource. Nucleic Acids Res 38: 1–14.
106. Puntervoll P, Linding R, Gemund C, Chabanis-Davidson S, Mattingsdal M, et al. (2003) ELM server: A new resource for investigating short functional sites in modular eukaryotic proteins. Nucleic Acids Res 31: 3625–3630.
107. Hsieh-Wilson LC, Allen PB, Watanabe T, Nairn AC, Greengard P (1999) Characterization of the neuronal targeting protein spinophilin and its interactions with protein phosphatase-1. Biochemistry 38: 4365–4373.
108. Schillace RV, Voltz JW, Sim AT, Shenolikar S, Scott JD (2001) Multiple interactions within the AKAP220 signaling complex contribute to protein phosphatase 1 regulation. J Biol Chem 276: 12128–12134.
109. Ajuh PM, Browne GJ, Hawkes NA, Cohen PT, Roberts SG, et al. (2000) Association of a protein phosphatase 1 activity with the human factor C1 (HCF) complex. Nucleic Acids Res 28: 678–686.
110. Kazemi S, Papadopoulou S, Li S, Su Q, Wang S, et al. (2004) Control of alpha subunit of eukaryotic translation initiation factor 2 (eIF2 alpha) phosphorylation by the human papillomavirus type 18 E6 oncoprotein: implications for eIF2 alpha-dependent gene expression and cell death. Mol Cell Biol 24: 3415–3429.
111. Rivera J, Abrams C, Hernaez B, Alcazar A, Escribano JM, et al. (2007) The MyD116 African swine fever virus homologue interacts with the catalytic subunit of protein phosphatase 1 and activates its phosphatase activity. J Virol 81: 2923–2929.
112. Brush MH, Weiser DC, Shenolikar S (2003) Growth arrest and DNA damage-inducible protein GADD34 targets protein phosphatase 1 alpha to the endoplasmic reticulum and promotes dephosphorylation of the alpha subunit of eukaryotic translation initiation factor 2. Mol Cell Biol 23: 1292–1303.
113. Novoa I, Zhang Y, Zeng H, Jungreis R, Harding HP, et al. (2003) Stress-induced gene expression requires programmed recovery from translational repression. EMBO J 22: 1180–1187.
114. Enjuanes L, Van der Zeijst BAM (1995) Molecular basis of transmissible gastroenteritis coronavirus epidemiology. In: Siddell SG, ed. The *Coronaviridae*. New York: Plenum Press. pp 337–376.
115. Saif LJ, Wesley RD (1992) Transmissible gastroenteritis. In: Leman AD, Straw BE, Mengeling WL, D'Allaire S, Taylor DJ, eds. Diseases of Swine. 7th ed. Ames. Iowa: Wolfe Publishing Ltd. pp 362–386.
116. Gantier MP, Williams BR (2007) The response of mammalian cells to double-stranded RNA. Cytokine Growth Factor Rev 18: 363–371.
117. Silverman RH (1985) Functional analysis of 2-5A-dependent RNase and 2-5a using 2′,5′-oligoadenylate-cellulose. Anal Biochem 144: 450–460.
118. Der SD, Yang YL, Weissmann C, Williams BR (1997) A double-stranded RNA-activated protein kinase-dependent pathway mediating stress-induced apoptosis. Proc Natl Acad Sci U S A 94: 3279–3283.
119. Zhou A, Paranjape J, Brown TL, Nie H, Naik S, et al. (1997) Interferon action and apoptosis are defective in mice devoid of 2′,5′-oligoadenylate-dependent RNase L. EMBO J 16: 6355–6363.
120. Rusch L, Zhou A, Silverman RH (2000) Caspase-dependent apoptosis by 2′,5′-oligoadenylate activation of RNase L is enhanced by IFN-beta. J Interferon Cytokine Res 20: 1091–1100.

121. Krahling V, Stein DA, Spiegel M, Weber F, Muhlberger E (2009) Severe acute respiratory syndrome coronavirus triggers apoptosis via protein kinase R but is resistant to its antiviral activity. J Virol 83: 2298–2309.
122. Kopecky-Bromberg SA, Martinez-Sobrido L, Frieman M, Baric RA, Palese P (2007) Severe acute respiratory syndrome coronavirus open reading frame (ORF) 3b, ORF 6, and nucleocapsid proteins function as interferon antagonists. J Virol 81: 548–557.
123. Wathelet MG, Orr M, Frieman MB, Baric RS (2007) Severe acute respiratory syndrome coronavirus evades antiviral signaling: role of nsp1 and rational design of an attenuated strain. J Virol 81: 11620–11633.
124. Garcia-Sastre A, Biron CA (2006) Type 1 interferons and the virus-host relationship: a lesson in detente. Science 312: 879–882.
125. Bantel H, Schulze-Osthoff K (2003) Apoptosis in hepatitis C virus infection. Cell Death Differ 10(Suppl 1): S48–S58.
126. Delmas B, Gelfi J, Sjöström H, Noren O, Laude H (1993) Further characterization of aminopeptidase-N as a receptor for coronaviruses. Adv Exp Med Biol 342: 293–298.
127. McClurkin AW, Norman JO (1966) Studies on transmissible gastroenteritis of swine. II. Selected characteristics of a cytopathogenic virus common to five isolates from transmissible gastroenteritis. Can J Comp Med Vet Sci 30: 190–198.
128. Penzes Z, Gonzalez JM, Calvo E, Izeta A, Smerdou C, et al. (2001) Complete genome sequence of transmissible gastroenteritis coronavirus PUR46-MAD clone and evolution of the purdue virus cluster. Virus Genes 23: 105–118.
129. Almazan F, Gonzalez JM, Penzes Z, Izeta A, Calvo E, et al. (2000) Engineering the largest RNA virus genome as an infectious bacterial artificial chromosome. Proc Natl Acad Sci USA 97: 5516–5521.
130. Jimenez G, Correa I, Melgosa MP, Bullido MJ, Enjuanes L (1986) Critical epitopes in transmissible gastroenteritis virus neutralization. J Virol 60: 131–139.
131. Zuñiga S, Sola I, Alonso S, Enjuanes L (2004) Sequence motifs involved in the regulation of discontinuous coronavirus subgenomic RNA synthesis. J Virol 78: 980–994.
132. Moreno JL, Zuniga S, Enjuanes L, Sola I (2008) Identification of a coronavirus transcription enhancer. J Virol 82: 3882–3893.
133. Diaz-Guerra M, Rivas C, Esteban M (1997) Inducible expression of the 2-5A synthetase/RNase L system results in inhibition of vaccinia virus replication. Virology 227: 220–228.
134. Sambrook J, Russell DW (2001) Molecular cloning: A laboratory manual. Cold Spring Harbor, New York: Cold Spring Harbor Laboratory Press.
135. Notredame C, Higgins DG, Heringa J (2000) T-Coffee: A novel method for fast and accurate multiple sequence alignment. J Mol Biol 302: 205–217.
136. Rost B, Yachdav G, Liu J (2004) The PredictProtein server. Nucleic Acids Res 32: W321–W326.
137. Bendtsen JD, Nielsen H, von Heijne G, Brunak S (2004) Improved prediction of signal peptides: SignalP 3.0. J Mol Biol 340: 783–795.
138. Blom N, Gammeltoft S, Brunak S (1999) Sequence and structure-based prediction of eukaryotic protein phosphorylation sites. J Mol Biol 294: 1351–1362.
139. Nakai K, Horton P (1999) PSORT: a program for detecting sorting signals in proteins and predicting their subcellular localization. Trends Biochem Sci 24: 34–36.

Virus Research 154 (2010) 150–160

Contents lists available at ScienceDirect

Virus Research

journal homepage: www.elsevier.com/locate/virusres

Review

Vectored vaccines to protect against PRRSV

Jazmina L.G. Cruz[a,1], Sonia Zúñiga[a,1], Martina Bécares[a], Isabel Sola[a], Juan E. Ceriani[b], Sandra Juanola[b], Juan Plana[b], Luis Enjuanes[a,*]

[a] Centro Nacional de Biotecnología, CSIC, Department of Molecular and Cell Biology, Campus Universidad Autónoma de Madrid, Darwin 3, 28049 Madrid, Spain
[b] Pfizer Animal Health, Girona, Spain

ARTICLE INFO

Article history:
Available online 25 June 2010

Keywords:
PRRSV
vectored vaccine
PRRSV vaccine
TGEV
coronavirus vector

ABSTRACT

PRRSV is the causative agent of the most important infectious disease affecting swine herds worldwide, producing great economic losses. Commercially available vaccines are only partially effective in protection against PRRSV. Moreover, modified live vaccines may allow virus shedding, and could revert generating virulent phenotypes. Therefore, new efficient vaccines are required. Vaccines based on recombinant virus genomes (virus vectored vaccines) against PRRSV could represent a safe alternative for the generation of modified live vaccines. In this paper, current vectored vaccines to protect against PRRSV are revised, including those based on pseudorabies virus, poxvirus, adenovirus, and virus replicons. Special attention has been provided to the use of transmissible gastroenteritis virus (TGEV) as vector for the expression of PRRSV antigens. This vector has the capability of expressing high levels of heterologous genes, is a potent interferon-α inducer, and presents antigens in mucosal surfaces, eliciting both secretory and systemic immunity. A TGEV derived vector (rTGEV) was generated, expressing PRRSV wild type or modified GP5 and M proteins, described as the main inducers of neutralizing antibodies and cellular immune response, respectively. Protection experiments showed that vaccinated animals developed a faster and stronger humoral immune response than the non-vaccinated ones. Partial protection in challenged animals was observed, as vaccinated pigs showed decreased lung damage when compared with the non-vaccinated ones. Nevertheless, the level of neutralizing antibodies was low, what may explain the limited protection observed. Several strategies are proposed to improve current rTGEV vectors expressing PRRSV antigens.

Contents

* Corresponding author. Tel.: +34 91 585 4555; fax: +34 91 585 4915.
E-mail address: L.Enjuanes@cnb.csic.es (L. Enjuanes).
[1] These authors contributed equally to this work.

0168-1702/$ – see front matter © 2010 Elsevier B.V. All rights reserved.
doi:10.1016/j.virusres.2010.06.017

1. Introduction

PRRSV is the causative agent of the most important infectious disease affecting the porcine herds worldwide. The immune response to PRRSV is poorly understood but, in spite of this, some vaccines are being commercialized. Commercial vaccines are mostly modified live vaccines based on attenuated European or North American PRRSV strains (i.e., Ingelvac®-PRRS from Boehringer Ingelheim, Amervac®-PRRS from Hipra, or Pyrsvac-183 from Syva labs). Nevertheless, some inactivated vaccines are also available (i.e., Progressis® from Merial, Ingelvac®-PRRS KV from Boehringer Ingelheim, or Suipravac®-PRRS from Hipra). Modified live vaccines have been preferentially used, as they can establish protective immunity, measured by viral load in blood and tissues. Nevertheless, current vaccines against PRRSV have several limitations. In general, modified live vaccines protect against challenge with homologous isolates. They could also protect against heterologous viruses (Diaz et al., 2006; Zuckermann et al., 2007). Furthermore, live vaccines provide partial protection against clinical disease but did not prevent infection (Osorio et al., 1998) and, more importantly, they can revert to virulence (Botner et al., 1997; Nielsen et al., 2001). As the attenuated vaccines induce an immune response resembling that induced by PRRSV natural infection, they do not induce high levels of neutralizing antibodies. Killed PRRSV vaccines, on the other hand, in general, have been less effective in prevention of both infection and disease (Ostrowski et al., 2002).

1.1. Immunity of PRRSV

The innate immune response against PRRSV is very weak, probably contributing to the delay in subsequent humoral and cellular immune responses, and also to virus persistence (Kimman et al., 2009). PRRSV does not induce interferon (IFN)-α production (Albina et al., 1998; Calzada-Nova et al., 2010), a key element in host antiviral response, leading to a minimal production of inflammatory cytokines and activation and recruitment of natural killer (NK) cells (Murtaugh et al., 2002). PRRSV-induced suppression of type I IFN production is due to the interference in the activation of IFN-β promoter stimulator 1 (IPS-1), located downstream of sensor molecule RNA helicase RIG-I. The inactivation of IPS-1 avoids IFN regulatory factor (IRF) 3 activation and, consequently, type I IFN production (Luo et al., 2008). Therefore, to design an effective vaccine against PRRSV, it would be advisable to increase the production of type I IFN. To date, different adjuvants promoting the production of IFN have been tested, in addition to the current vaccines formulations, with limited success (Charerntantanakul, 2009).

A hallmark of the swine humoral response against PRRSV is the production of non-neutralizing antibodies detected early in the infection, followed by a low neutralizing antibody (NAb) titer that is detected more than 3 weeks after infection (Kimman et al., 2009; Murtaugh et al., 2002). One possible explanation for the late detection of NAbs is the difference on technique sensitivity, as ELISA has higher sensitivity than neutralization assays. Therefore, the presence of very low titers of NAbs early in the infection cannot be completely discarded. Early non-neutralizing antibodies are mainly induced by nucleocapsid (N), M and GP5 proteins, and have been involved in antibody-dependent enhancement of PRRSV infection (Mateu and Diaz, 2008; Murtaugh et al., 2002). NAbs are induced by GP3, GP4, GP5 and M proteins, although the ones recognizing GP5 are the most relevant for protection (Kim and Yoon, 2008; Ostrowski et al., 2002). Two B cell epitopes were identified in GP5 protein ectodomain: an immunodominant epitope (IDE), that has been proposed to act as a decoy epitope, and an epitope critical for neutralization (ECN), that is recognized by NAbs (Ostrowski et al., 2002). Several hypothesis have been proposed to explain the delay in NAbs induction by GP5 protein, such as the presence of the IDE, and glican-shielding of the ECN (Lopez and Osorio, 2004). The role of NAbs in protection was demonstrated by passive transfer of these antibodies (Osorio et al., 2002). Protection of swine against PRRSV infection correlated with the level of NAbs and it was proposed that an efficient vaccine must induce NAb titers of 1:32 to prevent PRRSV infection (Lopez et al., 2007).

PRRSV infection results in a weak and delayed T cell mediated immune response that should be necessary for the elimination of the virus (Mateu and Diaz, 2008; Murtaugh et al., 2002). It has been shown that the induction of IFN-γ secreting cells, complementing neutralizing antibodies, provides partial protection against PRRSV (Zuckermann et al., 2007). As interleukin (IL)-10 levels inversely correlate with IFN-γ response, it has been proposed that the expression of IL-10 may be responsible for the suppression of T cell responses (Charerntantanakul et al., 2006; Kimman et al., 2009). M protein is the most potent inducer of T cell proliferation, followed by GP5, GP3 and GP2 (Bautista et al., 1999), and may play a role in protection. Different vaccine adjuvants have been tested to improve T cell responses to PRRSV. Nevertheless, in addition to the adjuvants included in vaccine formulation, only IL-2 and CpG oligodeoxynucleotides enhanced protection conferred by current vaccines (Charerntantanakul, 2009).

1.2. Factors affecting PRRSV vaccine development

There are three main problems for the development of more efficient vaccines against PRRSV: the correlates of protection are not well known, PRRSV may induce negative regulatory signals for the immune system, and there is a extremely large antigenic variability in PRRSV structural proteins. As indicated above, the PRRSV heterodimer GP5-M must be the main inducer of protective humoral and cellular responses. Nevertheless, minor structural proteins are also required for PRRSV virion infectivity (Wissink et al., 2005) and may play a role in protection. Also, there is limited information about the T cell epitopes implicated in the induction of a protective T cell response (Mateu and Diaz, 2008).

One of the mechanisms used by viruses to suppress or evade the host immune response is the induction of regulatory T cells (Treg). Porcine Treg phenotype is $CD4^+$ $CD25^+$ $Foxp3^+$ (Kaser et al., 2008), as that described for human and mice (Belkaid, 2007). Tregs have been classified in natural and induced. The latter ones can be subdivided in three subtypes: Treg1 (TR1) secreting IL-10, T helper 3 (Th3) secreting transforming growth factor (TGF)-β, and converted Tregs (Belkaid, 2007). It has been recently described that American

type PRRSV-infected dendritic cells induced Tregs, an effect that was reverted by the addition of IFN-α. The induced Treg population is a Th3 type, as it promotes TGF-β but not IL-10 expression (Silva-Campa et al., 2009). In contrast, dendritic cells infected with EU type PRRSV viruses did not induce Treg cells, although they exhibited an unbalanced ability to stimulate T cell immune responses (Silva-Campa et al., 2010). The impact of Treg induction on delayed immune responses after PRRSV infection remains to be established, as well as the viral proteins involved in this process.

PRRSV strains are extremely diverse, even when they belong to the same genotype. Among the structural proteins, M protein is the most conserved one, while GP5 is the most variable one (Dea et al., 2000). This high antigenic variability represents a problem for the development of universal vaccines against PRRSV, as shown by the low efficacy of current vaccines against heterologous challenge. To solve this problem, common critical B and T cell epitopes must be identified (Mateu and Diaz, 2008). Nevertheless, it has been reported that the ability of a vaccine to induce a strong cellular immune response may be more important for protection than the genetic similarity with the challenge strain (Diaz et al., 2006). An additional problem is the difference in the immune responses elicited by PRRSV in animals with different host genetic background (Lewis et al., 2007). Therefore, the knowledge of host responses to PRRSV infection is required for the development of an efficient vaccine.

2. Vectored vaccines

As mentioned above, both modified live and inactivated vaccines have been developed for PRRSV. Live vaccines led to better results than killed-virus based vaccines. Nevertheless, the live attenuated vaccines have several problems such as incomplete protection, virus shedding and possible reversion to virulence (Kimman et al., 2009). This problem was increased by the use of potentially hazardous methods to control the disease, such as the use of live field virus to vaccinate pigs. Vector-based vaccines could represent an advantage to stimulate both humoral and cell immune responses against PRRSV, and for the design of a marker vaccine. Nevertheless, the results reported to date using viral vectors are not fully satisfactory and new vectors, or antigenic combinations, must be explored.

2.1. Pseudorabies virus (PRV)

PRV, also known as Aujeszky's disease virus (ADV) is an alphaherpesvirus, classified within the family *Herpesviridae*. PRV is the causing agent of pseudorabies that was a worldwide-spread economically important disease. Swine is the natural host of PRV, but the virus also infects a broad range of vertebrates, including farm animals (Pomeranz et al., 2005). In order to eradicate the virus, modified live vaccines have been successfully used. All the vaccine strains were gE^- phenotype, i.e., have a gE gene deletion. The elimination of gE causes virus attenuation by reducing the virus transmission, but does not reduce virus production in cell culture nor the induction of protective immunity (Nauwynck et al., 2007). These live attenuated PRV have been used as vectors to protect against swine infectious diseases, such as classical swine fever (Hooft van Iddekinge et al., 1996), or porcine circovirus (Ju et al., 2005).

A recombinant PRV, based on the attenuated Bartha strain, was constructed expressing PRRSV GP5 protein (Qiu et al., 2005). Protection was evaluated by inoculation of 4-week-old piglets and homologous challenge with PRRSV CH-1 strain. None of the animals, even those inoculated with a commercially available inactivated vaccine, developed anti-GP5 antibodies before challenge. After challenge, the production of anti-GP5 antibodies was detected in all animals. Nevertheless, none of them produced neutralizing antibodies against PRRSV (Qiu et al., 2005). Reduced lung lesions and viremia, and faster virus elimination from tissues was observed in animals inoculated with PRV vaccine vector, similar to that found in animals inoculated with the commercial vaccine (Qiu et al., 2005).

Alternative recombinant attenuated PRV vaccine vectors expressing different combinations of PRRSV antigens have also been generated. These vectors expressed GP5 alone or together with M protein, or modified GP5 (GP5m), containing a Pan DR T-helper cell epitope (PADRE) between the decoy epitope and the ECN, recognized by NAbs (Fang et al., 2006), alone or co-expressed with M protein. The GP5-M heterodimer was detected in the recombinant PRVs co-expressing both proteins, suggesting that PRRSV antigenic structures were not changed (Jiang et al., 2007c). The PRV co-expressing GP5m and M proteins was the most promising candidate in the induction of neutralizing antibodies and lymphocyte proliferation, as tested in the mouse model. As a consequence, the protection conferred by this vector was evaluated in the porcine respiratory model, in relation to the protection provided by a commercially available PRRSV killed vaccine. Animals inoculated with the recombinant PRV expressing PRRSV proteins developed NAbs before the challenge. Furthermore, after challenge, the NAb titer was up to 4-fold higher in animals inoculated with recombinant PRRSV compared with those inoculated with the killed vaccine. None of the animals inoculated with the empty PRV developed neutralizing antibodies at any time during the experiment (Jiang et al., 2007c). Lymphocyte proliferative responses were also higher in animals inoculated with the recombinant PRV expressing GP5m and M proteins. Accordingly, lung lesions and viremia were lower in these animals, indicating a certain protection against the homologous challenge (Jiang et al., 2007c).

2.2. Adenovirus

Adenoviruses are currently one of the most extended systems for gene delivery. As vectors, they have high capacity for the insertion of foreign genes (from 5 Kb up to 36 Kb, depending on the system), and are able to transduce a broad range of cell types (Bantounas and Uney, 2007). Different replication-defective recombinant adenoviruses (rAd) have been used as vectors for PRRSV, both for vaccine development and for analysis of immunogenic properties of PRRSV wt or modified structural proteins.

A set of rAds expressing PRRSV GP5, M and a M-Gly-Thr-Thr-GP5 fusion protein were generated. These rAds were tested in the mouse model. The rAd expressing M-GP5 fusion protein induced and increased neutralizing antibodies humoral immune response, compared with mice inoculated with rAd expressing GP5 and M proteins independently or empty adenovirus vector (Jiang et al., 2006). The rAd expressing M-GP5 fusion protein also induced enhanced lymphocyte proliferation and cytotoxic T-lymphocyte (CTL) responses (Jiang et al., 2006). Unfortunately, protection conferred by these vectors was not evaluated in the porcine system.

The same authors also generated a set of rAds expressing other PRRSV structural protein combinations, such as GP3, GP4 or GP5 alone, and GP3-GP5, GP4-GP5 or GP3-GP4-GP5 fusion proteins (Jiang et al., 2008). Mice inoculated with rAds expressing fusion proteins developed higher NAb titers and lymphocyte proliferation responses than those inoculated with rAds expressing independent PRRSV proteins. Interestingly, specific CTL responses were higher in mice inoculated with rAds expressing GP3-GP5 or GP3-GP4-GP5 fusion proteins (Jiang et al., 2008). In fact, authors selected the recombinant rAd GP3-GP5 as the best vaccine candidate for testing protection in pigs. This recombinant induces NAbs in vaccinated piglets before challenge, and higher lymphocyte proliferation responses, IL-4 and IFN-γ production. Nevertheless, the

rAd expressing GP3-GP5 fusion protein did not fully protect against homologous challenge, as only a moderate decrease in lung lesions and viremia was observed (Li et al., 2009; Wang et al., 2009).

To improve the efficacy of the rAd-based vaccine, heat shock protein (HSP) 70 and granulocyte-macrophage colony stimulating factor (GM-CSF) were co-expressed as genetic adjuvants (Li et al., 2009; Wang et al., 2009). A set of rAds was obtained, expressing HSP70-5xGly-GP3-GP5 and HSP70-2A-GP3-GP5 fusion proteins, with a five glycine or a 2A protease linker, respectively. Piglets inoculated with rAd expressing fusion proteins induced higher NAb titers, produced higher IFN-γ levels, and presented reduced lung lesions, than those inoculated with rAd expressing GP3-GP5 protein (Li et al., 2009). Introduction of 2A protease between the HSP70 and PRRSV fusion protein resulted in a better production of IL-4 by inoculated animals, and also lower viremia. This could be due to the release of native HSP70 with higher adjuvant activity (Li et al., 2009).

GM-CSF has been widely used as an effective mucosal adjuvant (Toka et al., 2004). Intranasal inoculation of vectors expressing GM-CSF stimulates IFN-γ and IL-12 production in lung tissues (Bukreyev et al., 2001). A rAd expressing GM-CSF-Leu-Glu-GP3-Lys-Leu-GP5 fusion protein was generated. A moderate increase in NAb levels was observed before challenge in piglets inoculated with this rAd vector, compared with animals inoculated with empty rAd or rAd expressing GP3-GP5 fusion protein alone. After challenge, animals inoculated with rAd expressing the fusion protein containing the adjuvant developed significantly higher NAbs than the control animals (Wang et al., 2009). Lymphocyte proliferation responses and IFN-γ and IL-4 production were also enhanced in those animals. These enhanced immune responses correlated with a significant decrease in the viremia and lung lesions, indicating that GM-CSF enhanced the immunogenicity of rAd-based GP3-GP5 vaccine (Wang et al., 2009).

Adenovirus vectors have also been used to evaluate the antigenicity of PRRSV structural proteins, such as GP3 and GP5, and the role of GP5 glycosylation on immune responses (Jiang et al., 2007a,b). Unfortunately, these studies have been performed using the mouse model. The effect of IFN-α for protection against PRRSV has recently been analyzed using rAd. Piglets were inoculated with a rAd expressing porcine IFN-α and challenged with PRRSV (Brockmeier et al., 2009). Results obtained indicate that the presence of IFN-α has a moderate protective effect against PRRSV infection.

2.3. Poxvirus

Poxviruses are the largest known animal DNA viruses. They have been extensively used as expression vectors for vaccination, allow expression of large foreign genes, induce strong cell mediated and humoral immune responses, and safe poxvirus vectors are available (Paoletti, 1996; Wang et al., 2007).

Fowlpox was the first poxvirus used as vaccine vector for PRRSV (Guoshun et al., 2007). Fowlpox virus (FPV) belongs to the Avipoxvirus genus, and its replication is restricted to avian species. Nevertheless, attenuated strains of FPV have been used as vectors for poultry and mammals, resulting in strong and protective immune responses (Paoletti, 1996; Wang et al., 2007). A GP5-Pro-Pro-Ser-GP3 fusion protein, alone or combined with porcine IL-18, was expressed using recombinant FPV. Piglets inoculated with recombinant FPV expressing PRRSV antigens induced neutralizing antibodies at 42 dpi, and higher lymphocyte proliferation response, than those inoculated with the empty vector (Guoshun et al., 2007). Vaccinated animals also showed increased IFN-γ production, compared with non-vaccinated ones. Piglets vaccinated with FPV co-expressing PRRSV antigens and IL-18 produced higher IFN-γ amount than those inoculated with FPV expressing GP5-GP3 fusion protein alone (Guoshun et al., 2007). Partial protection was also observed after challenge with an homologous strain, as viremia was decreased in vaccinated animals (Guoshun et al., 2007).

Modified vaccinia virus Ankara (MVA), a member of the Orthopoxvirus genus, has also been used as a vector for PRRSV (Zheng et al., 2007). MVA was used as the vaccine agent for the prevention of smallpox, and has been extensively used as viral vector for infectious diseases and cancer. MVA is highly attenuated, even in immunosuppressed animals, but induces strong humoral and cellular immune responses (Wang et al., 2007). Four recombinant MVA viruses expressing PRRSV antigens were constructed, expressing GP5 or M proteins alone, GP5-M fusion protein, or co-expressing GP5 and M proteins (Zheng et al., 2007). These vectors were tested in the mouse model. Mice inoculated with recombinant MVA expressing heterologous antigens developed PRRSV neutralizing antibodies, with the highest antibody titers found in mice inoculated with the recombinant MVA co-expressing GP5 and M proteins. Similar results were obtained when IFN-γ and IL-2 production was analyzed, indicating a Th1 type cellular immune response (Zheng et al., 2007). Unfortunately, authors did not perform protection experiments in piglets. Therefore, the usefulness of MVA as vector for PRRSV vaccination remains to be determined.

2.4. Virus replicons

Expression vectors have been engineered using different viral replicons, by replacing the virus structural genes by heterologous ones. These RNA vectors, or replicons, express high levels of the foreign proteins, and replicate but are not packaged into virus-like particles unless structural proteins are provided *in trans*. Therefore, replicons do not spread into neighbor cells and are safe for their use as vaccines (Nagai et al., 2007; Rayner et al., 2002).

An alphavirus replicon derived from Venezuelan equine encephalitis virus (VEEV) has been successfully used as a vaccine against different pathogens, including swine influenza (Vander Veen et al., 2009). VEEV-derived vaccines induce robust humoral, mucosal and cellular immunity (Rayner et al., 2002). It has been recently described that a VEEV replicon expressing PRRSV GP5 and M proteins reduced viremia after PRRSV challenge and provides partial protection (Mogler et al., 2008, 2009).

Replicons from classical swine fever virus (CSFV) and vesicular stomatitis virus (VSV) expressing GP5 and M proteins have also been generated, expressing high levels of PRRSV antigens (N. Ruggli, personal communication).

3. TGEV as a vector

Coronaviruses have several advantages as vectors over other viral expression systems: (i) they are single-stranded RNA viruses that replicate in the cytoplasm without a DNA intermediary, making integration of the virus genome into the host cell chromosome unlikely (Lai and Cavanagh, 1997); (ii) these viruses have the largest RNA virus genome and, in principle, have room for the insertion of large foreign genes (Enjuanes et al., 2001, 2005); (iii) a pleiotropic secretory immune response is best induced by the stimulation of gut associated lymphoid tissues. Since coronaviruses in general infect both respiratory and enteric mucosal surfaces, these viruses may be used to target the antigen to the enteric and respiratory areas to induce a strong secretory immune response; (iv) the tropism of coronaviruses may be engineered by modifying the S gene (Ballesteros et al., 1997; Kuo et al., 2000; Sanchez et al., 1999); (v) non-pathogenic coronavirus strains infecting most species of interest (human, porcine, bovine, canine, feline, and avian) are available and therefore are suitable to develop safe virus vectors; and (vi) infectious coronavirus cDNA clones are available to design expression systems.

Our group obtained the first infectious coronavirus cDNA clone, for TGEV. This cDNA was propagated as a bacterial artificial chromosome (BAC) (Almazán et al., 2000; Gonzalez et al., 2002). Vectors based on this infectious cDNA were engineered by cloning foreign genes in the place previously occupied by non-essential genes 3a and 3b, leading to high (>50 μg/10^6 cells) and stable (>30 passages) expression levels of specific heterologous genes (Enjuanes et al., 2005; Ortego et al., 2003; Sola et al., 2003). Foreign gene expression levels were optimized by the study of the transcription-regulating sequences (TRSs), involved in coronavirus gene expression. Our group has generated a set of TRSs ranging from intermediate to high foreign gene expression levels (Alonso et al., 2002), a combination of these TRSs could be used to drive the expression of two or three heterologous genes from just one infectious cDNA (i.e., dicistronic or tricistronic vectors). TGEV derived vector biosafety was improved by the generation of replication-competent, propagation-deficient viruses (Ortego et al., 2002).

Porcine respiratory coronavirus (PRCV) is a mutant of TGEV that replicates in the respiratory tract and causes no or mild clinical signs. PRCV is spread worldwide and induces antibodies that can also neutralize TGEV (Saif et al., 1994). Therefore, preexisting immunity against the TGEV vector could have been a problem. Nevertheless, in vivo experiments showed that antibody titers against TGEV increased even after two re-infections of pigs with rTGEV vector (Alonso S., Sola I. and Enjuanes L., unpublished results). One of the main advantages of recombinant TGEV (rTGEV) as a vector for PRRSV is that TGEV is a potent inducer of IFN-α in a process that is mediated by the virus transmembrane (M) protein (Calzada-Nova et al., 2010; Charley and Laude, 1988). In addition, as mentioned above, TGEV vectors may present antigens at mucosal sites, eliciting mucosal and systemic immune responses. Therefore, rTGEV vectors will represent a novel strategy to study the induction of protection against PRRSV.

4. Engineered TGEV vectors expressing PRRSV antigens

4.1. The GP5-M antigenic platform

PRRSV structural proteins GP5 and M accumulate in the endoplasmic reticulum of infected cells, where they form disulfide-linked heterodimers that are incorporated into the virion. M protein

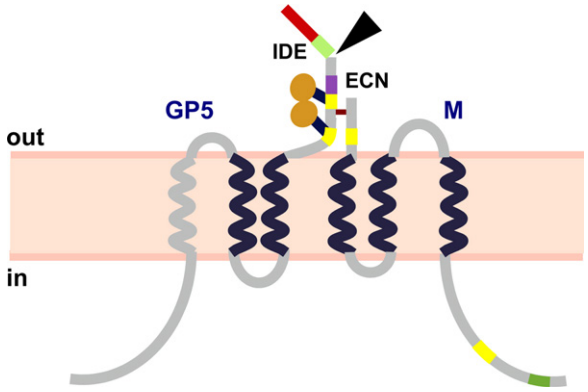

Fig. 1. Predicted GP5-M heterodimer topology. The PRRSV GP5-M heterodimer may be anchored in membranes, with both proteins exposing to the surface a short N-terminal ectodomain. The GP5 protein ectodomain contains the protein motives relevant in antigenicity, such as the epitope critical in neutralization (ECN, purple) and the decoy immunodominant epitope (IDE, green). Signal peptide (red) cleavage is represented by a black arrowhead. Both GP5 and M proteins contain predicted glycosylation sites (yellow), although only GP5 protein is glycosylated (represented by orange circles). M protein contains in its C-terminal an endoplasmic reticulum retention signal (dark green).

homodimers are also detected in infected cells, but are not incorporated into the virus particle (Dea et al., 2000; Meulenberg, 2000). GP5 and M proteins are essential for the production of viral particles, although additional minor envelope proteins are required for virion infectivity (Wissink et al., 2005). According to the accepted topology of the GP5-M heterodimer (Fig. 1), both GP5 and M proteins expose a short ectodomain on the virion surface, being involved in receptor recognition. GP5 ectodomain contains several glycosylation sites, depending on the viral strain. It has been described that GP5-M protein heterodimer formation is previous to GP5 glycosylation (Mardassi et al., 1996). GP5 glycosylation sites are close to the ECN epitope, and it has been proposed that the steric hindrance caused by the glycosylation is one of the causes for the potential delay in the production of NAbs after PRRSV infection (see below). It has been recently described that GP5-M heterodimer interacts with the PRRSV receptor, porcine

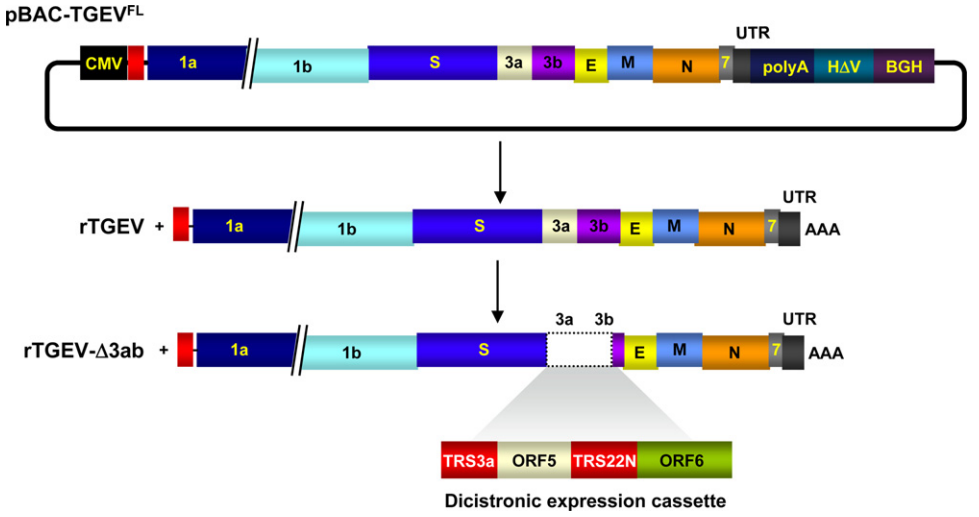

Fig. 2. Design of rTGEV expressing PRRSV antigens. Scheme of the TGEV infectious cDNA clone, cloned in a BAC (pBAC-TGEV^{FL}). After transfection of cells, a full-length virus genome is generated (rTGEV). CMV, cytomegalovirus immediate-early promoter; polyA, tail of 24 A residues; HDV, hepatitis delta virus ribozyme; BGH, bovine growth hormone termination and polyadenylation sequences. The TGEV derived vectors are based on a TGEV genome in which non-essential 3ab genes were deleted (rTGEV-Δ3ab). Genes encoding PRRSV heterologous proteins were cloned in this position. Expression of the foreign genes was driven by transcription regulatory sequences (TRSs) from genes 3a and N.

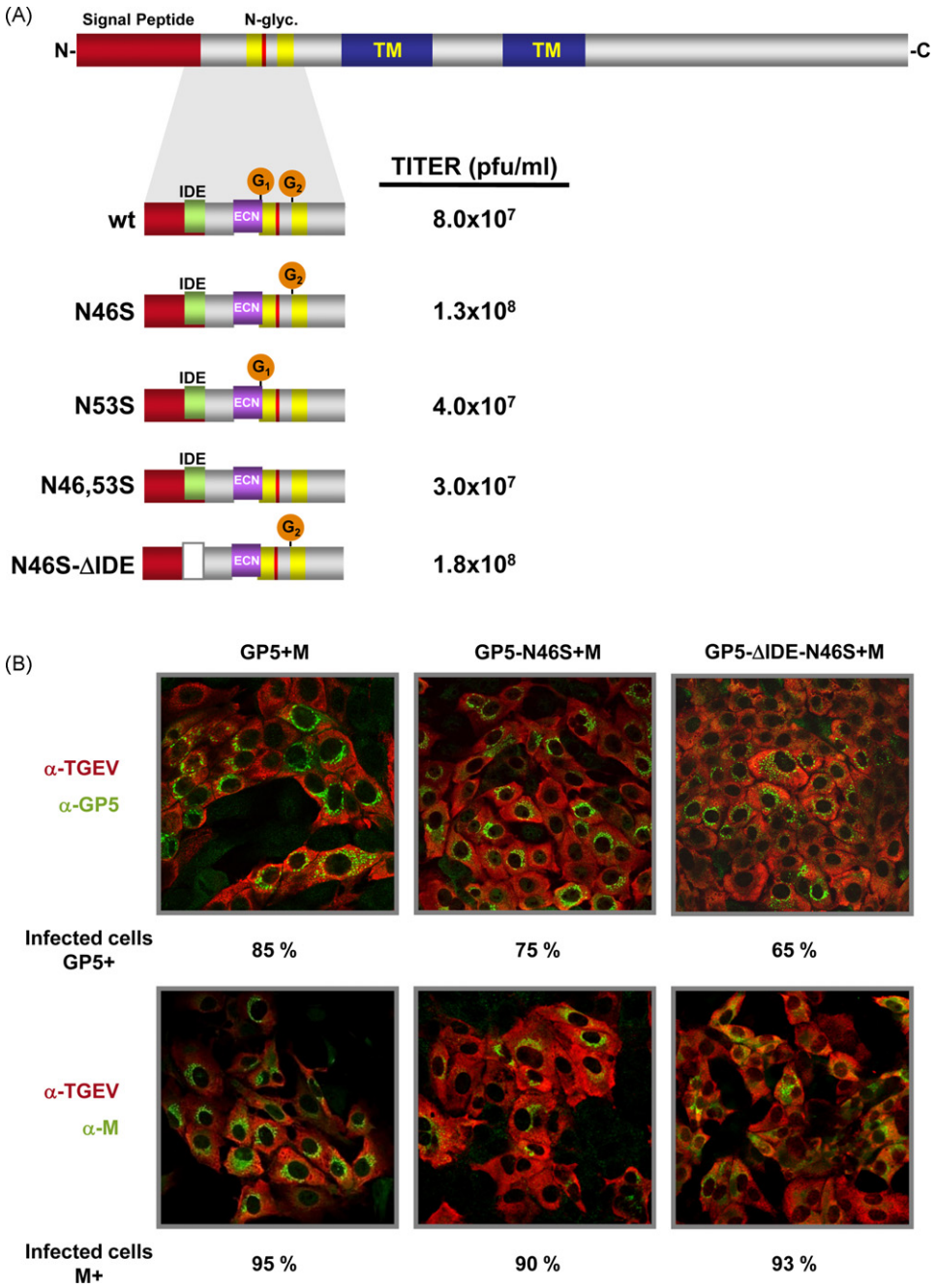

Fig. 3. Generation of rTGEV co-expressing GP5 and M proteins. (A) Schematic representation of PRRSVOlot91 GP5 domains. A detail of the domain containing the epitopes inducing non-neutralizing (IDE) and neutralizing (ECN) antibodies is shown. Two N-glycosylation sites, N46 (G1) and N53 (G2), are located within this domain. Three different mutants were generated, substituting Asn 46 and 53 by Ser, avoiding the glycosylation at these positions (N46S, N53S, and N46,53S). An additional mutant, lacking N46 glycosylation site and decoy epitope, was obtained (N46S-ΔIDE). In all cases, rTGEV viruses were recovered with high titers. (B) ST cells were infected with the rTGEVs and double immunofluorescence staining was performed. TGEV N protein specific monoclonal antibodies and a secondary antibody staining red were used to identify virus-infected cells. Expression of GP5 was detected with rabbit antiserum specific for a GP5 peptide coupled to a secondary antibody staining green (upper panels). Expression of M protein was detected with a rabbit antiserum specific for an M protein peptide, coupled to a secondary antibody staining green (lower panels). The percentage of infected cells expressing PRRSV antigens was estimated by the analysis 10 different microscopic fields.

sialoadhesin, and that this interaction is dependent on GP5 glycosylation, most likely at the glycosylation site overlapping with the epitope recognized by neutralizing antibodies (Van Breedam et al., 2010). As described above, GP5 and M proteins have been involved in the induction of PRRSV neutralizing antibodies and a strong cellular immune response, respectively (Bautista et al., 1999; Ostrowski et al., 2002). These data indicate that the GP5-M heterodimer is the most promising antigenic structure that could be used in the construction of an efficacious vaccine against PRRSV.

4.2. rTGEV expressing GP5 and M proteins

A dicistronic TGEV cDNA encoding PRRSV GP5 and M proteins was engineered (Fig. 2). PRRSV genes were cloned in the place of non-essential genes 3a and 3b. GP5 expression was driven by the transcription-regulating sequence of gene 3a (TRS3a), while M protein was expressed from an optimized TRS partially derived from gene N (TRS22N) (Alonso et al., 2002). Therefore, PRRSV genes were expressed from independent subgenomic mRNAs. The recovered virus expressed GP5 and M proteins in 85% and 95% of the

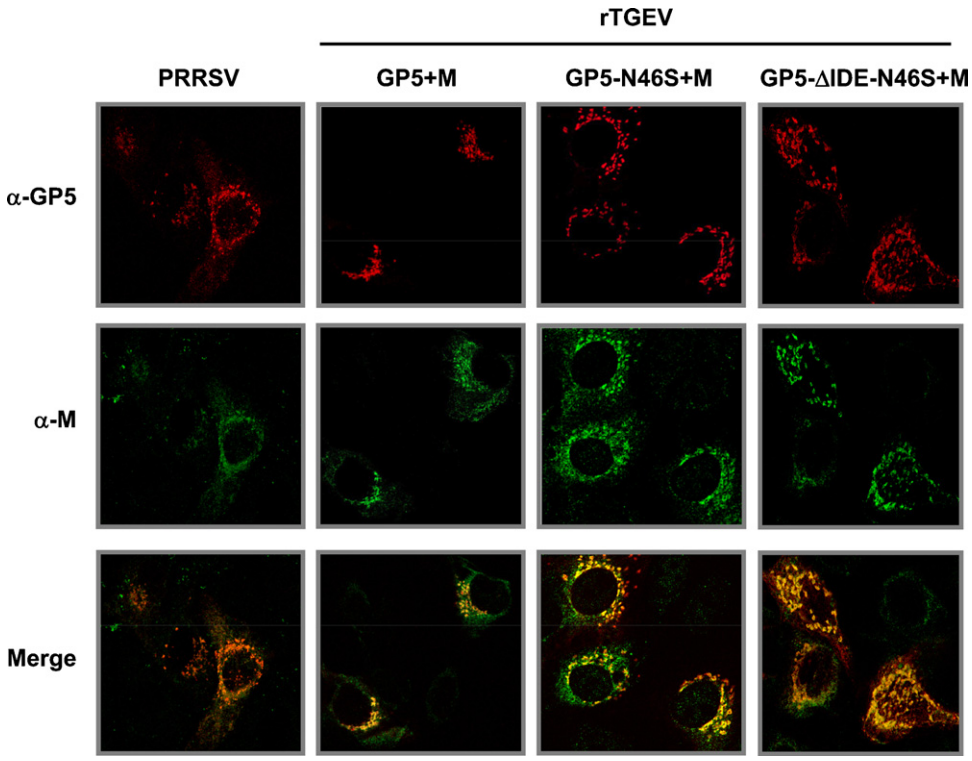

Fig. 4. Colocalization of GP5 and M proteins. To study if GP5 and M proteins expressed by rTGEVs also colocalize, confocal microscopy analysis was performed. MA-104 or ST cells were infected with PRRSV and the rTGEVs, respectively, and double immunofluorescence staining was performed. Expression of GP5 was detected with a monoclonal antibody specific for GP5, coupled to a secondary antibody staining red (upper panels). Expression of M protein was detected with a rabbit antiserum specific for an M protein peptide, coupled to a secondary antibody staining green (medium panels). As shown in the merge, colocalization of GP5 and M proteins was observed both in the PRRSV and rTGEV infected cells (lower panels). Mutant GP5 proteins (GP5-N46S and GP5-ΔIDE-N46S) expressed by rTGEVs also colocalized with M protein.

rTGEV infected cells, respectively (Fig. 3(B)). Expression levels were maintained even in virus recovered from tissues after infection of piglets with the rTGEV. This result substantially advanced the efficacy of previous rTGEVs expressing individually PRRSV antigens, showing high expression levels of GP5, but with limited stability. Co-expression of M protein with GP5 reduced GP5 toxicity and probably will elicit a better T cell immune response. The protection conferred by this vector was tested in vivo. One-week-old piglets were inoculated with 1×10^8 pfu of the rTGEV by three routes: oral, nasal and intragastric. Nine weeks later, a challenge was perfomed with 1×10^7 $TCID_{50}$ of a virulent European PRRSV strain. Blood samples were collected at different times post-inoculation, and humoral immune responses were evaluated by ELISA. All animals presented a high antibody response against TGEV, therefore, the vector infected target tissues as expected. Vaccinated animals also showed a clear humoral response against PRRSV GP5 and M proteins. A fast recall of the immune response was observed after the challenge, as vaccinated animals induced higher antibody titers against PRRSV antigens and earlier than control ones. Nevertheless, the immune response elicited by this rTGEV provided very limited protection, and antibody titers decreased before challenge. The lack of protection against challenge was likely due to the relatively low levels of neutralizing antibodies produced before challenge. Nevertheless, results using rTGEV as a platform were promising, as a humoral immune response against PRRSV antigens was elicited.

4.3. Generation of rTGEV based vaccines expressing modified GP5 protein

GP5 antigenicity may be a problem for the obtention of efficient vaccines. Therefore, several strategies to change GP5 antigenic structure were performed (Fig. 3(A)). In all cases, the GP5 mutants were co-expressed with M protein using a dicistronic vector, to minimize toxicity problems due to GP5 production.

4.3.1. Expression of GP5 mutants with a modified glycosylation pattern

The ectodomain of GP5 protein is N-glycosylated. There are three or four predicted glycosylation sites in the GP5 from the North American strains of PRRSV, whereas there are only two sites in the GP5 protein from European strains (wt, Fig. 3(A)). The relevance of the N-glycans in GP5 antigenicity is not clear. It has been proposed that the removal of the glycosylation sites could lead to the improvement of the immune response against PRRSV, due to the elimination of the steric hindrance raised by the carbohydrate on the epitope inducing NAbs (Ansari et al., 2006). Elimination of the glycosylation sites present only in the North American strains, both in engineered and natural PRRSV mutants, led to an increase in the levels of NAbs induced by the mutant viruses (Ansari et al., 2006; Faaberg et al., 2006). Nevertheless, it is worth noting that these sites are not present in European PRRSV strains. Although the elimination of the glycosylation site overlapping the epitope critical for neutralization (G1) (Fig. 3(A)) often leads to non-infectious viruses (Ansari et al., 2006; Wissink et al., 2005), natural North American strain mutants lacking this glycosylation site were found (2.1% of the sequenced GP5 proteins). Surprisingly, one of this natural mutants elicited lower neutralizing antibody response than the wild-type PRRSV strain (Faaberg et al., 2006). This is in contrast with the data obtained with lactate dehydrogenase-elevating virus (LDV), where deletion of the N-glycan enhanced the NAbs response (Plagemann and Moenngin, 1997). Elimination of the most conserved N-glycosylation site (G2, Fig. 3(A)) (only 0.2% of the sequenced North American GP5 proteins lack this motif) led to higher levels of neutralizing antibodies compared with the response elicited by the wild-type virus (Ansari

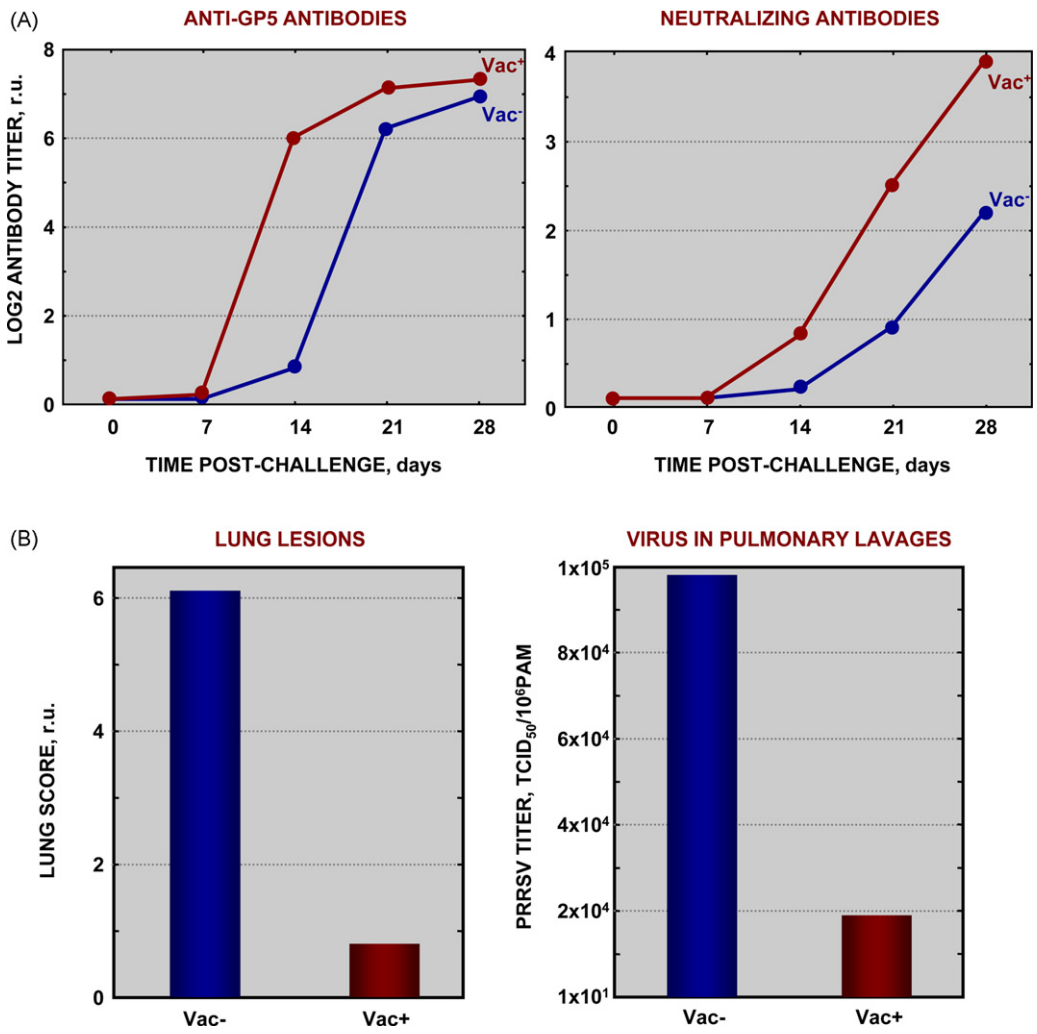

Fig. 5. Protection conferred by rTGEV based inactivated vaccine expressing GP5 with altered glycosylation pattern. (A) Killed vaccine was formulated from rTGEVs expressing GP5 with altered glycosylation pattern. Protection was analyzed and blood samples of animals were collected at indicated times post-challenge. Samples were analyzed by immunoperoxidase monolayer assay (IPMA) specific to detect antibodies against GP5 (left panel). Cells expressing recombinant GP5 were used as antigens for the IPMA assay. Neutralizing antibodies titers were calculated from neutralization assays of PRRSV Olot91 strain infecting MA-104 cells (right panel). (B) Lung damage caused by PRRSV infection (left panel). The lungs from vaccinated and non-vaccinated animals were analyzed. Lung lesions observed in all the pigs, with different degree of severity, included a craneo-ventral consolidation of apical and medial lung lobes. Viremia was also analyzed (right panel) by PRRSV quantification in samples, using Q-RT-PCR. Results were expressed as PRRSV $TCID_{50}$ per million of pulmonary lavages (PAM).

et al., 2006). As glycosylation of GP5 is probably also involved in virus infectivity, it is difficult to analyze the influence of N-glycans on the immunogenicity of the protein. In the rTGEV system, PRRSV GP5 and M are not involved in infectivity and, therefore, the relevance of these proteins antigenicity in protection could be analyzed in our laboratory using the rTGEV vector.

GP5 mutants lacking glycosylation site G1 (N46S), G2 (N53S) or both (N46,53S) were generated (Fig. 3(A)). The mutation Asn by Ser was selected in all cases, as this substitution most likely introduced little secondary structure modifications. Also, some PRRSV field strains bear similar Asn by Ser aminoacid mutations in putative glycosylation sites. All rTGEV viruses were recovered with high titers (Fig. 3(A)). Nevertheless, only the N46S mutant, lacking the glycosylation site partially overlapping the ECN, was stable (Fig. 3(B)). This rTGEV vector expressed high levels of GP5-N46S and M PRRSV proteins in 75% and 90% of the infected cells, respectively (Fig. 3(B)).

4.3.2. Generation of GP5 mutants lacking the decoy epitope

Several B cell epitopes have been found in GP5 protein. An immunodominant epitope is located in the endodomain and, therefore, has probably limited effect on the antigenicity of the ECN epitope, as it is not exposed in the viral surface (Dea et al., 2000; Oleksiewicz et al., 2002; Rodriguez et al., 2001). A second immunodominant epitope (IDE) was described in the ectodomain of GP5, close to the ECN (Fig. 3(A)) (Ostrowski et al., 2002). It has been suggested that this immunodominant site could be responsible for the delay in the production of NAbs against PRRSV acting as a decoy epitope. Antibodies against IDE and ECN epitopes were found in the sera of PRRSV infected pigs, appearing at different times post-infection. Furthermore, an increase in the titers against ECN correlates with a decrease in the level of antibodies specific for IDE (Lopez and Osorio, 2004; Ostrowski et al., 2002). An enhanced immunogenicity of a recombinant GP5 protein in which a synthetic sequence spacer has been introduced between IDE and ECN epitopes, to better display the neutralizing epitope has been reported. The data suggests that IDE is in fact acting as a decoy epitope (Fang et al., 2006).

rTGEV vectors were engineered expressing GP5 mutants lacking IDE, in order to clarify whether this epitope is acting as a decoy epitope, enhancing the production of PRRSV specific NAbs. This approach represents an advance over similar constructions made in a PRRSV infectious cDNA clone, as in this case the deletion of the decoy epitope prevents the recovery of the recombinant virus (Ansari et al., 2006). Two GP5 modifications were combined within

the same construct, expressing GP5 protein lacking the decoy epitope and the glycosylation site overlapping the epitope recognized by neutralizing antibodies (N46S-ΔIDE, Fig. 3(A)). The rTGEV virus was recovered with high titer (Fig. 3(A)), and expressed modified GP5 and M proteins in 65% and 93% of the infected cells, respectively (Fig. 3(B)).

4.4. Stability of PRRSV proteins expression in the rTGEV system

The data obtained in cultured cells suggest that rTGEV vectors expressing PRRSV antigens were not fully stable, mainly due to GP5 protein toxicity resulting in a significant lost of GP5 expression after 8–10 virus vector passages in cell culture. In contrast, M protein expression was fully stable, with at least 95% of infected cells expressing M protein for more than 10 passages in tissue culture. A decrease in GP5 expression was also observed after the introduction of modifications in this protein (upper panels, Fig. 3(B)). Again, M protein expression remained constant, independently of GP5 mutant co-expressed (lower panels, Fig. 3(B)). The reduction in GP5 expression could be responsible of the modest results in protection observed with the live rTGEV vectors, in comparison to the protection elicited with non-infectious antigens expressed using rTGEV vectors.

As described above, the rTGEV vector expressing PRRSV GP5 and M proteins represents a substantial advance on the efficacy of previous rTGEVs expressing PRRSV antigens (i.e., GP5 alone). We postulated that co-expression of M protein with GP5 reduces GP5 toxicity by the formation of GP5-M heterodimer. To clarify this issue, confocal microscopy analysis was performed (Fig. 4). MA-104 or ST cells were infected with PRRSV and the rTGEVs, respectively, and double immunofluorescence staining was performed. As shown in the merge (Fig. 4, lower panels), colocalization of GP5 and M proteins was observed both in the PRRSV and rTGEV infected cells. This result suggests that the GP5-M heterodimer is formed in both cases. The decrease in GP5 expression levels by the introduction of GP5 mutations suggested that the modifications could affect heterodimer formation. Colocalization of GP5 and M proteins was also observed when a mutant GP5 protein (i.e., GP5-N46S, or GP5-ΔIDE-N46S) was expressed by the rTGEV vector (Fig. 4), suggesting that a heterodimer was also formed by mutant GP5 proteins. Co-immunoprecipitation of GP5 and M proteins to fully demonstrated GP5-M heterodimer formation is in progress.

4.5. Protection conferred by rTGEV derived vaccines

4.5.1. Formulation of a killed vaccine expressing GP5 mutants with alterations in the glycosylation pattern

As a complementary approach, a killed vaccine was developed based on the rTGEV-GP5-N46S-M virus, co-expressing GP5 lacking the first glycosylation site and M proteins. ST cells were infected with this rTGEV, and the culture medium was harvested at 48 hpi. Soluble antigens were inactivated by incubation with binary ethylenimine (BEI), and a vaccine was formulated. Groups of six 1-week-old piglets were intramuscularly inoculated with the formulation to evaluate the protection conferred by this vaccine. A boost was performed 3 weeks after inoculation. Six weeks after the first inoculation, animals were challenged by intranasal inoculation with 10^7 $TCID_{50}$ of PRRSV/Olot91 strain. Blood samples were collected at different times post-inoculation to determine the levels of specific antibodies by ELISA. Vaccinated animals induced higher and faster antibody titers against PRRSV antigens than control animals (Fig. 5(A), left panel). Neutralizing antibody titers were also higher in the vaccinated animals when compared with non-vaccinated animals (Fig. 5(A), right panel). Viremia, gross lesions, and histopathology in the lungs of vaccinated and non-vaccinated animals were analyzed. A clear degree of protection

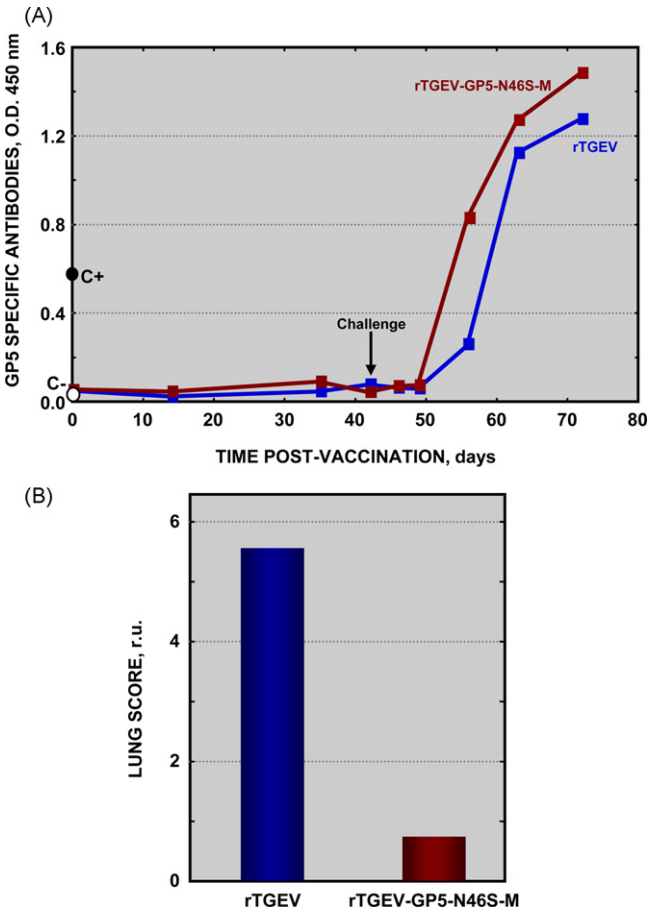

Fig. 6. Protection conferred by rTGEV based live vaccine expressing GP5 with altered glycosylation pattern. (A) Humoral immune response elicited by live rTGEV based vaccine. Blood samples of animals we collected at indicated times post-inoculation. Samples were analyzed by enzyme-linked immunosorbent assays (ELISAs) specific to detect antibodies against TGEV, GP5 and M. To evaluate response against GP5, GP5 protein from PRRSV Olot91 strain was expressed and purified from insect cells and used as antigen for the ELISA. (B) Lung damage caused by PRRSV infection. The lungs from animals inoculated with empty rTGEV vector, or rTGEV expressing GP5-N46S and M proteins, were analyzed. Lung lesions observed in all the pigs, with different degree of severity, included a craneo-ventral consolidation of apical and medial lung lobes.

was observed, as the lungs from vaccinated animals showed a significantly lower degree of lung damage than those from non-vaccinated ones (Fig. 5(B), left panel). Furthermore, a reduction in viremia was also observed in vaccinated animals (Fig. 5(B), right panel). Altogether, these data suggested that the elimination of the glycosylation site close to the neutralizing epitope improves protective immune response against PRRSV.

4.5.2. In vivo testing of rTGEV expressing PRRSV M protein and GP5 mutant with altered glycosylation

The protection conferred by rTGEV-GP5-N46S-M was tested in vivo. One-week-old piglets were inoculated with 1×10^8 pfu of the rTGEV by three routes: oral, nasal and intragastric. A boost was performed 3 weeks after inoculation. Six weeks later, a challenge was performed with 1×10^7 $TCID_{50}$ of PRRSV/Olot91 strain. Blood samples were collected at different times post-inoculation, and humoral immune responses were evaluated by ELISA. All the animals produced a high antibody response against TGEV (data not shown), therefore, the vector infected target tissues as expected. After challenge, vaccinated animals showed a clear humoral response against PRRSV antigens (Fig. 6(A)). A moderately faster recall response was observed, as vaccinated animals

induced higher antibody titers against PRRSV antigens and earlier than control animals (Fig. 6(A)).

The protection conferred by this TGEV based vaccine was also evaluated. A certain degree of protection was observed, as the lungs from vaccinated animals showed a lower degree of lung damage than those from non-vaccinated ones (Fig. 6(B)). Nevertheless, the immune response was not strong enough to provide full protection, probably because the levels of neutralizing antibodies were similar in vaccinated and non-vaccinated animals (data not shown).

4.6. Strategies for the improvement of TGEV derived vectors

To date, rTGEV expressing PRRSV antigens only provided partial protection. This could be due to the fact that the expression of PRRSV antigens by rTGEV vectors was not fully stable, mainly due to GP5 protein toxicity resulting in a significant lost of GP5 expression in 8–10 passages. In contrast, M protein expression was fully stable, with at least 95% of infected cells expressing M protein for more than 10 passages in tissue culture.

The lack of full protection using rTGEV expressing PRRSV antigens could also be due to the presence of domains in the expressed proteins inducing negative regulatory T cells (Treg). As the vector used in the immunization (rTGEV) efficiently induced the production of IFN, it is likely that either PRRSV GP5 or M proteins could contain negative signals inducing Treg. This negative regulation of the immune response elicited could also be a major cause for the delay in the development of a protective immune response against PRRSV.

To improve rTGEV vector stability different strategies can be developed, such as the expression of small domains of GP5 containing the epitopes relevant for protection but lacking domains responsible for instability in their expression. Alternatively, the generation of a library of point mutants in GP5 fragments in which the epitopes eliciting negative Treg have been eliminated may overcome what we consider the second most relevant limitation in the protection against PRRSV. These approaches are currently in progress in our laboratory.

5. Conclusions

An improvement of vaccination strategies against PRRSV is required, as current vaccines have limited efficacy. Best results have been obtained using modified live vaccines and virus vectored vaccines could represent an advantage to stimulate immune responses against PRRSV. The results reported to date using viral vectors are not fully satisfactory and new vectors must be explored. TGEV based vector vaccines expressing different PRRSV antigenic combinations represent a promising candidate to provide protection against two porcine viruses: PRRSV and TGEV. The use of rTGEV vectors led to promising results, similar to those obtained with other vectored vaccines. Nevertheless, as reported for other RNA viruses, data obtained indicate that heterologous protein expression stability was limited. Therefore, increase of PRRSV antigens expression stability, and removal of domains eliciting Treg, represent new avenues to improve the development of an efficient PRRSV vaccine.

Acknowledgements

We thank C.M. Sánchez, S. Ros, and M. González for technical assistance. This work was supported by grants from the Comisión Interministerial de Ciencia y Tecnología (CICYT, BIO2007-60978), the National Pork Board (NPB#07-112 and NPB#08-197), and the European Union (FP7, PLAPROVA-227056, and PoRRSCon-245141). S.Z., I.S. and M.B. received contracts from the EU. J.L.G.C. received contract from Community of Madrid.

References

Albina, E., Carrat, C., Charley, B., 1998. Interferon-alpha response to swine arterivirus (PoAV), the porcine reproductive and respiratory syndrome virus. J. Interferon Cytokine Res. 18, 485–490.

Almazán, F., González, J.M., Pénzes, Z., Izeta, A., Calvo, E., Plana-Durán, J., Enjuanes, L., 2000. Engineering the largest RNA virus genome as an infectious bacterial artificial chromosome. Proc. Natl. Acad. Sci. U.S.A. 97, 5516–5521.

Alonso, S., Izeta, A., Sola, I., Enjuanes, L., 2002. Transcription regulatory sequences and mRNA expression levels in the coronavirus transmissible gastroenteritis virus. J. Virol. 76, 1293–1308.

Ansari, I.H., Kwon, B., Osorio, F.A., Pattnaik, A.K., 2006. Influence of N-linked glycosylation of porcine reproductive and respiratory syndrome virus GP5 on virus infectivity, antigenicity, and ability to induce neutralizing antibodies. J. Virol. 80, 3994–4004.

Ballesteros, M.L., Sanchez, C.M., Enjuanes, L., 1997. Two amino acid changes at the N-terminus of transmissible gastroenteritis coronavirus spike protein result in the loss of enteric tropism. Virology 227, 378–388.

Bantounas, I., Uney, J.B., 2007. The evolution of adenoviral vectors and their application to gene delivery and RNAi in the CNS. In: Hefferon, K.L. (Ed.), Virus Expression Vectors. Transworld Research Network, Kerala, India, pp. 1–36.

Bautista, E.M., Suarez, P., Molitor, T.W., 1999. T cell responses to the structural polypeptides of porcine reproductive and respiratory syndrome virus. Arch. Virol. 144, 117–134.

Belkaid, Y., 2007. Regulatory T cells and infection: a dangerous necessity. Nat. Rev. Immunol. 7, 875–888.

Botner, A., Strandbygaard, B., Sorensen, K.J., Have, P., Madsen, K.G., Madsen, E.S., Alexandersen, S., 1997. Appearance of acute PRRS-like symptoms in sow herds after vaccination with a modified live PRRS vaccine. Vet. Rec. 141, 497–499.

Brockmeier, S.L., Lager, K.M., Grubman, M.J., Brough, D.E., Ettyreddy, D., Sacco, R.E., Gauger, P.C., Loving, C.L., Vorwald, A.C., Kehrli, M.E., Lehmkuhl, H.D., 2009. Adenovirus-mediated expression of interferon-alpha delays viral replication and reduces disease signs in swine challenged with porcine reproductive and respiratory syndrome virus. Viral Immunol. 22, 173–180.

Bukreyev, A., Belyakov, I.M., Berzofsky, J.A., Murphy, B.R., Collins, P.L., 2001. Granulocyte-macrophage colony-stimulating factor expressed by recombinant respiratory syncytial virus attenuated viral replication and increases the level of pulmonary antigen-presenting cells. J. Virol. 75, 12128–12140.

Calzada-Nova, G., Schnitzlein, W., Husmann, R., Zuckermann, F.A., 2010. Characterization of the cytokine and maturation responses of pure populations of procine plasmacytoid dendritic cells to porcine viruses and toll-like receptor agonists. Vet. Immunol. Immunopathol. 135, 20–33.

Charerntantanakul, W., 2009. Adjuvants for porcine reproductive and respiratory syndrome virus vaccines. Vet. Immunol. Immunopathol. 129, 1–13.

Charerntantanakul, W., Platt, R., Roth, J.A., 2006. Effects of porcine reproductive and respiratory syndrome virus-infected antigen-presenting cells on T cell activation and antiviral cytokine production. Viral Immunol. 19, 646–661.

Charley, B., Laude, H., 1988. Induction of alpha-interferon by transmissible gastroenteritis coronavirus: role of transmembrane glycoprotein E1. J. Virol. 62, 8–10.

Dea, S., Gagnon, C.A., Mardassi, H., Pirzadeh, B., Rogan, D., 2000. Current knowledge on the structural proteins of porcine reproductive and respiratory syndrome (PRRS) virus: comparison of the North American and European isolates. Arch. Virol. 145, 659–688.

Diaz, I., Darwich, L., Pappaterra, G., Pujols, J., Mateu, E., 2006. Different European-type vaccines against porcine reproductive and respiratory syndrome virus have different immunological properties and confer different protection to pigs. Virology 351, 249–259.

Enjuanes, L., Sola, I., Almazán, F., Ortego, J., Izeta, A., González, J.M., Alonso, S., Sánchez-Morgado, J.M., Escors, D., Calvo, E., Riquelme, C., Sánchez, C.M., 2001. Coronavirus derived expression systems. J. Biotechnol. 88, 183–204.

Enjuanes, L., Sola, I., Alonso, S., Escors, D., Zuñiga, S., 2005. Coronavirus reverse genetics and development of vectors for gene expression. In: Enjuanes, L. (Ed.), Coronavirus Replication and Reverse Genetics, vol. 287. Springer, pp. 161–197.

Faaberg, K.S., Hocker, J.D., Erdman, M.M., Harris, D.L., Nelson, E.A., Torremorell, M., Plagemann, P.G., 2006. Neutralizing antibody responses of pigs infected with natural GP5 N-glycan mutants of porcine reproductive and respiratory syndrome virus. Viral. Immunol. 19, 294–304.

Fang, L.R., Jiang, Y.B., Xiao, S.B., Niu, C.S., Zhang, H., Chen, H.C., 2006. Enhanced immunogenicity of the modified GP5 of porcine reproductive and respiratory syndrome virus. Virus Genes 32, 5–11.

Gonzalez, J.M., Penzes, Z., Almazan, F., Calvo, E., Enjuanes, L., 2002. Stabilization of a full-length infectious cDNA clone of transmissible gastroenteritis coronavirus by the insertion of an intron. J. Virol. 76, 4655–4661.

Guoshun, S., Ningyi, J., Mingxiao, M., Kuoshi, J., Min, Z., Tianzhong, Z., Huijun, L., Guangze, Z., Hongtao, J., Minglan, J., Xiaowei, H., Xiaoguang, Q., Ronglan, Y., Chang, L., Hongwen, L., Yang, L., Zhenzhen, H., Yifeng, C., Miaomiao, J., 2007. Immune responses of pigs inoculated with a recombinant fowlpox virus coexpressing GP5/GP3 of porcine reproductive and respiratory syndrome virus and swine IL-18. Vaccine 25, 4193–42002.

Hooft van Iddekinge, B.J., de Wind, N., Wensvoort, G., Kimman, T.G., Gielkens, A.L., Moormann, R.J., 1996. Comparison of the protective efficacy of recombinant pseudorabies viruses against pseudorabies and classical swine fever in pigs; influence of different promoters on gene expression and on protection. Vaccine 14, 6–12.

Jiang, W., Jiang, P., Li, Y., Tang, J., Wang, X., Ma, S., 2006. Recombinant adenovirus expressing GP5 and M fusion proteins of porcine reproductive and respiratory syndrome virus induce both humoral and cell-mediated immune responses in mice. Vet. Immunol. Immunopathol. 113, 169–180.

Jiang, W., Jiang, P., Li, Y., Wang, X., Du, Y., 2007a. Analysis of immunogenicity of minor envelope protein GP3 of porcine reproductive and respiratory syndrome virus in mice. Virus Genes 35, 695–704.

Jiang, W., Jiang, P., Wang, X., Li, Y., Wang, X., Du, Y., 2007b. Influence of porcine reproductive and respiratory syndrome virus GP5 glycoprotein N-linked glycans on immune responses in mice. Virus Genes 35, 663–671.

Jiang, Y., Fang, L., Xiao, S., Zhang, H., Pan, Y., Luo, R., Li, B., Chen, H., 2007c. Immunogenicity and protective efficacy of recombinant pseudorabies virus expressing the two major membrane-associated proteins of porcine reproductive and respiratory syndrome virus. Vaccine 25, 547–560.

Jiang, W., Jiang, P., Wang, X., Li, Y., Du, Y., Wang, X., 2008. Enhanced immune responses of mice inoculated recombinant adenoviruses expressing GP5 by fussion with GP3 and/or GP4 of PRRS virus. Virus Res. 136, 50–57.

Ju, c., Fan, H., Tan, Y., Liu, Z., Xi, X., Cao, S., Wu, B., Chen, H., 2005. Immunogenicity of a recombinant pseudorabies virus expressing ORF1-ORF2 fusion protein of porcine circovirus type 2. Vet. Microbiol. 109, 179–190.

Kaser, T., Gerner, W., Hammer, S.E., Patzl, M., Saalmüller, A., 2008. Detection of Foxp3 protein expression in porcine T lymphocytes. Vet. Immunol. Immunopathol. 125, 92–101.

Kim, W.I., Yoon, K.J., 2008. Molecular assessment of the role of envelope-associated structural proteins in cross neutralization among different PRRS viruses. Virus Genes 37, 380–391.

Kimman, T.G., Cornelissen, L.A., Moormann, R.J., Rebel, J.M., Stockhofe-Zurwieden, N., 2009. Challenges for porcine reproductive and respiratory syndrome virus (PRRSV) vaccinology. Vaccine 27, 3704–3718.

Kuo, L., Godeke, G.-J., Raamsman, M.J.B., Masters, P.S., Rottier, P.J.M., 2000. Retargeting of coronavirus by substitution of the spike glycoprotein ectodomain: crossing the host cell species barrier. J. Virol. 74, 1393–1406.

Lai, M.M.C., Cavanagh, D., 1997. The molecular biology of coronaviruses. Adv. Virus Res. 48, 1–100.

Lewis, C.R.G., Ait-Ali, T., Clapperton, M., Archibald, A.L., Bishop, S., 2007. Genetic perspectives on host responses to porcine reproductive and respiratory syndrome (PRRS). Viral Immunol. 20, 343–357.

Li, J., Jiang, P., Li, Y., Wang, X., Cao, J., Wang, X., Zeshan, B., 2009. HSP70 fused with GP3 and GP5 of porcine reproductive and respiratory syndrome virus enhanced the immune responses and protective efficacy against virulent PRRSV challenge in pigs. Vaccine 27, 825–832.

Lopez, O.J., Osorio, F.A., 2004. Role of neutralizing antibodies in PRRSV protective immunity. Vet. Immunol. Immunopathol. 102, 155–163.

Lopez, O.J., Oliveira, M.F., Garcia, E.A., Kwon, B.J., Doster, A., Osorio, F.A., 2007. Protection against porcine reproductive and respiratory syndrome virus (PRRSV) infection through passive transfer of PRRSV-neutralizing antibodies is dose dependent. Clin. Vaccine Immunol. 14, 269–275.

Luo, R., Xiao, S., Jiang, Y., Jin, H., Wang, D., Liu, M., Chen, H., Fang, L., 2008. Porcine reproductive and respiratory syndrome virus (PRRSV) suppresses interferon-beta production by interfering with the RIG-I signaling pathway. Mol. Immunol. 45, 2839–2846.

Mardassi, H., Massie, B., Dea, S., 1996. Intracellular synthesis, processing, and transport of proteins encoded by ORFs 5 to 7 of porcine reproductive and respiratory syndrome virus. Virology 221, 98–112.

Mateu, E., Diaz, I., 2008. The challenge of PRRS immunology. Vet. J. 177, 345–351.

Meulenberg, J.J., 2000. PRRSV, the virus. Vet. Res. 31, 11–21.

Mogler, M.A., Erdman, M.M., Vander Veen, R.L., Owens, G., Kamrud, K., Smith, J., Harris, D.L., 2008. Replicon particle PRRSV vaccine provides partial protection from challenge. In: International PRRS Symposium.

Mogler, M.A., Vander Veen, R.L., Erdman, M.M., Harris, D.L., 2009. Replicon particles expressing PRRSV GP5 and matrix reduce viremia following homologous and heterologous challenge. In: International PRRS Symposium.

Murtaugh, M.P., Xiao, Z., Zuckermann, F., 2002. Immunological responses of swine to porcine reproductive and respiratory syndrome virus infection. Viral Immunol. 15, 533–547.

Nagai, Y., Inoue, M., Iida, A., Zhu, Y.F., Hasegawa, M., Kato, A., Matano, T., 2007. Sendai virus engineering: from reverse genetics to vector development. In: Hefferon, K.L. (Ed.), Virus Expression Vectors. Transworld Research Network, Kerala, India, pp. 123–146.

Nauwynck, H., Glorieux, S., Favoreel, H., Pensaert, M., 2007. Cell biological and molecular characteristics of pseudorabies virus infections in cell cultures and in pigs with emphasis on the respiratory tract. Vet. Res. 38, 229–241.

Nielsen, H.S., Oleksiewicz, M.B., Forsberg, R., Stadejek, T., Botner, A., Storgaard, T., 2001. Reversion of a live porcine reproductive and respiratory syndrome virus vaccine investigated by parallel mutations. J. Gen. Virol. 82, 1263–1272.

Oleksiewicz, M.B., Botner, A., Normann, P., 2002. Pocine B-cells recognize epitopes that are conserved between the structural proteins of American- and European-type porcine reproductive and respiratory syndrome virus. J. Gen. Virol. 83, 1407–1418.

Ortego, J., Escors, D., Laude, H., Enjuanes, L., 2002. Generation of a replication-competent, propagation-deficient virus vector based on the transmissible gastroenteritis coronavirus genome. J. Virol. 76, 11518–11529.

Ortego, J., Sola, I., Almazan, F., Ceriani, J.E., Riquelme, C., Balasch, M., Plana-Durán, J., Enjuanes, L., 2003. Transmissible gastroenteritis coronavirus gene 7 is not essential but influences *in vivo* virus replication and virulence. Virology 308, 13–22.

Osorio, F.A., Zuckermann, F., Wills, R., Meier, W., Christion, S., Galeota, S., Doster, A.R., 1998. PRRSV: comparison of commercial vaccines in their ability to induce protection against current PRRSV strains of high virulence. In: Allen D. Lennan Swine Conference 25, 178–182.

Osorio, F.A., Galeota, J.A., Nelson, E., Brodersen, B., Doster, A., Wills, R., Zuckermann, F., Laegreid, W.W., 2002. Passive transfer of virus-specific antibodies confers protection against reproductive failure induced by a virulent strain of porcine reproductive and respiratory syndrome virus and establishes sterilizing immunity. Virology 302, 9–20.

Ostrowski, M., Galeota, J.A., Jar, A.M., Platt, K.B., Osorio, F.A., Lopez, O.J., 2002. Identification of neutralizing and nonneutralizing epitopes in the porcine reproductive and respiratory syndrome virus GP5 ectodomain. J. Virol. 76, 4241–4250.

Paoletti, E., 1996. Applications of pox virus vectors to vaccination: an update. Proc. Natl. Acad. Sci. U.S.A. 93, 11349–11353.

Plagemann, P.G.W., Moenngin, v., 1997. Lactate dehydrogenase-elevating virus, equine arteritis virus and simian haemorrhagic fever virus, a new group of positive strand RNA viruses. Adv. Virus Res. 41, 99–192.

Pomeranz, L.E., Reynolds, A.E., Hengartner, C.J., 2005. Molecular biology of pseudorabies virus: impact on neurovirology and veterinary medicine. Microbiol. Mol. Biol. Rev. 69, 462–500.

Qiu, H.J., Tian, Z.J., Tong, G.Z., Zhou, Y.J., Ni, J.Q., Luo, Y.Z., Cai, X.H., 2005. Protective immunity induced by a recombinant pseudorabies virus expressing the GP5 of procine reproductive and respiratory syndrome virus in piglets. Vet. Immunol. Immunopathol. 106, 309–319.

Rayner, J.O., Dryga, S.A., Kamrud, K.I., 2002. Alphavirus vectors and vaccination. Rev. Med. Virol. 12, 279–296.

Rodriguez, F., Harkins, S., Redwine, J.M., de Pereda, J.M., Whitton, J.L., 2001. CD4(+) T cells induced by a DNA vaccine: immunological consequences of epitope-specific lysosomal targeting. J. Virol. 75, 10421–10430.

Saif, L.J., van Cott, J.L., Brim, T.A., 1994. Immunity to transmissible gastroenteritis virus and porcine respiratory coronavirus infections in swine. Vet. Immunol. Immmunopathol. 43, 89–97.

Sanchez, C.M., Izeta, A., Sánchez-Morgado, J.M., Alonso, S., Sola, I., Balasch, M., Plana-Duran, J., Enjuanes, L., 1999. Targeted recombination demonstrates that the spike gene of transmissible gastroenteritis coronavirus is a determinant of its enteric tropism and virulence. J. Virol. 73, 7607–7618.

Silva-Campa, E., Flores-Mendoza, L., Resendiz, M., Pinelli-Saavedra, A., Mata-Haro, V., Mwangi, W., Hernandez, J., 2009. Induction of T helper 3 regulatory cells by dendritic cells infected with porcine reproductive and respiratory syndrome virus. Virology 387, 373–379.

Silva-Campa, E., Cordoba, L., Fraile, L., Flores-Mendoza, L., Montoya, M., Hernandez, J., 2010. European genotype of porcine reproductive and respiratory syndrome (PRRSV) infects monocyte-derived dendritic cells but does not induce Treg cells. Virology 396, 264–271.

Sola, I., Alonso, S., Zúñiga, S., Balach, M., Plana-Durán, J., Enjuanes, L., 2003. Engineering transmissible gastroenteritis virus genome as an expression vector inducing latogenic immunity. J. Virol. 77, 4357–4369.

Toka, F.N., Pack, C.D., Rouse, B.T., 2004. Molecular adjuvants for mucosal immunity. Immunol Rev. 199, 100–112.

Van Breedam, W., Van Gorp, H., Zhang, J.Q., Crocker, P.R., Delputte, P.L., Nauwynck, H.J., 2010. The M/GP_5 glycoprotein complex of porcine reproductive and respiratory syndrome virus binds the sialoadhesin receptor in a sialic acid-dependent manner. PLoS Pathogens 6, e1000730.

Vander Veen, R., Kamrud, K., Mogler, M., Loynachan, A.T., McVicker, J., Berglund, P., Owens, G., Timberlake, S., Lewis, W., Smith, J., Harris, D.L., 2009. Rapid development of an efficacious swine vaccine for novel H1N1. PLoS Curr. Influenza 29, RRN1123.

Wang, Q., Moroziewicz, D., Kaufman, H.L., 2007. Poxvirus expression vectors. In: Hefferon, K.L. (Ed.), Virus Expression Vectors. Transworld Research Network, Kerala, India, pp. 267–298.

Wang, X., Li, J., Jiang, P., Li, Y., Zeshan, B., Cao, J., Wang, X., 2009. GM-CSF fused with GP3 and GP5 of porcine reproductive and respiratory syndrome virus increased the immune responses and protective efficacy against virulent PRRSV challenge. Virus Res. 143, 24–32.

Wissink, E.H., Kroese, M.V., van Wijk, H.A., Rijsewijk, F.A., Meulenberg, J.J., Rottier, P.J., 2005. Envelope protein requirements for the assembly of infectious virions of porcine reproductive and respiratory syndrome virus. J. Virol. 79, 12495–12506.

Zheng, Q., Chen, D., Li, P., Bi, Z., Cao, R., Zhou, B., Chen, P., 2007. Co-expressing GP5 and M proteins under different promoters in recombinant modified vaccinia virus ankara (rMVA)-based vaccine vector enhanced the humoral and cellular immune response of porcine reproductive and respiratory syndrome virus (PRRSV). Virus Genes 35, 585–595.

Zuckermann, F.A., Alvarez Garcia, E., Diaz Luque, I., Christopher-Hennings, J., Doster, A., Brito, M., Osorio, F., 2007. Assessment of the efficacy of commercial porcine reproductive and respiratory syndrome virus (PRRSV) vaccines based on measurement of serologic response, frequency of gamma-IFN-producing cells and virological parameters of protection upon challenge. Vet. Microbiol. 123, 69–85.

JOURNAL OF VIROLOGY, Feb. 2010, p. 2169–2175 Vol. 84, No. 4
0022-538X/10/$12.00 doi:10.1128/JVI.02011-09

Coronavirus Nucleocapsid Protein Facilitates Template Switching and Is Required for Efficient Transcription▽

Sonia Zúñiga, Jazmina L. G. Cruz, Isabel Sola, Pedro A. Mateos-Gómez, Lorena Palacio, and Luis Enjuanes*

Centro Nacional de Biotecnología, CSIC, Department of Molecular and Cell Biology, Darwin 3, Campus Universidad Autónoma de Madrid, Cantoblanco, Madrid, Spain

Received 24 September 2009/Accepted 18 November 2009

Purified nucleocapsid protein (N protein) from transmissible gastroenteritis virus (TGEV) enhanced hammerhead ribozyme self-cleavage and favored nucleic acid annealing, properties that define RNA chaperones, as previously reported. Several TGEV N-protein deletion mutants were expressed in *Escherichia coli* and purified, and their RNA binding ability and RNA chaperone activity were evaluated. The smallest N-protein domain analyzed with RNA chaperone activity, facilitating DNA and RNA annealing, contained the central unstructured region (amino acids 117 to 268). Interestingly, N protein and its deletion mutants with RNA chaperone activity enhanced template switching in a retrovirus-derived heterologous system, reinforcing the concept that TGEV N protein is an RNA chaperone that could be involved in template switching. This result is in agreement with the observation that *in vivo*, N protein is not necessary for TGEV replication, but it is required for efficient transcription.

RNA chaperones are proteins that allow the proper folding of nucleic acids (4, 12). Several characteristics distinguish RNA chaperones from other RNA binding proteins: a lack of specificity; they are transiently needed; and there is no energy requirement for their function (19). RNA chaperone activity cannot be predicted based on the protein domain structure or the existence of discrete motifs. In the case of virus-encoded RNA chaperones, even RNA chaperone proteins of the same viral genus have little sequence similarity. Nevertheless, RNA chaperones have the highest frequency of disordered regions, and it has been proposed that they act according to an entropy transfer model, allowing correct RNA folding by successive cycles of protein-substrate order-disorder (5, 32). In fact, protein disorder has been the selected criterion for investigating the chaperone activity of candidate viral RNA chaperone proteins (14, 36). The list of virus-encoded RNA chaperones has been quickly growing. Nevertheless, their role in the viral life cycle as RNA chaperones is still unclear, mainly due to the difficulty of analyzing *in vivo* the chaperone activity of these proteins in viral infection.

Coronaviruses are enveloped viruses of the *Coronaviridae* family, included in the *Nidovirales* order (7, 10). Their genomes are positive-sense, single-stranded RNAs (ssRNAs) of around 30 kb, the largest known viral RNA genomes. The 5′ two-thirds of the genomic RNA encodes the replicase proteins. The 3′ third of the genome encodes structural and nonstructural proteins. Coronavirus transcription leads to a nested set of subgenomic (sg) mRNAs that are generated by a discontinuous mechanism. This process implies base pairing of nascent RNAs of negative polarity, synthesized under the control of transcription-regulating sequences (TRSs) preceding each gene, with sequences located at the 3′ end of the leader within the genomic RNA (21, 23, 35).

Coronavirus nucleocapsid protein (N protein) has a structural role and is involved in RNA synthesis (1, 6). The N proteins from different coronaviruses vary in length and primary sequence. Nevertheless, some motifs with functional relevance are conserved, and N proteins share a three-domain organization according to sequence similarity (18). Recently, based on disorder predictions, a modular organization including two structured domains separated by a long disordered region was proposed for coronavirus N protein (2, 36). Using transmissible gastroenteritis virus (TGEV) as a model, RNA chaperone activity has been demonstrated for N protein (36). RNA chaperone activity was also reported for severe and acute respiratory syndrome virus (SARS-CoV) N protein, and it was postulated as a general activity of all coronavirus nucleocapsid proteins (36).

The template switch during discontinuous RNA synthesis in coronavirus transcription is a complex process that includes several steps: the slowing down and stopping of nucleic acid synthesis, the template switch itself, reassociation of the nascent nucleic acid strand with the acceptor sequence, and elongation of the nascent strand using the acceptor nucleic acid as a template (8). To accomplish some of these steps, we have proposed that RNA chaperones, such as TGEV N protein, could decrease the energy barrier needed to dissociate the nascent minus RNA chain from the genomic RNA template (36). This decrease in the energy threshold would facilitate the nascent RNA chain template switch to hybridize with the TRS of the leader sequence during discontinuous transcription.

The role of coronavirus N protein in RNA synthesis has been controversial. On one hand, it has been reported that viral replicase gene products suffice for coronavirus replication (30). On the other, the same authors and others have reported

* Corresponding author. Mailing address: Department of Molecular and Cell Biology, Centro Nacional de Biotecnología, CSIC, Darwin, 3, Ciudad Universitaria de Cantoblanco, 28049 Madrid, Spain. Phone: 34-91-585 4555. Fax: 34-91-585 4915. E-mail: L.Enjuanes@cnb.csic.es.
▽ Published ahead of print on 2 December 2009.

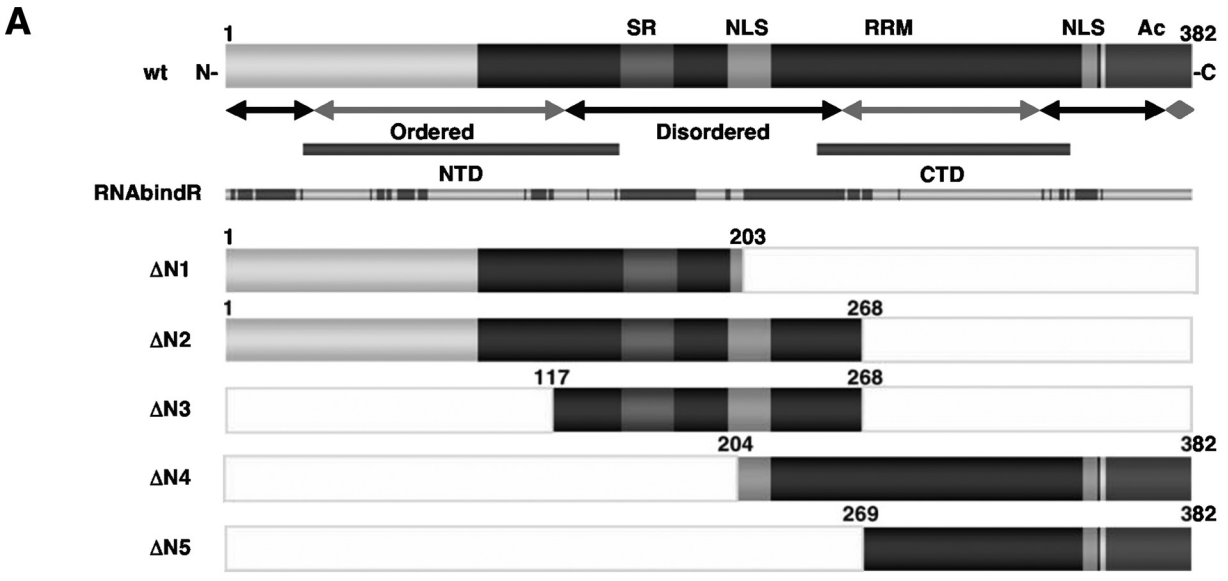

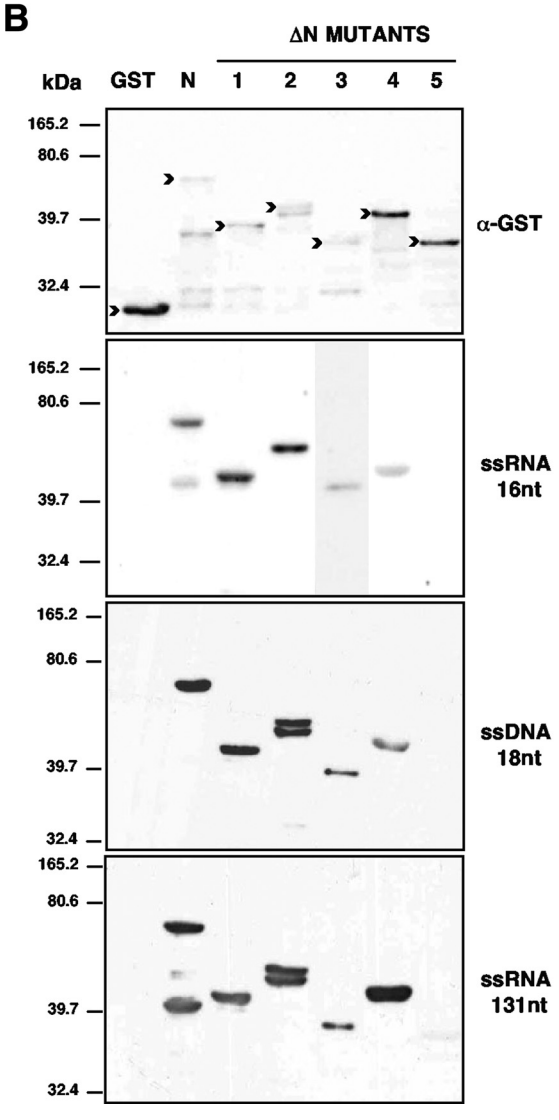

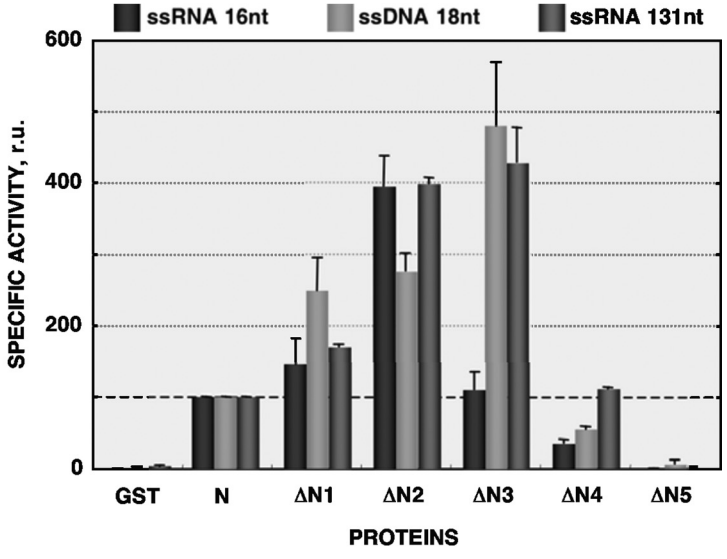

that addition of N protein enhances RNA synthesis (1, 22, 31). Whether this enhancement is due to an increase in replication, transcription, or both has not been clearly established.

In this article, we report the generation of a set of TGEV N-protein deletion mutants and the analysis of their RNA chaperone activity, using annealing assays. The role of wild-type (wt) N protein and deletion mutants in template switching was evaluated *in vitro* using a retrovirus-derived strand transfer system. Our data indicated that the central disordered domain of the TGEV N protein has RNA chaperone activity and facilitates template switching *in vitro*. Moreover, the role of N protein *in vivo* in TGEV replication and transcription was evaluated. Interestingly, the results reported in this paper indicate that N protein is not essential for TGEV RNA replication. In contrast, it is required for efficient transcription. These data reinforce the hypothesis of N protein having a role in template switching.

Nucleic acid binding of N protein deletion mutants. To locate a TGEV N protein domain with nucleic acid chaperone activity, a set of deletion mutants was designed according to several criteria: predicted domain distribution, order-disorder pattern, predicted location of crystallized N-terminal (NTD) and C-terminal (CTD) domains from other coronavirus N proteins, and predicted RNA-binding residues (Fig. 1A). The corresponding fragments of TGEV N-protein coding sequence were amplified by PCR and cloned into the plasmid pGEX-4T-2. The N-protein mutants ΔN1, ΔN2, ΔN3, ΔN4, and ΔN5 (Fig. 1A) were successfully expressed and purified from *Escherichia coli* as previously described (36).

RNA chaperone activity requires nucleic acid binding, and the ability of the constructed N protein deletion mutants to bind different nucleic acid species was evaluated by Northwestern blotting. Purified protein fractions were separated in 10% SDS-PAGE gels and transferred to nitrocellulose membranes. Blocking and incubation with biotin-labeled probes was performed as previously described (26). Three types of probes were used: 16-nucleotide (nt) single-stranded RNAs of both viral (leader TRS) and cellular (glyceraldehyde 3-phosphate dehydrogenase) origins, 18-nt single-stranded DNAs (ssDNAs), and longer ssRNAs of around 130 nt (acceptor and donor RNAs from the retrovirus-derived template switch system). Probe sequences are available from the authors upon request. Biotinylated RNAs were detected using the BrightStar BioDetect kit (Ambion) (Fig. 1B). The intensity of the binding was estimated by band densitometry. Since full-length TGEV N protein and its deletion mutants were prone to degradation, a property related to the disordered nature of the protein (16, 27, 34), binding values were calculated with reference to the amount of each intact protein fragment (Fig. 1B, top panel). As expected, the glutathione *S*-transferase (GST) control protein did not bind to any nucleic acid probe, while N protein bound to all nucleic acid species (Fig. 1C). N-protein mutants lacking the C-terminal domain (ΔN1 and ΔN2) and mutant ΔN3, containing just the central disorder domain of N protein, bound to all nucleic acid probes as well as or even better than N protein. The mutant ΔN4 hardly bound short nucleic acids, but it bound long ssRNAs as well as N protein. Finally, the mutant ΔN5, containing just the C-terminal domain of N protein, did not bind any nucleic acid (Fig. 1C). These results are in agreement with previously reported RNA binding domains for other coronavirus N proteins (2, 3, 9, 13, 17, 20, 24–27).

RNA chaperone activity of N-protein deletion mutants determined by nucleic acid annealing assays. Facilitation of rapid and accurate nucleic acid annealing is one of the properties of RNA chaperones in general and coronavirus N protein in particular (36). Both DNA and RNA annealing assays, followed by proteinase K treatment to rule out nucleic acid aggregation mediated by protein binding, were performed as previously described (36). In the absence of protein or in the presence of GST, background levels of double-stranded DNA (dsDNA) were obtained (Fig. 2A). The amount of dsDNA was increased in the presence of full-length N protein, as expected. The mutants ΔN1 and ΔN2 also increased the formation of dsDNA. Incubation with the mutant ΔN3, containing the central disordered domain of N protein, showed the largest increase in dsDNA levels. In contrast, incubation with the mutants ΔN4 and ΔN5 provided background levels of dsDNA (Fig. 2A). Similar results were obtained when the base pairing of viral TRS RNAs was analyzed (Fig. 2B). Altogether, these data suggested that the mutants ΔN1, ΔN2, and ΔN3 may have RNA chaperone activity.

Role of N protein in *in vitro* template switching. An *in vitro* template switch system based on human immunodeficiency virus (HIV) was used to evaluate the involvement of N protein in template switching (11). Using a labeled DNA primer, HIV reverse transcriptase (RT) synthesizes a cDNA copy of a donor RNA of 131 nt (strong-stop DNA [SSDNA]). In the presence of an RNA chaperone, template switching occurs, and a labeled transfer product of 185 nt was obtained (Fig. 3A). This system has strong RNA chaperone activity requirements in different steps, such as the unwinding of stable nucleic acid secondary structures, inhibition of self-priming, enhancement of template switching, an increase in RNase H activity, and improvement in RT processivity (15). Template switch reactions were performed as previously described (11), except for

FIG. 1. Nucleic acid binding of N protein mutants. (A) Scheme of TGEV full-length N protein (wt, upper bar) and deletion mutants (ΔN, lower bars). Disorder-order pattern, residues corresponding to crystallized amino- and carboxy-terminal domains (NTD and CTD, respectively), and prediction of RNA binding residues according to the RNAbindR server (28, 29) are indicated. Labels on the left indicate the protein name. SR, Ser-rich domain; RRM, RNA recognition motif; NLS, nuclear localization signal; Ac, acidic domain. The numbers indicate the corresponding amino acids in N protein. (B) Western blot of protein fractions (upper panel) and Northwestern blot using different biotin-labeled probes (lower panels). Proteins were detected with an antibody specific for the GST tag (α-GST). Nondegraded protein species are indicated by black arrowheads. The nature of the nucleic acid probe is indicated at the right of the figure. The numbers on the left indicate molecular masses in kDa. (C) The intensity of the bands binding the probe was estimated by densitometry and corrected by the amount of intact protein in each case. Binding of N protein was considered to be 100 relative units (r.u.) of activity in each case; this threshold is indicated by the black dashed line. Error bars represent the standard deviations from four independent experiments.

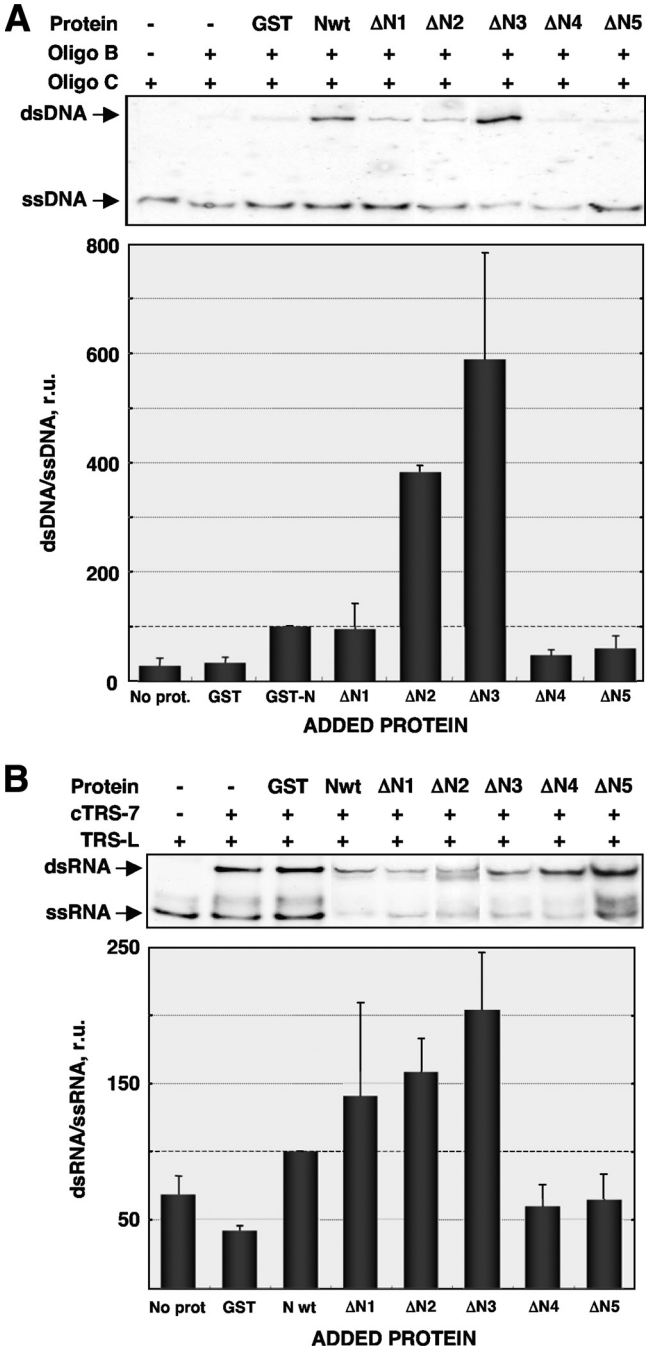

FIG. 2. Nucleic acid annealing assays. (A) DNA annealing assays were performed using an 18-mer biotin-labeled DNA oligonucleotide (Oligo C) and a 56-mer unlabeled DNA oligonucleotide (Oligo B) that under reaction conditions forms a stable secondary structure that must be unwound to allow double-stranded DNA formation. The ratio of dsDNA to ssDNA was estimated by densitometry (graph) and referenced to that obtained in the presence of wt N protein, considered 100 relative units (r.u.) (indicated by the black dashed line). (B) RNA annealing assays were performed using a biotin-labeled 16-mer RNA oligonucleotide representing the transcription regulating sequence of the leader (TRS-L) and an unlabeled 16-mer RNA oligonucleotide with the complementary sequence to the gene 7 TRS (cTRS-7). The ratio of dsRNA to ssRNA was estimated as for panel A. Error bars in panels A and B represent the standard deviations for results from four independent experiments.

the use of a biotin-labeled DNA primer and detection of biotinylated reaction products with the BrightStar BioDetect kit.

In the presence of increasing amounts of HIV nucleocapsid protein (NCp7), a well-known RNA chaperone, an increase in the formation of transfer product was observed (Fig. 3B). In contrast, the levels of transfer product remained constant in the presence of the GST negative control protein (Fig. 3B). The generation of transfer product as the result of template switching was monitored in the presence of full-length N protein and its deletion mutants (Fig. 3B). Template switch efficiency was estimated by densitometry as previously described (11) (Fig. 3C). An increase in the TGEV N protein concentration led to an increase in the amounts of transfer product (Fig. 3C). This result indicated that TGEV N protein acts as an RNA chaperone in the HIV-derived system, facilitating template switching *in vitro*. Incubation with N-protein mutants lacking the C terminus (ΔN1 and ΔN2) and the mutant ΔN3, containing the central disorder domain of N protein, also produced an increase in the levels of transfer product (Fig. 3C). In contrast, the mutants ΔN4 and ΔN5 did not produce an increase in the amounts of transfer product (Fig. 3C). It is worth noting that at the higher concentrations analyzed, wt N protein and mutants ΔN2 and ΔN3 led to a decrease in the amount of transfer product (Fig. 3C). This effect is probably a consequence of the RNA chaperone activity of the proteins, enhancing the RNA degradation due to nucleases present in the protein fractions (15, 36).

The purification of *in vitro* active coronavirus replication-transcription complexes was recently described (33). Unfortunately, these systems cannot be used to analyze the role of chaperones in template switching, since their chemical components are not fully defined. Most importantly, it is likely that these systems will already include the N protein with the RNA chaperone activity that we would like to evaluate, in addition to other cellular proteins that also have RNA chaperone activity.

Role of N protein in *in vivo* coronavirus RNA synthesis. Using TGEV-derived replicons, our group has previously reported the requirement of N protein for efficient RNA synthesis (1). To dissect the role of N protein in coronavirus replication and transcription, TGEV replicons containing full-length N protein (N wt) or lacking N protein (ΔN) were used (Fig. 4A). Their replication and transcription levels were analyzed by quantitative RT-PCR using specific TaqMan assays for negative and positive strands, respectively. RNA levels were compared in all cases with the levels obtained from a nonreplicative replicon (NR) (Fig. 4A), leading to background reference levels of replication (Fig. 4B) and transcription (Fig. 4C). In the absence of N protein, genomic RNA levels of the replicons including or lacking N protein were similar when both negative and positive RNA strands were analyzed. Furthermore, addition of N protein in *trans* led to an up to 10-fold increase of replication levels for both replicons (Fig. 4B). These data indicate that N protein is not essential for coronavirus replication, and they are in agreement with previous observations (30). The TGEV replicon containing full-length N protein transcribed very efficiently (Fig. 4C). In contrast, replicon ΔN, lacking N protein, led to basal levels of transcription that were increased up to 100-fold by adding N protein in *trans* (Fig. 4C). These data indicate that although not absolutely essential, N protein is required for efficient coronavirus

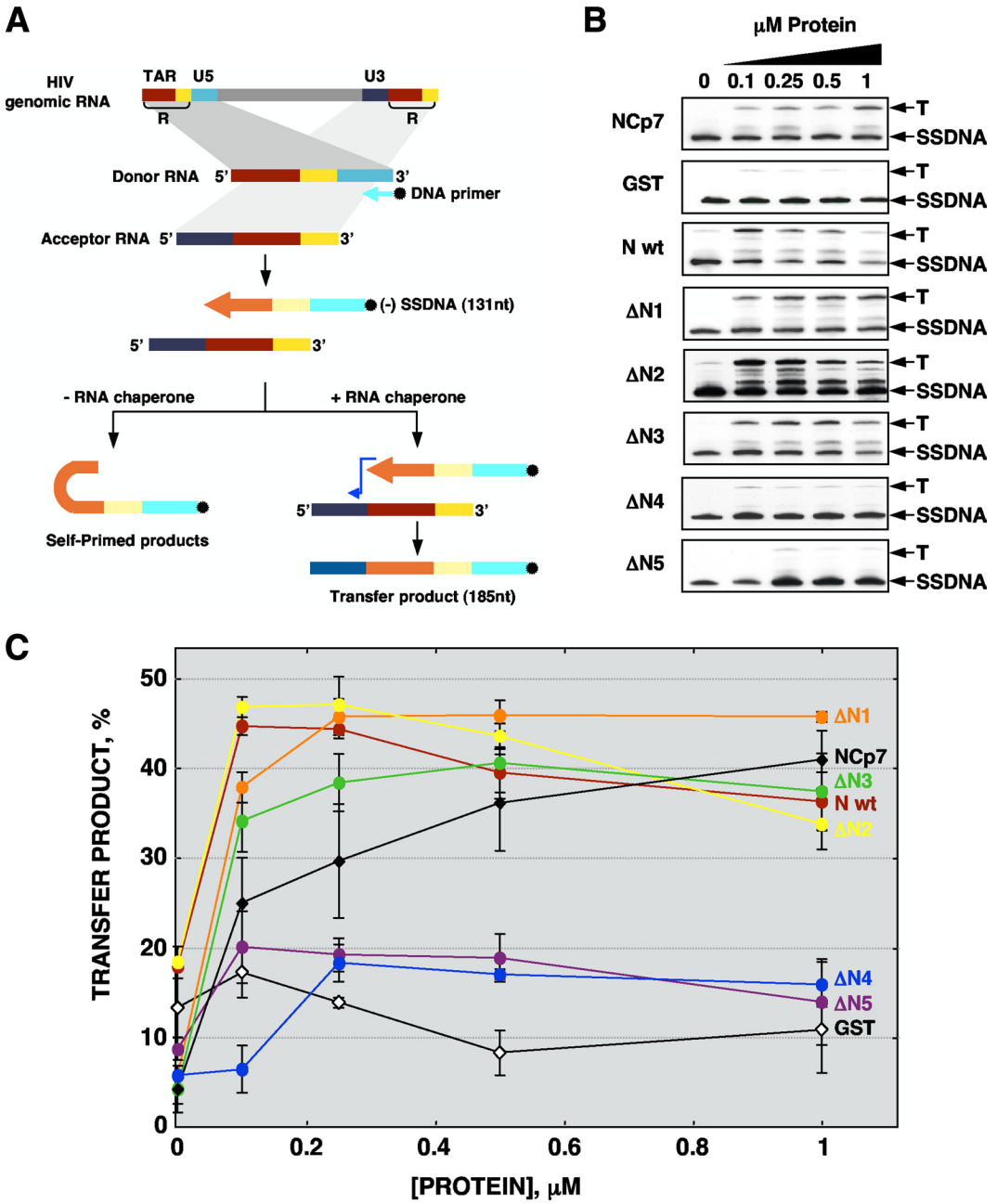

FIG. 3. *In vitro* template switching assay. (A) HIV-derived template switching system. Using a biotin-labeled DNA primer, HIV RT synthesizes a cDNA copy of a donor RNA of 131 nt (strong-stop DNA [SSDNA]). In the presence of an RNA chaperone, template switching occurs and a labeled transfer product (T) of 185 nt was obtained. R, repeated sequences, including transactivation response (TAR) element sequence. (B) Template switch assay in the presence of control NCp7 and GST proteins or TGEV N protein deletion mutants. (C) Template switch efficiency was estimated by densitometry of labeled T and SSDNA bands, and the transfer product amount was calculated as a percentage of the ratio T/(T + SSDNA) in each case. Error bars represent the standard deviations from four independent experiments.

transcription. The obtained results confirm previous data on the enhancement of RNA synthesis by N protein (1, 31), indicating that the increase in RNA synthesis from the presence of N protein is due mainly to an increase in transcription levels.

Overall, the results shown indicate that the RNA chaperone activity of TGEV N protein is located in its central disordered domain (aa 117 to 268) and that this activity requires the ability to bind RNA and additional characteristics present in the ΔN3 N-protein fragment. To our knowledge, this is the first demonstration of a nonretroviral RNA chaperone acting in an *in vitro* template switching system. The results obtained confirm the RNA chaperone activity of TGEV N protein and its potential role in template switching. In agreement with this, *in vivo* results indicated that N protein is required for efficient transcription. Nevertheless, additional experimental evidence will be required to defin-

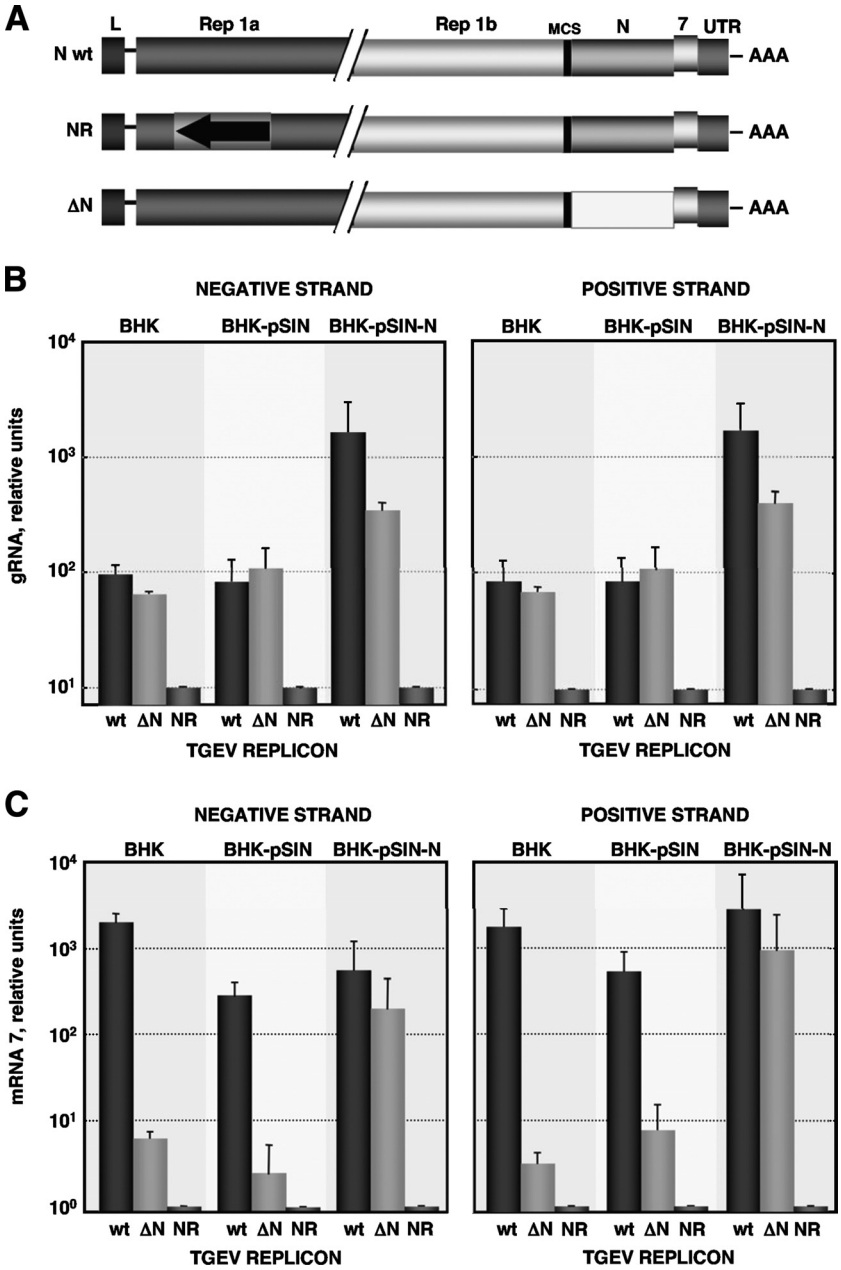

FIG. 4. *In vivo* coronavirus RNA synthesis. (A) Scheme of TGEV-derived replicons, containing full-length N protein (N wt) or lacking N protein (ΔN). A nonreplicative replicon (NR) containing full-length N protein, but unable to replicate due to a mutation affecting several replicase genes, was also used. All replicons contain gene 7 to allow measurement of transcription (1). (B) Quantification of negative and positive strands of genomic RNA (gRNA) using specific TaqMan assays. Experiments were performed as previously described (1), including a DNase I treatment to eliminate DNA from transfection. BHK-pSIN, BHK cells transfected with Sindbis virus replicon; BHK-pSIN-N, BHK cells expressing N protein from Sindbis virus replicon. (C) Transcription levels measured by quantification of subgenomic mRNA of gene 7, both negative and positive strand, using specific TaqMan assays. Error bars represent the standard deviations from five independent experiments.

itively establish the implication of N protein in coronavirus template switching.

We thank F. Almazan for critically reading the manuscript and helpful discussions. We are also grateful to J. G. Levin and R. J. Gorelick for kindly providing plasmids for the HIV-derived template switch assay and purified NCp7, respectively.

This work was supported by grants from Comisión Interministerial de Ciencia y Tecnología (CICYT) (no. BIO2007-60978), the Consejeria de Educación y Cultura de la Comunidad de Madrid (S-SAL-0185/06), the European Communities (PoRRSCon, EU-245141), and the National Pork Board (NPB#08-197). S.Z., I.S., and J.L.G.C. received contracts from the Consejo Superior de Investigaciones Científicas (CSIC) and Comunidad Autónoma de Madrid.

REFERENCES

1. **Almazan, F., C. Galan, and L. Enjuanes.** 2004. The nucleoprotein is required for efficient coronavirus genome replication. J. Virol. **78:**12683–12688.
2. **Chang, C. K., S. C. Sue, T. H. Yu, C. M. Hsieh, C. K. Tsai, Y. C. Chiang, S. J.**

Lee, H. H. Hsiao, W. J. Wu, W. L. Chang, C. H. Lin, and T. H. Huang. 2006. Modular organization of SARS coronavirus nucleocapsid protein. J. Biomed. Sci. **13:**59–72.
3. **Chen, C. Y., C. Chang, Y. W. Chang, S. C. Sue, H. Bai, L. Riang, C. D. Hsiao, and T. Huang.** 2007. Structure of the SARS coronavirus nucleocapsid protein RNA-binding dimerization domain suggests a mechanism for helical packaging of viral RNA. J. Mol. Biol. **368:**1075–1086.
4. **Cristofari, G., and J. L. Darlix.** 2002. The ubiquitous nature of RNA chaperone proteins. Prog. Nucleic Acid Res. Mol. Biol. **72:**223–268.
5. **Dyson, H. J., and P. E. Wright.** 2005. Intrinsically unstructured proteins and their functions. Nat. Rev. **6:**197–208.
6. **Enjuanes, L., F. Almazan, I. Sola, and S. Zuñiga.** 2006. Biochemical aspects of coronavirus replication and virus-host interaction. Annu. Rev. Microbiol. **60:**211–230.
7. **Enjuanes, L., A. E. Gorbalenya, R. J. de Groot, J. A. Cowley, J. Ziebuhr, and E. J. Snijder.** 2008. The Nidovirales, p. 419–430. *In* B. W. J. Mahy, M. Van Regenmortel, P. Walker, and D. Majumder-Russell (ed.), Encyclopedia of virology, 3rd ed. Elsevier Ltd., Oxford, United Kingdom.
8. **Enjuanes, L., I. Sola, S. Zuñiga, and J. L. Moreno.** 2007. Coronavirus RNA synthesis: transcription, p. 81–107. *In* V. Thiel (ed.), Coronaviruses: molecular and cellular biology. Caister Academic Press, Norfolk, United Kingdom.
9. **Fan, H., A. Ooi, Y. W. Tan, S. Wang, S. Fang, D. X. Liu, and J. Lescar.** 2005. The nucleocapsid protein of coronavirus infectious bronchitis virus: crystal structure of its N-terminal domain and multimerization properties. Structure **13:**1859–1868.
10. **Gorbalenya, A. E., L. Enjuanes, J. Ziebuhr, and E. J. Snijder.** 2006. Nidovirales: evolving the largest RNA virus genome. Virus Res. **117:**17–37.
11. **Guo, J., L. E. Henderson, J. Bess, B. Kane, and J. G. Levin.** 1997. Human immunodeficiency virus type 1 nucleocapsid protein promotes efficient strand transfer and specific viral DNA synthesis by inhibiting TAR-dependent self-priming from minus-strand strong-stop DNA. J. Virol. **71:**5178–5188.
12. **Herschlag, D.** 1995. RNA chaperones and the RNA folding problem. J. Biol. Chem. **270:**20871–20874.
13. **Huang, Q., L. Yu, A. M. Petros, A. Gunasekera, Z. Liu, N. Xu, P. Hajduk, J. Mack, S. W. Fesik, and E. T. Olejniczak.** 2004. Structure of the N-terminal RNA-binding domain of the SARS CoV nucleocapsid protein. Biochemistry **43:**6059–6063.
14. **Ivanyi-Nagy, R., J. Lavergne, C. Gabus, D. Ficheux, and J. Darlix.** 2008. RNA chaperoning and intrinsic disorder in the core proteins of *Flaviviridae*. Nucleic Acids Res. **36:**2618–2633.
15. **Levin, J. G., J. Guo, I. Rouzina, and K. Musier-Forsyth.** 2005. Nucleic acid chaperone activity of HIV-1 nucleocapsid protein: critical role in reverse transcription and molecular mechanism. Prog. Nucleic. Acids Res. Mol. Biol. **80:**217–286.
16. **Mark, J., X. Li, T. Cyr, S. Fournier, B. Jaentschke, and M. A. Hefford.** 2008. SARS coronavirus: unusual lability of the nucleocapsid protein. Biochem. Biophys. Res. Commun. **377:**429–433.
17. **Nelson, G. W., S. A. Stohlman, and S. M. Tahara.** 2000. High affinity interaction between nucleocapsid protein and leader/intergenic sequence of mouse hepatitis virus RNA. J. Gen. Virol. **81:**181–188.
18. **Parker, M. M., and P. S. Masters.** 1990. Sequence comparison of the N genes of five strains of the coronavirus mouse hepatitis virus suggests a three domain structure for the nucleocapsid protein. Virology **179:**463–468.
19. **Rajkowitsch, L., D. Chen, S. Stampfl, K. Semrad, C. Waldsich, O. Mayer, M. F. Jantsch, R. Konrat, U. Bläsi, and R. Schroeder.** 2007. RNA chaperones, RNA annealers and RNA helicases. RNA Biol. **4:**118–130.
20. **Saikatendu, K. S., J. S. Joseph, V. Subramanian, B. W. Neuman, M. J. Buchmeier, R. C. Stevens, and P. Kuhn.** 2007. Ribonucleocapsid formation of severe acute respiratory syndrome coronavirus through molecular action of the N-terminal domain of N protein. J. Virol. **81:**3913–3921.
21. **Sawicki, S. G., D. L. Sawicki, and S. G. Siddell.** 2007. A contemporary view of coronavirus transcription. J. Virol. **81:**20–29.
22. **Schelle, B., N. Karl, B. Ludewig, S. G. Siddell, and V. Thiel.** 2005. Selective replication of coronavirus genomes that express nucleocapsid protein. J. Virol. **79:**6620–6630.
23. **Sola, I., J. L. Moreno, S. Zuñiga, S. Alonso, and L. Enjuanes.** 2005. Role of nucleotides immediately flanking the transcription-regulating sequence core in coronavirus subgenomic mRNA synthesis. J. Virol. **79:**2506–2516.
24. **Spencer, K., and J. A. Hiscox.** 2006. Characterisation of the RNA binding properties of the coronavirus infectious bronchitis virus nucleocapsid protein amino-terminal region. FEBS Lett. **580:**5993–5998.
25. **Takeda, M., C. Chang, T. Ikeya, P. Güntert, Y. Chang, Y. I. Hsu, T. Huang, and M. Kainosho.** 2008. Solution structure of the C-terminal dimerization domain of SARS coronavirus nucleocapsid protein solved by the SAIL-NMR method. J. Mol. Biol. **380:**608–622.
26. **Tan, Y. W., S. Fang, H. Fan, J. Lescar, and D. X. Liu.** 2006. Amino acid residues critical for RNA-binding in the N-terminal domain of the nucleocapsid protein are essential determinants for the infectivity of coronavirus in cultured cells. Nucleic Acids Res. **34:**4816–4825.
27. **Tang, T. K., M. P. Wu, S. T. Chen, M. H. Hou, M. H. Hong, F. M. Pan, H. M. Yu, J. H. Chen, C. W. Yao, and A. H. Wang.** 2005. Biochemical and immunological studies of nucleocapsid proteins of severe acute respiratory syndrome and 229E human coronaviruses. Proteomics **5:**925–937.
28. **Terribilini, M., J. H. Lee, C. Yan, R. L. Jernigan, V. Honavar, and D. Dobbs.** 2006. Prediction of RNA binding sites in proteins from amino acid sequence. RNA **12:**1450–1462.
29. **Terribilini, M., J. D. Sander, J. H. Lee, P. Zaback, R. L. Jernigan, V. Honavar, and D. Dobbs.** 2007. RNABindR: a server for analyzing and predicting RNA-binding sites in proteins. Nucleic Acids Res. **35:**W578–W584.
30. **Thiel, V., J. Herold, B. Schelle, and S. G. Siddell.** 2001. Viral replicase gene products suffice for coronavirus discontinuous transcription. J. Virol. **75:**6676–6681.
31. **Thiel, V., N. Karl, B. Schelle, P. Disterer, I. Klagge, and S. G. Siddell.** 2003. Multigene RNA vector based on coronavirus transcription. J. Virol. **77:**9790–9798.
32. **Tompa, P., and P. Csermely.** 2004. The role of structural disorder in the function of RNA and protein chaperones. FASEB J. **18:**1169–1175.
33. **van Hemert, M. J., S. H. van den Worm, K. Knoops, A. M. Mommaas, A. E. Gorbalenya, and E. J. Snijder.** 2008. SARS-coronavirus replication/transcription complexes are membrane-protected and need a host factor for activity in vitro. PLoS Pathog. **4:**e1000054.
34. **Wang, Y., X. Wu, Y. Wang, B. Li, H. Zhou, G. Yuan, Y. Fu, and Y. Luo.** 2004. Low stability of nucleocapsid protein in SARS virus. Biochemistry **43:**11103–11108.
35. **Zuñiga, S., I. Sola, S. Alonso, and L. Enjuanes.** 2004. Sequence motifs involved in the regulation of discontinuous coronavirus subgenomic RNA synthesis. J. Virol. **78:**980–994.
36. **Zuñiga, S., I. Sola, J. L. Moreno, P. Sabella, J. Plana-Duran, and L. Enjuanes.** 2007. Coronavirus nucleocapsid protein is an RNA chaperone. Virology **357:**215–227.

JOURNAL OF VIROLOGY, May 2011, p. 5136–5149 Vol. 85, No. 10
0022-538X/11/$12.00 doi:10.1128/JVI.00195-11

The Polypyrimidine Tract-Binding Protein Affects Coronavirus RNA Accumulation Levels and Relocalizes Viral RNAs to Novel Cytoplasmic Domains Different from Replication-Transcription Sites[▽]

Isabel Sola, Carmen Galán,† Pedro A. Mateos-Gómez, Lorena Palacio, Sonia Zúñiga, Jazmina L. Cruz, Fernando Almazán, and Luis Enjuanes*

Department of Molecular and Cell Biology, Centro Nacional de Biotecnología, CSIC, Darwin 3, Cantoblanco, 28049 Madrid, Spain

Received 28 January 2011/Accepted 2 March 2011

The coronavirus (CoV) discontinuous transcription mechanism is driven by long-distance RNA-RNA interactions between transcription-regulating sequences (TRSs) located at the 5′ terminal leader (TRS-L) and also preceding each mRNA-coding sequence (TRS-B). The contribution of host cell proteins to CoV transcription needs additional information. Polypyrimidine tract-binding protein (PTB) was reproducibly identified in association with positive-sense RNAs of transmissible gastroenteritis coronavirus (TGEV) TRS-L and TRS-B by affinity chromatography and mass spectrometry. A temporal regulation of PTB cytoplasmic levels was observed during infection, with a significant increase from 7 to 16 h postinfection being inversely associated with a decrease in viral replication and transcription. Silencing the expression of PTB with small interfering RNA in two cell lines (Huh7 and HEK 293T) led to a significant increase of up to 4-fold in mRNA levels and virus titer, indicating a negative effect of PTB on CoV RNA accumulation. During CoV infection, PTB relocalized from the nucleus to novel cytoplasmic structures different from replication-transcription sites in which stress granule markers T-cell intracellular antigen-1 (TIA-1) and TIA-1-related protein (TIAR) colocalized. PTB was detected in these modified stress granules in TGEV-infected swine testis cells but not in stress granules induced by oxidative stress. Furthermore, viral genomic and subgenomic RNAs were detected in association with PTB and TIAR. These cytoplasmic ribonucleoprotein complexes might be involved in post-transcriptional regulation of virus gene expression.

Transmissible gastroenteritis virus (TGEV) is a member of the *Coronaviridae* family, included in the *Nidovirales* order (25, 26). Coronaviruses (CoVs) are the causative agents of a variety of respiratory and enteric diseases in humans and animals (22, 53). The emergence of severe acute respiratory syndrome coronavirus (SARS-CoV) revealed the potential high pathogenicity of CoVs for humans by infecting 8,000 people and killing about 10% of them (52). Common ancestors of CoVs have been identified in bats distributed worldwide, suggesting that they may represent a natural reservoir from which viruses may be reintroduced into the human population (20, 42, 46, 54, 55).

CoVs have the largest known RNA genome, consisting of a single-stranded positive-sense RNA of about 30 kb in length (19, 25, 50). The CoV replicase gene, which occupies the 5′ two-thirds of the genome, is extremely complex, and besides the RNA-dependent RNA polymerase (RdRp) and helicase activities, it encodes other enzymes less frequent or exclusive among RNA viruses (50, 62, 67), such as an endoribonuclease, a 3′-5′ exoribonuclease, a 2′-*O*-ribose methyltransferase, a ribose ADP 1″-phosphatase, and a second RNA-dependent RNA polymerase residing in nonstructural protein 8 (nsp8) (31). In addition to the replicase components, the viral nucleoprotein has been shown to play a major role in CoV RNA synthesis (3, 60, 70). The structures of the CoV genomic and subgenomic RNAs resemble the structure of most cellular mRNAs, containing a cap structure at the 5′ end, a poly(A) tail at the 3′ end, and 5′ and 3′ untranslated regions (UTRs). CoV gene expression depends on a discontinuous transcription process leading to a collection of subgenomic mRNAs (sgmRNAs), consisting of the 5′ terminal leader sequence (L) joined to distant genomic sequences. This complex process is associated with transcription-regulating sequences (TRSs), located at the 3′ end of the leader (TRS-L) and preceding each gene (body TRS or TRS-B). TRSs include the conserved core sequence (CS) (5′-CUAAAC-3′), identical in all TGEV genes, and the 5′ and 3′ flanking sequences (5′ TRS and 3′ TRS, respectively) (24).

In agreement with the proposed working model for CoV transcription (63, 69), TRS-B would act as an attenuation and dissociation signal for the transcription complex during the synthesis of the minus-strand RNA. This transcription step would promote a template switch of the nascent RNA, complementary to the coding sequences, to the genome 5′ leader region. Then, the synthesis of minus-strand subgenomic RNA (sgRNA) would resume, adding a copy of the leader. The resulting chimeric sgRNAs of minus sense serve as templates to yield sgmRNAs that share both 5′ and 3′ terminal sequences

* Corresponding author. Mailing address: Department of Molecular and Cell Biology, Centro Nacional de Biotecnología, CSIC, Darwin 3, Cantoblanco, 28049 Madrid, Spain. Phone: 34 91 585 4555. Fax: 34 91 585 4506. E-mail: L.Enjuanes@cnb.csic.es.

† Present address: Max-Planck Institute of Immunobiology, Department of Epigenetics, Laboratory Jenuwein, Stübeweg 51, D-79108 Freiburg, Germany.

▽ Published ahead of print on 16 March 2011.

with the genome RNA. Previous studies on the TGEV transcription mechanism have shown that complementarity between TRS-L and complement of TRS-B (cTRS-B) in the nascent RNA is a determinant factor during template switch (63, 69). Presumably, host cell proteins also contribute to transcriptional regulation by RNA-protein and protein-protein interactions involving TRSs (24, 50).

To date, limited information on cellular proteins involved in CoV transcription is available. The heterogeneous nuclear ribonucleoproteins (hnRNPs) A1 and Q were identified through their interaction with TRSs of the mouse hepatitis virus (MHV), a member of CoV genus β. These proteins were characterized as possible positive regulators for viral RNA synthesis (16, 45). The polypyrimidine tract-binding protein (PTB) was also described to bind the MHV leader TRS (30). However, analysis of the role of PTB in MHV replication and transcription did not lead to clear conclusions (15).

PTB, also known as hnRNP I, is a member of the hnRNP family of RNA-binding proteins, which regulate different aspects of RNA metabolism both in the nucleus and in the cytoplasm of eukaryotic cells (59). In the nucleus, PTB acts as a pre-mRNA splicing repressor associated with tissue-specific exons (12). It has been proposed that PTB interferes with molecular interactions across the exon between protein complexes that mediate exon definition (33) or, alternatively, by precluding the association of splicing factors required for exon RNA removal (64). In the cytoplasm, PTB is involved in the regulation of cap-independent translation of viral and cellular mRNAs driven by internal ribosome entry site (IRES) (61), mRNA location (47), and stability (41).

We have recently reported on the interaction of cellular proteins with the 5′ and 3′ UTRs of the TGEV RNA genome, a member of CoV genus α. The binding of PTB to the 5′ end of the viral genome was shown (28). In the study described in this report, PTB interaction with TGEV TRSs has been shown by RNA affinity chromatography and mass spectrometry analysis. The functional relevance of PTB on TGEV transcription was analyzed by small interfering RNA (siRNA) approaches in human Huh7 cells infected with TGEV and in HEK 293T cells transfected with a TGEV-derived replicon. A significant increase of up to 4-fold in mRNA levels and virus titer was observed after silencing of the expression of PTB, suggesting a negative effect of PTB in TGEV infection. In TGEV-infected cells, PTB localized to novel discrete cytoplasmic granules at the time that RNA synthesis ceased. Neither double-stranded RNA (dsRNA), intermediates of viral RNA synthesis, nor components of the viral replication-transcription complex were detected in these cytoplasmic structures. However, cellular RNA-binding proteins such as T-cell intracellular antigen-1 (TIA-1) and the TIA-1-related protein (TIAR) were identified in PTB-containing granules. PTB was not detected in TIAR-containing stress granules (SGs) induced in swine testis (ST) cells by oxidative stress, suggesting that PTB might be a specific component of cytoplasmic granules induced by TGEV infection. Interestingly, viral genomic RNA (gRNA) and sgmRNA were detected in association with PTB and TIAR. These data indicate that viral RNAs and cellular proteins such as PTB, TIA-1, and TIAR form cytoplasmic ribonucleoprotein complexes that are most likely involved in the posttranscriptional regulation of virus gene expression during infection.

TABLE 1. Oligonucleotides used for PCR amplifications

Oligonucleotide	Oligonucleotide sequence (5′ → 3′)[a]
T7-TRSL-EcoRI-VS	CCG*GAATTC***TAATACGACTCACTATAGG**GTTCTTTTACTTTAACTAGCCTTGTG**
TRSL-HindIII-DraI-RS	CCC*AAGCTT TTTAAA*CTGAATGGAAATAATC
cTRSL-EcoRI-SacI-VS	CCG*GAATTC GAGCTC*TTCTTTTACTTTAAC
T3-cTRSL-HindIII-RS	CCC*AAGCTT***AATTAACCCTCACTAAAGG**GGAATGGAAATAATCAACGCTTG**

[a] Restriction endonuclease sites used for cloning are in italics. Transcription promoters are in boldface.

MATERIALS AND METHODS

Cells and viruses. ST cells (51) were grown in Dulbecco modified Eagle medium (DMEM) supplemented with 10% fetal bovine serum (FBS). Human liver-derived Huh7 cells were kindly provided by R. Bartenschlager (University of Heidelberg, Heidelberg, Germany) and were grown in DMEM supplemented with 10% heat-inactivated FBS. Human HEK 293T cells were grown in DMEM supplemented with 5% FBS. The TGEV PUR46-MAD strain (58) was used to infect ST cells, and the TGEV PUR46-C11 strain (57) was used to infect Huh7 cells. Virus titration was performed on ST cell monolayers as previously described (35). For oxidative stress induction, ST cells were exposed to 1 and 3 mM sodium arsenite (Sigma) in complete medium for 60 and 90 min at 37°C. For endoplasmic reticulum (ER) stress induction, ST cells were exposed to 1 and 2 μM thapsigargin (Sigma) in complete medium for 1.5, 8, and 16 h at 37°C. For activation of RNA-activated protein kinase (PKR), ST cells were transfected with 2 and 4 μg of poly(I:C) (Sigma) by a reverse transfection protocol with Lipofectamine 2000 (Invitrogen), following the manufacturer's instructions. Stress granule formation was analyzed by immunofluorescence at 2, 6, and 16 h posttransfection.

DNA constructs. To generate a DNA template for the *in vitro* transcription of an RNA including TRS-L, nucleotides (nt) 39 to 159 of the TGEV genome were amplified by PCR from plasmid pBAC-TGEV-ΔCla (4) with the oligonucleotides T7-TRSL-EcoRI-VS (where VS indicates virus sense and which includes the T7 promoter) and TRSL-HindIII-DraI-RS (where RS indicates reverse sense) (Table 1). For the *in vitro* transcription of a minus-sense RNA including the complement of TRS-L (cTRS-L), TGEV genome nt 38 to 154 were amplified from the same plasmid by PCR with the oligonucleotides cTRSL-EcoRI-SacI-VS and T3-cTRSL-HindIII-RS, which includes the T3 promoter (Table 1). Both PCR amplicons were digested with EcoRI and HindIII and cloned into the same restriction sites of the vector pSL-1190 to generate plasmids pSL-T7-TRSL and pSL-T3-cTRSL, respectively. pSL-T7-TRSL and pSL-T3-cTRSL were linearized with DraI and SacI, respectively. Linearized plasmid pSL-T3-cTRSL-SacI was treated with T4 DNA polymerase (New England BioLabs) to generate blunt ends, following the manufacturer's conditions. The DNA templates were purified with QIAquick reagent (Qiagen) and then used for the *in vitro* transcription reactions. PCRs were performed with platinum *Pfx* DNA polymerase (Invitrogen), following the manufacturer's recommended conditions. All cloning steps were checked by sequencing the PCR-amplified fragments and cloning junctions.

***In vitro* transcription.** *In vitro* transcription reactions to generate TRS-L-121 (TGEV nt 39 to 159) and cTRS-L-117 (the complement of TGEV nt 38 to 154) RNAs were performed from 1.5 μg of linearized pSL-T7-TRSL and pSL-T3-cTRSL templates using a MAXIscript T7/T3 transcription kit (Ambion), according to the manufacturer's instructions. Biotin-14-CTP (Invitrogen) was added at a final concentration of 0.16 mM in a 1:6.25 ratio to unlabeled CTP. The transcription reaction mixtures were incubated for 2 h at 37°C and treated with 10 units of DNase I for 15 min at 37°C. The resulting transcripts were purified with an RNeasy kit (Qiagen), following the RNA cleanup protocol, analyzed by denaturing electrophoresis in 2% (wt/vol) agarose–2.2 M formaldehyde gels, and quantified spectrophotometrically.

Cell extracts. For proteomics analysis, Huh7 cells were grown in 15-cm-diameter dishes to confluence and infected at a multiplicity of infection (MOI) of 5 with TGEV PUR46-C11. After an adsorption period of 1 h, the inoculum medium was replaced by fresh medium and the cell extracts were prepared at

TABLE 2. Biotin-labeled RNA sequences used in affinity chromatography experiments

Name	TRS	Sequence (5′ → 3′)[a]	Polarity	Size (nt)
TRS-L-30	TRS-L	CACCAACUCGAA**CUAA AC**GAAAUAUUUGUC	+	30
cTRS-L-16	TRS-L	AUUUC**GUUUAG**UUCGA	−	16
TRS-S2-30	TRS-S2	GAAACCUUCCUU**CUAA AC**UAUAGUAGUAGG	+	30
cTRS-S2-16	TRS-S2	CUAUA**GUUUAG**AAGGA	−	16
TRS-N-30	TRS-N	CAUAUGGUAUAA**CUAA AC**UUCUAAAUGGCC	+	30
cTRS-N-30	TRS-N	GCCAUUUAGAAG**GUUU AG**UUAUACCAUAUG	−	30

[a] The conserved CS (in boldface) is the central motif of RNA oligonucleotides.

72 h postinfection (hpi). The cells were then washed with cold phosphate-buffered saline (PBS), scraped off the plates, centrifuged at 1,000 × *g* for 5 min at 4°C, and stored at −80°C. Cytoplasmic extracts were prepared from infected cells as previously described (28). Extracts were stored in 10% glycerol at −80°C. Total protein concentration was determined with a Coomassie plus protein assay (Pierce).

5′ Biotinylated RNA oligonucleotides. 5′ Biotinylated RNA oligonucleotides 16 or 30 nt long, including sequences of TGEV TRS-L and TRS-B with positive or negative polarity (Table 2) and the CS as the central motif, were purchased from CureVac (Tübingen, Germany).

RNA affinity chromatography. Cell extracts (250 μg) were diluted 1:3 in binding-washing (BW) buffer (50 mM HEPES, pH 7.9, 150 mM KCl, 5% glycerol, 0.01% NP-40) and precleared three times with 20 μl of streptavidin-coupled Dynabeads (M-80; Dynal) for 4 h at 4°C. *In vitro*-transcribed RNAs (3 μg) or 5′ biotinylated RNA oligonucleotides (400 pmol) were diluted in 20 μl of RNA-binding buffer (5 mM Tris HCl, pH 7.5, 0.5 mM EDTA, 1 M NaCl) and incubated with 20 μl of fresh streptavidin-coupled Dynabeads for 30 min at room temperature. The immobilized RNA was washed three times with 200 μl of BW buffer and then incubated with the precleared protein extract overnight. The RNA-protein complexes were washed three times with 200 μl of BW buffer. RNA-interacting proteins were eluted with 12 μl of KCl, 2 M, dialyzed against water on nitrocellulose membranes (VSWP01300; Millipore), resuspended in NuPage sample buffer (Invitrogen), and analyzed by denaturing electrophoresis using NuPAGE 4 to 12% bis-Tris gels and morpholinepropanesulfonic acid (MOPS)-SDS running buffer (Invitrogen). The gels were washed three times in deionized water and stained with Coomassie blue Simply Blue Safe stain (Invitrogen), and the protein bands of interest were excised from the gels for their identification by mass spectrometry.

Identification of proteins by mass spectrometry. Protein samples from excised bands were analyzed by matrix-assisted laser desorption ionization–time of flight (MALDI TOF) mass spectrometry in an ABI 4800 MALDI TOF/TOF mass spectrometer (Applied Biosystems), followed by comparative data analysis with the NCBI human protein nonredundant database using the Mascot program, as previously described (28).

siRNA transfection. Human Huh7 cells were transfected following a reverse transfection protocol. Briefly, for each well of a 24-well plate, 5×10^4 cells were incubated in suspension with 50 nM PTBP1-specific siRNA (sense sequence 5′GGAUUCAAGUUCUUCCAGAtt3′ and antisense sequence 5′UCUGGAA GAACUUGAAUCCtt 3′ [lowercase indicates nucleotide protruding at the 3′ ends]; catalog no. 12337; Ambion) and 2 μl of siPORT amine (Ambion) diluted in 50 μl of Opti-MEM I reduced serum medium (GibcoBRL-Invitrogen), following the manufacturer's instructions. As a negative control, an irrelevant validated siRNA (sequence not available; siRNA sequence identifier 4390843; Ambion) was transfected. Cells were plated onto each well using DMEM with 10% heat-inactivated FBS, incubated at 37°C for 48 h, and then infected with TGEV PUR46-C11 at an MOI of 5. At 24, 48, and 72 hpi, total RNA, protein, and cell supernatants were collected for further analysis. HEK 293T cells were transfected as previously described (28). Briefly, cells grown to 60% confluence were transfected with 100 nM the same PTBP1-specific siRNA and RNAiMax (Invitrogen), according to the manufacturer's specifications. Cells were incubated at 37°C for 24 h and then trypsinized and seeded in 24-well plates at a confluence of 2×10^5 cells per well. The cells were retransfected with 50 nM siRNAs at 48 h after the first transfection and incubated for 5 h at 37°C. Then, the transfection medium was discarded and the cells were transfected with 800 ng of the TGEV-derived replicon REP 2 and Lipofectamine 2000 (Invitrogen) as previously described (3). Total RNA was collected for further analysis at 19, 28, and 47 h after the replicon transfection (72, 92, and 100 h after the first transfe ction of siRNA, respectively).

Analysis of cellular gene expression and viral RNA levels. Cellular gene expression and viral RNA levels were quantified by quantitative real-time reverse transcription-PCR (qRT-PCR). Total RNA was prepared with an RNeasy kit (Qiagen), according to the manufacturer's instructions. cDNA was synthesized with random hexamers from 100 ng of total RNA using a high-capacity cDNA transcription kit (Applied Biosystems). Cellular gene expression was analyzed using a human PTB-specific TaqMan gene expression assay (Hs00259176_m1 PTBP1; Applied Biosystems). To analyze viral RNA levels, a custom TaqMan assay (Applied Biosystems) specific for TGEV mRNA 7 was used (28). Data were acquired with an ABI Prism 7000 sequence detection system (Applied Biosystems) and analyzed with ABI Prism 7000 SDS, version 1.0, software. Relative gene expression was referred to that for cells treated with a validated negative-control siRNA (Ambion) for each time point. The data represent the averages of biological triplicates.

Western blot analysis. Cell lysates were analyzed by denaturing electrophoresis in NuPAGE 4 to 12% bis-Tris gels with MOPS-SDS running buffer (Invitrogen). Proteins were transferred to a nitrocellulose membrane (Hybond-C extra nitrocellulose; Amersham Biosciences) with a Bio-Rad Mini protean II electroblotting apparatus at 100 V for 1 h in bis-Tris transfer buffer (25 mM bis-Tris, 25 mM bicine, 1 mM EDTA) containing 20% methanol. Membranes were blocked for 1 h with 5% dried skim milk in Tris-buffered saline (20 mM Tris-HCl, pH 7.5, 150 mM NaCl) and then probed with antibodies specific for PTB (mouse monoclonal antibody [MAb] from hybridoma BB7; ATCC), TGEV nucleoprotein (N; mouse MAb 3DC10) (48), and β-actin (mouse MAb ab8226; Abcam). Bound antibodies were detected with horseradish peroxidase-conjugated rabbit anti-mouse secondary antibody and the Immobilon Western chemiluminescent substrate (Millipore), following the manufacturer's recommendations. Densitometric analysis of PTB and β-actin bands from at least four different experiments was performed using Quantity One, version 4.5.1, software (Bio-Rad).

Immunofluorescence. TGEV-infected (MOI, 10) or noninfected ST cells were fixed with 100% chilled methanol for 10 min at room temperature, washed three times in PBS, and incubated with blocking buffer (PBS containing 10% bovine serum albumin) for 1 h at room temperature. Primary antibodies (anti-PTB MAb from hybridoma BB7 from ATCC; anti-TIAR and anti-TIA-1 from Santa Cruz Biotechnology; anti-Dcp1a kindly provided by J. Lykke-Anderson, University of Colorado; anti-HCoV 229E nsp8 kindly provided by J. Ziebuhr, Giessen University, Giessen, Germany; anti-N-protein MAb 3DC10 [48]; anti-dsRNA MAb from English & Scientific Consulting, Hungary) were diluted in PBS–5% bovine serum albumin (1:1,000 for anti-TIAR, anti-TIA-1, and anti-Dcp1a; 1:300 for anti-nsp8; 1:200 for anti-dsRNA and anti-PTB; 1:100 for anti-N) and incubated with cells at room temperature for 1 h. Cells were then washed four times for 10 min each time with PBS and incubated for 1 h at room temperature with secondary antibodies conjugated to Alexa Fluor 488 or Alexa Fluor 594 diluted 1:500 in PBS–5% bovine serum albumin. For double-labeling experiments with MAbs against PTB and dsRNA, affinity-purified anti-PTB MAb BB7 was directly labeled with Zenon labeling reagent (Molecular Probes, Invitrogen) following the manufacturer's instructions. Cells were first incubated with the primary MAb IgG2a anti-dsRNA and secondary antibody conjugated to Alexa Fluor 594. Then, cells were incubated with the complexes formed by MAb BB7 bound to goat anti-mouse IgG2b Fab fragments conjugated to Alexa Fluor 488. To prevent transfer of the Zenon label between antibodies, a fixation with 4% formaldehyde solution in PBS for 15 min at room temperature was performed. Nuclear DNA was visualized with 4′,6-diamidino-2-phenylindole (DAPI). Coverslips were mounted in Prolong Gold antifade reagent (Invitrogen) and analyzed with a confocal fluorescence microscope (TCS SP5; Leica). For each experimental series, images were acquired with the same instrument settings and analyzed with Leica software.

RNA IP. Isolation of PTB and TIAR-associated RNAs under native conditions was performed by immunoprecipitation (IP) using anti-PTB MAb BB7 and goat anti-TIAR antibody, respectively. Cytoplasmic extracts were prepared from ST cells uninfected or infected with TGEV PUR46-MAD at an MOI of 10. ST cells grown in 15-cm-diameter dishes to confluence were washed with cold PBS, scraped off the plates, and centrifuged at 2,000 × *g* for 2 min at 4°C, and the cell pellets were resuspended in 1 ml cold PBS. Then, the cell suspension was mixed with 1 ml lysis buffer (150 mM NaCl, 3 mM $MgCl_2$, 20 mM Tris-HCl, pH 7.5, 1% NP-40, protease inhibitor cocktail [Roche], 1.6 U/μl RNasin RNase inhibitor [Promega]) by gentle pipetting, incubated at 4°C for 10 min, and centrifuged at 3,000 × *g* for 2 min at 4°C. The supernatant, corresponding to the cytosolic

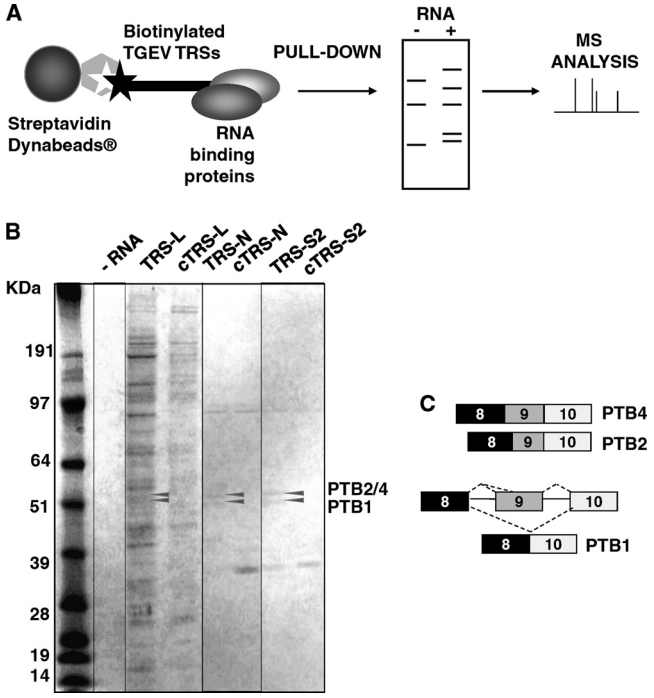

FIG. 1. RNA affinity chromatography assays for isolation of proteins interacting with TGEV TRS. (A) Scheme of the RNA affinity chromatography assay. (B) Proteins from the cytoplasmic extracts of infected Huh7 cells were pulled down, separated by SDS-PAGE, and stained with Coomassie blue. Bands detected in the presence of TRS RNAs and absent in samples without RNA were excised and analyzed by mass spectrometry (MS). Arrows indicate isoforms of PTB. Molecular size markers are shown. TRS-L, TRS-L 121-nt RNA; cTRS-L, cTRS-L 117-nt RNA complementary to leader TRS; TRS-N, 30-nt RNA including the N-gene TRS; cTRS-N, 30-nt RNA complementary to TRS-N; TRS-S2, 30-nt RNA including TRS-S2 within S gene; cTRS-S2, 16-nt RNA complementary to TRS-S2. (C) Scheme showing three isoforms of PTB generated by alternative splicing of exon 9. Complete skipping of exon 9 produces PTB1. Inclusion of exon 9 from two alternative splice sites produces PTB2 and PTB4, which have an extra 19- and 26-amino-acid insert, respectively, between exons 8 and 10.

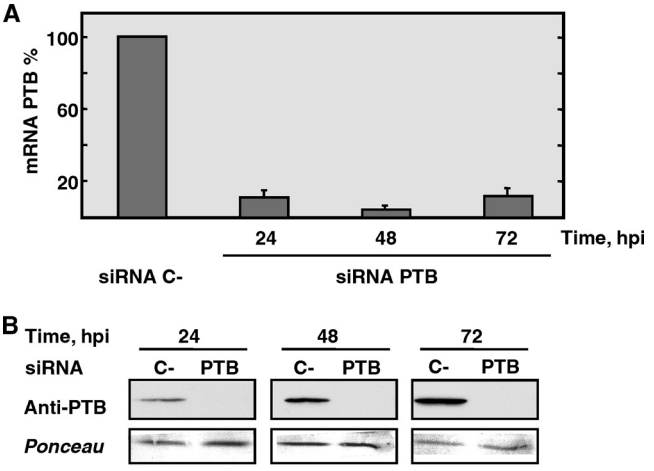

FIG. 2. Silencing of PTB expression in TGEV-infected cells. Human Huh7 cells were transfected with siRNAs and infected with the TGEV PUR46-C11 strain at 48 h posttransfection. Total RNA and protein extracts were collected at 24, 48, and 72 hpi (72, 96, and 120 h posttransfection, respectively) to analyze PTB silencing. (A) Analysis of PTB silencing at the mRNA level. The amount of PTB mRNA in cells transfected with PTB-specific siRNA was quantified by qRT-PCR and expressed as a percentage of mRNA reference levels in cells transfected with a validated negative-control siRNA (siRNA C−) for each time postinfection. (B) Analysis of PTB silencing at the protein level by immunoblotting with anti-PTB antibody. Ponceau staining was used as a loading control.

fraction, was collected and precleared before RNA IP on protein A/G plates (protein A/G plate IP kit; Pierce), following the manufacturer's instructions. Purified anti-PTB, anti-TIAR, or anti-green fluorescent protein (anti-GFP; Boehringer Mannheim) antibodies were first bound to A/G plates diluted (20 μg/μl) in IP buffer (PBS, 1% Triton X-100), and then cytoplasmic extracts were added to the protein A/G-antibody plates. Immunoprecipitated RNA-protein complexes were eluted according to the manufacturer's instructions. RNA was isolated by an RNeasy kit (Qiagen) and subjected to qRT-PCR for the detection of PTB-, TIAR-, or GFP-associated viral or cellular RNAs. Viral gRNA was detected with a custom TaqMan assay (forward primer, 5′-TTTAACTAGCCT TGTGCTAGATTTTGTC-3′; reverse primer, 5′-AAATAATCAACGCTTGTC CTCTATGA-3′; minor groove binder DNA probe, 5′-CAACTCGAACTAAA CGAAAT-3′). sgmRNA 7 was quantified as described above.

RESULTS

Interaction of PTB with TGEV transcription-regulating sequences. Since TRSs are specifically associated with transcription, they were selected to isolate TRS-interacting cellular proteins potentially involved in viral transcription by RNA affinity chromatography. Biotin-labeled RNAs, including viral TRS (Table 2), were used to capture proteins from cytoplasmic extracts of CoV-infected human Huh7 cells (MOI, 5). A human cell line was selected for proteomic analysis to improve protein identification, since human sequences are better represented in public databases than those from porcine species (28). RNA-protein complexes were immobilized on streptavidin-coupled paramagnetic beads and eluted proteins were resolved by SDS-PAGE. Bands detected in the presence of TRS RNAs and absent in samples without RNA were excised, digested with trypsin, and subjected to MALDI-TOF mass spectrometry analysis (Fig. 1A). PTB was reproducibly associated with positive-sense RNAs containing TRS-L sequences of 30 nt (TRS-L-30) or 121 nt (TRS-L-121), as well as 30-nt TRS-B sequences (TRS-S2-30 and TRS-N-30). In contrast, PTB was not detected when the minus-strand RNA complementary to these TRSs (cTRS-L-117, cTRS-S2-30, cTRS-N-30) was used. Two bands with apparent molecular masses of 57 and 59 kDa, compatible with isoforms PTB1 and PTB2/4, respectively, generated by alternative splicing of PTB mRNA (66) were identified with significant scores ($P < 0.05$) and sequence coverage (47 to 88%) (Fig. 1B and C).

Effect of PTB expression silencing on TGEV RNA levels and infectious virus production. To analyze the functional relevance of PTB on TGEV transcription and infectious virus production, its expression was silenced with specific siRNAs in the human cell line Huh7, which is susceptible to TGEV strain PUR46-C11 infection. Additionally, the effect of PTB on TGEV RNA levels was evaluated in human HEK 293T cells transfected with a TGEV-derived replicon (3, 28). A human cell line was selected for functional assays because gene silencing and gene expression reagents were not available for the porcine PTB gene, whereas they were available for the human gene. Furthermore, the design of porcine-specific custom

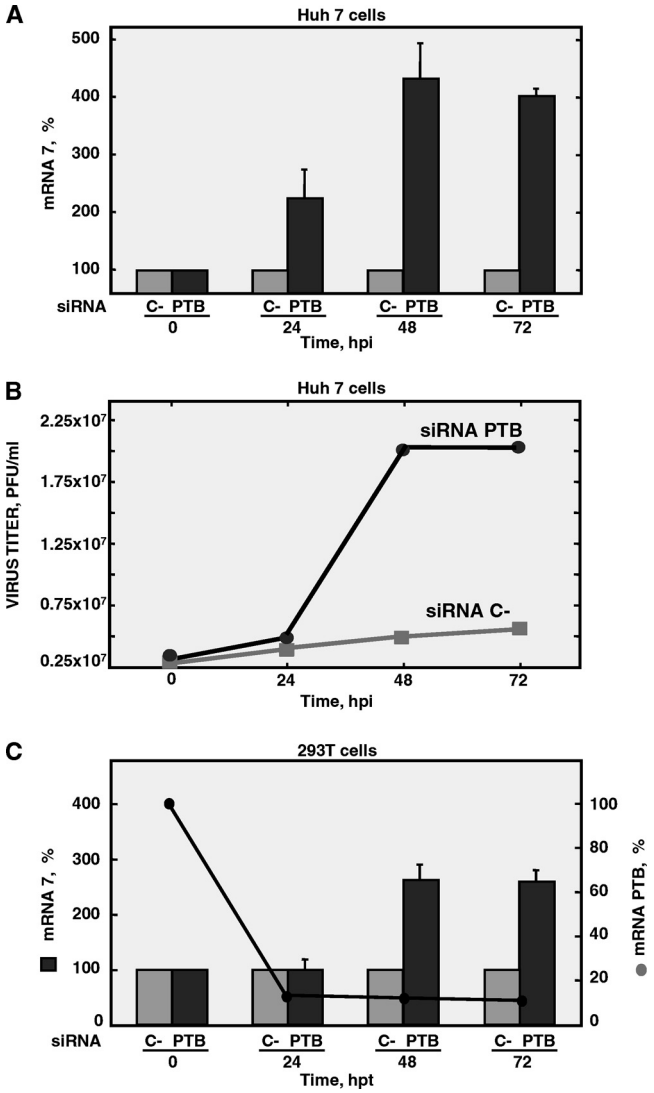

FIG. 3. Effect of silencing PTB expression on TGEV-infected human Huh7 cells and HEK 293T cells transfected with a TGEV-derived replicon. To analyze the viral phenotype, total RNA and supernatants were collected at the indicated times from human Huh7 cells which had been transfected with siRNAs and infected with TGEV PUR46-C11 and human HEK 293T cells transfected with siRNAs and subsequently with the TGEV-derived replicon. (A) Quantification by qRT-PCR of viral mRNA 7 accumulation in cells transfected with PTB-specific siRNA compared to reference levels from cells transfected with a validated negative-control siRNA (C−) at each time postinfection. (B) Virus production in Huh7 cells was quantified by titration of the supernatants on ST cells. (C) Effect of silencing PTB expression on human HEK 293T cells transfected with a TGEV-derived replicon. PTB mRNA and viral mRNA 7 accumulation levels were quantified by qRT-PCR at 19, 28, and 47 h after the replicon transfection (hpt; 72, 92, and 100 h after the first transfection of siRNA, respectively) and expressed as percentages of mRNA reference levels in cells transfected with a validated negative-control siRNA (C−) for each time postinfection. The experiment was performed three times, and the data represent the averages of triplicates. Standard deviations are indicated as error bars.

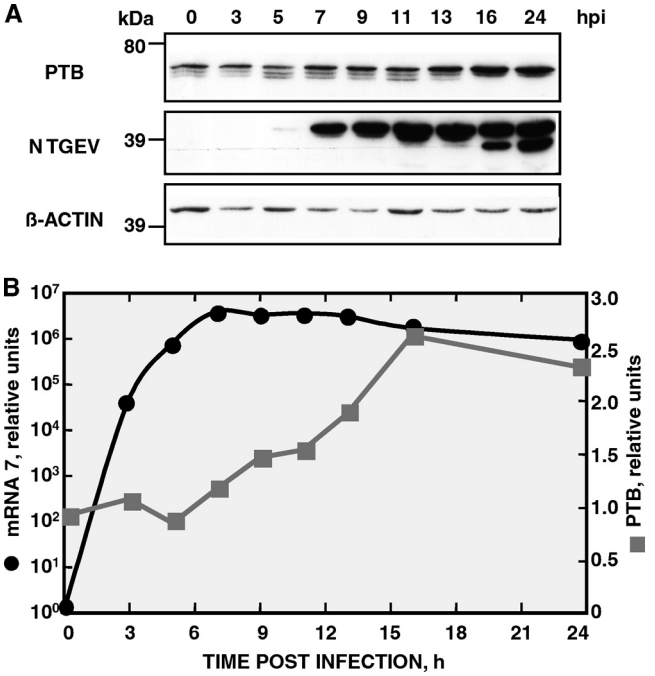

FIG. 4. Kinetic analysis of PTB cytoplasmic levels and viral markers in TGEV-infected ST cells. Total RNA and cytoplasmic protein extracts were collected from ST cells infected with the TGEV PUR46-MAD strain at the indicated hpi. (A) Western blot detection of PTB in cytoplasmic extracts from infected ST cells at different times postinfection. The smallest band detected with anti-PTB MAb in porcine ST cells corresponds to a nonspecific product. TGEV N was detected as a control of viral infection. The smaller band corresponds to a product of caspase-mediated proteolysis of TGEV nucleocapsid protein (23). β-Actin was used as a loading control. Protein molecular masses are given in kDa. (B) Quantification of viral mRNA 7 and cytoplasmic PTB levels in TGEV-infected ST cells. Viral mRNA 7 levels at different times postinfection were determined by qRT-PCR and expressed as relative units in reference to the amount at 0 hpi. Cytoplasmic PTB levels were quantified by densitometry of the PTB2/4 band (upper band) and normalized against the amount of β-actin. Densitometric analysis of PTB and β-actin bands from at least four different experiments was performed, with similar results.

siRNAs is restricted since information on porcine genomic sequences in public databases is very limited and currently available computer algorithms have been developed by taking as a reference only human, mouse, and rat sequences. Synthetic siRNAs were transfected into Huh7 cells by reverse transfection. After 48 h, the cells were infected with the TGEV strain PUR46-C11 at an MOI of 5. Silencing experiments were optimized to select the minimal concentration of siRNA and transfection reagent providing maximum gene silencing and minimum cytotoxicity. From previous PTB-silencing experiments (data not shown), one out of three specific siRNAs providing the highest silencing efficiency (>90%) was chosen for further analysis. Moreover, a single siRNA transfection was sufficient to achieve sustained PTB silencing at both the mRNA and protein levels at the times of the phenotypic analysis. PTB silencing did not have a significant impact on cell viability, as confirmed by the observed growth kinetics of transfected cells. Samples were collected for analysis at 24, 48, and 72 hpi (i.e., 72, 96, and 120 h after transfection of the siRNAs, respectively). PTB mRNA levels showed a significant reduction (90 to 95%) in PTB-silenced cells, in relation to the cells transfected with a validated negative-control siRNA, as determined by qRT-PCR with specific TaqMan gene expression

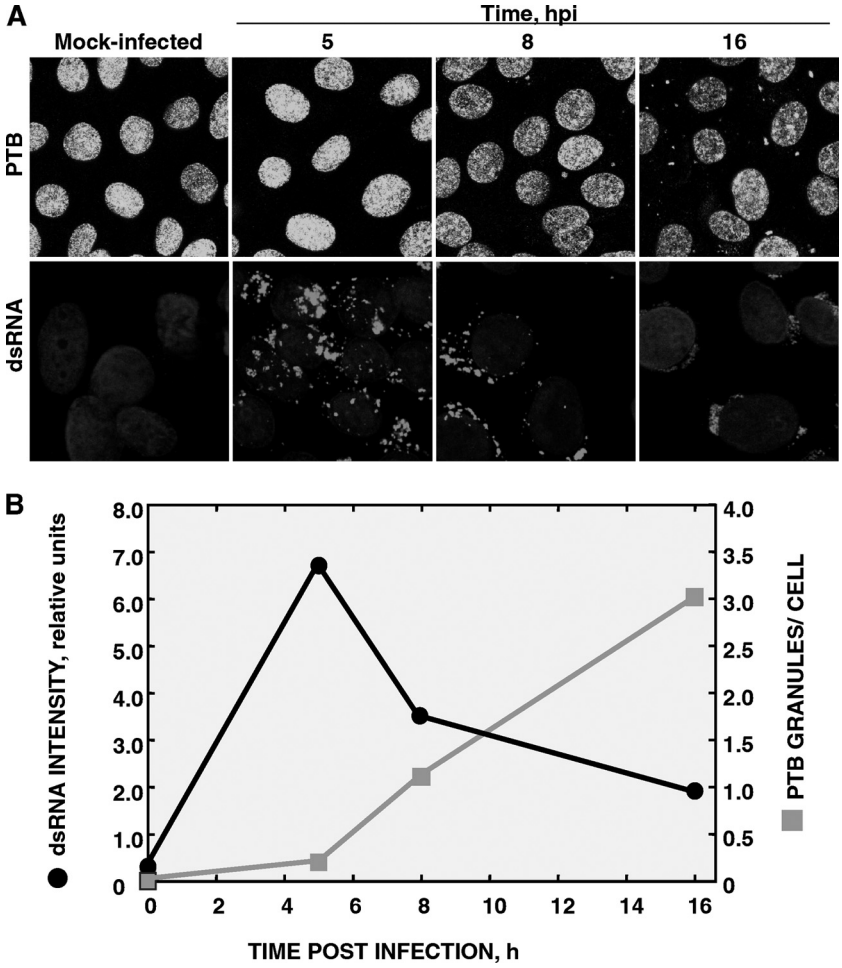

FIG. 5. Visualization of PTB and dsRNA intermediates for viral RNA synthesis in TGEV-infected ST cells. (A) Confocal immunomicroscopy analysis of ST cells mock infected or infected with the TGEV PUR46-MAD strain (MOI, 10) at 5, 8, and 16 hpi. PTB (green) and dsRNA (red) were detected with MAb BB7 and MAb J2, respectively. Nuclear DNA (blue) was stained with DAPI. (B) Quantification of the amount of dsRNA and PTB granules at different times postinfection. The relative intensity of the dsRNA signal in the cytoplasm of noninfected and TGEV-infected cells and the number of cytoplasmic PTB-containing granules per cell were determined in 10 randomly selected microscope fields for each time postinfection. Average values from three independent experiments are represented.

assays (Fig. 2A). Accordingly, PTB levels evaluated by Western blotting were also significantly reduced in PTB-silenced cells and maintained at the different times postinfection analyzed (Fig. 2B).

To determine the extent of viral transcription, the amount of viral mRNA 7 was quantified at the same time points by qRT-PCR. A reproducible and significant 2- to 4-fold increase in mRNA 7 levels was observed in relation to the levels for cells transfected with the negative-control siRNA (Fig. 3A). The maximum increase in viral RNA levels (higher than 4-fold) was observed at 48 and 72 hpi, which correspond to times of maximum TGEV PUR46-C11 RNA synthesis in human Huh7 cells (data not shown). Virus titers in the supernatants of PTB-silenced cells were determined at 24, 48, and 72 hpi. Accordingly, with the effects observed in viral RNA synthesis, a reproducible and significant increase in virus production (3.5-fold) was evident at 48 and 72 hpi in comparison to reference levels in cells transfected with the validated negative-control siRNA (Fig. 3B). To reduce the possibility of having off-target effects, the observed viral phenotype was confirmed in gene silencing experiments with two alternative PTB-specific siRNAs (data not shown). The results of PTB silencing in TGEV-infected cells indicated that PTB had a negative effect on both viral mRNA accumulation and infectious virus production. To confirm that the negative effect of PTB on TGEV accumulation was not indirectly caused by the inhibition of other viral processes distinct from RNA synthesis, PTB expression was silenced in human HEK 293T cells transfected with a TGEV-derived replicon (3, 28). Synthetic siRNAs were transfected twice into HEK 293T cells for a sustained silencing at the mRNA and protein levels. The TGEV-derived replicon was transfected into HEK 293T cells 6 h after the second siRNA transfection, and RNA samples were collected at 19, 28, and 47 h after the replicon transfection (72, 92, and 100 h after the first transfection of siRNA, respectively). A reduction in the PTB mRNA level of 85% was detected in cells transfected with the specific PTB siRNA. The viral mRNA 7 level was quantified as a measure of replicon activity. A reproduc-

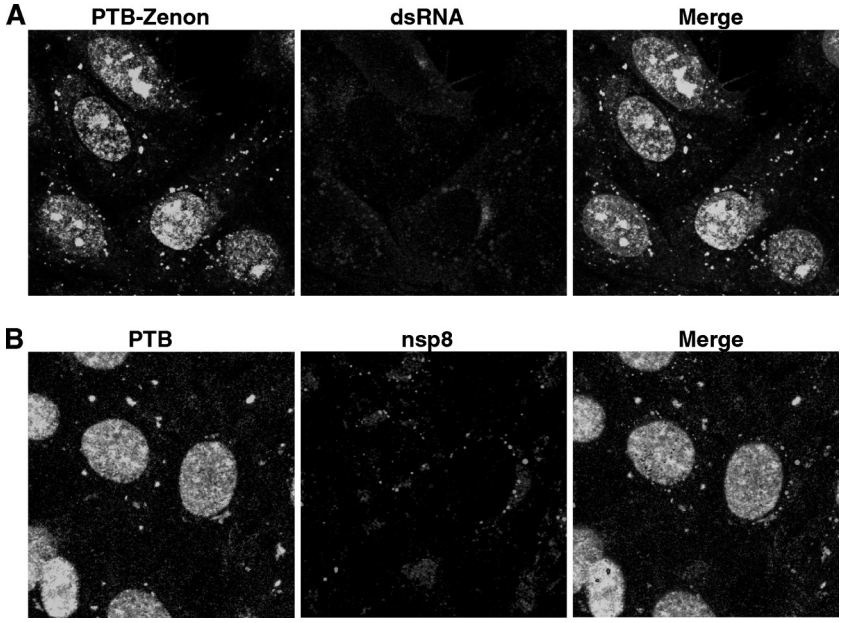

FIG. 6. Colocalization studies of PTB and viral replication markers in TGEV-infected cells. Confocal immunomicroscopy analysis was performed on ST cells infected with the TGEV PUR46-MAD strain (MOI, 10) at 16 hpi. (A) Colocalization analysis of PTB and dsRNA. Since both PTB- and dsRNA-specific antibodies are mouse MAbs, PTB (green) was detected with MAb BB7 directly labeled with Zenon labeling reagent conjugated to Alexa Fluor 488 and dsRNA (red) was visualized with MAb J2 and a secondary antibody conjugated to Alexa Fluor 594. (B) Colocalization analysis of PTB and nsp8. PTB (green) was detected with MAb BB7 and a secondary antibody conjugated to Alexa Fluor 488. Viral nsp8 (red) was visualized with a rabbit polyclonal antibody and a secondary antibody conjugated to Alexa Fluor 594. Nuclear DNA (blue) was stained with DAPI.

ible and significant increase in replicon activity of 2.5-fold was observed in comparison to reference levels of activity from cells transfected with a negative-control siRNA (Fig. 3C). These results confirmed the negative effect of PTB on virus mRNA accumulation previously shown in human Huh7 cells.

Cytoplasmic levels of PTB in TGEV-infected ST cells. PTB is mainly located in the cell nucleus, whereas CoVs are cytoplasmic viruses. If PTB has some function during TGEV infection, it should be present in the cytoplasm of infected cells, where TGEV replicates. Although the human Huh7 cell line is susceptible to TGEV infection, viral production in these cells was lower than that in ST cells. In addition, virus showed a delayed growth rate compared to that observed in TGEV-infected ST cells (data not shown). In order to study whether the subcellular localization of PTB was modified during TGEV infection, cytoplasmic extracts from TGEV-infected ST cells collected at different times postinfection were analyzed by Western blotting (Fig. 4A). As a control of viral infection, the expression of viral nucleoprotein was also analyzed. Levels of β-actin were used as an internal control for the amount of total protein. Cytoplasmic PTB levels were quantified by densitometry of the corresponding Western blot bands and normalized to the amount of β-actin (Fig. 4A). The levels of PTB in the cytoplasm of infected cells did not significantly change from 0 to 7 hpi. In contrast, from 7 hpi, PTB levels in the cytoplasm progressively increased up to 2.5-fold at 16 hpi compared to those in noninfected cells (Fig. 4). These results indicated that the intracellular distribution of PTB was modified in the course of infection, with an increase in cytoplasmic levels starting at 7 hpi.

An analysis of the kinetics of viral sgmRNA 7 accumulation was performed in TGEV-infected cells at different times postinfection by qRT-PCR (Fig. 4B). Viral sgmRNA 7 levels increased exponentially during the first hours of infection to reach a maximum at 7 hpi. From this time point, sgmRNA 7 levels did not increase further and started to decrease at 16 hpi. Altogether the results showed that active synthesis of viral sgmRNAs between 0 and 7 hpi was associated with low levels of cytoplasmic PTB, while the reduction in sgmRNA accumulation from 7 hpi was accompanied by a significant increase in PTB cytoplasmic levels (Fig. 4B).

Subcellular distribution of PTB in TGEV-infected ST cells. To confirm the subcellular redistribution of PTB during TGEV infection, immunofluorescence analysis was performed on mock-infected and infected ST cells at 5, 8, and 16 hpi. In noninfected cells and at 5 hpi, PTB was visualized almost exclusively in the nucleus of the cells (Fig. 5A). In contrast, at 8 hpi, PTB was also detected in discrete granules in the cytoplasm of some cells (7%), and at 16 hpi, these granules were visible in the cytoplasm of a large proportion of cells (63%) (Fig. 5A). The presence of PTB-containing granules in the cytoplasm of infected cells was also quantified by determining the number of PTB granules per cell (Fig. 5B). At 8 hpi, an evident increase in the amount of cytoplasmic granules containing PTB was observed (1.1 granules per cell), whereas at 5 hpi, granules were absent from mock-infected and infected cells. At 16 hpi, an additional significant increase in cytoplasmic PTB-containing granules was observed (about three granules per cell) (Fig. 5B). These results confirmed that at late times of TGEV infection, PTB localized to discrete granules

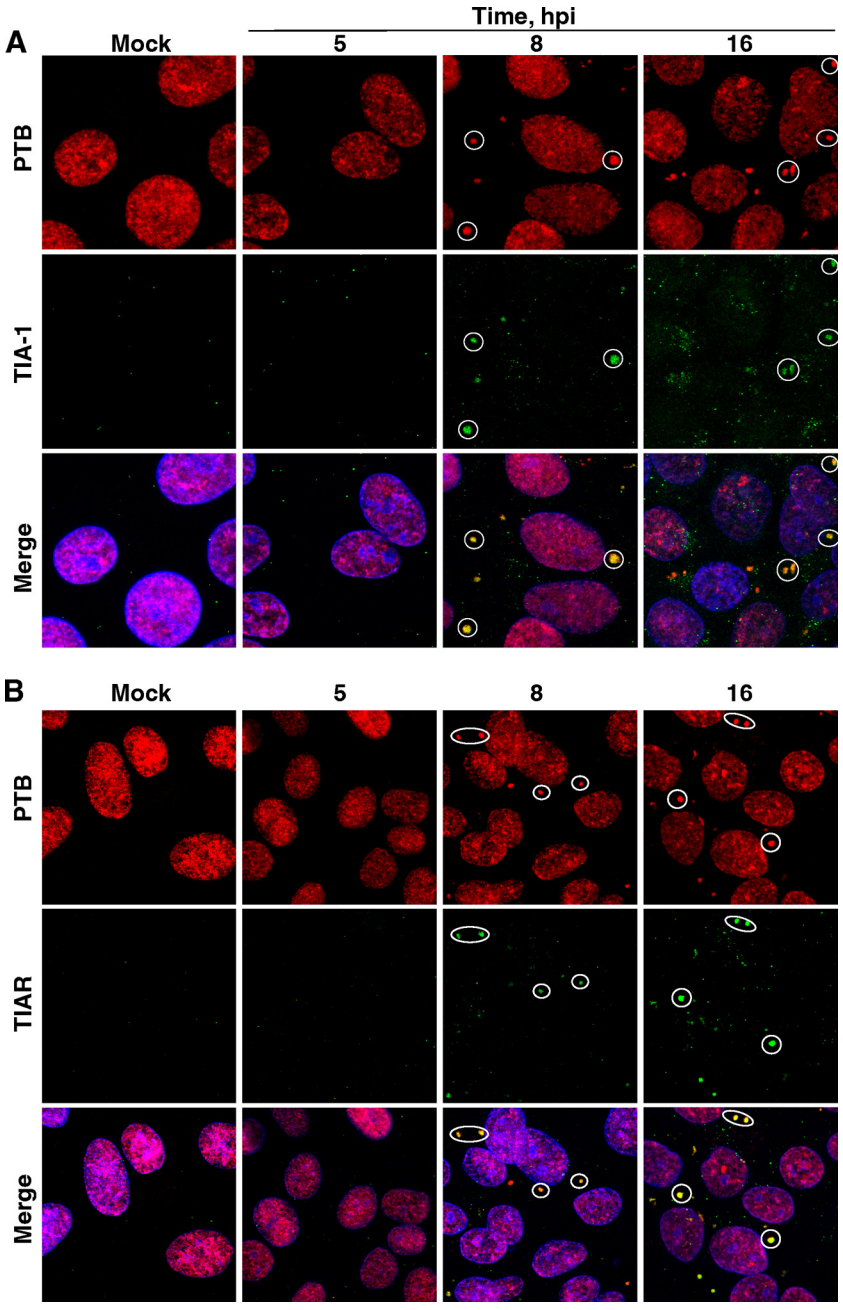

FIG. 7. Colocalization of PTB and the stress granule markers TIA-1 and TIAR in cytoplasmic granules induced by TGEV infection. Confocal immunomicroscopy analysis of ST cells mock infected or infected with the TGEV PUR46-MAD strain (MOI, 10) at 5, 8, and 16 hpi. PTB (red) was detected with MAb BB7. The stress granule markers TIA-1 (A) and TIAR (B) (green) were visualized with specific polyclonal antibodies. Nuclear DNA (blue) was stained with DAPI. Circles indicate representative granules in which PTB and TIA-1 or TIAR colocalize.

accumulated in the cell cytoplasm. Additionally, viral RNA synthesis was visualized in infected cells with a dsRNA-specific antibody that does not detect either cellular rRNA or tRNA (Fig. 5A) (65). This antibody detects dsRNA intermediates in viral RNA synthesis. The mean value of dsRNA intensity was determined in mock-infected ST cells and at 5, 8, and 16 hpi. The level of dsRNA reached a relative maximum at 5 hpi and significantly decreased at 8 and 16 hpi (Fig. 5B). These results confirmed the previously observed kinetics for viral mRNA levels (Fig. 4B), indicating that viral RNA synthesis occurs in the first hours of infection and decreased from 5 hpi. PTB-containing granules appeared in the cytoplasm of infected cells subsequent to that time, when active viral RNA synthesis decreased.

Absence of dsRNA and proteins from the virus replication-transcription complex in the cytoplasmic granules containing PTB. To study the association of cytoplasmic PTB with coronavirus replication-transcription complexes, confocal microscopy analysis was performed in ST cells at 5, 8, and 16 hpi using specific antibodies to identify dsRNA and nonstructural pro-

tein nsp8, a virus-encoded primase required for RNA synthesis (31). Previous studies have shown the localization of nsp8 in MHV (13, 14), TGEV (A. Nogales, L. Enjuanes, and F. Almazán, unpublished results), and SARS-CoV (40) replication complexes. No colocalization was observed between PTB-containing granules detected in the cell cytoplasm at late times of infection (16 hpi) and either dsRNA or nsp8 (Fig. 6A and B), indicating that PTB was not accumulated in replication-transcription complexes responsible for viral RNA synthesis. This observation does not exclude a temporary presence of PTB in the sites of active RNA synthesis to perform its inhibitory effect on TGEV transcription.

Absence of P-body marker Dcp1a in cytoplasmic granules containing PTB. The function of PTB in cytoplasmic granules is probably dependent on the binding to other regulatory *trans*-acting factors. To identify additional components of cytoplasmic granules induced by TGEV infection, immunofluorescence microscopy analysis was performed with ST cells. The morphology of PTB-containing granules resembled that of other known cytoplasmic structures associated with RNA metabolism in eukaryotic cells, such as processing bodies (P-bodies) and SGs, consisting of RNA-protein complexes including nontranslating mRNAs (38). PTB has not previously been related either to P-bodies or to SGs (36). The presence of the P-body marker Dcp1a in PTB-containing cytoplasmic granules was analyzed by confocal microscopy. Dcp1a protein did not colocalize with PTB in cytoplasmic granules at any time postinfection. Furthermore, P-body kinetics in TGEV-infected ST cells was the opposite of that observed for cytoplasmic granules containing PTB. The number of P-bodies strongly decreased at 16 hpi, almost disappearing completely, suggesting that TGEV infection interfered with P-body formation in ST cells (data not shown). Since Dcp1a is considered a unique marker specific to P-bodies (36), these results indicated that PTB cytoplasmic granules were not P-bodies. In addition, Dcp1a did not colocalize with either dsRNA intermediates of virus RNA synthesis or the viral nucleoprotein, thus excluding a direct association between P-bodies and virus components (data not shown).

Presence of stress granule markers TIA-1 and TIAR in cytoplasmic granules containing PTB. TIA-1 and the related protein TIAR are RNA-binding proteins with self-oligomerization properties and have been described to be markers of SGs induced in eukaryotic cells under stress conditions. It has been suggested that SG formation may be a consequence of translation initiation inhibition (5). Unlike P-bodies, SGs are heterogeneous in size and shape. SG assembly starts with the simultaneous formation of numerous small SGs, which progressively fuse into larger and fewer structures (7). The presence of TIA-1 and TIAR in PTB-containing cytoplasmic granules was analyzed by confocal microscopy in mock-infected or infected ST cells at different times postinfection. In unstressed, mock-infected cells, as expected, cytoplasmic granules including TIA-1 and TIAR were not detected (7) (Fig. 7). Small granules observed at 5 hpi evolved to larger structures at later times of infection. Furthermore, TIA-1 and TIAR extensively colocalized with PTB, mainly in larger granules observed at 8 and 16 hpi (Fig. 7A and B). Therefore, TGEV infection induced the formation of cytoplasmic granules containing PTB, TIA-1, and TIAR in ST cells at late times of infection. Cytoplasmic granules containing TIA-1 or TIAR significantly increased in number from 5 to 16 hpi, with kinetics being similar to that observed for PTB granules (Fig. 8). In agreement with our previous observations on PTB, TIA-1 and TIAR did not colocalize with either dsRNA intermediates or the viral proteins nsp8 (Fig. 9A and B) and N (data not shown). These results are in line with the conclusion that the three cellular RNA-binding proteins localized in similar subcellular compartments during infection. Although TIA-1 and TIAR have been established to be markers of SGs, PTB has not been related to these cytoplasmic ribonucleoprotein particles before, suggesting that TGEV infection in ST cells led to the generation of novel cytoplasmic granules differentiable from conventional SGs by the presence of PTB.

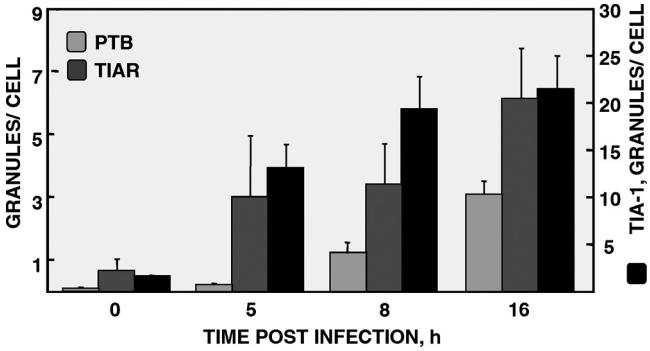

FIG. 8. Quantification of cytoplasmic granules induced by TGEV infection containing PTB, TIA-1, or TIAR. Confocal immunomicroscopy analysis of ST cells mock infected or infected with the TGEV PUR46-MAD strain (MOI, 10) at 5, 8, and 16 hpi. Cytoplasmic granules containing PTB, TIA-1, or TIAR in 10 randomly selected microscope fields were counted for each time point, and the average number of granules from three independent experiments is represented. Error bars indicate the standard deviations.

Specific presence of PTB in TGEV-induced cytoplasmic granules. Translation inhibition and SG formation have mainly been related to phosphorylation of eukaryotic factor 2α (eIF2α) by distinct kinases, including PKR, heme-regulated kinase (HRI), and PKR-like ER kinase (PERK), activated during viral infection and oxidative and ER stress, respectively (36). To determine whether PTB was also present in SGs induced by other stress conditions, ST cells were exposed to poly(I:C), sodium arsenite, and thapsigargin, leading to activation of PKR, HRI, and PERK, respectively. Neither the ER stress inducer thapsigargin nor the dsRNA synthetic analog poly(I:C) led to the formation of SGs positive for TIAR in ST cells under the assay conditions used (Fig. 10). In contrast, sodium arsenite induced the formation of SGs positive for TIAR in ST cells (Fig. 10). However, PTB was not detected in these cytoplasmic granules induced in ST cells by oxidative stress. These results indicated that PTB accumulated to a significant extent only in cytoplasmic granules induced by TGEV infection. Furthermore, TGEV infection in another cell line, human Huh7 cells (MOI, 20), also induced the formation of cytoplasmic granules containing PTB and TIAR (Fig. 11).

Association of PTB with viral gRNA and mRNA 7 during TGEV infection. Since PTB is an RNA-binding protein involved in regulating RNA metabolism processes in the cytoplasm of eukaryotic cells, its association with viral RNAs *in vivo* during TGEV infection was analyzed by RNA immuno-

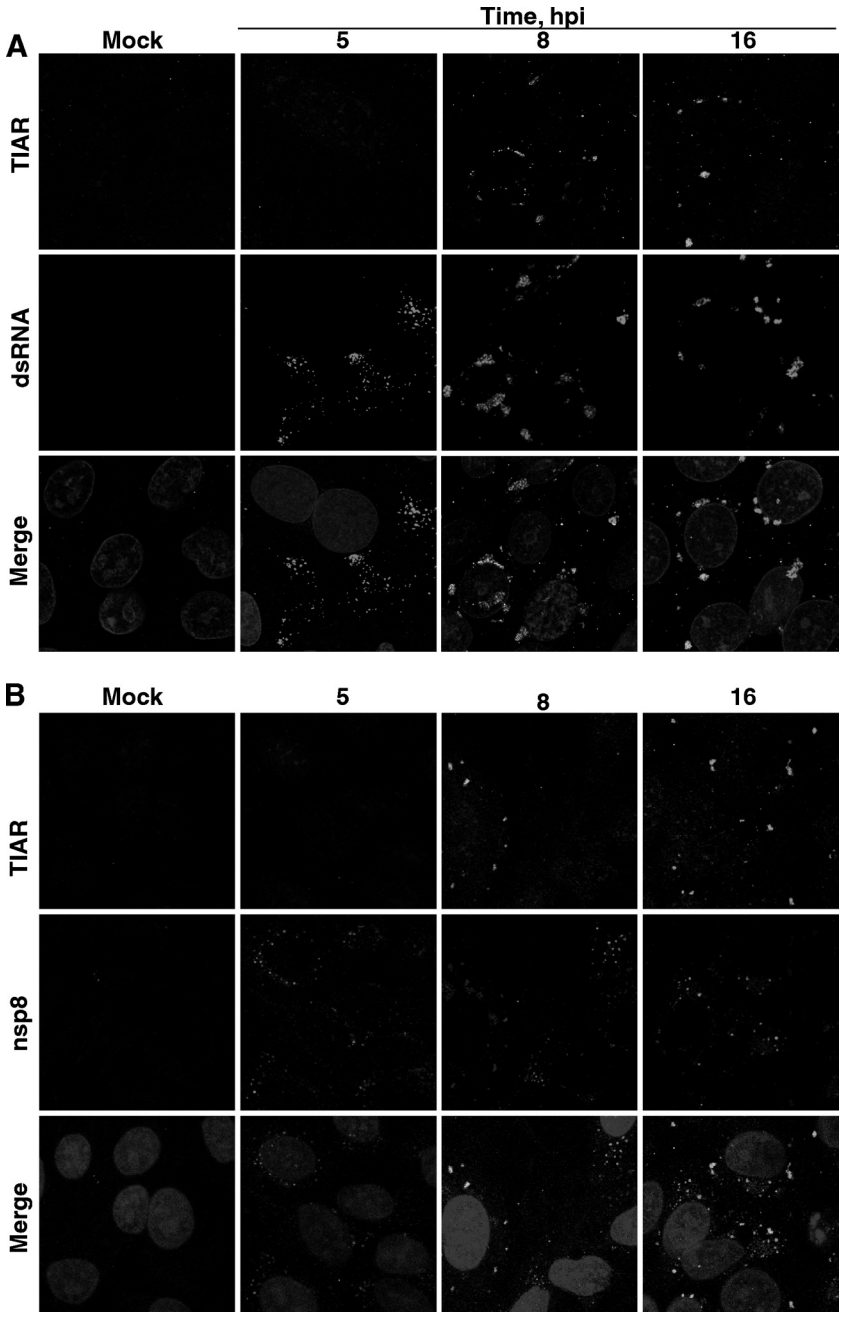

FIG. 9. Colocalization analysis of the stress granule marker TIAR and viral markers during TGEV infection. Confocal immunomicroscopy analysis of ST cells mock infected or infected with the TGEV PUR46-MAD strain (MOI, 10) at 5, 8, and 16 hpi. TIAR (green) was visualized with a specific polyclonal antibody. dsRNA intermediates of RNA synthesis (A) and viral nsp8 (B) (red) were visualized with MAb J2 and a specific polyclonal antibody, respectively. Nuclear DNA (blue) was stained with DAPI.

precipitation assays. These assays were performed on cytoplasmic extracts of noninfected or TGEV-infected cells with PTB- and TIAR-specific antibodies. Extracts from TGEV-infected ST cells collected at 16 hpi were analyzed in RNA immunoprecipitation experiments because PTB relocalization to the cytoplasm was maximum at late times of infection. The presence of viral RNAs in RNP complexes eluted from RNA immunoprecipitation was quantified by qRT-PCR and specific TaqMan assays for genomic and subgenomic mRNA 7. The level of viral gRNA immunoprecipitated from infected cells with anti-PTB or anti-TIAR antibodies was significantly increased compared to that precipitated with a negative-control antibody (anti-GFP) or no antibody (>150-fold increase for anti-PTB and >7-fold increase for anti-TIAR) (Fig. 12). Similarly, viral mRNA 7 was also significantly increased in cytoplasmic extracts from infected cells immunoprecipitated with anti-PTB (>800-fold) or anti-TIAR (>40-fold) antibodies in relation to that for the negative controls (Fig. 12). In contrast,

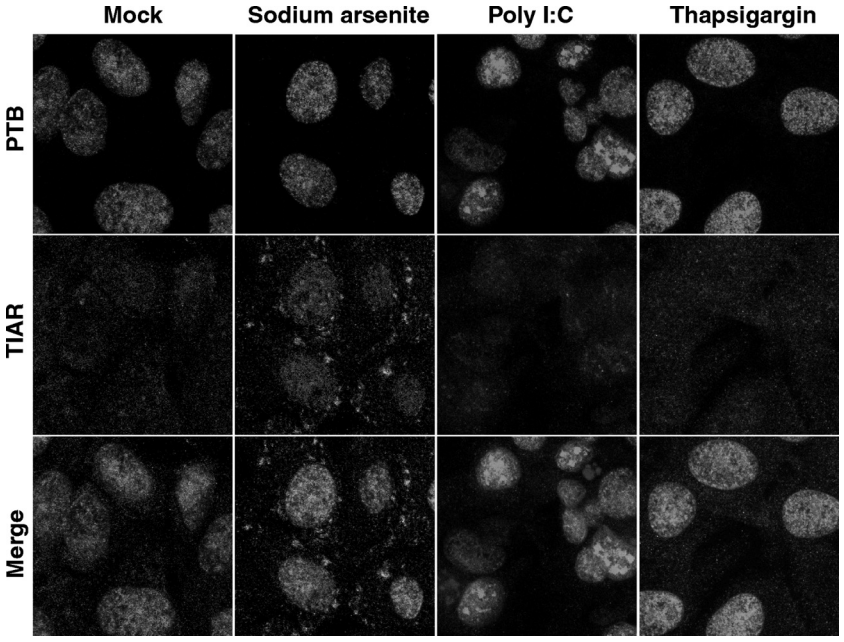

FIG. 10. Induction of stress granules in ST cells. ST cells were exposed to different stress conditions: (i) oxidative stress induced by 1 mM sodium arsenite for 60 min, (ii) PKR activation by 4 μg poly(I:C) for 6 h, or (iii) ER stress induced by 2 μM thapsigargin for 1.5 h. The presence of PTB (red) and TIAR (green) proteins in mock-treated or stressed ST cells was analyzed by confocal microscopy with specific antibodies.

the amount of cellular mRNA hnRNP U was not significantly increased in cytoplasmic extracts by immunoprecipitation with anti-PTB or anti-TIAR antibodies (data not shown). These results indicated that during infection, viral gRNA and sgmRNA were associated with PTB and TIAR in cytoplasmic RNA-protein complexes and probably regulate viral RNA and protein synthesis during viral infection.

DISCUSSION

This paper reports on the identification of PTB as a cellular protein directly or indirectly binding to CoV TRSs and analyzes PTB intracellular interactions during TGEV infection. Functional experiments showed that PTB had a negative effect on viral RNA accumulation and virus production, as silencing of PTB expression with specific siRNAs in the human Huh7 cell line led to a reproducible and significant increase (up to 4-fold) in viral mRNA 7 levels and in virus titers (3.5-fold) in relation to those for cells transfected with the negative-control siRNA. A possible effect of PTB on viral mRNA stability cannot be excluded. In addition, there was an inverse correlation between PTB cytoplasmic levels and RNA accumulation. Furthermore, PTB silencing in human HEK 293T cells transfected with a TGEV-derived replicon also led to a similar increase in viral mRNA 7, confirming the negative effect of PTB on viral RNA accumulation. After TGEV infection, PTB relocalized from the nucleus to discrete, temporally regulated, cytoplasmic granules. These PTB-containing granules accumulated in the cytoplasm of infected cells at the same time that active viral RNA synthesis decreased. In line with this observation, no colocalization between PTB in cytoplasmic granules and dsRNA or the replicase component nsp8 was observed, indicating that PTB was not accumulated in active replication-transcription complexes responsible for viral RNA synthesis. Other cellular RNA-binding proteins, such as the stress granule markers TIA-1 and TIAR, colocalized with PTB in cytoplasmic structures. In contrast, SGs induced in ST cells by oxidative stress contained TIAR but did not include significant levels of PTB, suggesting that PTB is a specific component of cytoplasmic granules induced by TGEV infection. Interestingly, virus gRNA and sgmRNA were detected in RNA immunoprecipitation assays in association with PTB and TIAR, indicating that PTB and TIAR were components of ribonucleoprotein complexes induced by TGEV infection and that those complexes included viral RNAs.

During infection by TGEV, a member of CoV genus α, the binding of PTB to viral RNA sequences involved in transcription, such as TRS-L and several TRS-Bs, has been shown. These results are in line with those described for MHV, a member of CoV genus β, in which PTB binds to the leader TRS and also to the complement of the 3′ UTR (30, 44). Using functional studies, we have shown that PTB-specific silencing during TGEV infection led to increases in RNA levels and virus infectivity. These results are consistent with the previously reported decrease in MHV RNA synthesis subsequent to PTB overexpression (15). Since PTB overexpression caused an unexpected inhibitory effect on viral RNA synthesis, these authors hypothesized that the excess of PTB would deplete other essential factors, indirectly affecting MHV replication and transcription, but no experimental evidence supporting this hypothesis was provided. PTB has been associated with other single-stranded positive-sense RNA viruses. In hepatitis C virus (HCV) and picornaviruses, PTB functions as an IRES *trans*-acting factor, activating viral translation initiation (34, 49). However, the role of PTB in RNA replication of positive-sense RNA viruses is still controversial. In HCV, it has been

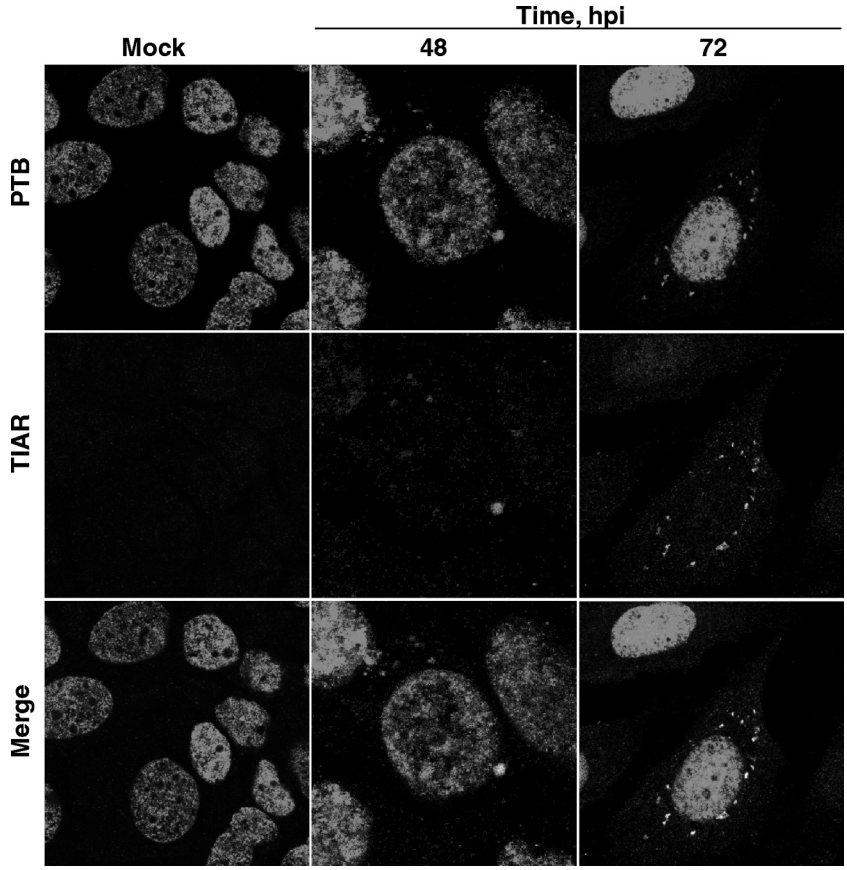

FIG. 11. Presence of PTB in cytoplasmic granules induced by TGEV infection in Huh7 cells. Huh7 cells were infected with the TGEV PUR46-C11 strain (MOI, 20). The presence of PTB (red) and TIAR (green) in mock-infected and infected Huh7 cells at 48 and 72 hpi was analyzed by confocal microscopy using specific antibodies.

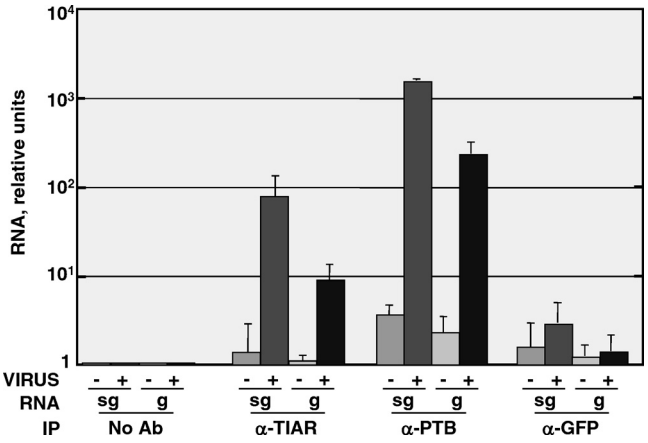

FIG. 12. RNA immunoprecipitation of viral RNAs with specific anti-PTB or anti-TIAR antibodies. ST cells were either noninfected (−) or infected (+) with the TGEV PUR46-MAD strain (MOI, 10). Cytoplasmic extracts were prepared at 16 hpi. RNA-protein complexes were immunoprecipitated in the absence of antibodies (No Ab) or the presence of anti-PTB (α-PTB) or anti-TIAR (α-TIAR) antibodies or the negative-control antibody anti-GFP (α-GFP). RNAs eluted from immunoprecipitated RNA-protein complexes were analyzed by qRT-PCR for the presence of associated viral genomic RNA (g) or subgenomic mRNA 7 (sg). The amount of viral RNAs in immunoprecipitated ribonucleoprotein complexes was expressed in relation to RNA levels in the absence of antibody. Quantifications were from three independent RNA immunoprecipitation assays. Error bars indicate the standard deviations.

reported that PTB is part of the RNA replication complex and participates in viral RNA synthesis (2). In contrast with these results, it has also been reported that PTB partially represses HCV replication and inhibits binding of RdRp to the 3′ UTR (21). In dengue virus, PTB has been shown to be involved exclusively with the virus replication machinery (8) and in replication or translation (1). In summary, the activity of PTB in the replication of CoVs seems to follow a uniform effect of reducing viral RNA levels, which is variable in the replication of other positive-sense RNA viruses.

In this paper, we report PTB redistribution to cytoplasmic structures during TGEV infection and that viral RNAs (gRNA and sgmRNA) were associated with PTB within these novel cytoplasmic structures potentially derived from SGs. In contrast, nucleus-to-cytoplasm relocalization of PTB during MHV infection was not described (15). During TGEV infection of ST cells, PTB, TIA-1, and TIAR were identified in temporally regulated cytoplasmic granules directly or indirectly associated with virus RNAs. Furthermore, TGEV infection of human Huh7 cells also led to the formation of cytoplasmic granules containing PTB and TIAR, similar to those detected in porcine ST cells. Although SGs formed in response to different stress conditions share many common factors, some components are unique to a particular stress (39). TIAR is a common component of SGs induced in ST cells by TGEV infection and oxi-

dative stress, whereas PTB is accumulated to significant levels only in TGEV-induced SGs. These results indicate that PTB might be a unique marker of cytoplasmic granules formed in ST cells during TGEV infection.

PTB, TIA-1, and TIAR are RNA-binding proteins associated with RNA metabolism events in the nucleus and the cytoplasm (9, 37). In the nucleus, PTB acts as a regulator repressing alternative splicing (12, 33), possibly by interfering with molecular interactions between protein complexes that mediate exon definition (10, 33) or, alternatively, by precluding the association of splicing factors (17, 64, 68). Also, TIA-1 and TIAR function in the nucleus as splicing regulators (27, 43). In the cytoplasm, in response to environmental stress, TIA-1 and TIAR contribute to translational arrest, polysome disassembly, and aggregation of nontranslated polyadenylated mRNAs to form SGs (6). Our paper describes for the first time that during TGEV infection, PTB is associated with cytoplasmic structures, including the SG markers TIA-1 and TIAR (38). These structures are differentiable from conventional SGs by the presence of PTB. One possibility is that these structures might be modified stress granules containing RNP complexes induced by TGEV infection. The binding of PTB to viral RNA may promote RNA-RNA or RNA-protein interactions required for the assembly of these RNP complexes. At the same time, TIA-1 and TIAR, defined to be SG nucleators (7), might contribute to concentrate viral RNAs and cellular RNA-binding proteins in cytoplasmic subdomains. In fact, TIA-1 and TIAR together with PTB have recently been shown to be involved in the posttranscriptional regulation of β-F1 ATPase mRNA expression at the translation level, mediated by its specific binding to the 3′ UTR of this mRNA (32, 56). It has been proposed that PTB may enhance (56) or repress (11) translation of specific cellular mRNAs, depending on the cellular context and on the binding of other regulatory *trans*-acting factors (9).

In recent years, the subcellular localization of mRNAs in ribonucleoprotein complexes has been demonstrated to be a powerful mechanism to spatially and temporally regulate various RNA processing events in the cell (29). PTB has been revealed to be a key structural component of RNP particles involved in regulating the spatiotemporal pattern of gene expression during the development of eukaryotic organisms (11). Accordingly, in the context of TGEV infection, PTB might (i) inhibit viral RNA accumulation, possibly by interfering with essential long-distance RNA-RNA and RNA-protein interactions established throughout the genome during discontinuous transcription between TRS-L and TRS-B, as previously described in our CoV transcription model (63, 69), and (ii) subsequently, at later times postinfection, PTB could relocalize and concentrate together with viral RNAs at cytoplasmic RNP complexes different from replication-transcription sites, including TIA-1 and TIAR, where translation or other posttranscriptional processes proceed. Since these cytoplasmic structures included not only SG markers but also PTB and viral RNAs, they could be named modified SGs. The two proposed activities for PTB in the context of TGEV replication, repression of template switch and relocalization with viral RNAs to modified SGs, mimic the dual cellular function of PTB (11, 59) as a splicing repressor in the nucleus (12) and a regulator of cytoplasmic mRNA stability, localization (18), and translation (11, 56), respectively. Therefore, PTB might be one of the factors involved in the transition of viral RNAs from transcription to a subsequent stage in the viral cycle. That being the case, the cytoplasmic granules observed after TGEV infection might contribute to the spatiotemporal regulation of viral RNAs to enter different steps, including translation or encapsidation. Alternatively, cytoplasmic granules might function to limit viral infection as part of the host response by reducing viral RNA stability and subsequently repressing translation of viral mRNAs.

In this paper, we provide evidence for changes induced in cell RNA-binding proteins associated with mRNA metabolism. These changes create dynamic cytoplasmic domains in which TIA-1 and TIAR accumulate in modified cytoplasmic granules with PTB, in association with viral RNAs. In addition, we have shown that viral infection interfered with P-body formation. Knowledge of the interactions between viral RNA and cellular proteins will enable us to understand the molecular basis of viral pathogenesis and to develop better therapeutic strategies to interfere with virus replication.

ACKNOWLEDGMENTS

This work was supported by grants from the Ministry of Science and Innovation of Spain (BIO2007-60978 and PET2008-0310), the Community of Madrid, Spain (S-SAL-0185-2006), the U.S. National Institutes of Health (ARRA-W000151845), and Pfizer Animal Health. The research leading to these results has received funding from the European Community's (EC's) Seventh Framework Programme (FP7/2007-2013) under the projects EMPERIE (EC grant agreement number 223498) and PoRRSCon (EC grant agreement number 245141). I.S. received a contract supported by grants from the Ministry of Science and Innovation of Spain (BIO2007-60978).

We gratefully acknowledge J. Lykke-Anderson and J. Ziebuhr for providing the indicated antibodies and M. González for technical assistance.

REFERENCES

1. **Agis-Juarez, R. A., et al.** 2009. Polypyrimidine tract-binding protein is relocated to the cytoplasm and is required during dengue virus infection in Vero cells. J. Gen. Virol. **90:**2893–2901.
2. **Aizaki, H., K. S. Choi, M. Liu, Y. J. Li, and M. M. Lai.** 2006. Polypyrimidine-tract-binding protein is a component of the HCV RNA replication complex and necessary for RNA synthesis. J. Biomed. Sci. **13:**469–480.
3. **Almazan, F., C. Galan, and L. Enjuanes.** 2004. The nucleoprotein is required for efficient coronavirus genome replication. J. Virol. **78:**12683–12688.
4. **Almazan, F., et al.** 2000. Engineering the largest RNA virus genome as an infectious bacterial artificial chromosome. Proc. Natl. Acad. Sci. U. S. A. **97:**5516–5521.
5. **Anderson, P., and N. Kedersha.** 2006. RNA granules. J. Cell Biol. **172:**803–808.
6. **Anderson, P., and N. Kedersha.** 2009. RNA granules: post-transcriptional and epigenetic modulators of gene expression. Nat. Rev. Mol. Cell Biol. **10:**430–436.
7. **Anderson, P., and N. Kedersha.** 2008. Stress granules: the Tao of RNA triage. Trends Biochem. Sci. **33:**141–150.
8. **Anwar, A., K. M. Leong, M. L. Ng, J. J. Chu, and M. A. Garcia-Blanco.** 2009. The polypyrimidine tract-binding protein is required for efficient dengue virus propagation and associates with the viral replication machinery. J. Biol. Chem. **284:**17021–17029.
9. **Beckham, C. J., and R. Parker.** 2008. P bodies, stress granules, and viral life cycles. Cell Host Microbe **3:**206–212.
10. **Berget, S. M.** 1995. Exon recognition in vertebrate splicing. J. Biol. Chem. **270:**2411–2414.
11. **Besse, F., S. Lopez de Quinto, V. Marchand, A. Trucco, and A. Ephrussi.** 2009. Drosophila PTB promotes formation of high-order RNP particles and represses oskar translation. Genes Dev. **23:**195–207.
12. **Black, D. L.** 2003. Mechanisms of alternative pre-messenger RNA splicing. Annu. Rev. Biochem. **72:**291–336.
13. **Bost, A. G., R. H. Carnahan, X. T. Lu, and M. R. Denison.** 2000. Four proteins processed from the replicase gene polyprotein of mouse hepatitis virus colocalize in the cell periphery and adjacent to sites of virion assembly. J. Virol. **74:**3379–3387.

14. **Bost, A. G., E. Prentice, and M. R. Denison.** 2001. Mouse hepatitis virus replicase protein complexes are translocated to sites of M protein accumulation in the ERGIC at late times of infection. Virology **285:**21–29.
15. **Choi, K. S., P. Huang, and M. M. Lai.** 2002. Polypyrimidine-tract-binding protein affects transcription but not translation of mouse hepatitis virus RNA. Virology **303:**58–68.
16. **Choi, K. S., A. Mizutani, and M. M. Lai.** 2004. SYNCRIP, a member of the heterogeneous nuclear ribonucleoprotein family, is involved in mouse hepatitis virus RNA synthesis. J. Virol. **78:**13153–13162.
17. **Chou, M. Y., J. G. Underwood, J. Nikolic, M. H. Luu, and D. L. Black.** 2000. Multisite RNA binding and release of polypyrimidine tract binding protein during the regulation of c-src neural-specific splicing. Mol. Cell **5:**949–957.
18. **Cote, C. A., et al.** 1999. A Xenopus protein related to hnRNP I has a role in cytoplasmic RNA localization. Mol. Cell **4:**431–437.
19. **de Groot, R. J., et al.** 2008. Revision of the family Coronaviridae. Report 2008.085-126V. International Committee on Taxonomy of Viruses London, United Kingdom.
20. **Dominguez, S. R., T. J. O'Shea, L. M. Oko, and K. V. Holmes.** 2007. Detection of group 1 coronaviruses in bats in North America. Emerg. Infect. Dis. **13:**1295–1300.
21. **Domitrovich, A. M., K. W. Diebel, N. Ali, S. Sarker, and A. Siddiqui.** 2005. Role of La autoantigen and polypyrimidine tract-binding protein in HCV replication. Virology **335:**72–86.
22. **Drosten, C., et al.** 2003. Identification of a novel coronavirus in patients with severe acute respiratory syndrome. N. Engl. J. Med. **348:**1967–1976.
23. **Eleouet, J. F., et al.** 2000. The viral nucleocapsid protein of transmissible gastroenteritis coronavirus (TGEV) is cleaved by caspase-6 and -7 during TGEV-induced apoptosis. J. Virol. **74:**3975–3983.
24. **Enjuanes, L., F. Almazan, I. Sola, and S. Zuniga.** 2006. Biochemical aspects of coronavirus replication and virus-host interaction. Annu. Rev. Microbiol. **60:**211–230.
25. **Enjuanes, L., et al.** 2008. The Nidovirales, p. 419–430. *In* B. W. J. Mahy, M. Van Regenmortel, P. Walker, and D. Majumder-Russell (ed.), Encyclopedia of virology, 3rd ed. Elsevier Ltd., Oxford, United Kingdom.
26. **Enjuanes, L., W. Spaan, E. Snijder, and D. Cavanagh.** 2000. *Nidovirales*, p. 827–834. *In* M. H. V. van Regenmortel, et al. (ed.), Virus taxonomy. Classification and nomenclature of viruses. Academic Press, San Diego, CA.
27. **Forch, P., O. Puig, C. Martinez, B. Seraphin, and J. Valcarcel.** 2002. The splicing regulator TIA-1 interacts with U1-C to promote U1 snRNP recruitment to 5′ splice sites. EMBO J. **21:**6882–6892.
28. **Galan, C., et al.** 2009. Host cell proteins interacting with the 3′ end of TGEV coronavirus genome influence virus replication. Virology **391:**304–314.
29. **Glisovic, T., J. L. Bachorik, J. Yong, and G. Dreyfuss.** 2008. RNA-binding proteins and post-transcriptional gene regulation. FEBS Lett. **582:**1977–1986.
30. **Huang, P., and M. M. C. Lai.** 1999. Polypyrimidine tract-binding protein binds to the complementary strand of the mouse hepatitis virus 3′ untranslated region, thereby altering RNA conformation. J. Virol. **73:**9110–9116.
31. **Imbert, I., et al.** 2006. A second, non-canonical RNA-dependent RNA polymerase in SARS coronavirus. EMBO J. **25:**4933–4942.
32. **Izquierdo, J. M.** 2006. Control of the ATP synthase beta subunit expression by RNA-binding proteins TIA-1, TIAR, and HuR. Biochem. Biophys. Res. Commun. **348:**703–711.
33. **Izquierdo, J. M., et al.** 2005. Regulation of Fas alternative splicing by antagonistic effects of TIA-1 and PTB on exon definition. Mol. Cell **19:**475–484.
34. **Jang, S. K.** 2006. Internal initiation: IRES elements of picornaviruses and hepatitis C virus. Virus Res. **119:**2–15.
35. **Jiménez, G., I. Correa, M. P. Melgosa, M. J. Bullido, and L. Enjuanes.** 1986. Critical epitopes in transmissible gastroenteritis virus neutralization. J. Virol. **60:**131–139.
36. **Kedersha, N., and P. Anderson.** 2007. Mammalian stress granules and processing bodies. Methods Enzymol. **431:**61–81.
37. **Kedersha, N., and P. Anderson.** 2002. Stress granules: sites of mRNA triage that regulate mRNA stability and translatability. Biochem. Soc. Trans. **30:**963–969.
38. **Kedersha, N., et al.** 2005. Stress granules and processing bodies are dynamically linked sites of mRNP remodeling. J. Cell Biol. **169:**871–884.
39. **Kedersha, N. L., M. Gupta, W. Li, I. Miller, and P. Anderson.** 1999. RNA-binding proteins TIA-1 and TIAR link the phosphorylation of eIF-2 alpha to the assembly of mammalian stress granules. J. Cell Biol. **147:**1431–1442.
40. **Knoops, K., et al.** 2008. SARS-coronavirus replication is supported by a reticulovesicular network of modified endoplasmic reticulum. PLoS Biol. **6:**e226.
41. **Kosinski, P. A., J. Laughlin, K. Singh, and L. R. Covey.** 2003. A complex containing polypyrimidine tract-binding protein is involved in regulating the stability of CD40 ligand (CD154) mRNA. J. Immunol. **170:**979–988.
42. **Lau, S. K., et al.** 2005. Severe acute respiratory syndrome coronavirus-like virus in Chinese horseshoe bats. Proc. Natl. Acad. Sci. U. S. A. **102:**14040–14045.
43. **Le Guiner, C., et al.** 2001. TIA-1 and TIAR activate splicing of alternative exons with weak 5′ splice sites followed by a U-rich stretch on their own pre-mRNAs. J. Biol. Chem. **276:**40638–40646.
44. **Li, H. P., P. Huang, S. Park, and M. M. C. Lai.** 1999. Polypyrimidine tract-binding protein binds to the leader RNA of mouse hepatitis virus and serves as a regulator of viral transcription. J. Virol. **73:**772–777.
45. **Li, H. P., X. Zhang, R. Duncan, L. Comai, and M. M. C. Lai.** 1997. Heterogeneous nuclear ribonucleoprotein A1 binds to the transcription-regulatory region of mouse hepatitis virus RNA. Proc. Natl. Acad. Sci. U. S. A. **94:**9544–9549.
46. **Li, W., et al.** 2005. Bats are natural reservoirs of SARS-like coronaviruses. Science **310:**676–679.
47. **Ma, S., G. Liu, Y. Sun, and J. Xie.** 2007. Relocalization of the polypyrimidine tract-binding protein during PKA-induced neurite growth. Biochim. Biophys. Acta **1773:**912–923.
48. **Martin Alonso, J. M., et al.** 1992. Antigenic structure of transmissible gastroenteritis virus nucleoprotein. Virology **188:**168–174.
49. **Martinez-Salas, E., A. Pacheco, P. Serrano, and N. Fernandez.** 2008. New insights into internal ribosome entry site elements relevant for viral gene expression. J. Gen. Virol. **89:**611–626.
50. **Masters, P. S.** 2006. The molecular biology of coronaviruses. Adv. Virus Res. **66:**193–292.
51. **McClurkin, A. W., and J. O. Norman.** 1966. Studies on transmissible gastroenteritis of swine. II. Selected characteristics of a cytopathogenic virus common to five isolates from transmissible gastroenteritis. Can. J. Comp. Med. Vet. Sci. **30:**190–198.
52. **Peiris, J. S., Y. Guan, and K. Y. Yuen.** 2004. Severe acute respiratory syndrome. Nat. Med. **10:**S88–S97.
53. **Perlman, S., T. E. Lane, and M. J. Buchmeier.** 2000. Coronavirus: hepatitis, peritonitis, and central nervous system disease, p. 331–348. *In* M. W. Cunningham and R. S. Fujinami (ed.), Effects of microbes on the immune system. Lippincott Williams & Wilkins, Philadelphia, PA.
54. **Pfefferle, S., et al.** 2009. Distant relatives of severe acute respiratory syndrome coronavirus and close relatives of human coronavirus 229E in bats, Ghana. Emerg. Infect. Dis. **15:**1377–1384.
55. **Poon, L. L., et al.** 2005. Identification of a novel coronavirus in bats. J. Virol. **79:**2001–2009.
56. **Reyes, R., and J. M. Izquierdo.** 2007. The RNA-binding protein PTB exerts translational control on 3′-untranslated region of the mRNA for the ATP synthase beta-subunit. Biochem. Biophys. Res. Commun. **357:**1107–1112.
57. **Sánchez, C. M., et al.** 1999. Targeted recombination demonstrates that the spike gene of transmissible gastroenteritis coronavirus is a determinant of its enteric tropism and virulence. J. Virol. **73:**7607–7618.
58. **Sánchez, C. M., et al.** 1990. Antigenic homology among coronaviruses related to transmissible gastroenteritis virus. Virology **174:**410–417.
59. **Sawicka, K., M. Bushell, K. A. Spriggs, and A. E. Willis.** 2008. Polypyrimidine-tract-binding protein: a multifunctional RNA-binding protein. Biochem. Soc. Trans. **36:**641–647.
60. **Schelle, B., N. Karl, B. Ludewig, S. G. Siddell, and V. Thiel.** 2005. Selective replication of coronavirus genomes that express nucleocapsid protein. J. Virol. **79:**6620–6630.
61. **Schepens, B., S. A. Tinton, Y. Bruynooghe, R. Beyaert, and S. Cornelis.** 2005. The polypyrimidine tract-binding protein stimulates HIF-1alpha IRES-mediated translation during hypoxia. Nucleic Acids Res. **33:**6884–6894.
62. **Snijder, E. J., et al.** 2003. Unique and conserved features of genome and proteome of SARS-coronavirus, an early split-off from the coronavirus group 2 lineage. J. Mol. Biol. **331:**991–1004.
63. **Sola, I., J. L. Moreno, S. Zuñiga, S. Alonso, and L. Enjuanes.** 2005. Role of nucleotides immediately flanking the transcription-regulating sequence core in coronavirus subgenomic mRNA synthesis. J. Virol. **79:**2506–2516.
64. **Wagner, E. J., and M. A. Garcia-Blanco.** 2001. Polypyrimidine tract binding protein antagonizes exon definition. Mol. Cell. Biol. **21:**3281–3288.
65. **Weber, F., V. Wagner, S. B. Rasmussen, R. Hartmann, and S. R. Paludan.** 2006. Double-stranded RNA is produced by positive-strand RNA viruses and DNA viruses but not in detectable amounts by negative-strand RNA viruses. J. Virol. **80:**5059–5064.
66. **Wollerton, M. C., et al.** 2001. Differential alternative splicing activity of isoforms of polypyrimidine tract binding protein (PTB). RNA **7:**819–832.
67. **Ziebuhr, J.** 2005. The coronavirus replicase, p. 57–94. *In* L. Enjuanes (ed.), Coronavirus replication and reverse genetics, vol. 287. Springer-Verlag, Berlin, Germany.
68. **Zuccato, E., E. Buratti, C. Stuani, F. E. Baralle, and F. Pagani.** 2004. An intronic polypyrimidine-rich element downstream of the donor site modulates cystic fibrosis transmembrane conductance regulator exon 9 alternative splicing. J. Biol. Chem. **279:**16980–16988.
69. **Zuñiga, S., I. Sola, S. Alonso, and L. Enjuanes.** 2004. Sequence motifs involved in the regulation of discontinuous coronavirus subgenomic RNA synthesis. J. Virol. **78:**980–994.
70. **Zuñiga, S., I. Sola, J. L. Cruz, and L. Enjuanes.** 2009. Role of RNA chaperones in virus replication. Virus Res. **139:**253–266.

Virus Research 139 (2009) 253–266

Contents lists available at ScienceDirect

Virus Research

journal homepage: www.elsevier.com/locate/virusres

Role of RNA chaperones in virus replication

Sonia Zúñiga, Isabel Sola, Jazmina L.G. Cruz, Luis Enjuanes*

Centro Nacional de Biotecnología, CSIC, Department of Molecular and Cell Biology, Campus Universitario de Cantoblanco, Darwin 3, 28049 Madrid, Spain

ARTICLE INFO

Article history:
Available online 8 August 2008

Keywords:
RNA viruses
Template switch

ABSTRACT

RNA molecules are functionally diverse in part due to their extreme structural flexibility that allows rapid regulation by refolding. RNA folding could be a difficult process as often molecules adopt a spatial conformation that is very stable but not biologically functional, named a kinetic trap. RNA chaperones are non-specific RNA binding proteins that help RNA folding by resolving misfolded structures or preventing their formation. There is a large number of viruses whose genome is RNA that allows some evolutionary advantages, such as rapid genome mutation. On the other hand, regions of the viral RNA genomes can adopt different structural conformations, some of them lacking functional relevance and acting as misfolded intermediates. In fact, for an efficient replication, they often require RNA chaperone activities. There is a growing list of RNA chaperones encoded by viruses involved in different steps of the viral cycle. Also, cellular RNA chaperones have been involved in replication of RNA viruses. This review briefly describes RNA chaperone activities and is focused in the roles that viral or cellular nucleic acid chaperones have in RNA virus replication, particularly in those viruses that require discontinuous RNA synthesis.

1. Introduction

Some RNA molecules easily become trapped in inactive conformations (kinetic traps) because of their structural and functional flexibility. These unproductive folds can be very stable and persistent. RNA chaperones existence was postulated to solve this RNA folding problem (Herschlag, 1995). Although RNA chaperone activity has been shown using different in vitro assays (see below), their in vivo activity was only recently demonstrated (Lorsch, 2002). RNA chaperones are non-specific nucleic acid binding proteins that rescue RNAs trapped in unproductive folding states (Cristofari and Darlix, 2002; Schroeder et al., 2004). One of the most important characteristics of RNA chaperones is that, once the RNA has been folded, they can be removed without alteration in the RNA conformation (Cristofari and Darlix, 2002; Rajkowitsch et al., 2005). RNA chaperone activity cannot be predicted based on the protein domain structure or the existence of discrete motifs. Nevertheless, RNA chaperones have the highest frequency of disordered regions, and it has been proposed that they act according to an entropy transfer model, allowing correct RNA folding by successive cycles of protein–substrate order–disorder (Fig. 1) (Dyson and Wright, 2005; Ivanyi-Nagy et al., 2005; Tompa and Csermely, 2004). In fact, viral proteins with large disordered regions, postulated as RNA chaperones based on this criteria, act as nucleic acid chaperones, at least in vitro (Ivanyi-Nagy et al., 2008; Zuñiga et al., 2007). The number of proteins with RNA chaperone activity is steadily growing [(Rajkowitsch et al., 2005), RCA website: http://www.projects.mfpl.ac.at/rnachaperones], but there is no consensus on the definition of RNA chaperone activity or the minimum assays required to establish the nucleic acid activity of a protein. Furthermore, the mode of action of RNA chaperones remains to be determined and a careful mechanistic comparison of several nucleic acid chaperones should be essential to achieve this objective (Rajkowitsch et al., 2005).

2. RNA chaperone activities

A number of in vitro assays, with different technical difficulty, have been used through the years to analyze the RNA chaperone activity of a protein [for a review see Cristofari and Darlix, 2002; Rajkowitsch et al., 2005]. In vitro conditions differ from intracellular conditions, and very few in vivo RNA chaperone assays have been reported. This could be due, at least in part, to the pleiotropic effects that RNA chaperones can cause, and to the difficulty in analyzing their activity in the context of a whole cell.

2.1. In vitro activities

The in vitro assays to analyze the nucleic acid chaperone activity of a protein could be divided into: simple assays, with relatively low technical difficulty as they are focused on a single aspect of chaperone activity (i.e., annealing and strand transfer assays), and

* Corresponding author. Tel.: +34 91 585 4555; fax: +34 91 585 4915.
E-mail address: L.Enjuanes@cnb.csic.es (L. Enjuanes).

0168-1702/$ – see front matter © 2008 Elsevier B.V. All rights reserved.
doi:10.1016/j.virusres.2008.06.015

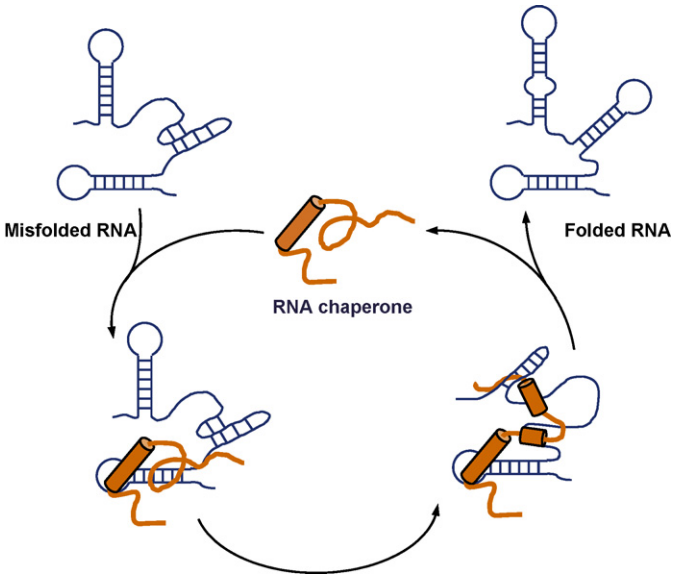

Fig. 1. Model of RNA chaperone mechanism. Entropy transfer model of the action of RNA chaperones, adapted from Tompa and Csermely (2004). RNA chaperones (orange) have long intrinsically disordered regions. In the first step of the model, this kind of proteins bind misfolded RNAs, in general, non-specifically. Disordered domains of the protein become ordered while domains of the substrate are unfolded (entropy transfer from protein to substrate). The RNA is correctly folded while the protein is disordered again (entropy transfer from RNA substrate to protein). Finally, after several cycles of order–disorder, the RNA substrate, correctly folded, is released, and the RNA chaperone is free to act again.

advanced assays, in which several chaperone activities are analyzed simultaneously (i.e., ribozyme or intron cleavage) (Cristofari and Darlix, 2002; Rajkowitsch and Schroeder, 2007; Rajkowitsch et al., 2005). Although there is no consensus, at least two different positive assays should be required to establish the RNA chaperone activity of a protein. In the simple assays, it should be at least desirable to show the absence of protein requirement after it has acted as nucleic acid chaperone, as this is the main difference between an RNA chaperone and an RNA binding protein that stabilizes a determined RNA folding while remaining bound. In some cases, biophysical technologies, such as fluorescence resonance energy transfer (FRET), NMR spectroscopy, fluorescence correlation spectroscopy (FCS), or single-molecule spectroscopy (SMS), have been applied to investigate the chaperone mechanism of action in in vitro assays providing precise information on the RNA chaperone mode of action (Égelé et al., 2005; Hong et al., 2003; Liu et al., 2007; Rajkowitsch and Schroeder, 2007; Ramalanjaona et al., 2007; Tisne et al., 2004; Zeng et al., 2007).

2.1.1. Nucleic acid annealing and strand displacement assays

The effect of proteins on RNA or DNA hybridization has been widely used to determine their nucleic acid chaperone activity (Cristofari et al., 2004; DeStefano and Titilope, 2006; Henriet et al., 2007; Huang et al., 2003; Ivanyi-Nagy et al., 2008; Pontius and Berg, 1992; Tsuchihashi and Brown, 1994; Vo et al., 2006; Zuñiga et al., 2007). It has been shown that RNA chaperones facilitate nucleic acid annealing. Nevertheless, annealing experiments must be carefully planned, as RNA annealing may occur in the absence of RNA chaperone activity. It is necessary to study activities including more than one step, and to perform the reactions in stringent conditions, such that only proteins with RNA chaperone activity could overcome all the requirements. To test activities that only RNA chaperones, but no other kind of proteins, could display, two strategies have been developed: (i) use of highly structured nucleic acid molecules, which requires a previous unwinding step by the RNA chaperone prior to the annealing, or (ii) protein elimination after base pairing has taken place (i.e., by treatment with proteinase K).

Nucleic acid chaperones also facilitate nucleic acid unwinding and strand displacement, and RNA chaperone activity could be clearly monitored within this kind of in vitro reactions (Cristofari et al., 2004; DeStefano and Titilope, 2006; Huang et al., 2003; Mir and Panganiban, 2006a,b; Pontius and Berg, 1992; Tsuchihashi and Brown, 1994). Recently, an experimental approach consisting on detection of double-stranded molecules by FRET has been described. This technique includes a first annealing step and a second strand displacement reaction, mediated by the addition of an excess of non-labeled nucleic acid competitor. Therefore, this process combines real-time analysis of both reactions within the same experiment, measuring annealing and strand displacement before and after the addition of the competitor RNA, respectively (Rajkowitsch and Schroeder, 2007). These type of experiments should be more informative about RNA chaperone activity and could avoid the problems of simple assays that could lead to a misinterpretation of the results.

2.1.2. Ribozyme cleavage

A more complex assay is the study of the cleavage, in *cis* or in *trans*, of a ribozyme. Hammerhead ribozymes have been widely used to monitor RNA chaperone activity, as nucleic acid chaperones enhance ribozyme cleavage (Bertrand and Rossi, 1994; Daros and Flores, 2002; Herschlag et al., 1994; Ivanyi-Nagy et al., 2008; Zuñiga et al., 2007). This assay implies more restrictive conditions for chaperone activity, as it requires unwinding and annealing steps that must finally render an RNA conformation capable of self-cleavage.

2.1.3. Group I intron splicing

Group I intron splicing is a special case of splicing that may occur within the introns of some organisms, in the absence of proteins. It depends on the folding of the RNA in a defined three-dimensional structure, as these type of introns are able of self-splice. This reaction could be very inefficient and slow in vitro, unless an RNA chaperone is present. Both *cis* and *trans* splicing assays have been used to demonstrate RNA chaperone activity of several proteins, especially bacterial proteins (Belisova et al., 2005; Coetzee et al., 1994; Grohman et al., 2007; Mayer et al., 2002; Semrad et al., 2004; Zheng et al., 1995).

2.1.4. Template switch

This assay has been used to study the RNA chaperone activity of human immunodeficiency virus (HIV)-1 nucleocapsid (NC) protein (Guo et al., 1997, 2002; Heilman-Miller et al., 2004; Henriet et al., 2007; Hong et al., 2003; Wu et al., 2007) and, more recently, to analyze the RNA chaperone activity of TGEV N protein (S. Zuñiga, I. Sola, L. Enjuanes, unpublished results). The synthesis of different cDNA species is analyzed, including a cDNA generated by a switch from the donor RNA template to an acceptor RNA. This assay involves a second level of complexity, as unwinding of very stable secondary RNA structures, efficient RNase H activity, inhibition of self-priming, and annealing of separate RNAs are required. This type of assay is considered below in detail.

2.2. In vivo activities

Evaluation of nucleic acid chaperone activity in vivo, using a physiological system, almost requires a “customized” assay, depending on the RNA chaperone tested. Therefore, as previously indicated, just a few in vivo RNA chaperone activity assays have been reported to date. The first system described was based on an

in vivo RNA folding trap existing in the bacteriophage T4 thymidylate synthase (td) group I intron (Clodi et al., 1999). Several RNA chaperones, overexpressed in *Escherichia coli*, are able to resolve the kinetic trap or impede the formation of misfolded structures, therefore promoting intron splicing. This system has been successfully used to test nucleic acid chaperone activity in vivo (Belisova et al., 2005; Clodi et al., 1999). Nevertheless, its physiological relevance remains uncertain (Lorsch, 2002) and, it also has a great limitation when overexpression of the RNA chaperone is toxic for *E. coli*.

Other reported assays, with more physiological relevance are based on: (i) transcription antitermination in vivo, for *E. coli* CspA-family nucleic acid chaperone proteins (Bae et al., 2000); (ii) *Neurospora crassa* group I intron splicing by CYT-19 protein, data that were also supported by the splicing phenotype of several mutants (Mohr et al., 2002); (iii) in vivo hepatitis delta ribozyme activity (Jeng et al., 1996); and (iv) in vivo reverse transcriptase template switching assay, using a MLV-based retroviral vector (Zhang et al., 2002).

An ideal assay for RNA chaperone activity is the in vivo demonstration of function associated with the natural RNA partner. Nevertheless, the analysis of RNA chaperone activity in vivo is quite difficult mainly because of the pleiotropic effects that RNA chaperones could have in the cell, and also because they act in different steps of a single biological process. All these reasons are in part responsible for the lack of appropriate in vivo systems for the analysis of RNA chaperone activity, and for a tendency to use complex in vitro systems with defined components.

3. Virus-encoded RNA chaperones and their roles in viral life cycle

The first viral RNA chaperone activities were reported in 1988, and were associated with the retrovirus nucleocapsid proteins. These activities have been extensively studied, and their nucleic acid chaperone activity was clearly established using different types of assays. Ten years have passed until another virus-encoded RNA chaperone was described, the HDV delta antigen. Then the list of virus-encoded RNA chaperones has been quickly growing, starting with the identification in 2004 of another viral RNA chaperone, the HCV core protein. Thus, in 2007, five new viral nucleic acid chaperones were described (Table 1). Nevertheless, the role of some of these proteins on viral life cycle, as RNA chaperones, is still unclear. This is mostly due to the difficulty in analyzing in an in vivo viral context the chaperone activity of these proteins.

Virus-encoded RNA chaperones have no common motif features (Fig. 2) and, sometimes, even RNA chaperone proteins of the same viral genus have little sequence similarity. Nevertheless, they fulfill the rule of having long disordered regions, with more than 50% of the protein being disordered in some cases. In fact, protein disorder has been the selected criterion to investigate the chaperone activity of several candidate viral RNA chaperone proteins.

3.1. Retrovirus-encoded RNA chaperones

Retroviruses are enveloped viruses infecting avian and mammalian species. Their genome is a dimer of two positive-sense single-stranded (ss) RNAs of around 10 kb, with a capped 5′-end and a poly-A at the 3′-end (Frankel and Young, 1998; ICTVdB-The Universal Virus Database, version 4; http://www.ncbi.nlm.nih.gov/ICTVdb/ICTVdB/). The viral genome can also be integrated into a host cell chromosome, and viral replication and transcription occurs in the host cell nucleus. Subsequent steps of the viral life cycle take place in the cell cytoplasm, i.e., viral protein translation and production of infectious viral particles. HIV-1 could be taken as a retrovirus model. Its genome encodes nine open reading frames (ORFs) (Fig. 3A). Three of these, Gag, Pol and Env polyproteins, are proteolyzed to generate mature structural proteins (from Gag and Env) and proteins with enzymatic functions (from Pol) such as protease, reverse transcriptase (RT) and integrase. The other six ORFs, encode accessory proteins, some of them found in the viral particle (Vif, Vpr and Nef) (Frankel and Young, 1998).

Avian and murine retrovirus NC proteins were the first virus-encoded RNA chaperones described (Prats et al., 1988). Later, the chaperone activity of HIV-1 NC was reported (Bertrand and Rossi, 1994; Tsuchihashi and Brown, 1994) and most of the current data on NC chaperone function came from HIV [for comprehensive reviews see Darlix et al., 2002; Levin et al., 2005]. The scenario has recently been complicated, as HIV-1 viral infectivity factor (Vif) and transcription activator (Tat) also have RNA chaperone activity (Henriet et al., 2007; Kuciak et al., 2008).

3.1.1. NC protein

The mature HIV-1 NC protein (usually named NCp7) is a short (55 aa), basic protein, produced by the proteolytic cleavage of the Gag precursor (Fig. 3B). It is found in the interior of the viral

Table 1
RNA chaperones involved in virus life cycle

Protein[a]	Virus[b]	Function	Reference
Virus encoded			
NC	Retrovirus	Reverse transcription, template switch	Levin et al. (2005)
SdAg	HDV	Replication	Huang et al. (2003)
Core	Flaviviridae	Replication	Ivanyi-Nagy et al. (2008)
N	Coronavirus	RNA synthesis	Zuñiga et al. (2007)
N	Hantavirus	Replication	Mir and Panganiban (2006a)
3AB	Poliovirus	Replication, recombination	DeStefano and Titilope (2006)
Vif	HIV-1	Temporal regulation of reverse transcription	Henriet et al. (2007)
Tat	HIV-1	Viral DNA transcription	Kuciak et al. (2008)
Host factors			
PTB	Picornavirus, HCV, coronavirus, calicivirus	Translation, RNA synthesis	Anderson et al. (2007); Domitrovich et al. (2005); Karakasiliotis et al. (2006); Shi and Lai (2005)
hnRNP A1	Coronavirus	RNA synthesis	Shi and Lai (2005)
La	HCV, poliovirus	Translation, replication	Domitrovich et al. (2005)
Unr	HRV-2	Translation	Hunt et al. (1999)
PARBP33	ASBVd	Replication	Daros and Flores (2002)

[a] NC, nucleocapsid protein; SdAg, small delta antigen; N, nucleocapsid protein; Vif, viral infectivity factor; Tat, transcription activation factor; PTB, polypyrimidine tract-binding protein; hnRNP A1, heterogeneous nuclear ribonucleoprotein A1; Unr, upstream of N-ras.
[b] HDV, hepatitis delta virus; HIV-1, human immunodeficiency virus-1; HCV, hepatitis C virus; HRV-2, human rhinovirus-2; ASBVd, avocado sunblotch viroid.

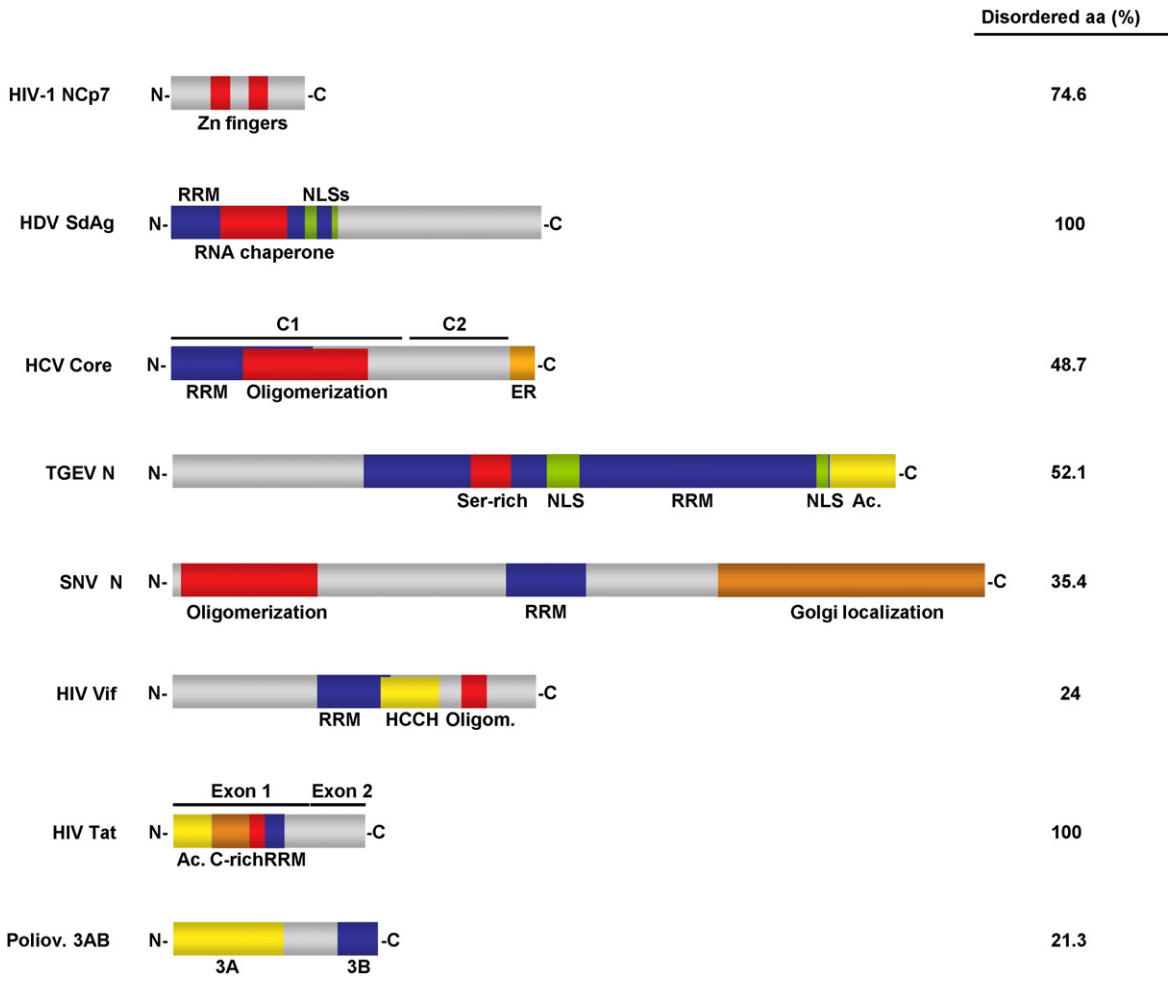

Fig. 2. Virus-encoded RNA chaperones. The left part of the figure schematically represents domain organization of viral RNA chaperones described to date. Numbers in the right column show the percentage of disordered aminoacids in each case, calculated using DisProt Predictor VL3H (Obradovic et al., 2003; Peng et al., 2005). Sequences used and GeneBank accession numbers: human immunodeficiency virus (HIV)-1 nucleocapsid protein (NCp7) (AAB21888), hepatitis delta virus (HDV) small delta antigen (SdAg) (AAQ09794), hepatitis C virus (HCV) core protein (AAX11912), transmissible gastroenteritis virus (TGEV) N protein (AJ271965), hantavirus Sin Nombre (SNV) N protein (M14626), HIV-1 viral infectivity factor (Vif) (AAC05239), HIV-1 transcriptional activator (Tat) (AAL01567) and human poliovirus 1 Mahoney 3AB polypeptide (P03300). RRM, RNA recognition or binding motif; NLS, nuclear localization signal; ER, endoplasmic reticulum retention signal; Ac., acidic domain; HCCH, HCCH motif; C-rich, cysteine rich domain.

particle, bound to the genomic RNA. NC contains two conserved zinc-finger domains with the CCHC Zn binding motif. Both Zn fingers are required for virus replication, but mutations on the first CCHC motif had a greater impact on RNA chaperone activity and virus replication (Guo et al., 2002).

NC plays a role in almost all the steps of retrovirus replication cycle, from reverse transcription to RNA packaging (Levin et al., 2005). As an RNA chaperone, NC facilitates dimerization of genomic RNA (Darlix et al., 1990), initiation of the reverse transcription and transfer events during reverse transcription. The effect of NC in these processes will be discussed below in more detail. Also, NC improves the processivity of the RT by reducing polymerase pausing during transcription (Ji et al., 1996; Wu et al., 1996) and stimulates RNase H activity of the RT (Levin et al., 2005).

3.1.1.1. Initiation of reverse transcription. Reverse transcription is initiated by annealing of a cellular tRNA with the primer binding site (PBS), located in the 5′ untranslated region (UTR) of the viral genome (Fig. 4A). The tRNA, specific for each retrovirus, will act as primer for the reverse transcriptase. These tRNAs are selectively incorporated into the viral particle where they are already placed onto the viral RNA. NC protein is required for the formation of an initiation-competent complex by facilitating tRNA–PBS annealing and unwinding of local domains. It was shown that NC induces conformational changes in the tRNA structure, allowing annealing with the viral genome and also additional interactions between the RNA genome and the tRNA (Tisne et al., 2004).

3.1.1.2. Minus strand transfer. Following initiation of the reverse transcription, RT synthesizes the negative strong-stop DNA [(−) SSDNA], that must be translocated to the 3′-end of the viral genome (Fig. 4B). This step is guided by the annealing between the complementary repeat regions (R) in each case, that contain the highly structured trans-activation response (TAR) element sequence. This step is highly efficient in vivo, as (−) SSDNA is not accumulated in infected cells. NC promotes the minus strand transfer by facilitating the annealing of the complementary TAR sequences in the (−) SSDNA and the acceptor RNA (Liu et al., 2007; Vo et al., 2006; Zeng et al., 2007), inhibiting self-priming of (−) SSDNA (Guo et al., 1997; Hong et al., 2003), and promoting RNase H cleavage of the donor RNA (Levin et al., 2005). After strand transfer, (−) SSDNA is elongated by the RT (Fig. 4B). NC increases the elongation efficiency by reducing RT pausing at genomic RNA secondary structures (Ji et al., 1996; Wu et al., 1996).

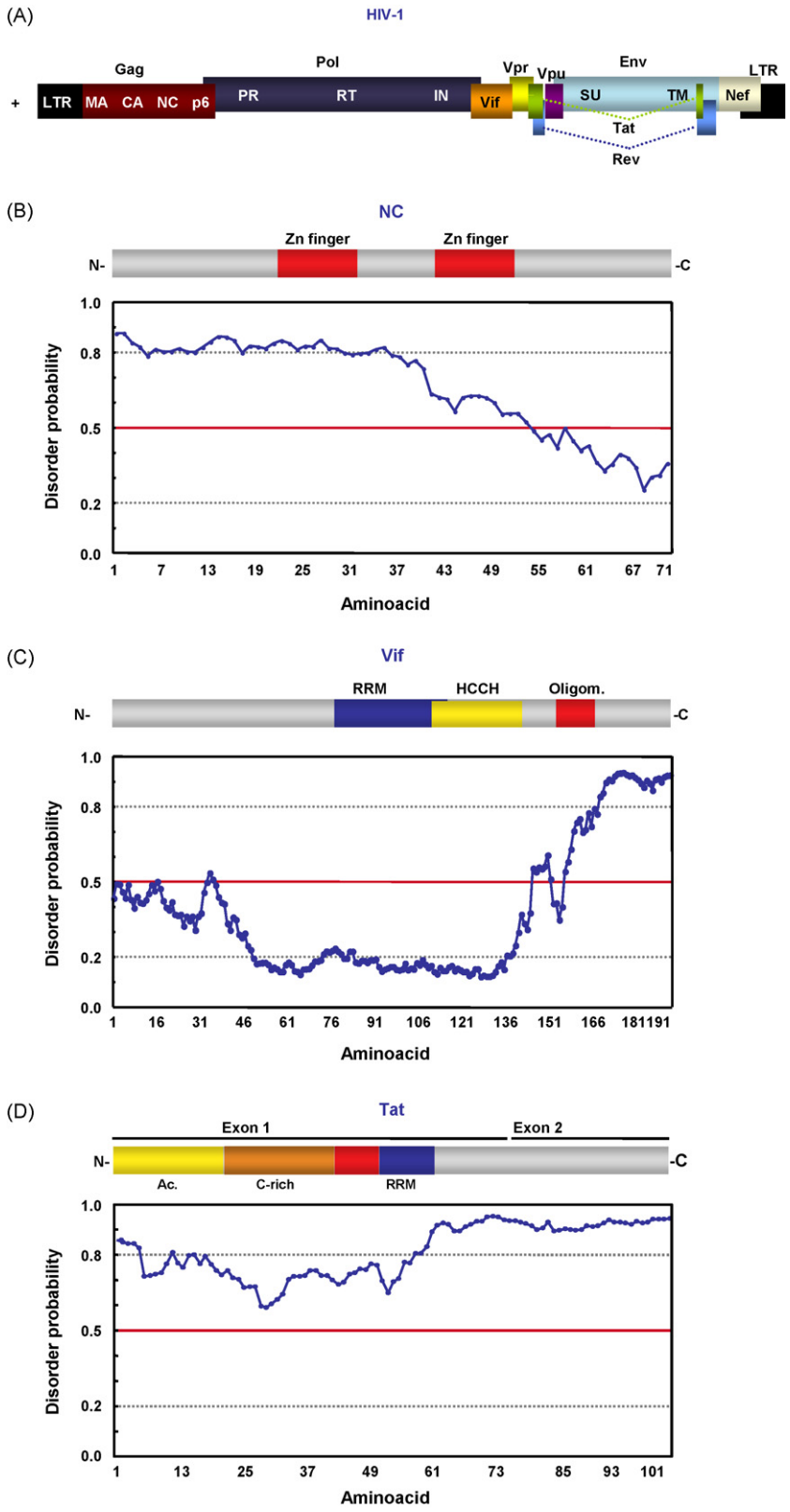

Fig. 3. Retrovirus-encoded RNA chaperones. (A) Schematic representation of HIV-1 genome. Gag, Pol and Env polyproteins, and their processing products are represented. LTR, long terminal repeat; MA, matrix protein; CA, capsid protein; NC, nucleocapsid; PR, protease; RT, reverse transcriptase; IN, integrase; Vif, viral infectivity factor; Vpr, viral protein R; Vpu, viral protein U; Tat, transactivator protein; SU, surface glycoprotein gp120; TM, transmembrane protein gp41; Nef, negative replication factor. Domain organization and disorder prediction, calculated using DisProt Predictor VL3H (Obradovic et al., 2003; Peng et al., 2005), for HIV NC (B), Vif (C) and Tat (D) proteins. Aminoacids with a disorder score equal or above 0.5 are considered to be in a disordered environment, while a value below 0.5 is considered ordered. GeneBank accession numbers and acronyms are as in Fig. 2.

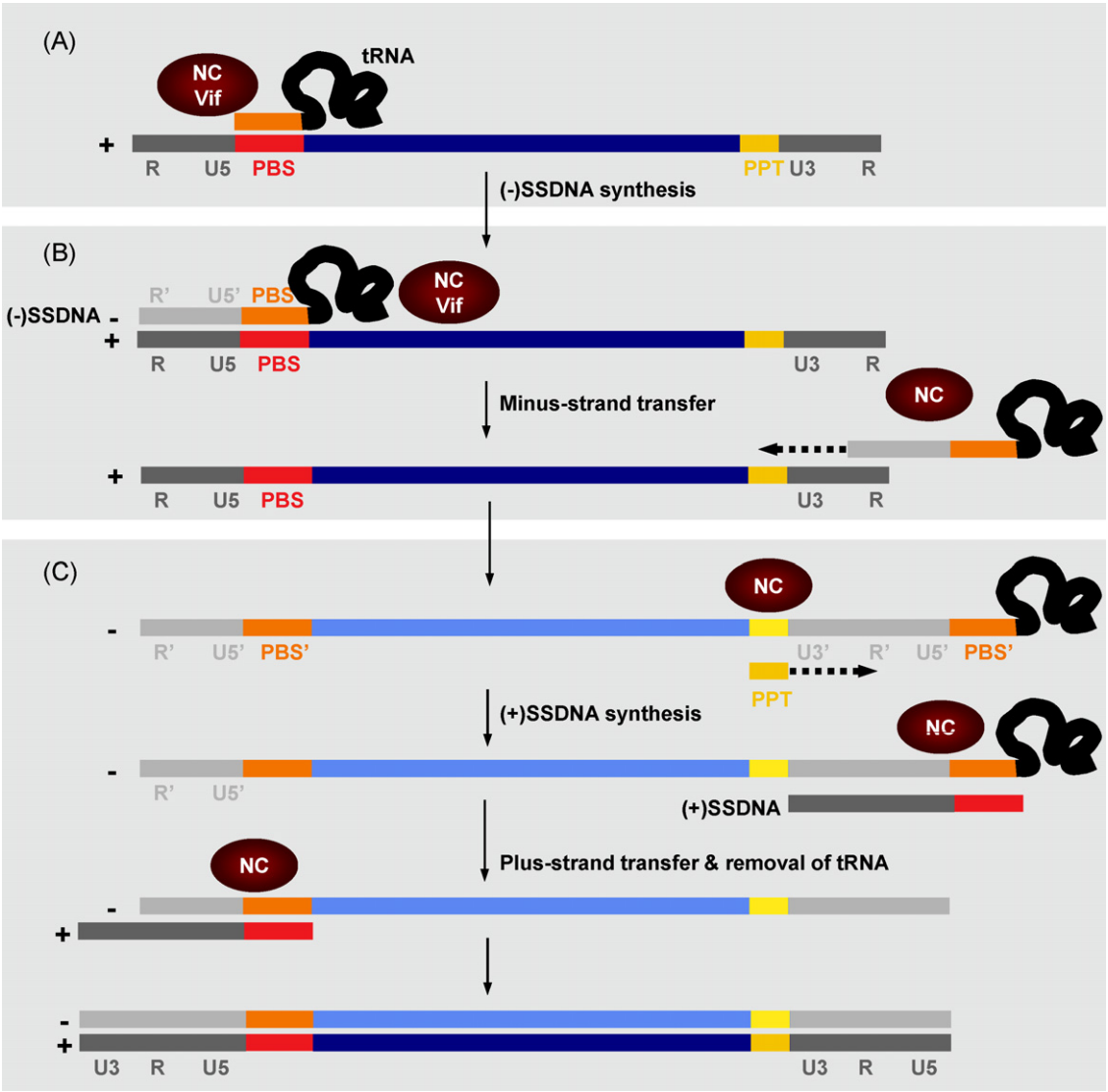

Fig. 4. Retrovirus replication. Representation of the key steps in retrovirus replication. Negative polarity DNA synthesis is initiated using a partially unwound tRNA annealed to the primer-binding site (PBS, in red) at the 5′-end of the viral genomic RNA. The reverse transcriptase elongates the 3′-end of tRNA, synthesizing the (−) strong-stop DNA (SSDNA), complementary to U5 and R. RNase H activity of RT degrades R and U5 sequences in the retroviral genomic RNA. The first RT template switch occurs, and the minus strand DNA anneals with R sequences at the 3′-end of the genomic RNA. RT elongates the negative-strand DNA to synthesize a (−) DNA strand complementary to the viral genome. RNase H degrades all viral genomic RNA except the polypurine tract (PPT, in yellow) sequence. The RT begins the synthesis of positive strand DNA using PPT RNA as a primer. The RNA primer is degraded by RNase H, and the second RT template switch occurs, annealing the (+) DNA PBS (in red) with its complementary sequence on the (−) DNA strand. Finally, RT elongates both strands to complete synthesis of a double-stranded proviral DNA. Positive polarity RNA and DNA strands are represented in dark colors. Negative polarity DNA strands are shown in light colors. Long terminal repeat (LTR) sequences are shown in grey. Steps in which RNA chaperones have a role are indicated by the red ellipses.

3.1.1.3. Plus strand transfer. While synthesis of minus strand DNA occurs, RT initiates the plus strand DNA synthesis. Similarly to minus strand DNA synthesis, a short DNA product, termed positive strong-stop DNA [(+) SSDNA] is produced by elongation of a polypurine tract (PPT), used as a primer (Fig. 4C). The synthesis of (+) SSDNA is followed by a plus strand transfer event, required for the subsequent elongation of plus strand DNA. During this transfer process, the complementary PBS sequences, present in the minus strand DNA and (+) SSDNA, anneal to form a circular intermediate. As an RNA chaperone, NC facilitates plus strand transfer by contributing to tRNA primer removal from the minus strand DNA donor, and enhancing the PBS sequences annealing (Égelé et al., 2005; Ramalanjaona et al., 2007; Wu et al., 1999).

3.1.2. Vif protein

HIV-1 Vif is an accessory 192 aa protein (Fig. 3C), important for the efficient viral DNA synthesis in certain cell types, named "non-permissive" (Frankel and Young, 1998; Sakai et al., 1993; Sova and Volsky, 1993). Vif is required in non-permissive cells to counteract cellular inhibitors of viral infection, such as APOBEC3G and APOBEC3F (Opi et al., 2006; Wiegand et al., 2004). It has been recently shown that Vif has RNA chaperone activity, and that it is involved in the early steps of reverse transcription. Vif enhances tRNA primer–PBS annealing, decreases RT pausing and enhances SSDNA synthesis. Nevertheless, it has modest effects in NC-mediated strand transfer events that are different depending on the maturation product of NC used in the assays. It has been proposed that Vif could act as a negative temporal regulator pre-

venting premature initiation of reverse transcription (Henriet et al., 2007).

3.1.3. Tat protein

HIV-1 Tat is a small nuclear regulatory protein that acts as a transcriptional activator (Fig. 3D). It is required for the transcription of integrated proviral DNA, driven by the 5′ long terminal repeat (LTR) sequence and the interaction of Tat with TAR element. Interaction of Tat with TAR recruits several transcription factors such as the TATA-binding protein, transcription factor TFIIB and positive transcription elongation factor B (P-TEFB). These interactions favor the hyperphosphorylation of the carboxy terminus domain (CTD) of the RNA polymerase II by the cyclin-dependent kinase 9 (CDK9) component of P-TEFB, allowing the elongation of the nascent RNA (Gatignol, 2007). Tat is a highly unstructured protein, and its RNA chaperone activity has been recently demonstrated (Kuciak et al., 2008). As an RNA chaperone, Tat enhances TAR DNA annealing, RNA–DNA exchange, ribozyme cleavage and RNA trans-splicing. It has been proposed that, as an RNA chaperone, Tat may act at the levels of proviral DNA transcription, viral RNA splicing and suppression of silencing (Kuciak et al., 2008).

3.2. Hepatitis delta virus delta antigen

Hepatitis delta virus (HDV) is an enveloped subviral satellite agent with hepatitis B virus (HBV) as its natural helper virus. Viral genome is a 1679 nt negative-sense, ssRNA with a circular rod-like conformation (Kos et al., 1986; Wang et al., 1986). The genome contains several ORFs, but only two proteins are produced from a single ORF: the small (195 aa) and large (214 aa) delta antigens. The large delta antigen isoform is generated later in the infection by post-transcriptional RNA editing, acts as an inhibitor of virus replication, and is required for viral assembly (Cornillez-Ty and Lazinski, 2003).

The small delta antigen (SdAg) is required for viral replication (Kuo et al., 1989). The RNA chaperone activity of SdAg was shown in different in vitro assays. This activity was proportional to the RNA binding activity of the protein, and was located in a domain from aa 24 to 59 (Huang et al., 2003; Huang and Wu, 1998; Wang et al., 2003).

During HDV replication, monomeric size RNA molecules must be generated. The ribozyme activity present in the viral RNA allows *cis* cleavage of both genome and antigenome RNAs. It was shown that, although delta antigen is not essential for the in vivo cleavage of HDV RNA, it enhances HDV ribozyme activity both in vitro and in vivo (Huang et al., 2003; Jeng et al., 1996).

3.3. Flaviviridae core proteins

Flaviviruses are enveloped viruses that infect vertebrates and are transmitted by an arthropod vector. Their genome is a positive-sense ssRNA close to 11 kb. The family comprises three genera: flavivirus, pestivirus and hepacivirus (Lindenbach and Rice, 2001). RNA chaperone activity was reported for hepacivirus (hepatitis C virus, HCV) core protein (Cristofari et al., 2004). Recently, based on disorder conservation in *Flaviviridae* core proteins, the RNA chaperone activity of core proteins from different members of each genera has been analyzed. It has been found that, although core proteins from different *Flaviviridae* genera have low sequence similarity, all of them have RNA chaperone activity (Ivanyi-Nagy et al., 2008). Furthermore, data strongly suggest that nucleic acid chaperone activity resides in disordered regions of *Flaviviridae* core proteins as their RNA chaperone activity is resistant to heat denaturation of the protein (Ivanyi-Nagy et al., 2008).

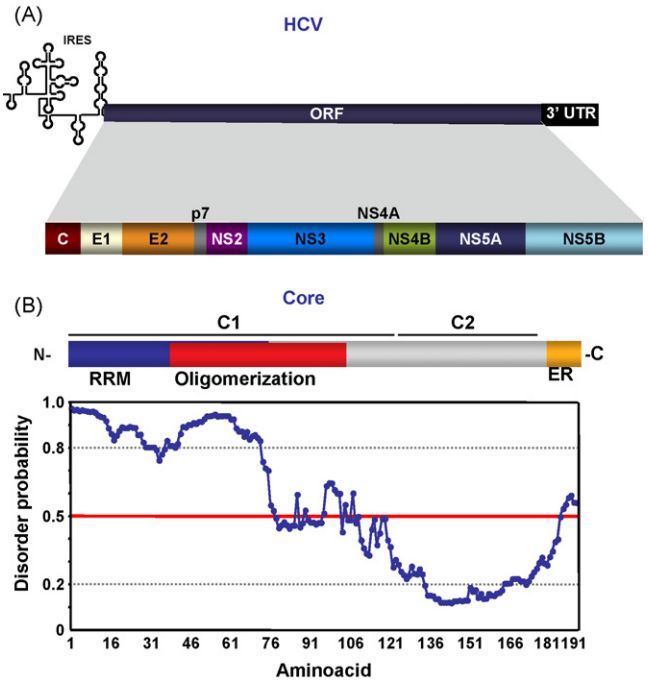

Fig. 5. Hepacivirus-encoded RNA chaperone. (A) Representation of HCV genome. C, core protein; E1, envelope protein 1; E2, envelope protein 2; NS, non-structural protein. (B) Domain organization and disorder prediction plot for HCV core protein. Plot obtention and interpretation as in Fig. 3. GeneBank accession number and acronyms are as in Fig. 2.

HCV has a 9.6 kb RNA genome, with a unique ORF encoding a long polyprotein (Fig. 5A). Structural and non-structural proteins are generated by co- and post-translational processing of the polyprotein. The 5′ and 3′ UTR regions contain RNA domains involved in viral replication. The 5′ UTR is folded with an IRES structure that promotes cap-independent translation. The 3′ UTR consists on a short variable region, a U/(UC) motif, and a X tail with highly conserved stem loop structures (Moradpour et al., 2007). The mature 178 aa core protein is produced by cleavage of the polyprotein and further signal peptide processing. Core protein could be divided in two different domains: C1, involved in RNA binding and oligomerization, and C2, involved in association with lipid droplets (Moradpour et al., 2007) (Fig. 5B).

HCV core protein has RNA chaperone activity that has been demonstrated using different approaches (Cristofari et al., 2004). It was also shown that, acting as a nucleic acid chaperone, core protein allows dimerization of the HCV RNA 3′ UTR (Cristofari et al., 2004; Ivanyi-Nagy et al., 2006). This HCV RNA region could adopt different conformations, with unknown role on viral life cycle. It has been suggested that HCV RNA 3′ UTR interconversion between different structures could act by regulating transitions between translation–replication and replication–packaging of the genomic RNA. In this context, the RNA chaperone activity of the core protein could regulate these riboswitches by facilitating interconversion of the different RNA structures (Ivanyi-Nagy et al., 2006).

3.4. Coronavirus nucleocapsid protein

Coronaviruses are enveloped viruses, of the *Coronaviridae* family, included in the *Nidovirales* order (Enjuanes et al., 2008; Gorbalenya et al., 2006). Their genomes are positive-sense, ssRNAs of around 30 kb, the largest known viral RNA genomes. The 5′ two-thirds of the genomic RNA encode the replicase genes (rep1a and rep1ab). The 3′ one-third of the genome encodes structural and

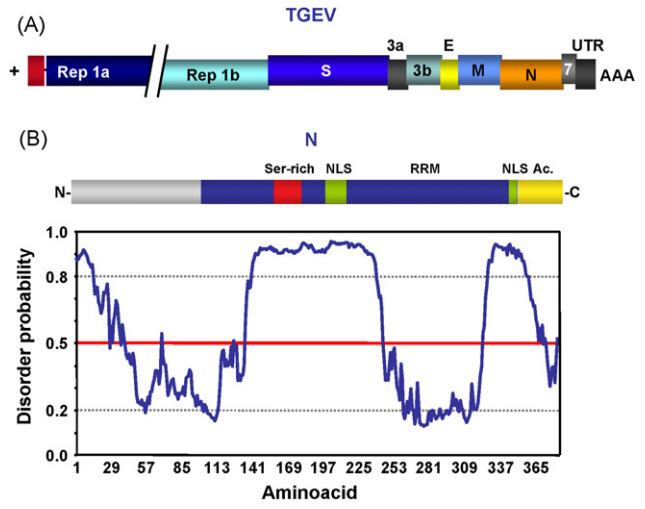

Fig. 6. Coronavirus-encoded RNA chaperone. (A) Schematic representation of TGEV genome, as a model for coronavirus genomes. Rep, replicase polyproteins; S, spike protein; E, envelope protein; M, membrane protein; N, nucleocapsid protein. (B) Domain organization and disorder prediction for TGEV N protein. Plot obtention and interpretation as in Fig. 3. GeneBank accession number and acronyms are as in Fig. 2.

non-structural proteins (Fig. 6A). Coronavirus replication and transcription occur in the cytoplasm of infected cells, and are based on RNA-dependent RNA synthesis. Transcription leads to a nested set of subgenomic (sg) mRNAs that are 5′- and 3′-coterminal with the viral genome. These sg mRNAs are generated by a discontinuous process (Fig. 7) that implies base pairing of nascent RNAs of negative polarity, driven by the transcription-regulating sequences (TRSs) preceeding each gene, and sequences located at the 3′-end of the leader within the genomic RNA (Sawicki and Sawicki, 2005; Sawicki et al., 2007; Sola et al., 2005; Zuñiga et al., 2004).

It has been shown that the free energy of duplex formation between nascent RNA sequences complementary to the body (donor) TRS and the leader (acceptor) TRS is the main factor driving coronavirus discontinuous transcription (Sola et al., 2005; Zuñiga et al., 2004) (Fig. 7). Nevertheless, on top of this mechanism operating in the synthesis of all sg mRNAs, the transcription of specific genes, such as N gene, is regulated by a recently described enchancer mechanism (Moreno et al., 2008).

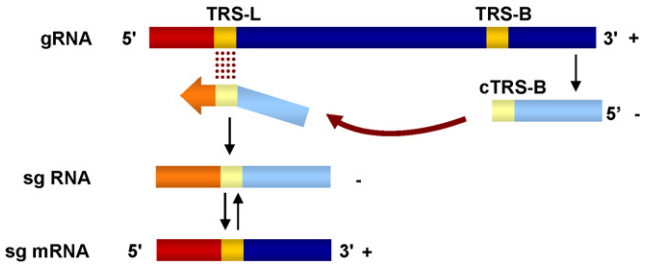

Fig. 7. Coronavirus transcription. Representation of the coronavirus discontinuous transcription during negative-strand synthesis. Transcription regulating sequences from the leader (TRS-L) and preceding a gene (TRS-B) are shown in yellow. Negative polarity RNA synthesis begins from 3′-end of the coronavirus genome. Once the transcription complex copies the TRS-B template switch of the nascent RNA to the leader sequence (red) takes place and the sequence complementary to the TRS-B (cTRS-B) hybridizes with the TRS-L. This process is indicated by the dark red arrow. Nascent RNA synthesis continues with the copy of the leader sequence (red), leading to a negative polarity subgenomic RNA (sg RNA) that will be used as a template for the generation of the sg mRNAs of positive polarity. Genomic RNA and sg mRNA strands are shown in dark colors. Negative polarity RNA strands are shown in light colors.

Coronavirus nucleocapsid (N) protein has a structural role and has also been involved in RNA synthesis (Almazan et al., 2004; Enjuanes et al., 2006). The N proteins from different coronaviruses are variable in length and primary sequence. Nevertheless, some motifs with functional relevance are conserved, and the proteins share a common domain organization. A three-domain structure has been proposed for N protein (Parker and Masters, 1990). Recently, based on disorder predictions, a modular organization including two structured domains separated by a long disordered region has been proposed for coronavirus N protein (Chang et al., 2006; Zuñiga et al., 2007) (Fig. 6B).

Using transmissible gastroenteritis virus (TGEV) as a model, RNA chaperone activity has been demonstrated for N protein (Zuñiga et al., 2007). RNA chaperone activity was also reported for severe and acute respiratory syndrome virus (SARS-CoV) (Zuñiga et al., 2007). Based on these results and on the high conservation of disorder patterns for different coronavirus N proteins, RNA chaperone was postulated as a general activity of all coronavirus nucleoproteins. In fact, it has been recently shown that the central disordered domain of TGEV N protein includes the nucleic acid chaperone activity of the protein (S. Zuñiga, I. Sola, L. Enjuanes, unpublished results).

The template switch involved during the discontinuous RNA synthesis in coronavirus transcription is a complex process that includes numerous steps (see below). To accomplish some of these steps we have proposed that RNA chaperones, such as the N protein, could decrease the energy barrier needed to dissociate the nascent minus RNA chain from the genomic RNA template, in order to perform a template switch leading to the hybridization with the TRS of the leader sequence during discontinuous transcription (Zuñiga et al., 2007). In fact, we have recently shown that TGEV N protein enhanced template switch in vitro using the HIV-derived system (S. Zuñiga, I. Sola, L. Enjuanes, unpublished results).

It is worth noting that the number of coronavirus-encoded RNA chaperones could grow with the addition of some non-structural proteins, such as SARS-CoV nsp3 (Neuman et al., 2008).

3.5. *Hantavirus nucleocapsid protein*

Hantaviruses are enveloped viruses included within the *Bunyaviridae* family. Their genome is composed of three segments of negative-sense, ssRNA (Khaiboullina et al., 2005). The large (L), medium (M) and small (S) segments, encode RNA dependent RNA polymerase, the glycoprotein precursor yielding surface glycoproteins G1 and G2, and the nucleocapsid (N) protein, respectively (Plyusnin et al., 1996). These RNA segments have complementary 5′ and 3′ termini that are base-paired, forming a panhandle structure leading to circular, supercoiled RNAs. Formation of the panhandle structure is important for bunyavirus replication, but the precise role in viral RNA synthesis is unclear (Barr and Wertz, 2005).

Hantavirus N proteins have around 433 aa, and interact with viral RNA, plus strand cRNA, and mRNAs (Mir and Panganiban, 2005; Plyusnin et al., 1996). Hantavirus N protein has been found to be involved in viral RNA packaging and virus replication (Mir and Panganiban, 2006b). The RNA chaperone activity of the hantavirus Sin Nombre (SNV) N protein was recently reported (Mir and Panganiban, 2006b). It has been proposed that N protein facilitates panhandle formation and mediates panhandle dissociation during replication initiation, acting as an RNA chaperone (Mir and Panganiban, 2006a,b).

Hantavirus N protein is the first RNA chaperone described encoded by a negative-stranded RNA virus. Genomic RNA panhandle formation and dissociation during virus replication could be a common feature of other negative strand RNA viruses. Nevertheless, influenza A virus nucleocapsid protein has no RNA chaperone

activity, at least in in vivo assays based on an RNA folding trap (Clodi et al., 1999).

3.6. Poliovirus 3AB protein

Polioviruses belong to the *Picornaviridae* family. Their genome is a positive-sense ssRNA of around 8 kb, encoding a single polypeptide. This polyprotein is processed leading, at least, to 10 different protein products (Agol, 2006). Processing intermediates of the polyprotein often have specific functions. RNA chaperone activity was recently reported for one of these products, the 3AB precursor, that has annealing and helix-destabilizing activities (DeStefano and Titilope, 2006). 3B protein, also named as VPg, is linked to the 5′-end of the viral genome and acts as primer for viral RNA synthesis. 3A protein was proposed as the protein that anchors the replication complexes to membranes. 3AB precursor stimulates RNA synthesis by the RNA-dependent RNA polymerase, and has RNA chaperone activity. Nevertheless, its role as RNA chaperone in the viral life cycle is unclear.

4. Cellular RNA chaperones involved in viral replication

A large collection of cellular factors has been found to be involved in virus replication (Table 1). Most of them were first identified using viral RNA–protein binding assays, followed by functional assays, i.e., silencing of cell protein expression and relevance on virus replication. Most of the cellular proteins identified using these approaches are common for unrelated viruses. RNA chaperone activity has been associated to several proteins identified using these strategies. Nevertheless, some of these proteins do not act as real RNA chaperones, as they need to remain bound to the RNA to achieve the expected functional activity. In fact, their relevance in viral replication acting as canonical RNA chaperones has been clearly demonstrated only in a reduced number of cases. Therefore, the exact role of these proteins, as RNA chaperones, on viral life cycle still needs to be elucidated. The activity of some of these proteins is described below.

4.1. Heterogeneous nuclear ribonucleoprotein A1 (hnRNP A1)

hnRNP A1 is a cellular RNA binding protein involved in different aspects of RNA metabolism. It is predominantly nuclear, but also shuttles to the cytoplasm (Dreyfuss, 1986; Dreyfuss et al., 1993). hnRNP A1 is a well-characterized RNA chaperone (Herschlag et al., 1994; Pontius and Berg, 1992; Portman and Dreyfuss, 1994) that promotes RNA annealing and enhances ribozyme cleavage.

Mouse hepatitis coronavirus (MHV) RNAs and N protein bind hnRNP A1 (Zhang et al., 1999). It has been found that the binding of hnRNP A1 to viral TRSs correlates with the sg mRNA level transcribed from these TRSs (Zhang and Lai, 1995). hnRNP A1 has also been involved in 5′–3′-end cross-talk (Huang and Lai, 2001). All data reported indicated that hnRNP A1 plays a role in vivo in coronavirus RNA synthesis, as over-expression of the protein facilitates MHV replication and dominant-negative mutants of hnRNP A1 reduce virus replication (Shi and Lai, 2005). Nevertheless, its role, as nucleic acid chaperone, in viral replication has not been fully established. That was mostly due to the fact that other hnRNP proteins could substitute for hnRNP A1 in vivo (Shen and Masters, 2001; Shi and Lai, 2005), making it very difficult to evaluate the precise role of hnRNP A1 even in its cellular functions.

4.2. Polypyrimidine tract-binding protein (PTB)

PTB is an RNA binding protein involved in regulation of alternative splicing and translation of cellular RNAs. Similarly to hnRNP A1, it is mainly located in the nucleus, although it can shuttle to cell cytoplasm under different conditions (i.e., viral infections). There are at least three different PTB isoforms: PTB1, PTB2 and PTB3 (Gil et al., 1991), and differences in the activity of these proteins in cellular RNA splicing have been reported (Wollerton et al., 2001). Only PTB3, also known as hnRNP I (Ghetti et al., 1992), has a well-established RNA chaperone activity based on group I splicing assays (Belisova et al., 2005). Nevertheless, the RNA chaperone activity of other PTB isoforms is not clear. In fact, when analyzed, PTB1 did not enhance nucleic acids annealing and hammerhead ribozyme cleavage (Zuñiga et al., 2007).

PTBs are the most recurrent proteins reported to bind viral RNAs. It is difficult to identify the specific PTB isoform involved in each case, due to the small aa difference between them, and because in most cases, it has been identified by proteomic approaches that do not distinguish PTB isoforms. PTBs bind picornavirus IRES, both entero-rhinovirus group (including poliovirus and HRV-2) and cardio-aphthovirus (including encephalomyocarditis virus [ECMV] and foot-and-mouth disease virus [FMDV]) (Florez et al., 2005; Hunt et al., 1999; Song et al., 2005). PTBs also bind HCV UTR regions (Domitrovich et al., 2005), calicivirus RNA (Karakasiliotis et al., 2006) and coronavirus RNAs (Shi and Lai, 2005).

In viral life cycle, PTBs mainly act by facilitating translation. For picornavirus and HCV, it has been proposed that PTBs, acting as RNA chaperones, may help IRES folding into a translation-competent conformation (Anderson et al., 2007; Domitrovich et al., 2005; Gosert et al., 2000; Hunt and Jackson, 1999; Song et al., 2005). Nevertheless, in these cases, it has not been shown whether PTBs could be eliminated after the IRES has folded properly. Therefore, a key property of RNA chaperones has not been demonstrated.

The role of PTBs in viral RNA synthesis seems to depend on virus taxonomy. It was reported that PTBs modulate coronavirus RNA synthesis and also could facilitate 5′–3′-end interactions (Shi and Lai, 2005). A positive effect on feline calicivirus RNA synthesis was observed, but only at temperatures proposed to difficult functional folding of calicivirus RNA (Karakasiliotis et al., 2006). In HCV RNA synthesis the role of PTBs as RNA chaperones needs additional work. It has been shown that PTBs have an inhibitory effect on HCV RNA synthesis (Domitrovich et al., 2005) and it has been proposed that they block replication initiation while enhancing IRES-promoted translation, facilitating the replication–translation switch. At the same time, it has also been reported that PTBs are required for an efficient HCV RNA replication (Aizaki et al., 2006; Chang and Luo, 2006).

4.3. La autoantigen

La is a nuclear RNA-binding phosphoprotein that is associated with RNA polymerase III transcripts (Maraia and Intine, 2001; Pannone et al., 1998). La has RNA chaperone activity, as it facilitates group I intron splicing both in vitro and in vivo (Belisova et al., 2005). La interacts with the UTR regions of HCV and poliovirus, and enhances translation from the IRES of these viruses (Domitrovich et al., 2005; Meerovitch et al., 1993). In addition, La autoantigen is also required for efficient replication of HCV viral RNA (Domitrovich et al., 2005). Nevertheless, the relevance of La autoantigen RNA chaperone activity in these processes has not been clarified.

4.4. Upstream of N-ras (Unr)

Unr is a cytoplasmic RNA binding protein essential for transcriptional regulation and mRNA metabolism. Unr contains five cold-shock domains and, therefore, is predicted to act as RNA chaperone by similarity with prokaryotic cold-shock domain containing proteins (Rajkowitsch et al., 2007). Unr binds and stimulates trans-

lation from human rhinovirus-2 (HRV-2) IRES (Brown and Jackson, 2004; Hunt et al., 1999). It has been proposed that Unr could act as an RNA chaperone to allow folding of HRV-2 IRES into a translation-competent structure that could bind PTB and ribosome (Anderson et al., 2007), similarly to cellular Apaf-1 IRES (Mitchell et al., 2003).

4.5. PARBP33

PARBP33 is a chloroplast RNA binding protein identified by UV-crosslinking of avocado sunblotch viroid (ASBVd) infected leaves and purification of the RNA–protein complexes obtained. It has been reported that PARBP33 acts as an RNA chaperone in vitro, enhancing ASBVd hammerhead ribozyme cleavage (Daros and Flores, 2002). According to this report, PARBP33 should act in vivo facilitating ribozyme-mediated cleavage of oligomeric ASBVd RNA, a key step in the replication mechanism of this viroid.

5. RNA chaperones, template switch and transcription

Template switch is a complex process in which different steps could be differentiated: (i) slow down or stop of nucleic acid synthesis; (ii) template switch itself; (iii) reassociation of the nascent nucleic acid strand with the acceptor sequence; and (iv) elongation of the nascent strand using the acceptor nucleic acid as template (Enjuanes et al., 2007). Some aspects of these steps will be expanded below, specially focused on the two viral systems where template switch is an essential process of their life cycle: coronavirus discontinuous transcription and retrovirus reverse transcription.

5.1. Polymerase pausing

Two different slow-down or stop signals could be acting, both in coronavirus transcription and retrovirus reverse transcription. First, the termination of nascent strand synthesis might be mediated by secondary RNA structures located either in the template or in the nascent strand, as described for prokaryotic (Wilson and von Hippel, 1995) or eukaryotic (Reeder and Lang, 1997) RNA polymerases. Extensive studies have been made on HIV RT pausing and on secondary RNA structures influencing this process. It has been shown that the RT pausing could be promoted by a highly structured hairpin. This RT slow-down should increase RNase H cleavages at the site of pausing, increasing template switch at this location (Basu et al., 2008; Roda et al., 2003). In coronavirus little is known about secondary structures and pausing sites, although 5′ TRS sequence secondary structures are good candidates for stopping signals (Enjuanes et al., 2007). TRS secondary structures could be specially relevant in the case of torovirus non-discontinuous transcription (Smits et al., 2005), that resembles the premature transcription termination mechanism of tombusviruses (Lin and White, 2004; White, 2002; White and Nagy, 2004). In these viruses, it has been proposed that RNA secondary structures formed in the genome, upstream to the transcription initiation sites, could facilitate transcription termination (White and Nagy, 2004).

Alternatively, sequence complementarity of nascent nucleic acid with the acceptor molecule could have a role on pausing decision. According to this model, in coronavirus, both the CS and the TRS 3′-flanking sequences combine their complementarity to decide whether template switch would take place. This model fits with the results obtained for bovine coronavirus (BCoV) (Ozdarendeli et al., 2001) and TGEV (Sola et al., 2005; Zuñiga et al., 2004) showing that sequences downstream the CS exert a dominant influence on the template-switching decision. Similar results were obtained in HIV systems, in which increased complementarity before the pausing site facilitates acceptor invasion (Basu et al., 2008; Gao et al., 2007). In HIV it was also reported that a pause-independent strand transfer occurs in low structured RNA regions (Basu et al., 2008; Derebail and DeStefano, 2004), although the relevance of sequence complementarity on this process has not been established.

The role of RNA chaperones on the RNA secondary structure mediated pausing is not obvious, as this kind of proteins are expected to unwind secondary structures. In fact, reduction of polymerase pausing has been shown for NC (Levin et al., 2005), and proposed for coronavirus N protein (Sawicki et al., 2007). Nevertheless, in HIV it has been shown that NC enhances RNase H cleavage, that is a key step of RT hairpin-mediated pausing, as mentioned above (Levin et al., 2005). The possible role of RNA chaperones in sequence complementarity mediated pausing seems a probable event, as RNA chaperones enhance nucleic acids annealing.

5.2. Template switch

Template switch both in corona and retrovirus resembles a similarity-assisted high-frequency copy-choice recombination (Negroni and Buc, 2000; Sawicki et al., 2007). A copy-choice mechanism implies that the polymerase leaves the first template (the donor) and continues synthesis on a second template (the acceptor) (Kim and Kao, 2001). In similarity-assisted recombination, sequence similarity between nucleic acids influences the frequency and site of the recombination event, but additional structure determinants, generally only present in one of the nucleic acids, are essential for efficient recombination (Nagy and Simon, 1997). For instance, in turnip crinkle virus (TCV), efficient recombination needs RNA sequence similarity and a hairpin structure present only in the acceptor RNA (Nagy et al., 1998).

In retroviruses, a secondary DNA structure present in the donor strand, that allows acceptor invasion, has been postulated in the recombination process (Negroni and Buc, 2000). Similar increase in recombination levels has been found when only the acceptor or both the donor and acceptor molecules are coated with NC protein, indicating that this protein could display its chaperone activity when coating a nucleic acid molecule (Negroni and Buc, 2000). In contrast, a secondary structure on one of the nucleic acid molecules is not required for either the minus or the plus strand transfer events. In fact, for an efficient template switch, the unwinding of a stable secondary structure must occur, both in the minus and plus strand transfer (Basu et al., 2008; Levin et al., 2005). NC protein plays a key role in this process, acting as an RNA chaperone (Hong et al., 2003; Wu et al., 1999). One of the determinant steps in HIV minus strand transfer is the annealing of the two highly structured TAR sequences (Basu et al., 2008; Levin et al., 2005). Without the nucleic acid chaperone activity of NC, the annealing reactions would occur much more slowly, as NC increases the annealing of structured sequences around 3000-fold, depending on the assays (Basu et al., 2008; Levin et al., 2005; Vo et al., 2006; Zeng et al., 2007).

According to the current model of coronavirus transcription there is a structural requirement for the leader TRS, that should be in an adequate context to serve as the acceptor for the nascent minus RNA strand transfer (Enjuanes et al., 2007; Sawicki et al., 2007). In fact, a leader stem-loop structure was predicted for several nidovirus, and its existence and relevance on RNA synthesis has been shown for equine arteritis arterivirus (EAV) (van den Born et al., 2004, 2005) and for TGEV coronavirus (J.L. Moreno, D. Dufour, I. Sola, J. Gallego, L. Enjuanes, unpublished results). In coronavirus template switch, the annealing of the leader and nascent minus RNA sequences complementary to the body TRSs is one of the main factors regulating transcription. It has been demonstrated that the free-energy of the duplex formation between those sequences is

the driving force of template switch, regulating the amount of each sg mRNA, and the places where template switch takes place (Sola et al., 2005; Zuñiga et al., 2004). Acting as an RNA chaperone, N protein could be involved in the correct folding of the leader structure. In fact, it has been proposed that N protein could mediate the annealing of TRSs by decreasing the energy barrier required for this process (Zuñiga et al., 2007). Nowadays, our group is working on the design of an in vivo system to analyze template switch step during coronavirus transcription.

5.3. Experimental systems to analyze coronavirus template switch

In the case of retroviruses, there are several experimental systems concerning just one step of the transfer events. These kind of approaches have been essential to develop extensive knowledge on the role of retrovirus NC RNA chaperone on strand transfer (Levin et al., 2005). In contrast, the experimental system to study coronavirus template switch at the molecular level needs to be developed.

Coronaviruses have the longest viral RNA genome known, but it is possible to perform reverse genetics on these viruses, as infectious cDNA clones are available for several coronaviruses (Enjuanes, 2005). Nevertheless, the analysis of RNA chaperone activity in the context of the whole infectious virus represents a challenge. An alternative approach is the use of coronavirus replicons. In the case of TGEV, a set of replicons has been generated (Almazan et al., 2004), that may be used for in vivo testing the chaperone activity of the candidate protein.

In vitro systems are required to precisely define the role that RNA chaperones have on the different steps of coronavirus template switch. The purification of in vitro active coronavirus replication–transcription complexes has been recently described (van Hemert et al., 2008). These systems could be used to analyze the role of chaperones on template switch. The main limitation of these in vitro systems is that the precise components required to reproduce the activity still need to be identified and, very likely, in addition to viral RNA chaperones, cellular ones could be part of the purified active complexes. An alternative is to develop in vitro systems based on defined components, similarly to the current retrovirus in vitro systems. Acceptor and donor RNAs must be carefully selected, attending to the features to be assayed. Probably, the key difficulty in the development of these in vitro systems is the precise number of protein components required. The RNA-dependent RNA-polymerase (RdRp) from SARS-CoV has been purified and its polymerization activity has been shown (Cheng et al., 2005). In addition RNA chaperones and other still unidentified proteins will be required for a fully functional in vitro system.

6. Perspectives

There is little evidence of the in vivo folding mechanism of RNA molecules, but it is generally accepted that RNAs exist bound to proteins within the cells. In 1995, based on some in vitro observations, and from the point of view of the existence of a functional association between RNA and proteins, RNA chaperone activity was postulated (Herschlag, 1995). Since then, several RNA chaperones have been identified using diverse in vitro assays, or postulated, based on the effects observed when these proteins are mutated. A helpful attempt to provide a precise and restricted definition of RNA chaperone activity has recently been reported (Rajkowitsch et al., 2007). According to this definition, RNA chaperones are proteins that resolve misfolded RNAs, and that also must fulfill several requirements: (i) transient interaction with the nucleic acid, mainly due to a weak and low specificity RNA–protein binding; (ii) lack of requirement of an external energy input, such as ATP hydrolysis; and (iii) lack of RNA–protein interaction requirement to maintain the functional RNA conformation.

Previous confusion in the precise identification of RNA chaperones has arised in large extent due to the experimental difficulty in analyzing RNA chaperone activity. As mentioned above, simple studies such as annealing or strand displacement assays could involve other non-chaperone activities (i.e., RNA crowding or matchmaker activities) (Rajkowitsch et al., 2007). New technologies that monitor single molecules have been used to clarify the mechanism of RNA chaperone activity by measuring RNA folding in real-time. These approaches include force spectroscopy and single-molecule stretching using optical tweezers, and time-resolved NMR (Furtig et al., 2007; Williams et al., 2002, 2001). Nevertheless, performance and interpretation of the results provided by these technologies require highly specialized personnel and equipment.

Complex refolding events, such as ribozyme cleavage or intron splicing, are in general suited for the assessment of candidate proteins and to evaluate RNA chaperone mutant activity. Nevertheless, several assays are needed to avoid misinterpretation of the results, such as combination of ribozyme cleavage and transcription activity. These assays must be concentrated on measurements performed using RNA, it also must be shown that after the initial steps protein can be removed, and that the process is independent of external energy sources (Rajkowitsch et al., 2007). In more advanced systems, RNA chaperone should be also tested in vivo, using its natural RNA partner. The analysis of RNA chaperone activity in vivo has the additional difficulty of the pleiotropic effects that RNA chaperones could have in the cell. Nevertheless, the development of in vivo systems is possible. In coronaviruses progress is being made to develop a homologous template switch system that could be easily evaluated.

Acknowledgements

This work was supported by grants from the *Comisión Interministerial de Ciencia y Tecnología* (CICYT, BIO2007-60978), the Community of Madrid (S-SAL-0185/06), the Ministry of Science and Innovation (MICINN, CIT-010000-2007-8) and the European Union (Frame VI, DISSECT Project, SP22-CT-2004-511060). S.Z. and I.S. received contracts from Highest Council of Scientific Research (CSIC). J.L.G.C. received contract from Community of Madrid.

References

Agol, V.I., 2006. Molecular mechanisms of poliovirus variation and evolution. Curr. Top. Microbiol. Immunol. 299, 211–259.
Aizaki, H., Choi, K.S., Liu, M., Li, Y.J., Lai, M.M., 2006. Polypyrimidine-tract-binding protein is a component of the HCV RNA replication complex and necessary for RNA synthesis. J. Biomed. Sci. 13, 469–480.
Almazan, F., Galan, C., Enjuanes, L., 2004. The nucleoprotein is required for efficient coronavirus genome replication. J. Virol. 78, 12683–12688.
Anderson, E.C., Hunt, S.L., Jackson, R.J., 2007. Internal initiation of translation from the human rhinovirus-2 internal ribosome entry site requires the binding of Unr to two distinct sites on the 5′ untranslated region. J. Gen. Virol. 88, 3043–3052.
Bae, W., Xia, B., Inouye, M., Severinov, K., 2000. *Escherichia coli* CspA-family RNA chaperones are transcription antiterminators. Proc. Natl. Acad. Sci. U.S.A. 97, 7784–7789.
Barr, J.N., Wertz, G.W., 2005. Role of the conserved nucleotide mismatch within 3′- and 5′-terminal regions of Bunyamwera virus in signaling transcription. J. Virol. 79, 3586–3594.
Basu, V.P., Song, M., Gao, L., Rigby, S.T., Hanson, M.N., Bambara, R.A., 2008. Strand transfer events during HIV-1 reverse transcription. Virus Res. 134, 19–38.
Belisova, A., Semrad, K., Mayer, O., Kocian, G., Waigmann, E., Schroeder, R., Steiner, G., 2005. RNA chaperone activity of protein components of human Ro RNPs. RNA 11, 1084–1094.
Bertrand, E.L., Rossi, J.J., 1994. Facilitation of hammerhead ribozyme catalysis by the nucleocapsid protein of HIV-1 and the heterogeneous nuclear ribonucleoprotein A1. EMBO J. 13, 2904–2912.

Brown, E.C., Jackson, R.J., 2004. All five cold-shock domains of unr (upstream of N-ras) are required for stimulation of human rhinovirus RNA translation. J. Gen. Virol. 85, 2279–2287.
Chang, C.K., Sue, S.C., Yu, T.H., Hsieh, C.M., Tsai, C.K., Chiang, Y.C., Lee, S.J., Hsiao, H.H., Wu, W.J., Chang, W.L., Lin, C.H., Huang, T.H., 2006. Modular organization of SARS coronavirus nucleocapsid protein. J. Biomed. Sci. 13, 59–72.
Chang, K.S., Luo, G., 2006. The polypyrimidine tract-binding protein (PTB) is required for efficient replication of hepatitis C virus (HCV) RNA. Virus Res. 115, 1–8.
Cheng, A., Zhang, W., Xie, Y., Jiang, W., Arnold, E., Sarafianos, S.G., Ding, J., 2005. Expression, purification, and characterization of SARS coronavirus RNA polymerase. Virology 335, 165–176.
Clodi, E., Semrad, K., Schroeder, R., 1999. Assaying RNA chaperone activity in vivo using a novel RNA folding trap. EMBO J. 18, 3776–3782.
Coetzee, T., Herschlag, D., Belfort, M., 1994. *Escherichia coli* proteins, including ribosomal protein S12, facilitate in vitro splicing of phage T4 introns by acting as RNA chaperones. Genes Dev. 8, 1575–1588.
Cornillez-Ty, C.T., Lazinski, D.W., 2003. Determination of the multimerization state of the hepatitis delta virus antigens in vivo. J. Virol. 77, 10314–10326.
Cristofari, G., Darlix, J.L., 2002. The ubiquitous nature of RNA chaperone proteins. Prog. Nucleic Acid Res. Mol. Biol. 72, 223–268.
Cristofari, G., Ivanyi-Nagy, R., Gabus, C., Boulant, S., Lavergne, J.P., Penin, F., Darlix, J.L., 2004. The hepatitis C virus core protein is a potent nucleic acid chaperone that directs dimerization of the viral (+) strand RNA in vitro. Nucleic Acids Res. 32, 2623–2631.
Darlix, J.L., Gabus, C., Nugeyre, M.T., Clavel, F., Barré-Sinoussi, F., 1990. *Cis* elements and *trans*-acting factors involved in the RNA dimerization of the human immunodeficiency virus HIV-1. J. Mol. Biol. 216, 689–699.
Darlix, J.L., Lastra, M.L., Mély, Y., Roques, B., 2002. Nucleocapsid protein chaperoning of nucleic acids at the heart of HIV structure, assembly and cDNA synthesis. In: Kuiken, C., Foley, B., Freed, E., Hahn, B., Marx, P., McCutchan, F., Mellors, J.W., Wolinsky, S., Korber, B. (Eds.), HIV Sequence Compendium. Los Alamos, NM, pp. 69–88.
Daros, J.A., Flores, R., 2002. A chloroplast protein binds a viroid RNA in vivo and facilitates its hammerhead-mediated self-cleavage. EMBO J. 21, 749–759.
Derebail, S.S., DeStefano, J.J., 2004. Mechanistic analysis of pause site-dependent and -independent recombinogenic strand transfer from structurally diverse regions of the HIV genome. J. Biol. Chem. 279, 47446–47454.
DeStefano, J.J., Titilope, O., 2006. Poliovirus protein 3AB displays nucleic acid chaperone and helix-destabilizing activities. J. Virol. 80, 1662–1671.
Domitrovich, A.M., Diebel, K.W., Ali, N., Sarker, S., Siddiqui, A., 2005. Role of La autoantigen and polypyrimidine tract-binding protein in HCV replication. Virology 335, 72–86.
Dreyfuss, G., 1986. Structure and function of nuclear and cytoplasmic ribonucleoprotein particles. Annu. Rev. Cell Biol. 2, 459–498.
Dreyfuss, G., Matunis, M.J., Pinol-Roma, S., Burd, C.G., 1993. hnRNP proteins and the biogenesis of mRNA. Annu. Rev. Biochem. 62, 289–321.
Dyson, H.J., Wright, P.E., 2005. Intrinsically unstructured proteins and their functions. Nat. Rev. 6, 197–208.
Égelé, C., Schaub, E., Piémont, E., Rocquigny, H., Mély, Y., 2005. Investigation by fluorescence correlation spectroscopy of the chaperoning interactions of HIV-1 nucleocapsid protein with the viral DNA initiation sequences. C. R. Biol. 328, 1041–1051.
Enjuanes, L. (Ed.), 2005. Coronavirus replication and reverse genetics, vol. 287. Curr. Top. Microbiol. Immunol. Springer, Berlin.
Enjuanes, L., Almazan, F., Sola, I., Zuñiga, S., 2006. Biochemical aspects of coronavirus replication and virus-host interaction. Annu. Rev. Microbiol. 60, 211–230.
Enjuanes, L., Gorbalenya, A.E., de Groot, R.J., Cowley, J.A., Ziebuhr, J., Snijder, E.J., 2008. The Nidovirales. In: Mahy, B.W.J., Van Regenmortel, M., Walker, P., Majumder-Russell, D. (Eds.), Encyclopedia of Virology, 3rd ed. Elsevier Ltd, Oxford, pp. 419–430.
Enjuanes, L., Sola, I., Zuñiga, S., Moreno, J.L., 2007. Coronavirus RNA synthesis: transcription. In: Thiel, V. (Ed.), Coronaviruses: Molecular and Cellular Biology. Caister Academic Press, Norfolk, pp. 81–107.
Florez, P.M., Sessions, O.M., Wagner, E.J., Gromeier, M., Garcia-Blanco, M.A., 2005. The polypyrimidine tract binding protein is required for efficient picornavirus gene expression and propagation. J. Virol. 79, 6172–6179.
Frankel, A.D., Young, J.A.T., 1998. HIV-1: fifteen proteins and an RNA. Annu. Rev. Biochem. 67, 1–25.
Furtig, B., Buck, J., Manoharan, V., Bermel, W., Jaschke, A., Wenter, P., Pitsch, S., Schwalbe, H., 2007. Time-resolved NMR studies of RNA folding. Biopolymers 86, 360–383.
Gao, L., Balakrishnan, M., Roques, B.P., Bambara, R.A., 2007. Insights into the multiple roles of pausing in HIV-1 reverse transcriptase-promoted strand transfers. J. Biol. Chem. 282, 6222–6231.
Gatignol, A., 2007. Transcription of HIV: Tat and cellular chromatin. Adv. Pharmacol. 55, 137–159.
Ghetti, A., Piñol-Roma, S., Michael, W.M., Morandi, C., Dreyfuss, G., 1992. hnRNP I, the polypyrimidine tract-binding protein: distinct nuclear localization and association with hnRNAs. Nucleic Acids Res. 20, 3671–3678.
Gil, A., Sharp, P.A., Jamison, S.F., Garcia-Blanco, M.A., 1991. Characterization of cDNAs encoding the polypyrimidine tract-binding protein. Genes Dev. 5, 1224–1236.
Gorbalenya, A.E., Enjuanes, L., Ziebuhr, J., Snijder, E.J., 2006. Nidovirales: evolving the largest RNA virus genome. Virus Res. 117, 17–37.
Gosert, R., Chang, K.H., Rijnbrand, R., Yi, M., Sangar, D.V., Lemon, S.M., 2000. Transient expression of cellular polypyrimidine-tract binding protein stimulates cap-independent translation directed by both picornaviral and flaviviral internal ribosome entry sites in vivo. Mol. Cell. Biol. 20, 1583–1595.
Grohman, J.K., Del Campo, M., Bhaskaran, H., Tijerina, P., Lambowitz, A.M., Russell, R., 2007. Probing the mechanisms of DEAD-box proteins as general RNA chaperones: the C-terminal domain of CYT-19 mediates general recognition of RNA. Biochemistry 46, 3013–3022.
Guo, J., Henderson, L.E., Bess, J., Kane, B., Levin, J.G., 1997. Human immunodeficiency virus type 1 nucleocapsid protein promotes efficient strand transfer and specific viral DNA synthesis by inhibiting TAR-dependent self-priming from minus-strand strong-stop DNA. J. Virol. 71, 5178–5188.
Guo, J., Wu, T., Kane, B.F., Johnson, D.G., Henderson, L.E., Gorelick, R.J., Levin, J.G., 2002. Subtle alterations of the native zinc finger structures have dramatic effects on the nucleic acid chaperone activity of human immunodeficiency virus type 1 nucleocapsid protein. J. Virol. 76, 4370–4378.
Heilman-Miller, S.L., Wu, T., Levin, J.G., 2004. Alteration of nucleic acid structure and stability modulates the efficiency of minus-strand transfer mediated by the HIV-1 nucleocapsid protein. J. Biol. Chem. 279, 44154–44165.
Henriet, S., Sinck, L., Bec, G., Gorelick, R.J., Marquet, R., Paillart, J.C., 2007. Vif is a RNA chaperone that could temporally regulate RNA dimerization and the early steps of HIV-1 reverse transcription. Nucleic Acids Res. 35, 5141–5153.
Herschlag, D., 1995. RNA chaperones and the RNA folding problem. J. Biol. Chem. 270, 20871–20874.
Herschlag, D., Khosla, M., Tsuchihashi, Z., Karpel, R.L., 1994. An RNA chaperone activity of non-specific RNA binding proteins in hammerhead ribozyme catalysis. EMBO J. 13, 2913–2924.
Hong, M.K., Harbron, E.J., O'Connor, D.B., Guo, J., Barbara, P.F., Levin, J.G., Musier-Forsyth, K., 2003. Nucleic acid conformational changes essential for HIV-I nucleocapsid protein-mediated inhibition of self-priming in minus-strand transfer. J. Mol. Biol. 325, 1–10.
Huang, P., Lai, M.M.C., 2001. Heterogeneous nuclear ribonucleoprotein A1 binds to the 3′-untranslated region and mediates potential 5′–3′-end cross talks of mouse hepatitis virus RNA. J. Virol. 75, 5009–5017.
Huang, Z.S., Su, W.H., Wang, J.L., Wu, H.N., 2003. Selective strand annealing and selective strand exchange promoted by the N-terminal domain of hepatitis delta antigen. J. Biol. Chem. 278, 5685–5693.
Huang, Z.S., Wu, H.N., 1998. Identification and characterization of the RNA chaperone activity of hepatitis delta antigen peptides. J. Biol. Chem. 273, 26455–26461.
Hunt, S.L., Hsuan, J.J., Totty, N., Jackson, R.J., 1999. unr, a cellular cytoplasmic RNA-binding protein with five cold shock domains, is required for internal initiation of translation of human rhinovirus RNA. Genes Dev. 13, 437–448.
Hunt, S.L., Jackson, R.J., 1999. Polypyrimidine-tract binding protein (PTB) is necessary, but not sufficient, for efficient internal initiation of translation of human rhinovirus-2 RNA. RNA 5, 344–359.
Ivanyi-Nagy, R., Davidovic, L., Khandjian, E.W., Darlix, J.L., 2005. Disordered RNA chaperone proteins: from functions to disease. Cell. Mol. Life Sci. 62, 1409–1417.
Ivanyi-Nagy, R., Kanevsky, I., Gabus, C., Lavergne, J.P., Ficheux, D., Penin, F., Fossé, P., Darlix, J.L., 2006. Analysis of hepatitis C virus RNA dimerization and core–RNA interactions. Nucleic Acids Res. 34, 2618–2633.
Ivanyi-Nagy, R., Lavergne, J., Gabus, C., Ficheux, D., Darlix, J., 2008. RNA chaperoning and intrinsic disorder in the core proteins of *Flaviviridae*. Nucleic Acids Res. 36, 2618–2633.
Jeng, K.S., Su, P.Y., Lai, M.M.C., 1996. Hepatitis delta antigens enhance the ribozyme activities of hepatitis delta virus RNA in vivo. J. Virol. 70, 4205–4209.
Ji, X., Klarmann, G.J., Preston, B.D., 1996. Effect of human immunodeficiency virus type 1 (HIV-1) nucleocapsid protein on HIV-1 reverse transcriptase activity in vitro. Biochemistry 35, 132–143.
Karakasiliotis, I., Chaudhry, Y., Roberts, L.O., Goodfellow, I.G., 2006. Feline calicivirus replication: requirement for polypyrimidine tract-binding protein is temperature-dependent. J. Gen. Virol. 87, 3339–3347.
Khaiboullina, S.F., Morzunov, S.P., St Jeor, S.C., 2005. Hantaviruses: molecular biology, evolution and pathogenesis. Curr. Mol. Med. 5, 773–790.
Kim, M.J., Kao, C., 2001. Factors regulating template switch *in vitro* by viral RNA-dependent RNA polymerases: implications for RNA–RNA recombination. Proc. Natl. Acad. Sci. U.S.A. 98, 4972–4977.
Kos, A., Dijkema, R., Arnberg, A.C., van der Meide, P.H., Schellekens, H., 1986. The hepatitis delta (d) virus possesses a circular RNA. Nature 323, 558–560.
Kuciak, M., Gabus, C., Ivanyi-Nagy, R., Semrad, K., Storchak, R., Chaloin, O., Muller, S., Mély, Y., Darlix, J.L., 2008. The HIV-1 transcriptional activator Tat has potent nucleic acid chaperoning activities in vitro. Nucleic Acids Res. 36, 3389–3400.
Kuo, M.Y., Chao, M., Taylor, J., 1989. Initiation of replication of the human hepatitis delta virus genome from cloned DNA: role of delta antigen. J. Virol. 63, 1945–1950.
Levin, J.G., Guo, J., Rouzina, I., Musier-Forsyth, K., 2005. Nucleic acid chaperone activity of HIV-1 nucleocapsid protein: critical role in reverse transcription and molecular mechanism. Prog. Nucleic Acid Res. Mol. Biol. 80, 217–286.
Lin, H.X., White, K.A., 2004. A complex network of RNA–RNA interactions controls subgenomic mRNA transcription in a tombusvirus. EMBO J. 23, 3365–3374.
Lindenbach, B.D., Rice, C.M., 2001. Flaviviridae: the viruses and their replication. In: Knipe, D.M., Howley, P.M. (Eds.), Fields Virology, 4th ed. Lippincott Williams and Wilkins, Philadelphia, pp. 991–1041.
Liu, H.W., Zeng, Y., Landes, C.F., Kim, Y.J., Zhu, Y., Ma, X., Vo, M.N., Musier-Forsyth, K., Barbara, P.F., 2007. Insights on the role of nucleic acid/protein interactions in chaperoned nucleic acid rearrangements of HIV-1 reverse transcription. Proc. Natl. Acad. Sci. U.S.A. 104, 5261–5267.

Lorsch, J.R., 2002. RNA chaperones exist and DEAD box proteins get a life. Cell 109, 797–800.
Maraia, R.J., Intine, R.V.A., 2001. Recognition of nascent RNA by the human La antigen: conserved and divergent features of structure and function. Mol. Cell. Biol. 21, 367–379.
Mayer, O., Waldsich, C., Grossberger, R., Schoeder, R., 2002. Folding of the td pre-RNA with the help of the RNA chaperone StpA. Biochem. Soc. Trans. 30, 1175–1180.
Meerovitch, K., Svitkin, Y.V., Lee, H.S., Lejbkowicz, F., Kenan, D.J., Chan, E.K., Agol, V.I., Keene, J.D., Sonenberg, N., 1993. La autoantigen enhances and corrects aberrant translation of poliovirus RNA in reticulocyte lysate. J. Virol. 67, 3798–3807.
Mir, M.A., Panganiban, A.T., 2005. The hantavirus nucleocapsid protein recognizes specific features of the viral RNA panhandle and is altered in conformation upon RNA binding. J. Virol. 79, 1824–1835.
Mir, M.A., Panganiban, A.T., 2006a. Characterization of the RNA chaperone activity of hantavirus nucleocapsid protein. J. Virol. 80, 6276–6285.
Mir, M.A., Panganiban, A.T., 2006b. The bunyavirus nucleocapsid protein is an RNA chaperone: possible roles in viral RNA panhandle formation and genome replication. RNA 12, 272–282.
Mitchell, S.A., Spriggs, K.A., Coldwell, M.J., Jackson, R.J., Willis, A.E., 2003. The Apaf-1 internal ribosome entry segment attains the correct structural conformation for function via interactions with PTB and Unr. Mol. Cell 11, 757–771.
Mohr, S., Stryker, J.M., Lambowitz, A.M., 2002. A DEAD-box protein functions as an ATP-dependent RNA chaperone in group I intron splicing. Cell 109 (6), 769–779.
Moradpour, D., Penin, F., Rice, C.M., 2007. Replication of hepatitis C virus. Nat. Rev. Microbiol. 5, 453–463.
Moreno, J.L., Zuñiga, S., Enjuanes, L., Sola, I., 2008. Identification of a coronavirus transcription enhancer. J. Virol. 82, 3882–3893.
Nagy, P.D., Simon, A.E., 1997. New insights into the mechanisms of RNA recombination. Virology 235, 1–9.
Nagy, P.D., Zhang, C., Simon, A.E., 1998. Dissecting RNA recombination in vitro: role of RNA sequences and the viral replicase. EMBO J. 17, 2392–2403.
Negroni, M., Buc, H., 2000. Copy-choice recombination by reverse transcriptases: reshuffling of genetic markers mediated by RNA chaperones. Proc. Natl. Acad. Sci. U.S.A. 97, 6385–6390.
Neuman, B.W., Joseph, J.S., Saikatendu, K.S., Serrano, P., Chatterjee, A., Johnson, M.A., Liao, L., Klaus, J.P., Yates, J.R., Wüthrich, K., Stevens, R.C., Buchmeier, M.J., Kuhn, P., 2008. Proteomics analysis unravels the functional repertoire of coronavirus nonstructural protein 3. J. Virol. 82, 5279–5294.
Obradovic, Z., Peng, K., Vucetic, S., Radivojac, P., Brown, C., Dunker, A.K., 2003. Predicting intrinsic disorder from aminoacid sequence. Proteins 53, 566–572.
Opi, S., Takeuchi, H., Kao, S., Khan, M.A., Miyagi, E., Goila-Gaur, R., Iwatani, Y., Levin, J.G., Strebel, K., 2006. Monomeric APOBEC3G is catalytically active and has antiviral activity. J. Virol. 80, 4673–4682.
Ozdarendeli, A., Ku, S., Rochat, S., Williams, G.D., Senanayake, S.D., Brian, D.A., 2001. Downstream sequences influence the choice between a naturally occurring noncanonical and closely positioned upstream canonical heptameric fusion motif during bovine coronavirus subgenomic mRNA synthesis. J. Virol. 75, 7362–7374.
Pannone, B., Xue, D., Wollin, S.L., 1998. A role for the yeast La protein in U6 snRNP assembly: evidence that the La protein is a molecular chaperone for RNA polymerase III transcripts. EMBO J. 17, 7442–7453.
Parker, M.M., Masters, P.S., 1990. Sequence comparison of the N genes of five strains of the coronavirus mouse hepatitis virus suggests a three domain structure for the nucleocapsid protein. Virology 179, 463–468.
Peng, K., Vucetic, S., Radivojac, P., Brown, C.J., Dunker, A.K., Obradovic, Z., 2005. Optimizing intrinsic disorder predictors with protein evolutionary information. J. Bioinform. Comput. Biol. 3, 35–60.
Plyusnin, A., Vapalahti, O., Vaheri, A., 1996. Hantaviruses: genome structure, expression and evolution. J. Gen. Virol. 77, 2677–2687.
Pontius, B.W., Berg, P., 1992. Rapid assembly and disassembly of complementary DNA strands through as equilibrium. J. Biol. Chem. 267, 13815–13818.
Portman, D.S., Dreyfuss, G., 1994. RNA annealing activities in HeLa nuclei. EMBO J. 13, 213–221.
Prats, A.C., Sarih, L., Gabus, C., Litvak, S., Keith, G., Darlix, J.L., 1988. Small finger protein of avian and murine retrovirus has nucleic acid annealing activity and positions the replication primer tRNA onto genomic RNA. EMBO J. 7, 1777–1783.
Rajkowitsch, L., Chen, D., Stampfl, S., Semrad, K., Waldsich, C., Mayer, O., Jantsch, M.F., Konrat, R., Bläsi, U., Schroeder, R., 2007. RNA chaperones, RNA annealers and RNA helicases. RNA Biol. 4, 118–130.
Rajkowitsch, L., Schroeder, R., 2007. Dissecting RNA chaperone activity. RNA 13, 1–8.
Rajkowitsch, L., Semrad, K., Mayer, O., Schroeder, R., 2005. Assays for the RNA chaperone activity of proteins. Biochem. Soc. Trans. 33, 450–456.
Ramalanjaona, N., de Rocquigny, H., Millet, A., Ficheux, D., Darlix, J.L., Mély, Y., 2007. Investigating the mechanism of the nucleocapsid protein chaperoning of the second strand transfer during HIV-1 DNA synthesis. J. Mol. Biol. 374, 1041–1053.
Reeder, R.H., Lang, W.H., 1997. Terminating transcription in eukaryotes: lessons learned from RNA polymerase I. Trends Biochem. Sci. 22, 473–477.
Roda, R.H., Balakrishnan, M., Hanson, M.N., Wöhrl, B.M., Le Grice, S.F.J., Roques, B.P., Gorelick, R.J., Bambara, R.A., 2003. Role of the reverse transcriptase, nucleocapsid protein, and template structure in the two-step transfer mechanism in retroviral recombination. J. Biol. Chem. 278, 31536–31546.
Sakai, H., Shibata, R., Sakuragi, J., Kawamura, M., Adachi, A., 1993. Cell-dependent requirement of human immunodeficiency virus type 1 Vif protein for maturation of virus particles. J. Virol. 67, 1663–1666.
Sawicki, S.G., Sawicki, D.L., 2005. Coronavirus transcription: a perspective. Curr. Top. Microbiol. Immunol. 287, 31–55.
Sawicki, S.G., Sawicki, D.L., Siddell, S.G., 2007. A contemporary view of coronavirus transcription. J. Virol. 81, 20–29.
Schroeder, R., Barta, A., Semrad, K., 2004. Strategies for RNA folding and assembly. Nat. Rev. Mol. Cell. Biol. 5, 908–919.
Semrad, K., Green, R., Schoeder, R., 2004. RNA chaperone activity of large ribosomal subunit proteins from *Escherichia coli*. RNA 10, 1855–1860.
Shen, X., Masters, P.S., 2001. Evaluation of the role of heterogeneous nuclear ribonucleoprotein A1 as a host factor in murine coronavirus discontinuous transcription and genome replication. Proc. Natl. Acad. Sci. U.S.A. 98, 2717–2722.
Shi, S.T., Lai, M.M., 2005. Viral and cellular proteins involved in coronavirus replication. In: Enjuanes, L. (Ed.), Curr. Top. Microbiol. Immunol., vol. 287, pp. 95–131.
Smits, S.L., van Vliet, A.L., Segeren, K., el Azzouzi, H., van Essen, M., de Groot, R.J., 2005. Torovirus non-discontinuous transcription: mutational analysis of a subgenomic mRNA promoter. J. Virol. 79, 8275–8281.
Sola, I., Moreno, J.L., Zuñiga, S., Alonso, S., Enjuanes, L., 2005. Role of nucleotides immediately flanking the transcription-regulating sequence core in coronavirus subgenomic mRNA synthesis. J. Virol. 79, 2506–2516.
Song, Y., Tzima, E., Ochs, K., Bassili, G., Trusheim, H., Linder, M., Preissner, K.T., Niepmann, M., 2005. Evidence for an RNA chaperone function of polypyrimidine tract-binding protein in picornavirus translation. RNA 11, 1809–1824.
Sova, P., Volsky, D.J., 1993. Efficiency of viral DNA synthesis during infection of permissive and nonpermissive cells with vif-negative human immunodeficiency virus type 1. J. Virol. 67, 6322–6326.
Tisne, C., Roques, B.P., Dardel, F., 2004. The annealing mechanism of HIV-1 reverse transcription primer onto the viral genome. J. Biol. Chem. 279, 3588–3595.
Tompa, P., Csermely, P., 2004. The role of structural disorder in the function of RNA and protein chaperones. FASEB J. 18, 1169–1175.
Tsuchihashi, Z., Brown, P.O., 1994. DNA strand exchange and selective DNA annealing promoted by the human immunodeficiency virus type I nucleocapsid protein. J. Virol. 68, 5863–5870.
van den Born, E., Gultyaev, A.P., Snijder, E.J., 2004. Secondary structure and function of the 5′-proximal region of the equine arteritis virus RNA genome. RNA 10, 424–437.
van den Born, E., Posthuma, C.C., Gultyaev, A.P., Snijder, E.J., 2005. Discontinuous subgenomic RNA synthesis in arteriviruses is guided by an RNA hairpin structure located in the genomic leader region. J. Virol. 79, 6312–6324.
van Hemert, M.J., van den Worm, S.H., Knoops, K., Mommaas, A.M., Gorbalenya, A.E., Snijder, E.J., 2008. SARS–coronavirus replication/transcription complexes are membrane-protected and need a host factor for activity in vitro. PLoS Pathog. 4, e1000054.
Vo, M.N., Barany, G., Rouzina, I., Musier-Forsyth, K., 2006. Mechanistic studies of mini-TAR RNA/DNA annealing in the absence and presence of HIV-1 nucleocapsid protein. J. Mol. Biol. 363, 244–261.
Wang, C.C., Chang, T.C., Lin, C.W., Tsui, H.L., Chu, P.B., Chen, B.S., Huang, Z.S., Wu, H.N., 2003. Nucleic acid binding properties of the nucleic acid chaperone domain of hepatitis delta antigen. Nucleic Acids Res. 31, 6481–6492.
Wang, K.S., Choo, Q.L., Weiner, A.J., Ou, J.H., Najarian, R.C., Thayer, R.M., Mullenbach, G.T., Denniston, K.J., Gerin, J.L., Houghton, M., 1986. Structure, sequence and expression of the hepatitis delta (d) viral genome. Nature 323, 508–514.
White, K.A., 2002. The premature termination model: a possible third mechanism for subgenomic mRNA transcription in (+)-strand RNA viruses. Virology 304, 147–154.
White, K.A., Nagy, P.D., 2004. Advances in the molecular biology of tombusviruses: gene expression, genome replication, and recombination. Prog. Nucleic Acid Res. Mol. Biol. 78, 187–226.
Wiegand, H.L., Doehle, B.P., Bogerd, H.P., Cullen, B.R., 2004. A second human antiretroviral factor, APOBEC3F, is suppressed by the HIV-1 and HIV-2 Vif proteins. EMBO J. 23, 2451–2458.
Williams, M.C., Gorelick, R.J., Musier-Forsyth, K., 2002. Specific zinc-finger architecture required for HIV-1 nucleocapsid protein's nucleic acid chaperone functions. Proc. Natl. Acad. Sci. U.S.A. 99, 8614–8619.
Williams, M.C., Rouzina, I., Wenner, J.R., Gorelick, R.J., Musier-Forsyth, K., 2001. Mechanism for nucleic acid chaperone activity of HIV-1 nucleocapsid protein revealed by single molecule stretching. Proc. Natl. Acad. Sci. U.S.A. 98, 6121–6126.
Wilson, K.S., von Hippel, P.H., 1995. Transcription termination at intrinsic terminators: the role of the RNA hairpin. Proc. Natl. Acad. Sci. U.S.A. 92, 8793–8797.
Wollerton, M.C., Gooding, C., Robinson, F., Brown, E.C., Jackson, R.J., Smith, C.W., 2001. Differential alternative splicing activity of isoforms of polypyrimidine tract binding protein (PTB). RNA 7, 819–832.
Wu, T., Guo, J., Bess, J., Henderson, L.E., Levin, J.G., 1999. Molecular requirements for human immunodeficiency virus type 1 plus-strand transfer: analysis in reconstituted and endogenous reverse transcription systems. J. Virol. 73, 4794–4805.
Wu, T., Heilman-Miller, S.L., Levin, J.G., 2007. Effects of nucleic acid local structure and magnesium ions on minus-strand transfer mediated by the nucleic acid chaperone activity of HIV-1 nucleocapsid protein. Nucleic Acids Res. 35, 3974–3987.
Wu, W., Henderson, L.E., Copeland, T.D., Gorelick, R.J., Bosche, W.J., Rein, A., Levin, J.G., 1996. Human immunodeficiency virus type 1 nucleocapsid protein reduces reverse transcriptase pausing at a secondary structure near the murine leukemia virus polypurine tract. J. Virol. 70, 7132–7142.
Zeng, Y., Liu, H.W., Landes, C.F., Kim, Y.J., Ma, X., Zhu, Y., Musier-Forsyth, K., Barbara, P.F., 2007. Probing nucleation, reverse annealing, and chaperone function along

the reaction path of HIV-1 single-strand transfer. Proc. Natl. Acad. Sci. U.S.A. 104, 12651–12656.
Zhang, W., Hwang, C.K., Hu, W.S., Gorelick, R.J., Pathnak, V., 2002. Zinc finger domain of murine leukemia virus nucleocapsid protein enhances the rate of viral DNA synthesis in vivo. J. Virol. 76, 7473–7484.
Zhang, X., Lai, M.M.C., 1995. Interactions between the cytoplasmic proteins and the intergenic (promoter) sequence of mouse hepatitis virus RNA: correlation with the amounts of subgenomic mRNA transcribed. J. Virol. 69, 1637–1644.
Zhang, X., Li, H.P., Xue, W., Lai, M.C.C., 1999. Formation of a ribonucleoprotein complex of mouse hepatitis virus involving heterogeneous nuclear ribonucleoprotein A1 and transcription-regulatory elements of viral RNA. Virology 264, 115–124.
Zheng, A., Derbyshire, V., Salvo, J.L., Belfort, M., 1995. *Escherichia coli* protein StpA stimulates self-splicing by promoting RNA assembly in vitro. RNA 1, 783–793.
Zuñiga, S., Sola, I., Alonso, S., Enjuanes, L., 2004. Sequence motifs involved in the regulation of discontinuous coronavirus subgenomic RNA synthesis. J. Virol. 78, 980–994.
Zuñiga, S., Sola, I., Moreno, J.L., Sabella, P., Plana-Duran, J., Enjuanes, L., 2007. Coronavirus nucleocapsid protein is an RNA chaperone. Virology 357, 215–227.